Petrology and geochronology of an arc sequence, Bonaire, Dutch Antilles, and its relationship to the Caribbean Plateau

By

Patricia Maeve Eleanor Thompson BSc.

(Edinburgh)

A thesis submitted for the degree of

Doctor of Philosophy

at the University of Leicester

Department of Geology

University of Leicester

January 2002

Abstract

Petrology and geochronology of an arc sequence, Bonaire, Dutch Antilles, and its relationship to the Caribbean Plateau

Patricia M. E. Thompson

Oceanic plateau rocks, island arc fragments and tonalitic batholiths are juxtaposed on the southern Caribbean margin, and appear to be both spatially and temporally related. It is widely accepted that the plateau originated in the Pacific realm, and although there is no consensus as to which hotspot it was derived from, Galápagos is frequently cited. A previous study concluded that one of the tonalitic batholiths, the 85 Ma Aruba batholith was generated from the first stages of subduction beneath the 90 Ma plateau, following a subduction polarity reversal.

Until this study, little was known about the genesis of the arc sequences associated with the plateau, and their tectonic significance. This work focuses on the volcanic sequence exposed on Bonaire, and uses field, geochemical, isotopic and geochronological constraints to confirm that it is an arc sequence, and to reveal that the arc sequence is genetically unrelated to the plateau and the batholith. It formed as part of an intra oceanic arc at 95 ± 2 Ma, prior to plateau formation.

In addition, Hf-Nd isotopes are used to fingerprint both the Caribbean plateau and the Galápagos plume, and support a genetic link between the two. The arc most likely originated in the Pacific, along with the Caribbean plateau, and was later swept up in front of the eastwards moving plateau, and eventually accreted onto the Southern Caribbean margin.

Acknowledgments

I must first give huge thanks to my supervisors, John Tarney, Andy Saunders and Andrew Kerr, along with my semi-unofficial supervisor, Roz White, for devising the project, for their support and for all the discussions we've had over the years. In particular, John is thanked for his company and assistance in the field, Andrew for allowing me to become his "Monday girl" for those weekly 8am discussions on the Caribbean, Roz for allowing me to pester her for "quick questions", and Andy for always having sound words of advice.

I am really grateful to Pamela Kempton for all her patience, enthusiasm (and amazing efficiency!) for the radiogenic isotope side of the project, and for encouraging me to spend last summer in the middle of the Pacific. A big thanks also goes to Malcolm Pringle for his great help and enthusiasm with the Ar-Ar analysis, for teaching me the joys of isotopes by night, and for making my visit to East Kilbride much more fun.

I 'd like to thank all the people on Bonaire who assisted us in the field- especially Kerenza Rannou-Frenz from Stinapa, and the folk at DROB for their assistance with obtaining topographic maps and arranging access, and Bas Tol for dutifully arranging the return of my rocks every year. And thanks to Julian Henty for his field assistance and company in my first field season, and for not destroying our "poor leettle car" on rough dirt tracks despite the 200kg of rock on the back seat!

I am really grateful to all the Leicester folk who have shown interest in my project and discussed things with me: Norry, for his encyclopaedic knowledge on partition coefficients etc, Dickson, for some great chats, Richard England, for spending hours on those gravity maps and for his enthusiasm, Randy, for helping me round the strontium problem, and others elsewhere- Henriette Lapierre, Nick Arndt, Sido, Jean Hernandez and anyone else I haven't mentioned. Other Leicester folk who have helped me with rock preparation/analysis are sincerely thanked too- Emma, Nick, Rob, Colin, Lyn, and Rob Wilson, and I owe Loz at Cardiff a lot of beers for his assistance with ICP-MS analysis.

I also owe a huge thanks to my long-suffering housemates Bloomers, Butch and Storey (and honorary housemate Gav), for putting up with my writing up, as well as the occasional drunken blonde break-in attempts. Thanks too to Roz for being the best landlady ever. Craig B deserves a special mention for three years of verbal abuse, computer troubleshooting, advice and also for last-minute map assistance. You're a star! My officemates are also thanked for the occasional distraction and those Friday afternoon you-know-what championships- Matt H, Hanananah, Andrew and particularly Little Dave, as he's had to bear the brunt of me for the last few months. A special mention must go to my circuits team- Heike, Brownboy, Gav and Little Dave, for encouraging me to do pressups instead of thesis writing, and for the other distractors around the department- Matt H, James T, James H, Natalie, Big Dave, Annabel, Marc Moocow, Mike M and all the rest at Leicester. Thanks too to my mates at the end of email- my shipmates Jill and Claire, to Bev and Chrissy.

Finally, I am also really indebted to my thesis support team- to James, for being my personal chauffeur, proofreader, and destresser (and for the endless 2am thesis formatting!), to Stozz for his office visits and support, and especially to my family for their support (and cash injections!).

Contents

Appendix F

Publications and presentations resulting from this study

List of Figures

List of Tables

Chapter 1

Introduction

1.1. Rationale of the project

The southern Caribbean represents a complex accretionary margin, where island arc-derived sequences are found in close association with oceanic plateau fragments and tonalitic batholiths (e.g. Beets et al., 1984). The arcs, plateaux and related rocks are all of Upper Cretaceous age. Similar island arc sequences are found all round the margins of the plateau, but their origin remains enigmatic, particularly given their close spatial and temporal association with the Caribbean plateau. This study aims to document one such arc sequence, the Washikemba Formation, on the island of Bonaire, with the aim of using field, geochronological and isotopic techniques to evaluate its origin and the nature of its relationship with the Caribbean plateau and tonalitic batholith on the neighbouring island of Aruba.

The Washikemba Formation was selected for this study because of its geographical proximity to both plateau and tonalitic batholith lithologies. A plateau sequence is exposed on Curaçao, only ~50 km away, and a tonalitic batholith intrudes the plateau lavas on the nearby island of Aruba. Both of these islands are well characterised by previous studies (Kerr et al., 1997; White, 1999; White et al., 1999), and are similar in age to the most reliable existing ages of the Washikemba Formation. Hence, an investigation of the Washikemba Formation may help to place important constraints on the relationship between the Caribbean plateau, batholith and arc sequences, and thereby give further insights into the origin and evolution of the Caribbean plate.

Within this study, three basic models of the origin of the arc-related sequences are considered and evaluated. These are presented in Fig.1.1, and summarised below:

A. *Subduction beneath the Caribbean plateau.* This model requires that the arc has resulted from normal oceanic crust being subducted beneath the Caribbean plateau, and that the resulting arc has developed on top of the plateau. This model has been invoked for the Aruba batholith, which clearly intrudes the plateau sequence (White, 1999).

B. *Remelting of the Caribbean plateau.* In this scenario, the "arc" is generated through remelting of the mafic plateau sequences, resulting in the development of an arc-like geochemical signature, but no actual arc. This model has been proposed for the generation of the siliceous rocks on Iceland (Marsh et al., 1991; Jonasson et al., 1992; Jonasson, 1994).

C. *Accreted arc sequence unrelated to the Caribbean plateau.* This third model proposes that the arc sequences are entirely unrelated to the Caribbean plateau, despite the similarity in their ages.

These three hypotheses are returned to in Chapter 7, where each one is assessed for its applicability to the new data presented in this study, before they are discriminated between, and a new model for the origin of the Washikemba Formation is presented.

The results of this study may have wider implications. The Southern Caribbean margin has many features common to Archaean granite greenstone belts: tonalites, komatiites and arc-related sequences. Granite greenstone belts represent a significant amount of the earliest continental crust preserved, and thus the Southern Caribbean margin may prove to be a natural laboratory for gaining a greater understanding of crustal development and evolution. In particular, the role of arc magmatism in continental crust generation is widely lauded, partly due to the broad geochemical similarity between arcs and average continental crust, (Tarney et al., 1976; Taylor et al., 1977). Thus, gaining an insight into the role of the arc sequences (including Bonaire) in the evolution of the Southern Caribbean margin could help constrain models of crustal generation.

1.2. Methodology

As previous studies of the Washikemba Formation have been extremely limited in extent, a detailed field, geochemical, geochronological study was undertaken, in order to gain a greater understanding of the detailed characteristics of the Formation. These are outlined below.

Chapter 2 presents an overview of Caribbean plateau, island arc and silicic batholith lithologies exposed around the margins of the Caribbean. Emphasis is placed on the island arc sequences, in order to place the Washikemba Formation into a wider tectonic context. This section has been incorporated into a co-authored review paper of the Caribbean plateau and arc sequences, to be published in a memoir of the American Association of Petroleum

Geologists (AAPG) entitled *"No Oceanic Plateau - No Caribbean Plate? The Seminal Role of Oceanic Plateau(s) in Caribbean Plate Evolution"*.

The results of a field study of the lithological characteristics of the Washikemba Formation, based on two field seasons carried out in 1999 and 2000, is presented in Chapter 3. This aims to present the first geological map of the Southern Complex, the more poorly studied of the two inliers of the Formation, and to evaluate in detail the relationship between the different lithological components.

Chapter 4 presents the results of a new $^{40}Ar - ^{39}Ar$ study of the Formation, undertaken at Scottish Universities Research and Reactor Centre (SURRC) during March 2001. Despite the difficulties usually associated with obtaining reliable $^{40}Ar - ^{39}Ar$ ages for lithologies as altered as those of the Washikemba Formation, new minimum ages obtained allow useful constraints to be placed on the origin of the Formation. These will be returned to in Chapter 7.

A comprehensive geochemical investigation of the different lithologies of the Washikemba Formation is presented in Chapter 5. This comprises major, trace element and Pb-Sr-Nd-Hf isotope data, along with some preliminary interpretations of the relationship of different members of the Formation. Isotopic analysis was undertaken at the NERC Isotope Geosciences Laboratories (NIGL), Keyworth, under the guidance of Dr Pamela Kempton, and major and trace element data were obtained at the Universities of Leicester and Cardiff. Emphasis was placed on Hf and Nd isotopic data, rather than Pb and Sr, due to the levels of alteration experienced by the Formation (discussed within Chapter 5).

Chapter 6 aims to place the Washikemba Formation into a wider reference frame, by presenting the results of the first Hf-Nd isotope study of the Caribbean plateau. It then goes on further to use Hf-Nd isotopes to evaluate the relationship between the Caribbean plateau the Galápagos plume (widely thought to be responsible for generating the plateau lavas), in order to establish its origin. A version of this chapter has been submitted to *Earth and Planetary Science Letters*, in a paper co-authored by Pamela Kempton, Rosalind White, Andrew Kerr, John Tarney, Andrew Saunders and Godfrey Fitton (Edinburgh).

In Chapter 7, entitled *"The petrogenesis of the Washikemba Formation and its relationship to the Caribbean plateau"*, the geochemical data presented in Chapter 5 is integrated with the geochronological and field data, in order to formulate a model for the formation and evolution of the arc sequence exposed on the island of Bonaire. This chapter returns to the models first outlined in Section 1.1, and uses the integrated data discussed in the first part of Chapter 7 to discriminate between them. Finally, the chapter discusses the implications this new model for the origin of the Washikemba Formation has on the Mesozoic evolution of the Caribbean region.

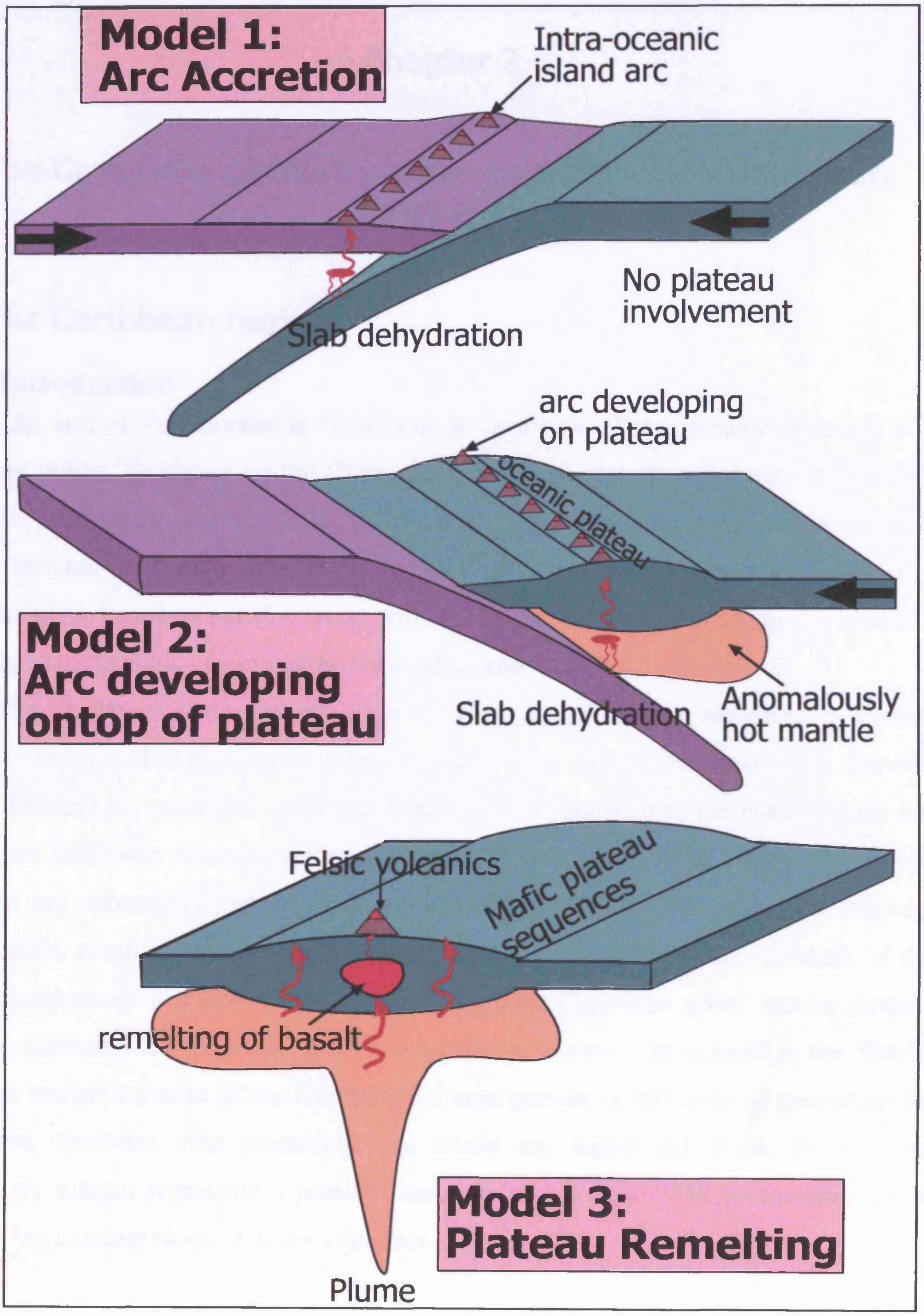

Fig. 1.1. Cartoon showing three possible models for the origin of the island arc sequences associated with the Caribbean plateau. Discussed in Section 1.1.

Chapter 2

The Caribbean oceanic plateau and associated island arc sequences

2.1 The Caribbean region

2.1.1 Introduction

The aim of this chapter is to present an overview of the tectonic elements of the Caribbean region, focussing on the Cretaceous Caribbean plateau and associated island arc sequences, in order to place the geology of Bonaire, in particular the Washikemba Formation, into its tectonic framework. A tectonic model for the formation and evolution of the Caribbean plate, based on existing work, will also be presented, in order to give a context for this study. This tectonic model will be returned to, and modified, in Chapter 7.

The Caribbean region represents a complex assemblage of Mesozoic to Cenozoic oceanic terranes, including oceanic plateaux, island arcs, and oceanic crust. The Caribbean Plateau, forming the main part of the Caribbean plate, is bounded to the north and the south by complex strike-slip zones (Mann et al., 1990, Avè Lallemant, 1996; 1997), where plateau fragments are subaerially exposed and tectonically associated with island arc sequences, oceanic crust, tonalitic batholiths and high pressure metamorphic rocks. A study of these various components will help unravel the origin of the Caribbean plate, and constrain the Mesozoic-Cenozoic evolution of the intra-American region. Additionally, the Southern Caribbean margin contains all the individual terranes present in Precambrian greenstone belts (komatiites, tonalities, iron formations and island arc sequences). Thus, the Caribbean accretionary margin represents a possible analogue of a Precambrian greenstone belt, and therefore the building block of a new continent.

2.1.2 Neotectonic regime of the broader Caribbean region

The limits of the Caribbean plate have been defined seismically through earthquake focal mechanisms (Mann et al., 1990; Mann, 1999; Fig. 2.1). The Caribbean plate is bordered to the east and the west by subduction zones: Pacific lithosphere is consumed on the western margin (the Central American arc) and Atlantic lithosphere on the eastern side (the Lesser Antilles island arc). The precise positions of the northern and southern boundaries are not as

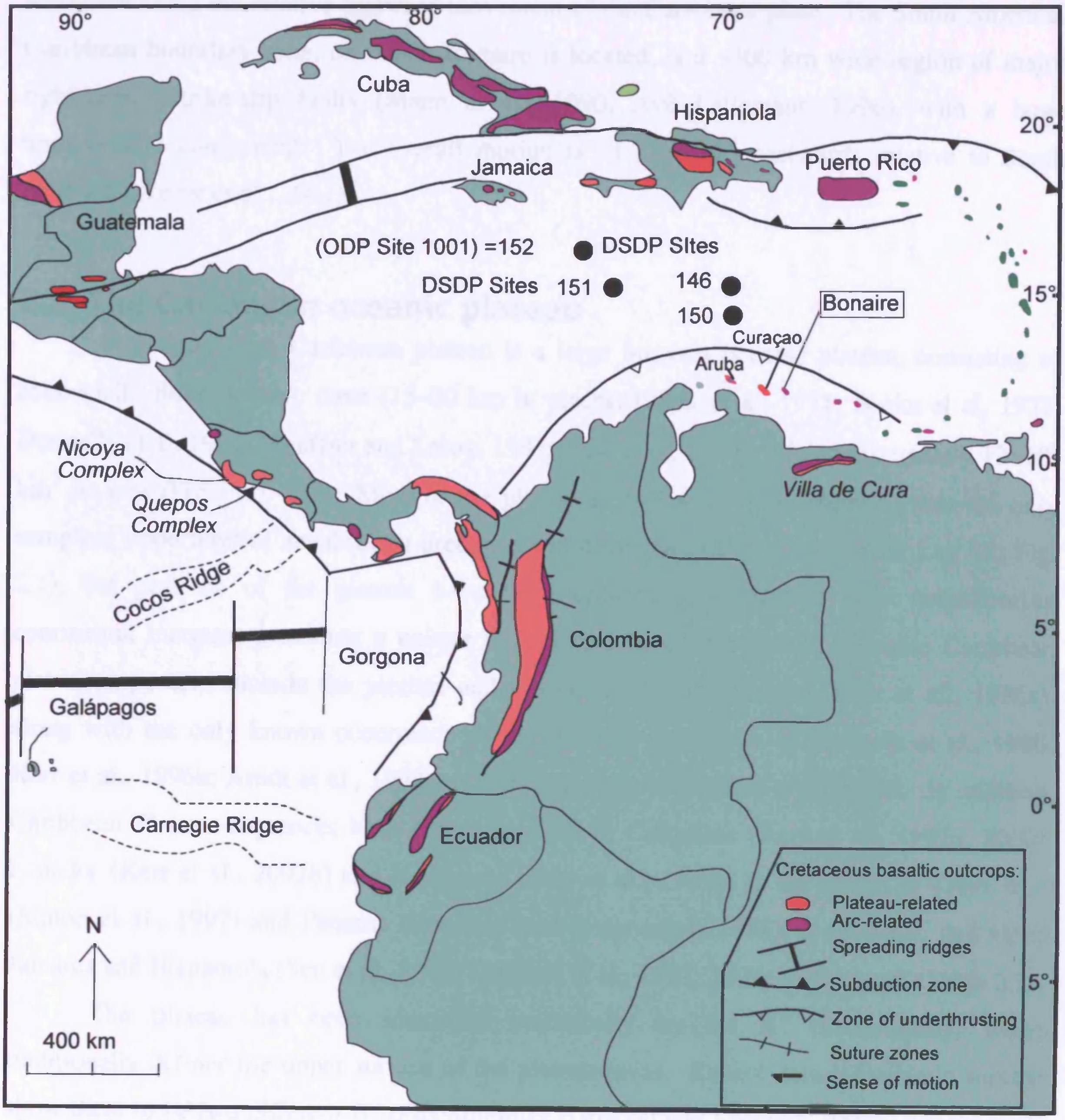

Fig. 2.1. Tectonic map of the Caribbean, showing different oceanic terranes. After Mann et al. (1990), White et al. (1999) and Kerr et al. (2002).

well defined as the eastern and western ones, due to the lack of earthquakes to yield focal mechanisms. Each boundary consists of a broad (250–300 km) zone of strike slip faults, accommodating the relative eastward movement of the Caribbean plate. The South America-Caribbean boundary zone, on which Bonaire is located, is a ~300 km wide region of major right-lateral strike-slip faults (Mann et al., 1990; Avè Lallemant, 1996), with a large transpressive component. The overall motion is ~1.3 cm yr^{-1} eastwards relative to South America (Weber et al., 2001).

2.2 The Caribbean oceanic plateau

The Cretaceous Caribbean plateau is a large buoyant oceanic plateau, consisting of abnormally thick oceanic crust (15–20 km in places; Edgar et al, 1971; Burke et al. 1978, Donnelly et al. 1989; Mauffret and Leroy, 1997; Case et al, 1990). It is approximately 12×10^5 km^2 in area (Figs. 2.1–2.3). Most of the plateau is still submarine, meaning that the only sampling opportunities are through dredging and deep sea drilling (e.g. DSDP Leg 15; Fig. 2.1), but portions of the plateau have been uplifted and accreted onto neighbouring continental margins, providing a unique insight into its deeper levels. Notable Caribbean plateau exposures include the picrites and pillow basalts on Curaçao (Kerr et al., 1996a), along with the only known occurrence of Phanerozoic komatiites (Echeverría et al., 1980; Kerr et al., 1996b; Arndt et al., 1997), which outcrop on the island of Gorgona. In addition, Caribbean Plateau sequences have been identified in Colombia (Kerr et al., 1997a; 2000), Ecuador (Kerr et al., 2002b) and Venezuela (Kerr et al., 1997a) to the south, in Costa Rica (Sinton et al., 1997) and Panama (Bowland and Rosencranz, 1988) to the west, and Haiti, Jamaica and Hispaniola (Sen et al., 1988; Lapierre et al., 1997; 2000) to the north (Table 2.1).

The plateau has been identified seismically by the B″ discontinuity, which traditionally defines the upper surface of the plateau lavas. Recent detailed seismic surveys show there to be two different B" discontinuities (Driscoll and Diebold, 1998; Diebold et al., 1999): a thick (15–20 km) smooth one which is interpreted as representing the upper limit of the large-scale homogeneous plateau flows and sills (i.e. the plateau, sensu stricto), and a thin (~4 km) rough horizon consisting of local highs and ridges which is much more reminiscent of typical - albeit abnormally thin - oceanic crust (Diebold et al., 1999).

The smooth B" horizon has been drilled in five localities: DSDP Sites 146, 150, 151 and 153, and ODP Site 1001. Unfortunately the rough B" discontinuity has never been penetrated. At DSDP Site 152 and ODP Site 1001 (40 km apart), a thin basalt sill overlying basement was drilled (Driscoll et al., 1999) but basement was not reached (Diebold, pers. com., 2001). The basalts from Site 1001 have been dated by ^{40}Ar–^{39}Ar techniques at around

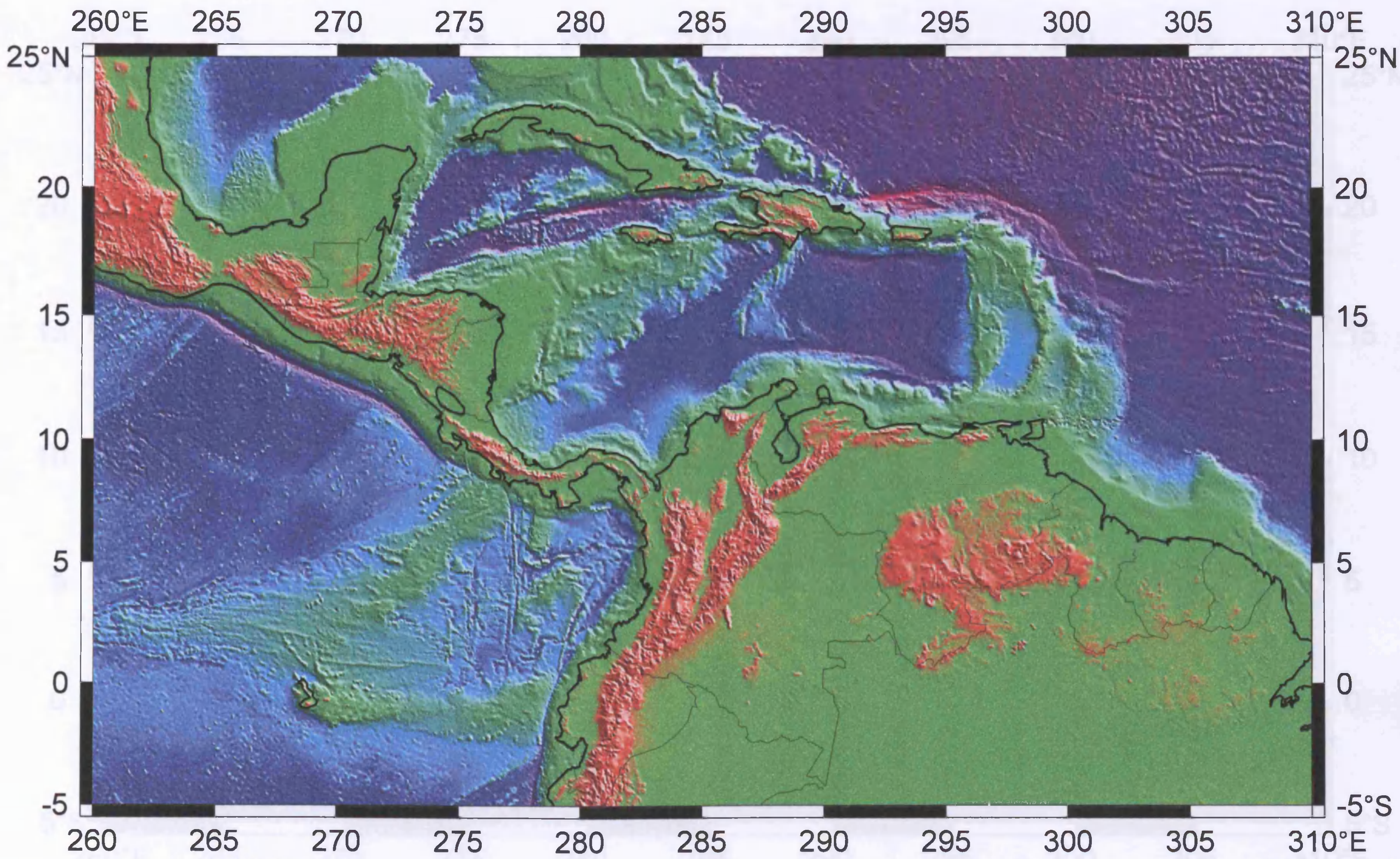

Fig. 2. Map showing satellite topographic data for the Caribbean region. Data from GMT, taken at 2 second intervals.

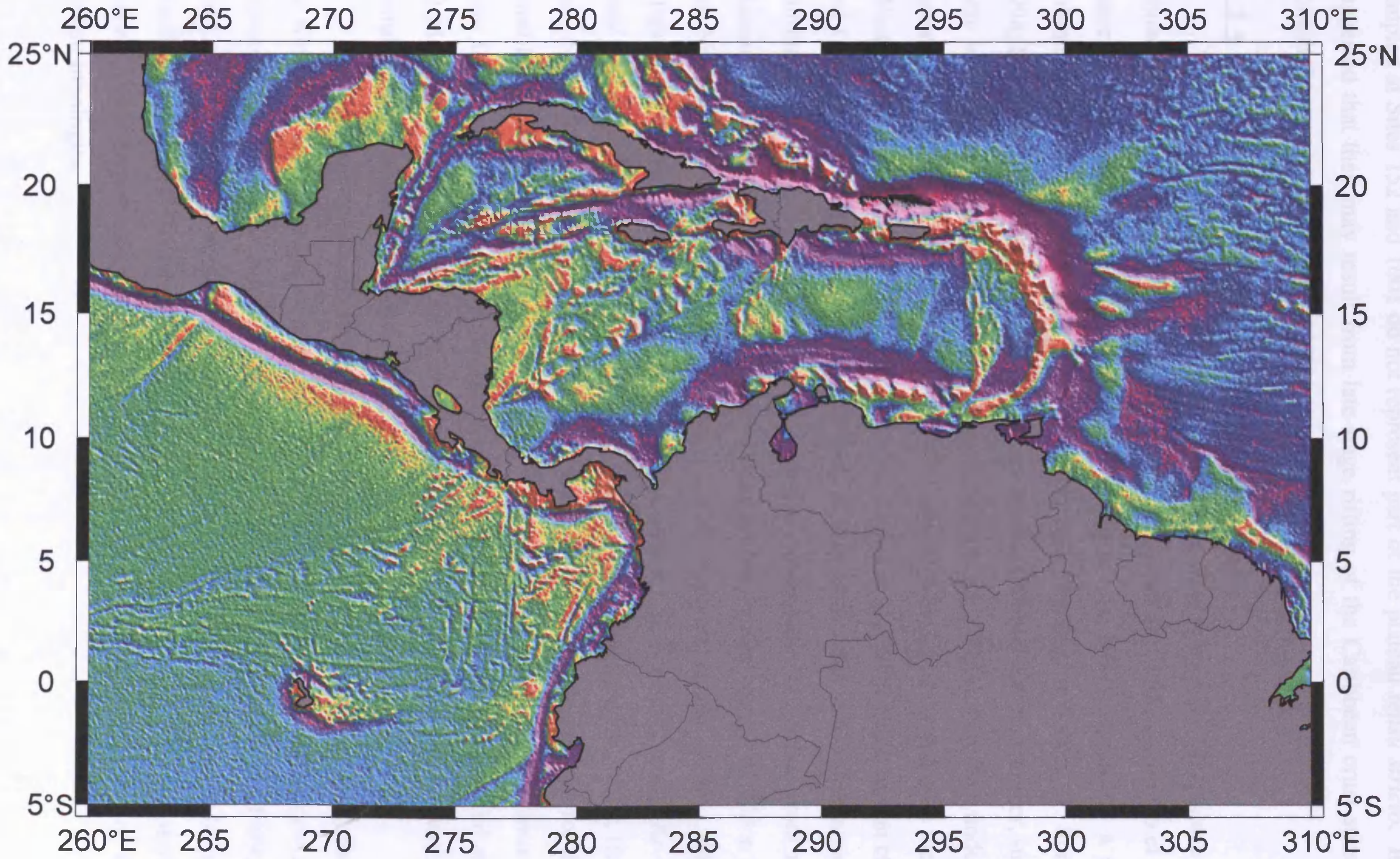

Fig. 2.3. Map showing satellite gravity data for the Caribbean region. Data from GMT, taken at 2 second intervals.

81 Ma (Sinton et al., 2000), and are therefore younger than the bulk of the plateau, and therefore the majority of the rough B" layer which underlies the plateau. Thus the basalts sampled at Sites 152 and 1001 do not represent part of the plateau *sensu stricto*. It has been suggested that they may result from late-stage rifting of the Caribbean crust subsequent to plateau formation (Sinton et al., 1998).

2.2.1 Age constraints on the Caribbean Plateau

Until recently, all the available ^{40}Ar–^{39}Ar and Re–Os ages for the plateau clustered around 90 Ma (Sen et al., 1988; Sinton et al., 1993; Kerr et al., 1997a; Alvarado et al., 1997; Lapierre et al., 1999; Lewis et al., 1999; Walker et al., 1999) suggesting a short and voluminous burst of magmatism. New ^{40}Ar–^{39}Ar ages (outlined in Table 2.1; Sinton et al., 1998; Lapierre et al., 1999) and seismic interpretations (Diebold, 1999), however, suggest that there were at least two main phases of plateau magmatism. Whilst there was undoubtedly a major plateau-wide magmatic event at ~90 Ma, abundant evidence from across the province (Western Colombia: Kerr et al., 1997a; Curaçao: Sinton et al., 1998; Haiti: Sinton et al., 1998 and Costa Rica: Hauff et al., 2000a) suggests a secondary, but still voluminous plateau-building phase occurred around 76 Ma. A primary magmatic hornblende from a possible plateau-related small ultramafic sequence in Ecuador has yielded an age of 123 ± 13 Ma by Sm–Nd isochron methods (Lapierre et al., 1999, Lapierre et al., 2000), although its relationship to the Caribbean plateau remains uncertain. In addition, new ^{40}Ar–^{39}Ar ages from plateau sequences in Costa Rica and Central America (Sinton et al., 1997; Hauff et al., pers. com., 2001) fall in the ranges of 93–84 Ma and 76–72 Ma, and new ages for the Central Cordillera of Colombia place its formation at 93–88 Ma (Kerr et al., 2002a). These new ages show that Caribbean plateau magmatism occurred from 95 to 72 Ma, and peaked around 88–92 Ma, rather than occurring in one voluminous burst at around 90 Ma, as was originally postulated (Kerr et al., 1997; Sinton et al., 1998; Hauff et al., 2000a).

A similar story is beginning to emerge for other large igneous provinces, for example the Kerguelen and Ontong Java plateaux. This has important implications for new models of plateau generation as the simple starting plume head model (Richards et al., 1989; Griffiths and Campbell, 1990; Campbell and Griffiths, 1990; Hill, 1993) may no longer be applicable. Mauffret and Leroy (1997) and Révillon et al. (1999), for example have invoked a multi-headed plume hypothesis to explain the age and geographical distribution of Caribbean plateau lithologies.

Locality	Unit name	Age	Lithologies	Reference	Comments
Dominican Republic	Duarte Complex	81.6 & 86.7 Ma	Metabasic to ultramafic rocks intruded by Cretaceous to Eocene plutons	Lapierre et al., 1999	Metabasites are of oceanic crustal affinity.
Dominican Republic	Siete Cabezas Formation	68.5 & 69 Ma	Basalts and cherts	Sinton et al., 1998	
Tobago	North Coast Schists	>120 Ma	Metabasites, andesites and volcaniclastics	Snoke et al., 1998; 2001	
Tobago	Tobago Dykes	91& 103–105 Ma	Basic dykes	Snoke et al., 1998; 2001	
Venezuela	Tiara Formation, Villa de Cura	Albian (97–112)	Mafic and picritic metalavas, tuffs and volcanic conglomerates	Beck et al., 1984	
Cuba	Margot & Encrucijada Formations	Aptian– Cenomanian (90–124 Ma)	Ophiolite melange	Kerr et al., 1999	
Ecuador	Pinon Formation	At least Turonian	Tholeiitic pillows and volcaniclastics	Jaillard et al., 1995; Reynaud et al., 1999	
Ecuador	Pallatanga Unit	Santonian–Campanian (86.5–83 Ma)	Pillow basalts, dolerites, hyaloclastites and sediments	Kerr et al., 2002	
Ecuador	San Juan Unit	123 ± 13 Ma	Peridotites and gabbros, intruded by dykes	Lapierre et al., 2000	
Colombia	Central Cordillera	93–88 Ma	Basalts and subordinate picrites with sediments	Kerr et al., 2001	
Colombia	Western Cordillera	92.7 & 77.2 Ma	Basalts and metasediments	Kerr et al., 1997; Sinton et al., 1998	*Recorrected to new age of Taylor Creek rhyolite (28.34 Ma).*
Colombia	Serranía de Baudó	72.5–77.9 Ma	Basalts and metasediments	Kerr et al., 1997	*Recorrected to new age of Taylor Creek rhyolite (28.34 Ma).*
Colombia	Gorgona	88.1–89.3/ 89.2 ± 5.2 Ma (Ar-Ar & Re-Os)	Komatiites, picrites, breccias, pillow basalts and gabbros	Echeverria, 1980 Walker et al., 1999	*Recorrected to new age of Taylor Creek rhyolite (28.34 Ma).*
Haiti	Dumisseau Fm	89.7–93.0 Ma	Basalt and dolerites	Sen et al., 1988; Sinton & Duncan, 1992	*Recorrected to new age of Taylor Creek rhyolite (28.34 Ma).*
Trinidad	Sans Souci Formation	87± 4 Ma (K–Ar)	Basalts, gabbros, volcaniclastics	Wadge & McDonald, 1985	
Jamaica	Bath–Dunrobin Fm	83–74 Ma (fossil age)	Deformed basalts, dolerites and gabbros with some sediments	Wadge et al., 1982	

Table 2.1a. Summary of oceanic plateau outcrops of the Caribbean region (continued overleaf)

DSDP Leg 15	Site 146	91.6–93.1 Ma	Basalts, dolerites. Correlates with smooth B" layer.	Sinton et al., 1998	*Recorrected to new age of Taylor Creek rhyolite (28.34 Ma).*
DSDP Leg 15	Site 150	95.4 Ma	Basalts dolerites. Correlates with smooth B" layer.	Sinton et al., 1998	*Recorrected to new age of Taylor Creek rhyolite (28.34 Ma).*
DSDP Leg 15	Site 151		Basalts dolerites. Correlates with smooth B" layer.	Sinton et al., 1998	
DSDP Leg 15	Site 152		Basalts dolerites. Correlates with rough B" layer.	Sinton et al., 1998	
DSDP Leg 165	Site 1001	80.8–81.3	Basalts dolerites. Correlates with rough B" layer.	Sinton et al., 1998	
Guatemala	El Tambor Group	Cenomanian (90–97 Ma)	Metamorphosed mafics	Donnelly 1990	
Panama	Azuero Complex	<58 Ma	Metabasites	Goosens et al., 1977, Hauff, pers. comm., 2001.	
Panama	Sona Complex	74.6 Ma	Metabasites	Goosens et al., 1977, Hauff, pers. comm., 2001.	
Curaçao	Curaçao Lava Formation	89.0–90.8 & 76.9	Picrites, pillow basalts and volcaniclastics	Kerr et al., 1997; Sinton et al., 1998	*Recorrected to new age of Taylor Creek rhyolite (28.34 Ma).*
Aruba	Aruba Lava Formation	88–91 Ma	Basalts and amphibolites	White, 1999 White et al., 1999	
Costa Rica	Nicoya Complex	94.7–84.5 Ma	Pillow basalts, grabbro and plagiogranite intrusions	Sinton et al., 1997 Hauff et al., 2000	Intrusives are 84.1 Ma in age *Recorrected to new age of Taylor Creek rhyolite (28.34 Ma)*
Costa Rica	Tortugal Complex	89.7 Ma	Picrites and basalts	Alvarado et al., 1997	
Costa Rica	Herradura Complex	83.4–86.0 Ma	Pillow basalts, grabbro and plagiogranite intrusions	Sinton et al., 1997 Hauff et al., 2000	
Costa Rica	Quepos Complex	59 & 63.9 Ma	Pillow basalts, grabbro and plagiogranite intrusions	Sinton et al., 1997 Hauff et al., 2000	
Costa Rica	Osa Complex	62.1 Ma	Pillow basalts, grabbro and plagiogranite intrusions	Hauff et al., 2000	
Costa Rica	Golfito & Burica Complexes	Maastrichtian (68–74 Ma)	Pillow basalts, grabbro and plagiogranite intrusions	Di Marco et al., 1994	

Table 2.1b. Summary of oceanic plateau outcrops of the Caribbean region (ctd.)

2.2.2 How and where did the Caribbean plateau form?

The widespread magmatism occurring within a relatively short timescale, the abnormally thick oceanic crust and the enriched (relative to chondrite) geochemical character of the lithologies (Kerr et al., 1996a), along with the presence of picrites and komatiites (which require an ambient mantle temperature up to 200–300°C hotter than normal; McKenzie and Bickle, 1988), has led most workers to suggest that the Caribbean plateau represents the eruptive products of a mantle plume (e.g. Kerr et al., 1997; Sinton et al., 1998). Determining which mantle plume was responsible for the Caribbean Plateau is still somewhat uncertain.

Existing models for the origin of the Caribbean plate can be divided into two types: the intra-American and the Pacific models. The intra-American class of model (e.g., Ball et al., 1969; Donnelly, 1985; Meschede, 1998) proposes that the plateau formed essentially *in situ* relative to the two Americas along the Caribbean spreading axis, and therefore is considered autochthonous. A more common view amongst Caribbean workers is that the Caribbean Plateau originated in the Pacific, and has since moved eastwards relative to the two Americas (e.g. Burke et al., 1978, 1984; Duncan and Hargreaves, 1984; Pindell and Barrett, 1990; Pindell et al., 1998; Kerr et al., 1999). This is supported by the present day eastward motion of the Caribbean plate along well-developed strike-slip zones, implying a long duration of eastward movement. The oldest rocks of the present-day Lesser Antilles island arc are Eocene in age, indicating that Atlantic crust (as opposed to Caribbean crust) has been consumed since at least then. In addition, in several localities around the Caribbean, sedimentary intercalations in Cretaceous volcanic sequences contain radiolaria with a clear Pacific affinity (Montgomery et al., 1994).

2.2.3 Initial outpourings of the Galápagos plume?

Many workers suggest the Galápagos plume may have been responsible for the extrusion of the Caribbean plateau (e.g. Duncan and Hargreaves, 1984; Richards et al., 1989; Hill, 1993; Hauff et al., 1997), an argument which is strengthened by the occurrence of the 65 Ma Quepos terrane, an accreted oceanic island complex on the Costa Rican margin, sharing geochemical affinities with both the Caribbean plateau and the Galápagos plume (e.g. Sallares et al., 2001; Hauff et al., 2000). This shows isotopic (Pb, Sr, Nd) and trace element similarities to both the neighbouring Caribbean plateau sequences found on the Costa Rican margin (e.g., the Nicoya Complex), and the Miocene Cocos and Carnegie aseismic ridges that are believed to form part of the Galápagos hotspot track (Hauff et al., 1997), hinting at a common origin. In addition, komatiites from Gorgona (Révillion et al., 2002, in press) and picrites from the Costa Rican Quepos Complex (Hauff et al., 2000) both have high $^{3}He/^{4}He$

signatures: the Galápagos plume is one of the relatively few plumes in existence today that also displays this feature (Graham et al., 1993), strengthening the connection between the Galápagos plume and the Caribbean Plateau, and the Quepos Complex.

Whilst trace element and existing isotope data for the Caribbean plateau do not exclude a Galápagos origin, the hypothesis nonetheless still remains controversial amongst tectonics workers. Recent kinematic and palinspastic reconstructions (Pindell, pers. com., 2001) suggest the Caribbean plateau formed much closer to the Americas than the Galápagos hotspot, which was as far away as 1000 km to the west. New paleomagnetic data (Acton et al., 2000) are consistent with the Caribbean plate being at the present latitude of the Galápagos hotspot at the time of plateau formation; however the estimated paleolongitudes, as determined from plate motion estimates and palinspastic reconstructions (Meschede and Frisch, 1998; Meschede, 1998), indicate that the Caribbean plate was probably much closer to the Americas than Galápagos was at that time. In addition, the oldest proven manifestations of the Galápagos plume, parts of the Galapagos islands, are 15–20 Ma old (Christie et al., 1992), yet the youngest Caribbean plateau sequences identified are at least 65 Ma (Sinton et al., 1998; Hauff et al., 2000b). This requires a long hotspot duration of >90 Ma (Sinton et al., 1998; Kerr et al., 1999; Walker et al., 1999), with an absence of any magmatic record for ca. 25 My of that time, possibly as a consequence of subduction at the Central American trench.

2.3 Mesozoic-Cenozoic tectonic reconstruction of the Caribbean region

Assuming a Pacific origin of the Caribbean plate, as seems to be the general consensus today, the following model is discussed, based on an amalgamation of existing tectonic models (Duncan and Hargreaves, 1984; Kerr et al., 1997; Mann et al., 2000; Pindell and Barrett, 1998; Pindell et al., 2001).

Since the Jurassic (Fig. 2.4), a long-lived subduction zone has been present between the Americas and the Pacific region, subducting Farallon (Pacific) crust beneath the Americas. In the Jurassic, North and South America started to break apart, extending the length of this subduction zone. Around 90 Ma, normal Farallon oceanic crust drifted over a Pacific hotspot (not necessarily the Galápagos hotspot), where the crust became thickened and underplated, forming the present-day Caribbean Plateau. As this thick (and therefore buoyant) crust collided with the subduction zone (ca. 85 Ma; White et al., 1999), it temporarily choked it, ultimately causing a polarity reversal, with subduction resuming in the opposite direction (Farallon /Caribbean plate consuming Atlantic crust; i.e. the proto-Lesser Antilles). The Caribbean plate then continued to move eastwards relative to the two

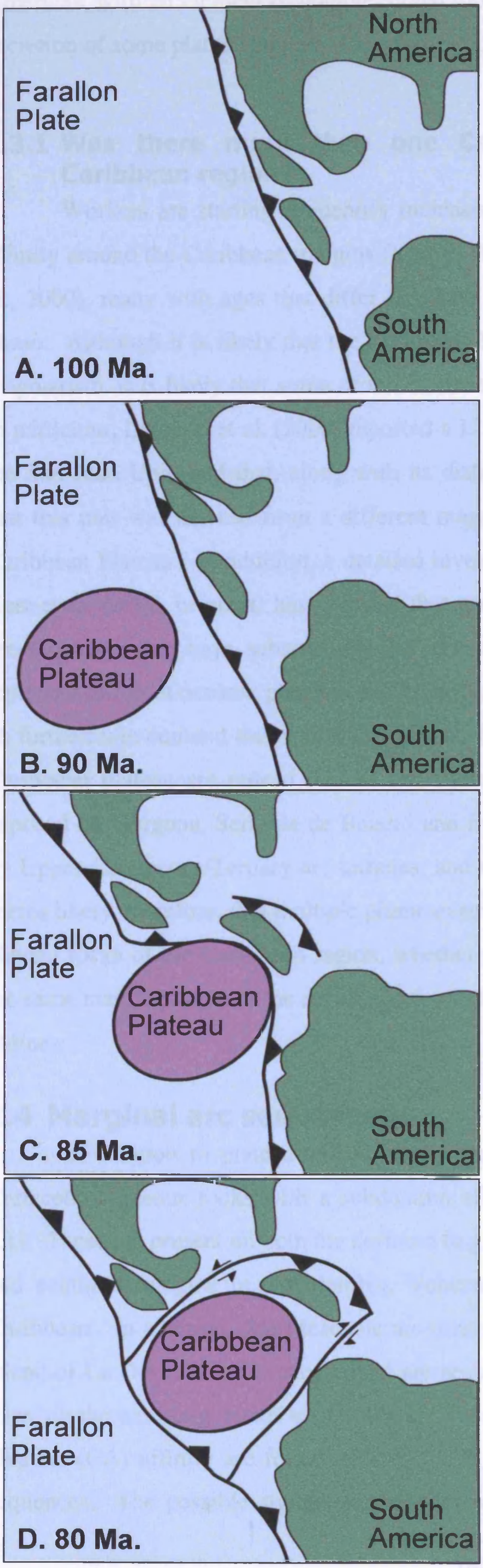

A. North and South America start to diverge, extending the length of the long-lived intra-American subduction zone.

B. As the Pacific plate drifts eastwards over a hotspot, the Caribbean Plateau is extruded onto Pacific crust.

C. The Caribbean plateau reaches the subduction zone, causing it to jam and ultimately backstep and reverse polarity.

D. The Caribbean Plateau continues to move eastwards between the two Americas, and fragments dock against the American margins.

Fig. 2.4. Simplified Upper Cretaceous tectonic reconstruction of the Caribbean region, after Pindell et al. (1990); White et al. (1999).

Americas, with an element of compressional motion against the Americas causing uplift and accretion of some plateau and arc-derived rocks onto the neighbouring continental margins.

2.3.1 Was there more than one Cretaceous oceanic plateau in the Caribbean region?

Workers are starting to identify increasing numbers of terranes with oceanic plateau affinity around the Caribbean margins (Kerr et al., 1999; 2000; Hauff et al., 2000; Lapierre et al., 2000), many with ages that differ from the main 88–91 Ma Caribbean plateau building phase. Although it is likely that the Caribbean Plateau was produced from several pulses of magmatism, it is likely that some of these terranes do not represent a single oceanic plateau. In particular, Lapierre et al. (2000) reported a 123 Ma 3-point isochron age for a gabbro from the San Juan Unit, and that, along with its distinct Pb isotopic signature provided evidence that this unit was derived from a different magmatic source (and at a different time) to the Caribbean Plateau. In addition, a detailed investigation of the different Ecuador terranes by Kerr et al. (2002, in press) has revealed that oceanic plateau slices are separated by distinct arc sequences and have substantially different accretion ages, providing evidence that two represent different oceanic plateaux events of similar age are represented in Ecuador. Kerr et al. furthermore contend that whilst the bulk of the 88–91 Ma ages previously ascribed to the Caribbean Plateau are indeed part of the plateau, the westernmost terranes (such as those exposed on Gorgona, Serranía de Baudió and Piñon) are separated from other plateau rocks by Upper Cretaceous/Tertiary arc terranes, and thus represent a separate magmatic event. It seems likely, therefore, that multiple plume events were involved in the genesis of the oceanic plateau rocks of the Caribbean region, whether through multiple pulses of magmatism from the same mantle plume, or the accretion of oceanic plateaux originating from different mantle plumes.

2.4 Marginal arc sequences

In addition to plateau-related exposures, many outcrops of intrusive and extrusive Cretaceous igneous rocks with a subduction affinity outcrop in the Caribbean region (Fig. 2.1). These are present on both the northern (e.g. Puerto Rico, Cuba, Hispaniola and Jamaica) and southern margins (e.g. Colombia, Venezuela, Ecuador, Tobago and Bonaire) of the Caribbean. In addition, one Mesozoic arc-related sequence is present on the Lesser Antilles island of La Desirade, and many island arc sequences have been recently identified in Costa Rica, on the west (e.g. Hauff et al., 2000a). Units of both island arc tholeiite (IAT) and calc-alkaline (CA) affinity are found, although IAT predominates, especially amongst the older sequences. The possible significance of this will be discussed in Section 2.6. Bonaire is omitted from the section below, as it is the focus of this thesis, and its field geology is discussed in detail in Chapter 3.

2.4.1 Bonaire

The Washikemba Formation on Bonaire is considered to represent a typical island arc sequence. It is the focus of this thesis, and a summary of previous work on the island is outlined in Chapter 3.1.

2.4.2 Virgin Islands

The Water Islands Formation is considered the type example of the IAT or PIA series in the Caribbean (Donnelly 1966; 1972; 1994; Donnelly and Rogers, 1967), and consists of three kilometres of interlayered mafic and siliceous lavas. The mafic rocks are termed spilites (Donnelly, 1966), due to their modal albite and chlorite, whereas the siliceous rocks (known as keratophyres) tend to be more dominant. It has been postulated (Donnelly, 1972), that this Formation has formed largely as the result of the eruption of water-rich melts at abyssal depths, sufficient to prevent volatile separation and encourage reaction between the seawater and the alkalis. There appears to have been a sea level rise over time, culminating in pyroclastic deposits at the top of the succession. Donnelly et al. (1990) have reported radiolarian ages of upper Aptian to lowermost Albian (115–110 Ma) for the top of the Formation.

An angular unconformity separates the Water Island Formation from the overlying Louisenhoj Formation, which consists of subaerially erupted andesite and its epiclastic derivatives. These appear to have accumulated in shallow water around an emergent volcano (Donnelly, 1972). Pb isotopes show the Water Island Formation to be one of the least radiogenic arc sequences in the world, indicating very little contamination of subducted sediment (Lewis et al., 1995). A sedimentary succession immediately overlying the Louisenhoj Formation apparently contains late Albian ammonites (Young, 1972).

2.4.3 Hispaniola

Hispaniola is a geologically very complex area (Mann et al., 1991), consisting of eleven distinct tectonic arc-related terranes, including belts of serpentised peridotites, blueschists and granodiorite plutons. In a general sense, in the north of the island an extensive Cretaceous-Eocene arc sequence is found. It consists of components of the forearc, magmatic arc, oceanic basement and a possible closed Upper Cretaceous back-arc basin (Draper et al., 1991). The magmatic arc is best represented by the hydrothermally metamorphosed rocks of the Los Ranchos formation (Mann et al., 1991; Kesler et al. 1991 including rhyolites, tuffs, andesites, volcanic breccias and pillowed basalts. Geochemically, these volcanic rocks are of tholeiitic affinity, and there is some evidence of sub-aerial eruption in the final volcanic stages. K–Ar dating yields imprecise ages ranging from Aptian to Santonian, and a granodiorite pluton of calc-alkaline affinity has a Santonian (86.5–83 Ma) K–Ar age (reported in Mann et al., 1991). Unfortunately no trace element data for the volcanics of the Los Ranchos Formation have been published.

Island arc tholeiite sequences of this age, known as the Guamira volcanics, are uncomformably overlain by the Loma La Vega volcanics and the Las Guajabas tuffs (Lebron and Perfit, 1993; 1994). These latter two units are arc-derived sequences of calc-alkaline affinity, and the unconformity between them and the IAT sequence beneath is thought to represent the subduction flip event (Lebron and Perfit, 1993; 1994). This unconformity can be constrained to Albian-Aptian times, due to the presence of a fossiliferous limestone containing Albian-Aptian fauna occurring directly above the unconformity. No equivalent unconformity is found in other Caribbean arc-related units, however, implying that it may not be a Caribbean-wide event, meaning that the unconformity probably cannot be correlated with any major tectonic episode such as a subduction polarity reversal.

2.4.4 Puerto Rico

Like Hispaniola, Puerto Rico consists of a complex amalgamation of arc terranes, which represent one of the longest known records (120–45 Ma) of continual arc activity in the world (Jolly et al., 2001). The island is divided into three volcanic provinces, and in each of these provinces a broad progression from primitive island arc to calc-alkaline and shoshonitic geochemical affinity is observed (Jolly et al., 1998). The central volcanic province is the most extensive, and consists of five east-west tectonic belts that migrated northward over time (Jolly et al., 1998). The oldest lithologies are Aptian volcanic breccias, and the sequence continues until the Mastrichtian, where volcaniclastic tuffs are abundant. The southwestern volcanic province is underlain by a Lower-Upper Jurassic basement complex known as the Bermeja complex (Section 2.6; Schellekens, 1998a). The volcanic province is dominated by detrital volcanic units containing the remnants of two sequential island arc belts of Campanian-Mastrichtian to Eocene age. In contrast, the northeastern volcanic province contains an older Lower-Albian to Eocene volcanic arc sequence and associated sediments, although folding and large-scale strike-slip faulting makes correlation of different units difficult.

There is a gradual geochemical change from exclusively IAT series to the CA series (with some continuing IAT activity) over time, as evidenced by the progressive increase in La/Sm and Th/Hf ratios (Schellekens, 1998b; Jolly et al., 1998). The first calc-alkaline products appeared about 100 Ma (Schellekens, 1998b). This is interpreted as reflecting the addition of a sedimentary component, which is supported by the broad increase in negative Ce anomalies over time (Schellekens, 1998b). Radiogenic isotope evidence also reveals a gradual change from IAT to CA in the Puerto Rico arc sequences (Frost et al., 1998). Once again, there is no evidence for a sudden change in geochemical affinity which could be attributed to a subduction flip. Additionally, in the northeastern province no unconformity has been identified until 85 Ma (Jolly et al., 1998), meaning that it is highly probable that the subduction flip did not occur until at least the Santonian (86.5–83 Ma), and the earliest island-wide hiatus is observed at ~60 Ma.

Pb, Nd and Sr isotopes, along with Th/La element ratios, suggest that there was a systematic increase in the amount of sediment subducted over the Mesozoic, whilst the absolute abundance of terriginous sediment in the system stayed constant. This suggests that neighbouring continents, including South American craton, did not significantly contribute to the Mesozoic subduction zone (Jolly et al., 2001).

2.4.5 Ecuador

Ecuador represents a complex accretionary margin consisting of several juxtaposed oceanic plateau and island arc terranes. There is evidence in Ecuador for several oceanic arc events during the Mesozoic, of which the most well-known is the Macuchi arc. This unit consists of a 2–2.5 km volcaniclastic submarine arc sequence with intercalated pillow lavas and minor mafic intrusions (McCourt et al. (1997). Palaeontological dating places it as Eocene in age. The sequence shows IAT characteristics, with $(La/Yb)_N$ ratios of 2–5 and pronounced negative Nb anomalies (Lebras et al., 1987, Kerr et al., 2002b). The rocks appear to be more primitive and depleted than other arc sequences from Ecuador, leading Kerr et al. (2002) to speculate that they may have formed in a back-arc basin setting.

The Naranjal Unit includes rocks of both oceanic plateau and arc-related origin. The arc-related rocks occur as mafic pillow lavas and intrusives, yielding radiolaria with a Late Campanian-Maastrichtian age (Boland et al. 2000). They have IAT affinity, with $(La/Yb)_N$ ratios >2 and Zr/Th ratios <180. The unit has been directly correlated (Kerr et al., 2002b) with the Ricaurte arc in Southern Colombia (Spadea and Espinosa 1996).

The San Lorenzo arc sequence outcrops in Coastal Ecuador. This sequence includes basaltic flows and volcaniclastics, and sedimentary intercalations containing fauna of a late Campanian to Maastrichtian age (83–65 Ma; Jaillard et al. 1995). Geochemically, the sequence shows pronounced LREE enrichment with $(La/Yb)_N$ ratios of around 4–5 (Lebras et al., 1987), typical of a calc alkaline signature. These lavas, along with those of the Las Orquideas Unit described beneath, directly overly the Piñon Unit (a unit with an oceanic plateau affinity) suggesting the arcs may have formed from melting beneath the plateau (Kerr et al., 2002b).

The thin Las Orquideas unit of Coastal Ecuador is made up of pillow basalts and dolerites. It shows calc-alkaline affinities, negative Nb anomalies, and typically high $(La/Yb)_N$ ratios of around 5 (Reynaud, 1996). Biostratigraphic constaints place it as pre-Cenomanian (Reynaud et al., 1999). Field relations coupled with the steep chondrite-normalised REE patterns are consistent with the arc forming on top of an oceanic plateau sequence (Kerr et al., 2002b).

2.4.6 Colombia

Subduction-related sequences are also associated with the complex accretionary margin of Colombia, along with units of oceanic plateau affinity. In the Central Cordillera, an intermediate to basic volcanosedimentary sequence is found, known as the Quebradagrande Complex (Nivia et al., 1996). The sequence is metamorphosed to prehnite-pumpellyite facies, and shows a clear subduction related signature with high amounts of LREE and LILE's relative to Nb and Zr, as evidenced by the high La/Nb ratios (A. Nivia and A. C. Kerr, unpubl.). A diverse marine assemblage found in the Complex, including ammonites, radiolaria and brachiopods, yield Valanginian-Albian (140–97 Ma) ages, attesting to its Lower Cretaceous origin (Gomez et al., 1995).

The Western Cordillera contains at least two separate arc-related sequence: an Upper Cretaceous IAT suite and a younger CA one. The Ricaurte-Altaquer area in the south of the Western Cordillera consists of variably metamorphosed submarine basaltic to andesitic flows and volcaniclastics, along with minor shallow intrusives (Spadea and Espinosa, 1996). The sequence shows IAT affinities, and well preserved radiolaria from sedimentary intercalations yield Campanian ages (Spadea and Espinosa, 1996). The similarity in age and to the upper Macuchi Formation in northern Ecuador has led Spadea and Espinosa (1996) to suggest that the two units are correlative. However, Kerr et al. (2002) argued that the lack of CA lavas in the Macuchi Formation contradicts this, and suggested that instead the Ricuarte arc may instead be correlative with the Naranjal arc of Ecuador, based on the similarity of trace element ratios and ages.

Younger arc sequences are also found. The Dabeiba volcanic arc outcrops on the flank of the Western Cordillerra (Tistl and Salazar, 1994), and yields Lower Tertiary Ar–Ar ages of 43 ± 1 Ma (Kerr et al., 1997a). The few analysed samples suggest that it has a calc-alkaline affinity. The exposures consist of mafic to felsic flows intruded by an almost coeval dioritic batholith (Tistl and Salazar, 1994). A late Paleocene planktonic assemblage with Central American affinity attests to its allocthonous origin.

2.4.7 Cuba

Cuba consists of a series of accreted Jurassic and Cretaceous terranes of varying tectonic provenance (Kerr et al., 1999). Many of these terranes contain rocks of island arc affinities, albeit highly deformed and metamorphosed. Rocks of boninitic, IAT, CA and back-arc affinity are all identified within the Cuban tectonic melange. The presence of latest Jurassic-Early Cretaceous boninites is thought to be indicative of an early volcanic arc distinct from the main Cretaceous Caribbean arc, as represented by the remainder of the arc-related rocks. Rocks of the IAT series are found as basalt and andesite blocks in an ophiolitic melange to the north. Like the Virgin Islands, spilitilisation (Kerr et al., 1999) has occurred, but despite alteration, these lavas display close similarities to the other IAT rocks situated around the Caribbean (Kerr et al., 1999).

Rocks of calc-alkaline affinity are found predominantly in south-central and south-east Cuba (Iturralde-Vinent, 1996). Albian-Turonian tuffs, limestones and andesite-dacites comprise the main lithologies, intruded and metamorphosed by extensive plutonic bodies (Ituralde-Vinent, 1997). These suites were followed by eruption of a shoshonitic (high potassium) group from Santonian to Campanian times. Geochemically, rocks of the CA series possess less TiO_2 than the IAT series (Kerr et al., 1999), along with a more enriched LREE signature. Kerr et al. (1999) have also shown that the change from IAT to CA geochemical character was more gradual than previously believed, implying that the source region of IAT was still present during the later stages of CA magmatism.

2.4.8 Tobago

Tobago is separated from other islands on the South American margin by a strike-slip fault to the north, and the island consists of two separate units of Mesozoic island arc rocks, intruded by a mafic to ultramafic batholith and late stage mafic dykes (Frost and Snoke; 1989, Snoke 1991). The underlying unit, the North Coast Schist, is comprised of variably metamorphosed volcaniclastics, chert and andesite dykes. There are no age constraints on the sequence itself, but new biostratigraphical ages for sedimentary intercalations associated with the overlying Tobago Volcanic Group place it at pre-105 Ma, when the overlying group was deposited (Snoke et al., 2001). The biostratigraphical ages are consistent with the Ar-Ar data (Sharp and Snoke 1988). The Tobago Volcanic Group, which is composed of undeformed volcaniclastic sediments, occasional lavas and fossiliferous sedimentary intercalations (Frost and Snoke, 1989), is intruded and contact metamorphosed by rocks of the Tobago Plutonic Suite. The Tobago Volcanic Group is of IAT affinity and possesses LREE enrichments. Initial εNd values for the Mesozoic rocks on Tobago range from +6.6 to +9.4 (Frost and

Snoke, 1989), similar to other Mesozoic Caribbean rocks. Thus, the geochemical, isotopic and geochronological data indicate that the plutonic suite is cosanguinous with the volcanics and possibly the late-stage dykes: therefore the pluton is interpreted as intruding its own carapace (Snoke et al., 2000).

2.4.9 Villa de Cura

Both plateau related and island-arc related terranes are found in Venezuela as part of the Villa de Cura Group. The terranes that appear to show island arc-like characteristics are the Santa Isabel, the El Chino and the El Cano formations (Kerr et al., 2002a). The El Cano and the El Chino Formations consist of finely-bedded volcaniclastic rocks, lavas and cherts, all metamorphosed to low grade facies (Navarro, 1983, reported in Smith et al., 1999), whereas the Santa Isabel Formation consists mostly of siliceous volcaniclastic rocks (Shagam 1960; Donnelly et al., 1990; Smith et al., 1999). The lavas and volcaniclastic rocks of the three formations possess flat- to-moderately LREE enriched normalised patterns, thus placing them in the IAT suite. Beets et al. (1984) have proposed that the group was obducted on to the continental margin in the Late Cretaceous or Early Tertiary.

In addition, the Las Hermanas Formation outcrops as part of the Villa de Cura Nappe. It consists of a series of basaltic flows and associated volcaniclastic sediments (Navarro, 1983, reported in Smith 1999). No geochemical data on this Formation has been published.

2.4.10 Jamaica

Jamaica, like other northern Caribbean islands, consists of a complex amalgamation of different Mesozoic and Cenozoic island arc terranes: the best known units are summarised here. The lower Cretaceous Devils Racehorse Formation is probably the oldest unit exposed on the island (Lewis and Draper, 1990), and has a tholeiitic character, although metamorphism and alteration has rendered interpretation of its primary magmatic affinity difficult. Although only limited geochemical data have been published, (Donnelly et al., 1990), note that the Devils Racehorse Formation has some characteristics of the IAT series, in particular flat to slightly LREE enriched patterns.

The Eocene Wagwater belt comprises a 7 km thick sequence of conglomerates and sandstones interbedded in places with bimodal volcanics and volcaniclastics (Lewis and Draper, 1990; Jackson and Smith, 1979). The mafic lithologies are termed the Halberstadt Volcanics, and show tholeiitic affinities (Jackson and Smith, 1979) whereas the felsic units are calc-alkaline in character and are termed the Newcastle Volcanics. Both units show strong LREE enrichments, supporting an island arc derived origin, but only limited geochemical data is available.

2.4.11 La Desirade

The island of La Desirade, east of Guadeloupe is the only island in the Lesser Antilles in which pre-Tertiary basement is exposed. Three different units make up the igneous basement: the Central Acid Massif is comprised of a quartz diorite intrusion and associated rhyolite flows, all of calc-alkaline affinity (J. Hernandez, pers. com; 2001), the Northeast Complex consists of interbedded pillow basalt and radiolarian cherts, intruded by trondhemitic to dioritic dykes (Bouysse et al., 1983), and finally a group of east-west orientated andesite dykes crosscut the entire sequence (Bouysse et al., 1983). The age of the basement is constrained by palaentological and radiometric methods: radiolaria from cherts in the Northeast Complex denote an Upper Jurassic age (Montgomery et al., 1992), and U-Pb dating of igneous zircons from the acidic intrusions again yield a Late Jurassic (145–150 Ma) age.

There is much debate about the tectonic origin of the basement: Mattinson et al. (1980) considered it to represent oceanic crust, rather like the Bermeja complex in Puerto Rico (also associated with Jurassic radiolaria, Montgomery et al., 1980). New work by Hernandez et al. (pers com) demonstrates a calk-alkaline affinity for the entire igneous basement, attesting to its arc-related origin

2.4.12 Southern Mexico

The Guerrero terrane is recognised as an Upper Jurassic-Early Cretaceous island arc sequence (Tardy et al., 1994, Freydier et al., 2000), which bears close lithological and geochemical resemblances to the Caribbean arc sequences, and appears to be coeval with at least some (e.g. Puerto Rico). Tardy et al. (1994) have identified five distinct arc related lithological units, four of which show oceanic affinities and are composed of a sequence of bimodal lavas, intrusives and siliceous volcaniclastic rocks. The geochemical character of these units shows an evolution from tholeiitic basalts to calc-alkaline pillow basalts and andesites, whilst a back arc sequence yields shoshonitic olivine basalts. The tholeiitic units generally show relatively flat REE plot (typically 10× chondrite) whereas the calc alkaline rocks are LREE enriched. However, the negative Nb anomaly typically associated with arc-related rocks is not observed.

A fifth lithological type, exposed on the Pacific coast, consists of a calc-alkaline volcanic sequence (with strong negative Nb anomalies) interbedded with subaerial ignimbrites and continental red beds, said to represent an arc sequence formed on continental crust (Tardy et al., 1994). This is contradicted by Kerr et al. (2002), who consider an intra-oceanic origin for the subduction system to still be likely, based on the lack of unequivocal evidence to the contrary.

2.4.13 Costa Rica-Santa Elena complex

The Santa Elena nappe in Costa Rica is made up of several distinct lithological units, including a volcano-sedimentary succession of possible oceanic plateau affinity, pillow basalts and intrusive mafic bodies (Hauff et al., 2000b; Frisch et al., 1992). The pillow basalts and intrusives all have similar arc-like geochemical signatures, with moderate negative Nb and P anomalies, and a general depletion in incompatible elements $(La/Yb)_N = 0.45$ (Hauff et al., 2000b). New Ar–Ar dating indicates an age of 109 ± 2 Ma for a pillow basalt, and 124 ± 4 Ma for a plagioclase separate from an intrusive gabbro. These members of the Santa Elena Complex are therefore interpreted to represent an early-mid Cretaceous IAT sequence.

2.4.14 Venezuelan Antilles

The Venezuelan Antilles form the eastern continuation of the Dutch Antilles (Aruba-Curaçao-Bonaire) island chain. They consist of metamorphosed volcanosedimentary rocks intruded by silicic plutons and unconformably overlain by Tertiary to Recent limestones (Jackson, 1994). The islands are detailed below, but in general interpretation of their tectonic affinity is hindered by the lack of geochemical data.

Margarita Island is composed of two metamorphic/igneous cores, overlain by variably metamorphosed Eocene-Recent sediments. The two main units are the Juan Griego Group, comprising high-grade crystalline basement with a Paleozoic U–Pb age (Stockhert et al., 1995) and the La Rinconada Group, of uncertain Cretaceous age, consisting of 2–3 km stratigraphic thickness of amphibolites and eclogites. Boccio et al. (1990) found the La Rinconada Group to have a MORB-like geochemical signature, however, the limited geochemical data available and low Nb values (1–3 ppm) ensures that an island arc setting cannot be ruled out on a geochemical basis. The Juan Griego Group is chemically very homogeneous and again is interpreted by Boccio et al. (1990) as reflecting a MORB source. The higher levels of Nb (7–8 ppm) may hint at this but once again, existing geochemical data is very limited. On the basis of P-T-t evidence, Stockhert et al. (1995) proposed that these units may have formed the basement of an island arc in upper Cretaceous times. The La Rinconada Group is intruded by the El Salado calc-alkaline granite at around 86 Ma (U–Pb age), which is said to be arc related (Stockhert et al., 1995). The island of Los Frailes consists of extrusive tholeiitic basalts and their intrusive equivalents, and dolerite, metamorphosed to prehnite-pumpellyite facies (Speed and Smith-Horowitz, 1998). The lack of geochemical data for the sequence, however, means that its tectonic affinity is uncertain.

The rocks on La Orchilla are considered to be amongst the oldest on the southern Caribbean margin, and consist of schists, amphibolites and gneiss, intruded by dolerites, granodiorites and granites, and pegmatite and aplite dykes (Santamaria and Schubert, 1974).

Serpentinite and peridotite also crop out, although their relationship to the other lithologies is unclear.

On Gran Roque basic igneous rocks (diabase and lamprophyre) have been intruded by a coarse-grained quartz diorite and numerous aplite and pegmatite dykes (Santamaria and Schubert, 1974).

Finally, on the island of Los Testigos, a meta-andesite volcanic complex is intruded by a metagranitic pluton, with a clear intrusive relationship (Santamaria and Schubert, 1974).

2.5 Siliceous batholiths associated with the Caribbean Plateau

Cretaceous and Tertiary siliceous plutonic rocks also occur on the margins of the Caribbean. Lidiak and Jolly (1996) defined two main types: low-K suites dominated by tonalite, and more potassic calc-alkaline suites typified by granodiorite. With a few exceptions, geochemical data for these plutonic suites is limited; nevertheless all data supports a subduction-related origin, with negative Nb anomalies relative to LREE (White et al., 1999). There is no correlation between the limited Sr isotopic data and K content, indicating that the two groups do not simply indicate varying amounts of subducted sediment (Lidiak and Jolly; 1996).

2.5.1 The Aruba batholith

Of the circum-Caribbean siliceous plutons, the Aruba batholith is described in detail, partly because of its geographical proximity to Bonaire and also because it represents probably the best studied Cretaceous plutonic suite of the Caribbean. It is returned to in Chapter 7, and its geochemical characteristics are discussed further, where it is considered as a possible analogue of the Washikemba Formation.

The Aruba batholith is principally tonalitic in composition, with associated granite, diorite, granodiorite, mela-diorite, norite and gabbro members. Field relations confirm that it intrudes and metamorphoses the Caribbean plateau sequences, and intrusion is said to be contemporaneous with deformation of the plateau (White, 1999; White et al., 1999). All members of the batholith have similar abundances of incompatible elements, with high La/Yb ratios, high Sr, Ba and low Nb, attesting to a subduction-related origin (White et al., 1999). The suite also has a clear calc-alkaline signature, and has affinities with Precambrian tonalite-trondjhemite-granodiorite suites (White, 1999). Recent ^{40}Ar–^{39}Ar dating of hornblende and biotite separates reveal that the batholith was emplaced between 84.9 ±0.2 and 81.8 ± 0.3 Ma, perhaps only 5–10 Ma after plateau formation. The batholith is thus interpreted as representing the first stages of subduction beneath the plateau following the polarity reversal (White, 1999). The negative correlation between La/Nb and $^{206}Pb/^{204}Pb$ for all members of the batholith is attributed to mixing between subduction related (high La/Nb) and plateau-related (high $^{206}Pb/^{204}Pb$) endmembers, with the gabbros possessing more of a subduction signature, and the tonalities possessing more of a plume signature (White, 1999). A summary of geochemical data for the Aruba batholith, and a summary model for its formation (derived from White, 1999) is presented in Figs. 8.6–7.

2.6 The Subduction Polarity Reversal

Most Caribbean reconstructions (Pindell, 1985; Pindell and Barrett, 1990) require a eastward-dipping subduction zone between the Americas in the early late Cretaceous, with Pacific crust moving eastwards relative to the Americas and being subducted beneath Atlantic crust. A subduction polarity reversal is therefore required, as in the present-day configuration Atlantic crust is being consumed beneath Caribbean crust, in a west-dipping subduction zone. Most workers consider this subduction polarity reversal to be triggered by the arrival of the Caribbean Plateau at the subduction zone. The inherent buoyancy and abnormal thickness of the oceanic plateau would have rendered the oceanic plateau unsubductable (Cloos et al., 1993; Saunders et al., 1986), clogging the subduction zone, and forcing the polarity to ultimately reverse, in a situation analogous to the modern-day Ontong Java Plateau colliding with the Solomon Arc (Petterson et al., 1997; 1999). This constrains the timing of the reversal to younger than 88 Ma, i.e. the age of the bulk of the Caribbean Plateau (Sinton et al., 1998; Kerr et al., 1997). There is, however, no Caribbean-wide evidence for a major tectonic event such as a subduction polarity reversal at this time. Likely manifestations of a subduction polarity reversal in the volcanosedimentary record would be as follows:

1. Major Caribbean-wide tectonic breaks and unconformities in the island arc sequences, produced as the subduction zone jams and results in major tectonic uplift. These are unlikely to be synchronous throughout the whole Caribbean region, but probably instead occur as a series of stepped unconformities.
2. Evidence of large amounts of uplift of the upper plate, as subduction is attempted, perhaps involving the accretion and uplift of high pressure rocks.
3. A possible change in the geochemical signature of the island arc rocks at the event. It is reasonable to suppose that both subducting plates and associated sediments will have different geochemical characteristics, and hence a change in the composition of the subducted material will result in a change in the geochemical character of the volcanic products.

There is evidence for some or all of these features around the Caribbean region. Lebron and Perfit (1993; 1994) noted that in the Cordillera Oriental, Dominican Republic, a change from island arc tholeiite to calc-alkaline geochemical character of the arc rocks at the Albian-Aptian boundary (112 Ma; Harland et al., 1990) is accompanied by a major unconformity, and postulated that this represents the Caribbean subduction polarity reversal. Unfortunately, at this time the Caribbean Plateau did not exist, and hence the timing of the reversal it too early for the Caribbean plateau to be the trigger.

In recent years much emphasis has been placed on the significance of the tholeiitic to calc-alkaline transition: sequences of island arc tholeiite affinity are said to belong to the pre-polarity reversal arc, whereas the calc-alkaline sequences are thought to represent an arc or arcs formed after the polarity reversal (Lebron and Perfit, 1994; Donnelly 1994). However, increasing evidence suggest that the change from island arc tholeiite to calc-alkaline character is not as abrupt nor as regional as originally suggested (Schellekens et al., 1998; Kerr et al, 1999), and instead may represent a more gradual chemical evolution based on differing amounts of sediment or another input in the source of the island arc, rather than a sudden subduction flip (Donnelly et al., 1990). In addition, many of the chemical parameters used to define arc tholeiite vs. calc-alkaline character are based on elements susceptible to mobilisation via secondary alteration (e.g. K_2O, FeO, MgO), and most Caribbean rocks are known to have suffered such a fate, rendering recognition of their original geochemical character difficult.

2.7 Normal oceanic crustal sequences

In addition to oceanic plateaux and island arc rocks, the Caribbean region is also typified by occurrences of "normal" oceanic crust: Jurassic to Early Cretaceous oceanic crust is found as accreted fragments on the margins of the Caribbean plate. In addition to these subaerial exposures, the pre-existing oceanic crust of the Caribbean Plateau has been identified through seismic studies of the Caribbean basin (Diebold et al., 1999), and it is likely that the subaerial exposures are correlative with this.

The Bermeja Complex (Puerto Rico) consists of a melange of serpentinite, amphibolite, chert and metabasalt, and has been identified as having a MORB-like affinity (Schellekens et al., 1990; 1998). Radiolaria found in the cherts have been identified as Pleinsbachian (195–187 Ma) and Kimmeridgian–Tithonian (155–146 Ma) in age (Montgomery et al., 1984; Schellekens et al., 1998), substantially older than surrounding Caribbean plateau or arc rocks. In addition, the radiolarian fauna has been identified as Pacific in origin (Montgomery et al., 1984), meaning that it is likely that the Bermeja Complex represents the Pacific oceanic crust onto which the Caribbean plateau was extruded.

Lapierre et al. (1999) and Kerr et al. (2002) identified several other units of normal oceanic crustal affinity, including part of the Duarte Complex (Hispaniola), part of the La Rinconada Group (Margarita Island), and the El Sabalo Formation and part of the Encrucijada

Formation (Cuba), on the basis of geochemical characteristics. All of these sequences appear to be Early Cretaceous or older in age, which is consistent with their oceanic crust interpretation.

2.8 Summary

- The Caribbean Plateau, which is dated at ~86–93 Ma (although the bulk of the ages are concentrated around 88–91 Ma) originated in the Pacific as the initial eruptions of a Pacific mantle plume. It has since moved eastwards between the Americas as they diverged in the Upper Cretaceous, and the margins of the plateau have been dismembered.

- The northern and southern margins of the Caribbean plate are composed of a complex amalgamation of oceanic plateaux, island arc and oceanic crustal fragments.

- The arc associated with the leading edge of the plateau experienced a subduction polarity reversal to produce its present day configuration, probably as the oceanic plateau clogged the subduction zone.

- Subduction related sequences are found all round the margins of the plateau and there is a general transition from island arc tholeiite to calc-alkaline geochemical character over time. This is not, however, linked to the subduction flip and instead represents changing source characteristics over time. This thesis focuses on one such subduction sequence, the Washikemba Formation, on the island of Bonaire.

Chapter 3

Field Geology, Petrography and Mineralogy of the Washikemba Formation, Bonaire

3.1 Introduction

The island of Bonaire in the Dutch Antilles forms part of an east-west island chain situated on the Southern Caribbean margin (Fig. 3.1). It lies ~50 km offshore from South America. Its closest neighbouring islands are Aruba and Curaçao, both of which contain outcrops of Cretaceous volcanic rocks, and which are separated from Bonaire by strike-slip faults (Mann et al., 1990).

Bonaire is an elbow-shaped island, 43 km long at its maximum point (Fig. 3.2). It is 288 km^2 in area, and is of low elevation, the highest hill, Brandaris, being only 240 m high. Despite its tropical location, the island remains arid for most of the year, and the vegetation is dominated by cactus and scrub, which reduces the exposure and inhibits fieldwork.

Lithologically, it consists of two inliers of Cretaceous volcanic rocks, referred to in this study as the Northern and the Southern Complex. These are surrounded by Tertiary–Recent limestones, which are in turn fringed by modern-day coral reefs. There is plenty of evidence for a widely fluctuating sea level: marine terraces and wave-cut platforms are found up to 1 km inland, and many saline lakes (known as saliñas) in the northern area represent marine bays which have since been cut from the sea.

3.2 Previous geological studies of Bonaire

The first detailed study of the island was undertaken by Pijpers in 1933, who interpreted the Cretaceous volcanic rocks (which he termed the Washikemba Formation) as a continuous marine succession greater than 5 km thick. Pijpers described a heterogeneous succession of basic lavas, intermediate and acid volcanic rocks and dolerite sills, intercalated with cherts and radiolarites.

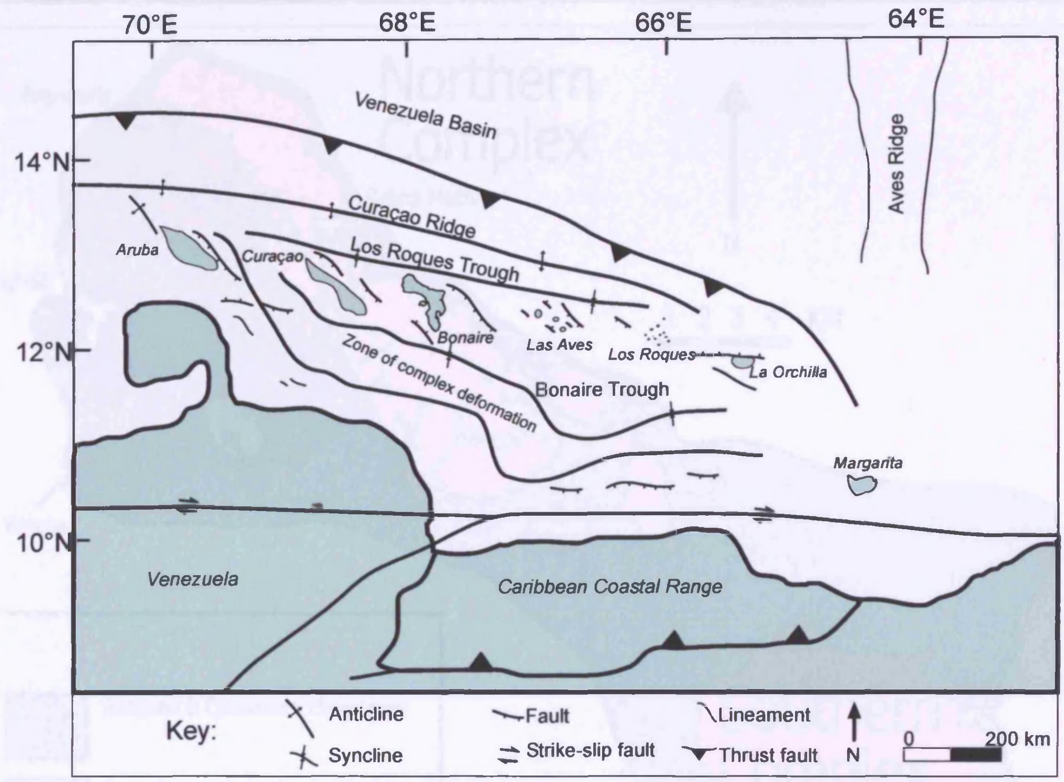

Fig. 3.1. Tectonic map of the Southern Caribbean margin, adapted from Silver et al. (1975) and Avè Lallemant et al. (1997).

The sequence was interpreted as an island arc succession by Klaver (1976), who studied the northern region extensively and produced a detailed geological map (Fig. 3.2) and undertook some preliminary geochemical analyses. Klaver noted the graduation from radiolarites and cherts in the lower half of the sequence, to limestones and cherty limestones in the upper portion, and concluded that this represented a change from below the Carbonate Compensation Depth (CCD) to above. He concluded this represented a shallowing depth of deposition from 3500 m at the base to 1000 m near the top of the section (Beets, 1984), using the best existing estimates of the depth of the Cretaceous CCD. The presence of boulder beds in the upper portion of the sequence was seen to indicate temporary emergence.

The Southern Complex has been much less studied. Pijpers (1933) also identified this as part of the Washikemba Formation, on the basis of lithological similarities between the two complexes. There are, however, several rhyodacite domes (Beets, 1984), which suggest a higher lava viscosity than the rhyodacites of the Northern Complex, which form laterally extensive flows and sills. A study and basic mapping programme of the Southern Complex was undertaken by Yonce (1997, unpublished) under the instruction of the Netherland Antilles government, in order to evaluate its economic resources.

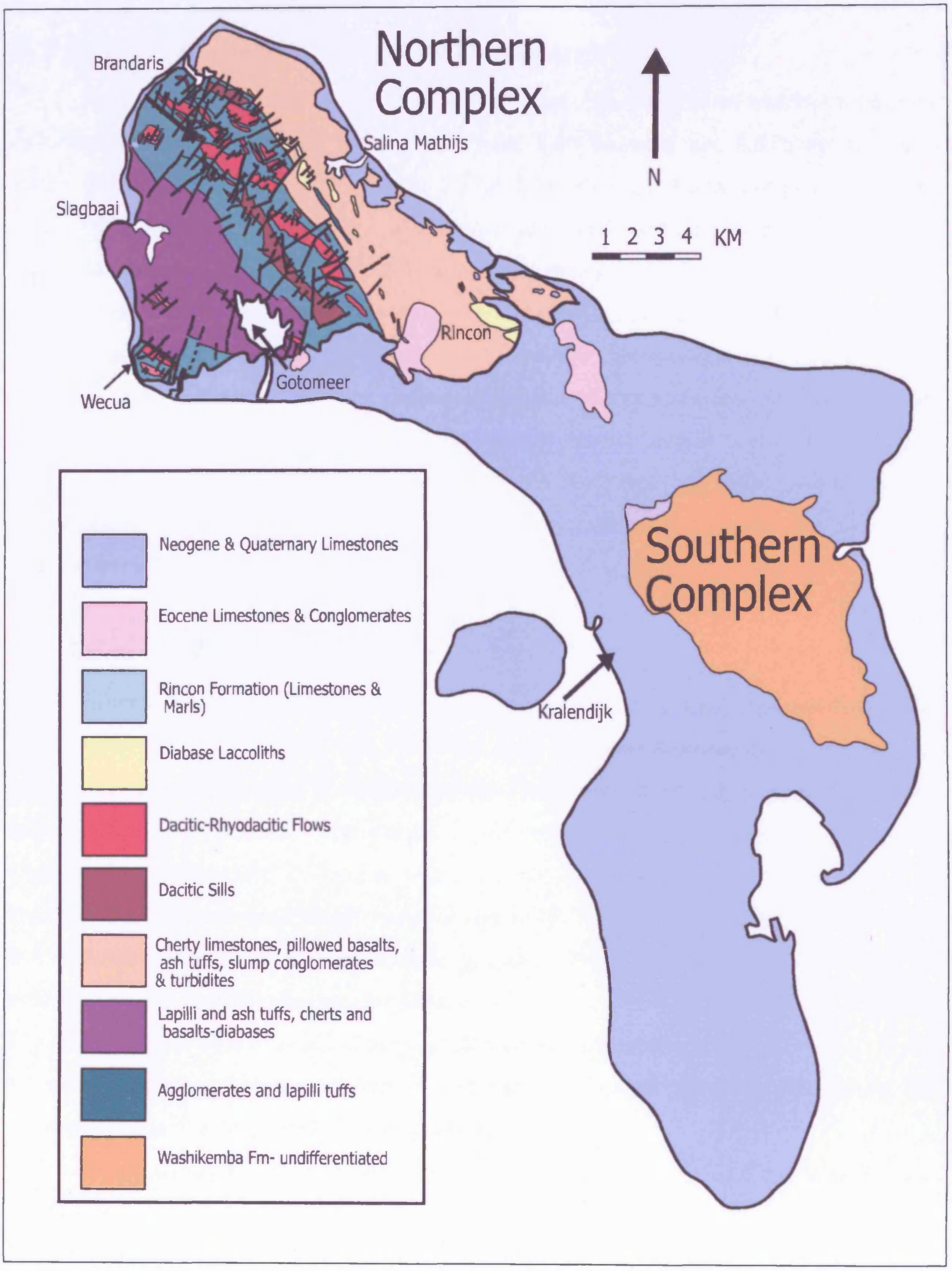

Fig. 3.2. Geological map of Bonaire, Dutch Antilles. After Klaver, 1976.

3.3 Nature of basement beneath Bonaire

Bonaire represents part of the Southern Caribbean boundary zone, which is a complex deformational belt marking the transition between the Caribbean and the South American plates. This zone is ~400 km in width (Fig. 3.1) and, from north to south, comprises deformed sediments, plateau and arc fragments, extensional basins and southward verging nappes. The Dutch Antilles represent discrete land platforms, separated by northwest-trending faults and broad sediment-filled basins (Silver et al. 1975; Case et al., 1972). Thus the tectonic relationship between the different islands is not obvious. Geophysical evidence, however, suggests the islands themselves are positioned on abnormally thick (ca. 32 km) basement (Silver et al., 1975). Whether this basement represents normal oceanic crust which has been tectonically thickened through convergence with the Southern Caribbean margin, oceanic plateau material, or even continental crust is only speculative, as is whether the islands all have the same basement lithologies.

3.4 Aims of fieldwork

Approximately 3 months of fieldwork in the Dutch Antilles was completed during two field seasons in 1999 and 2000. One week was spent on reconnaissance on the neighboring islands of Aruba and Curaçao, in order to provide a reference frame, and the remainder of the time was spent on Bonaire. The general objectives of the fieldwork were to determine whether the Washikemba Formation represents an island arc sequence, and if so, to investigate the volcanic architecture and evolution of the island arc, and to look for evidence of interaction with the Caribbean oceanic plateau. These general objectives would be achieved through the following specific aims:

1 Investigate the field relations of the Washikemba Formation.
2 Carry out an extensive geochemical and geochronological sampling programme for elemental and isotopic analysis and Ar–Ar dating.
3 Seek any stratigraphic or palaentological constraints on the age of the Washikemba Formation.
4 Investigate evidence of any tectonic contacts within the Washikemba Formation, and evidence for tectonic deformation of the island.
5 Produce a geological map of the Southern Complex.
6 Confirm or otherwise that the Southern Complex also represents part of the Washikemba Formation.

7 To look for the presence of plateau-type material on the island, or any structural evidence to suggest the involvement of an oceanic plateau.

Maps showing sampling localities are presented in Appendix A (Maps A.2 and A.3). A list of all samples obtained during this study, along with field and petrographic information, is presented in Table A.1.

3.5 Lithologies of the Northern Complex

The Northern Complex is better exposed and studied and forms the high relief portion of the island, the majority of which is now a national park, the Washington-Slagbaai Park. The Complex has been accurately mapped by Klaver in 1976 and subdivided into broad lithological units. These units were examined in detail, with the objective of mapping them in greater detail, but poor exposure meant this was an impractical task to complete for the entire Complex, and so the exercise was restricted to areas of greater exposure, such as the inland lakes. Paths and tracks provide further exposures, albeit infrequent and generally poor, but the number of paths have been reduced over the years by the park rangers, who have systematically allowed many old tracks to become overgrown, in an attempt to simplify navigation for tourists.

The study of the Northern Complex is facilitated by the presence of large saline lakes, which would originally have been connected to the sea. The margins of these lakes provide much-needed bands of near-continuous exposure, and so the Northern Complex has been subdivided into areas based upon these lakes, or other dominant topographic features. The entire sequence dips broadly 40° towards the northeast (040°), so the Wecua area, therefore, exposes the lowermost successions of the Washikemba Formation (Fig. 3.2). This is overlain by the rocks of the Gotomeer area, then the Brandaris lithologies, and finally the Salina Mathijs area, which contains the youngest exposed rocks of the Washikemba Formation. These different areas will be described in detail in their relevant sections, and will be subdivided into their different lithologies. In general, the Northern Complex consists of a 5 km succession of volcaniclastic sandstones and conglomero-breccias, intrusive dolerites, with abundant rhyodacite flows and shallow sills in the middle of the succession, with cherty limestones and pillow basalts being present towards the top (Fig. 3.3). Field photos of the Northern Complex are displayed in Figs. 3.4–3.7. Photomicrographs of lithologies from both the Northern and the Southern Complex are presented in Figs. 3.12–3.14.

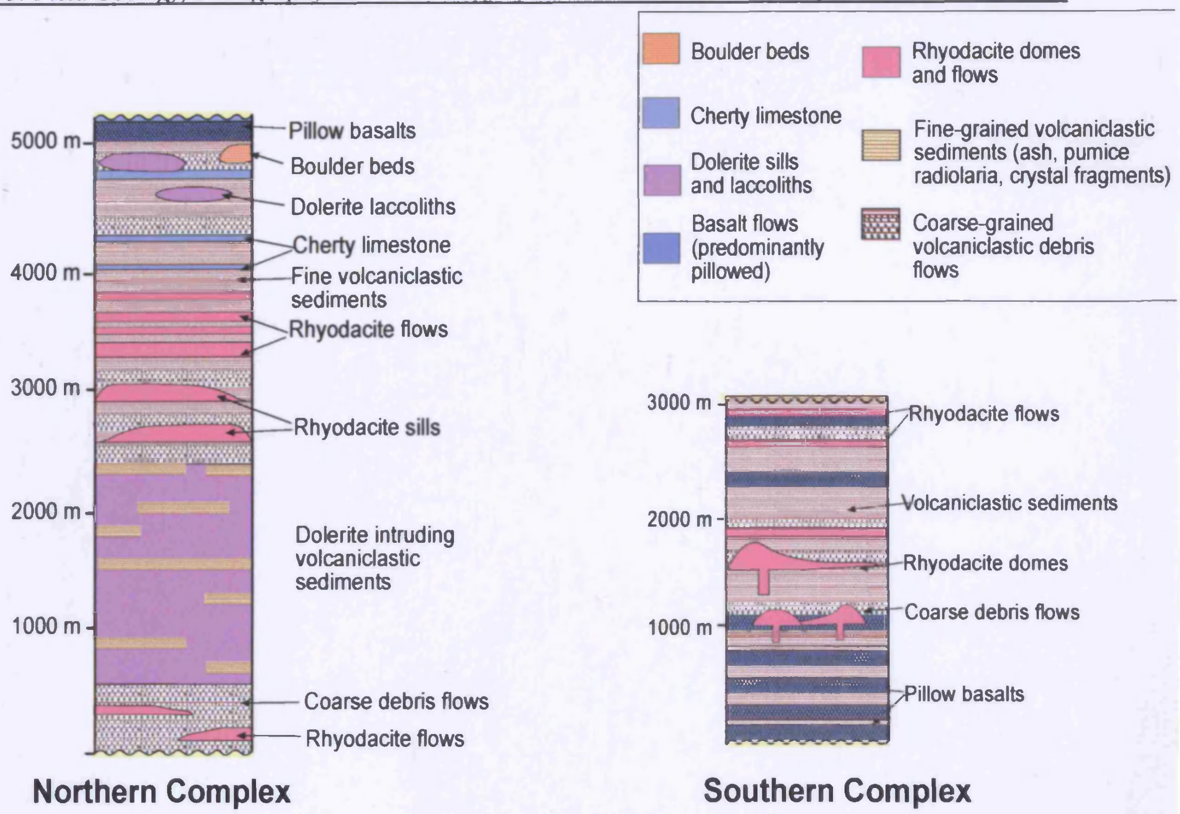

Fig. 3.3. Schematic stratigraphic sections through the Washikemba Formation, Bonaire. Based on this study and Klaver (1976).

3.5.1 Wecua Region

The Wecua region forms the lowermost exposed part of the Washikemba Formation. The base of the formation is not exposed, as it is unconformably overlain by the Neogene to Quaternary limestone. It broadly consists of several large rhyodacite flows, along with thick sequences of mainly coarse-grained volcaniclastic units.

3.5.1.1 Felsic igneous rocks

Several rhyodacite flows are found in this area. A major rhyodacite flow forms the Wecua hill. The impenetrable vegetation and scree obscures the basal contacts and means its extrusive nature cannot be confirmed, although it is implied by the lack of columnar jointing (given its thickness) and presence of vesicles.

The rhyodacites are generally a dull pink/orange colour, with elongate porphyritic feldspar laths up to 1 cm in length. Some of the less altered blocks contain a core of blue rhyodacite in the middle, indicating that the dull pink orange colour is simply the result of alteration. The rhyodacites are often very hard which suggests they may be silicified, and quartz, calcite and epidote veining are common.

Fig. 3.4a.
Slagbaai: Locality 99-127 (Bon 99-4-31). Layering seen in dolerite. Accentuated by degree of weathering. Note pencil for scale.

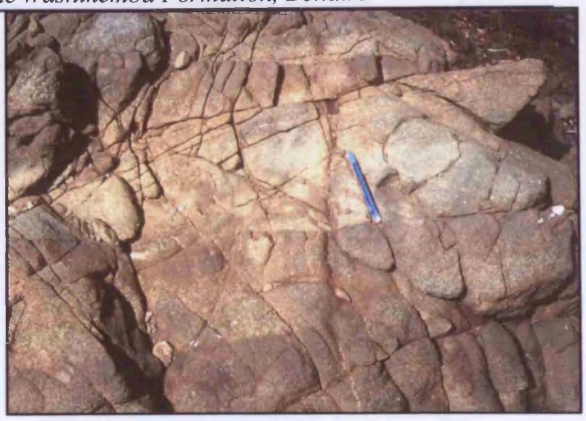

Fig. 3.4b.
Slagbaai: Locality 99-104 (Bon 99-4-20). Layering seen in dolerite. Defined by changes in grainsize and proportion of mafic minerals. Note pencil for scale.

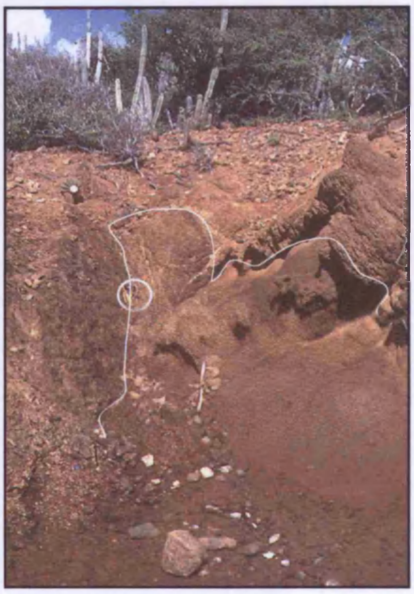

Fig. 3.4c.
Gotomeer: Locality 99-27 (Bon 99-3-19). Dolerite intruding into fine-grained volcaniclastic sandstone. White line follows the contact. Note compass for scale (ringed).

Fig. 3.4d.
Slagbaai: Locality 99-73 (Bon 99-4-15). Layering seen in dolerite. Defined by changes in grainsize and proportion of mafic minerals. Also note spheroidal weathering. Note pencil for scale.

Fig. 3.4e.
Gotomeer island (Bon 99-4-15).
Photo of Gotomeer island showing columnar jointing of rhyodacite sill.

Figs. 3.4a-e. Structures and features of the igneous rocks of the Gotomeer area.

Fig. 3.5a.
Gotomeer: Locality 99-65 (Bon 99-3-37). Alternating sedimentary sequence of coarse crystal-rich volcaniclastic sandstone and medium-grained volcaniclastic sandstones. Note hammer for scale.

Fig. 3.5b.
Gotomeer: Locality 99-24 (Bon 99-3-17) Typical outcrop of blue coarse-grained conglomerate/breccia. Note hammer for scale.

Fig. 3.5c.
Gotomeer: Locality 99-33 (Bon 99-3-21). Outcrop of volcaniclastic tuff with a pronounced fabric parallel to bedding defined by elongate clasts of volcaniclastic sandstone and rhyolite. Note pencil for scale.

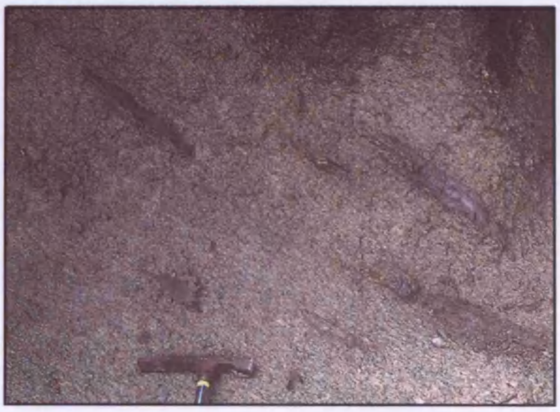

Fig. 3.5d.
Gotomeer: Locality 99-61 (Bon 99-3-34). Elongate rip-up clasts of fine-grained volcanic sandstone, parallel to bedding, within the basal part of the conglomerate-breccia. Note hammer head for scale.

Fig. 3.5e.
Gotomeer: Locality 99-26 (Bon 99-3-18). Asymmetric slump folds in chert. Pencil is orientated parallel to plunge of fold. Note pencil for scale.

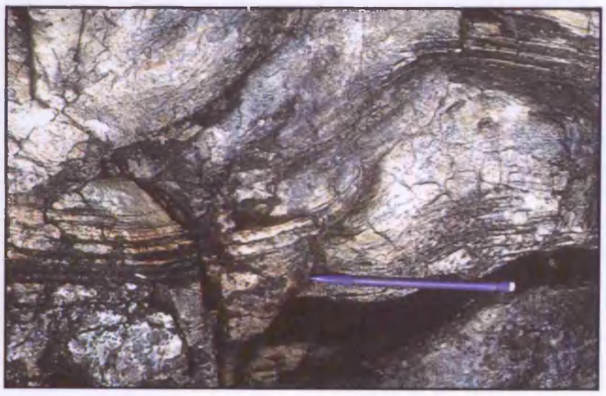

Fig. 3.5f.
Gotomeer: Locality 99-35 (Bon 99-3-22). Small-scale slump folds in sandstone. Note pencil for scale.

Figs. 3.5a-f. Sedimentary structures and features of the volcaniclastic rocks of the Gotomeer area.

Fig. 3.6a.
Brandaris: panorama taken from the summit looking towards Slagbaai (SSE). All the surrounding hills are comprised of rhyodacite flows and sills. Distance to sea is about 1 km.

Fig. 3.6b.
Summit to east of Brandaris. Highest point on island.
Well-defined columnar jointing on rhyodacite sill. Dividivi tree, for scale, is 3 m wide (Bon 99-4-02).

Fig. 3.6c.
Seru Juwa, Brandaris area (Bon 99-4-26). Well-defined columnar jointing on rhyodacite sill. Cactus in foreground (right hand side) is 2 m high.

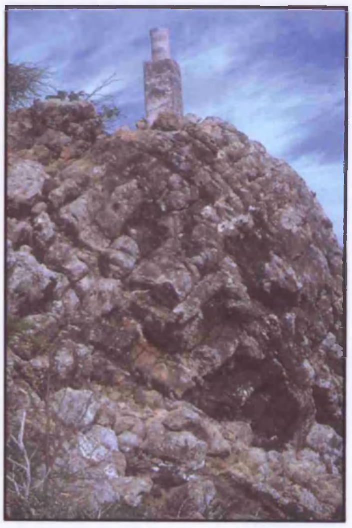

Figs. 3.6d.
Ceru Mangel summit. Pronounced stubby columnar jointing of rhyodacite flow. Triangulation point, for scale, is 1m high (Bon 99-4-06).

Figs. 3.6a-e. Structures and features of the rocks of the Brandaris area.

Fig. 3.7a.
Salina Mathijs (Bon 99-3-24).
Isolated large rounded limestone block within coarse-grained conglomerate-breccia. Note hammer in foreground for scale.

Fig. 3.7b.
Salina Mathijs (Bon 99-3-27).
Boulderbed consisting of chaotic piles of rounded cobbles of volcanic and plutonic origin. Note hammer for scale.

Figs. 3.7a-b. Sedimentary structures and features of the volcaniclastic rocks of the Salina Mathijs area.

3.5.1.1.1 Petrography

Both K-feldspar and plagioclase are present, along with variable amounts of quartz. It should be noted that in this study the rhyodacites are defined on geochemical (Section 5.5) rather than petrographical criteria, and thus, some rhyodacites contain less modal quartz than feldspar. Phenocrysts typically comprise up to 15% of the rock, and are 0.5–3 mm in size, and sometimes form glomerocrysts. The K-feldspar is frequently tabular, possibly microperthitic but considerably turbid, and alteration products such as sericite and clays are common along fractures and within the grains (e.g. Figs. 3.13g; 3.12h). Plagioclase often displays strong oscillatory zoning, fractures and resorbed margins, indicating it may often be xenocrystic in origin. Frequently grains are albitised or seriticised, but with selective sampling pristine plagioclase (andesite-oligioclase in composition) can be found. Some samples show glomerocrysts of feldspar with occasional corroded clinopyroxene associated- these may be xenocrystic in origin (e.g. Fig. 3.12d). Quartz phenocrysts are typically irregular in shape and often show signs of resorption. Some show undulose extinction indicative of straining.

The matrix is typically fine-grained to microcrystalline and consists of plagioclase and k-feldspar, quartz, magnetite and interstitial areas of chlorite/pumpellyite. A trachytic texture is common, and occasionally the matrix has partially devitrified or completely devitrified (producing a granophyric texture, common in ancient volcanic rocks, Mc Phie et al., 1983) and small spherulites, up to 5 mm in diameter are visible. Vesicles are often abundant, ranging from 0.2 to 200 mm in size. They are often rimmed with opaque minerals, and variably filled with quartz, calcite or pumpellyite (e.g. Fig. 3.13e). They are generally round, although in the field some are seen to be oriented parallel to bedding surfaces (~40° dip).

3.5.1.2 Mafic igneous rocks

Dolerites are also found on the shores of Salina Tan. They are poorly exposed and weathered, and clearly intrude into the coarse-grained conglomerates and mega-breccias. It must be noted that if the conglomerates are indeed related to reworking of the rhyodacite flows, as seems increasingly likely (Section 3.5.2.3), then this places some time constraints as they are intruded by dolerites, and hence the rhyodacites must represent a slightly earlier volcanic phase.

3.5.1.2.1 Petrography

The dolerites are easily distinguished due to their prominent spheroidal weathering, dark blue/green colour and their lumpy weathered surface. In thin section, an interlocking framework of plagioclase and clinopyroxene is apparent, with subordinate amounts of orthopyroxene and magnetite. Olivine is visible in some of the less altered sections, where it comprises up to 10% of the rock. The dolerites are typically very altered, and plagioclase laths are usually seriticised and turbid, whilst clinopyroxene is partially to completely altered to pumpellyite and cryptocrystalline clays (Figs 3.12a–b). Chlorite and Fe-oxyhydroxides are also present as secondary phases, probably replacing orthopyroxene and olivine respectively.

3.5.1.3 Rhyodacite mega-breccia

A distinctive lithology is seen at Salina Tan, southeast of Seru Wecua. It was described by Klaver (1987) as a "remarkable agglomerate". At its most "remarkable" (e.g. Locality 99-86), it consists of angular blocks of pink porphyritic and amygdular rhyodacite 10–70 cm in size, in a clast-supported finer-grained (0.1–2 cm diameter) matrix of rhyodacite, recrystalline ash and pumice. The unit often has a greenish tinge as a result of surface epidote mineralisation. Within 50 metres of this locality (e.g. Locality 99-79), the outcrops appear transitional to the coarse-grained conglomerate seen in other regions, although one outcrop (Locality 99-89) appears to have a slab-like form, and the matrix is harder and less easy to separate from the clasts. This was interpreted in the field as possible evidence for welding, but as no eutaxitic texture was observed petrographically, this interpretation is probably premature.

Whilst the unit was termed by Klaver an agglomerate, it clearly does not represent volcanic ejecta. The fact that the unit is situated in close proximity to coherent rhyodacite (Localities 99-82, 99-83) and adjacent to a major rhyodacite flow (which forms the hill Seru Wecua, to the northwest) suggests that it may represent a brecciated lava. This is supported by the fact that the rhyodacite clasts are up to 70 cm in diameter, angular (implying a local derivation), and are contained in a poorly-sorted matrix of rhyodacite and pumice (e.g. Figs 3.14g–h). The presence of abundant pumice in the matrix, however, means that the deposit cannot represent an autobrecciated rhyodacite, however. The observed transition to a more typical coarse-grained conglomerate/breccia (still with abundant clasts) within 100 m, and the similarity of the matrix to that of the conglomerate implies that the deposit is more likely to represent a particularly coarse-grained and high-volume debris flow, better described as an avalanche deposit. Avalanche flows are very rapid inertial granular flows resulting from large-volume landslides, and may be initiated by structural collapse of a volcanic centre (e.g. a dome) or precariously situated flow (Cas and Wright, 1986; Fisher and Smith, 1991; Kelslar and Bédard, 2001). An obvious source for this deposit would be the nearby Wecua rhyodacite flows, and in order to explain the presence of pumice within the deposit, the avalanche flow would have to remobilise a pyroclastic flow deposit or vice versa. This is a feasible situation as there is likely to be abundant pyroclastic debris on the flanks of the central volcano, which are likely to be intrinsically unstable and easily remobilised by earthquakes.

3.5.2 Gotomeer–Slagbaai Region

The Gotomeer–Slagbaai region is described by Klaver (1976) as consisting of "lapilli and ash tuffs, cherts and basalt-diabases", with occasional rhyodacite flows and outcrops of "agglomerates". Some of this terminology needs to be revised and will be discussed in the relevant sections. In general, doleritic lithologies are a lot more abundant than has been suggested by Klaver's work, and the whole sequence can be summarised as consisting of coarse-grained volcanic breccias, fine-grained volcanic sandstone with some chert development, all intruded by dolerite-diorite with occasional small rhyodacite flows. Photographs of the Gotomeer–Slagbaii lithologies are presented in Figures 3.4 and 3.5.

3.5.2.1 Mafic igneous rocks

Dolerites and basalts are also locally very abundant in the Gotomeer–Slagbaai region. Detailed examination of exposures around Lake Gotomeer (the lake margins represent the areas with the best exposure in the region) indicate that dolerite comprises more than 60% of the exposure, and is clearly intrusive into the fine-grained volcaniclastic turbidites (e.g. Localities 99-16, 99-17, 99-18). The sediments show a degree of low-angle folding and deformation near where the dolerites have intruded (see Section 3.9), which indicates that the sediments were not very consolidated at the time of intrusion, and that the intrusions were therefore occurring at very shallow levels, just below the sediment surface. At no point, however, was any contact seen between the dolerites and the rhyodacites, due to the poor levels of exposure.

The dolerite in the Gotomeer region is very different in outcrop to that found in the Salina Mathijs region, although they are petrographically similar (see Section 3.5.5.2.1). Here the dolerites show obvious spheroidal weathering, are visibly very altered and crumbly, and do not form any positive topographical features (Fig 3.14c). They are often transitional to basalts in grainsize, especially when chilled against the volcaniclastic turbidites and cherts. Geochemically, the dolerites are actually transitional to microdiorites, as suggested by the presence of quartz in the groundmass.

The dolerites surrounding Slagbaai lake are distinctive as faint layering on a 10–50 cm scale can be seen, defined by a subtle change from more mafic compositions at the base of each layer to more felsic compositions at the top (Figs. 3.14a,b,d). In one locality (Locality 99-126), a short distance along strike from a layered dolerite, an unlayered dolerite can be seen, with apparent columnar jointing. Unfortunately, the dolerites in the Slagbaai are very weathered, possibly hindering any meaningful geochemical or petrographical analysis of the origin of the layers.

Small outcrops of basalt are also found around the shores of Lakes Slagbaai and Gotomeer. The basalt is very difficult to distinguish, as it has suffered severe alteration and resembles a fine-grained mudstone, and also tends to form the lowest relief areas and therefore be covered in vegetation. Locality 99-76 is a good example of this, where the basalt is red in colour, but has been demonstrated to represent the finer-grained margins of the dolerite. Klaver (1976) discovered some pillows, especially around Salina Frans, but no such structures were found in the Gotomeer-Slagbaai area in this study. Klaver (1976) has suggested that these basalts are flows, and represent the extrusive equivalent of the dolerites. This may indeed be the case, but the pervasive surface weathering (in most cases the basalts can be plucked off the outcrop by hand) inhibits any meaningful geochemical analysis and confirmation of this hypothesis. The fact the dolerites appear to represent intrusion just below the sediment surface does provide support to this idea, however, as it seems likely that some magma will penetrate the surface and subsequently chilled by sea water to form pillow basalts. If there was some degree of mixing between wet sediment and lava, one might expect to find peperite horizons. This is never seen, but may be disguised by the degree of weathering of the basalts, and the fact that often the actual contact between the two is never exposed, and is simply represented by an area of modern-day soil and scree.

In addition, in the Slagbaai region, basalt is seen clearly intruding the dolerite (e.g. Locality 99-127). These intrusions are mainly orientated parallel to regional bedding, and therefore are more accurately described as small sills (ca. 30 cm thick), although there are some small offshoots which clearly intrude and cross-cut the dolerite. The intrusions are distinctive as they appear to have some form of banding (defined by paler and darker laminations parallel to the symmetrically-chilled margins), but the significance of these is not clear. The banding appears to be the result of changes in modal abundance or grain size variation, rather than superficial staining of the rockface. These intrusions must be significantly younger than the intrusion of the dolerite, as they have chilled against the dolerite, which in itself is chilled against the rhyodacite sediments.

3.5.2.1.1 Petrography

The dolerites of the Gotomeer area are indistinguishable from those of the Wecua region, and hence are discussed in Section 3.5.1.2.1. The basalts/andesites are typically very altered in thin section, and are dominated by turbid glomerocrystic plagioclase, in a matrix of cubic opaque minerals, quartz, and occasional clinopyroxene that is variably altered to pumpellyite and/or green clays.

3.5.2.2 Miscellaneous Igneous Rocks

Some small outcrops of rhyodacite are also apparent within the region (e.g. Fig. 3.4e). In one locality (Locality 99-49, Slagbaai) a dacite can be seen, and adjacent to this is situated what appears to be its autobreccia, which consists of angular clasts of dacite in a matrix comprised of smaller (<5 cm) fragments of dacite. This suggests that the unit may be a flow rather than an intrusion, and the similarity between the autobreccia and the coarse conglomerate/breccia seen in other localities implies that the coarse conglomerate/breccia may sometimes result from reworking of an autoclastic breccia. In other localities small outcrops of rhyodacite are also seen, but the limited exposure means that its emplacement origin is unclear.

3.5.2.3 Coarse-grained conglomerate-breccia

The lithological unit described by Klaver as "agglomerate" is actually a coarse-grained conglomerate-breccia found throughout the Washikemba Formation, both in the Northern and the Southern Complexes. The unit broadly fines up and consists of a large proportion of rhyodacite, porphyritic rhyodacite and indeterminate clasts of igneous or volcaniclastic origin, varying in size from several mm to 10 cm, in a brown crumbly heterogeneous matrix.

The unit has a distinctive blue/green patchy colour (e.g. Fig 3.5b), which is attributed to the presence of chlorite. Very little evidence for internal structure or bedding is preserved, although at certain horizons a parallel orientation of clasts is apparent (e.g. Fig 3.5c). In addition, at several localities, large (up to 1 m in length) rafts of fine-grained volcaniclastic sandstone are present, all with an elongation direction consistent with bedding. In places (e.g. Locality 99-19) the unit shows a clear erosive contact with the underlying fine-grained volcaniclastic sediments, and contains rip-up clasts of these sediments up to 20 cm in length (e.g. Fig 3.5d). These are orientated parallel to the weak-bedding fabric, and indicate that the fine-grained volcaniclastic sediments must have been fairly consolidated before deposition of the conglomerate/breccia. In places it can be seen that the unit grades up into a crystal-rich medium-grained volcaniclastic unit (e.g. Fig. 3.5a), and this unit is also seen to grade in places into a fine-grained volcaniclastic sandstone. At one locality (Locality 99-129A) the whole sequence is seen, ranging from a coarse conglomerate containing angular blocks of amygdular basalt (and occasionally chert) up to 20 cm in size, which are particularly abundant in the first metre thickness, and fining up over 10 m until it reaches a fine-grained well-bedded ash deposit.

3.5.2.3.1 Petrography

Petrographically, the coarse-grained conglomerate-breccia is comprised of a heterogeneous mix of angular fragments of quartz and feldspar (some showing complex zoning), surrounding a variety of lithic clasts including fine-grained igneous examples, scoria, mudstones and some relic glass (with classical perlite fractures). These are surrounded by a heterogeneous matrix of brownish microcrystalline quartz (recrystallized ash?). Recrystallisation of the matrix has destroyed any original structure so no shards are identifiable. Tube pumice is abundant (<60%) in some thin sections, and is often apparent both as elongate sheaves and masses of spherical structures in the same sections (Fig 3.14a,b,e), signifying that it occurs in random orientations within a deposit. This is an important observation as it confirms the non-welded nature of the deposit. In addition, as the tube morphologies are retained, despite the age of the deposit, it is likely that the texture was preserved by infilling with quartz, prior to compaction.

3.5.2.3.2 Interpretation of mode of origin

The variety of clasts, lack of internal structure and thickness of the unit all point towards it being some form of mass flow deposit. The abundance of pumice suggests that the deposit may be an ignimbrite, but there is no evidence for welding and the pumice clearly does not display a eutaxitic fabric, implying that the deposit was not hotter than 600°C. It has been emphasised in the literature (Cas and Wright, 1987), that the classification of a unit as an ignimbrite should be restricted to lithologies where a pyroclastic mode of origin *and* emplacement can be unequivocally demonstrated. This is particularly difficult to ascertain for ancient rocks, where primary petrographic textures and sedimentary structures may not be preserved (Cousineau and Bédard, 2000), and thus the unit is interpreted as a subaqueous volcaniclastic mass-flow deposit.

This contradicts Klaver's classification of the unit as an agglomerate, which, according to McPhie et al. (1993), is "a coarse-grained (>64 mm) pyroclastic fall deposit that contains a significant proportion of volcanic bombs and blocks, and is restricted, in general, to very proximal settings". It is therefore suggested that the unit would be more accurately termed a "volcaniclastic debris flow", and represents subaqueous reworking of volcanogenic sediment. This is consistent with the commonly non-erosive based of the deposit, as debris flows commonly are in sharp contact with easily erodable underlying material, whereas pyroclastic flows tend to be erosive (Fisher, 1984a,b). Further evidence for a secondary, rather than primary, pyroclastic origin includes the abundance of rip-up clasts in the base of the deposit and the lack of grading in the size of the tube pumice (Fiske, 1964; Yamada, 1984; Druitt; 1998).

This interpretation of the deposit as a volcaniclastic debris flow also directly contradicts Beets (1967), who classified it as an ignimbrite, based on petrographic identification of apparent welding textures. In particular, he cited the presence of elongate pumice fragments, which he identified as collapsed pumice. However, in this study the elongated pumice fragments are interpreted as tube pumice, as they are seen in conflicting orientations in thin-section (Figs 3.14a,b,e), and are believed to represent primary eruptive structures, rather than being as the result of heat-aided compaction. Klaver (1976) said the agglomerates were pyroclastic flow deposits but conceded that the main transport mechanisms were debris flows, making it apparent that his use of the term "pyroclastic flow" did not in this case imply a primary pyroclastic origin.

The question therefore arises, how were the debris flows generated? Debris flows are often associated with dome collapse events (e.g. Fisher and Smith, 1991). This is probably unlikely in the case of the Washikemba Formation, as the debris flow deposits contain abundant non dome-derived clasts, including plentiful pumice. In addition, the domes preserved today are small-scale features (e.g. Doyle and McPhie, 2000)- too small to generate debris flow deposits of the volume in question. Given the resemblance of the deposits to primary pyroclastic flow deposits (discussed above) and the abundance of pumice, it seems more feasible that the deposits are at least partially derived from remobilised pyroclastic flow material, and hence essentially represent secondary pyroclastic flows.

3.5.2.4 Fine-grained volcaniclastic sandstones

Fine-grained volcaniclastic sandstones are also present, and can be seen in places (e.g., Localities 99-021; 99-035) to grade up from the crystal-rich volcaniclastic units, and in one locality (Locality 99-129A) to grade up from the coarse conglomerate/breccia over a scale of 10 metres. The sandstones are yellow/brown in colour and are finely laminated, some showing convolute laminations, ripples and graded bedding. Individual beds are between 3 and 20 cm thick, and the cyclicity of these sandstones along with the sedimentary features present suggest that they represent the upper divisions of low-density turbidity currents. Some volcaniclastic sandstones contain lenses or beds of chert, suggesting that at least some of the cherts are secondary, formed by the remobilisation of silica from the silica-rich volcaniclastic turbidites or radiolaria. The ripples and graded bedding are features typical of subaqueous deposition, probably resulting from the collapse of suspended sediment clouds generated as the debris flows waned in intensity (Lowe, 1988).

3.5.2.4.1 Petrography

The presence of secondary, rather than primary, cherts is supported by petrographic studies where occasional poorly-preserved radiolaria, foraminifera and sponge spicules are observed. An attempt was made to extract these for biostratigraphic dating, but specimens proved to be too poorly preserved to enable identification. The main constituents of the volcaniclastic sandstones, however, are angular fragments of quartz and feldspar in a microcrystalline quartz matrix, with some occasional patches of orange brown Fe-oxyhydroxide. Fine-scale laminae are defined by slight concentrations of opaque minerals or Fe-oxyhydroxide. A clear subaqueous mode of deposition (although not necessarily a subaqueous origin) is implied by the marine fauna present, along with the fine laminations.

3.5.2.5 Structural Features of the Gotomeer-Slagbaii Region

Many outcrops of volcaniclastic sandstone show evidence for syn-depositional slumping (Figs. 3.5e–f). In several localities, the bedding orientation can be seen to vary quite dramatically within less than a metre, but these discrete exposures of bedded sediments are separated by areas of non-exposure, meaning that low-angle folding can only be implied. In one locality, however, (Locality 99-017) small-scale convolute laminations and cross bedding can be seen in a fine-grained sandstone, which clearly show reverse way-up criteria, whereas in general the Washikemba Formation shows abundant evidence for being the correct way-up. The bed itself is steeply dipping (80/280) and dips in a contrasting direction to the general trend, which suggests that it represents an overturned limb of a fold. There are abundant examples of small scale folding (wavelength of less than 1 m) where no nearby intrusions are apparent (intrusions also appear to have deformed the sediments, and these have been attributed to soft-sediment deformation and slumping, as they only affect selected beds). This is discussed in Section 3.9. In Locality 99-052, a syn-depositional normal fault can be seen in fine-grained cherty sediment, with an offset of several centimetres. All of these structures suggest that the environment of deposition was extremely unstable, which is consistent with deposition on the flanks of a volcanic edifice.

3.5.3 Brandaris Region

This region forms the high relief part of the island, due to the large amount of rhyodacite flows and sills, intruded into volcaniclastic sandstones and debris flows (termed "agglomerates and lapilli tuffs" by Klaver, 1976). The sills and flows are often large-scale structures- one such flow has been said to be about 3 km long, according to Klaver (1976), and they are dissected by syn-volcanic faults. However, the poor exposure of the area means that individual flow units cannot be traced more than 50 or so metres, and many sills and flows may in reality comprise many smaller ones. Photographs of lithological features of the Brandaris region are displayed in Figures 3.6a–e.

3.5.3.1 Rhyodacites

Rhyodacites represent the dominant lithology in the Brandaris area (e.g. Fig. 3.6a), and are indistinguishable in hand specimen and thin section from those found in other areas of the Northern Complex (see description in Section 3.5.2.1).

There is very little distinction between the apparent flows and sills (as defined by Klaver). Some sills show crude to well-defined columns, with cooling surfaces parallel to bedding (Figs 3.6b–d). In one sill (Sumpina) a large lava feeder tube 20 m wide with well-defined radiating columns connects to the overlying Mangel flow. Intrusive (or other) contacts are almost impossible to find, as they are situated in the low relief and highly vegetated areas, and do not tend to be exposed.

3.5.3.1.1 Petrography

Rhyodacites are commonly similar to those seen in the Wecua area (Section 3.5.1.1.1). Another variety of intrusive rhyodacite, however, is also present. This typically contains abundant (10%) patches of brown fine-grained material, with irregular embayed margins, which in thin section are shown to consist of concentrations of acicular magnetite (Fig. 3.12e–f), and to therefore be patches of segregated material. The rocks also contain squat phenocrysts of quartz and feldspar along with clinopyroxene. In thin section, these have been seen to show abundant evidence for a xenocrystic origin (strongly resorbed margins, fragmented crystals, oscillatory zoning of plagioclase; e.g. Fig 3.13d), in contrast to many of the rhyodacites present in the remainder of the Washikemba Formation.

3.5.3.2 Volcaniclastic rocks

The low-lying volcaniclastic sandstones and debris flows appear identical in character to those described from the Gotomeer region (Section 2.2). They are not very well-exposed, as the rhyodacites are the only lithologies that seem to protrude from the vegetation. At Seru Camina (Locality 99-102), a >20 m thick sequence can be seen, visibly fining up from a coarse conglomerate to a fine volcaniclastic sandstone. Evidence is also seen here for channeling of the conglomerate into underlying sandstone. The channels are several metres wide, albeit very poorly exposed.

3.5.4 Salina Mathijs

As described by Klaver (1976), this region is typified by "cherty limestones, pillowed basalts, ash tuffs, slump conglomerates and turbidites" and is intruded by dolerite laccoliths. In general, there is a much greater variety of sedimentary units than in other regions, and conglomeratic units are much more dominant. However, exposure is once again restricted principally to lake margins (Salina Mathijs) and paths in the vegetated interior. Photographs of the lithologies of the Salina Mathijs area are displayed in Figures 3.7a–b.

3.5.4.1 Basaltic Flows

Small outcrops of basaltic flows are seen near the top of the succession. These are generally significantly weathered and are green in colour with extensive calcite veining. Generally they can be broken by hand, and there is very little evidence of the original mineralogy. Klaver identified these as pillow basalts, but in most cases the degree of weathering meant that no evidence for pillow structures was seen. However, on the road between Kraalendijk and Rincon one outcrop is visible, displaying well-formed pillow structures < 1 m wide. Some lobes display a clear radial structure, and others have sediment in the interstices. A correct "way up" can be determined from their morphology. One other outcrop (Locality 99-131A), on the northern margins of Salina Mathijs also shows faint pillow structures, but all other basalt outcrops are very weathered and any original pillow structure is likely to have been obscured.

3.5.4.1.1 Petrography

Salina Mathijs basalts are occasionally transitional to dolerites in terms of grainsize. Typically they consist of skeletal and frequently glomerocrystic plagioclase, with interstitial areas of clinopyroxene and opaque minerals. Some appear to contain pumpellyite/clay pseudomorphs of olivine and possibly orthopyroxene. Vesicles are frequently lined with brown clays and infilled with calcite.

3.5.4.2 Mafic igneous rocks

The dolerites in the Salina Mathijs region are different in character to those of the Gotomeer region. These appear unaltered in hand specimen, and are distinctive due to their blue-green colour. *In situ* samples are very difficult to obtain but relatively unaltered boulders appear to be effectively *in situ.* The dolerites take the form of elongate laccoliths and form the high relief parts of the area, in contrast to the Gotomeer dolerites, which are only exposed on the lake margins. In addition, there is no evidence of internal layering, also unlike the Gotomeer dolerites.

3.5.4.2.1 Petrography

The Salina Mathijs dolerites are petrographically similar to those of the Gotomeer-Slagbaii region (described in Section 3.5.2.1.1), but show more evidence of primary mineralogy than the other dolerites, rather than mineral replacement by pumpellyite/chlorite. In addition, in some sections olivine can be distinguished.

3.5.4.3 Fine-grained sediments

Fine-grained brown volcaniclastic sandstone is found throughout the Salina Mathijs region. It is similar to the sandstones found in other areas (i.e. Gotomeer), but has developed cherty horizons/nodules throughout and is also interbedded with a pale-coloured laminated limestone. Some horizons of cherty-limestones are found, in particular around Locality 99-130, which consist of yellow-grey coloured rocks with a cherty appearance but which react with hydrochloric acid. They display knife-edge small-scale jointing on bedding surfaces (probably due to limestone dissolution) and the interiors of the beds often contain a blue horizon (possibly indicating the more chertified layers). Some large (<1 m diameter), rounded slumped blocks of finely-laminated grey limestone are seen lying as rafts within the sandstone (e.g. Fig 3.7a), and there are some metre-scale slump folds visible within this unit, testifying to the unstable nature of the volcanic paleoenvironment. Inoceramids have been found within some of the cherty-limestone bedding planes (Klaver, 1976; discussed in Section 4.2.1).

3.5.4.4 Conglomerates

Towards the top of the unit (i.e. directly around Salina Mathijs) several distinctive lithologies are seen: a variety of conglomerates outcrop, distinctly different to the blue-green conglomerate/breccia described in Section 3.5.2.3. One of these outcrops on the north-western side of Salina Mathijs (Locality 99-039A; Fig. 3.7b), where a small chaotic patch of weathered boulders of igneous origin are seen with very little matrix in between. This has been termed a boulder bed (Klaver, 1976), and is said to represent the first signs of emergence of the island. The boulders are rounded, vary from 0.1 to 1 m in size, and show great variation: rhyodacite, basalt, unaltered dolerite and a distinctive extensively calcite-brecciated yet unaltered basalt are all visible. The outcrop is limited in extent, allowing little to be said about its origin. However, the roundness, variety and low levels of alteration of the clasts may point to them having a channelised fluvial origin, and hence they may well represent emergence of the volcanic centre, although the entire Washikemba Formation is likely to have remained in a subaqueous environment.

Other conglomerate/breccias are also seen, but their relationship with each other is not clear. Distinctly different lithologies outcrop along strike from one another, separated by only several metres of non-exposure. It is only possible to infer that they represent channel fills, although the presence of faulting cannot be ruled out due to the poor exposure.

3.5.5 Summary of field relations in the Northern Complex

- 5 km continuous sequence of volcaniclastic conglomerates, sandstones and cherts, with intrusive dolerite, rhyodacite flows and shallow sills. Cherty limestones, basaltic subaqueous flows (pillow lavas) and channel-fill conglomerates are present towards the top of the succession.
- Neither base nor top of the Formation exposed.
- Sequence intruded by dolerite- extensive shallow intrusions in south, more volumetrically minor dolerite laccoliths in north.
- Dolerite intrudes volcaniclastic lithologies at numerous localities but is never seen intruding rhyodacite, nor does the rhyodacite appear to intrude the dolerite.
- Coarse-grained conglomerates/breccias clearly grade all the way into fine-grained volcaniclastic sandstones over scale of tens of metres.
- The coarse-grained conglomerates/breccias contain abundant pumice, but are not likely to be primary ignimbrites (although they may represent redeposited ignimbrites) as there is no evidence for welding, and a pyroclastic mode of emplacement cannot be confirmed.
- Coarse-grained conglomerates/breccias appear to be formed (at least in part) from remobilisation of pyroclastic flow deposits, generating debris flows and turbidity currents.
- As volcaniclastics appear to be derived from rhyodacites, and the dolerites frequently intrude these but never do the rhyodacites intrude the dolerites, it appears that the rhyodacites represent a slightly earlier magmatic phase.
- The presence of marine fauna, pillow basalts and limestone confirm a subaqueous mode of deposition. The central volcanic edifice may have been periodically emergent.
- No major tectonic contacts are visible, nor evidence for extensive deformation of the sequence.

3.6 Lithologies of the Southern Complex

The southern outcrop of the Washikemba Formation is situated east of Kralendijk, and is approximately 45 km^2 in area (Fig. 3.2). It is low-lying and rhyodacite domes form the only small hills on the landscape. The low relief and its suitability for agriculture mean that exposure is considerable poorer than the Northern Complex, and much of the land is privately-owned. During this study, the area was mapped at a 1:12,500 scale. Detailed lithological mapping, however, was hampered by the limited exposure, which meant that very few detailed lithological contacts could be examined. In the low-lying areas, exposure is almost non-existent and the only routes are on an ever-reducing number of dirt tracks. For mapping purposes, I had to frequently rely on documenting the rock debris seen on these tracks. Caution had to be exercised, though, as basalt tends to be over-represented as it is used in the construction of these tracks, and greater emphasis is placed on any larger boulders (which are unlikely to have been used as road metal) and debris in field adjacent to the roads, which has been cleared from the fields in order to aid cultivation. If any exposures do occur, they tend to be seen in crevices and gulleys on the tracks. It must also be noted that the basal topographic maps were created in 1976, and many of the tracks have disappeared since then, through the effects of underuse and vigorous cactus growth. Where this has been found, it is noted on the map.

An additional hazard is that there are very few recognisable landmarks to aid mapreading. Fences and plantation boundaries, which are the dominant features on the map, rarely correspond to existing boundaries. Tracks remain the best source of landmarks, along with any topographic highs. This mapping program was completed with the aid of an Eagle Explorer GPS receiver, using the international WGS datum, but with a position correction factor of 0°00'05''S, 0°00'06''E, which gave accuracy to within approximately 30 m.

The Southern Complex was previously thought to consist of interbedded volcaniclastic sandstones and mudstones, with some cherty horizons, and intruded by a series of rhyodacite domes (Klaver, pers. com.). However, this study contradicts this, and the sequence could be summarised as being comprised of basaltic pillowed flows, with interstital chert (often showing secondary iron development) and interbedded with fine-grained volcaniclastic sediments, intruded by rhyodacite domes (Fig. 3.8). In addition, coarse-grained conglomerate-breccias are present, which locally grade up into crystal-rich coarse-grained sandstones and fine-grained turbiditic units.

The Southern Complex dips roughly 40° towards the northeast, identical to the Northern Complex, but tends to be a lot more variable. Locally, some folding exists as bedding reverts towards the south-southwest (ca. 200°). However, the near non-existent exposure means that the extent of folding cannot be determined with any confidence. It can only be assumed that the Washikemba Formation seen in the Southern Complex consists of a uniformly dipping sequence with no repetition of lithological units.

According to Yonce (1997), the Complex is bounded to the southwest by a fault, the Kibri Hacha fault, which coincidentally strikes parallel to bedding, being uniformly orientated

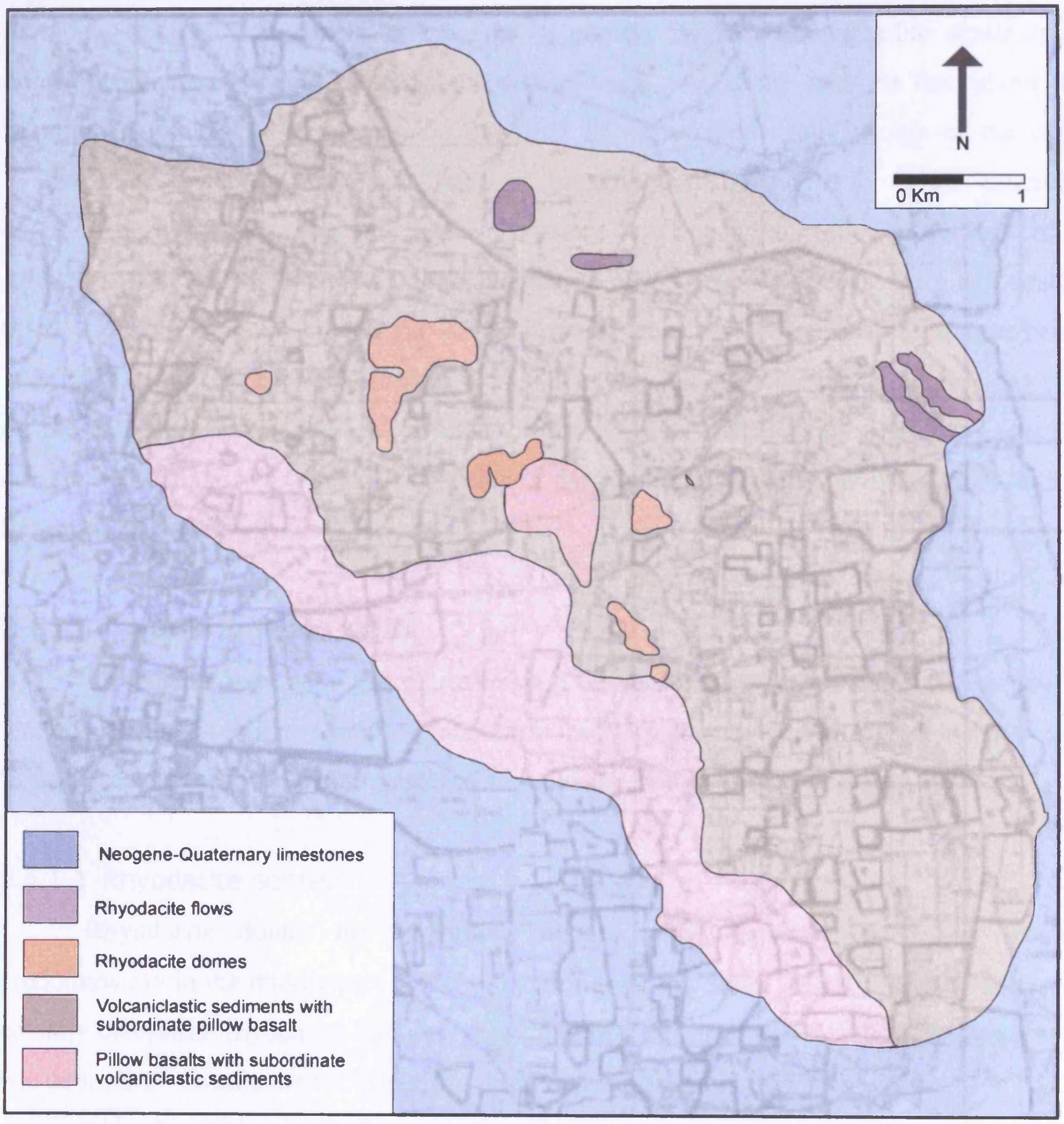

Fig. 3.8. Geological map of the Southern Complex, produced during this study. Limited exposure prevents lithological types being subdivided further.

310°–130°. However, no firm evidence was seen in this study of this fault, and it is believed that the Southern Complex is bounded in its entirety by an unconformable stratigraphic contact with the overlying Eocene-Recent limestones. As is the problem throughout the Southern Complex, there is no good exposure of the contact itself. Some of the main evidence for the existence of the fault, as invoked by Yonce (1997), is the extensive calcification of basalt adjacent to the limestone contact, giving the appearance of a calcite/basalt breccia. However, upon examination of the contact in places such as Locality 00-19-2, for example, the breccia appears to represent an erosive breccia with limestone being later deposited on the erosional surface. This is also seen in associated with a modern-day reef on the cliff face beside Slagbaai, in the Northern Complex. Therefore, it appears that the contact between the Washikemba Formation of the Southern Complex and the Eocene-Recent limestones is an unconformity.

3.6.1 Felsic igneous rocks

Rhyodacite intrusions and extrusions are the dominant geological and topographical features of the Southern Complex, and form both exogenous dome-shaped features and laterally extensive flows. Photographs of these features are presented in Figures 3.9a–f.

3.6.1.1 Rhyodacite domes

Rhyodacite domes are a feature unique to the Southern Complex, located predominantly in the middle part of the succession (e.g. Fig 3.9a). Many of these domes are actually composite rhyodacite features, consisting of a series of subordinate lava flows with one or several volcanic domes, which would have acted as minor volcanic edifices.

The rhyodacite is buff-coloured (grey on rare unaltered surfaces) and contains elongate laths of feldspar. In places it is vesicular, with vesicles mainly 0.5–1 mm in size, but large round ones exist up to 1 metre in size. Vesicles tend to be more common in the domes rather than the lavas. Vertical quartz veining is also locally abundant, and quartz and a green mineral (copper silicate?) occasionally infills the largest vesicles (e.g. Fig 3.9b). The presence of these copper silicate nodules is believed to indicate that the rhyodacite represents an eruptive centre (a dome, or vent).

The domes are also characterised by a rugged and spiny surface morphology (e.g. Figs 3.9b,f), frequently changing to a smoother "crazy paving" flow-like morphology on the dome margins (Fig 3.9e,f). Exposure on the rhyodacite hills is surprisingly poor, as it is obscured by large quantities of scree, and a rhyodacite contact can generally only be surmised from the abrupt change in gradient of the slope. However, on several rhyodacite hills (e.g. Seru

Fig. 3.9a.
Southern Complex (Bon 99-3-12).
Top of rhyodacite dome. Note spiny morphology of dome and low relief topography in the background. Width of view is ~4 m.

Fig. 3.9b.
Southern Complex (344530).
Rhyodacite lava dome. Quartz-rimmed vesicle is highlighted in white. Width of view is ~4 m.

Fig. 3.9c.
Southern Complex (Bon 00-04-06).
Successive lava flows at Seru Korai. Note hat for scale.

Fig. 3.9d.
Southern Complex (Bon 00-04-01).
Successive lava flows at Seru Korai. Note rucksack on left hand side for scale.

Fig. 3.9e.
Southern Complex (Bon 00-04-08).
Photograph showing surface morphology of lava flow with "crazy paving" texture. Note house for scale in background.

Fig. 3.9f.
Southern Complex (344530).
Morphology of lava dome. Cacti in background are ~2 m in height.

Figs. 3.9a-f. Structures and features of the rhyodacite lava flows and domes of the Southern Complex. Numbers in parentheses refer to photograph catalogue number.

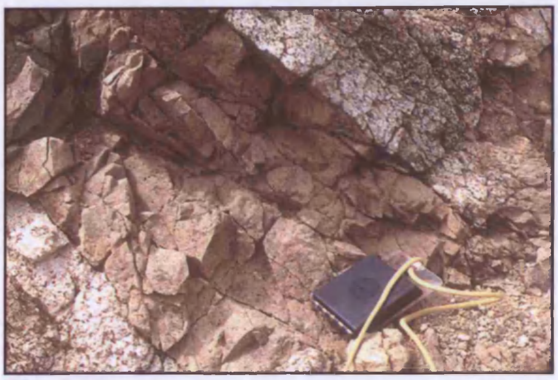

Fig. 3.10a.
Southern Complex (99-03-05).
Basaltic dyke intruding sediment and causing remobilisation of calcite giving a baked margins effect. Note compass for scale.

Fig 3.10b.
Southern Complex (99-03-09).
Pillow basalt flow overlain by fine-grained volcaniclastic sandstone. Note hat for scale.

Fig. 3.10c.
Southern Complex (99-03-06).
Poorly-exposed pillow basalts on hillside. Cactii in background are ~2 m tall.

Fig. 3.10d.
Southern Complex (99-03-08).
Angular blocks of rhyolite within coarse-grained conglomerate-breccia. Note hammer for scale.

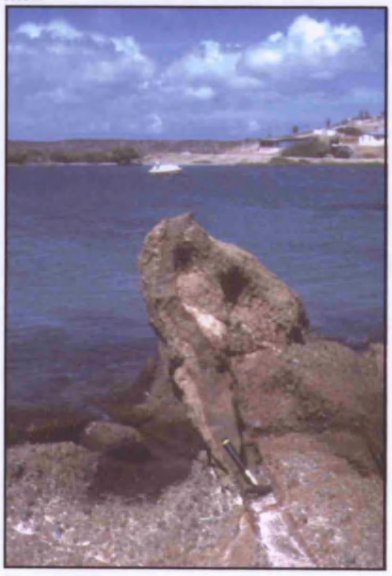

Fig. 3.10e.
Southern Complex (99-03-07).
Basaltic dyke forms promintory into sea at Lagoen. Note hammer for scale.

Fig. 3.10f.
Southern Complex (99-03-11).
Well-bedded sequence of volcaniclastic sediments at Lagoen. Note black rucksack for scale in foreground.

Fig. 3.10g.
Southern Complex (99-0.3-11).
Pillow basalt flow overlain by volcaniclastic sandstone. Note hammer for scale.

Figs. 3.10a-g. Structures and features of the volcaniclastic rocks and basalt lava flows (and intrusions) of the Southern Complex.

Grande and Barai Karta), fine-grained volcaniclastic sediment can be seen separating two main rhyodacite outcrops (a dome and a lava flow), but it remains unclear whether the sediment represents the outer margins of the dome (resedimented hyaloclastite, e.g. Lafrance et al., 2000), resedimented hyaloclastite/ash unrelated to the margins of the dome, or a block of sediment up-faulted after emplacement of the dome and lava.

The domes appear to intrude into fine-grained volcaniclastic sandstones and pillowed basalt, but the thick vegetation on the low-relief areas means that the actual contacts are never seen, although they can frequently be inferred to within a metre. They appear to be 50–100 m in height and up to 1 km in diameter, giving an aspect ratio of ~0.1. This is considerably smaller than many modern-day rhyodacite domes (e.g. McPhie, 1993; Doyle and McPhie, 2000) implying that these vents are minor volcanic features.

The domes are exogenous, rather than endogenous, in nature. This is suggested by the fact that no sediment is seen overlying the domes, and the spiny morphology (Fig. 3.9b) which would not be so well developed should the dome be entirely intrusive. In addition, the "crazy paving" surface texture most likely represents the original lava surface, formed by cooling of the upper surface in contact with water. A mechanism is invoked where cooling of the upper lava surface has led to a reduction in volume whilst the liquid interior continued to move below, resulting in the development of polygonal cracks and fractures (e.g. Christiansen and Lipman, 1966). Similar features have been documented in the Paleoproterozoic Flin Flon greenstone belt, where continued dome growth and quenching has resulted in the development of crackle breccia (Ayres and Peloquin, 2000).

3.6.1.1.1 Petrography

The rhyodacite domes are broadly petrographically similar to other rhyodacites from the Washikemba Formation (e.g. Section 3.5.1.1). There is one important textural difference however: the rhyodacite domes display a moderate to well-defined seriate texture. This is represented by a near continuous size range of feldspar from phenocryst to groundmass, and is in contrast to the rhyodacite flows (and sills) of the Formation, which have a well-defined porphyritic texture. This is consistent with the domes having a different magma chamber history to the rhyodacite flows of the Washikemba Formation.

3.6.1.2 Rhyodacite flows

Rhyodacite flows are also present in the middle and upper parts of the succession. These are distinguished by their conformable contact with the underlying sediments, their "crazy paving" surface texture (Fig. 3.9e), caused by the surface manifestation of columnar jointing, their undulating topography and the presence of the flow breccia seen on the tops and bases of the flows. Although there is no *a priori* reason why the cores of rhyodacite domes cannot also display this "crazy paving" surface, none showed evidence for it, possibly due to their small size inhibiting the development of columnar jointing. The flow breccias (e.g. Locality 00-11-04) consist of angular rhyodacite clasts 1–300 mm in size, in a rhyodacite lava matrix, and is distinct from the coarse-grained breccia/conglomerate seen elsewhere throughout the sequence. At one locality (00-18-01, Seru Korai), where construction development has exposed the rhyodacite flows, more than 30 individual lava flows are seen, ranging from 1–5 m in thickness. Interesting features can be found within the lava, for example large steam holes up to 2 m in diameter and pronounced columnar jointing (e.g. Figs. 3.9c,d). This contrasts with other flows, especially towards the top of the succession (e.g. the Washikemba area), where individual flows are seen to be at least 50 metres thick. In addition, several flows (e.g. Locality 00-5-02) show in places a spherulitic texture, which is apparent in hand specimen as well as in thin section, where the spherulites are defined by aggregates of anhedral quartz and feldspar (e.g. Fig. 3.13f).

On the southern side of the Lagoen Bay, several interesting exposures (e.g. Localities 99-08 and 99-09) of rhyodacite can be seen. Angular blocks of rhyodacite up to 2 m in length are seen in a coarse-grained conglomerate/breccia (detailed in Section 3.6.3.1), and directly beneath this angular rhyodacite blocks (<30 cm) comprising almost 100% of the rock are seen, only separated by small interstitial patches of the coarse-grained conglomerate/breccia (Fig. 3.9d). An apparent jigsaw-fit texture can be seen in places. I would interpret this as a rhyodacite flow breccia, which has then been partially reworked by a later conglomeratic debris flow. This is supported by the fact that ca. 300 m along strike from these localities more conventional rhyodacite flow breccias are seen with a similar clast size (e.g. Locality 00-11-04), without any evidence of interstitial coarse-grained conglomerate/ breccia, indicating that reworking did not occur at this point.

3.6.2 Mafic igneous rocks

Basaltic lithologies are far more abundant than previously recognised and are the dominant lithological unit of the succession. The basalt is particularly weathered and altered, however, and in most cases can be crumbled by hand. It is fine-grained, with a greenish tinge, and is amygdular with abundant calcite veining.

3.6.2.1 Mafic flows

In many different localities from different horizons throughout the succession unequivocal evidence for pillow (rather than pahoehoe) lobes was found, clearly indicating an extrusive (and subaqueous) origin (Figs 3.10b,c,g). The absence of visible pillow structures in the remainder of the succession is believed to be the result of alteration and weathering: in the known pillow outcrops, a complete transition from perfect pillow morphologies to a homogeneous crumbly rockface is seen within a few metres along strike. In addition, the basalts (due to their level of alteration) never form more resistant protrusions, and any basalt outcrops tend to be small and superficial, meaning that pillow structures are difficult to distinguish. Where present, the pillow lobes vary in size from 0.1 to 1 metre, and show evidence for being the correct way up. A red/blue chert, often with some ironstone development, is often present in the interstices, and in areas of negligible exposure, reasonably consistent mapping can be achieved by assuming basalt outcrops anywhere the distinctive resistant chert boulders lie.

The basalt flows are intercalated with fine-grained volcaniclastic sediment over a metre scale, and all available evidence confirms that they display conformable contacts (e.g. Localities 00-08-06, 00-08-07; Figs 3.10b,g). There is little evidence for interaction between the wet sediment and the basalt (i.e. peperites). Towards the (exposed) base of the succession basalt appears to comprise ca. 70% of the succession, as exposed in large quarries, whereas in the middle and upper parts of the succession, sediments become increasingly dominant although pillowed basalt is still present throughout.

3.6.2.2 Mafic Intrusives

At several localities throughout the succession (e.g. Locality 99-13), basalt (often transitional to dolerite in terms of grainsize) is clearly seen to intrude the fine-grained volcaniclastic sediment. This basalt is indistinguishable from the basaltic flows apart from the obvious absence of pillow structures. It is therefore impossible to determine the relative amounts of intrusive and extrusive basalt within the Southern Complex, other than noting that both are present.

In addition, abundant basaltic dykes are seen in the Lagoen area, where exposure is adequate (Figs. 3.10a,b,e). Some dykes contain large olivine phenocrysts, but are otherwise brown and weathered in appearance. The relationship between these basalt dykes, the pillow basalt flows and the more voluminous intrusions is unclear based on field evidence alone. The dykes may represent a late pulse of volcanic activity, but this would need to be confirmed by geochemical and geochronological data.

3.6.2.3 Petrography

Basalts of the Southern Complex are typified by elongate plagioclase laths surrounding patches of altered clinopyroxene, now partially replaced by chlorite and clay minerals. Pumpellyite appears to be pseudomorphing olivine, although the typically degree of alteration observed means this is only speculative. In the pillow basalts, plagioclase typically displays a skeletal and branching form, and a subvariolitic texture is often observed, indicative of quenching. Photographs of these features are presented in Figures 3.10a–g.

3.6.3 Volcaniclastic rocks

In the Lagoen area, volcaniclastic lithologies are dominant within the succession. The lithologies are very heterogeneous, and will be described below.

3.6.3.1 Coarse-grained conglomerate/breccia

These are pumaceous lithic-rich coarse-grained deposits with a distinctive blue-green colour. Whereas they were once thought to be a distinctive marker horizon, many different units have now been found over the island, including in the Northern Complex (first described in Section 3.5.2.3), and do not appear correlative. The description below is based on the best exposure of the deposit, at Lagoen Bay (Locality 99-01), and is detailed in the sedimentary log of Fig. 3.11.

The actual basal contact of the conglomerate is not exposed, although near the base, two small faults are seen which truncate it. Towards the base, it can be seen to consist of a basal layer (several metres exposed) rich in subangular to subrounded lithic clasts (mainly rhyodacite) 1–100 mm in diameter, with abundant tube pumice (displaying a blue-green hue and a weak fabric parallel to bedding), perlitic glass fragments and angular crystal fragments. Rip-up clasts of fine-grained ash are common, and are angular, up to 30 cm in length and are orientated parallel to bedding.

The main division of the deposit, up to 30 m in thickness, is massive, very poorly sorted conglomerate, containing abundant lithic fragments. These are predominantly purple rhyodacite (occasional scoreaceous rhyodacite, basalt, and tuffaceous clasts are also present), and appear moderately well rounded, although any roundness is accentuated by the way the matrix appears to encrust the lithic clasts. The lithic clasts vary from 2–10 cm in diameter, and locally comprise up to 90% of the deposit, although more commonly are found in diffuse bands comprising ~60% of the rock. They appear to show a crude normal size grading. Bedding is weakly-defined by concentrations of lithic-rich bands, which is parallel to the

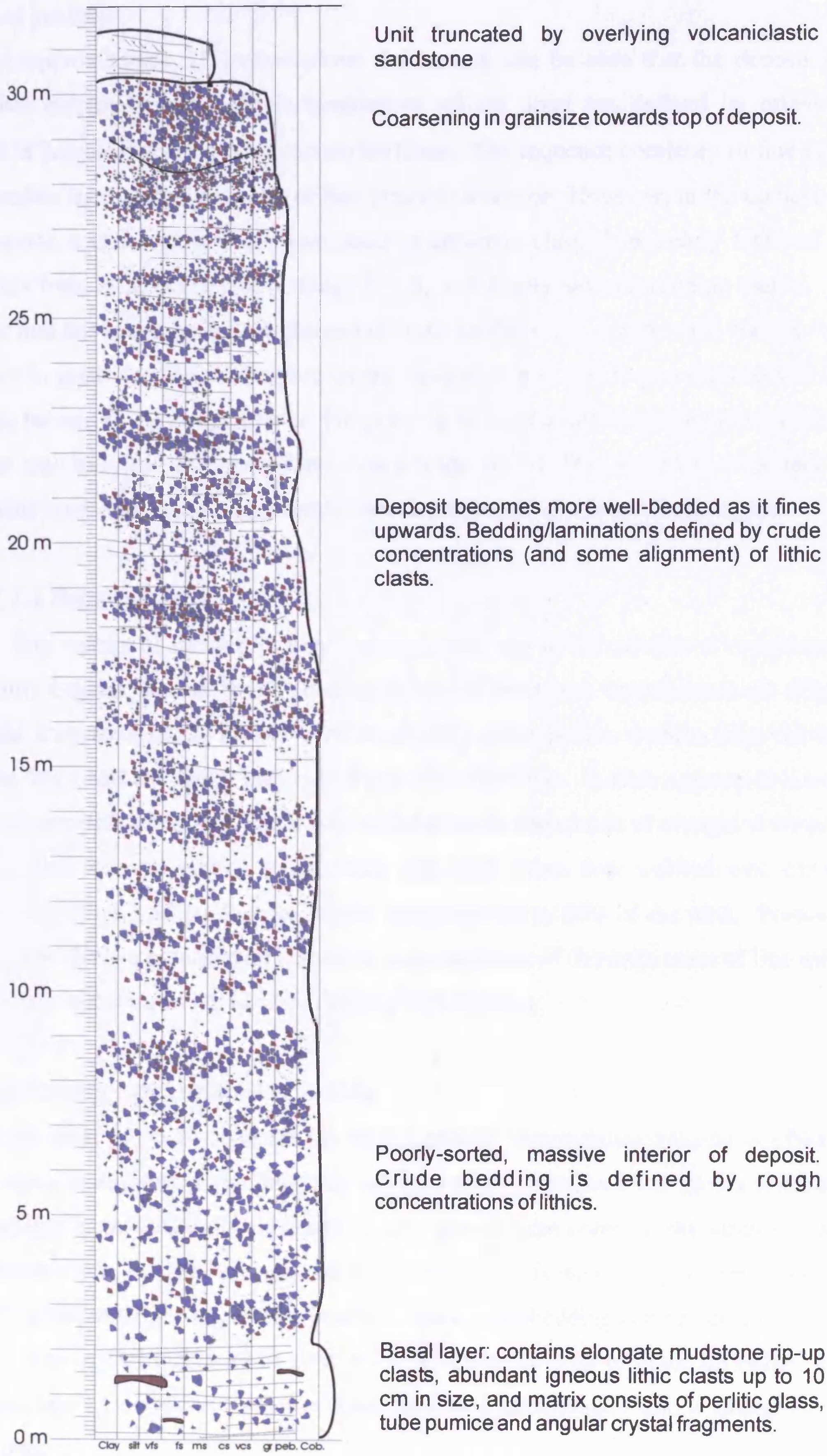

Fig. 3.11. Graphic sedimentary log of the coarse-grained conglomerate/breccia at the type locality (99-01), Lagoen bay. Vfs: very fine sand, fs: fine sand, ms: medium sand, cs: coarse sand, vcs: very coarse sand, gr: gravel, peb.: pebble, cob: cobble.

regional bedding direction. The beds are approximately 10 cm thick, and show no obvious signs of grading.

Approximately 15 metres above the base, it can be seen that the deposit suddenly becomes extremely well-bedded: laminations ~3 cm apart are defined by oriented clasts (38°/038°) and weathering in of certain horizons. The sequence continues to fine up, until it is truncated by the overlying unit of fine-grained sandstone. However, in the upmost metre of the deposit, a clear coarsening-up sequence is apparent: clasts form nearly 100% of the rock and vary from 2–20 cm in size (average 5 cm), with barely any surrounding matrix. It would appear that this unit represents a channel cut into the thick unit, but the fact that the "channel" appears to grade into the underlying conglomerate suggest that it was deposited at the same time as the rest of the conglomerate, but possibly through a different transport regime (eg. the current may have had a degree of turbulence at this point). This would be consistent with the overlying coarse-grained conglomerate-breccia representing a debris flow deposit.

3.6.3.1.1 Petrography

The matrix of the unit is very heterogeneous and in thin section it comprises smaller (<2 mm) angular igneous lithic fragments, sparse chert and mudstone clasts (Fig 3.14c), rounded fragments of devitrified glass showing a relict perlitic texture (Fig. 3.14a,c), and angular fragments of quartz, plagioclase and alkali feldspar. It often appears to have a weak foliation parallel to bedding, and this is defined by an abundance of elongated wisps of tube pumice, less than 10 mm in length, and with their tubes now infilled with chlorite and pumpellyite (Figs 3.8f, h). Pumice locally comprises up to 60% of the rock. Portions of the matrix often have a granophyric texture as a consequence of devitrification of fine ash shards. No primary ash textures are identified in any thin sections.

3.6.3.2 Crystal-rich volcaniclastic units

In areas of good exposure the coarse-grained conglomerate/breccia is often seen to grade into a crystal tuff. This commonly has an orange/tan colour. The matrix is usually well-lithified and is not easily distinguished on first glance from coherent rhyodacite. Bedding is sometimes crude, but often present on a 5 cm scale and is defined by a slight weathering in and out of the outcrop. In places a poorly defined cross-bedding can be seen, over a scale of 20 cm. The crystal tuff is up to 10 m thick, and is often seen to grade up (where exposure permits) into a fine-grained volcanic sandstone, and occasionally into a fine-grained fissile mudstone.

3.6.3.2.1 Petrography

The crystal-rich volcaniclastic units are typified by an abundance of plagioclase crystals with subordinate quartz and alkali feldspar, most of which are fragmented and less than 2 mm in size. On rare occasions fragments of olivine and augite crystals are visible. The matrix is similar to that of the coarse-grained conglomerate/breccia, being extremely poorly sorted and consisting of a heterogeneous mix of pumice, perlite, corroded igneous lithic clasts and devitrified ash shards.

3.6.3.3 Volcaniclastic Sandstones

The fine-grained volcanic sandstone is brown/tan in colour, and is finely bedded and laminated. In places (often where it is overlain by a coarse-grained crystal tuff) wildly convolute laminations are seen. These are interpreted as syn-depositional slumping, and are believed to result from the rapid deposition of the crystal tuff atop of the unlithified fine-grained sandstones, possibly on a moderately steep paleoslope.

At Lagoen, (Locality 99-01) overlying the type section of the coarse-grained conglomerate/breccia, is a thick (ca. 20 m) sequence of fine-grained volcaniclastic sandstone. This consists of alternating beds ca. 5 cm thick of finely-laminated fine-grained sandstone (possibly fining-up) and very fine-grained grey radiolarian chert displaying convolute laminations. These alternating units appear to represent the upper parts of a turbidite sequence, and are similar to the lithologies found elsewhere, except this is the best continuous sequence seen in the region. Towards the upper part of the sequence, however, blocks of volcaniclastic sandstone are found as rafts within the sediment. These blocks display contorted bedding, up to 50 cm in wavelength, and provide a good indication of the unstable submarine volcanic environment. Shortly above this, a conglomerate unit truncates the fine-grained sequence.

The southern side of Lagoen Bay also shows similar lithologies. It is a low-lying area with excellent exposure, and there are many outcrops showing the entire fining-up sequence from conglomerate to fine sandstone. In addition, fine-grained sandstone can be seen unconformably overlying conglomerate (e.g. Localities 99-02 and 99-03; Fig 3.10f). As it is unlikely that the current depositing the sandstone would be powerful enough to erode the coarse-grained conglomerate/breccia, it appears that it has been deposited into deep channels (ca. 100m in width) in the conglomerate. This indicates that there were significant time gaps in the formation of the Washikemba Formation, and provides further evidence that the coarse conglomerate is not a unique marker horizon.

3.6.3.3.1 Petrography

The fine-grained volcaniclastic lithologies consist of plagioclase and quartz crystals and pumice (e.g. Figs. 3.13a–c, 3.14a–b), along with variable amounts of poorly preserved foraminfera (Fig. 3.14d). The matrix is typically homogeneous and microcrystalline, that again probably represents the devitrification of glass shards.

3.6.4 Sedimentary Lithologies

As mentioned in Section 3.6.2, the basalt is found in the low-lying areas, which tend to be poorly exposed. Also associated with these areas is a red/blue cherty ironstone. This is usually found as loose fragments <50 cm in size on the ground surface, and appears to always be associated with the basalt. As it is never found actually in situ, determining the extent of chert development, and the nature of the chert (i.e. nodular or bedded) is difficult. The chert fragments are dark red or more uncommonly dark blue in colour. They show discontinuous parallel laminations, defined by changes in colour, and are distinct because of their high density.

3.6.4.1 Petrography

In thin section it can be seen that the rock predominantly consists of interlocking recrystalline quartz grains which vary in size from 0.2–0.6 mm, with irregular patches and small discontinuous veinlets of haematite. There are no signs of radiolaria or other fauna, and it is clear that the chert is secondary, and would perhaps be better termed a jasper. The rock strongly resembles the jaspers seen in the Gwna Formation on Anglesey (e.g. Greenly, 1940), and probably represents hydrothermal alteration of the basalts due to the proximity to the central volcanic vent. A similar association of jasper and iron oxide has been documented in the Archaean Hunter Mine group, part of the Abitibi greenstone belt. The association is thought to have been deposited directly on the sediment surface in a very proximal setting, with the fluids derived from the compaction of felsic tuffs (Chown et al., 2000), and a similar situation could be invoked for the Washikemba Formation.

3.6.5 Relationship between the different volcaniclastic lithologies

Whilst the coarse-grained conglomerate/breccia is locally seen to grade into the crystal tuff, which is also in places seen to grade into the fine-grained volcanic sandstone, the whole continuous sequence is never seen. This may be partly due to the poor exposure, but in several localities crystal tuff is found conformably overlying fine-grained sandstone and not grading up from the coarse conglomerate, and often thick sequences of sandstone are seen

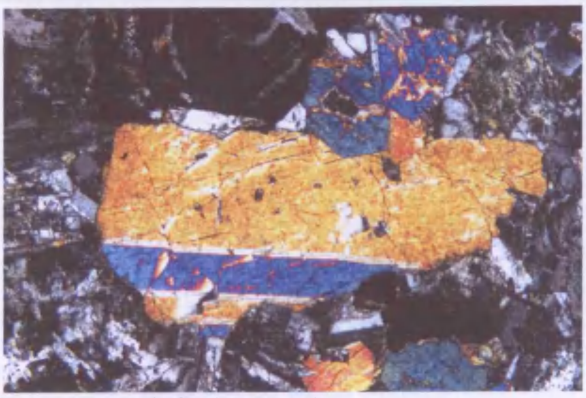

Fig. 3.12a. Dolerite (01-08-15).
Unaltered interlocking clinopyroxene and skeletal magnetite (top) in dolerite. Field of view: 5 mm, cross polarised light.

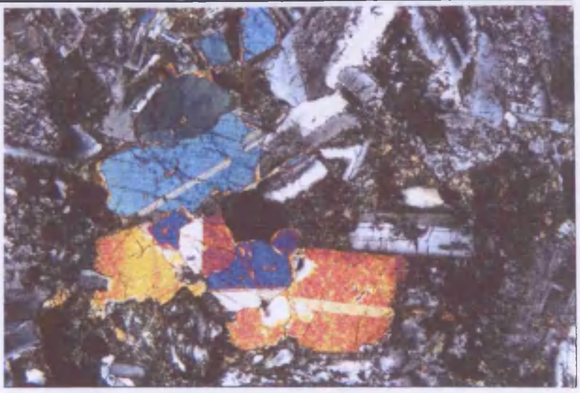

Fig. 3.12b. Dolerite (01-08-16).
Unaltered interlocking clinopyroxene (some displaying twinning) and plagioclase in dolerite. Field of view: 5 mm, cross polarised light.

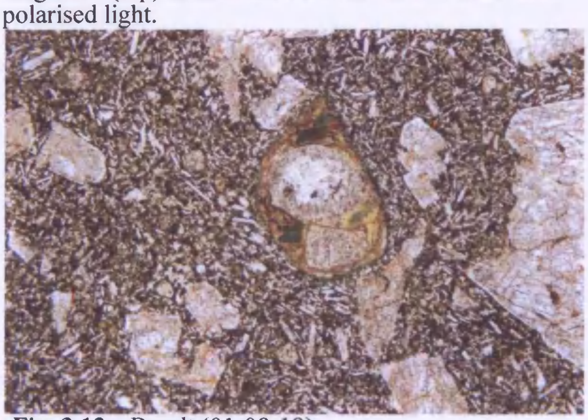

Fig. 3.12c. Basalt (01-08-19).
Relic olivine phenocryst (centre) now pseudomorphed by chlorite, calcite and Fe-oxyhydroxides. Field of view: 5 mm, plane polarised light.

Fig. 3.12d. Rhyodacite (01-08-11).
Plagioclase and relic clinopyroxene (higher relief, outlined in red) in porphyritic rhyodacite. Field of view: 5 mm, cross polarised light.

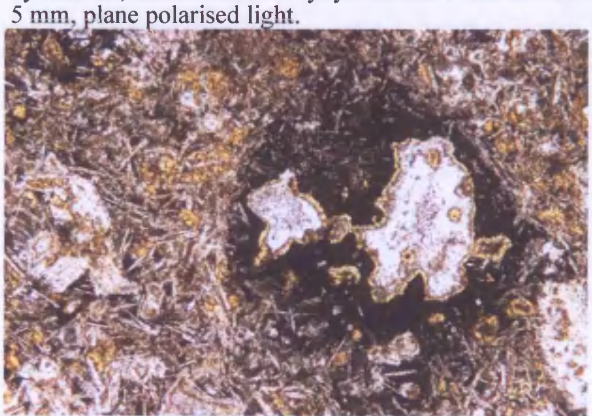

Fig. 3.12e. Vesicular Basalt (01-08-28).
Segregated material rich in magnetite surrounding vesicle. Field of view: 5 mm, plane polarised light.

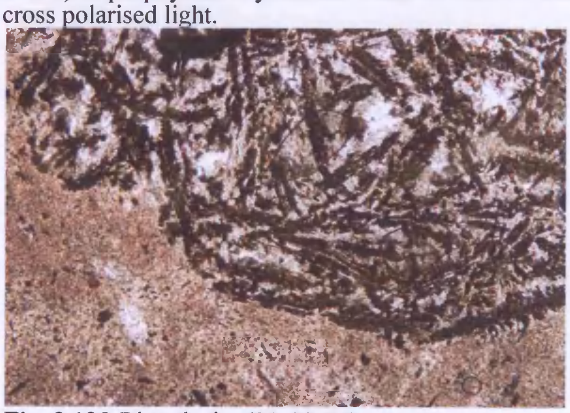

Fig. 3.12f. Rhyodacite (01-08-21).
Patch of segregated material in rhyodacite defined by concentration of skeletal and acicular magnetite. Field of view: 5 mm, plane polarised light.

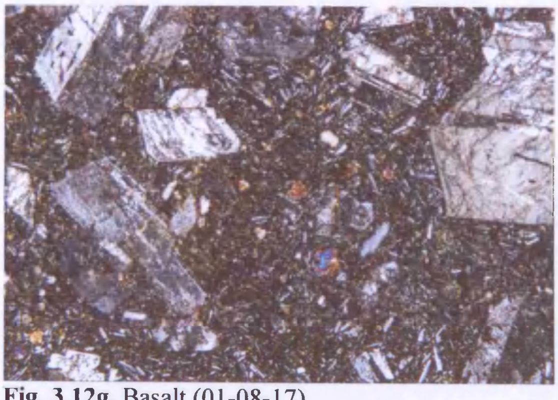

Fig. 3.12g. Basalt (01-08-17).
Typical texture of relatively unaltered basalt, with plagioclase phenocrysts in a groundmass of plagioclase, clinopyroxene and magnetite. Field of view: 5 mm, cross polarised light.

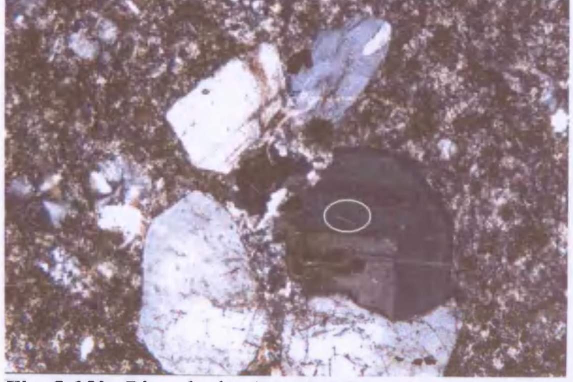

Fig. 3.12h. Rhyodacite (01-08-19).
Highly zoned and fractured plagioclase forming glomerocryst in rhyodacite. Note apatite needle (ringed). Field of view: 5 mm, cross polarised light.

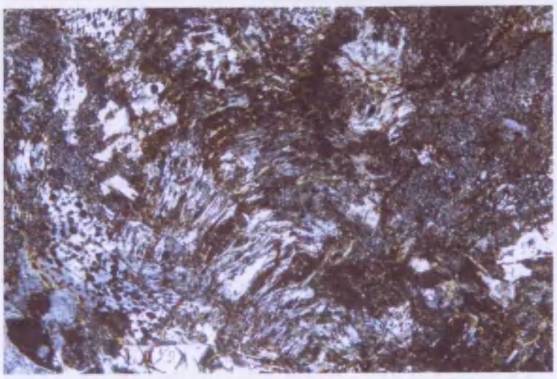

Fig. 3.13a. Volcaniclastic sandstone (00-07-21). showing twisted pumice and perlite in fine ashy matrix. Field of view: 5 mm, cross polarised light.

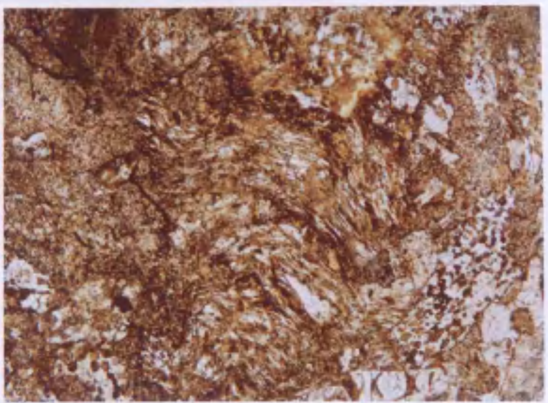

Fig. 3.13b. Volcaniclastic sandstone (00-07-22). showing twisted pumice and perlite in fine ashy matrix. Field of view: 5 mm, plane polarised light.

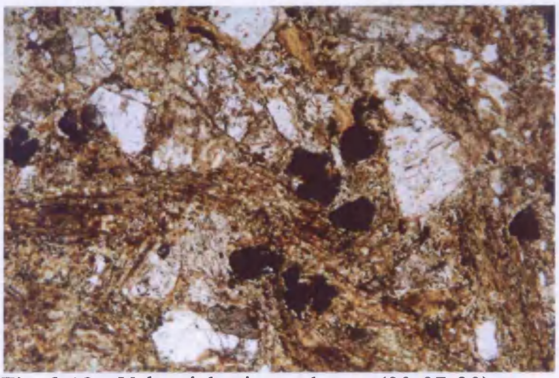

Fig. 3.13c. Volcaniclastic sandstone (00-07-30). showing twisted pumice, opaques and crystal fragments. Field of view: 5 mm, plane polarised light.

Fig. 3.13d. Rhyodacite (00-06-22). Quartz xenocryst displaying extremely resorbed margins. Field of view: 5 mm, plane polarised light.

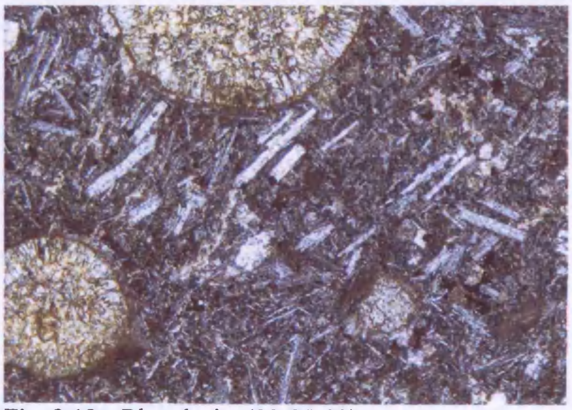

Fig. 3.13e. Rhyodacite (00-05-03). Vesicles infilled with chlorite and pumpellyite in feldspathic groundmass. Field of view: 5 mm, cross polarised light.

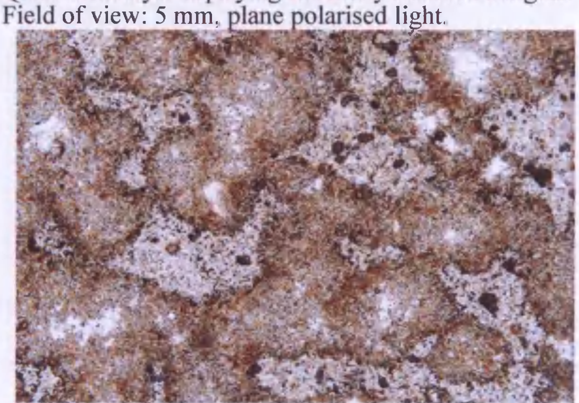

Fig. 3.13f. Rhyodacite (00-06-31). Development of spherulites (devitrification structures) in rhyodacite. Field of view: 5 mm, plane-polarised light.

Fig. 3.13g. Rhyodacite (00-06-30). Glomerocryst of sericitised feldspar in feldspathic matrix. Field of view: 5 mm, cross polarised light.

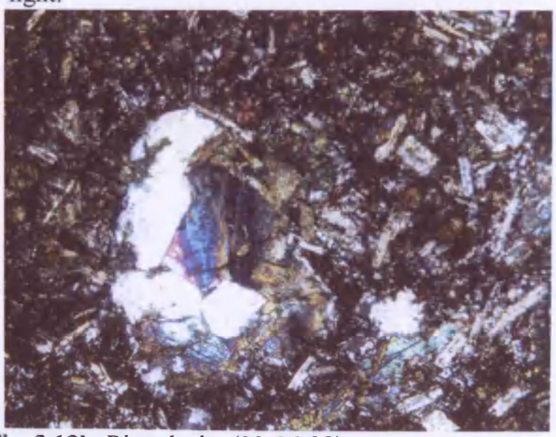

Fig. 3.13h. Rhyodacite (00-06-32). Resorbed quartz phenocryst (xenocryst?) with clinopyroxene. Field of view: 5 mm, cross polarised light.

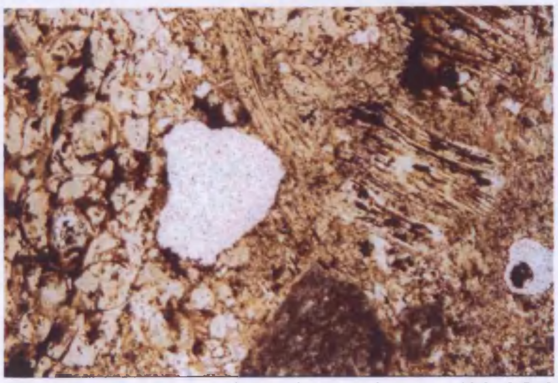

Fig. 3.14a. Volcaniclastic sandstone (00-05-07). Section showing fragment of perlite (left of centre), tube pumice (in conflicting orientations?) and an igneous lithic clast (bottom centre). Field of view: 5 mm, plane polarised light.

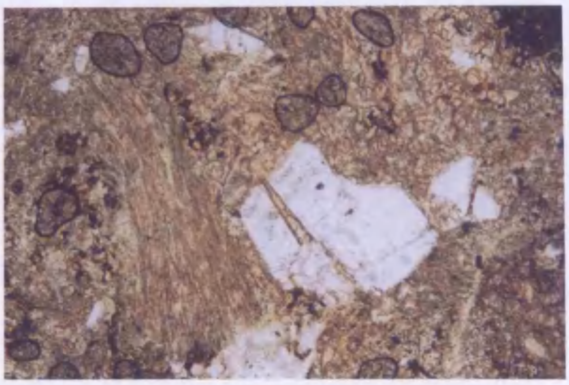

Fig. 3.14b. Volcaniclastic sandstone (00-05-03). Section showing tube pumice and crystal fragments in fine-grained devitrified ash matrix. Field of view: 5 mm, cross polarised light.

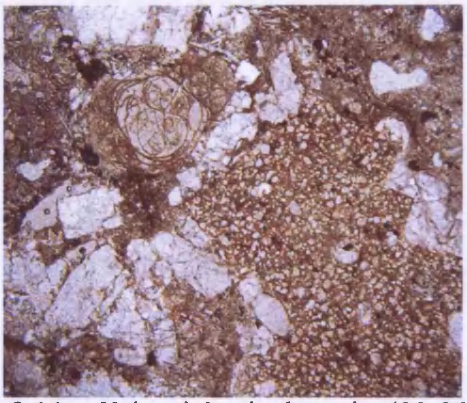

Fig. 3.14c. Volcaniclastic breccia (00-06-02). Section showing perlite fragment and radiolarian chert fragment in fine ashy matrix. Field of view: 5 mm, plane polarised light.

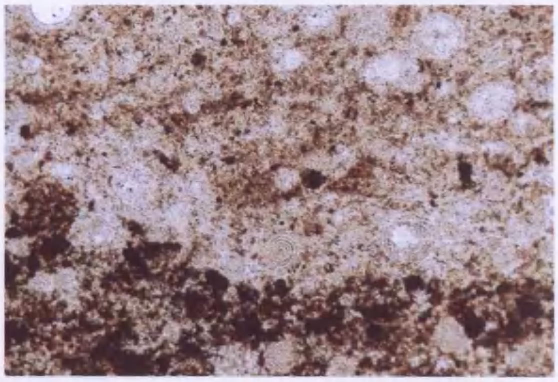

Fig. 3.14d. Volcaniclastic sandstone (00-06-09). Fine-grained turbidite showing well-preserved forams. Field of view: 5 mm, plane polarised light.

Fig. 3.14e. Volcaniclastic breccia (00-07-18). Tube pumice in conflicting orientations. Field of view: 5mm, plane polarised light.

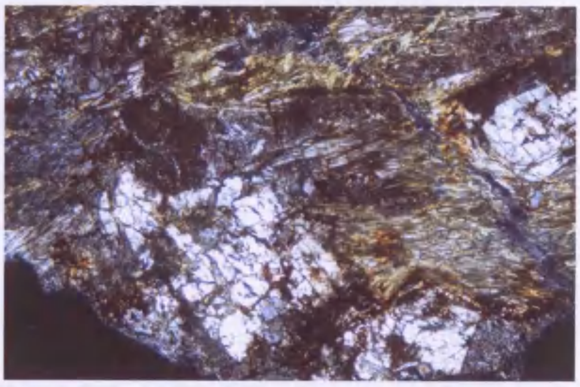

Fig. 3.14f. Volcaniclastic breccia (00-07-19). Section showing abundant pumice being replaced by pumpellyite. Field of view: 5 mm, cross polarised light.

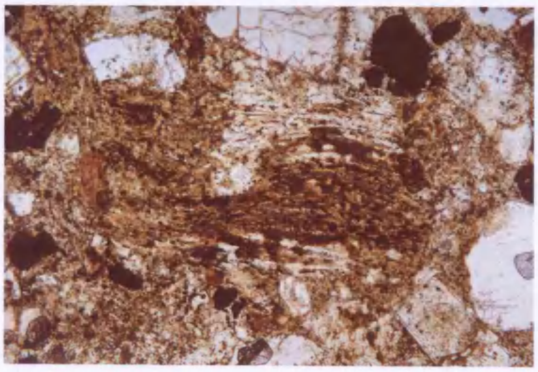

Fig. 3.14g. Volcaniclastic breccia (00-07-28). Tube pumice surrounded by crystal fragments. Field of view: 5 mm, plane polarised light.

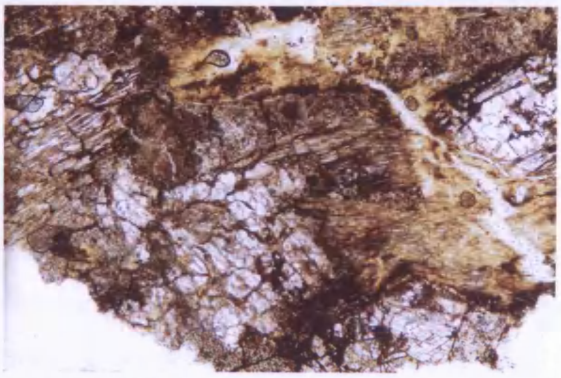

Fig. 3.14h. Volcaniclastic breccia (00-07-20). Section showing abundant pumice being replaced by pumpellyite. Field of view: 5 mm, plane polarised light.

with no underlying crystal tuff. This implies that although the units are often related, each can be deposited independently. This seems likely, as debris flows (responsible for the deposition of the coarse-grained conglomerate/breccia), can undergo flow transformations to turbidity currents as the flow wanes in intensity (Fisher, 1984b; Kesler and Bédard, 2000), thereby accounting for the gradation to fine-grained turbidites. Furthermore, turbidity currents can also be generated independently.

In addition, it is interesting that all rip-up clasts seen within the basal layers of the conglomerate/breccias are invariably fine sandstones and not basalt. This is surprising, as the basaltic flows were deposited synchronously with the sedimentary successions. This is most likely to be because the basalt flows were by their very nature more lithified than the (still-soft) sandstones, and were therefore more unlikely to be incorporated into the deposit.

In summary, it is important to note that the coarse-grained conglomerate unit appears identical to those observed in the Northern Complex, but should not be seen as a marker horizon: it seems to be found at many different horizons, and simply represents similar depositional processes occurring at different stratigraphic levels.

3.7 Degree of weathering/alteration of the Bonaire volcanics

The island is relatively low lying. Any hilly topography is due to the presence of more resistant igneous rocks, such as the rhyodacite sills/flows and dolerite laccoliths in the Northern Complex; the less resistant sediments form the more low-lying areas.

The lithologies appear very altered. Beets et al. (1984) noted that three phases of alteration have affected the volcanic rocks: low-grade metamorphism followed by seawater alteration and finally surface tropical weathering. From field evidence, only the presence of zeolites infilling vesicles and cavities provide any indication of the first phase; no prehnite or pumpellyite is seen. In addition, there is evidence for moderate hydrothermal alteration of the Bonaire volcanic rocks as some lithologies are veined with calcite, quartz and epidote, and hydrothermal jasper is found associated with the pillow basalts. However, some dolerites and basalts are so impregnated with calcite and clays that it is possible to crumble them by hand.

In thin section, feldspars are often cloudy and some are seriticised. Interstitial patches of a brown/green amorphous mineral phase are abundant, occasionally with a core of clinopyroxene, indicating it is probably replacing the primary igneous assemblage. Microprobe analysis identifies this mineral as chlorite, although some examples border with pumpellyite in composition, and others appear to show the characteristic oak leaf form typical of pumpellyite. This appears to suggest the prograde metamorphic reaction clinopyroxene

->pumpellyite-> chlorite has taken place, placing the assemblage well into the greenschist facies.

3.7.1 Summary of field relations in the Southern Complex

- The Southern Complex consists of a ~3 km apparently continuous sequence of pillow basalts, volcaniclastic conglomerates, sandstones and cherts, with occasional rhyodacite flows. The sequence is intruded by rhyodacite domes (which are concentrated in the middle portions of the sequence) and subordinate amounts of dolerite.
- The rhyodacite domes are very different in morphological character to the Northern Complex rhyodacite flows and sills, indicating a greater lava viscosity. In addition, the domes display a seriate texture, as opposed to the porphyritic texture displayed by the rhyodacite flows.
- Basalt lavas are the dominant lithology throughout the succession, but are poorly exposed due to their vulnerability to weathering. The basalt decreases in abundance upwards. Pillow lobes are commonly poorly preserved but are believed to be present throughout the succession.
- Neither base nor top of the sequence is exposed.
- The volcaniclastic sediments are of rhyodacite affinity, and are interlayered with the basalt flows, and therefore the two appear to be contemporaneous.
- Dolerite intrudes the volcaniclastic lithologies, but never the coherent rhyodacite, nor does the rhyodacite intrude any dolerite.
- The whole sequence is bimodal; this is unlikely to be an artefact of biased sampling methods.
- No visible tectonic contacts are present, nor evidence for extensive deformation of the sequence.
- The lithological similarity to the Northern Complex suggests both Complexes are part of the Washikemba Formation. However, some lithologies are unique to each, suggesting they each represent different levels of the Formation.

3.8 Relationship between the two Complexes

The two different outcrops of the Washikemba Formation are rather different in character and are separated and surrounded by Neogene and Quaternary limestone reef terraces.

The Northern Complex is typified by rugged topography, representing rhyodacite sills, flows and dolerite laccoliths. In the Southern Complex, however, the only topographic relief is formed by the small rhyodacite domes, intruding into basalt lavas, fine-grained volcaniclastic sandstones and cherts. One distinctive unit, however, is seen in both Complexes: the coarse-grained conglomerate. This is a thick conglomerate/breccia with a distinctive blue-green colour, and is interpreted as a subaqueous debris flow. However, although this appears lithologically identical in both Complexes, there is no evidence to say the two units are temporally related, and it would be inadvisable to treat it as a marker horizon.

The similarity of the sedimentary facies between the two Complexes and the similar bimodality of the volcanism suggests that the two Complexes must be related in some way. However, there are some lithological (and geochemical; as discussed in Chapter 5) differences between the two Complexes, suggesting that each may represent different levels of the Washikemba Formation (after all, neither the base nor the top of the Formation is exposed at any point), rather than a simple lateral variation in volcanic facies. The simplest explanation is that the Northern Complex is overlain directly by the Southern Complex. This is supported by the similarity in regional bedding directions, and the fact that the top of the Northern Complex is almost directly along strike from the base of the Southern Complex, meaning the Complexes combined could represent a near-continuous sequence. In addition, pillow basalts and cherts are found at the top of the Northern Complex and throughout the Southern Complex (particularly the base), supporting the idea of a progressive lithological sequence of >8 km in thickness. As the Southern Complex is not found directly above the Northern Complex, but outcrops along strike, some along-strike lithological variation between the two inliers is expected.

3.9 Structural evidence seen in the Northern and Southern Complexes

Very little evidence is seen for any structural deformation of either Complex, other than the regional tilt of the bedding, which trends 40°/040°. The Northern Complex, according to the existing map, appears to be dissected by many faults, with small amounts of displacement. However, the low level of exposure means that very little field evidence for this (such as definite offsets) is evident. It may be that single flows as marked on the map are in fact multiple flows, which makes correlating different units more difficult, and flow units may be truncated by topography rather than later faulting. According to the geological map (Klaver, 1976), faults are typically perpendicular to bedding orientation and therefore strike approximately 040°–060°, perhaps suggesting that faulting was synchronous with the tilting event, rather than being syn-volcanic.

There are some small-scale examples of folding, but all of these without exception appear to be syn-sedimentary folds. Convolute laminations on the scale of 1–100 mm are seen in many localities. A table of fold orientations seen is shown below, and many of them appear to relate to the nearby intrusion of dolerite. In addition, several small (centimetre) scale faults can be seen in various localities, but these are all undoubtedly syn-depositional in origin.

Locality	Fold Plunge	Wavelength	Amplitude	Related to intrusion?
99-026	20°/108°	30 cm	15 cm	?
99-030	20°/350°	10 m	2 m	Surrounded by dolerite
99-035	28°/038°	5 cm	20 cm	Surrounded by dolerite
99-039	64°/060°	4 m	30 cm	?
99-052	Convolute bedding	Several m	30 cm	?
99-078	Ca. 70°/110°	1 m	50 cm	Surrounded by dolerite
99-129	30°/178°	6m	2m	Surrounded by dolerite

Table 3.1. Fold orientations seen in Northern Complex.

In the Southern Complex, the poorer exposure means that in most cases the sedimentary lithologies are not exposed well enough to see any faulting/folding. Convolute laminations, where visible, appear irregular, and ripples and cross-bedding seen within the sedimentary sequences show no consistent paleo current directions.

The Southern Complex is intruded by a suite of basaltic dykes, which all strike approximately 040°.

The faulting, dip of the beds and the dyke orientations all appear to be roughly coincident, suggesting they all occurred during similar regional stress regimes. The fact that bedding strikes parallel in both Complexes suggests that they have both had similar histories, and were not rotated by any fault separating the two.

3.10 Interpretation of the Washikemba Formation, based on field evidence

3.10.1 The Northern Complex

The Northern Complex consists of a 5 km thick sequence of intrusive dolerites and rhyodacitic lava flows with intercalations of volcaniclastics, cherts and cherty limestones. The middle of the sequence also comprises shallow-level, columnar-jointed rhyodacitic sills, and both the basal and the upper portions of the sequence are heavily intruded by dolerites. The field observations are consistent with the Complex originating in a volcanic flank setting. The presence of radiolaria within both the volcaniclastics and the cherts, along with thinly bedded limestones and basaltic pillow lavas confirm a submarine depositional environment, albeit with temporary emergence of a nearby topographic high (probably the central volcanic edifice) resulting in boulder bed formation towards the top of the sequence.

There is no evidence in the Northern Complex for any volcanic edifice, so we conclude that it has not been preserved. The presence of abundant rhyodacite lavas, however, along with reworked volcaniclastic pyroclastic flow deposits is indicative of a relatively distal volcanic facies, probably 3–10 km away from the source (Mc Guire, 1996; Fisher and Smith, 1991).

The volcaniclastic sediments are of rhyodacite affinity and so the whole sequence is geochemically bimodal. However, as intrusion of the dolerite appears to be synchronous with sediment deposition (the sediments are locally deformed by the intrusion, indicating very shallow-level intrusives) then we conclude that the two magmatic sources were coeval.

3.10.2 The Southern Complex

The Southern Complex of the Washikemba Formation is rather different in character; a series of rhyodacite domes and flows form the higher relief areas, and intrude into a poorly exposed succession of intercalated volcaniclastic sediments and pillowed basalts. The volcaniclastic sediments appear indistinguishable from those of the Northern Complex and their mode of formation is considered identical. In addition, geochemical evidence indicates a related origin for the two Complexes.

Topographically, the 5 lava domes dominate the Southern Complex. The largest of these is less than 1 km in diameter, and although they are exogenous domes, their small size means they are unlikely to represent the vent responsible for many of the rhyodacite lavas of the Southern (or indeed Northern) Complex. One possibility is that the domes have been eroded drastically in size, but this is not supported by the spiny surface morphologies of the domes, nor the fact that many surrounding flows still have original carapace breccias present, indicating that surface erosion has been minimal. Therefore, it appears that the domes are more likely to be subsidiary, or flank fissure vents, marginal to a main volcanic centre. This is supported by data presented in Chapter 5, where the rhyodacite domes are found to have unique trace element characteristics, compared to the rest of the Washikemba Formation, and the petrographic textural differences between the two (Section 3.6.1.1.1) which is consistent with their evolution in subsidiary magma chambers. In addition, the lack of erosion associated with the domes means that these are likely to be late-stage features, and earlier ones may have been completely eroded away.

3.10.3 Central Volcanic edifice

Where would the central volcanic source have been? The typically poor levels of exposure of the Formation ensues that lateral facies variations cannot be used to infer vent location or direction (e.g. Francis, 1983). Evidence outlined above suggests that the Washikemba Formation (in particular the Southern Complex) represents a relatively proximal succession. Yet there is no indication of a central volcanic vent in either the Northern or the Southern Complexes. It is possible than the vague arcuate distribution of the domes (convex northwards) represents the outline of a large caldera (as suggested by Yonce, 1997), and the southern portion of this has been removed through erosion associated with tilting towards the northwest. However, there is no central topographic depression associated with this. It also possible that the central volcanic edifice was once situated immediately to the south of the domes, without invoking a caldera model, and has since been eroded away and unconformably overlain by limestone. The domes we see now would have developed on the flank of this edifice, at a late stage of volcanic evolution, and earlier ones may have been eroded away.

A question therefore arises: why the domes are present in the Southern Complex and not the Northern Complex? As mentioned above, silicic exogenous domes, which represent parasitic vents, are generally found within the order of one or two kilometres of a volcanic centre, partially due to the viscous nature of the magma. The Southern Complex, therefore, could represent a slightly more proximal volcanic setting than the Northern Complex. Alternative plausible explanations include a result of a greater magma viscosity, a flatter paleo-topography, or an external caldera wall restricting lava flow in the Southern Complex.

3.10.4 Was the Washikemba Formation entirely subaqueous?

Evidence for subaqueous deposition of the Washikemba Formation includes the following:

- presence of pillow lavas (not pahoehoe lobes) with interstital baked carbonate sediment
- volcaniclastic turbidites, showing grading, fine laminations, and some soft sediment deformation
- A marine fauna (including radiolaria) in the fine-grained sediments
- Presence of limestone towards the top of the sequence

Additionally, the presence of pumice, and vesicles in the pillow basalts implies that the water depth was less than 500 m in order for lava vesiculation to occur (Yamada, 1984). As the Washikemba Formation was most likely deposited on the basinal flanks of the volcanic centre, the central vent would have been situated at much shallower depths, and possibly emerged above sea level. This is supported by the presence of a probable fluvial-derived deposit towards the top of the sequence (Section 3.5.4.4), and the presence of pyroclastic flow deposits (now redeposited), as it is unlikely that pyroclastic flows can be generated underwater (e.g. Cas and Wright, 1987). Thereby, a model is envisaged where the volcanic centre became periodically emergent, but the volcanic products were deposited in a subaqueous setting.

3.11 Summary of the Volcanic Origin of the Washikemba Formation

The Washikemba Formation consists of two separate inliers which both represent the marginal flanks of a bimodal volcano. There is no evidence for any faulted offset between the two inliers. The volcanic edifice is believed to have been situated a kilometre or so south of the Southern Complex, but has since been eroded away due to tilting towards the northeast, and is only represented by a semi circle of domes or vents found on the southern confines of the Southern Complex. Hence the Southern Complex represents a slightly more proximal facies, as well as a slightly younger age.

The entire sequence appears to be subaqueous. The central volcanic edifice (which may have been emergent throughout the entire sequence) became conspicuously emergent towards the top of the succession, resulting in the boulder beds seen towards the top of the Northern Complex, as vent-derived material was reworked and remobilised by flash floods. Volcanism was dominated by pyroclastic sedimentation and lava flows, and dolerite was extensively intruded into the lava and sediment pile, just below the sediment-water interface. Pyroclastic flows were periodically generated at the volcanic edifice, and these were reworked to form debris flows or lahars, which plunged into the volcanic basin and were deposited as debris flow deposits, capped by turbidites as the flow waned. Basaltic pillow lavas first started to become apparent towards the middle of the succession, and became very abundant soon afterwards (seen at the base of the Southern Complex). As the volcano evolved, parasitic domes developed from congealing lava on the flanks of the edifice. The central vent continued to produce bimodal lavas throughout.

Chapter 4

Geochronology of the Washikemba Formation, Bonaire

4.1 Introduction

This chapter reviews existing age information for the Bonaire Washikemba Formation, and presents new ^{40}Ar–^{39}Ar ages. Previous geochronological studies of the Formation are extremely limited in extent and show contradictory ages. Poor preservation of fossil species coupled with possible misidentifications has meant that biostratigraphic dating of the Formation has been inconclusive. In addition, existing radiometric dating has relied on techniques which are vulnerable to resetting due to metamorphism or other factors, meaning that most – if not all – existing ages obtained actually represent later thermal resetting events, rather than primary magmatic crystallisation ages. However, constraining the age of the Formation is vital for interpreting the origin of the arc sequence and constraining its relationship to the neighbouring Caribbean plateau and tonalitic batholiths (both of which have well-constrained ^{40}Ar–^{39}Ar ages). In addition, as outlined in Chapter 3, there are two separate inliers ascribed to the Washikemba Formation outcropping on the island of Bonaire. Determining the relative ages of the two inliers is required in order to determine their stratigraphic relationship relative to one another, and to confirm their cogenetic origin as part of the Washikemba Formation.

4.2 Previous geochronological studies

4.2.1 Biostratigraphical studies

There exists a limited number of biostratigraphic studies of the sedimentary intercalations within the Northern Complex inlier of the Bonaire Washikemba Formation (Fig. 4.1). Sedimentary intercalations within the volcanic rocks are commonly chert or cherty limestone, and hence both siliceous and calcareous fauna are frequently associated with the sequence and preserved. Chert lithologies tend not to be primary cherts, but secondary cherts (e.g. Sections 3.5.2.4 and 3.6.4), i.e. they tend to comprise silicified volcaniclastic sediments rather than radiolaria. Nevertheless, small numbers of poorly-preserved forams and radiolaria were seen in this study, albeit too poorly preserved and fragmented to date (Sections 3.5.2.4 and 3.6.4), although previous studies detailed below have managed to place a biostratigraphical age on similar fauna. Two samples from a succession of cherty limestones and siliceous marls from the upper part of the Northern Complex (Smit, 1977) have yielded foraminifera with two apparent distinct ranges in ages, from Albian to Turonian and Turonian to Santonian (112–90.4 Ma and 90.4 Ma to 83 Ma; Harland et al., 1990). Because of the abundance of younger species, Smit (1977) judged these fauna to represent a Turonian–Santonian age, with the older species resulting from the mechanical reworking of older sediments. In particular, Smit ascribed the presence of *Globotruncana concavata Brotzen* and *Globotruncana angusticarinata Gandolfi* to strongly imply a Turonian–Santonian age. In addition, inoceramids yielding Coniacian ages were apparently found from the same lithological unit further to the northwest (Beets et al., 1977). However, Smit (1977) acknowledged that there were some difficulties with species identification, casting some doubts on the reliability of the biostratigraphic ages. Furthermore, evidence from this study (Chapter 3) suggests that tracing any lithological unit more than a few tens of metres is virtually impossible due to the poor exposure and numerous synvolcanic folds and faults, meaning that the inoceramids could potentially be derived from a completely different stratigraphic horizon to the radiolaria.

Macrofossils are also present within the Washikemba Formation. Intercalations of cherty sediment within the lower portions of the Formation yield sparse ammonites of a late Albian (112–97 Ma: Harland et al., 1990) age (Beets et al., 1977). The ammonites, however, are poorly preserved and reworking of these, or even misidentification of the individual species, would be very possible.

4.2.2 Radiometric age determinations

K–Ar and Rb–Sr geochronological studies of the Northern Complex were undertaken by Priem et al. (1979), but with only limited success. Analyses of a range of rock types from the Complex, including both whole-rock and hornblende mineral separate analyses, yielded ages ranging from 57.0–100 Ma. Most of the ages cluster around 78 Ma. Priem et al. attributed the older 100 Ma age to excess Ar, and the remainder of the ages to representing thermal resetting events, with the main metamorphic events occurring around 61± 4 and 78 ± 2 Ma. A K–Ar age of 88±2 Ma for four hornblende crystals from within a tuffaceous horizon towards the top of the sequence was taken as possibly representing a magmatic age (Priem et al., 1979). However, this only represents a minimum age of formation, and it is entirely possible that it represents a thermal resetting event rather than a primary igneous age. K–Ar radiometric dating relies on certain assumptions (detailed below), which may not be valid for rocks such as the Bonaire Washikemba Formation, that have suffered significant low-temperature alteration (Section 5.3). Ar–Ar radiometric dating relies on a reduced number of assumptions, and hence is much more suited to the altered rocks of the Bonaire Washikemba Formation. New Ar–Ar data are therefore presented in the next section.

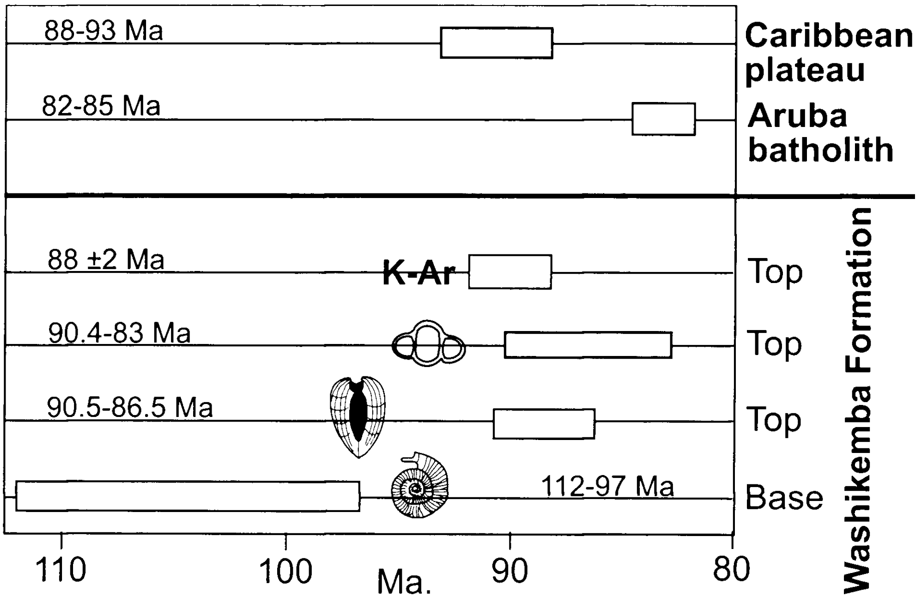

Fig. 4.1. Summary of existing age constraints on the Washikemba Formation. Note that dates only exist for the Northern Complex. Bonaire ages from Beets et al. (1977), Smit et al. (1977) and Priem et al. (1979). The Caribbean plateau age represents the apparent peak magmatic event based on a compilation of ages (as discussed in Chapter 2). Top and Base refer to the uppermost and lowermost exposed horizons of the Washikemba Formation in the Northern Complex, respectively.

4.3 An Ar–Ar geochronological study

As existing age constraints on the Bonaire Washikemba Formation appear to be mutually inconsistent (e.g. Fig. 4.1), further studies are clearly required. A new and more comprehensive geochronological study of the Formation is thus presented, using the more reliable ^{40}Ar –^{39}Ar technique.

4.3.1 The Ar–Ar technique

The Ar–Ar technique is based on the K–Ar radiometric technique, where naturally occurring ^{40}K decays to stable ^{40}Ar over time, and can be measured in a mass spectrometer. The time taken for the decay reaction to take place is calculated from the amount of ^{40}Ar measured, providing that the decay constant and the abundance of K in the sample are known. However, this technique assumes that all the ^{40}Ar has been derived from the radioactive decay of ^{40}K, and that no ^{40}Ar has subsequently escaped or been gained. Argon is a gaseous element, and this assumption may not be realistic, especially in rocks that have experienced secondary alteration and metamorphism. If the rock is heated above the Ar closure temperature (~300°C for plagioclase; Faure, 1986), the system can be reset, and hence yield erroneously young ages. This substantially reduces the reliability of K–Ar ages, especially for rocks such as those of the Bonaire Washikemba Formation, for which petrographic and geochemical studies confirm their altered nature (Chapter 3 and Section 5.3, respectively). In addition, both K and ^{40}Ar abundances are required for K–Ar studies. As they are determined on different aliquots of sample, sample inhomogeneity can be a significant source of error.

The equation for the growth of radiogenic Ar in a rock is:

$$^{40}Ar^* = \frac{\lambda e}{\lambda} {}^{40}K(e^{\lambda t} - 1)$$

where the recommended value for λ is 5.543×10^{-10} yr^{-1} and λe is 0.581×10^{-10} yr^{-1} (Steiger & Jaeger, 1977).

The ^{40}Ar –^{39}Ar technique is a variant of the K–Ar technique, where a portion of the ^{39}K is converted to ^{39}Ar by bombarding the sample with neutrons in a nuclear reactor. The $^{39}Ar/^{40}Ar$ ratio is then measured in a mass spectrometer. This eliminates the need for element abundances to be determined, and reduces the analytical error as isotopic ratios are more accurately determined than absolute abundances. ^{39}Ar gas can be either be extracted from the specimen using either a laser or a furnace in one of two ways: in incremental step heating, the temperature is increased sequentially until total fusion occurs, obtaining an age for each step. Total fusion, the alternative method, involves fusing the specimen in one step, releasing all the gas and analysing it to yield one overall age. Incremental step heating of a mineral grain has the added advantage that lower temperature steps can be used to release gas loosely held on the rims of the grain, i.e., sites which may potentially be affected by alteration. Ages can be obtained for all incremental steps, and the lower ones discounted, if necessary, meaning that this technique can be effective even for moderately altered rocks.

4.3.2 Sample selection

In ^{40}Ar–^{39}Ar dating, analysis usually involves either the whole rock or a K–rich phase such as feldspar, biotite, hornblende or phlogopite mineral separate. Given the level of secondary alteration seen in thin section (Chapter 3), it was decided that in the felsic lithologies, large phenocrystic feldspars represented the least altered components. These tended to be free of sericite and other K-rich secondary phases, which could contain excess Ar, and therefore lead to an artificially young age. In the mafic units, however, secondary alteration phases are uniformly abundant throughout the whole rock, and argon is likely to have been lost from the system. It was therefore decided that geochronological analysis should concentrate on the felsic units, as these represent the least altered lithological components and are found in abundance throughout the Formation. Eight samples were selected on the basis of the freshness and abundance of their phenocrystic feldspar, and care was taken to ensure that representative levels of the Formation from both inliers was sampled.

4.3.3 Mineral separation technique

Feldspar phenocrysts within the rhyodacites tend to be 0.5–2 mm in size, and comprise 5–20% of the rock. Both K-feldspar and plagioclase are present in variable proportions throughout. Both of these phases contain significant amounts of K, and are of potential use for ^{40}Ar–^{39}Ar dating, although as plagioclase contains less K, a greater quantity of mineral separate is required than for K-feldspar. As K-feldspar and plagioclase are difficult to distinguish optically without the aid of liquid refraction techniques, it was decided to separate both from the whole rock and to then select the freshest and cleanest crystals, regardless of their chemical composition. As both these phases are phenocrystic (0.5–2 mm in length), theoretically even the plagioclase should contain enough K to yield an analysis.

Samples were crushed in a cleaned flypress at the University of Leicester, to a coarse grit grain size. This material was then sieved in a series of clean mesh sieves and all fractions were collected. The two size fractions (1180–500 μm and 500–250 μm) which would yield the most phenocrystic feldspar (based on petrographical studies; Chapter 3; Appendix A, Table A.1) were then leached in warm 3 N HCl for 30 minutes in an ultrasonic bath, in order to remove any clays and secondary alteration products. These fractions were then rinsed in distilled and deionised water and dried in an oven at 100°C prior to picking. Feldspars were separated from the whole rock using a binocular microscope and fine tweezers. The most translucent grains were selected, which were free of inclusions and displayed good cleavage surfaces. The coarser fraction (1180–500 µm) tended to have rock debris adhering to the crystal surfaces whereas the 500–250 µm fraction tended to be debris-free, and hence in most cases only the finer fraction was selected for analysis.

4.3.4 Sample Irradiation and Analytical techniques

Approximately fifty handpicked mineral grains per sample were then wrapped in copper foil packets and placed in quartz vials, separated at intervals by monitor samples. In this study, the monitor materials used were sanidine crystals from sample TCR2 of the Taylor Creek rhyolite (Dalrymple and Duffield, 1988), with a new agreed age of 28 ± 0.34 Ma (M. Pringle, pers. com. 2002). These vials were then placed in a nuclear reactor for 24 hours in the cadmium-lined RODEO facility at the EC 45 megawatt reactor at Petten, Holland. They were then allowed to cool for three months before further preparation.

At the Scottish Universities Research and Reactor Centre (SURRC) they were then handpicked by Dr. Malcolm Pringle and the freshest-looking crystals were loaded into a copper pan with labelled holes. Individual crystals were heated with a 20 watt CO_2 laser for 2 minutes and cleaned for 3–8 minutes, and each crystal was heated incrementally in several steps, depending on the size and composition of the crystal. For crystals which appeared to be K-feldspar in composition on the basis of the initial degassing step, 2–4 incremental heating steps were undertaken before the final fusion, whereas small (<250 µm) plagioclases or altered k-feldspars were treated with just an initial degassing step (3.0–3.5 W) prior to total fusion. It should be noted that many small crystals experienced partial fusion at a temperature well below that expected for the minerals. Partial fusions tended to occur along small discontinuities along the crystal faces, indicating that secondary alteration products still remained along fractures and cleavage surfaces.

The cleaned gas was then released to a MAP 215 upgraded rare gas mass spectrometer, with a variable slit and an electrostatic filter. For each analysis, the peaks over the mass range 36–40 were measured over 9 cycles. Blanks were analysed at least every 6 steps which was usually at the end of each experiment. Typical blanks were 2×10^{-15} moles for ^{39}Ar.

Analyses were then corrected for these blanks. Monitor samples were analysed and their J curves were calculated from their positions within the vial. These curves were interpolated and J values were obtained for each sample, which was then used as a correction factor.

Step (a)	$^{40}Ar/^{39}Ar$ (b)	$^{37}Ar/^{39}Ar$ (b)	$^{36}Ar/^{39}Ar$ (b)	^{40}Ar s.d. (%)	^{39}Ar s.d. (%)	^{37}Ar s.d. (%)	^{36}Ar s.d. (%)	^{40}ArR (mol)	^{40}ArR (c)	^{40}ArK (c)	$^{39}ArCa$ (c)	$^{36}ArCa$ (c)	K/Ca (%)	^{39}Ar (%)	Apparent Age (Ma)	± (d)	1 s.d. (Ma)
BON94-09	NC	J = 0.01146 ± 0.0000229 (1 s.d.)						Exp. No.: pt1I0072.IHD			*Total gas age =*				*80.07*	±	*1.01*
3.5	130.74	0.979	0.4185	0.04	0.38	0.94	0.64	6.60E-16	5.5	0	0.07	0.06	0.5	2.5	142	±	18.3
3.6	15.802	3.052	0.0367	0.21	0.76	0.16	3.35	5.10E-16	33	0	0.21	2.25	0.16	2.7	104.83	±	6.75
3.7	57.62	2.893	0.1822	0.05	0.69	0.15	0.41	1.60E-15	7	0	0.2	0.43	0.17	11.2	81.49	±	5.1
3.8	16.76	4.234	0.0462	0.09	1	0.16	1.62	6.30E-16	20.5	0	0.29	2.48	0.12	5	69.94	±	4.27
3.9	8.39	3.764	0.017	0.15	0.89	0.27	3.89	7.30E-16	43.6	0	0.25	5.98	0.13	5.5	74.22	±	3.54
4.1	7.69	3.25	0.0162	0.05	0.8	0.07	2.29	1.00E-15	41	0	0.22	5.42	0.15	9.1	64.13	±	2.06
4.3	19.469	3.045	0.0546	0.06	0.71	0.06	0.21	4.20E-15	18.3	0	0.21	1.51	0.16	32.1	72.45	±	1.03
4.5	26.01	6.179	0.0764	0.03	1.43	0.09	0.5	1.40E-15	15.1	0	0.42	2.19	0.08	9.5	79.74	±	2.29
4.7	26.08	8.446	0.0779	0.06	1.96	0.1	0.99	6.40E-16	14.3	0	0.57	2.93	0.06	4.7	75.87	±	4.49
10	21.6	11.29	0.0604	0.06	2.62	0.07	0.46	3.00E-15	21.5	0	0.76	5.06	0.04	17.6	94.32	±	1.75
BON94-09	NC	J = 0.01146 ± 0.0000229 (1 s.d.)						Exp. No.: pt1I0061.IHD			*Total gas age =*				*90.11*	±	*2.85*
3.5	103.73	8.071	0.3398	0.11	1.88	0.1	0.38	6.10E-16	3.8	0	0.54	0.64	0.06	21	80.55	±	10.3
3.7	10.521	10.127	0.025	0.47	2.36	0.14	5	2.30E-16	37.6	0	0.68	10.98	0.05	8	80.56	±	6.37
3.8	19.134	8.655	0.0521	0.11	2	0.11	1.45	1.20E-15	23.1	0	0.58	4.49	0.06	35.9	89.76	±	4.12
10	12.133	12.494	0.028	0.12	2.9	0.11	2.03	1.30E-15	39.9	0	0.84	12.06	0.04	35.2	98.29	±	2.84
BON94-09	NC	J = 0.01146 ± 0.0000229 (1 s.d.)						Exp. No.: pt1I0062.IHD			*Total gas age =*				*71.9*	±	*3.95*
3.5	113.21	1.125	0.3725	0.34	0.66	0.8	0.36	2.50E-15	2.8	0	0.08	0.08	0.44	17.9	65.29	±	21.9
3.8	34.33	2.026	0.1038	0.05	0.49	0.14	0.5	2.40E-15	11.1	0	0.14	0.53	0.24	14.2	77.45	±	3.33
4.1	10.75	1.8007	0.0257	0.1	0.43	0.07	1.01	2.20E-15	30.6	0	0.12	1.89	0.27	15.6	66.93	±	1.5
4.3	12.468	1.6809	0.0316	0.06	0.4	0.1	0.77	1.80E-15	26.1	0	0.11	1.44	0.29	12.6	66.17	±	1.43
4.5	17.784	2.671	0.0489	0.04	0.62	0.08	0.26	4.50E-15	19.9	0	0.18	1.48	0.18	29.3	71.98	±	0.92
10	21.44	7.553	0.0596	0.08	1.75	0.1	0.5	2.00E-15	20.7	0	0.51	3.43	0.07	10.3	89.85	±	1.84
BON94-09	NC	J = 0.01146 ± 0.0000229 (1 s.d.)						Exp. No.: pt1I0183.IHD			*Total gas age =*				*69.09*	±	*1.52*
3.6	25.13	1.6623	0.0744	0.11	0.4	0.37	0.44	1.80E-15	13	0	0.11	0.6	0.29	43.1	66.38	±	2.17
3.8	15.207	2.207	0.0408	0.08	0.52	1.79	0.76	1.90E-15	21.9	0	0.15	1.46	0.22	46.1	67.69	±	1.88
4.2	30.08	8.861	0.0919	0.18	2.1	0.77	3.08	1.90E-16	12.1	0	0.6	2.61	0.06	4.2	74.23	±	16.3
12	29.29	8.421	0.0859	0.13	1.97	0.36	1.3	3.90E-16	15.6	0	0.57	2.65	0.06	6.7	92.74	±	6.72
BON94-09	NC	J = 0.01148 ± 0.0000229 (1 s.d.)						Exp. No.: pt1I0184.IHD			*Total gas age =*				*73.04*	±	*1.2*
3.7	34.25	2.84	0.1039	0.18	0.7	0.26	0.5	4.30E-15	11	0	0.19	0.74	0.17	26.9	76.4	±	4.06
3.9	6.381	3.041	0.0113	0.09	0.73	0.35	2.21	1.70E-15	51.3	0.01	0.21	7.25	0.16	12.3	66.62	±	1.39
4.2	11.682	2.577	0.0296	0.1	0.6	0.26	0.72	2.00E-15	26.8	0	0.17	2.35	0.19	15	63.86	±	1.29
4.5	16.141	3.67	0.0434	0.09	0.86	0.13	0.32	5.40E-15	22.4	0	0.25	2.29	0.13	34.8	73.68	±	1.09
12	15.352	10.129	0.041	0.1	2.35	0.16	0.68	1.90E-15	26.4	0	0.68	6.69	0.05	11	82.48	±	1.64
BON94-09	NC	J = 0.01146 ± 0.0000229 (1 s.d.)						Exp. No.: pt1I0060.IHD			*Total gas age =*				*42.9*	±	*3.09*
3.6	64.84	0.6477	0.2142	0.09	0.23	0.42	0.37	2.40E-15	2.5	0	0.04	0.08	0.76	51.4	32.69	±	5.99
3.7	5.362	0.875	0.0123	0.17	0.27	0.26	1.89	5.10E-16	33.6	0.01	0.06	1.93	0.56	9.9	36.87	±	1.35
3.9	6.568	0.9772	0.017	0.21	0.28	0.3	3.62	3.10E-16	24.7	0.01	0.07	1.56	0.5	6.6	33.24	±	3.5
4.2	9.404	1.3838	0.0219	0.07	0.33	0.1	0.65	2.20E-15	32.2	0	0.09	1.71	0.35	25	61.69	±	0.87
10	16.457	3.92	0.0456	0.1	0.93	0.17	1.25	6.80E-16	20	0	0.26	2.33	0.13	7.2	66.94	±	3.34
BON00-19	SC	J = 0.01145 ± 0.0000229 (1 s.d.)						Exp. No.: pt1I0066.IHD			*Total gas age =*				*79.18*	±	*0.85*
3.6	8.933	0.0277	0.0172	0.09	0.2	1.06	0.9	3.80E-15	43	0	0	0.04	17.7	56.5	77.69	±	0.99
3.9	6.951	0.0134	0.0089	0.4	0.13	30.25	13.04	4.50E-16	62.2	0.01	0	0.04	36.6	6	87.23	±	6.47
10	6.41	0.034	0.0083	0.11	0.08	1.21	2.76	2.60E-15	61.9	0.01	0	0.11	14.4	37.4	80.12	±	1.3

Table 4.1. Single Crystal Incremental Heating Ar-Ar data (ctd. overleaf).

Step (a)	$^{40}Ar/^{39}Ar$ (b)	$^{37}Ar/^{39}Ar$ (b)	$^{36}Ar/^{39}Ar$ (b)	^{40}Ar s.d. (%)	^{39}Ar s.d. (%)	^{37}Ar s.d. (%)	^{36}Ar s.d. (%)	^{40}ArR (mol)	^{40}ArR (c)	^{40}ArK (c)	$^{39}ArCa$ (c)	$^{36}ArCa$ (c)	K/Ca (%)	^{39}Ar (%)	Apparent Age (Ma)	± (d)	1 s.d. (Ma)
BON00-19	SC		J = 0.01145 ± 0.0000229 (1 s.d.)						Exp. No.: pt1l0068.IHD			*Total gas age =*			*83.57*	±	*3.59*
3.6	24.3	0.0403	0.0671	0.08	0.24	6.03	1.61	7.10E-16	18.4	0	0	0.02	12.2	41.8	90.15	±	6.24
3.8	6.84	0.087	0.0127	1.02	0.37	10.77	19.92	1.20E-16	45.4	0.01	0.01	0.19	5.63	10.2	63.08	±	14.3
4.2	13.377	0.1542	0.0315	0.21	0.52	1.72	2.25	5.10E-16	30.5	0	0.01	0.13	3.18	33	82.43	±	4.33
10	28.97	0.3683	0.0845	0.17	0.38	1.5	1.86	2.30E-16	13.9	0	0.02	0.12	1.33	15	81.53	±	9.27
Bon 00-19	SC		J = 0.01145 ± 0.0000229 (1 s.d.)						Exp. No.: pt1l0069.IHD			*Total gas age =*			*108.54*	±	*4.85*
3.4	30.85	0.0955	0.0894	0.12	0.29	3.56	1.09	4.30E-16	14.4	0	0.01	0.03	5.13	52.6	89.39	±	5.99
3.5	19.647	0.1714	0.0506	0.24	0.26	2.96	2.33	2.80E-16	24	0	0.01	0.09	2.86	32.8	94.85	±	6.73
10	53.65	0.7087	0.1461	0.19	0.54	1.84	2.39	2.80E-16	19.6	0	0.05	0.13	0.69	14.6	205.4	±	19.4
BON99-180	NC		J = 0.0115 ± 0.000023 (1 s.d.)						Exp. No.: pt1la070.IHD			*Total gas age =*			*86.9*	±	*6.07*
3.6	8.244	0.041	0.0134	0.51	0.28	11.5	13.47	3.00E-16	51.9	0	0	0.08	12	37	86.73	±	10.1
4.2	3.999	0.0931	0.0006	1.71	0.42	8.18	496.29	1.50E-16	95.4	0.23	0.01	4.1	5.26	20.2	77.51	±	16.5
10	13.246	0.2022	0.0296	0.25	0.27	1.88	4.86	3.70E-16	34.1	0	0.01	0.18	2.42	42.8	91.47	±	8.04
BON99-180	NC		J = 0.0115 ± 0.000023 (1 s.d.)						Exp. No.: pt1l0064.IHD			*Total gas age =*			*71.78*	±	*5.63*
3.5	68.05	1.1895	0.2251	0.08	0.46	0.38	0.67	1.40E-16	2.4	0	0.08	0.14	0.41	21.9	33.72	±	11.3
3.9	7.871	0.451	0.0154	0.76	0.7	1.88	18.26	1.50E-16	42.6	0	0.03	0.79	1.09	11.5	68.3	±	15.8
4.1	10.176	0.2592	0.017	0.41	0.42	1.85	10.41	3.40E-16	50.9	0	0.02	0.41	1.89	16.2	104.39	±	9.79
4.3	32.94	0.7272	0.0961	0.12	0.31	0.32	0.96	6.20E-16	14	0	0.05	0.2	0.67	33.3	93	±	5.72
10	144.97	3.208	0.4833	0.1	0.83	0.22	0.63	1.70E-16	1.7	0	0.22	0.18	0.15	17.2	49.51	±	23.7
BON99-180	NC		J = 0.0115 ± 0.000023 (1 s.d.)						Exp. No.: pt1l0065.IHD			*Total gas age =*			*64.11*	±	*10.8*
3.7	27.7	2.951	0.0896	0.2	0.83	0.4	3.31	7.80E-17	5.3	0	0.2	0.89	0.17	34	30.33	±	17.4
3.8	45.97	1.5802	0.1478	0.14	0.55	0.85	1.43	1.40E-16	5.3	0	0.11	0.29	0.31	36.5	49.82	±	13.2
10	155.04	3.565	0.5055	0.07	0.92	0.23	0.67	2.70E-16	3.8	0	0.24	0.19	0.14	29.4	119.62	±	25.7

Table 4.1. Single Crystal Incremental Heating Ar-Ar data (ctd.).

NC: Northern Complex, SC: Southern Complex.
(a) Steps labeled as laser power (W).
(b) Corrected for ^{37}Ar and ^{39}Ar decay, half-lives 35.1 days and 259 years, respectively.
(c) Radiogenic (R), calcium-derived (Ca), and potassium-derived (K) argon, respectively (percent).
(d) Ages calculated relative to 85G003 TCR Sanidine at 28.02 Ma with lambda e = 0.581E-10/yr and lambda b = 4.692E-10/yr.

Step (a)	$^{40}Ar/^{39}Ar$ (b)	$^{37}Ar/^{39}Ar$ (b)	$^{36}Ar/^{39}Ar$ (b)	^{40}Ar s.d. (%)	^{39}Ar s.d. (%)	^{37}Ar s.d. (%)	^{36}Ar s.d. (%)	^{40}ArR (mol)	^{40}ArR (c)	^{40}ArK (c)	$^{39}ArCa$ (c)	$^{36}ArCa$ (c)	K/Ca (%)	^{39}Ar (%)	Apparent Age (Ma)	± (d)	1 s.d. (Ma)
Bon 00-12	Feldspar		J =0.011 ± 0.0000227 (1 s.d.)					Exp. No.: pt1I7481.IHD				*Total gas age =*			*68.59*		*118.5*
dg1	132.13	0.2896	0.4342	0.24	1.5	10.93	2.9	3.70E-17	2.9	0	0.02	0.02	1.691	8.7	77.2	±	89.0
dg2	245.6	0.546	0.8197	0.06	0.58	2.59	0.96	7.20E-17	1.4	0	0.04	0.02	0.897	18.9	68.99	±	58.8
dg3	139.51	0.65	0.4699	0.27	1.96	7.29	4.65	5.20E-18	0.5	0	0.04	0.04	0.753	6.4	14.818	±	149.0
dg4	80.52	0.5842	0.251	0.36	1.49	5.99	5.34	6.10E-17	7.9	0	0.04	0.06	0.838	8.5	126.72	±	79.4
fs1	661.3	1.1173	2.218	0.07	1.28	1.87	0.62	1.00E-16	0.9	0	0.08	0.01	0.438	16.1	115.3	±	236.4
fs2	1596.9	1.6379	5.416	0.09	2.01	2.34	0.43	-3.90E-17	-0.2	0	0.11	0.01	0.299	10.5	-70.19	±	958.8
fs3	743.3	1.2268	2.44	0.07	2.77	3.39	1.25	1.80E-16	3	0	0.08	0.01	0.399	7.1	410	±	484.3
fs4	724.7	1.6186	2.458	0.06	0.95	0.74	0.08	-3.80E-17	-0.2	0	0.11	0.02	0.302	23.7	-29.93	±	186.9
Bon 00-23	Feldspar		J =0.011 ± 0.0000227 (1 s.d.)					Exp. No.: pt1I7582.IHD				*Total gas age =*			*83.46*	±	*16.7*
dg1	71.99	1.4182	0.22	0.29	1.05	2.41	4.65	9.20E-17	9.8	0	0.1	0.17	0.345	8.9	140.13	±	58.3
dg2	42.58	1.2256	0.1236	0.28	0.66	1.18	3.85	1.40E-16	14.5	0	0.08	0.27	0.399	16.1	122.45	±	26.8
dg3	40.36	1.7286	0.1263	0.14	0.51	0.55	2.38	1.90E-16	7.9	0	0.12	0.37	0.283	40	64.29	±	17.4
dg4	154.85	5.82	0.483	0.47	4.45	1.54	6.34	4.60E-17	8.1	0	0.39	0.33	0.084	2.5	242.9	±	223.3
fs1	74.18	3.361	0.2376	0.22	1.52	1.86	5.2	3.80E-17	5.7	0	0.23	0.38	0.145	6.1	85.03	±	73.6
fs2	143.63	2.313	0.4757	0.1	1.47	1.63	2.67	4.00E-17	2.3	0	0.16	0.13	0.211	8.4	65.85	±	89.8
fs3	87.96	5.485	0.2841	0.1	1.44	0.52	1.9	1.10E-16	5	0	0.37	0.52	0.089	16.3	89.28	±	34.2
fs4	169.54	3.797	0.6419	0.36	5.9	3.67	7.08	-4.70E-17	11.7	0	0.26	0.16	0.129	1.6	-463.5	±	520.7
Bon 00-29	Feldspar		J =0.011 ± 0.0000223 (1 s.d.)					Exp. No.: pt1I7683.IHD				*Total gas age =*			*157.56*	±	*67.4*
dg1	14.74	0.8391	-0.0953	-4.89	3.51	11.81	-36.62	5.00E-17	91.5	0	0.06	-0.24	0.584	7.4	258.1	±	178.7
dg2	50.14	0.9237	0.1373	0.75	1.92	5.05	11.31	6.90E-17	19.2	0	0.06	0.18	0.53	14.4	188.36	±	85.0
dg3	102.21	3.1	0.3001	0.43	2.18	1.96	5.96	8.30E-17	13.5	0	0.21	0.28	0.158	12	263.6	±	103.1
dg4	105.15	1.5302	0.3263	0.49	2.46	3.94	6.87	4.60E-17	8.4	0	0.1	0.13	0.32	10.3	173.51	±	135.5
fs1	602.6	1.9792	2.029	0.07	1.11	1.46	0.69	4.70E-17	0.6	0	0.13	0.03	0.247	28.3	67.09	±	187.1
fs2	223.6	2.014	0.7602	0.23	2.95	4.69	3.26	-4.10E-18	-0.4	0	0.14	0.07	0.243	9.8	-17.435	±	239.8
fs3	268.4	2.755	0.8697	0.13	2.65	3.17	2.73	5.80E-17	4.3	0	0.19	0.09	0.178	10	224.6	±	211.3
fs4	188.53	2.669	0.5945	0.18	4	3.22	4.68	5.10E-17	6.9	0	0.18	0.12	0.183	7.9	250.6	±	229.6
Bon 00-39	Feldspar		J =0.011 ± 0.0000227 (1 s.d.)					Exp. No.: pt1I7784.IHD				*Total gas age =*			*113.23*	±	*15.4*
dg1	38.06	0.2531	0.1066	0.55	1.24	8.86	7.79	8.60E-17	17.3	0	0.02	0.06	1.935	9.8	130.92	±	46.7
dg2	21.95	0.1919	0.0574	1.18	1.05	15.38	18.28	5.20E-17	22.8	0	0.01	0.09	2.55	7.7	100.17	±	58.4
dg3	43.93	0.2259	0.1332	0.33	0.8	7.65	4.32	8.60E-17	10.5	0	0.02	0.05	2.17	14	92.35	±	33.3
dg4	23.81	0.1269	0.0711	0.54	0.76	13.29	7.65	5.80E-17	11.8	0	0.01	0.05	3.86	15.4	57.16	±	31.2
fs1	93.92	0.6156	0.304	0.12	0.58	2.23	2.05	9.90E-17	4.4	0	0.04	0.05	0.796	17.9	83.02	±	37.8
fs2	152.72	0.8143	0.4861	0.12	1.05	2.66	1.61	1.40E-16	6	0	0.05	0.05	0.601	11.1	179.37	±	57.9
fs3	183.83	0.8529	0.5969	0.05	0.44	1.57	0.8	2.40E-16	4.1	0	0.06	0.04	0.574	24.1	148.48	±	32.3
Bon 99-050	Feldspar		J =0.011 ± 0.0000227 (1 s.d.)					Exp. No.: pt1I7885.IHD				*Total gas age =*			*17.494*	±	*71.6*
dg1	501.3	3.295	1.6937	0.05	1.64	1.44	0.95	1.00E-17	0.2	0	0.22	0.05	0.148	28.6	22.6	±	227.0
dg2	38.87	1.0304	0.1308	0.31	0.76	2.46	6.8	3.90E-18	0.8	0	0.07	0.21	0.475	39.5	6.264	±	52.4
dg3	76.9	1.3565	0.2561	0.2	1.45	2.22	4.09	1.30E-17	1.7	0	0.09	0.14	0.361	31.9	26.77	±	67.7
fs1	270.7	1.8647	0.9394	0.57	5.2	6.35	4.92	-1.90E-17	-2.5	0	0.13	0.05	0.262	7.5	144.65	±	532.2
fs2	285.5	2.572	0.941	0.09	1.05	1.24	0.91	1.40E-16	2.7	0	0.17	0.07	0.19	48	149.88	±	79.8
fs3	277.5	1.9907	0.9336	0.08	1.22	1.67	1.29	3.00E-17	0.7	0	0.13	0.06	0.246	44.5	36.56	±	112.6
Bon 99-185	Feldspar		J =0.011 ± 0.0000227 (1 s.d.)					Exp. No.: pt1I7986.IHD				*Total gas age =*			*76.15*	±	*6.5*
dg1	3.352	0.2074	0.0007	1.24	0.34	4.93	409	1.30E-16	94.1	0.01	0.01	7.77	2.36	10.9	63.48	±	15.4
dg3	4.439	0.11	0.0026	0.4	0.23	4.9	56.54	2.80E-16	82.7	0.01	0.01	1.13	4.45	20.3	73.66	±	8.2
dg2	6.556	0.2282	0.0122	0.59	0.27	3.61	27.89	1.10E-16	45.3	0.01	0.02	0.51	2.15	9.4	59.77	±	19.2
dg4	5.467	0.2086	0.0083	0.58	0.3	3.6	35.06	1.30E-16	55.4	0.01	0.01	0.68	2.35	10.9	61.03	±	16.3
fs1	30.73	0.2686	0.0868	0.13	0.35	2.55	3.64	2.70E-16	16.6	0	0.02	0.08	1.824	13.7	101.66	±	17.7
fs2	16.35	0.1809	0.0411	0.17	0.26	2.66	5.41	3.00E-16	25.7	0	0.01	0.12	2.71	18.9	84.18	±	12.4
fs3	24.38	0.2091	0.0644	0.23	0.6	6.38	10.16	1.40E-16	22	0	0.01	0.09	2.34	6.7	106.44	±	36.2
fs4	7.184	0.303	0.006	3.74	2.7	23.77	502.23	3.10E-17	75.7	0.01	0.02	1.37	1.617	1.5	108.11	±	163.0
fs4z	43.3	0.3579	0.1394	0.14	0.57	3.12	4.2	6.20E-17	4.9	0	0.02	0.07	1.369	7.7	43.24	±	34.1

Table 4.2. Degassing and fusion Ar-Ar data (ctd. overleaf).

Step (a)	$^{40}Ar/^{39}Ar$ (b)	$^{37}Ar/^{39}Ar$ (b)	$^{36}Ar/^{39}Ar$ (b)	^{40}Ar s.d. (%)	^{39}Ar s.d. (%)	^{37}Ar s.d. (%)	^{36}Ar s.d. (%)	^{40}ArR (mol)	^{40}ArR (c)	^{40}ArK (c)	$^{39}ArCa$ (c)	$^{36}ArCa$ (c)	K/Ca (%)	^{39}Ar (%)	Apparent Age (Ma)	± (d)	1 s.d. (Ma)
Bon 94-09	Feldspar		J =0.011 ± 0.0000227 (1 s.d.)						Exp. No.: pt1I8087.IHD			*Total gas age =*			*63.48*	±	*1.1*
dg1	85.48	1.7889	0.2809	0.13	0.57	0.54	0.97	1.20E-16	3.1	0	0.12	0.17	0.274	1	53.24	±	18.4
dg2	46.98	0.5843	0.1467	0.07	0.19	0.2	0.37	2.40E-15	7.9	0	0.04	0.11	0.838	14.3	74.73	±	3.8
dg3	73.43	1.8681	0.2395	0.1	0.44	0.17	0.22	1.10E-15	3.8	0	0.13	0.21	0.262	8.7	57.3	±	4.4
dg4	51.55	1.4591	0.1658	0.04	0.35	0.18	0.25	1.70E-15	5.2	0	0.1	0.24	0.335	14.5	54.32	±	3.3
dg5	42.87	0.6477	0.1355	0.06	0.17	0.12	0.21	2.60E-15	6.7	0	0.04	0.13	0.756	20.4	58.49	±	2.3
fs1	17.828	3.841	0.0506	0.06	0.91	0.18	2.39	5.80E-16	17.8	0	0.26	2.05	0.127	4.1	64.57	±	6.8
fs2	11.07	1.6694	0.0276	0.08	0.41	0.22	1.78	1.20E-15	27.5	0	0.11	1.64	0.293	8.5	62.02	±	2.8
fs3	17.962	4.066	0.0503	0.03	0.94	0.07	1.51	1.00E-15	19.1	0	0.27	2.19	0.12	6.8	69.64	±	4.2
fs4	12.763	3.113	0.0322	0.07	0.73	0.16	1.4	1.60E-15	27.3	0	0.21	2.61	0.157	10.4	70.85	±	2.5
fs5	9.179	1.8677	0.0206	0.06	0.46	0.17	1.58	1.60E-15	35.2	0	0.13	2.45	0.262	11.2	65.74	±	1.8
Bon 99-180	Feldspar		J =0.012 ± 0.0000227 (1 s.d.)						Exp. No.: pt1Ib070.IHD			*Total gas age =*			*107.94*	±	*96.6*
dg2a	3300.9	17.602	11.188	0.09	9.9	1.35	1.04	-6.40E-18	-0.1	0	1.19	0.04	0.028	1.2	-80.37	±	8993
dg3a	35.2	0.3578	0.103	0.31	0.59	4.23	4.49	1.20E-16	13.6	0	0.02	0.09	1.369	16.4	96.75	±	26.2
dg4a	392.8	2.306	0.8921	0.75	14.4	22.1	19.41	1.20E-16	32.9	0	0.16	0.07	0.212	0.6	1645.6	±	693.4
dg2b	180.9	6.729	0.603	0.26	2.58	0.73	2.83	2.30E-17	1.8	0	0.45	0.3	0.072	4.8	66.18	±	141.1
dg2b	14.588	0.6604	0.0503	0.48	0.83	1.19	6.1	-8.50E-18	-1.5	0	0.04	0.36	0.742	27.1	-4.468	±	18.3
dg2b	181.13	5.226	0.6386	0.2	2.39	0.82	3.01	-5.70E-17	-4	0	0.35	0.22	0.093	5.4	-155.55	±	171.4
fs2	148.09	3.252	0.4707	0.11	1.19	0.68	1.43	1.60E-16	6.3	0	0.22	0.19	0.15	11.8	182.92	±	49.7
fs3	189.5	2.1	0.6197	0.08	0.65	1.03	1.29	2.40E-16	3.5	0	0.14	0.09	0.233	24.8	131.29	±	49.1
fs4	193.31	3.618	0.5966	0.16	1.62	0.72	2.33	2.00E-16	9	0	0.24	0.16	0.135	7.9	328.1	±	92.1

Table 4.2. Degassing and fusion Ar-Ar data (ctd.).

(a) Steps labelled as degassing (dg) or total fusion (fs).
(b) Corrected for 37Ar and 39Ar decay, half-lives 35.1 days and 259 years, respectively.
(c) Radiogenic (R), calcium-derived (Ca), and potassium-derived (K) argon, respectively (percent).
(d) Ages calculated relative to 85G003 TCR Sanidine at 28.02 Ma with lambda e = 0.581E-10/yr and lambda b = 4.692E-10/yr.

Following blank correction, age spectra were plotted for each experiment. Unfortunately, in no instance was a good reliable plateau age attained. In most instances, the first few incremental heating steps were considered to be low-temperature (~3.0 W) degassing steps, as they yielded anomalously young ages with large errors, indicating that the ^{39}Ar–^{40}Ar system has been disturbed. These ages likely represent ^{39}Ar held in loosely-bound crystal sites, i.e. secondary alteration minerals, rather than the magmatic mineral itself. The early "cleaning and degassing" steps were discluded if they were deemed to have disproportionally large errors or have abnormally high K/Ca ratios (possibly indicating the fusion of low-temperature K-rich phases such as sericite). Where steps have been discluded from the final age calculation the ages were therefore calculated using the weighted mean plateau age. In some cases this resulted in only a small proportion of the ^{39}Ar gas released being included in the final age calculation. Consequently, all the ages presented in this study represent *minimum* ages, rather than absolute ages.

For all experiments, errors are quoted at the 1σ (67%) confidence level.

4.4 Results

Incremental step heating data for samples from the Washikemba Formation are presented in Table 4.1, whereas single crystal degassing and fusion data (a technique principally used for small plagioclases) are presented in Table 4.2. It is evident from Table 4.2 that the crystal degassing and fusion technique failed to yield worthwhile results, and the data that were obtained had errors that frequently greatly exceeded the age of the crystal itself. This is most likely a function of the size of the crystal, and therefore the amount of K (particularly as this technique was employed for plagioclases, which have a low K/Ca ratio). The degassing and fusion data were therefore disregarded in the discussion that follows, and emphasis is placed on the data obtained from the incremental step heating technique employed for larger plagioclase and sanidines (Table 4.1).

4.4.1 Northern Complex

Only two of the four samples selected for Ar–Ar analysis yielded any worthwhile results. The remainder consisted of small plagioclases and/or altered sanidines, which had suffered from Ar loss and therefore yielded results with huge errors, or alternatively absurdly young/old ages (Table 4.1). The two samples with geologically viable results are BON 99-180, a rhyodacite flow from the Wecua region in the base of the Complex, and BON 94-09, which is derived from a sill from the Brandaris area (Table 4.3). BON 94-09 yielded five different reasonable minimum ages (mean age 80.2 ± 3) with the greatest minimum age being

95.5 Ma. ± 2, obtained from a relatively fresh plagioclase feldspar (Fig. 4.2a). This was obtained in 4 steps, with 71% of the gas released in the last two steps and both yielding similar ages, suggesting that this age is geologically meaningful. Additionally, the K/Ca ratio remains uniformly low throughout the experiment, suggesting the mineral analysed is a relatively pristine sanidine crystal. Fig. 4.2b shows an age spectra for a second plagioclase from BON 94-09. It yields an age of 89.8± 1.8 Ma for the final incremental heating step. However, only 10% of ^{39}Ar was released in this final step, and earlier steps yielded substantially younger ages, implying that this age may not be reliable.

Sample BON 99-180 (Fig 4.2c, 4.3a&b) yielded 3 minimum ages, but no reasonable plateau ages. Of these, the greatest minimum age obtained was 95 ± 7 Ma, implying that middle part of the Washikemba Formation is at least 88 Ma (i.e. 95–7 Ma) in age.

4.4.2 Southern Complex

The Southern Complex again yielded only one sample with geologically meaningful results. Sample BON 00-19, from the base of the Complex, gave minimum ages averaging around 80 Ma from three different experiments. The best of these analyses is displayed in Fig. 4.3c. Over 90% of the ^{39}Ar released corresponded to a well-constrained age of around 78 Ma, with a very small error. Unfortunately, the second incremental step yielded an older 87 Ma age with a substantially larger error, reducing the reliability of the plateau age. As this step has a substantially greater K/Ca ratio, it is likely that ^{39}Ar has been lost by recoil, and therefore has yielded an abnormally old age. Given this, the weighted mean plateau age of 78±2 Ma must therefore be treated with caution.

The upper part of the Complex is represented by only one minimum age of 74±5 Ma, from Sample BON 99-50 (Table 4.3.)

Experiment number	Sample	Rock	Mineral	Increments used	$\%^{39}Ar$	Age	1σ error	MSWD	J Value
01L0061	BON 94-09	rhyodacite	plagioclase	2 of 4	70.1	95.5	2.3	2.9	0.01146
01L0062	BON 94-09	rhyodacite	plagioclase	2 of 6	39.6	89.9*	1.8	75.1	0.01146
01L0064	BON 99-180	rhyodacite	plagioclase	3 of 5	50.0	94.0	7.0	2.3	0.0115
01L0065	BON 99-180	rhyodacite	plagioclase	1 of 3	100.0	119.6*	25.7	4.2	0.0115
01L0066	BON 00-19	rhyodacite	plagioclase	3 of 3	100.0	78.7	0.8	2.0	0.01145
01L0068	BON 00-19	rhyodacite	Anorthoclase?	4 of 4	100.0	83.6	3.7	1.1	0.01145
01L0070	BON 99-180	rhyodacite	K-feldspar	1 of 3	45.0	86.2	5.8	1.1	0.0115

* denotes age obtained only from final total fusion step

Table 4.3. Summary of successful $^{40}Ar - ^{39}Ar$ experiments and ages obtained.

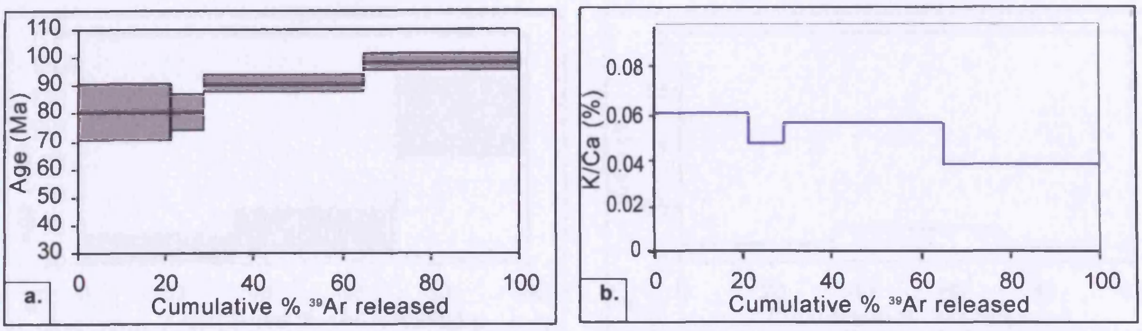

Experiment no: **0110061** Sample: **BON 94-09** Northern Complex rhyodacite sill
Plagioclase separate Weighted mean plateau age: **95±2 Ma**
Age based on final two steps (~71% ^{39}Ar) Treated as MINIMUM age

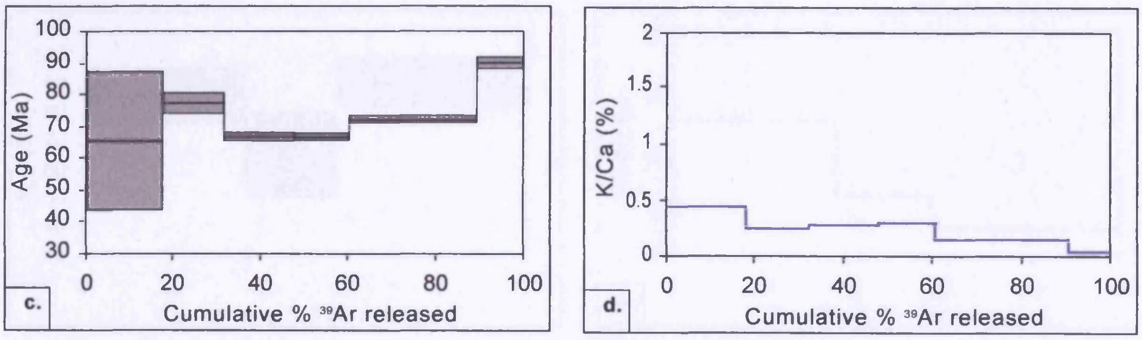

Experiment no: **0110062** Sample: **BON 94-09** Northern Complex rhyodacite sill
Plagioclase separate Age based on final heating step: **89.8±1.8 Ma**
(Earlier steps treated as degassing steps) Treated as MINIMUM age

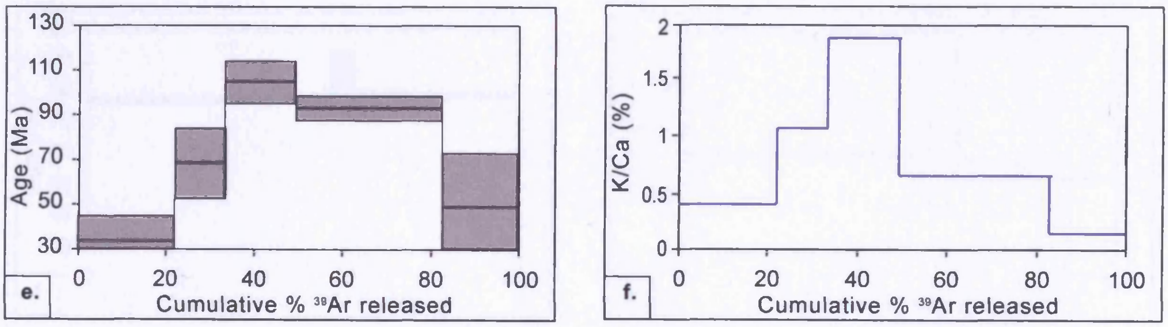

Experiment no: **0110064** Sample: **BON 99-180** Northern Complex rhyodacite flow
Plagioclase separate Weighted mean plateau age: **94.8±7 Ma**
Age based on final three steps (~50% ^{39}Ar) Treated as MINIMUM age

Fig. 4.2: Plots of age spectra for the Bonaire Washikemba Formation. Age spectra shown represent the best analyses.

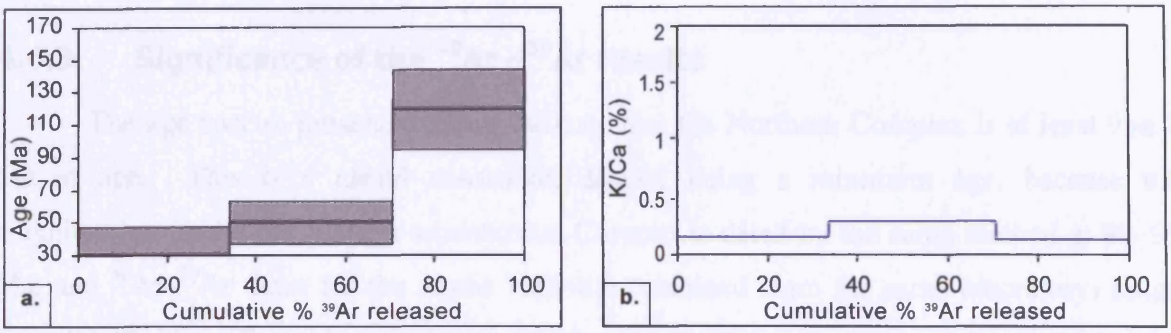

Experiment no: **0110065** Sample: **BON 99-180** Northern Complex rhyodacite flow
Plagioclase separate Weighted mean plateau age: **122±25 Ma**
Treated as MINIMUM age

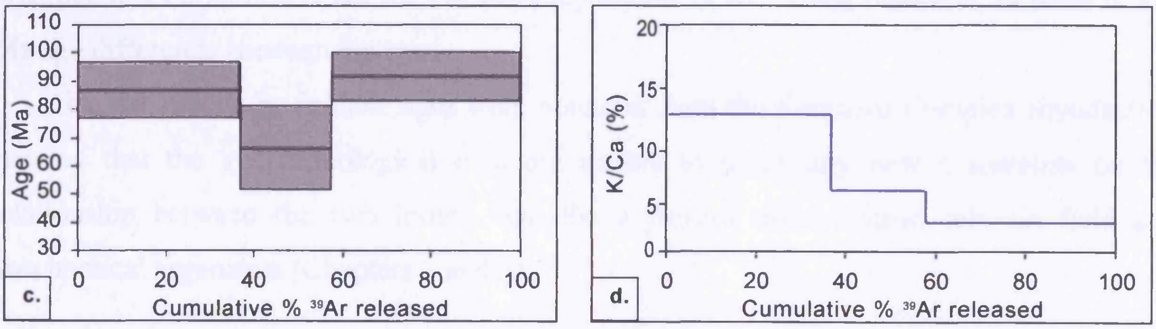

Experiment no: **0110070** Sample: **BON 99-180** Northern Complex rhyodacite flow
K-feldspar separate Age based on final step (43% ^{39}Ar): **91±8 Ma**
(Earlier steps treated as degassing steps) Treated as MINIMUM age

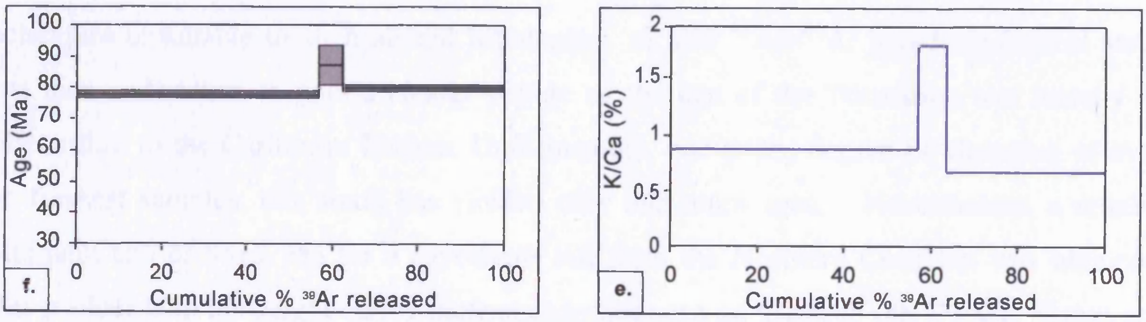

Experiment no: **0110066** Sample: **BON 00-19** Southern Complex rhyodacite dome
Sanidine separate Weighted mean plateau age: **78±2 Ma** Treated as MINIMUM age

Fig. 4.3: Plots of age spectra for the Bonaire Washikemba Formation. Age spectra shown represent the best analyses.

4.4.3 Significance of the $^{40}Ar-^{39}Ar$ results

The age spectra presented above indicate that the Northern Complex is at least 95± 2 Ma in age. This is a useful constraint, despite being a minimum age, because the neighbouring Caribbean plateau sequence on Curaçao is dated by the same method at 88–91 Ma, and $^{40}Ar-^{39}Ar$ dates for the Aruba batholith (obtained from the same laboratory) range from 82–85 Ma. The oldest minimum age for the Northern Complex of the Washikemba Formation, Bonaire is older than both the plateau and the Aruba batholith, which suggests there is no genetic relationship. These results imply that the arc is not built on top of the plateau, as it appears to have formed before the plateau. In addition, the results show that the Washikemba Formation is not the extrusive equivalent of the Aruba batholith, as there is >10 Ma age difference between the two.

Unfortunately, no reliable ages were obtained from the Southern Complex rhyodacites, ensuing that the geochronological data are unable to place any new constraints on the relationship between the two inliers, and the argument must instead rely on field and geochemical arguments (Chapters 3 and 5).

4.5 Conclusions

Existing biostratigraphic studies of the Washikemba Formation are limited, and show many inconsistencies. Previous attempts at radiometric dating of the Formation have used techniques unsuitable to such altered lithologies. A new $^{40}Ar-^{39}Ar$ geochronological study was thus undertaken to gain a clearer picture of the age of the Formation and thereby its relationship to the Caribbean Plateau. Unfortunately, due to the degree of alteration of even the freshest samples, this study has yielded only minimum ages. Nevertheless, a reliable minimum age of 95±2 Ma for a rhyodacite sill from the Northern Complex was obtained. This is older than the neighbouring plateau sequence seen on Curaçao (88–91 Ma, Sinton and Duncan, 1992; Sinton et al., 1998) and strongly suggests there is no genetic relationship between them. In addition, the new minimum age indicates that the Formation is at least 10 Ma older than the Aruba batholith, providing evidence that the Washikemba Formation is not the extrusive equivalent of the Aruba batholith, despite their close geographical proximity today.

Chapter 5

Major, Trace Element and Pb-Sr-Hf-Nd Isotope Geochemistry of the Bonaire Washikemba Formation

5.1. Introduction

A geochemical study of the Washikemba Formation is presented, in order to gain an understanding of the origin and evolution of the volcanic sequence exposed on Bonaire. This will help evaluate the nature of any relationship with the Caribbean plateau (e.g. the sequences exposed on Aruba and Curaçao), with which it is closely spatially and temporally associated.

As outlined in Chapter 3, field evidence suggests that two separate inliers of the Washikemba Formation are present on the island of Bonaire. The Northern Complex is subdivided into the Wecua-Gotomeer, Brandaris and Salina Mathijs areas, which show different lithological characteristics, and occur at different stratigraphic levels within the Formation. A primary aim is to resolve whether the geochemistry is consistent with the whole sequence being comagmatic or if there are any compositionally distinct components within the Washikemba Formation. A comparison of the geochemistry of the two inliers of the Washikemba Formation is also required, given that the relationship between the two is uncertain, including their volcanostratigraphic positions within the Washikemba Formation. If the two inliers show individual trends of geochemical evolution, their relative stratigraphic position within the Washikemba Formation may be determined.

In order to place the sequence into its wider tectonic framework, it is necessary to validate the proposed island arc affinity of the volcanic sequence, through geochemical comparison with other island arc sequences including modern day arcs. Additionally any possible relationship to other volcanic sequences of a similar age in the Southern Caribbean region such as the Caribbean plateau and the neighbouring Aruba batholith is investigated.

5.2. Summary of analytical techniques for major and trace element analysis

In total, 325 samples were obtained during 4 different field seasons on the island of Bonaire, Dutch Antilles; two undertaken by the author as part of this study, and two by previous studies (A.C. Kerr, 1994; R. V. White, 1996). Of these 325 samples, 120 were selected for geochemical analysis, the remainder being studied petrographically. All of the samples were analysed by XRF, and 58 were selected for analysis by ICP-OES and 26 for analysis by ICP-MS, specifically for the Rare Earth Elements (REE). In addition, a subset of 15 samples were chosen for isotopic (Hf, Nd, Pb and Sr) analysis. Where samples have been analysed by several methods, preference is given to data produced by ICP-MS over ICP-OES, and ICP-OES over XRF. Details of each analytical technique along with data quality are presented in Appendices B and C, and the data is presented in Appendix D.

5.3. Degree of alteration of the Washikemba Formation

Primary geochemical signatures can be masked by subsequent geochemical exchange such as that resulting from metamorphism or late-stage alteration. Determining the extent of this secondary geochemical overprinting for the Washikemba Formation is vital in order to unravel its primary geochemical signature and thereby place constraints on the origin of the sequence and its relationship to the rest of the Cretaceous Caribbean sequences. Field and thin section studies (Chapter 3) reveal that the lithologies have undergone several different stages of alteration and weathering, any of which may have affected their primary geochemical signatures.

1. Burial metamorphism, up to prehnite-pumpellyite facies, resulting in partial to complete replacement of phases such as olivine and pyroxene by pumpellyite, chlorite, prehnite, Fe-oxyhydroxides and clays.
2. Seawater alteration. This may be concurrent with metamorphism, and its effects are difficult to distinguish. The rocks, however have been submerged for most of their >90 Ma existence.
3. Surface tropical weathering. Bonaire has a hot, moist climate and surface weathering has affected many lithologies through extensive clay formation. This can penetrate to many centimetres or even metres below the present day erosional surface, and has resulted in a leached brown and rotten appearance to the surface of most samples.

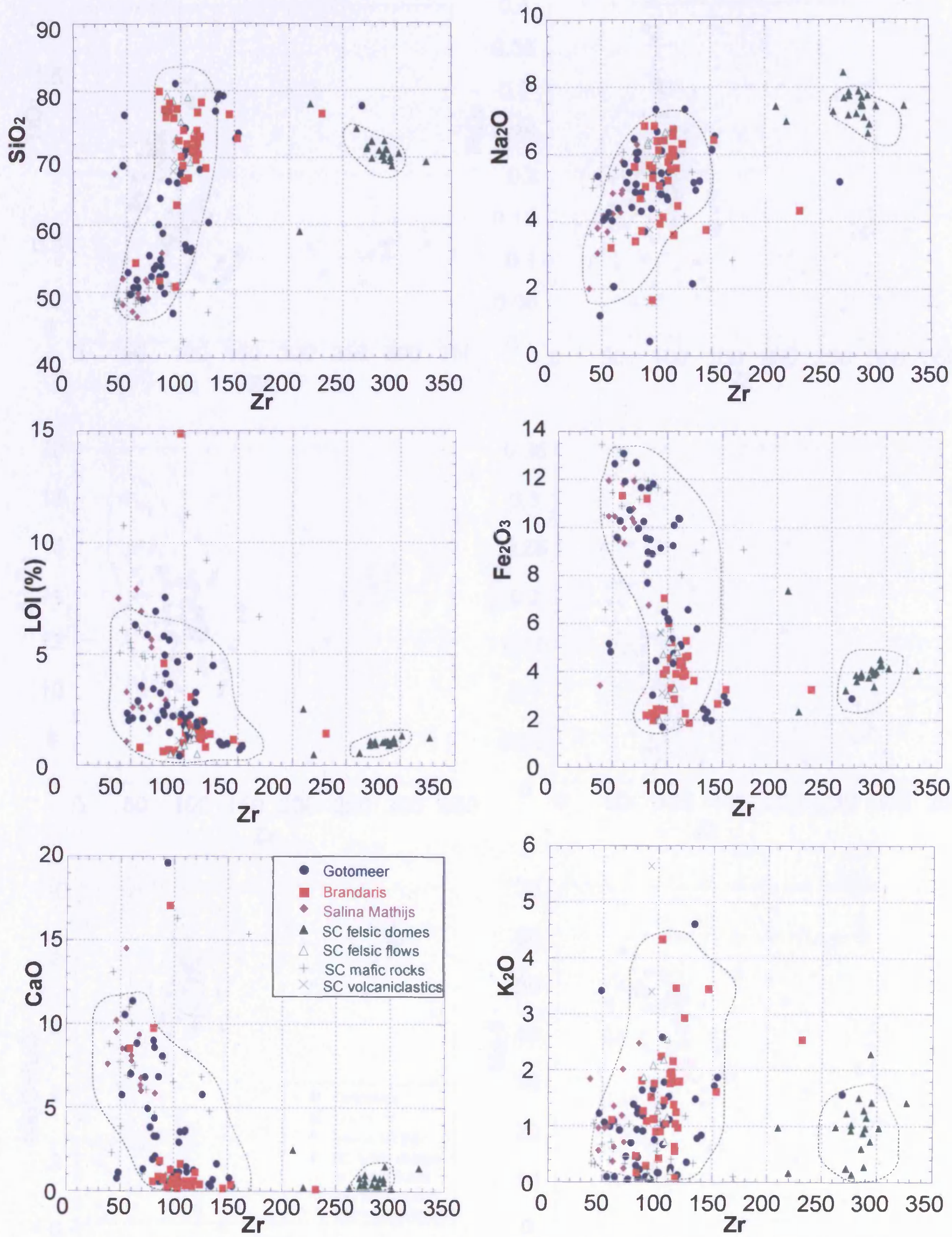

Fig. 5.1. Plots of major elements vs. Zr. An indication of the degree of mobility of an element is represented by its correlation with Zr: an immobile element will show a good positive correlation. The LOI represents loss on ignition. Zr values are quoted in parts per million (ppm); major elements are quoted in weight % (wt. %). All data obtained by XRF or ICP-MS where available, except for Zr (XRF). SC is an abbreviation for Southern Complex.

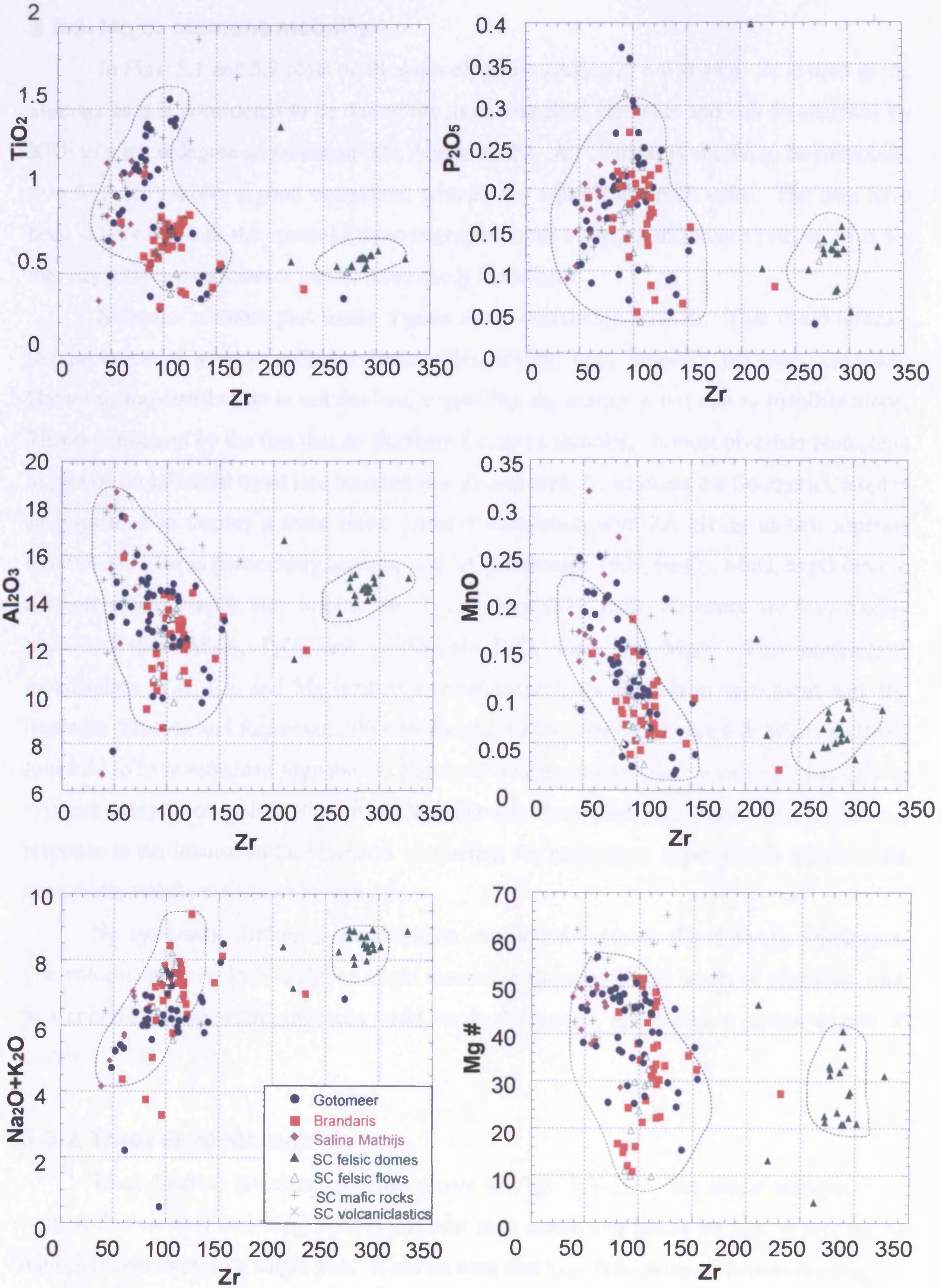

Fig. 5.2. Plots of major elements vs. Zr. An indication of the degree of mobility of an element is represented by its correlation with Zr: an immobile element will show a good positive correlation. All Zr values are quoted in parts per million (ppm); major elements are quoted in wt. %. Data obtained by XRF or ICP-MS where available, except for Zr (XRF). SC is an abbreviation for Southern Complex.

5.3.1. Major element mobility

In Figs. 5.1 and 5.2 plots of all major elements against Zr are shown. Zr is used as the abscissa as it is considered to be one of the most immobile elements and can be analysed by XRF to a good degree of precision (see Appendix B). An element is shown to be immobile, therefore, if it shows a good correlation with Zr for a particular rock suite. The data have been subdivided into the various lithostratigraphic units by using different symbols, in order that any different rock suites can be more easily identified.

No major element plot shows a good linear correlation with Zr. This could indicate the presence of several different rock suites, and/or high mobility of many elements. However, the distribution is not random, suggesting the scatter is not due to mobility alone. This is confirmed by the fact that all Northern Complex samples, on most bivariate plots, tend to plot on an inflected trend line between low Zr and high Zr, whereas the Southern Complex samples tend to display a more linear positive correlation with Zr, giving us two separate trend lines. This is particularly apparent for SiO_2, although TiO_2, Fe_2O_3, MnO, MgO (and to a lesser extent Na_2O) also display this trend, suggesting these elements are less readily mobilised than Al_2O_3, P_2O_5, and particularly K_2O, CaO and Mg#. This preferential mobilisation of K, Ca, and Mg (and to a lesser extent Al and P) is in agreement with the literature (Sharma and Rajamani, 2000; Rollinson, 1993), although Kerrich & Wyman (1996) found Al to have remained immobile in Precambrian greenstone belts, whereas Al has clearly suffered a degree of mobilisation in the Washikemba Formation lithologies. This could be a response to the intense surface tropical weathering the rocks have experienced, which could have preferentially mobilised Fe and Al.

No systematic difference in alteration was found between the different lithologies. The volcaniclastic rocks, which one might assume to show enhanced levels of alteration, plot as a coherent group within the main trend, as do the basalts, albeit with a greater degree of scatter.

5.3.2. Trace element mobility

Trace element bivariate plots are shown in Figs. 5.3–5.7. The major element plots suggest that we may be seeing several different rock suites, and hence we may expect to see multiple trend lines on a single plot. It can be seen that very few elements appear to correlate with Zr. The elements Nb, Nd, Hf, Y, La, Co and (to a lesser extent Sc) show good linear trends, with only several outlying samples, if any, which indicates these are the most

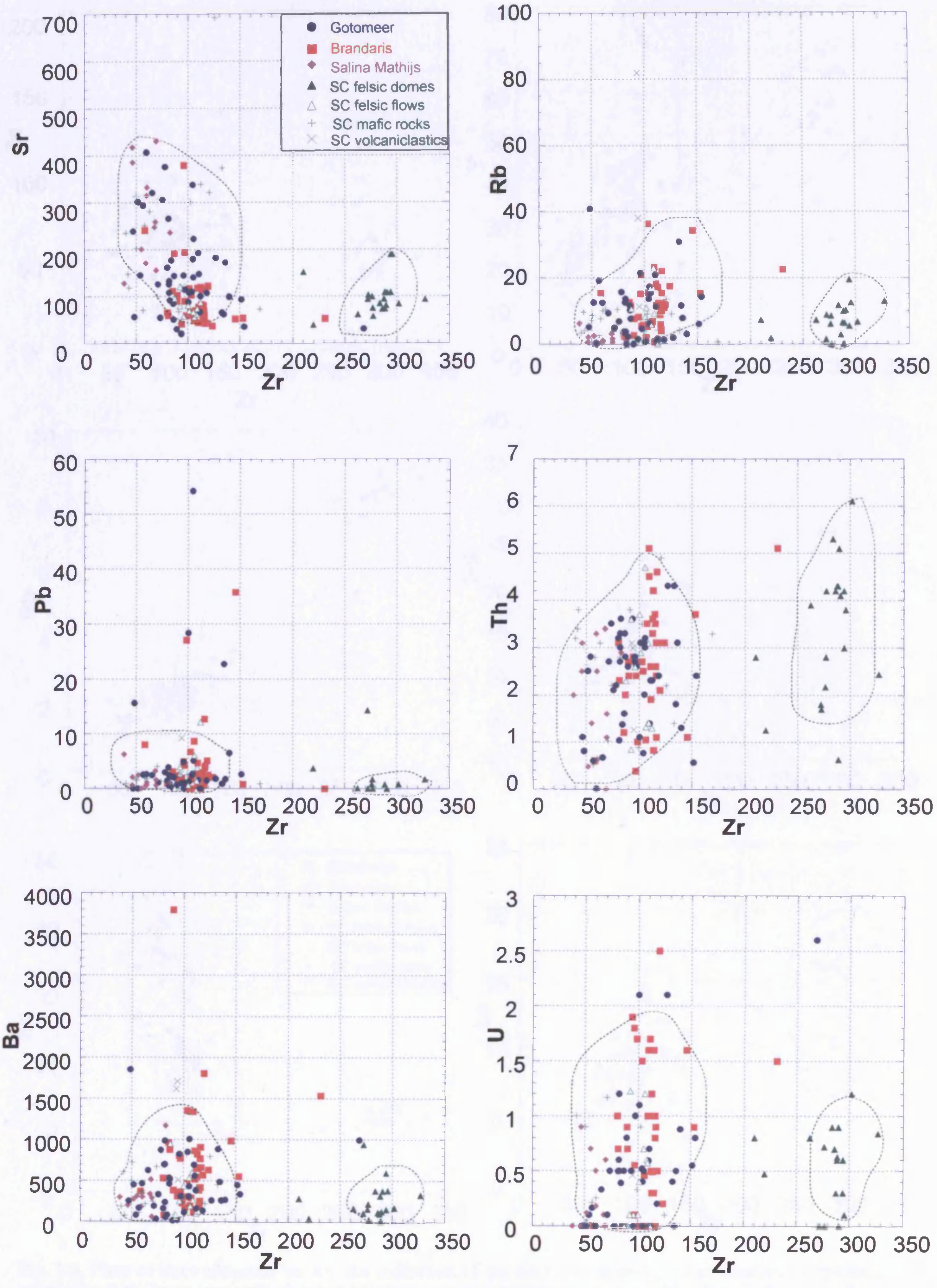

Fig. 5.3. Plots of trace elements vs. Zr. An indication of the degree of mobility of an element is represented by its correlation with Zr: an immobile element will show a good correlation, assuming that all rocks belong to the same suite and are related by crystal fractionation. All values are quoted in parts per million (ppm). All data obtained by XRF or ICP-MS where available, except for Zr (XRF). SC is an abbreviation for Southern Complex. Note that the Th, U and Pb plots show considerable scatter. These data are unfiltered, but serve to show the likely degree of alteration experienced by the Formation.

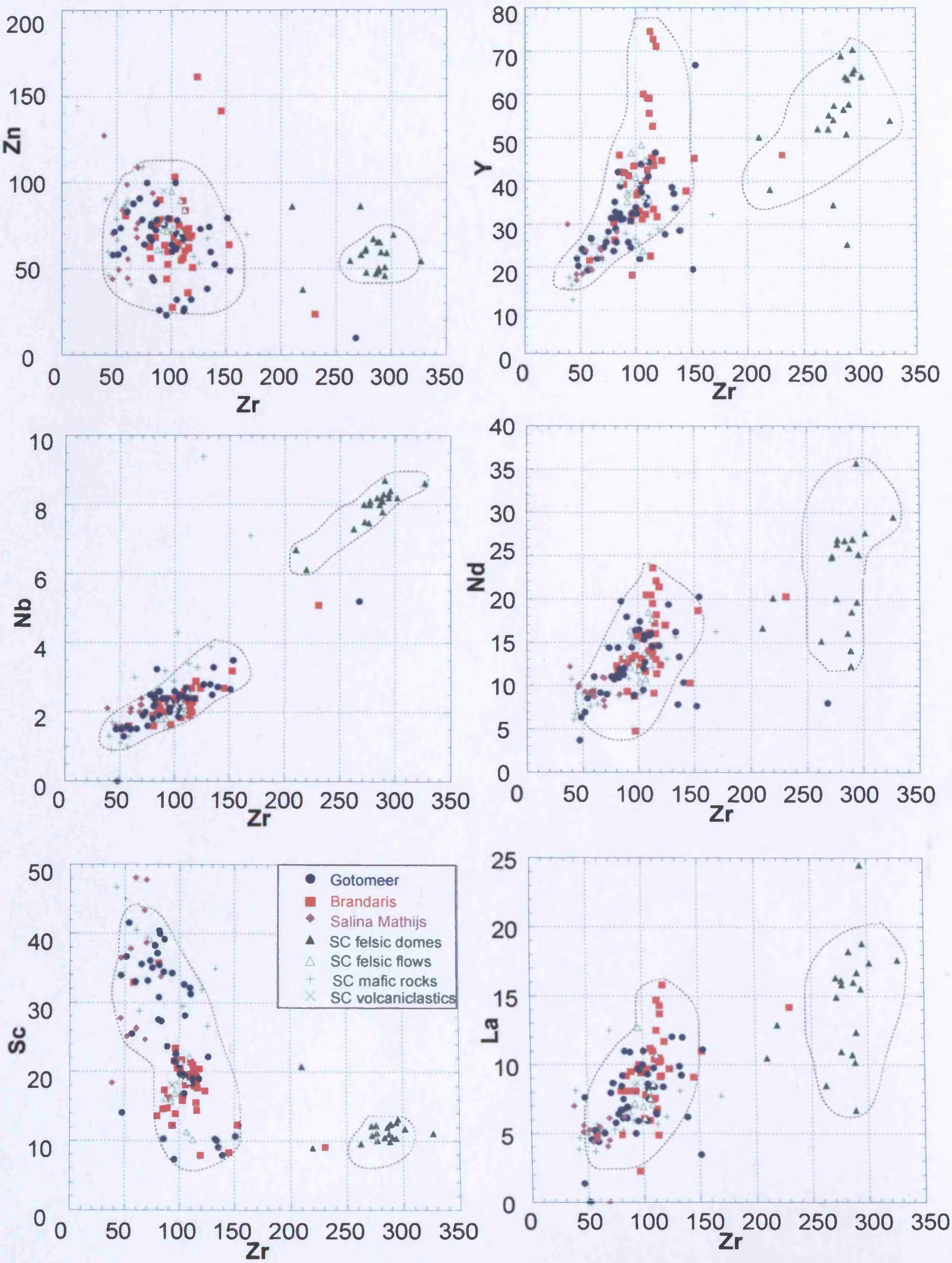

Fig. 5.4. Plots of trace elements vs. Zr. An indication of the degree of mobility of an element is represented by its correlation with Zr: an immobile element will show a good correlation, assuming that all rocks belong to the same suite and are related by crystal fractionation. All values are quoted in parts per million (ppm). All data obtained by XRF or ICP-MS where available, except for Zr (XRF). SC is an abbreviation for Southern Complex.

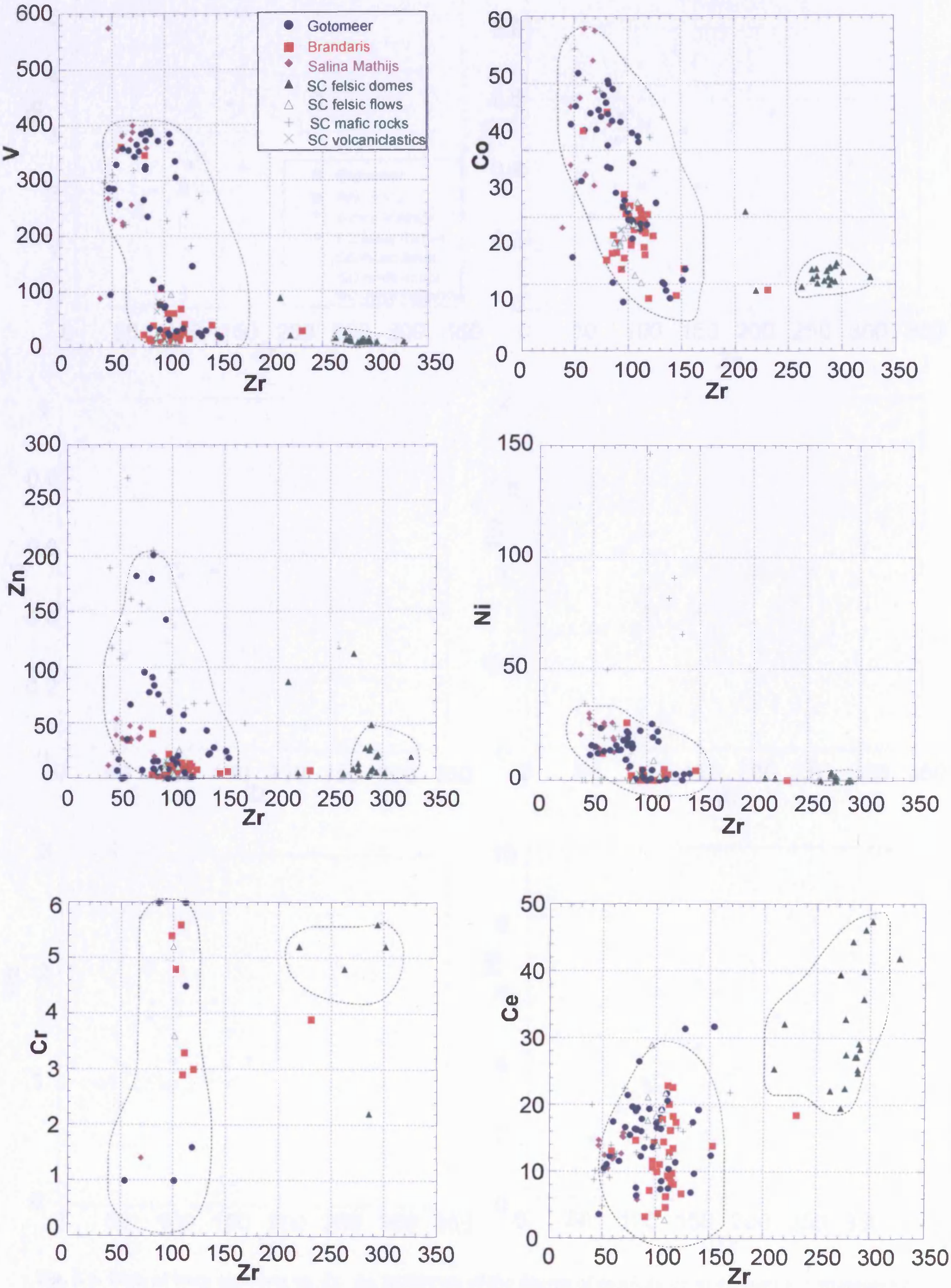

Fig. 5.5. Plots of trace elements vs. Zr. An indication of the degree of mobility of an element is represented by its correlation with Zr: an immobile element will show a good correlation, assuming that all rocks belong to the same suite and are related by crystal fractionation. All values are quoted in parts per million (ppm). All data obtained by XRF or ICP-MS where available, except for Zr (XRF). SC is an abbreviation for Southern Complex.

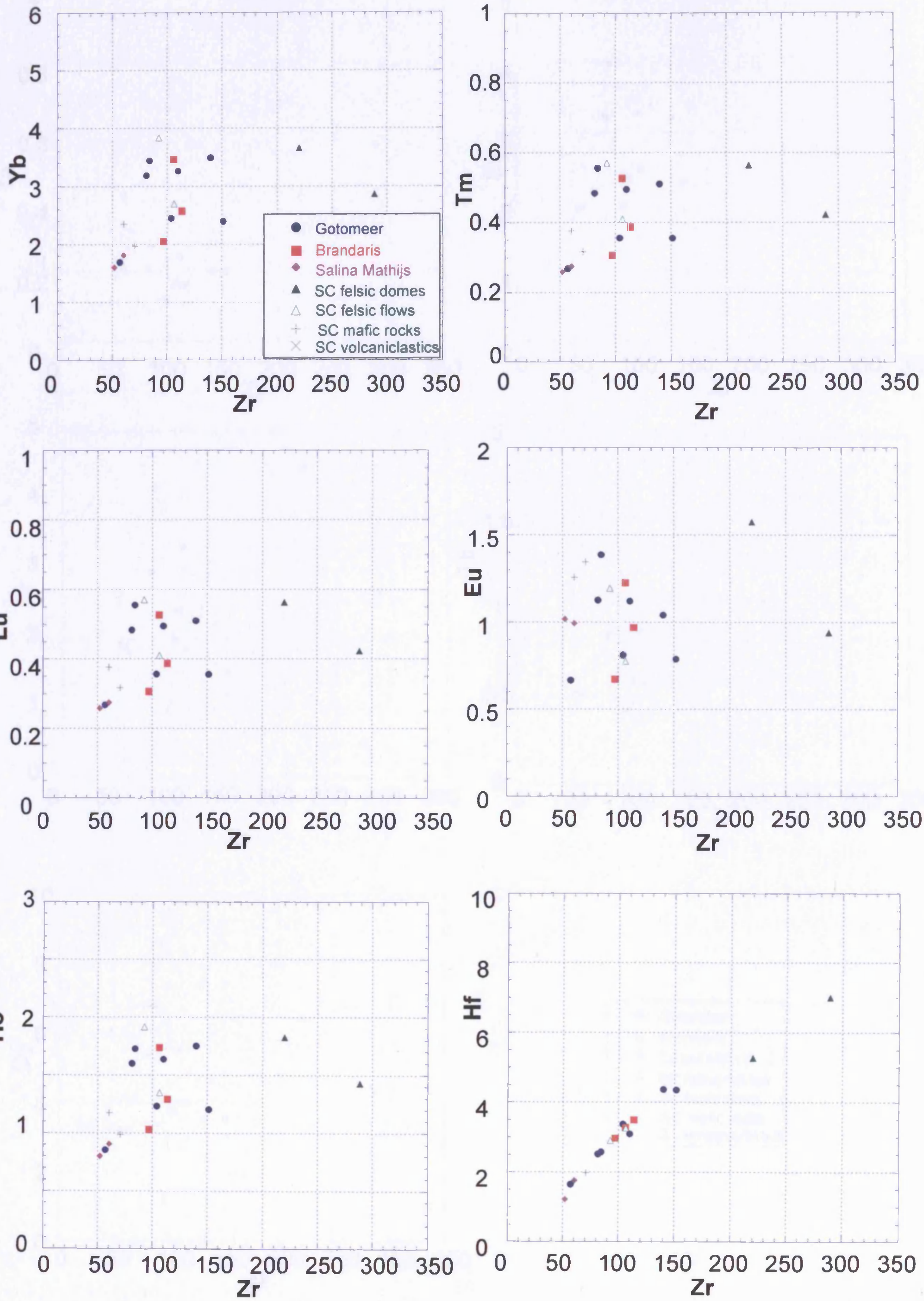

Fig. 5.6. Plots of trace elements vs. Zr. An indication of the degree of mobility of an element is represented by its correlation with Zr: an immobile element will show a good correlation, assuming that all rocks belong to the same suite and are related by crystal fractionation. All values are quoted in parts per million (ppm). All data obtained by XRF or ICP-MS where available, except for Zr (XRF). SC is an abbreviation for Southern Complex.

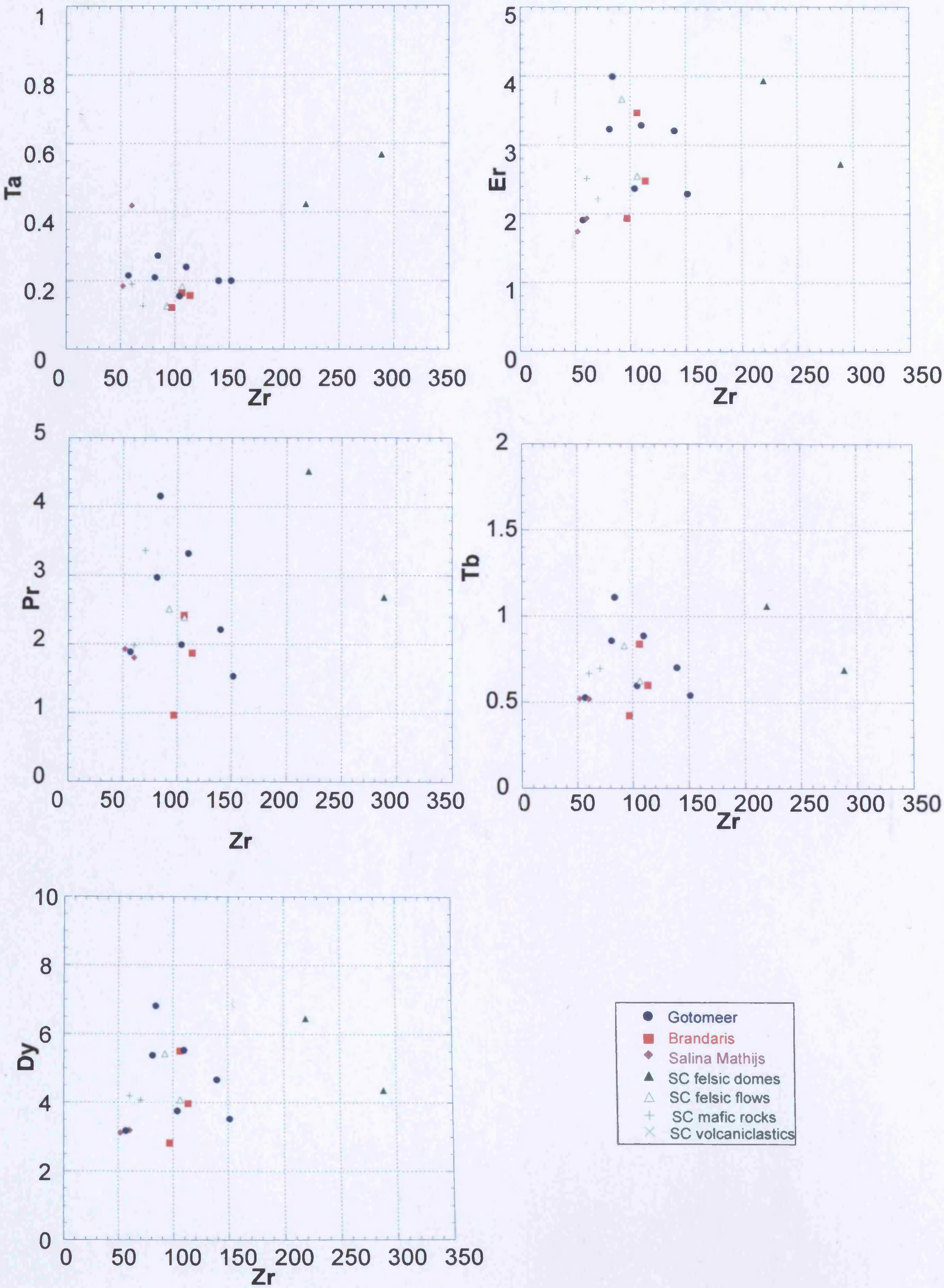

Fig. 5.7. Plots of trace elements vs. Zr. An indication of the degree of mobility of an element is represented by its correlation with Zr: an immobile element will show a good correlation, assuming that all rocks belong to the same suite and are related by crystal fractionation. All values are quoted in parts per million (ppm). All data obtained by XRF or ICP-MS where available, except for Zr (XRF). SC is an abbreviation for Southern Complex.

immobile of the trace elements. Hf displays a near perfect correlation with Zr, which can be attributed to its near-identical geochemical behaviour during most geochemical processes, and therefore it does not necessarily indicate that Hf is less immobile than, say, Nd or Nb. Elements such as Y, Sc, Cr, Co and V seem to display two separate subparallel trend lines, again one defined by the majority of the samples, including the whole Northern Complex, and the other trend defined by the Southern Complex rhyodacite domes. These elements therefore appear to be moderately immobile, but display evidence of several different magmatic differentiation events.

Some elements show a great deal of scatter when plotted against Zr, such as Pb, Rb, Ba, Th, U and Sr. This indicates that these elements have been mobilised, and we should exercise caution when using them in any geochemical interpretation. In particular, the Pb and Sr isotopic systems may have been at least partially reset, which may have implications for interpreting their isotopic signatures (Section 5.8).

Fewer data points exist for many of the Heavy Rare Earth Elements (HREE), due to analytical factors, and this limits their use in determining their immobility. As the Light Rare Earth Elements (LREE) such as La, Ce and Nd seem to be largely immobile, and as under normal conditions the HREE are expected to be even less mobile (Rollinson, 1993), then the heavy rare earth elements are likely to have not suffered significantly from the effects of alteration.

In conclusion, several points can be noted from these trace element plots:

1. As several elements show a well-defined correlation with Zr (e.g. Nd and Nb), the validity of using Zr to constrain mobility is confirmed, as it too appears to be relatively immobile for the Washikemba Formation.
2. Element mobility is variable: most low field strength elements show evidence for enhanced mobility within the Washikemba Formation, whereas all the high field strength elements essentially retain their primary geochemical values.
3. The elements Pb, Rb, Ba, Th, U and Sr have been extensively mobilised, and should only be used with caution in the interpretation of any primary magmatic trends. Accordingly, the Pb and Sr isotopic systems may have also been reset due to post-magmatic processes.
4. An apparent degree of scatter on a mobility plot can originate from different rock suites being plotted on the same diagram, and need not necessarily reflect the state of alteration.

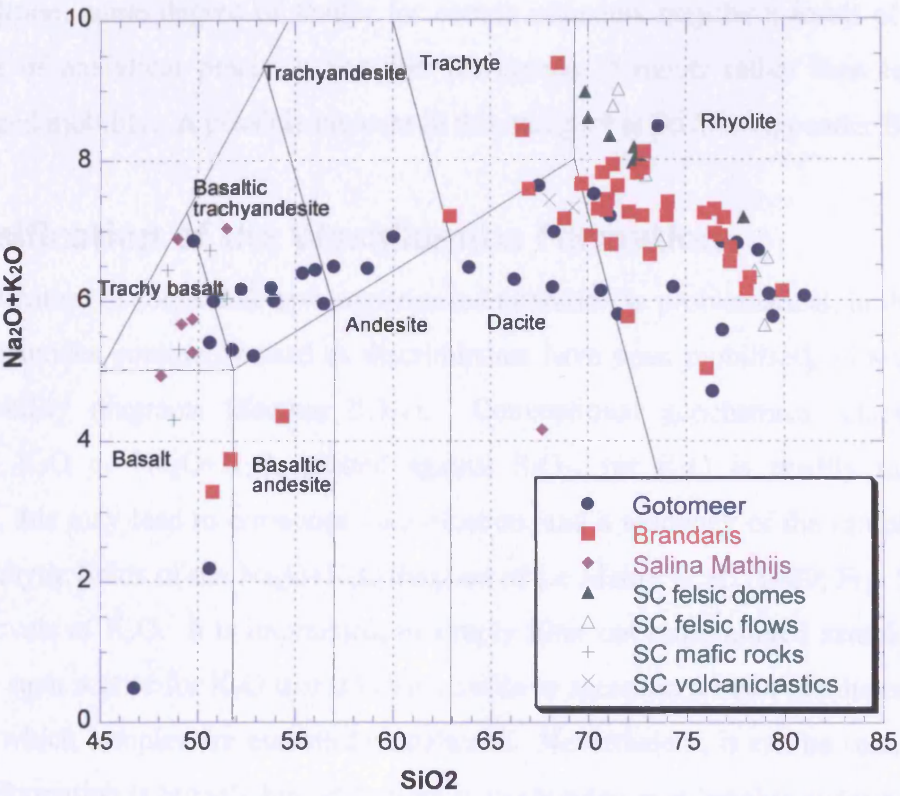

Fig. 5.8. Discrimination plot for rocks for the Washikemba Formation, Bonaire, using the plot developed by Le Maitre et al. (1989). The position of mafic rocks within the trachytic fields may be the result of elevated K2O contents due to alteration processes. SC is an abbreviation for Southern Complex.

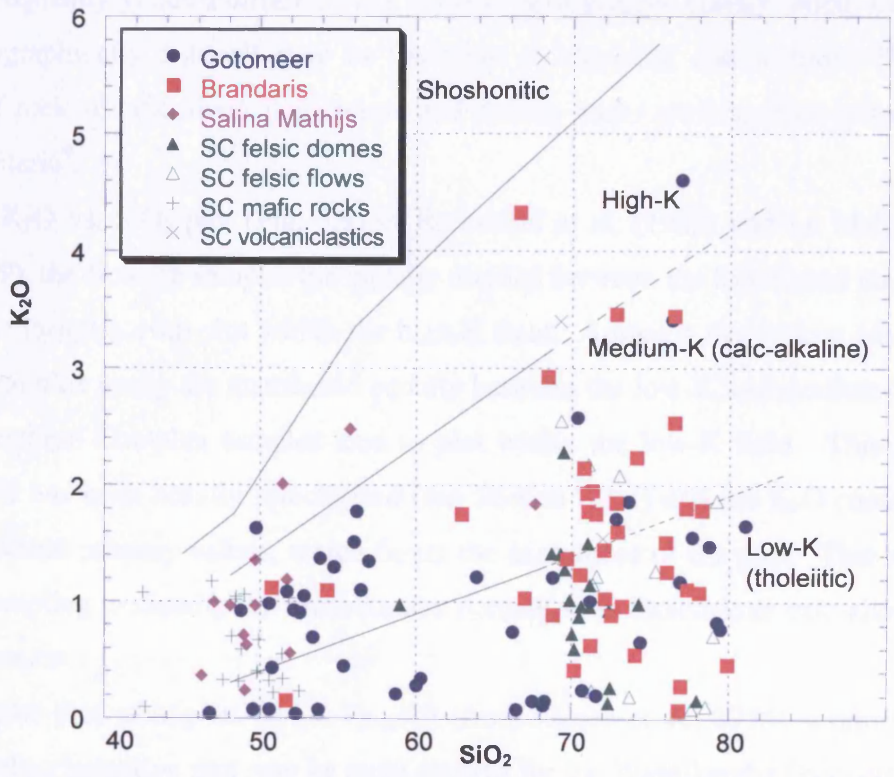

Fig. 5.9. Discrimination plot for rocks of the Washikemba Formation. Enhanced K2O and trend towards the calc-alkaline field may be the result of elevated K2O content due to alteration. Dividing lines were devised by Gill et al. (1970). SC is an abbreviation for Southern Complex.

5. In addition, some degree of scatter for certain elements may be a result of a lesser degree of analytical precision possible for certain elements rather than indicating enhanced mobility. A possible element in this category is Sc (see Appendix B).

5.4. Classification of the Washikemba Formation

Classification of rocks that have experienced alteration is problematical, in that many major element oxides commonly used as discriminants have been mobilised, as ascertained from the mobility diagrams (Section 5.3.1). Conventional geochemical classification diagrams use K_2O or Na_2O+K_2O, plotted against SiO_2, yet K_2O is readily mobilised. Consequently, this may lead to erroneous classification, and a tendency of the samples to lie within the trachytic fields of the Na_2O+K_2O diagram of Le Maitre et al. (1989; Fig. 5.8), due to enhanced levels of K_2O. It is impractical to simply filter out more altered samples, as all samples show such scatter for K_2O that it is impossible to ascertain a main (unaltered) trend, and therefore which samples are essentially unaltered. Nevertheless, it can be seen that the Washikemba Formation is broadly bimodal: there is an abundance of basaltic andesites (many of which plot as basaltic trachyandesites due to enhanced K_2O through alteration) and rhyolites/dacites, but only a few samples in between. It should be noted that geochemical classification frequently yields a different rock name to petrographic classification, i.e. a rock which is petrographically a basalt may be andesitic in chemical composition. This is a consequence of rock silicification/calcification, and thereby rocks are classified primarily on petrographic criteria[#].

On the K_2O vs. SiO_2 plot (Fig. 5.9) of Rickwood et al. (1989) and Le Maitre et al. (1989), (Fig. 5.9), the Bonaire samples are equally divided between the low-K and medium-K fields, and some samples even plot within the high-K field. Amongst the various categories, the Northern Complex group are distributed equally between the low-K and medium-K field, whereas the Southern Complex samples tend to plot within the low-K field. This poses a problem, as K_2O has been heavily remobilised (see Section 5.3.1) and the K_2O contents are unlikely to represent primary values, which limits the usefulness of the plot. This must be noted when attempting to classify the Washikemba Formation as tholeiitic or calc-alkaline on the basis of K content.

A trivariate plot of Mg vs. Al vs. Fe_{tot}+Ti (from Jensen et al., 1976) is presented in Fig. 5.10. This discrimination plot may be more suitable for the Washikemba Formation, as

[#] Throughout this chapter, lithologies are divided into broad lithological groups, e.g. the dolerite group includes rocks which are technically diorite in composition. This is for the purposes of simplicity of plotting and discussion.

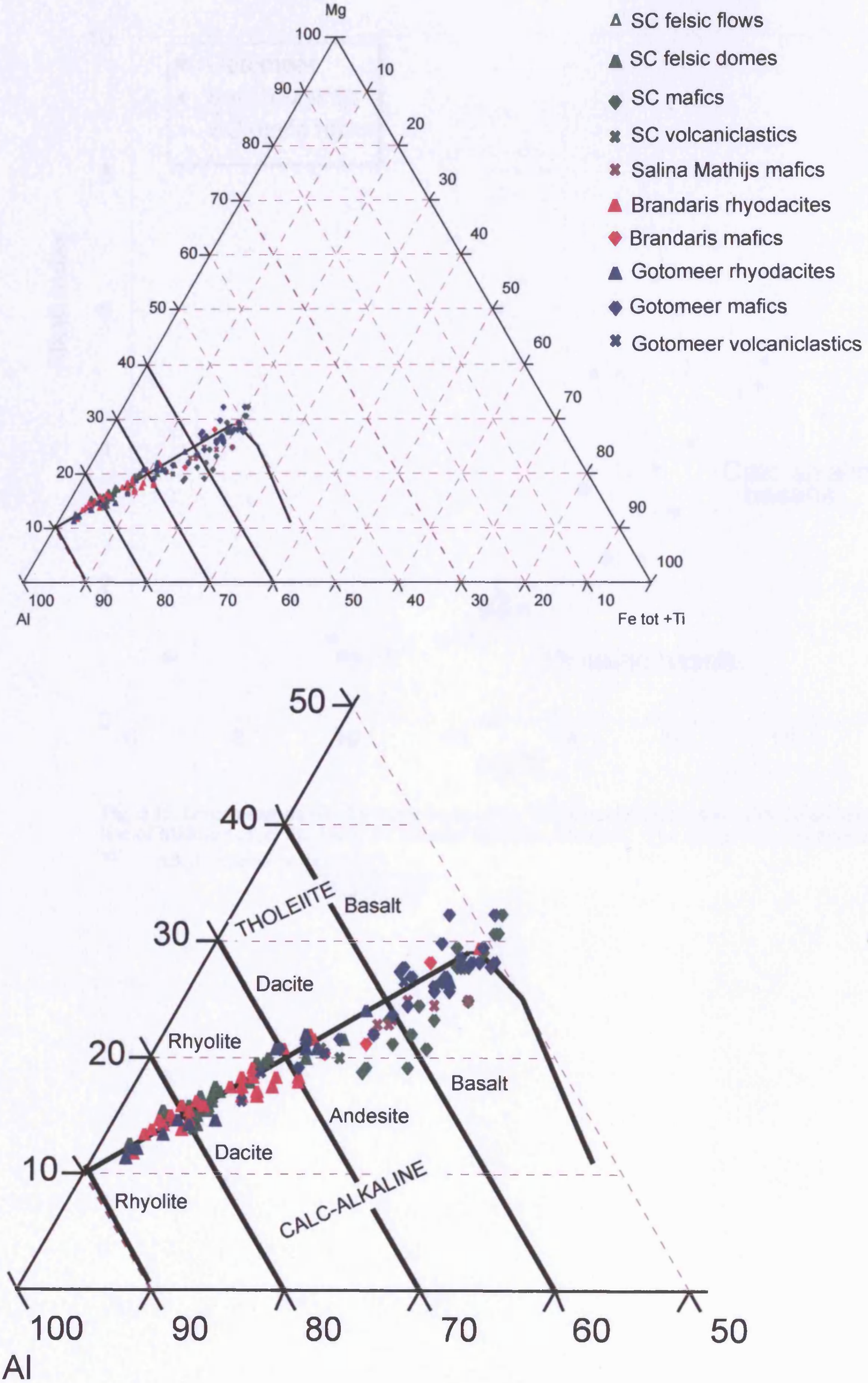

Fig. 5.10. Top- Classification plot of the Washikemba Formation, using the system of Jensen (1976). Co-ordinates of dividing lines from Rollinson (1993).

Bottom- enlargment of classification plot shown above.

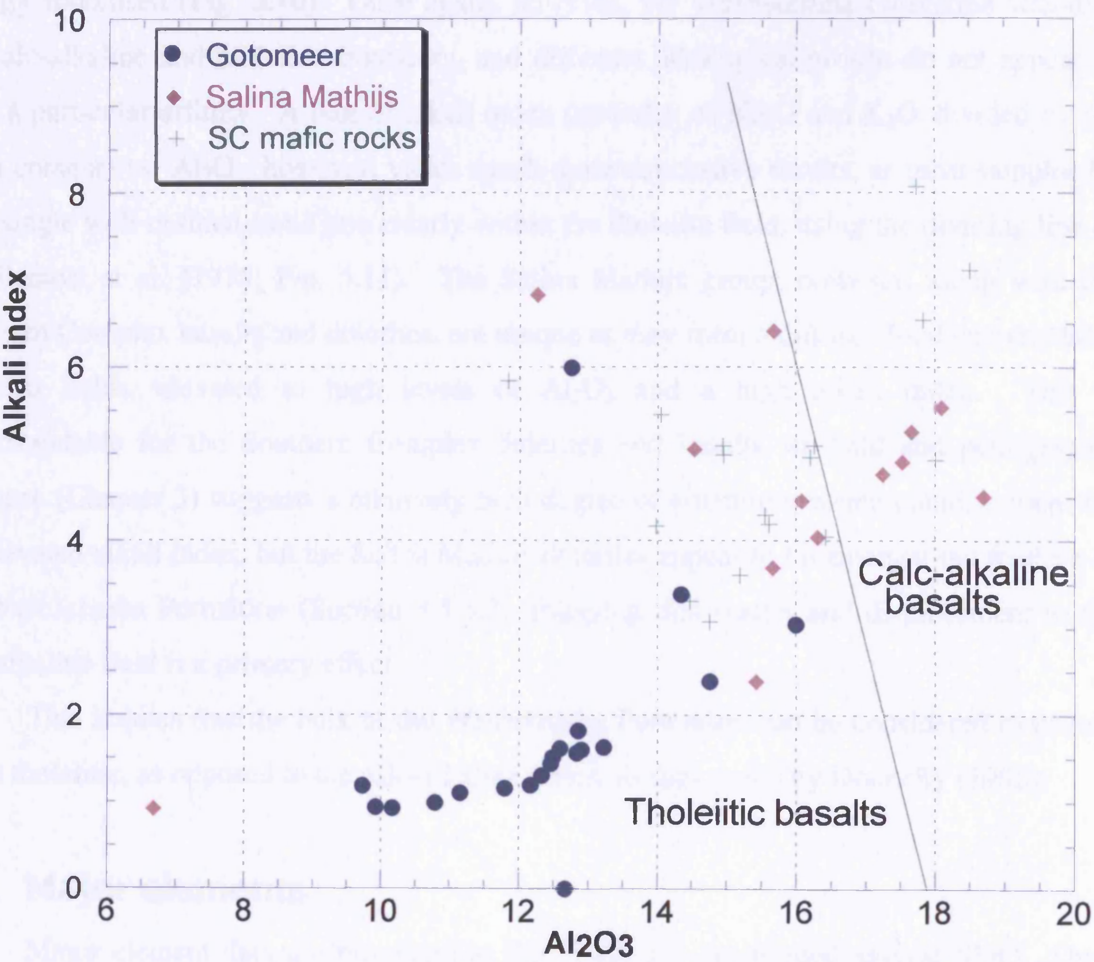

Fig. 5.11. Discrimination plot for mafic rocks of the Washikemba Formation, with the dividing line of Middlemost et al., 1975. SC denotes Southern Complex. The Alkali Index is defined as:

$$\text{Alkali Index} = \frac{Na_2O + K_2O}{0.17*(SiO_2-43)}$$

TiO_2 has been shown to be relatively immobile, whereas MgO, Fe_2O_3 and Al_2O_3 have been slightly mobilised (Fig. 5.10). Once again, however, the Washikemba Formation straddles the calc-alkaline and tholeiitic boundary, and different lithological groups do not appear to have a particular affinity. A plot of alkali index (an index of Na_2O and K_2O, divided by the silica content) vs. Al_2O_3, however, yields much more conclusive results, as most samples lie on a single well-defined trend line clearly within the tholeiite field, using the dividing line of Middlemost et al. (1975; Fig. 5.11). The Salina Mathijs group, however, along with the Southern Complex basalts and dolerites, are unique as they form a diffuse cloud that straddles the two fields, elevated to high levels of Al_2O_3 and a high alkali index. This is understandable for the Southern Complex dolerites and basalts, as field and petrographic evidence (Chapter 3) suggests a relatively high degree of alteration, which could account for the elevated alkali index, but the Salina Mathijs dolerites appear to be amongst the freshest of the Washikemba Formation (Section 3.5.5.2), implying this scatter and displacement to the calc-alkaline field is a primary effect.

This implies that the bulk of the Washikemba Formation can be considered to belong to the tholeiitic, as opposed to the calc-alkaline series, as first stated by Donnelly (1990).

5.5. Major elements

Major element data are presented in Fig. 5.12, and are plotted against MgO. On a SiO_2 vs. MgO plot, the rocks appear to be moderately bimodal, with one cluster ranging from 50–57 weight % (wt. %) SiO_2 and the other ranging from 67–80 wt.%, with very few samples in between. MgO contents range from zero to 8 wt.%. It must be noted that certain samples show either elevated or reduced levels of SiO_2 (which would directly affect modal SiO_2) due to abundant development of quartz or calcite amygdules/veins, and where these have been found, they have been noted in the lithological descriptions.

There is a continuum between dacite and rhyolite, and the silica content of the rhyodacites does not appear to be associated with a particular region. For example, the rhyodacite domes of the Southern Complex are known as the high-viscosity rhyodacites (Klaver, 1976), and one might expect them to have more SiO_2 than the sills and flows from the other outcrop of the Washikemba Formation. This was not found to be the case, however.

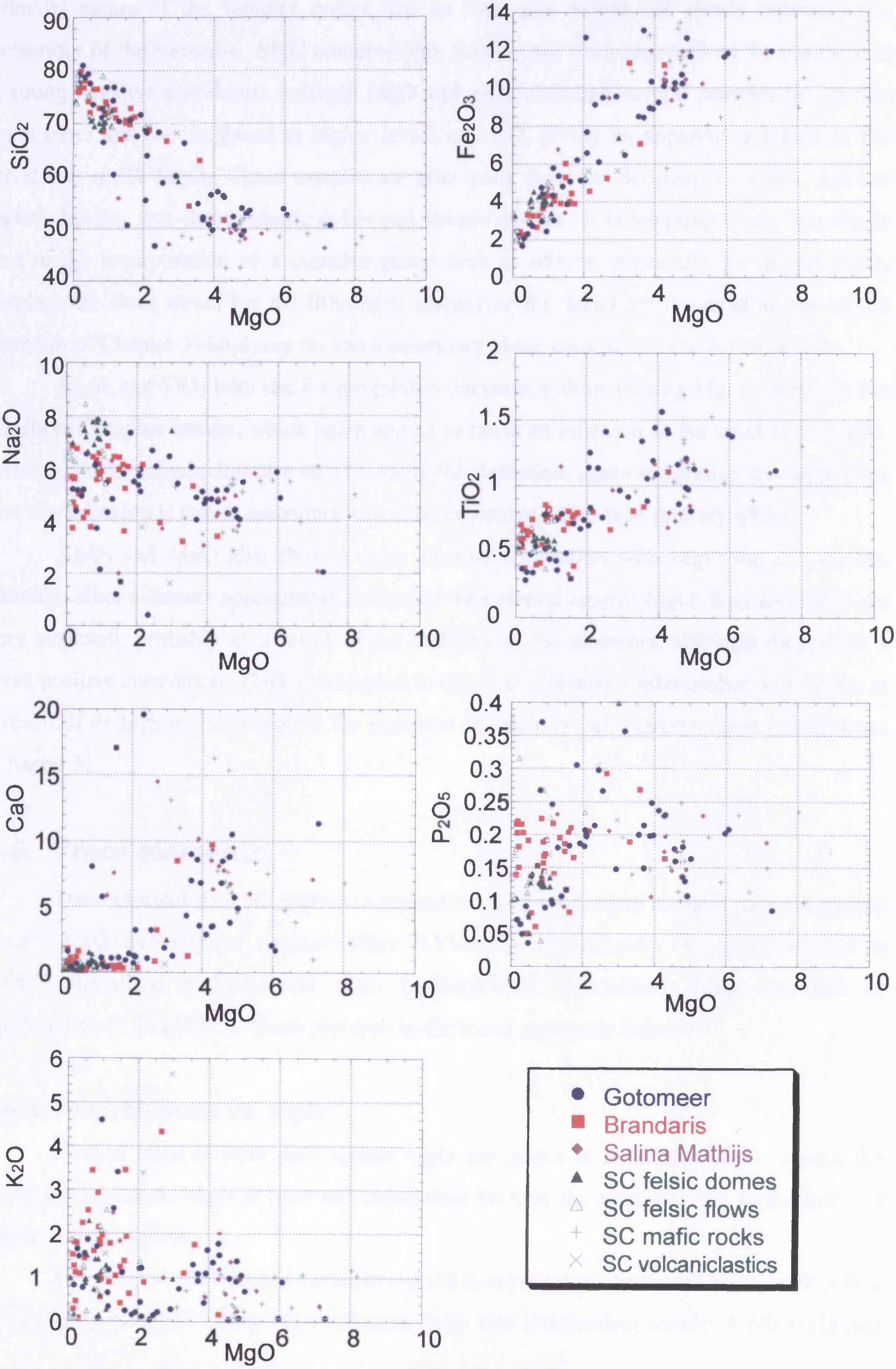

Fig. 5.12. Plots of major elements vs. MgO. All values in wt. %. SC is an abbreviation for Southern Complex.

5.5.3. Major Element vs. MgO

MgO is chosen as the abscissa rather than the more commonly used SiO_2, as the near-bimodal nature of the samples means that an SiO_2 plot would not clearly represent the behaviour of the elements. MgO contents (Fig. 5.12) range from zero to 8 wt.%, and there is a strong negative correlation between MgO and SiO_2, although several samples lie off this main trend and are displaced to higher levels of MgO, giving an apparent inflexion in the trend line at 5% MgO. These samples are principally from the Southern Complex, and are mainly basalts, late-stage basaltic dykes and volcaniclastics. It is tempting to say that this is due to the incorporation of a cumulus phase such as olivine, especially given that Fe_2O_3 displays the same trend, but the lithologies displaying this trend are the most altered of the Formation (Chapter 3) implying instead a secondary phase such as chlorite is responsible.

Fe_2O_3 and TiO_2 both show a progressive increase with increasing MgO, except for the Southern Complex basalts, which again appear to cause an inflexion in the trend at 5% MgO. Some of the Gotomeer dolerites also lie along this inflexion, again supporting the suggestion that this inflexion is due to secondary alteration processes rather than primary effects.

Al_2O_3 and MnO also show a clear positive correlation with MgO for all samples, although other elements appear more scattered when plotted against MgO: K_2O and Na_2O are very scattered, probably as a result of the mobility of the elements, although they show a weak positive correlation. CaO also appears to show no systematic relationship with MgO, as a result of its high mobility, and/or the presence of calcite as an alteration/vein filling phase (Chapter 3).

5.6. Trace elements

Trace element data are plotted in several ways: Firstly, trace element data are plotted against MgO, as for major elements (Figs. 5.13–5.17), and secondly they are presented as MORB-normalised multi-element plots (spidergrams), normalised using the data of McDonough & Sun (1995). Each plot type is discussed separately below.

5.6.1. Trace Element vs. MgO

Plots of trace element data against MgO are shown in Figs. 5.13–5.17. As for the major element data, MgO is favoured rather than SiO_2 as the abscissa, due to the bimodal nature of the samples.

The elements Sc, Co and Ga show a good positive correlation with MgO, with only a few outlying samples. Many other elements show two independent trends: A Nb-MgO plot

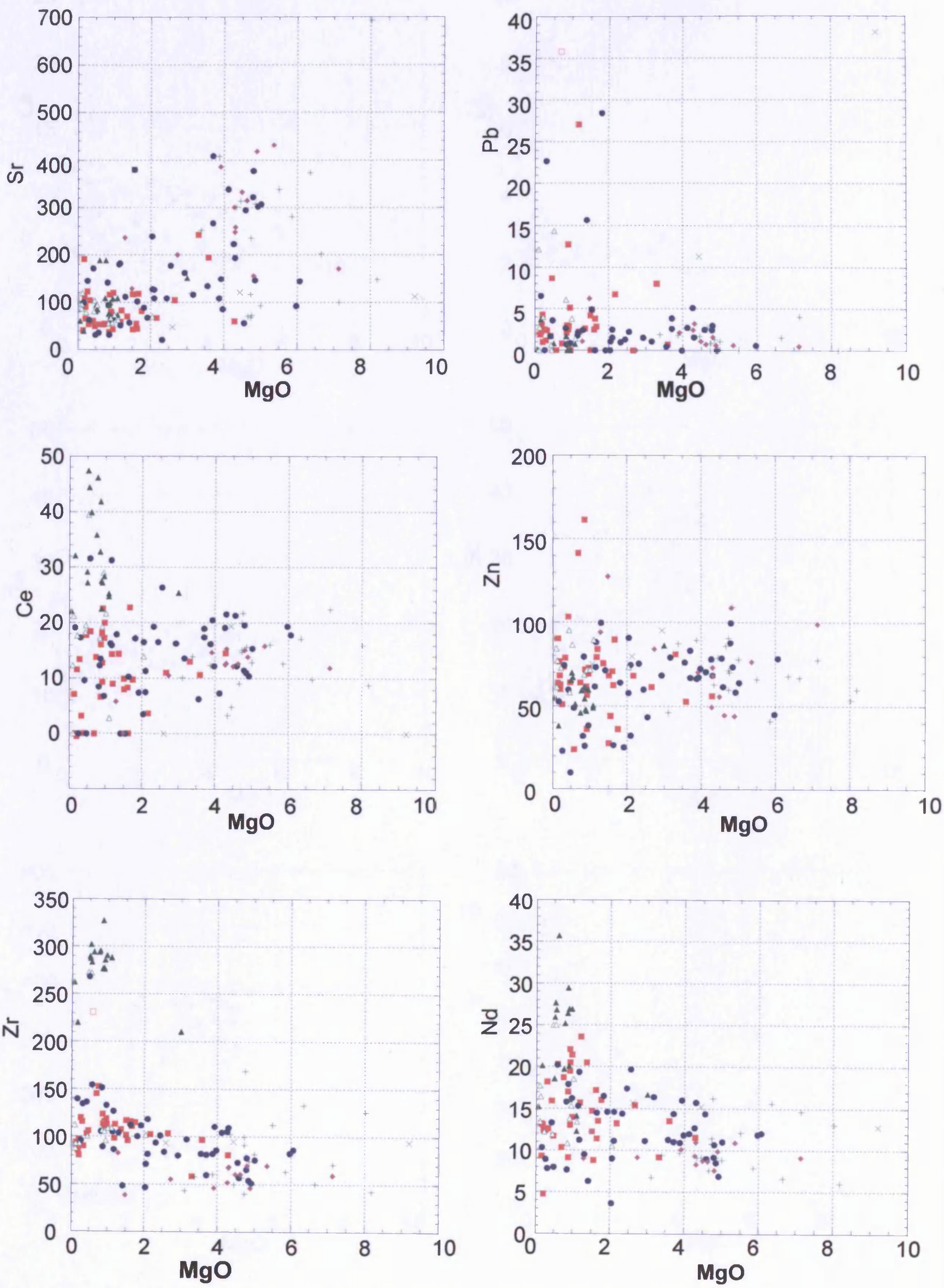

Fig. 5.13. Plots of trace elements vs. wt.% MgO. Trace element abundances are in parts per million (ppm). Symbols as in Fig. 5.12.

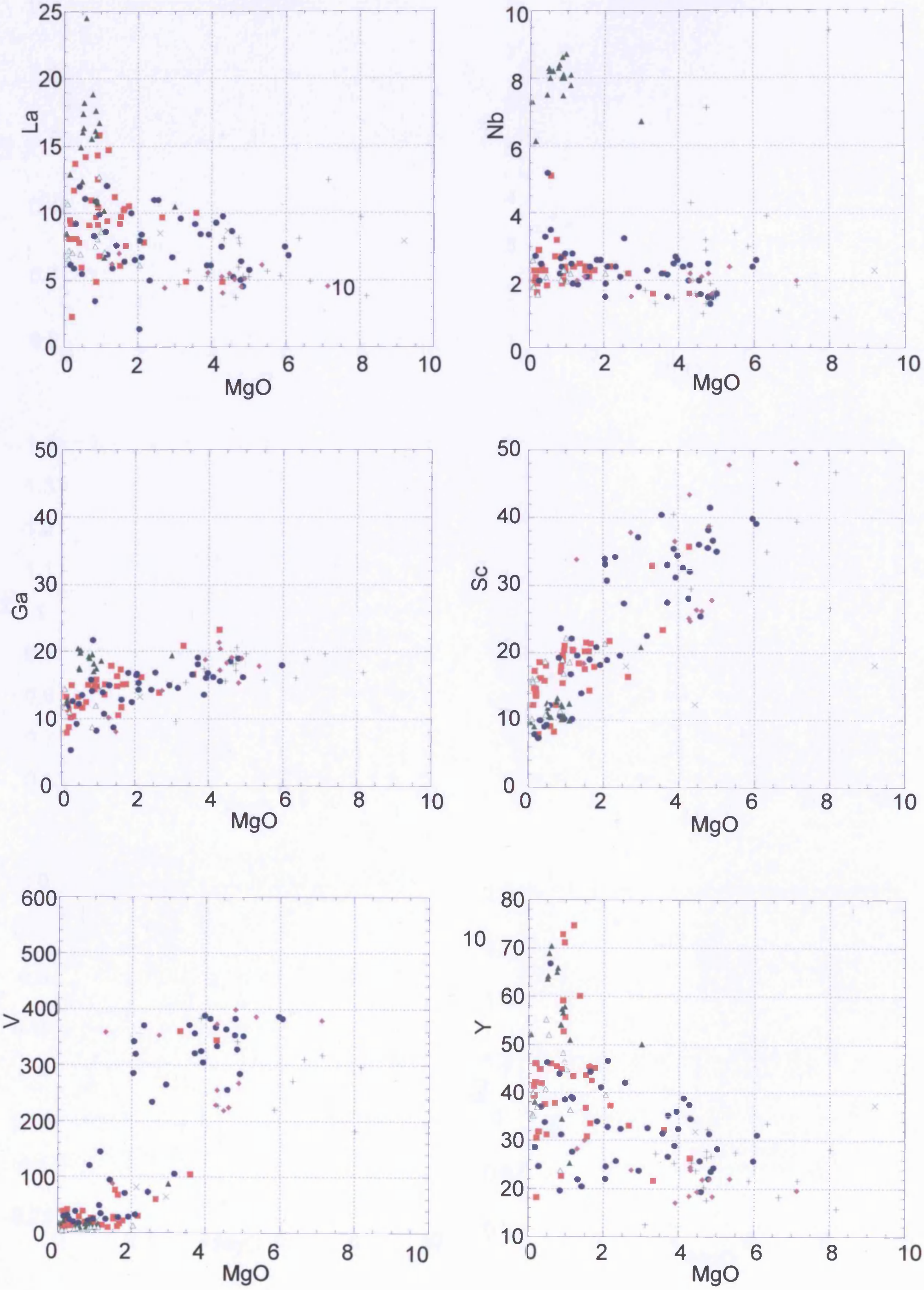

Fig. 5.14. Plots of trace elements vs. wt.% MgO. Trace element abundances are in parts per million (ppm). Symbols as in Fig. 5.12.

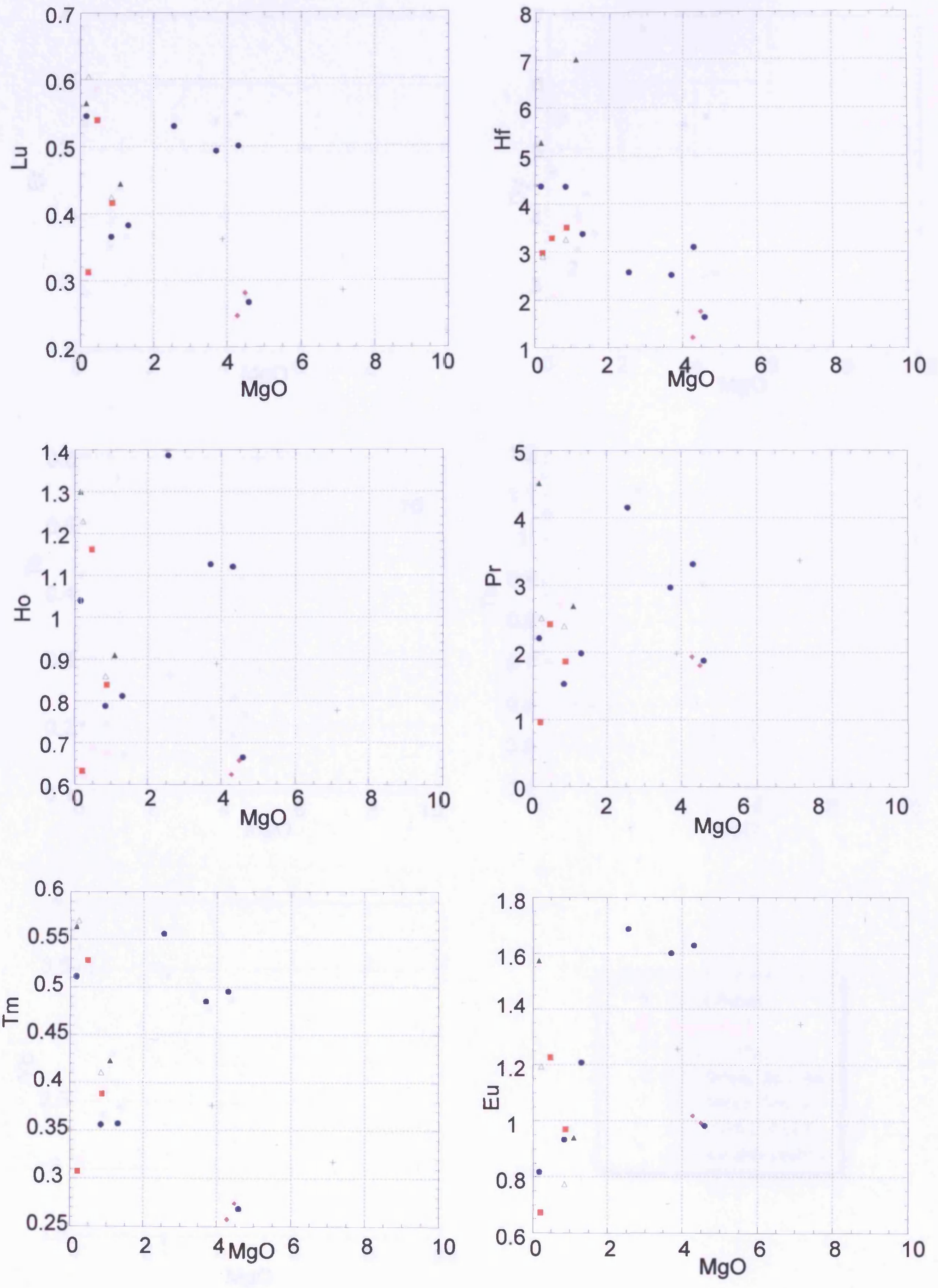

Fig. 5.15. Plots of trace elements vs. wt.% MgO. Trace element abundances are quoted in parts per million (ppm). Symbols as in Fig. 5.12.

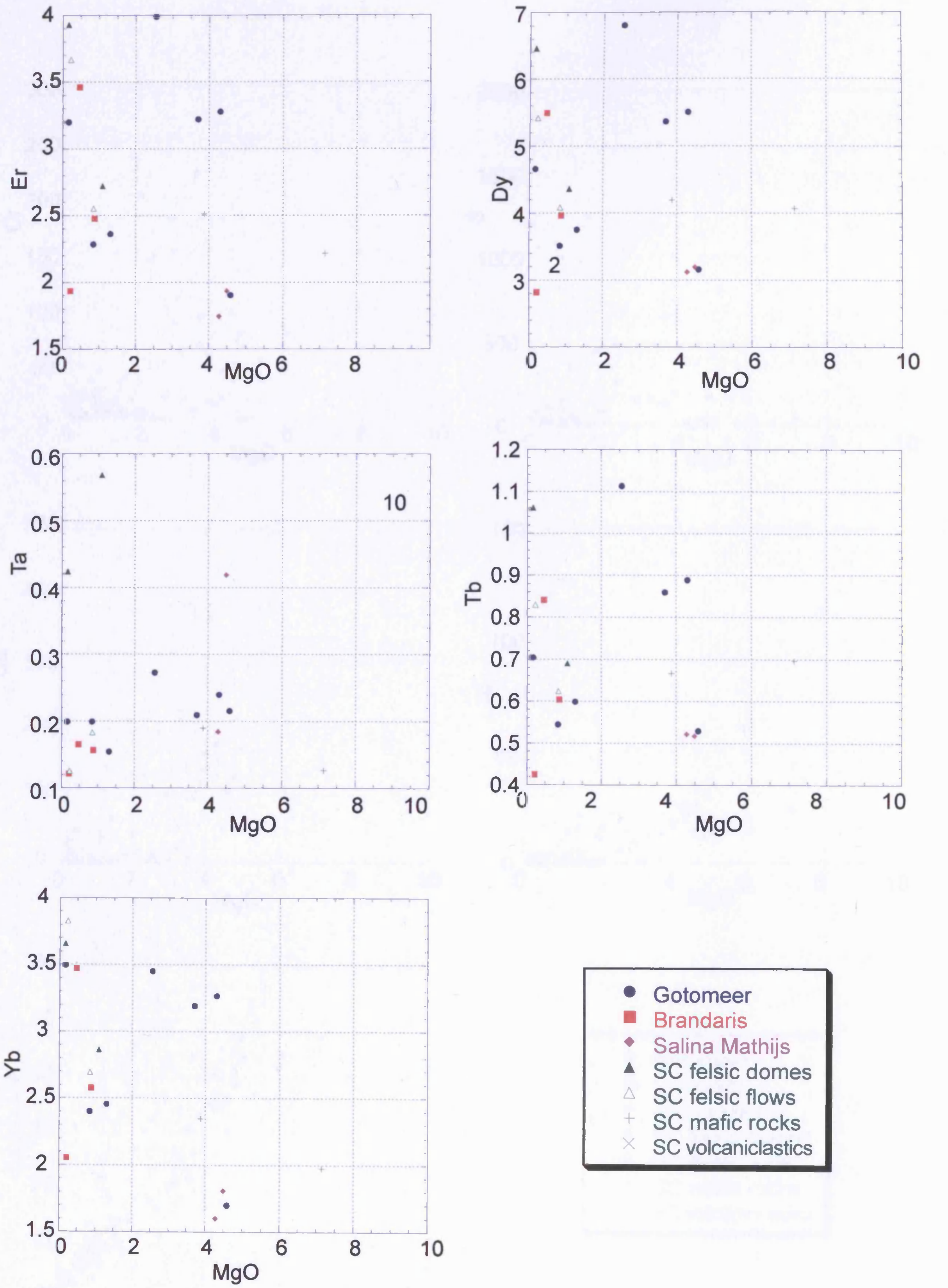

Fig. 5.16. Plots of trace elements vs. wt% MgO. Trace element abundances are in parts per million (ppm). Symbols as in Fig. 5.12.

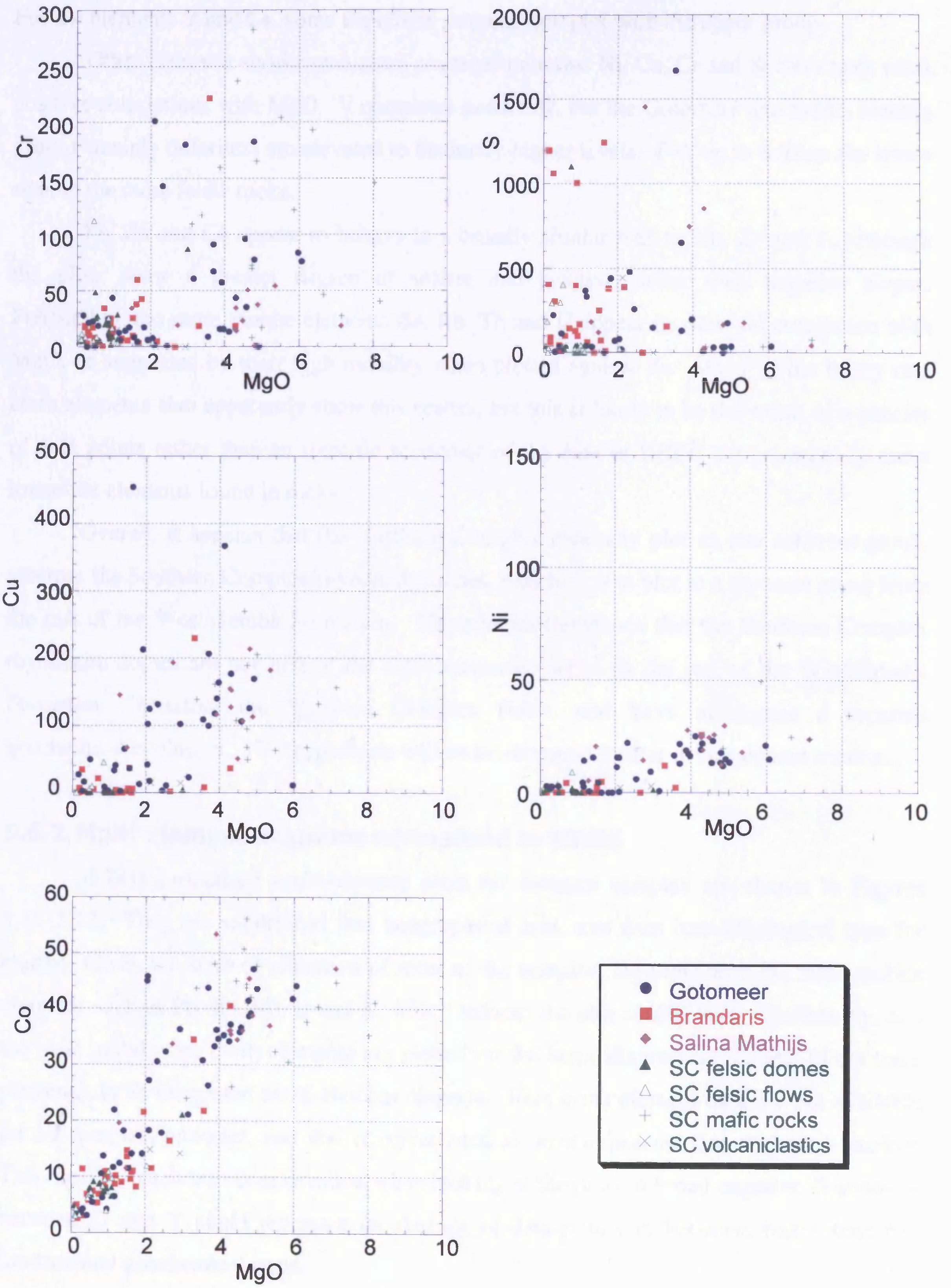

Fig. 5.17. Plots of trace elements vs. wt.% MgO. Trace element abundances are quoted in parts per million (ppm).

shows 2 separate trends: a flat well-defined trend is defined by most samples, and a subset of the Southern Complex rhyodacites form a distinct group at higher levels of Nb (>6 ppm). This distinct pattern is also displayed by Zr and Y, and to lesser degrees by Nd, La and Ce. For the elements Y and La, some Brandaris samples also plot with the upper group.

Other elements show much more scattered patterns: Ni, Cu, Cr and Sr have very weak positive correlations with MgO. V correlates positively, but the Gotomeer and Salina Mathijs groups (mainly dolerites) are elevated to distinctly higher levels of V, up to 8 times the levels seen in the more felsic rocks.

Pb, Zn and Ce appear to behave in a broadly similar way to Nb, Zr and Y, although the plots show a greater degree of scatter and positive rather than negative slopes. Predictably, the more mobile elements Ba, Rb, Th and U appear to show no correlation with MgO, as suggested by their high mobility when plotted against Zr. Many of the heavy rare earth elements also apparently show this scatter, but this is likely to be the result of a paucity of data points rather than an intrinsic scattering of the data as HREE are amongst the most immobile elements found in rocks.

Overall, it appears that the Northern Complex generally plot as one coherent group, whereas the Southern Complex rhyodacite domes, which tend to plot in a separate group from the rest of the Washikemba Formation. This provides evidence that the Southern Complex rhyodacite domes are not part of the same magmatic series as the rest of the Washikemba Formation, including the Southern Complex flows, and have undergone a separate geochemical evolution. This hypothesis will be investigated further in subsequent sections.

5.6.2. Multi-element diagrams normalised to MORB

MORB-normalised multi-element plots for Bonaire samples are shown in Figures 5.18–5.22. They are subdivided into geographical area, and then into lithological type for clarity. Given the state of alteration of most of the samples, the plots omit the more mobile elements such as Pb, Ba, Rb, U and K, which reduces the plot scatter level significantly, and the least mobile rare earth elements are plotted on the same diagram as the rest of the trace elements, in an integrated multi-element diagram. Rare earth element data are not available for all samples, however, and this is represented as an interpolated line without a marker. This must be taken into consideration when looking at the plots: a broad negative Ti anomaly between Zr and Y could represent an absence of data points in between, rather than any fundamental geochemical trend.

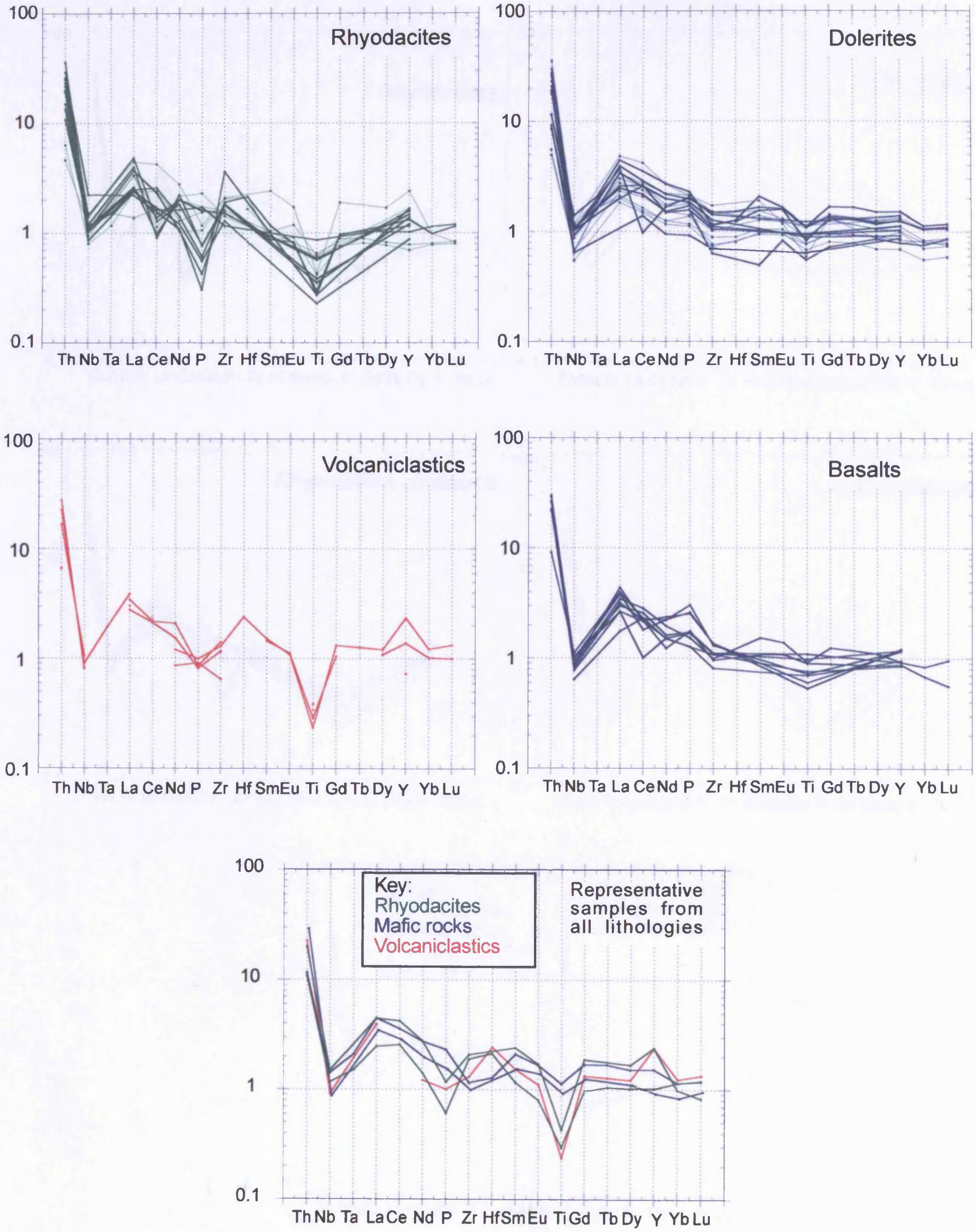

Fig. 5.18. MORB-normalised integrated multi-element plot for samples from the Gotomeer area, subdivided by lithology.

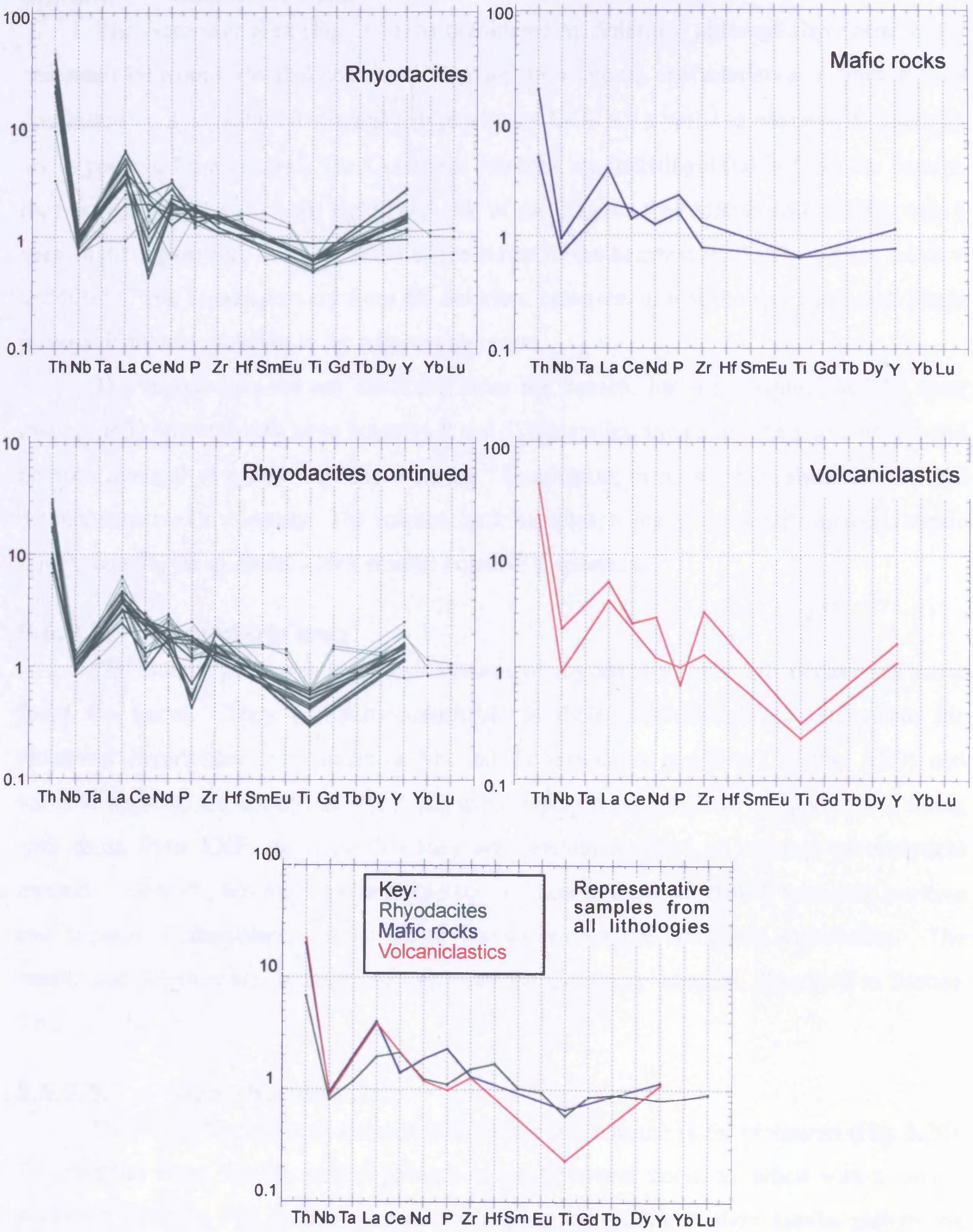

Fig. 5.19. MORB-normalised integrated multi-element plot for samples from the Brandaris area, subdivided by lithology.

The bulk of the Washikemba shows typical island arc trends such as a spiky profile with negative Nb and Ti anomalies. Any deviation from this trend for certain lithological groups is discussed in the sections beneath.

5.6.2.1. Gotomeer area

The Gotomeer area (Fig. 5.18) is dominated by dolerites, although rhyodacite flows and small intrusions are also abundant. They all show certain characteristics: a spiky profile dominated by a negative Nb anomaly (typically 1× MORB), a variable negative Ti anomaly and a positive La anomaly. The Gotomeer dolerites are indistinguishable from the basalts: they are essentially flat on the right hand side of the diagram (the MREE and HREE), with a very slight negative Ti anomaly and a slight deficit of the heaviest REE, Yb and Lu, relative to MORB. The basalts do vary from the dolerites, however, in that the basalts show a slight positive P anomaly relative to the adjacent elements.

The rhyodacites are not dissimilar from the basalts, but are distinguished by their distinct and comparatively large negative P and Ti anomalies, indicating the fractionation and obvious removal of apatite and Ti-Fe oxides. In addition, many samples show a small but distinct negative Ce anomaly. The volcaniclastic samples, being of rhyodacite affinity, mimic this rhyodacite trend, albeit with a smaller negative P anomaly.

5.6.2.2. Brandaris area

The Brandaris area is mainly comprised of rhyodacites, although occasional mafic rocks are found. They are indistinguishable in their geochemical character from the Gotomeer rhyodacites, with negative Nb and Ti anomalies, positive La (Fig. 5.19) and variable negative Ce anomalies. ICP-MS data display these negative Ce anomalies, along with those from XRF, implying that they are genuine and not an artefact of analytical methods. They do, however, show a marked variation in terms of their P contents: positive and negative P anomalies are distributed equally within the Brandaris rhyodacites. The basalts and dolerites are indistinguishable from the Gotomeer samples, described in Section 5.6.6.1.

5.6.2.3. Salina Mathijs area

The Salina Mathijs area consists of dolerites and volcaniclastic sediments (Fig. 5.20). The dolerites show broadly similar patterns to the Gotomeer dolerites, albeit with a greater positive P anomaly. The limited number of volcaniclastic sediments show similar patterns on the multi-element plots from the dolerites.

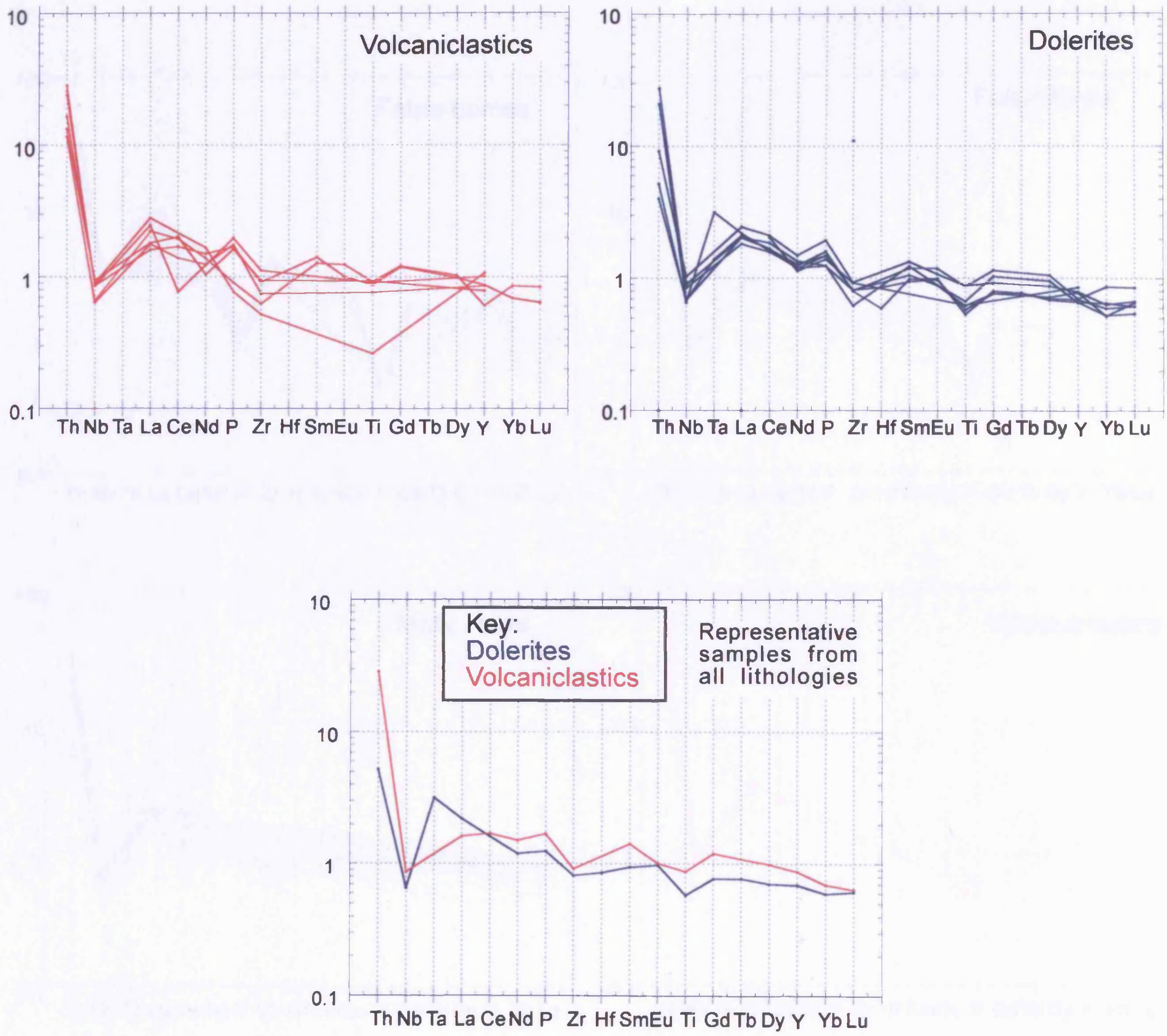

Fig. 5.20. MORB-normalised integrated multi-element plot for samples from the Salina Mathijs area, subdivided by lithology.

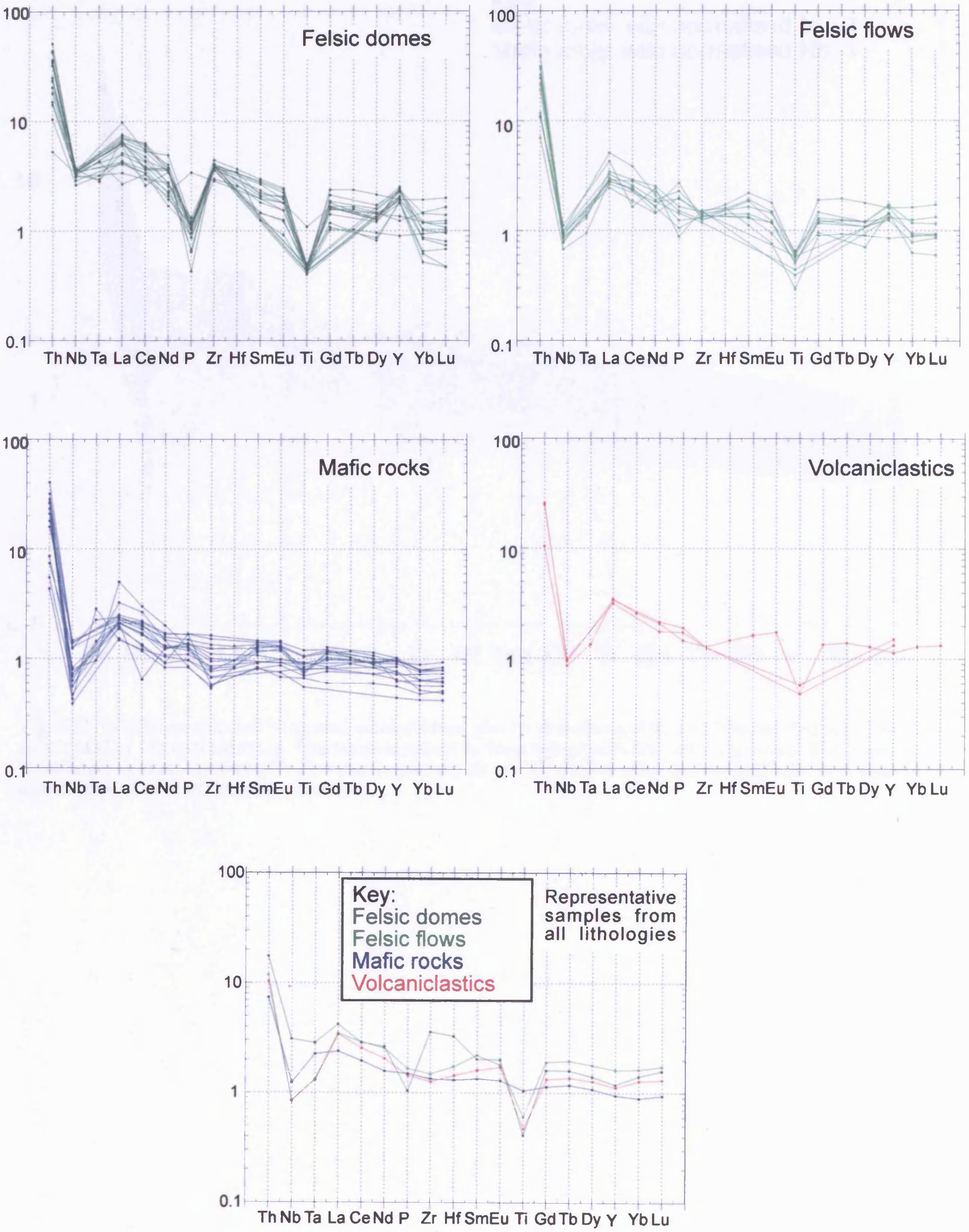

Fig. 5.21. MORB-normalised integrated multi-element plot for samples from the Southern Complex, subdivided by lithology.

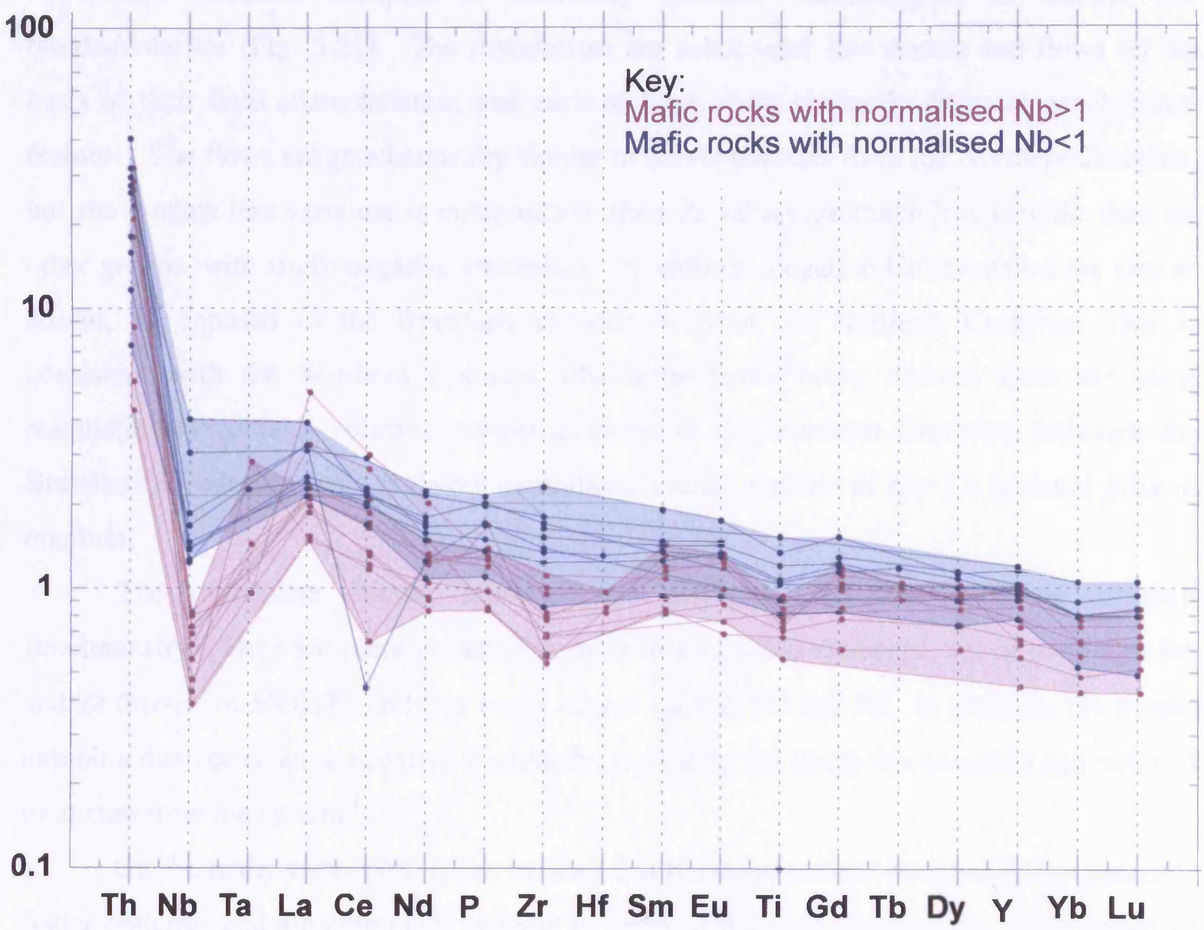

Fig. 5.22. MORB-normalised integrated multi-element plot for dolerites and basalts from the Southern Complex, subdivided by Nb concentration. The samples appear to form two groups: one with normalised Nb<1 and lower abundances of most incompatible elements (especially Zr and Ti) and the other with normalised Nb>1 and higher abundances of most incompatible elements.

5.6.2.4. Southern Complex

The Southern Complex is essentially bimodal, consisting of rhyodacites and basalts/dolerites (Fig. 5.21). The rhyodacites are subdivided into domes and flows on the basis of their field characteristics, and each of these show distinctly different geochemical features. The flows are geochemically similar to the rhyodacites from the Northern Complex, but show much less variation in composition: their Zr values are much less variable than for other groups, with slight negative anomalies. In addition, negative Ce anomalies are rare or absent, as opposed to the Brandaris rhyodacites from the Northern Complex. This is consistent with the Southern Complex rhyodacite flows being derived from the same magmatic source (and volcanic centre) as those of the Northern Complex, although the Brandaris rhyodacites have probably assimilated a small amount of low Ce material prior to eruption.

The rhyodacite domes, however, are distinctly different in terms of their geochemistry. They are more enriched in most incompatible elements, but in particular Nb and Zr (both ~3× MORB), and to a lesser degree La, Ce, Nd and Hf. In addition, the domes exhibit a distinctive large negative P anomaly, indicating the likely fractionation and removal of apatite from the system.

On the mafic rocks plot, it can be seen that the dolerites and basalts display generally flatter patterns, and are extremely variable in terms of their Nb composition. One subset of samples has a distinct negative Nb anomaly (normalised Nb<1), and has a spiky pattern with a negative Zr anomaly (Fig. 5.22). The other subset has Nb levels of up to 4× MORB, and a much flatter pattern with only a slight negative slope (i.e. a slight relative enrichment in LREE) and therefore is more MORB-like in appearance. There does not appear to be any lithological or other difference between the two geochemical groups. All the dolerites form part of the "flatter" high-Nb trend, but basalts from successive flows only metres apart can have contrasting trends, and there appears to be no geographical correlation. The geochemical variation is not a result of weathering since the freshest samples are found in both groups, and also the elements defining the trends are amongst the most immobile of elements (e.g. Zr). It is therefore apparent that both these geochemical trends are consanguineous and contemporaneous, and are indicative of two coeval yet compositionally distinct magma batches.

Only sparse data exist for the volcaniclastic lithologies of the Southern Complex. Nonetheless, it is evident that they appear geochemically indistinguishable from the rhyodacites flows, rather than the domes, as dictated by their MORB-like Nb concentrations.

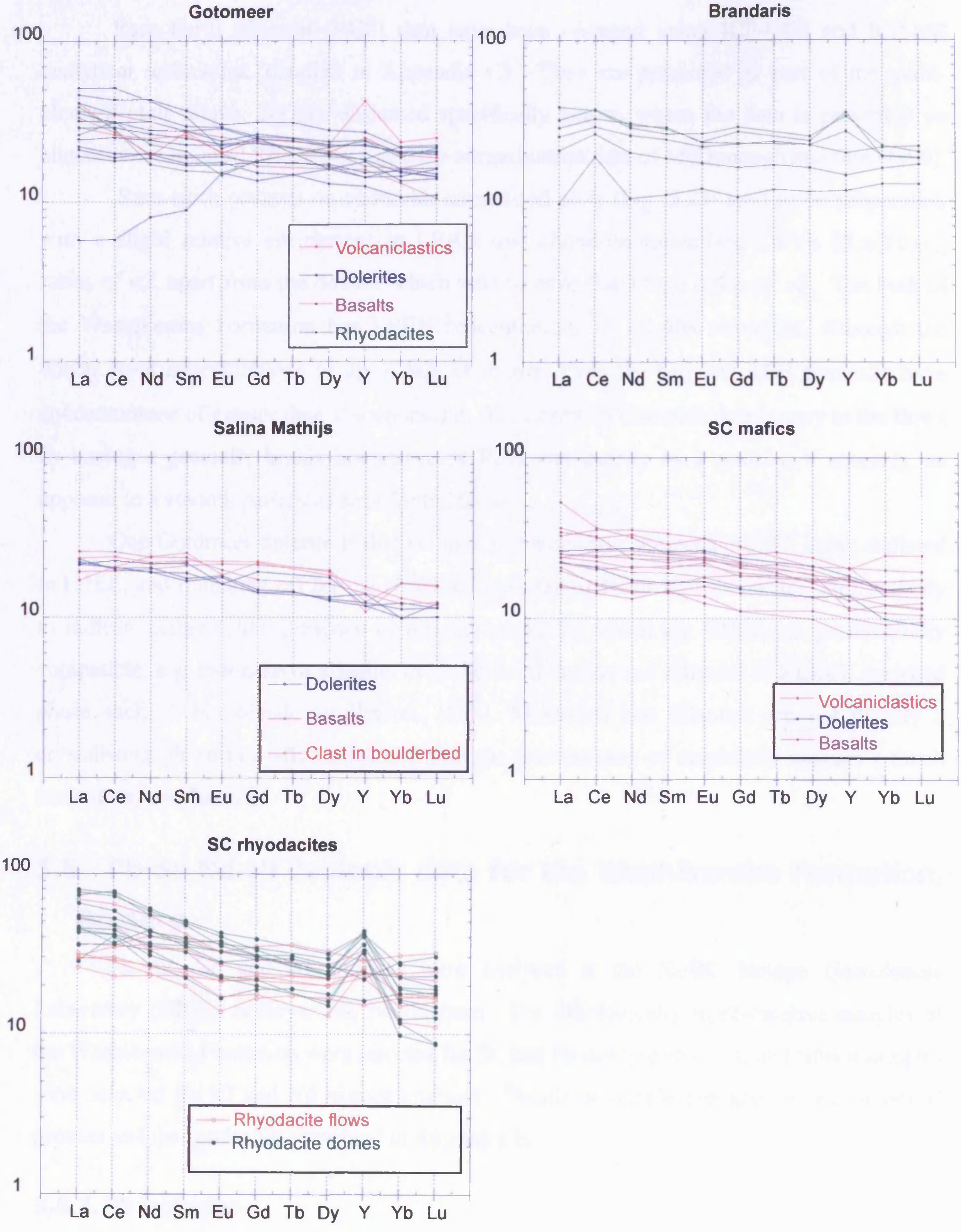

Fig. 5.23. Chondrite-normalised rare earth element plot for the Bonaire Washikemba Formation, subdivided by area.

5.7. Rare earth element data

Rare Earth Element (REE) data have been obtained using ICP-OES and ICP-MS analytical techniques (detailed in Appendix C). They are presented as part of the multi-element plots above, but are discussed specifically below, where the data is presented on chondrite-normalised REE plots, using the normalisation data of McDonough and Sun (1999).

Rare earth patterns on chondrite-normalised plots (Fig. 5.23) tend to be subparallel, with a slight relative enrichment in LREE, and chondrite-normalised La/Yb [$(La/Yb)_{CN}$] ratios of <2, apart from the domes, which tend to have $(La/Yb)_{CN}$ ratios of >3. The bulk of the Washikemba Formation has LREE concentrations of 20–40× chondrite, although the domes have concentrations of up to 80× chondrite. Even the heaviest REE generally have concentrations of greater than 10× chondrite. The Southern Complex domes vary to the flows by having a generally higher abundance of REE, and usually by a positive Y anomaly, as opposed to a smooth pattern as seen for the flows.

One Gotomeer dolerite is distinct as it has a concave upwards profile, being depleted in LREE, and flattening off for the HREE to a plateau of about 20× chondrite. This is likely to indicate either a. the presence of residual phase for which the HREE are preferentially compatible, e.g. monazite or allanite, or b. the fractionation and removal of a LREE enriched phase such as hornblende (Rollinson, 1993). Monazites and allanites are not usually a crystallising phase in mafic rocks, and thus the fractionation of amphibole appears a much more likely mechanism.

5.8. Pb-Sr-Nd-Hf Isotopic data for the Washikemba Formation, Bonaire

Pb, Sr, Nd and Hf isotopes were analysed at the NERC Isotope Geosciences Laboratory (NIGL) at Keyworth, Nottingham. Ten lithologically representative samples of the Washikemba Formation were selected for Sr, and Pb isotopic analysis, and fifteen samples were selected for Hf and Nd isotope analysis. Details of sample preparation, the analytical process and the results are presented in Appendix E.

5.8.1. Pb isotopes

Pb isotopes were analysed using both the Thermal Ionisation Mass Spectrometry (TIMS) and the Plasma Ionisation Multi-collector Mass Spectrometry (PIMMS) technique. A comparison of both sets of results is presented in Table E.7 and discussed in Section E.1.8 of the Appendix. All Pb data presented in this thesis were analysed using the PIMMS technique.

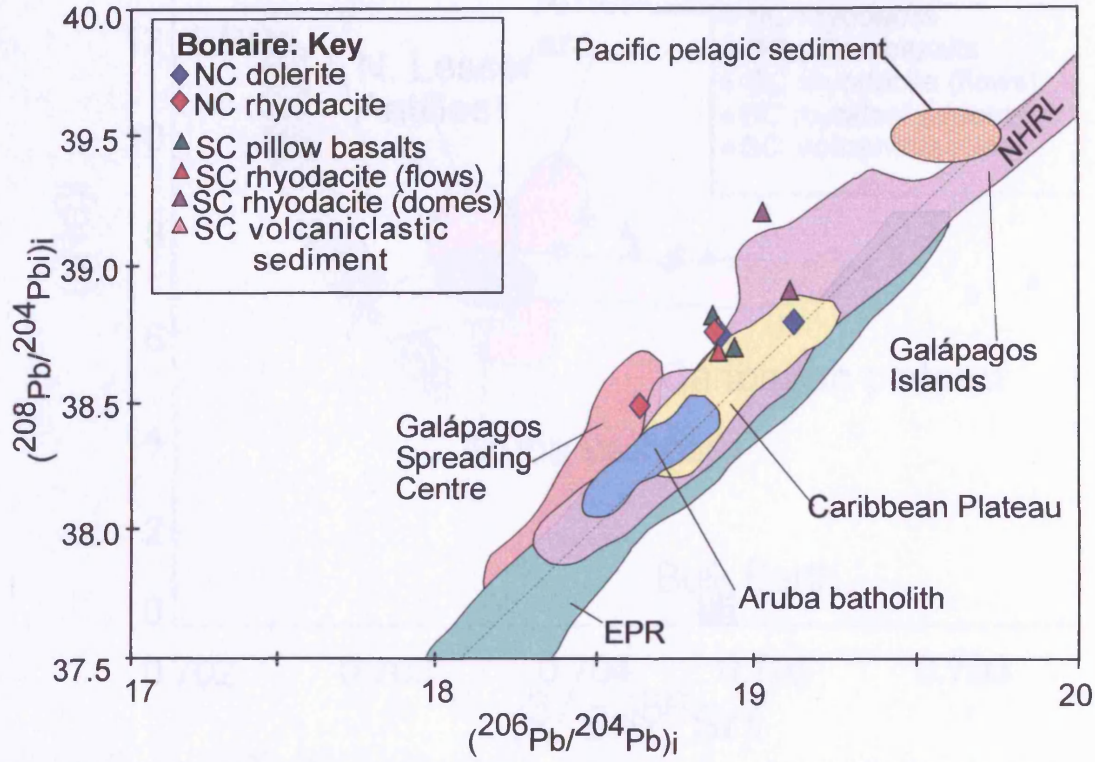

Fig. 5.24 a. Plot of $(^{208}Pb/^{204}Pb)i$ vs. $(^{206}Pb/^{204}Pb)i$ for samples from the Bonaire Washikemba Formation with other fields shown for reference, all age corrected to the time of emplacement. Data for the Aruba batholith from White (1999), Caribbean plateau data from White (1999) and Hauff et al. (2000). Galapagos data from White et al., 1993; Pelagic sediment data from Schmincke et al., 1998 and EPR data from Mahoney et al., 1993.

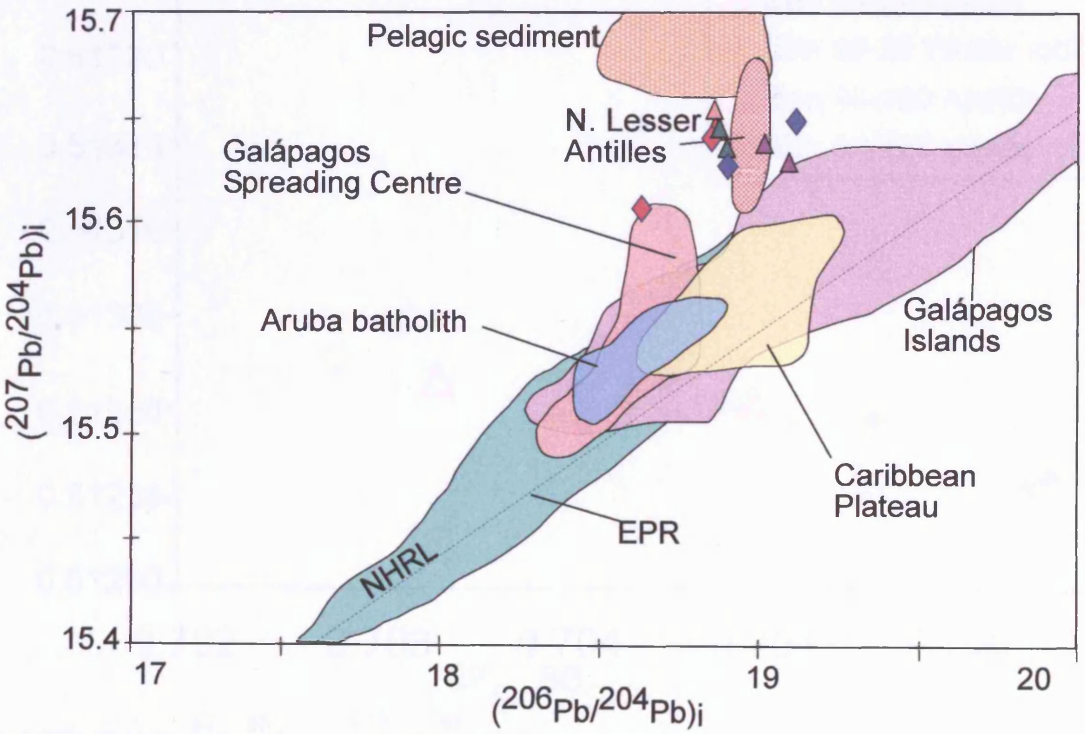

Fig. 5.24 b. Plot of $(^{207}Pb/^{204}Pb)i$ vs. $(^{206}Pb/^{204}Pb)i$ for samples from the Bonaire Washikemba Formation with other fields shown for reference. Data sources as for Fig. 5.25a., and Lesser Antilles data from White and Dupre (1983); Davidson (1987) and Davidson (1993).

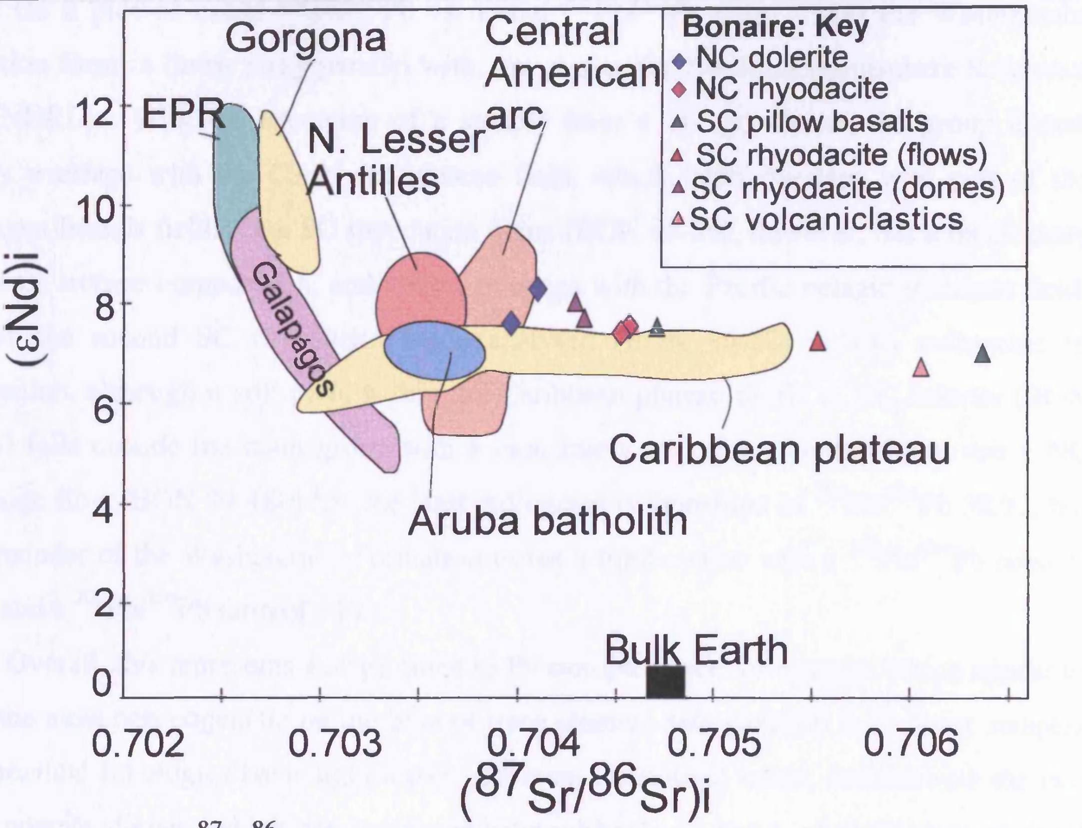

Fig. 5.25a. Plot of initial $^{87}Sr/^{86}Sr$ vs. initial εNd for samples from the Bonaire Washikemba Formation, with other fields shown for reference. All are age corrected to assumed age of emplacement (95 Ma for the Washikemba Formation; Section 4.3). Data sources as for Fig. 5.24a, and Central American arc data from Feigenson and Carr (1986).

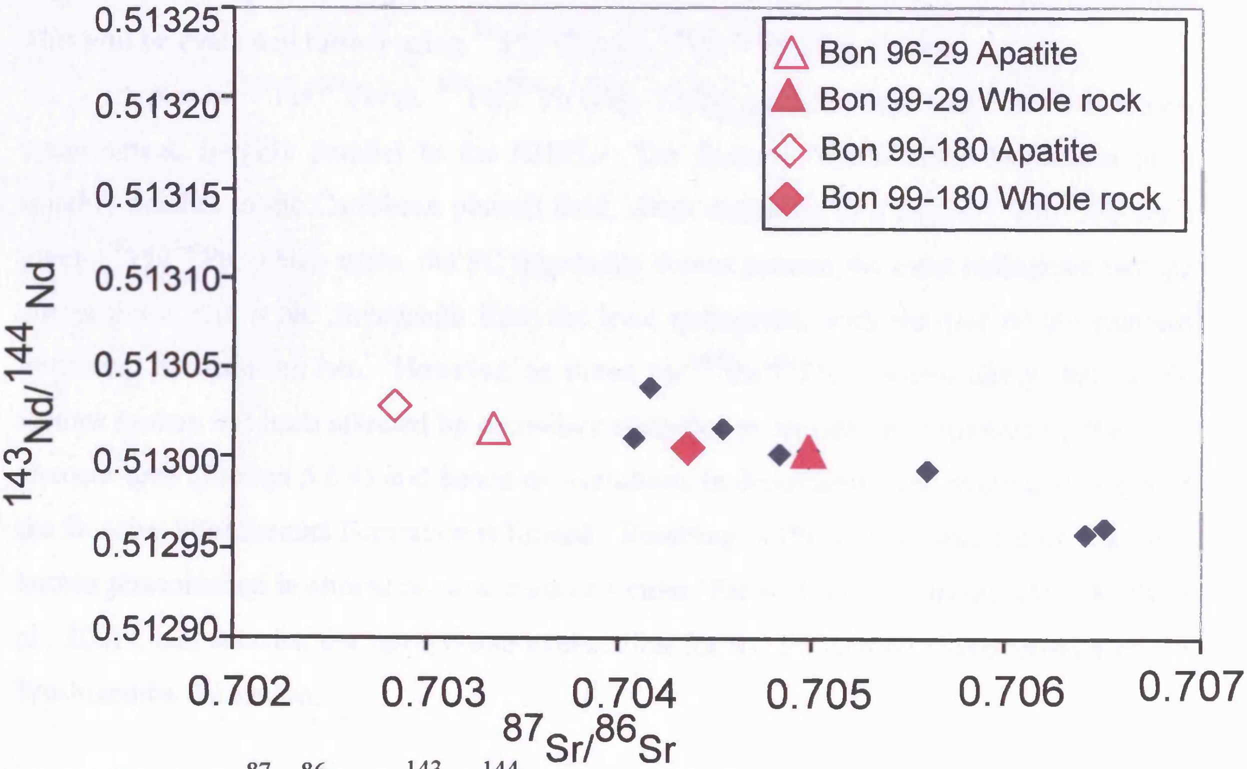

Fig. 5.25b. Plot of $^{87}Sr/^{86}Sr$ vs. $^{143}Nd/^{144}Nd$ for samples from the Bonaire Washiekmba Formation, showing results of analysis of apatite mineral separates compared with the whole rock data. Blue points denote age corrected data (shown above), for reference. Analyses have not been age corrected as for the plot above, as accurate Rb, Sr, Sm and Nd trace element data are not available for the apatite seperates.

On a plot of initial $^{208}Pb/^{204}Pb$ vs. initial $^{206}Pb/^{204}Pb$ (Fig. 5.24a) the Washikemba Formation forms a linear array parallel with, but above, the Northern Hemisphere Reference Line (NHRL). With the exception of a sample from a SC rhyodacite, the group almost entirely overlaps with the Caribbean plateau field, which itself overlaps with part of the Galápagos Islands field. One SC rhyodacite dome (BON 96-29), however, has a much more radiogenic isotope composition, and almost overlaps with the Pacific pelagic sediment field, whereas the second SC rhyodacite dome analysed (BON 96-22) is also radiogenic in composition, although it still plots within the Caribbean plateau field. A NC dolerite (BON 99-104) falls outside the main group with a moderately radiogenic composition, and a NC rhyodacite flow (BON 99-180) has the least radiogenic composition of $^{208}Pb/^{204}Pb$ 38.33, but the remainder of the Washikemba Formation forms a tight cluster with a $^{208}Pb/^{204}Pb$ ratio of ~38.8, and a $^{206}Pb/^{204}Pb$ ratio of ~19.

Overall, this represents a large range in Pb isotopic space for samples which appear to be for the most part cogenetic on the base of trace element data (Section 5.6). Some samples from identical lithologies have significantly different Pb isotope ratios, for example the two SC rhyodacite domes, which are largely indistinguishable in terms of their trace element characteristics. Consequently, it seems likely that the Pb isotopic system may have experienced isotope resetting due to secondary alteration and/or metamorphism processes. This will be evaluated further using $^{207}Pb/^{204}Pb$ vs. $^{206}Pb/^{204}Pb$ (Fig. 5.24b).

A plot of $^{207}Pb/^{204}Pb$ vs. $^{206}Pb/^{204}Pb$ (Fig. 5.24b) yields a large range in Pb isotopes, again spread roughly parallel to the NHRL. The Bonaire Washikemba Formation plots roughly parallel to the Caribbean plateau field, albeit displaced to a higher $^{207}Pb/^{204}Pb$ for a given $^{206}Pb/^{204}Pb$. Once again, the SC rhyodacite domes possess the most radiogenic isotope composition, and a NC rhyodacite flow the least radiogenic, with the rest of the samples clustering between the two. However, as stated for $^{208}Pb/^{204}Pb$, it seems likely that the Pb isotope system has been affected by secondary alteration processes, as suggested by the trace element data (Section 5.6.4) and hence its usefulness in determining the magmatic origin of the Bonaire Washikemba Formation is limited. Resetting of Pb isotope systematics is a well-known phenomenon in altered oceanic crust or similar (Faure, 1986; Rollinson, 1993; Kelly et al., 2001), and remains the most viable explanation for the Pb isotope characteristics of the Washikemba Formation.

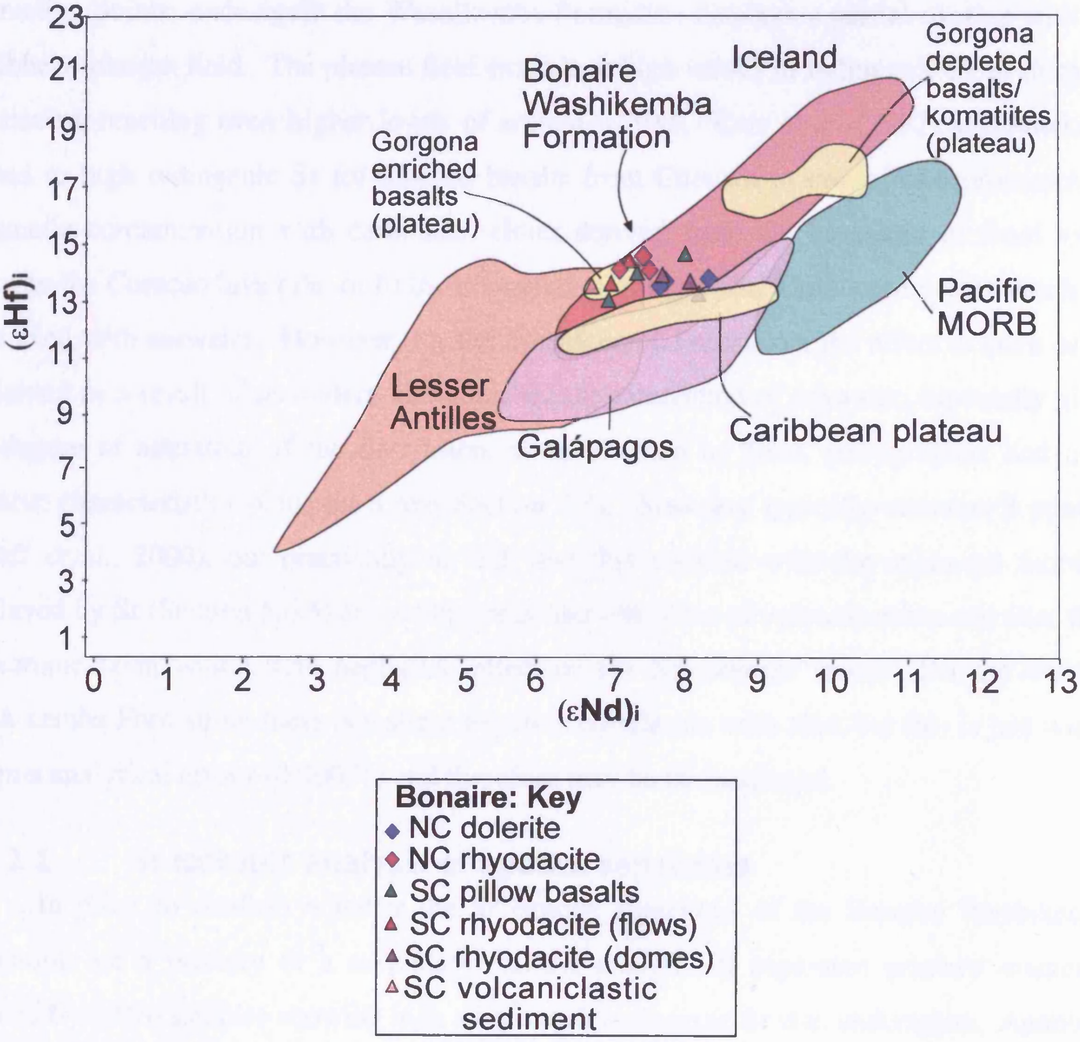

Fig. 5.26. Plot of initial εHf vs. initial εNd for samples from the Bonaire Washikemba Formation with other fields shown for reference, all age corrected to the assumed age of emplacement (95 Ma for the Washikemba Formation; Section 4.3). Key as above. Caribbean plateau and Galápagos data from this study (Chapter 6). Lesser Antilles data from Patchett and White (1984), Iceland data from Kempton (unpubl.) and Pacific MORB data from Nowell et al., 1999.

5.8.2. Sr –Nd systematics

A plot of initial $^{87}Sr/^{86}Sr$ vs. initial εNd is shown in Fig 5.25a. It demonstrates several interesting points: once again the Washikemba Formation displays a partial overlap with the Caribbean plateau field. The plateau field extends to high values of radiogenic Sr, as does the Formation, reaching even higher levels of around 0.7065. Kerr et al. (1997) attributed this spread to high radiogenic Sr for leached basalts from Curaçao to one of two processes: a) magmatic contamination with carbonate, either derived from the basement or from lower down in the Curaçao lava pile, or b) the assimilation of high $^{87}Sr/^{86}Sr$ altered basalt which has interacted with seawater. However, for the Washikemba Formation, the effect is more easily explained as a result of secondary alteration via the interaction of seawater, especially given the degree of alteration of the Formation, as ascertained by field, petrographic, and trace element characteristics (Chapter 3 and Section 5.3). Seawater typically contains 8 ppm Sr (Hauff et al., 2000), but practically no Nd, and this coupled with the enhanced mobility displayed by Sr (Section 5.6.5) ensues that seawater alteration of volcanic rocks can alter their Sr isotopic composition with negligible effect on the Nd isotopic ratios. For the Bonaire Washikemba Formation, there is a slight negative correlation with εNd, but this is just within 2 sigma analytical error (~0.00001) and therefore may be co-incidental.

5.8.2.1. Sr isotopic analysis of apatite separates

In order to confirm whether the Sr isotope signatures of the Bonaire Washikemba Formation are a primary or a secondary feature, analysis of separated primary magmatic apatites from two samples showing high whole rock radiogenic Sr was undertaken. Apatite is of particular use as it contains reasonable concentrations of Sr (~300 ppm for felsic rocks; Sha and Chappell, 1999), and is likely to remain unaltered even when the whole rock is extensively altered. Metamorphic apatites can also occur, but these are usually distinguished by their less acicular form and occurrence in more metamorphosed areas of the rock. Details of the technique used for sample selection, mineral separation and isotopic analysis is presented in Appendix E.

Apatite separated from two samples was analysed in this study. Both samples yielded much lower Sr isotopic ratios for the apatites alone than for the whole rock (Fig. 5.25b). The Nd isotopic ratio, however, remained almost identical (within analytical error), providing evidence that the Sr isotopic system has been reset due to alteration processes, whilst the Nd isotope systematics appear robust.

5.8.3. Nd-Hf systematics

Nd and Hf isotopes are thought remain immobile during moderate degrees of alteration (Pearce et al., 1999). The Sr-Nd isotopic study of apatite mineral separates presented in Section 5.8.2 confirms the robustness of the Nd isotope system in the rocks of the Washikemba Formation. Hf isotopes coupled with Nd are therefore particularly useful in characterising the Washikemba Formation, especially when other isotopic systems may have been partially reset. The problem until now, however, has been a limited dataset for the Caribbean region as a whole, which restricts the usefulness of the plot, as no comparisons with other relevant Caribbean rocks can be made. Comprehensive Hf isotopic analysis of Caribbean plateau rocks was undertaken, therefore, in order to characterise it in εHf-εNd space, and is detailed in Chapter 6.

A plot of εHf vs. εNd (Fig. 5.26) displays the Washikemba Formation compared with the Caribbean plateau, Galápagos, Pacific N-MORB and Icelandic data. The Washikemba Formation plots as a coherent group within Hf-Nd space. The SC domes plot at the high εNd end of the cluster, and overlap with the NC rhyodacites, suggesting that their distinctive trace element composition is not due to source variation. This provides some support for the idea postulated in Section 5.6.4, that the SC rhyodacites are the product of a separate magmatic differentiation event from the rest of the sequence.

5.9. Geochemical constraints on the origin and evolution of the Bonaire Washikemba Formation

5.9.1. Geochemical evolution of the Northern Complex

All trace element data presented supports a consanguineous origin of all members of the Northern Complex. The Complex forms a continuous trend on element–MgO (Figs. 5.12–5.17) and element–Zr plots (Figs. 5.1–5.7), indicating a continuous magmatic series. In addition, on chondrite-normalised multi-element plots (Figs. 5.18–5.21), different lithologies from the Northern Complex possess similar patterns, albeit with different overall abundances of trace elements. This supports the idea that the members of the Northern Complex (Washikemba Formation, Bonaire) are all related through fractional crystallisation of a single basaltic parental composition. This is frequently cited as a mechanism of generating rhyolite (e.g. Thorpe et al., 1993).

This conclusion is consistent with trace element modelling using TRACE3 of Nielsen et al. (1988). This DOS-based program uses a series of mathematical iterations to calculate hypothetical major and trace element compositions of the liquid and mineral phases at various

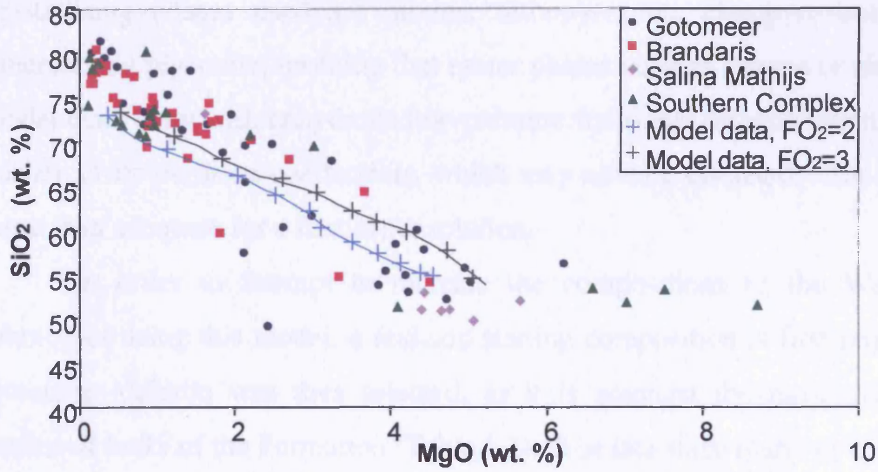

Fig. 5.27a. Plot showing results of modelling using TRACE3 (plotted as crosses) compared with the actual data for SiO2 and MgO. A fresh Salina Mathijs dolerite (BON 99-87) was used, with no assimilant. Further details of the modelling parameters are outlined below.

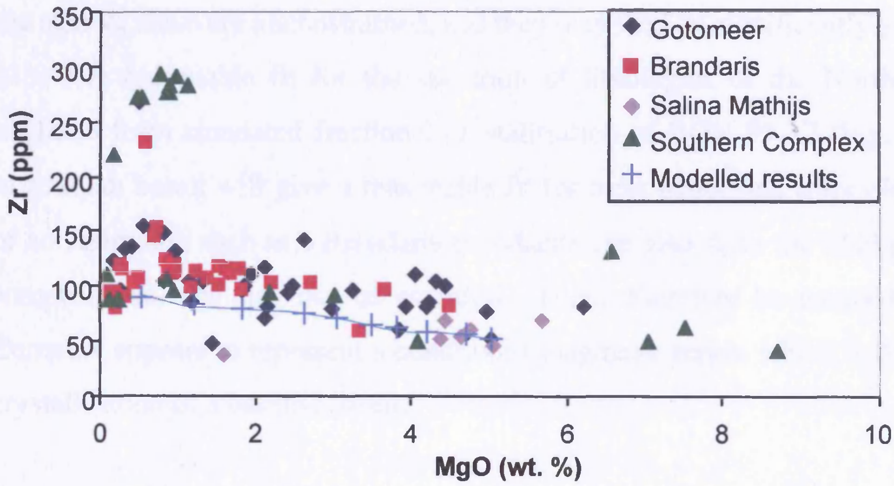

Fig. 5.27b. Plot showing results of modelling using TRACE3 (plotted as crosses) compared with the actual data for Zr and MgO. This model assumes an oxygen fugacity of +2, and no assimilant. Further details of the modelling parameters are outlined below.

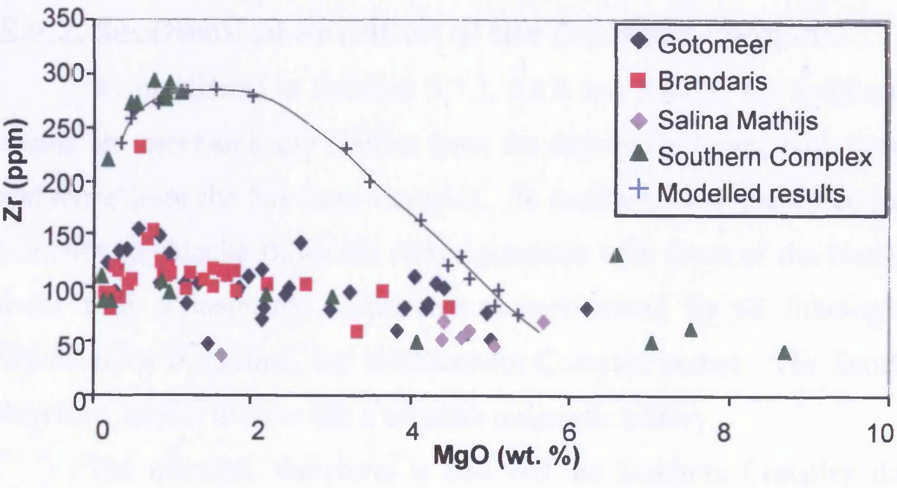

Fig. 5.27c. Plot showing results of modelling using TRACE3 (plotted as crosses) compared with the actual data for Zr and MgO. This model assumes an oxygen fugacity of +2, and extensive assimilation of a Caribbean Plateau basalt. Further details of the modelling parameters are outlined below.

Starting composition: a fresh Salina Mathijs dolerite, BON 99-87 was used. In Fig 5.27c, a Caribbean plateau sample from Curacao (CUR99-003) was used as an assimilant in the ratio 010 (i.e. no recharge, no eruption but assimilation of the same amount of material as that crystallised). This is probably not geologically reasonable, but illustrates that it is not possible to model such high Zr rhyodacites from fractional crystallsation using TRACE 3, unless geologically unreasonable parameters are used. FO_2=Oxygen fugacity, represented in log units above the QFM buffer.

crystallisation intervals, from any starting composition and using any assimilant. The crystallising phases used are olivine, orthopyroxene, clinopyroxene, plagioclase, spinel, ilmenite and pigeonite, meaning that minor phases such as sphene or zircon are ignored. The model deals only with anhydrous low-pressure fractional crystallisation, and is limited by the quality of its partition coefficients, which may now be outdated. The program is, however, more than adequate for a first order solution.

In order to attempt to recreate the compositions of the Washikemba Formation lithologies using this model, a realistic starting composition is first required. BON 99-87, a Gotomeer dolerite was thus selected, as it is amongst the most magnesian of the more unaltered rocks of the Formation (Table 5.1). The late stage mafic dykes were disregarded, as the ages of these are unconstrained, and they may well be significantly younger.

A reasonable fit for the spectrum of lithologies of the Northern Complex can be obtained from simulated fractional crystallisation of BON 99-87 (Fig. 5.27a), although any magnesian basalt will give a reasonable fit for most major and trace elements. The addition of an assimilant such as a Brandaris rhyodacite can also drive the final product to more felsic compositions, but may not be essential. It can therefore be concluded that the Northern Complex appears to represent a continuous magmatic series, which is derived from fractional crystallisation of a basaltic parent.

5.9.2. Geochemical evolution of the Southern Complex

As mentioned in Sections 5.3.2, 5.6.4 and 5.6.6.4, the Southern Complex rhyodacite domes are geochemically distinct from the rhyodacite flows, both those from the same area and those from the Northern Complex. In contrast, all evidence suggests that the Southern Complex rhyodacite flows are consanguineous with those of the Northern Complex. These rocks form a magmatic series that is represented by all lithologies from the Bonaire Washikemba Formation, bar the Southern Complex domes. The Southern Complex domes, therefore, appear to have had a separate magmatic history.

The question, therefore, is how did the Southern Complex domes originate? The rhyodacite domes are characterised by high Zr (typically three times that of the flows) along with elevated concentrations of most incompatible elements, including Nd, La, Y, and Nb. Trace element modelling using Nielsen's 1988 program (as detailed above) was unable to reproduce these geochemical compositions using the same parameters as for the Northern Complex, confirming that they represent a separate magmatic series. No starting composition from the Northern Complex will reproduce the high concentrations of Zr and other trace elements, without significant assimilation of another basaltic component. However, the only assimilant from the area that will reproduce these relatively enriched compositions is a Caribbean Plateau basalt from Curaçao (Fig 5.27c). An assimilation rate of 1 is required for optimum results, which means that the assimilation rate is equivalent to the crystallisation rate. This rate is thought to violate simple heat budget calculations (Nielsen, 1988) and therefore seems untenable. In addition, the Southern Complex rhyodacite domes are indistinguishable in terms of Hf-Nd isotopes from the rest of the sequence (Fig. 5.26) and yet the Caribbean Plateau has a distinct isotopic composition, implying that significant (if any) assimilation of plateau basalts did not occur. Thus, it is concluded that the Southern Complex domes have experienced a magmatic evolution distinct to the rest of the domes, and cannot be reproduced from a mafic parent through simple crystal fractionation models, nor through the coupled fractionation and assimilation of Caribbean Plateau. This theme will be discussed further, and alternative models presented in Chapter 7.

5.10. Relationship between the Northern and Southern Complexes

The two Complexes outcrop in completely different areas of Bonaire, and there is no obvious stratigraphic overlap between the two, nor does any field evidence suggest an obvious stratigraphic correlation. Whereas preliminary palaentological dating places the volcaniclastic rocks of the Northern Complex in the Upper Cretaceous, no such study has been completed on the Southern Complex, and in fact, it is only an assumption that they both represent part of the Washikemba Formation. Confirmation of this, and the determination of the relative stratigraphic level of each Complex relative to one another within the Washikemba Formation will therefore enable us to study the geochemical and volcanostratigraphical evolution of the arc sequence.

In terms of field relations, the two Complexes show broadly the same lithologies (rhyodacite flows and intrusives, volcaniclastic sediments, dolerites and basalts; see Chapter 3) but they vary substantially in terms of their abundance and distribution: pillow basalts are abundant in the Southern Complex, but are only found in two localities in the Northern Complex, and rhyodacite domes are unique to the Southern Complex, although sills predominate in the Northern Complex.

It is apparent that there are certain geochemical similarities between the two Complexes. Both Complexes are indistinguishable in terms of Hf-Nd isotope systematics (Fig. 5.26). Trace element geochemistry suggests that the Northern Complex rhyodacites are related to the mafic members through simple crystal fractionation (see Sections 5.9.1–5.9.2), and these are geochemically indistinguishable from the Southern Complex rhyodacite flows, thereby suggesting a similar magmatic origin for the two Complexes. It is likely therefore that the volcanic products from both Complexes (with the exception of the Southern Complex rhyodacites) were derived from the same volcano. The Southern Complex rhyodacite domes cannot represent part of the same crystallisation series (Section 5.9.2), but are isotopically indistinguishable from the bulk of the Washikemba Formation, implying a similar magmatic source.

Table 5.1. Geochemical parameters of model compositions used in liquid line of descent modelling (TRACE3; Nielsen, 1988). Na refers to samples not analysed.

	Starting composition: dolerite Salina Mathijs BON 99-87	**Assimilant:** dolerite Curaçao CUR 99-03
Na_2O	4.8	2.1
MgO	4.5	7.3
Al_2O_3	17.7	13.1
SiO_2	49.1	50.6
K_2O	0.6	0.1
CaO	8.1	11.4
TiO_2	0.7	1.1
Cr	23.2	90.9
FeO	6.1	7.7
Fe_2O_3	3.3	4.2
Ni	24.6	73.9
P_2O_5	0.1	0.1
MnO	0.2	0.2
Co	34.5	48.0
Sc	26.4	42.5
V	218.8	341.7
Sr	332.3	128.0
La	5.5	2.7
Ce	12.1	13.1
Nd	8.7	6.8
Sm	2.5	n.a.
Eu	0.9	1.0
Gd	2.7	3.9
Dy	3.1	4.0
Ho	0.7	n.a.
Er	1.9	2.6
Tm	0.3	n.a.
Yb	1.7	2.3
Lu	0.3	0.4
Y	19.9	20.6
Zr	60.4	61.1
Nb	1.5	5.0

Therefore, the entire Northern Complex and the Southern Complex rhyodacite flows, basalts and volcaniclastic sediments were derived from a central volcanic source, but the Southern Complex rhyodacite domes represent marginal flank vents which have a different geochemical character to the main volcanic source. Possible mechanisms for the generation of the distinct trace element geochemical characteristics displayed by the domes will be presented in the petrogenesis chapter (Chapter 7).

5.11. A comparison with other island arc rock series

All geochemical data so far suggests that the Washikemba Formation represents a typical island arc sequence. It seems logical therefore, to compare it with other island arc sequences in order to confirm this interpretation. Subduction zone signatures (Macdonald et al., 2000) are characterised by:

1. High water contents, as evidenced by the presence of hydrous phases such as hornblende and kaersurtite (Gill, 1981).
2. High oxidation states, expressed by high MgO/FeO ratios in mineral phases, and high Fe_2O_3/FeO whole rock ratios (Gill, 1981).
3. Enrichments of Large Ion Lithophile Elements (LILE) relative to LREE, Th and particularly the High Field Strength Elements (HFSE) (Tatsumi et al., 1986; Hawkesworth et al., 1993). This manifests itself as a positive Ba, Rb and K anomaly, and negative Nb anomaly relative to MORB.
4. Low abundances of Ni (Wilson, 1989).
5. Evidence for explosive eruptions (i.e. pyroclastic rocks)

Most of these above criteria are difficult to apply to ancient or altered rocks. In the lithologies of the Washikemba Formation, low temperature metamorphism means that primary hydrous mineral phases are either replaced, or are indistinguishable from secondary hydrous phases. Both MgO and FeO have been mobilised to some degree (Figs. 5.1–5.2), ruling out the second criterion, and in addition the LILE's have also been extensively mobilised (Fig. 5.3), limiting their use as a discriminant. In practice, therefore, negative Nb anomalies represent the best diagnostic indicator of a subduction zone signature.

Fig. 5.28 shows representative samples from the Washikemba Formation compared with a variety of arc-related rocks, and plotted on a MORB-normalised multi-element plot. As before, this plot excludes elements likely to be mobilised, such as the LILE's. It is evident that the Washikemba Formation displays the same overall trend as modern-day arcs. The

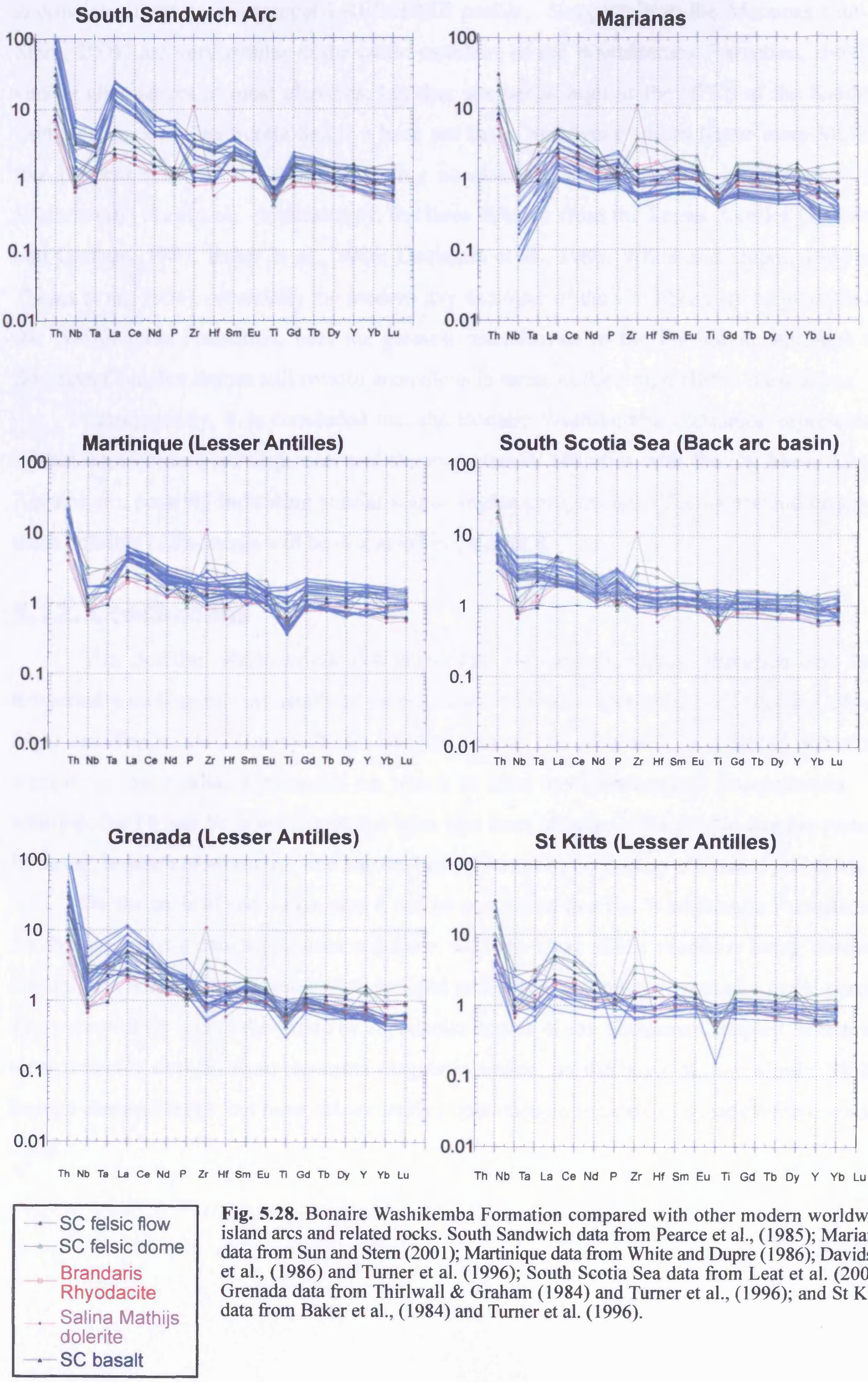

Fig. 5.28. Bonaire Washikemba Formation compared with other modern worldwide island arcs and related rocks. South Sandwich data from Pearce et al., (1985); Marianas data from Sun and Stern (2001); Martinique data from White and Dupre (1986); Davidson et al., (1986) and Turner et al. (1996); South Scotia Sea data from Leat et al. (2000); Grenada data from Thirlwall & Graham (1984) and Turner et al., (1996); and St Kitts data from Baker et al., (1984) and Turner et al. (1996).

South Sandwich arc (Pearce et al., 1985) displays similar patters of negative Nb and Ti anomalies, albeit with a steeper LREE/HREE profile. Samples from the Marianas (Sun & Stern, 2001) are very similar to the mafic members of the Washikemba Formation, showing similar abundances of most elements, but they are not as high as the HFSE of the Southern Complex domes. The Scotia Sea is a back arc basin, and hence shows flatter more MORB-like patterns (Leat et al., 2000), including no discernable Nb anomaly, in contrast to the Washikemba Formation. Interestingly, the three datasets from the Lesser Antilles (Thirlwall and Graham, 1984; Baker et al., 1986; Davidson et al., 1986; White and Dupré, 1986 and Turner et al., 1996), essentially the modern-day analogue of the Caribbean arc responsible for the Washikemba Formation, bear the greatest resemblance to the Formation, although the Southern Complex domes still remain anomalous in terms of their high HFSE abundances.

Consequently, it is concluded that the Bonaire Washikemba Formation represents a typical intra-oceanic arc sequence, and shows particular affinities with the Caribbean Lesser Antilles arc, possibly indicating similar source region components. The nature and origin of these possible components will be discussed in Chapter 8.

5.12. Conclusions

The Bonaire Washikemba Formation has suffered secondary alteration and low-temperature metamorphism, resulting in mobilisation in many elements, including K_2O, CaO, MgO and Fe_2O_3, the LILE's, Th, U, Ba, Rb, Sr and Pb. The REE and HFSE, therefore, remain the most reliable elements on which to base any geochemical interpretation. In addition, the Pb and Sr isotopic systems have also been affected. The Hf-Nd isotope system, however, is much more robust, and has not been affected by secondary alteration processes.

On the basis of these elements it can be concluded that the Washikemba Formation is for the most part a consanguineous sequence, with the more silicic members being obtained through fractional crystallisation of major (and probably anhydrous) phases of a mafic parent. The exception to this is the group of rhyodacite domes of the Southern Complex, which are most probably derived from the same magmatic source, on the basis of their similar Hf-Nd isotope characteristics, but have subsequently experienced a separate magmatic differentiation event.

Chapter 6

Hf-Nd isotope constraints on the origin of the Cretaceous Caribbean plateau and its relationship to the Galápagos plume

6.1. Foreword

This chapter has been formulated as a separate paper, submitted to *Earth and Planetary Science Letters*. The aim of this aspect of the study was to formulate a Hf-Nd isotope reference frame for the Caribbean region, in which to interpret the Bonaire Washikemba Formation, and thus, this work represents the first Hf-Nd isotopic study of the Caribbean plateau. In order to broaden the scope of the paper, it includes some introductory information about the Caribbean region already presented in Chapter 2, and in order to avoid duplication, the reader may wish to skip Sections 6.3 and 6.4. The co-authors on this paper are P. D. Kempton, R. V. White, A. C. Kerr, J. Tarney, A. D. Saunders and J. G. Fitton.

6.2. Introduction

The Caribbean plateau has played an important role in developing our understanding of oceanic large igneous provinces. It is unusual in that it has been tectonically uplifted, and portions are subaerially exposed, giving us an opportunity to study the three-dimensional structure of an oceanic plateau. Many workers have linked the Caribbean plateau to a "start-up" mantle plume (e.g. Duncan and Hargreaves, 1984), but there is no consensus as to which mantle plume is responsible. The Galápagos plume has, however, been repeatedly invoked (e.g. Kerr et al., 1996b; Sinton and Duncan, 1997; Hauff et al., 1997; Mauffret and Leroy, 1997; Lapierre et al., 2000; Hauff et al., 2000b). An absence of a clear plume track, probably because it has been subducted, has ensured that the relationship between the two can only be speculated upon without the use of geochemical fingerprinting. This problem is not restricted to the Caribbean plateau –the same dilemma applies to other Pacific large igneous provinces, including the Ontong Java Plateau (Mahoney and Spencer, 1991).

Although the Caribbean plateau is already well characterised in terms of trace elements and isotopes such as Sr, Nd and Pb (e.g. Hauff et al., 1997; Kerr et al., 1997; Lapierre et al., 1999; White et al., 1999; Hauff et al., 2000a; Lapierre et al., 2000), mobility of key elements during alteration, e.g., Sr and Pb, means that these isotope systems have been unable to resolve many important issues. In particular, is the Caribbean plateau the product of the Galápagos plume, and how do the apparently unique Gorgona rocks (including komatiites) relate to the other uplifted plateau sequences? These issues are vital for constraining plate reconstructions of the Mesozoic Caribbean and American region, and for evaluating the life cycle of mantle plume systems.

In this paper we use Hf-Nd isotope data to gain new insights into both the Cretaceous Caribbean plateau and the Galápagos mantle plume, in order to characterise their respective isotope systematics, and hence evaluate any relationship between the two. This technique has been successfully applied to other plume systems, for example the Iceland plume (Kempton et al., 2000). The relative immobility of Hf and Nd (compared to other isotopic systems) during alteration and metamorphism means that they are invaluable in tracing mantle sources and signatures in altered rocks (Pearce et al., 1999), and the long half-lives of Sm and Lu also mean that we can trace ancient (i.e. source?) characteristics rather than more recent magmatic differentiation processes. Hf and Nd isotopes thus can provide reasonably robust information about the source characteristics of altered plateau basalts.

Our new data suggest that both the Caribbean plateau and the Galápagos plume are compositionally heterogeneous, each comprising at least three distinct source components. Two of the three isotopic end members are common to both systems, suggesting that the Cretaceous Caribbean plateau is the product of the ancestral Galápagos mantle plume and therefore originated in the Pacific realm.

6.3. The Caribbean plateau

The Cretaceous Caribbean plateau comprises abnormally thick oceanic crust (15–20 km in places; Burke et al., 1978, Mauffret and Leroy, 1997; Case et al., 1990; Donnelly et al., 1990). It is approximately 12×10^5 km^2 in area, and forms much of the Caribbean plate (Fig. 6.1). Most of the plateau is presently submarine, meaning that the majority of sampling opportunities are through dredging and deep sea drilling (e.g. DSDP Leg 15), but portions of the plateau have been uplifted and accreted onto neighbouring continental margins, providing a unique insight into its deeper levels. The island of Gorgona, for example, contains what is interpreted as an obducted plateau sequence (Kerr et al., 1996; Arndt et al., 1997), which includes the only known example of Phanerozoic komatiites (Echeverría et al., 1980).

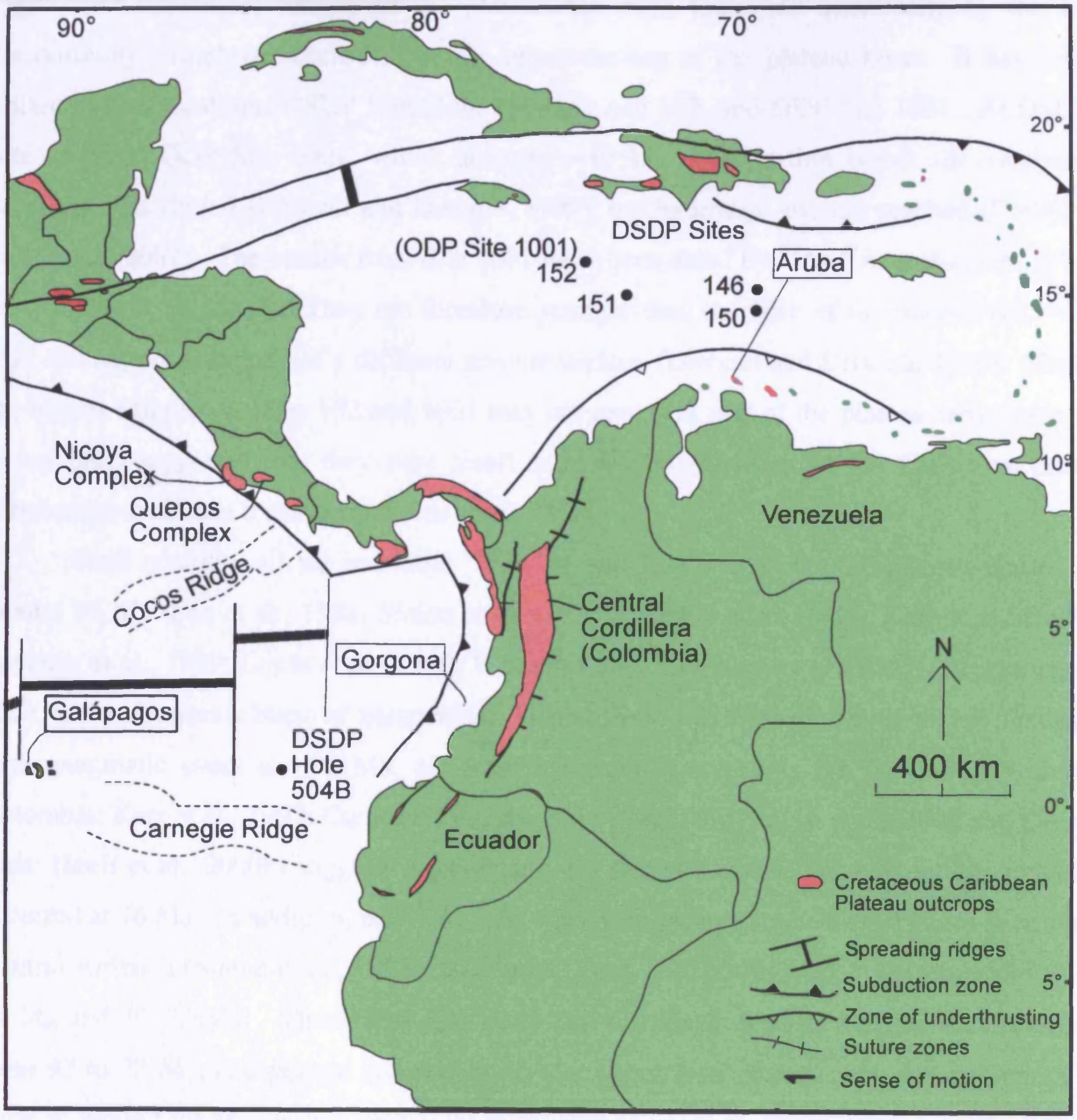

Fig. 6.1. Tectonic map of the Caribbean showing sampling sites. After Mann et al. (1990); White et al. (1999) and Hauff et al. (2000a). Boxed locality names denote sampling sites.

The uppermost surface of the plateau has been identified seismically by the B" discontinuity, which is inferred to be the upper surface of the plateau lavas. It has been drilled in five localities: DSDP Sites 146, 150, 151 and 153, and ODP Site 1001. At DSDP Site 152 and ODP Site 1001, which are only ~40 km apart, a thin basalt sill overlying basement was drilled (Driscoll and Diebold, 1999), but basement was not reached (Diebold, pers. com., 2001). The basalts from Site 1001 have been dated by ^{40}Ar-^{39}Ar techniques at 81 Ma (Sinton et al., 2000). They are therefore younger than the bulk of the plateau (i.e. ~90 Ma) and appear to be part of a different seismic horizon (Diebold and Driscoll, 1999). Thus, the basalts sampled at Sites 152 and 1001 may not represent part of the plateau *sensu stricto*. It has been suggested that they may result from late-stage rifting of the Caribbean crust subsequent to plateau formation (Sinton et al., 1998).

Until recently, all the available ^{40}Ar-^{39}Ar and Re-Os ages for the plateau clustered around 90 Ma (Sen et al., 1988; Sinton et al. 1993; Alvarado et al., 1997; Kerr et al., 1997; Lapierre et al., 1999; Lewis et al., 1999; Walker et al., 1999; Kerr et al., 2002), suggesting a short and voluminous burst of magmatism. Whilst there was undoubtedly a major plateau-wide magmatic event at ~90 Ma, abundant evidence from across the province (Western Colombia: Kerr et al., 1997; Curaçao: Sinton et al., 1998; Haiti: Sinton et al., 1998 and Costa Rica: Hauff et al., 2000b) suggests a secondary, but still voluminous, plateau-building phase occurred at 76 Ma. In addition, new ^{40}Ar-^{39}Ar ages from plateau sequences in Costa Rica and Central America (Sinton et al., 1997; Hauff et al., pers. com., 2001) fall in the ranges of 95–84 Ma and 76–72 Ma. These new ages show that Caribbean plateau magmatism occurred from 95 to 72 Ma, and peaked around 88–92 Ma, rather than occurring in one voluminous burst at around 90 Ma, as was originally postulated (Kerr et al., 1997; Sinton et al., 1998; Hauff et al., 2000b). A similar story is beginning to emerge for other large igneous provinces, for example the Kerguelen and Ontong Java plateaux (Nicolaysen et al., 2000). This has important implications for new models of plateau generation, as the simple starting plume head model (Richards et al., 1989; Griffiths and Campbell, 1990; Campbell and Griffiths, 1990; Hill, 1993) may no longer be applicable. Mauffret and Leroy (1997) and Révillion et al. (1999), for example, have invoked a multi-headed plume hypothesis to explain the age and geographical distribution of Caribbean plateau lithologies.

6.4. The Galápagos mantle plume

The Galápagos archipelago consists of a group of volcanic islands situated above the Galápagos plume. They are located ~100 km south of the Galápagos spreading centre, which is currently separating the Cocos and the Nazca plates (Figs. 6.1a&b). The spreading centre is

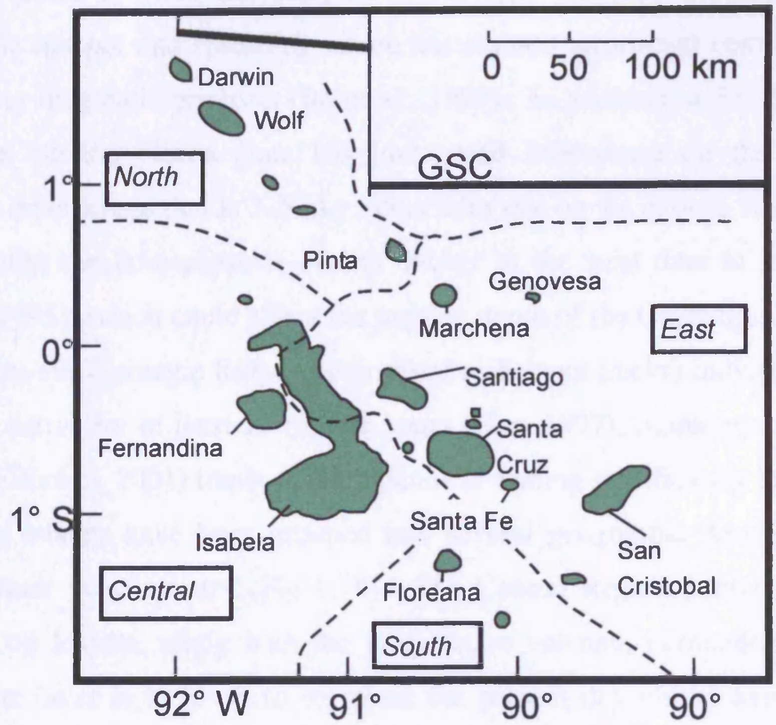

Fig. 6.1b. Map of the Galápagos islands, after Kurtz and Geist (1999). Geographic subdivisions are based on geochemical variations (McBirney et al., 1993). GSC is an abbreviation of Galápagos Spreading Centre.

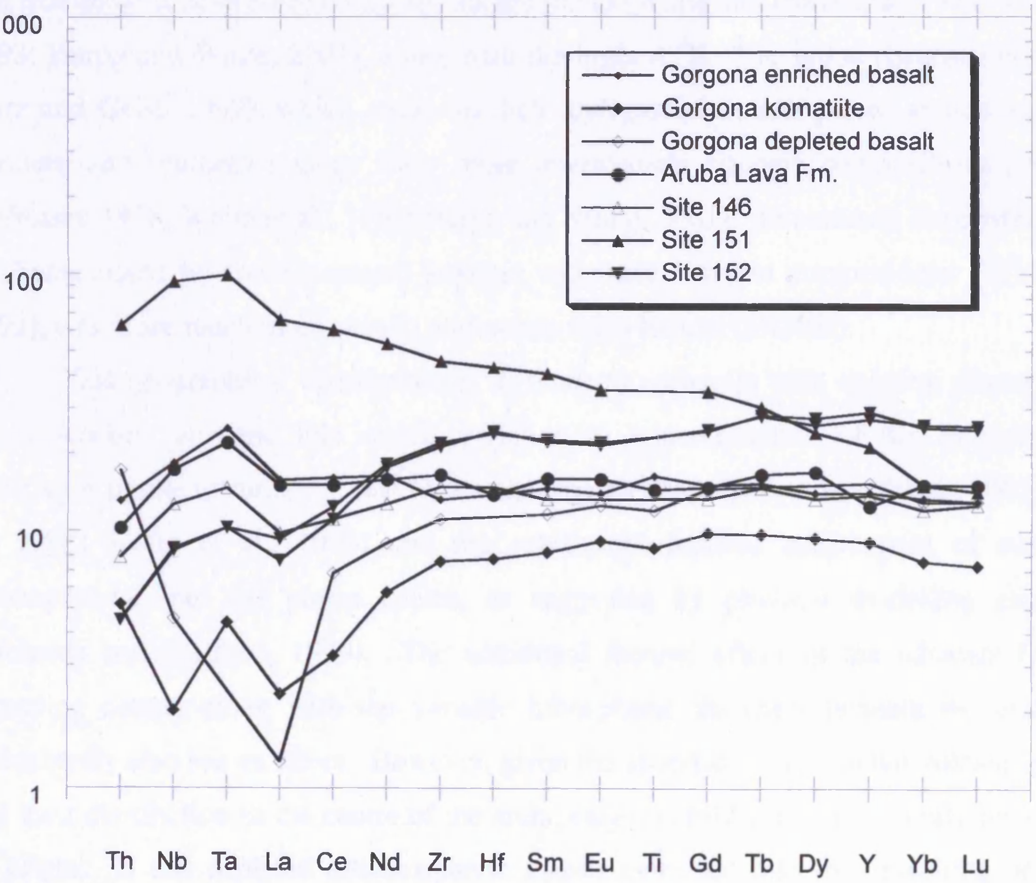

Fig. 6.2. Chondrite-normalised multi-element plot for Caribbean plateau samples using existing data. Data from Kerr et al. (submitted), White et al. (1999), Sinton et al. (1998) and Arndt et al. (1997). Normalising data from McDonough & Sun (1995). Note the extreme depletion of LREE displayed by the Gorgona komatiites and depleted basalts, and comparitive enrichment in LREE seen in basalts of DSDP Site 151. DSDP basalts also display depletion in LREE and similar $(La/Yb)_N$ ratios to Site 146.

thought to have overlain the hotspot ~8 Ma ago (Hey, 1977), and dynamic interaction between the hotspot and spreading centre has exerted significant control on the character of the resulting magmatic products (Ito et al., 1997). In addition, a 350 km sinistral transform fault offset on the Nazca plate has juxtaposed lithosphere on the western side of the Galápagos archipelago that is 3–5 m.y. older than that on the eastern side (White et al., 1993). Consequently, the lithosphere is ~6 km thicker in the west than in the east (Feighner and Richards, 1995), which could affect the melting depth of the Galápagos source. The presence of the Cocos and Carnegie Ridges (interpreted as hotspot tracks) indicate that the plume must have been active for at least 25 million years (Hey, 1977); moreover, new petrological data (Allan and Simkin, 2001) imply that the plume is waning significantly in intensity.

The islands have been grouped into several geographic domains (McBirney, 1993) based on their geochemistry (Fig 6.1b). The Central Region contains the majority of the volcanoes on Isabela, along with the most active volcano, Fernandina (Allan and Simkin, 2001). The latter is believed to represent the present day plume axis (White et al., 1993; Graham et al., 1993; Kurz and Geist, 1999). It is here that the most enriched trace element and isotopic (i.e. Sr-Nd-Pb) compositions are found (White and Hoffmann, 1978; White et al., 1993; Harpp and White, 2001), along with the highest $^{3}He/^{4}He$ ratios (Graham et al., 1993; Kurz and Geist, 1999), which attests to their undegassed mantle plume source region. The northern and southern regions show more intermediate isotopic compositions (White and Hofmann; 1978, White et al., 1993; Harpp and White, 2001). In contrast, the Eastern Region is characterised by more depleted isotopic and trace element compositions (White et al., 1993), which are much more akin to mid-ocean ridge basalts (MORB).

This geographical distribution is difficult to reconcile with existing plume theories. Many workers attribute this spatial variation to a combination of the dragging of the Galápagos plume towards the east by laminar mantle flow (Harpp and White, 2001; Geist et al. 1998; White et al., 1993) and the subsequent thermal entrainment of surrounding asthenosphere into the plume centre, as suggested by physical modelling experiments (Richards and Griffiths, 1989). The additional thermal effect of the adjacent Galápagos spreading centre, along with the variable lithospheric thickness beneath the archipelago, undoubtedly also has an effect. However, given the abundance of depleted volcanic products, and their distribution in the centre of the archipelago, considerable uncertainty remains as to its origin. Is this depleted asthenospheric mantle entrained into the upwelling plume or a depleted component intrinsic to the plume itself? Most workers agree that at least three components are required to explain the Galápagos system (White et al., 1993; Geist et al., 1998; Kurtz and Geist, 1999; Harpp and White, 2001), although new statistical analysis of

Galápagos lavas (Harpp and White, 2001) suggests that an additional minor component, characterised by elevated $^{207}Pb/^{204}Pb$ and $^{206}Pb/^{204}Pb$ for a given $^{208}Pb/^{204}Pb$, is also present. The nature of this component (or even confirmation of its presence) is unclear, as it is only defined in Pb isotope space.

6.5. Sampling strategy

For the purposes of this study, samples were selected from a wide range of Caribbean plateau-related outcrops, both submarine and subaerial. DSDP sites represent the only "in situ" plateau samples, and the others represent allochthonous uplifted plateau fragments now accreted onto the South American margin.

The DSDP samples are taken from three different sites (Table 6.1). The basalts at Site 146 are dated as part of the main plateau-building event at 90 Ma (Sinton et al., 1998), and exhibit essentially flat chondrite-normalised trace element patterns (Fig 6.2). Basalts from Site 151 show light and middle Rare Earth Element (REE) enrichments up to 100 × chondrite); these are undated. The basalts of Site 152, however, intrude Campanian (74–83 Ma; Harland et al., 1990) sediments (Edgar et al. 1971), and new ^{40}Ar-^{39}Ar dating of basalt from Site 1001 (located only 40 km from Site 152 and with similar trace element composition) yields ages of around 81 Ma (Sinton et al., 2000). These basalts show a depletion in light REE compared to the majority of the Caribbean plateau sequences.

The onland samples are from the Aruba Lava Formation, and the Gorgona komatiites and associated basalts. Each of these sequences is believed to represent a portion of the uplifted Caribbean plateau (Kerr et al., 1997; White et al., 1999), and are dated via ^{40}Ar-^{39}Ar methods (biostratigraphic methods for the Aruba Lava Formation) at around 90 Ma (Wiedmann, 1978; Kerr et al., 1997; Sinton et al., 1998). The Aruba Lava Formation displays flat chondrite-normalised REE patterns; the geochemical similarity and proximity to the well-characterised plateau sequence on Curaçao has led many workers (Beets et al., 1984; Klaver, 1987; White et al., 1999) to advocate that it may represent the top of the Curaçao sequence.

In contrast, the island of Gorgona boasts a heterogeneous mix of plateau-derived lithologies: komatiites, picrites, and basalts, with radiometric ages clustering around the age of the main plateau building phase at 88–91 Ma (Kerr et al., 1996b; Arndt et al., 1997). The komatiites, picrites and one basalt group are depleted in incompatible trace elements (in particular the LREE) relative to MORB. Another group of basalts, however, is geochemically distinct, with enriched patterns on chondrite-normalised trace element plots. In this study, Hf and Nd isotopes have been measured on a representative selection of these lithologies.

Galápagos lavas (Harpp and White, 2001) suggests that an additional minor component, characterised by elevated $^{207}Pb/^{204}Pb$ and $^{206}Pb/^{204}Pb$ for a given $^{208}Pb/^{204}Pb$, is also present. The nature of this component (or even confirmation of its presence) is unclear, as it is only defined in Pb isotope space.

6.5. Sampling strategy

For the purposes of this study, samples were selected from a wide range of Caribbean plateau-related outcrops, both submarine and subaerial. DSDP sites represent the only "in situ" plateau samples, and the others represent allochthonous uplifted plateau fragments now accreted onto the South American margin.

The DSDP samples are taken from three different sites (Table 6.1). The basalts at Site 146 are dated as part of the main plateau-building event at 90 Ma (Sinton et al., 1998), and exhibit essentially flat chondrite-normalised trace element patterns (Fig 6.2). Basalts from Site 151 show light and middle Rare Earth Element (REE) enrichments up to 100 × chondrite); these are undated. The basalts of Site 152, however, intrude Campanian (74–83 Ma; Harland et al., 1990) sediments (Edgar et al. 1971), and new ^{40}Ar-^{39}Ar dating of basalt from Site 1001 (located only 40 km from Site 152 and with similar trace element composition) yields ages of around 81 Ma (Sinton et al., 2000). These basalts show a depletion in light REE compared to the majority of the Caribbean plateau sequences.

The onland samples are from the Aruba Lava Formation, and the Gorgona komatiites and associated basalts. Each of these sequences is believed to represent a portion of the uplifted Caribbean plateau (Kerr et al., 1997; White et al., 1999), and are dated via ^{40}Ar-^{39}Ar methods (biostratigraphic methods for the Aruba Lava Formation) at around 90 Ma (Wiedmann, 1978; Kerr et al., 1997; Sinton et al., 1998). The Aruba Lava Formation displays flat chondrite-normalised REE patterns; the geochemical similarity and proximity to the well-characterised plateau sequence on Curaçao has led many workers (Beets et al., 1984; Klaver, 1987; White et al., 1999) to advocate that it may represent the top of the Curaçao sequence.

In contrast, the island of Gorgona boasts a heterogeneous mix of plateau-derived lithologies: komatiites, picrites, and basalts, with radiometric ages clustering around the age of the main plateau building phase at 88–91 Ma (Kerr et al., 1996b; Arndt et al., 1997). The komatiites, picrites and one basalt group are depleted in incompatible trace elements (in particular the LREE) relative to MORB. Another group of basalts, however, is geochemically distinct, with enriched patterns on chondrite-normalised trace element plots. In this study, Hf and Nd isotopes have been measured on a representative selection of these lithologies.

	Age	Lithology	Geochemical Character	ΔNb	References
Aruba Lava Formation	88-91 Ma	Basalts,	Flat chondrite-normalised patterns	+ve	White et al., 1999.
DSDP Site 146	88-91 Ma	Basalt flows	Flat chondrite-normalised patterns	+ve	Sinton et al., 2000.
DSDP Site 151	(88-91 Ma??)	Basalt flows	LREE and MREE enriched	+ve	Sinton et al., 2000.
DSDP Site 152	81 Ma	Basalt flows	LREE depleted	-ve	Sinton et al., 2000.
Gorgona Island	88-91 Ma.	Komatiites/ Picrites	LREE depleted	-ve	Kerr et al., 1996. Arndt et al., 1997. Walker et al., 1999.
	88-91 Ma.	Depleted Basalts	LREE depleted	-ve	
	88-91 Ma.	Enriched Basalts	LREE enriched	+ve	

Table 6.1. Table summarizing the location, lithology and geochemistry of Caribbean plateau rocks used in this study. For definition of ΔNb see text and Fig. 6.7.

6.6. Analytical Techniques

New trace element data were obtained by ICP-MS on a Perkin Elmer Elan 5000 at the University of Cardiff, Wales. 0.1g of rock powder was digested in concentrated HF. After evaporation the residue was dissolved with concentrated HNO_3, evaporated again and dissolved in 6 cm^3 of 5M HNO_3. The sample solution was accurately made up to 50cm^3 with deionised water and a 2cm^3 aliquot was spiked with a 100pb solution of Re and Rh and made up to 10cm^3 volume. A selection of international standard reference materials were used to calibrate the machine and W-2 was used as a drift monitor during analysis. Representative data are presented in Table 6.2. A complete data set is available from the authors on request.

Nd, Pb and Hf isotope ratios were determined at the NERC Isotope Geosciences Laboratory (NIGL). The data are presented in Table 6.2. Procedures used in the analysis of Nd, Pb and Hf isotopes are given in Royse et al. (1998), Kempton (1995) and Kempton et al., (2001). Nd was run as the metal species on double Re-Ta filaments using a Finnigan MAT 262 multicollector mass spectrometer in static mode. The effects of fractionation during runs were eliminated by normalising $^{143}Nd/^{144}Nd$ to a $^{146}Nd/^{144}Nd$ value of 0.7219. Sample values for $^{143}Nd/^{144}Nd$ are reported relative to an accepted value for La Jolla of 0.51186. Minimum uncertainty is derived from external precision of standard measurements that over the course of analysis average 43 ppm (2σ) for $^{143}Nd/^{144}Nd$. Pb isotopes were analysed on the VG P54

MC-ICP-MS, since this instrument allows us to correct for mass fractionation during the run using the Tl-doping method. We have used a $^{203}Tl/^{205}Tl$ value of 0.41876, which was determined empirically by cross calibration with NBS 981. All Pb isotope ratios have been corrected relative to the NBS 981 composition of Todt et al. (1996). Based on repeated runs of NBS 981, the reproducibility of whole rock Pb isotope measurements is better than ±0.01% (2σ).

Within-run standard error for Hf isotope measurements is normally less than 22 ppm (2σ). Minimum uncertainties are derived from external precision of standard measurements, which average 44 ppm (2σ). Replicate analysis of our internal rock standard, pk-G-D12, over the course of analysis yields 0.283050±12 (2σ, n=45), which is indistinguishable from our previously reported value determined by TIMS (Nowell et al., 1998) (0.283046±16, 2σ, n=9) and the previously reported value determined by PIMMS (0.283049±18, 2σ, n=27; Kempton et al., 2000). The data are corrected for mass fractionation during the run by normalization to $^{179}Hf/^{177}Hf$ of 0.7325 and are reported relative to an accepted value of JMC 475 of 0.282160, as recommended by Nowell et al. (1998).

6.7. Analytical Results

6.7.1. Sr-Nd-Pb isotopic characteristics of the Caribbean plateau basalts

The Caribbean plateau has a restricted range of εNd_i compositions, typically between +6 and +8 (Fig. 6.3), similar to other Pacific Cretaceous oceanic plateaux, e.g., Ontong Java and Manihiki, (Mahoney, 1987). Basalts that plot within this range include those from the Western Cordillera and Serranía de Baudo (Colombia), Curaçao, Aruba and Nicoya. Gorgona komatiites, however, are atypical in that they have much more depleted compositions, with εNd values (t= 90 Ma) ranging between +9 and +12. The Quepos terrane in Costa Rica, which some claim represents the oldest known manifestation of the Galápagos hotspot track (e.g. Hauff et al., 2000b), overlaps with the bulk of the plateau rocks in Nd-Sr isotope space. Of the DSDP samples, basalts from Site 151 have εNd_i of around +6. Basalts from Site 152 are more depleted, with εNd_i of above +10, and Site 146 plots within the main plateau cluster, with an εNd_i of +9.

$(^{87}Sr/^{86}Sr)_i$ shows a far greater range than εNd_i. Most plateau sequences have a $^{87}Sr/^{86}Sr$ composition ranging from 0.7035 to much more radiogenic values, up to 0.706 (e.g. Serranía de Baudo: 0.706, (Hauff et al., 2000a); Aruba: 0.7053, (White et al., 1999); Curaçao: 0.7045, (Kerr et al., 1996a); and Western Cordillera: 0.7045, (Hauff et al., 2000a). This spread to high levels of radiogenic Sr with little change in εNd has been attributed to several

Rock	Sample	Age in Ma	Sm	Nd	$^{147}Sm/^{144}Nd$	$^{143}Nd/^{144}Nd$ meas	$^{143}Nd/^{144}Nd$ init.	εNd	$^{206}Pb/^{204}Pb$	$^{207}Pb/^{204}Pb$	$^{208}Pb/^{204}Pb$
DSDP Site 151 basalt	15-151-15R-1, 110-113	88	5.94	24.34	0.1475	0.512947	0.512862	6.54			
DSDP Site 152 basalt	15-152-24R-2, 22-25	75	3.05	6.91	0.2669	0.513236	0.513105	10.95			
DSDP Site 146 basalt	15-146-42R-1, 29-32	88	2.26	6.43	0.2125	0.513111	0.512988	9.01			
DSDP Site 146 basalt	15-146-43R-3, 33-36	88	2.12	6.11	0.2098	0.513087	0.512966	8.57			
DSDP Site 146 basalt	15-146-43R-4, 90-93	88	2.12	8.60	0.1491	0.513077	0.512991	9.06			
Aruba Lava Formation	ARU 96-2	88	2.23	6.88	0.1962	0.512997	0.512884	6.97			
Aruba Lava Formation	ARU 96-30	88	1.61	4.86	0.2005	0.513013	0.512898	7.23			
Aruba Lava Formation	ARU 96-21	88	1.79	5.47	0.1979	0.513044	0.512930	7.87			
Gorgona depleted basalt	GOR 92-12 D basalt	88	2.31	5.28	0.2645	0.513135	0.512982	8.89	18.449	15.586	38.274
Gorgona depleted basalt	GOR 92-20 d bas	88	1.74	3.49	0.3014	0.513147	0.512973	8.71			
Gorgona komatiite	GOR 94-26 kom	88	1.19	2.44	0.2949	0.513226	0.513056	10.33			
Gorgona komatiite	GOR 94-29 kom	88	1.26	2.38	0.3201	0.513224	0.513039	10.00			
Gorgona komatiite	GOR 94-1 kom	88	1.38	2.95	0.2828	0.513197	0.513034	9.90			
Gorgona komatiite	GOR 94-19 kom	88	1.22	2.63	0.2805	0.513199	0.513038	9.97			
Gorgona picrite	GOR 94-32 picrite	88	0.59	0.87	0.4101	0.513294	0.513058	10.36			
Gorgona picrite	GOR 94-34 picrite	88	0.90	1.58	0.3444	0.51319605	0.512998	9.19	17.417	15.535	37.274
Gorgona enriched basalt	GOR 94-37 e basalt	88	2.40	7.48	0.1940	0.5129916	0.512880	6.89	18.855	15.576	38.590
Gorgona enriched basalt	GOR 94-38 e basalt	88	2.17	7.75	0.1693	0.51299538	0.512898	7.24	18.897	15.579	38.701

Rock	Sample	Age in Ma	Lu	Hf	$^{176}Lu/^{177}Hf$	$^{176}Hf/^{177}Hf$ measured	$^{176}Hf/^{177}Hf$ Init	εHf	Nb high prec. XRF	Zr high prec. XRF	Y high prec. XRF
DSDP Site 151 basalt	15-151-15R-1, 110-113	88	0.36	5.39	0.009467854	0.2830393	0.28302321	10.88			
DSDP Site 152 basalt	15-152-24R-2, 22-25	88	0.55	2.43	0.032085407	0.28320633	0.28315179	15.43			
DSDP Site 146 basalt	15-146-42R-1, 29-32	88	0.37	1.63	0.032177985	0.28312578	0.28307108	12.58			
DSDP Site 146 basalt	15-146-43R-3, 33-36	88	0.35	1.57	0.031601843	0.283117	0.28306328	12.30			
DSDP Site 146 basalt	15-146-43R-4, 90-93	88	0.31	1.53	0.028721966	0.28311558	0.28306676	12.42			
Aruba Lava Formation	ARU 96-2	88	0.37	1.35	0.038851789	0.28310502	0.28303897	11.44			
Aruba Lava Formation	ARU 96-30	88	0.27	1.14	0.033573943	0.28310961	0.28305254	11.92			
Aruba Lava Formation	ARU 96-21	88	0.26	1.06	0.0347705	0.28310981	0.28305071	11.85			
Gorgona depleted basalt	GOR 92-12	88	0.32	0.94	0.048258868	0.28325498	0.28317295	16.18	1.29	48.0	24.8
Gorgona depleted basalt	GOR 92-20	88	0.35	1.05	0.047253518	0.28326	0.28317968	16.42	0.93	43.1	25.0
Gorgona komatiite	GOR 94-26	88	0.22	0.95	0.03282876	0.28326	0.2832042	17.28	0.40	29.4	14.0
Gorgona komatiite	GOR 94-29	88	0.22	0.89	0.035041948	0.283262	0.28320243	17.22	0.44	31.5	15.1
Gorgona komatiite	GOR 94-1	88	0.204	0.923	0.031331739	0.283268	0.28321474	17.66	0.47	31.8	15.2
Gorgona komatiite	GOR 94-19	88	0.177	0.802	0.031286313	0.283261	0.28320782	17.41	0.44	28.6	13.6
Gorgona picrite	GOR 94-32	88	0.24	0.4	0.08505741	0.28332912	0.28318454	16.59	0.27	13.4	14.1
Gorgona picrite	GOR 94-34	88	0.2	0.36	0.078756758	0.28332198	0.28318811	16.71	0.34	15.1	13.4
Gorgona enriched basalt	GOR 94-37	88	0.38	1.64	0.032846229	0.28313898	0.28308315	13.00	4.69	61.6	24.3
Gorgona enriched basalt	GOR 94-38	88	0.32	1.35	0.033601849	0.28315398	0.28309686	13.49	4.16	56.9	22.9

Table 6.2. Isotope and trace element data for the Caribbean Plateau determined in this study.

possible factors. In a study of picrites and basalts from Curaçao, Kerr et al. (1996a) found that $^{87}Sr/^{86}Sr$ was not reduced by repeated leaching, and therefore argued that this is a primary feature, due to the assimilation of altered basalt. Révillion et al. (2001, submitted) found that unaltered clinopyroxenes from Gorgona had much lower values of radiogenic Sr than the whole rock, and therefore concluded that the displacement to high $^{87}Sr/^{86}Sr$ was the result of subsolidus alteration. Thus, interpretation of Sr isotope variations is ambiguous.

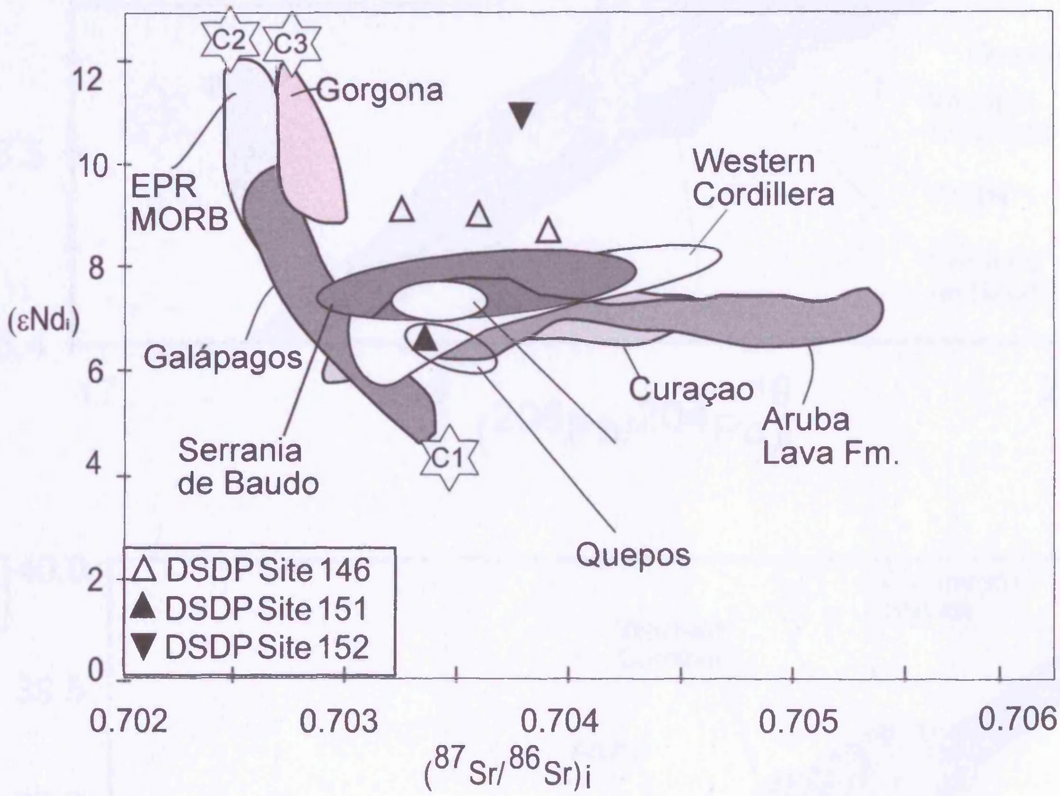

Fig. 6.3. εNd_i versus initial $^{87}Sr/^{86}Sr$ for various Caribbean plateau rocks compared with EPR MORB and the Galápagos Islands. Symbols C1, C2 & C3 refer to Caribbean endmembers referred to in the text. MORB data from Mahoney et al. (1993); Galápagos data from White et al. (1993). Other Caribbean data from Kerr et al. (1996b), White et al. (1999), Hauff et al. (2000a), Hauff et al. (2000b) and Kerr et al. (2002).

Pb isotope data are shown in Fig. 6.4. This figure shows that the majority of the basalts from the plateau plot within a restricted range, with a $^{206}Pb/^{204}Pb$ of 18.5–19.25, and a $^{207}Pb/^{204}Pb$ of 15.55–15.6 (Fig. 6.4a). Again, samples from Curaçao, Aruba and Serranía de Baudo appear to have very similar Pb isotopic compositions. The DSDP Site 151 sample also lies within this range. Basalts from Sites 152 and 146, however, appear to have elevated $^{207}Pb/^{204}Pb$, possibly due to post magmatic processes (Hauff et al., 2000a). Similarly, new data for four samples from Gorgona show a wide range in Pb isotope compositions, with $^{206}Pb/^{204}Pb$ ranging from 17.4 to 18.9 and significantly higher $^{207}Pb/^{204}Pb$ than other plateau rocks. A plot of $^{208}Pb/^{204}Pb$ vs. $^{206}Pb/^{204}Pb$ (Fig. 6.4b) shows a similar scenario: all samples from the plateau have a similar range in $^{208}Pb/^{204}Pb$, from ~38.2 to ~38.7. Within that array, the DSDP Sites are compositionally distinct: Site 151 has a more radiogenic isotope

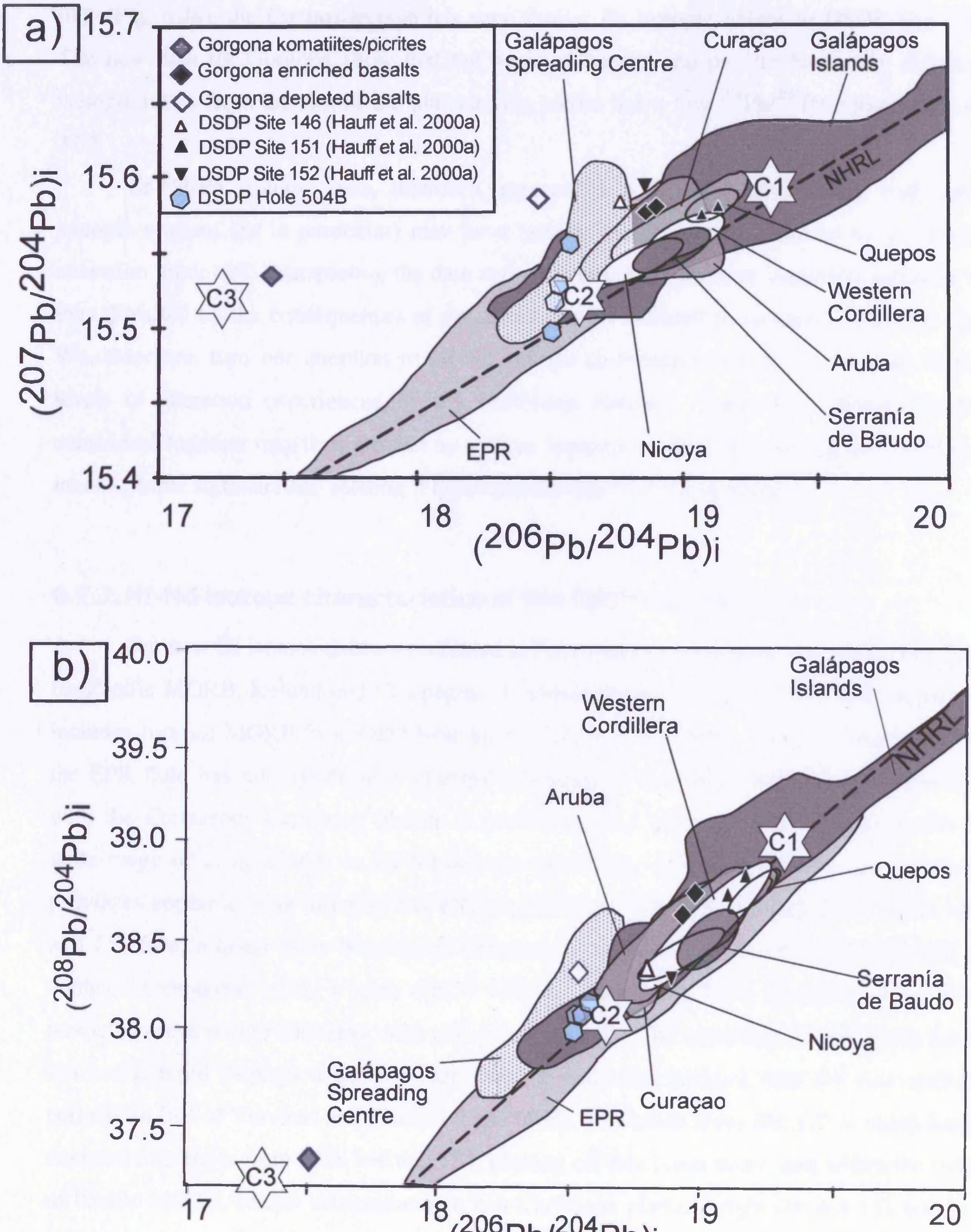

Figure 6.4. a) Initial $^{207}Pb/^{204}Pb$ versus $^{206}Pb/^{204}Pb$ for Caribbean plateau samples compared with EPR MORB and the Galápagos Islands. New data for Gorgona is un age corrected to to uncertainty about U-Pb concentrations. Symbols C1, C2 & C3 represent Caribbean plateau endmembers referred to in the text. b) Initial $^{208}Pb/^{204}Pb$ versus $^{206}Pb/^{204}Pb$ for Caribbean plateau samples compared with EPR MORB and the Galápagos Islands. EPR MORB data from Mahoney et al. (1993), Galápagos data from White et al. (1993). Other Caribbean data from Kerr et al. (1996), White et al. (1999), Hauff et al. (2000a), Hauff et al. (2000b), and Kerr et al. (2002).

composition ($^{206}Pb/^{204}Pb \approx 19.2$) than Sites 146 and 152. As also displayed on the $^{207}Pb/^{204}Pb$ plot (Fig. 6.4a), the Quepos terrane has very similar Pb isotopic values to DSDP Site 151. The new data for Gorgona show that the depleted basalts and picrites have very different isotopic ratios from the rest of the plateau –the picrite has a low $^{208}Pb/^{204}Pb$ composition of 37.3.

Sr-Nd-Pb isotopic data, therefore, present us with some ambiguities, and some isotopic systems (Sr in particular) may have been at least partially disturbed by secondary alteration processes. Interpreting the data and unravelling the primary magmatic signature is thus thwarted by the consequences of processes that are difficult to constrain quantitatively. We, therefore, turn our attention to Hf-Nd isotope systematics, which are resistant to the levels of alteration experienced by the Caribbean plateau. These two isotope systems considered together may thus provide us with an important tool in deciphering the Caribbean mantle plume signature and relating it to the present-day Galápagos plume.

6.7.2. Hf-Nd isotope characteristics of the Caribbean plateau

Our new Hf isotope data are presented in Figure 6.5 and compared with published data for Pacific MORB, Iceland and Galapagos. It should be noted that the EPR field displayed includes Jurassic MORB from ODP Hole 801C (Pearce et al., 1999). This demonstrates that the EPR field has not significantly changed composition over time, and hence comparison with the Cretaceous Caribbean plateau is justified. The Caribbean plateau encompasses a wide range of compositions in Hf-Nd isotope space (Fig. 6.5), and different geographical provinces appear to have different εHf-εNd compositions. The basalts from DSDP Sites 146 and 151 form a linear array between an enriched component ($\varepsilon Nd_i = +6$, $\varepsilon Hf_i = +8$) and a depleted component (εNd_i, $= +10$, $\varepsilon Hf_i = +13.5$). The Aruba Lava Formation plots in a restricted range within this array, with εHf of around +12. The combined DSDP-Aruba Lava Formation trend displays a positive slope with a shallower gradient than the crust-mantle correlation line of Vervoort and Blichert-Toft (1999). The basalt from Site 152 is much more depleted than those from Sites 146 and 151, plotting off this linear array, and within the field of Pacific MORB, further substantiating a non-Caribbean plateau origin for Site 152 basalts. The variable degree of depletion of Sm relative to Nd and Lu relative to Hf implied by the range of isotope ratios is consistent with the trace element geochemistry of these samples; for example, La/Yb, Sm/Nd and Lu/Hf ratios correlate well with εNd and εHf (see Table 6.2).

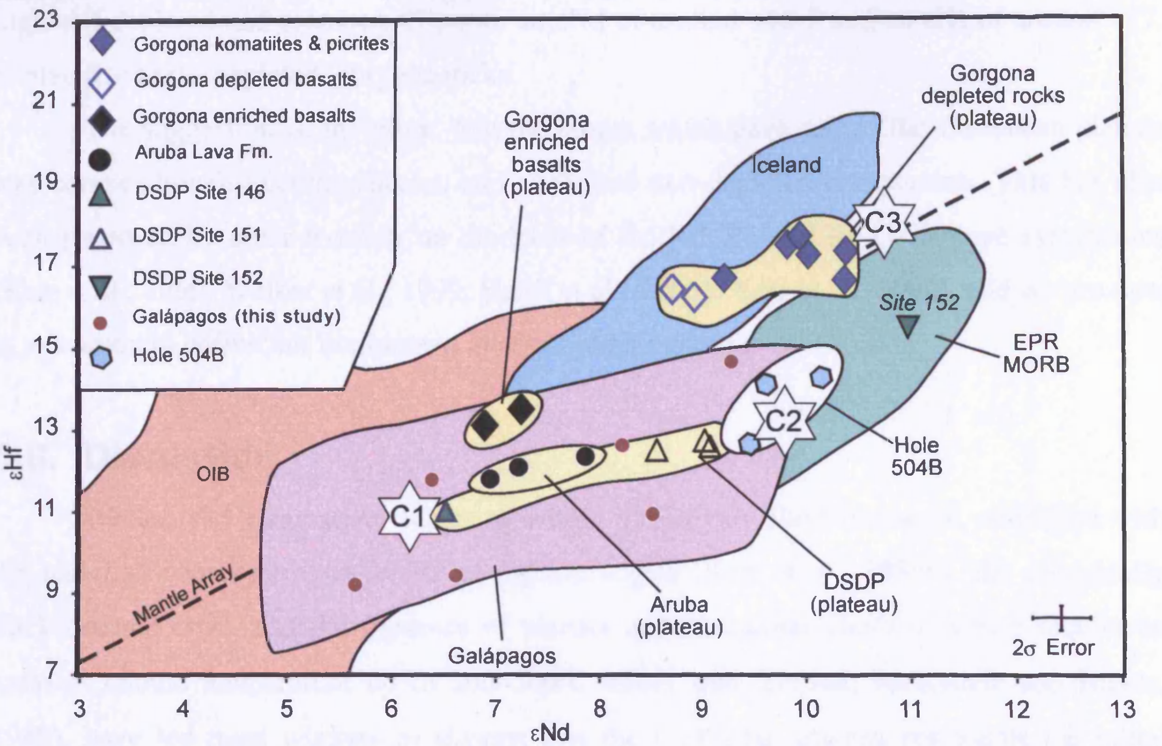

Fig. 6.5. Initial εNd vs. εHf for rocks of the Caribbean plateau and Galápagos islands, with EPR MORB, Iceland and existing Galápagos data (Blichert-Toft et al., 2001) fields shown for comparison. New data for DSDP Hole 504B is also presented. Symbols C1, C2 and C3 refer to Caribbean end members referred to in text. EPR MORB data from Kempton (unpublished), OIB data from Kempton et al. (2000) and Iceland data from Kempton (unpubl.). The Caribbean plateau is subdivided into geographical provinces: Aruba, drilled DSDP rocks, and both the depleted and enriched rocks from Isla Gorgona (Colombia). The fields of Aruba and DSDP Sites overlap, indicating derivation from a similar magmatic source. The Gorgona enriched basalts plot at the enriched end of the DSDP/Aruba array, albeit displaced to slightly higher eHf, and the depleted Gorgona rocks have distinctive depleted high εHf compositions. This requires a heterogeneous source for rocks of the Caribbean plateau, comprising at least three mantle components, including two isotopically distinct depleted ones.

Rocks from Gorgona plot in two distinct areas: komatiites, picrites and depleted basalts form a tight cluster with εNd_i between +9 and +10.5, and εHf_i between +15 and +17. The field is at the depleted end of the mantle array, but displaced to slightly higher εHf for a given εNd for all samples but one. Within this field, the komatiites and picrites plot at the high εNd, εHf end, whereas the "depleted basalts" (as defined by Kerr et al., 1995, and Arndt et al., 1997) have slightly less depleted εHf and εNd compositions. The enriched basalts from Gorgona plot as a distinct cluster at lower εHf-εNd (~+13 and ~+7, respectively), and overlap or lie just slightly above the "enriched" end of the Caribbean DSDP-Aruba array.

These data reveal that the Caribbean plateau is compositionally heterogeneous, and encompasses a wide range of Hf and Nd isotopic compositions. At least three end members must be invoked to explain the variation in Hf-Nd isotopic space (Table 6.2): one enriched end member, C1, with an εHf of around +11 and an εNd of around +6.5, one isotopically depleted end member, C2, with an εNd of around +10 and an εHf of around +13.5, and one high εHf depleted end member, C3, with an εNd of around +10.5 and an εHf of around +17, to give rise to the depleted Gorgona rocks.

The suggestion is, therefore, that the plume which gave rise to the Caribbean plateau was compositionally heterogeneous, and contained two depleted components. This has also been proposed by other workers on the basis of Sr, Nd, Pb and Re-Os isotope systematics (Kerr et al., 1999; Walker et al., 1999; Hauff et al., 2000a; Kerr et al., 2002), and we are now in a position to define this component in terms of Hf isotopes.

6.8. Discussion

Widespread magmatism occurring within a relatively short timescale, combined with the enriched geochemical character of the lithologies (Kerr et al., 1996b), the abnormally thick oceanic crust, and the presence of picrites and komatiites (both of which require an ambient mantle temperature up to 200–300°C hotter than normal; McKenzie and Bickle, 1988), have led most workers to suggest that the Caribbean plateau represents the initial outpourings from a mantle plume (e.g. Kerr et al., 1997; Sinton et al., 1998).

The isotopic and trace element data presented rule out a MORB-source region, and are consistent with a plume origin using the Nb-Zr-Y plot of Fitton et al., 1997 (Fig. 6.6). This geochemical discriminant has been used to great effect for the Icelandic plume system to distinguish between entrained MORB-sourced depleted mantle and a depleted component intrinsic to the plume. In Fig. 6.6, all plume-derived basalts from Iceland lie within two parallel lines (known as the Iceland array), whereas N-MORB plots outside. From this diagram, ΔNb can be defined as the deviation from the lower of the two parallel lines, i.e., a positive ΔNb indicates a plume-related source, whereas negative values relate to N-MORB. This diagram is independent of the degree and depth of partial melting and low-pressure fractional crystallisation, and hence discriminates between different mantle sources (Fitton et al., 1997) in most cases. In addition, the elements Zr, Nb and Y are amongst those most resistant to low temperature alteration processes. Fig. 6.6 shows that most basalts from the Caribbean plateau clearly plot within the Iceland array. Exceptions include the basalts from Site 152 and depleted basalts and komatiites from Gorgona, which plot slightly beneath the Iceland array, overlapping the field for the Reykjanes Ridge.

Consequently, the Nb-Zr-Y systematics of Caribbean plateau samples are consistent with a plume-derived origin, and are not sourced by MORB-like mantle unrelated to the plume, with the possible exception of basalts of Site 152, and the Gorgona depleted basalts and komatiites. For Site 152, this is substantiated by existing geochemical, geochronological and geophysical evidence (Sections 2, 6.2), and it would therefore appear that the basalts from

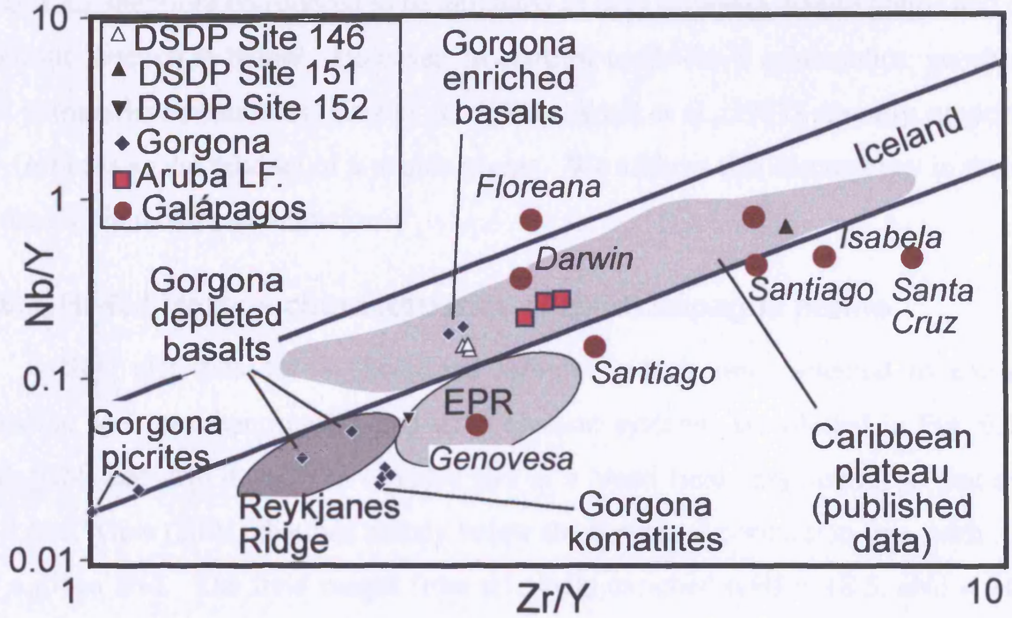

Fig. 6.6. Plot of Nb/Y vs. Zr/Y for Caribbean plateau samples from this study, with the Iceland array, East Pacific Rise (EPR) MORB and Reykjanes Ridge (south of 61°N) fields for reference (Fitton et al., 1997). Gorgona data was obtained by XRF at the University of Edinburgh, using extra-long count times. Aruba data from White (1999) and DSDP data from Marriner (unpubl.). ll Caribbean plateau basalts analysed plot within the Iceland array, denoting an enriched plume source, with the exception of depleted basalts, picrites and komatiites from Gorgona, and a ODP Site 152 basalt. The significance of this is explained in the text.

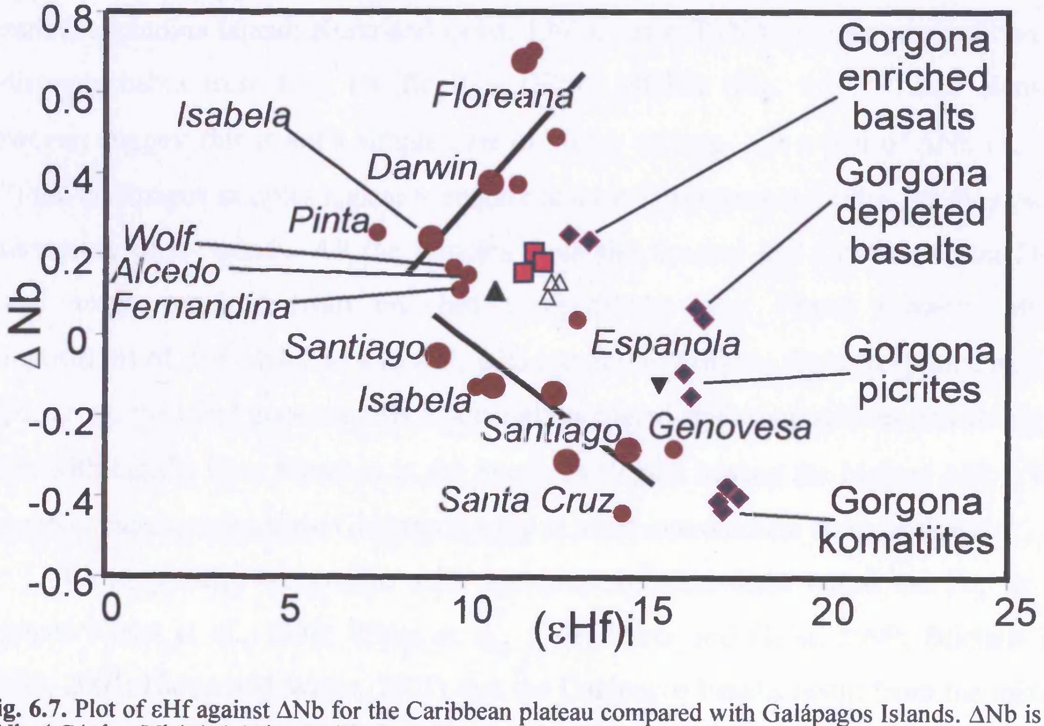

Fig. 6.7. Plot of εHf against ΔNb for the Caribbean plateau compared with Galápagos Islands. ΔNb is defined as ΔNb=1.74+log(Nb/Y)-1.92log(Zr/Y) from Fitton et al., 1997. For Galápagos, larger symbols denote new daya, smaller symbols denote data from Blichert-Toft and White, 2001. Galápagos trace element data is from Fitton (unpublished) and was obtained using the XRF at the University of Edinburgh with extra long count times. Other data sources as above. Lines denote two trend lines observed.

Site 152 are derived from a younger magmatic event, possibly associated with small scale rifting of the Caribbean crust, resulting in MORB-like geochemical affinities. Site 152 basalts are therefore considered to be unrelated to the Caribbean mantle plume and discounted from the discussion below. However, in contrast to Zr-Nb-Y systematics, geochronological and petrological arguments (Kerr et al., 1996b; Arndt et al., 1997) strongly support an origin for Gorgona as the product of a mantle plume. We address this discrepancy in the discussion of the Hf-Nd isotope systematics.

6.8.1. Hf-Nd isotope characteristics of the Galápagos plume

New εHf data for 8 Galápagos samples, which were selected to encompass the variation seen in other isotopic and trace element systems, are plotted in Fig. 6.5, together with published εNd data. The samples plot in a broad field very similar to that of Blichert-Toft and White (2001) that lies mainly below the terrestrial correlation line, with a lower εHf for a given εNd. The field ranges from relatively enriched (εHf = +8.5, εNd = +6) to more depleted MORB-like compositions (εHf = +14, εNd = +10). Samples from close to the modern-day plume centre situated under Fernandina (Kurtz and Geist, 1999) are the most isotopically enriched (e.g. samples from Sierra Negra, Isabella I), whereas with increasing distance from the hypothesised plume head the isotopic compositions become more MORB-like. For example, the island of Genovesa, situated ~150 km east of the hypothesised plume centre (Fernandina Island; Kurtz and Geist, 1999), has a Hf-Nd isotopic composition virtually indistinguishable from East Pacific Rise (EPR) MORB (Fig. 6.5). Trace element data, however, suggest this is not a simple case of binary mixing. On a plot of ΔNb vs. εHf, (Fig. 6.7) the Galápagos samples appear to require at least 3 component mixing, as they plot on two intersecting linear trends. All the samples from the Eastern and Central region fall on the lower array, trending from enriched compositions (e.g. Pinta) towards MORB-like compositions of -0.4 ΔNb and +15 εHf, with increasing distance from the plume axis. On the upper array, the trend goes towards moderately depleted εHf compositions and strong positive ΔNb, with basalts from Floreana in the Southern Region having the highest ΔNb. The trend appears to intersect the main Galápagos array at more intermediate compositions.

Consequently, we concur with previous interpretations based on Pb, Sr and Nd isotopes (Geist et al., 1998; White et al., 1993; Kurtz and Geist, 1999; Blichert-Toft and White, 2001; Harpp and White, 2001) that the Galápagos basalts result from the mixing of at least three components (Table 6.3). One component, G2, is a depleted MORB-like component, as represented by the samples from Genovesa Island; one is a moderately enriched, high ΔNb component sampled on Floreana (G3); and at least one is a low εHf component with intermediate ΔNb values. As both high and low $^3He/^4He$ ratios are associated with this low εHf component, it is likely that there are actually two separate enriched components with different $^3He/^4He$ ratios, G1a and G1b, as suggested by Blichert-Toft and White (2001) and White et al. (2001).

The depleted end member G2 is most likely entrained depleted asthenospheric mantle, as has been previously suggested (Geist et al., 1998; White et al., 1993; Hoernle et al., 2000; Blichert-Toft and White, 2001). The entrainment of this material into the plume would be facilitated by the close proximity of the Galápagos spreading centre, and the moderately fast plate movement of 4–5 mm per year (Gripp and Gordon, 1990), which could encourage laminar mantle flow.

The origin of the high ΔNb and high εHf Floreana end member (G3) is more problematic. Blichert-Toft and White (2001) put forward two hypotheses for the origin of the Floreana end member: it could signify a component of subducted marine sediment, which has resided in the mantle for a relatively short time (several hundred million years), based on its high $^{206}Pb/^{204}Pb$ composition, and high abundance of elements such as Ba, Ta, Rb, Sr, Th and Pb relative to the HFSE (Harrp and White, 2001). A second possibility is that the Hf and Nd isotopic systems may have become decoupled through mantle melting processes having occurred at a greater depth than usual, where garnet would be more abundant, increasing the (Lu/Hf)/(Sm/Nd) ratio of the residue. Neither of these scenarios is particularly satisfactory at explaining the high ΔNb characteristics, however, as the Zr-Nb-Y ratios are unlikely to be affected by either process. Harrp and White (2001) have suggested that the preferential enrichment in incompatible trace elements relative to Nd isotope ratios is due to the incorporation of metasomatic LREE-enriched fluids into the asthenosphere beneath Floreana, meaning that radiogenic ^{143}Nd has not had time to accumulate. This speculation is contradicted by the high εHf values of the Floreana end member, as ^{176}Hf should accumulate at an even slower rate than ^{143}Nd. We acknowledge that metasomatism, or more specifically, the involvement of hydrous phases such as amphibole, may play a role in generating these Floreana compositions, as amphibole can readily fractionate both Nb and Lu/Hf but not Sm/Nd (Moine et al., 2001). Amphibole can fractionate Lu/Hf by as much as 0.25, and Nb by up to four times. This could provide a mechanism for allowing ^{176}Hf and Nb to accumulate without ^{143}Nd, and thereby generating Floreana-like compositions (Table 6.3).

6.8.1.1. The depleted Caribbean plateau end members: entrained MORB mantle?

Trace element and isotope depletion is not traditionally associated with mantle plumes, which are generally considered to be enriched in incompatible trace elements. Recently, however, workers have identified depleted source components (distinct from MORB-source) in many plumes (e.g. Geldmacher et al., 2000). In Iceland, for example, Kempton et al. (2000) identified two distinct plume-related depleted components: one attributed to a depleted sheath of material entrained from the base of the upper mantle, and the other representing depleted streaks of material intrinsic to the plume itself. The depleted end members of the Caribbean plateau array could have arisen from either of these possibilities, and therefore be related to the plume itself. Alternatively, at least one of them could represent shallowly entrained MORB. The possible origins of both depleted end members are therefore discussed in detail below.

Basalts, picrites and komatiites from Gorgona have high εHf characteristics that are distinct from Pacific MORB, and are thus unlikely to represent entrained upper mantle. On Fig. 6.5 they overlap in Hf-Nd isotope space with basalts from Iceland and the Reykajnes Ridge, which are interpreted as being derived from, or associated with, a depleted plume source (Kempton et al., 2000). Recent studies (Révillion et al., in press) have shown the Gorgona picrites and komatiites to have high $^{3}He/^{4}He$, up to 18× atmospheric values, which indicates derivation from an undegassed, presumably deep, mantle source and precludes a shallow asthenospheric MORB-like source. All existing isotope and trace element evidence therefore suggests that the Gorgona rocks represent a very depleted end member intrinsic to the plume, derived from deep within the mantle. However, they do not appear to form the depleted end member for the main Caribbean plateau array (Figs. 6.5 and 6.6).

The main Caribbean depleted end member, C2, (Table 6.3) has an isotopic composition which overlaps with Pacific MORB in εHf-εNd isotopic space (Fig. 6.5), and appears to be isotopically indistinguishable from basalts from DSDP Hole 504B (Figs. 6.4 & 6.5). Is this depleted end member related to MORB, or does it represent a depleted plume-derived component, rather like that sampled at Iceland (e.g. Fitton et al., 1997)? On the main Caribbean array, the trend towards more depleted Hf-Nd isotopic compositions is not accompanied by a corresponding trend to more MORB-like values on the Zr-Nb-Y plot (Fig. 6.3), which might imply the endmember is distinct to MORB-source. However, binary mixing calculations between the hypothesised endmembers of the main Caribbean array (C1 and C2) suggest that the resulting mixing curve will not be linear in terms of Nb-Zr-Y systematics, and that a reduction in ΔNb will not be discernable until nearly 90% mixing with the depleted source has occurred. In fact, binary mixing of the enriched C1 endmember with a depleted basalt from DSDP Hole 504B (arguably a likely analogue, as suggested by the Hf-Nd-Pb isotopes) yields a mixing trajectory that overlaps with the actual Caribbean array in ΔNb-Hf space. The origin of the depleted component C2, therefore, is uncertain, but it at least resembles shallow entrained depleted upper mantle, and most likely is.

6.8.1.2. Implications for plume composition and differentiation

Our new εHf-εNd results indicate that the mantle source responsible for the formation of the Caribbean plateau was intrinsically heterogeneous, comprising at least three different components, including two distinct depleted ones. A potential flaw in this argument is the implicit assumption that the DSDP and Aruba samples are derived from the same plume as Gorgona. We consider that this assumption is justified, particularly given that the Gorgona suite appears to lie on a mixing line between the depleted C3 component and a component common to the main Caribbean array, the enriched C1 component, implying a related origin. This trend is also apparent for our new Pb data (Fig. 6.4). The identical ages for all of these different sequences further strengthens the connection between them. These components of the Caribbean plume are all detailed below, and summarised in Table 6.3:

C1. Enriched Caribbean end member. This has a ΔNb of >0, εHf_i of ≤+10, and εNd_i of ≤+6.5. It is best represented by samples from DSDP Site 151, and the enriched basalts from Gorgona. We interpret it as being derived from an enriched deep-seated mantle source, which has been tapped by an ascending mantle plume.

C2. Depleted main Caribbean end member. A depleted component with a similar Hf-Nd isotopic composition (εHf_i ~+13.5; εNd_i ~+10) to MORB, and which has mixed extensively with the enriched component to produce the main DSDP-Aruba trend. This component most likely represents depleted upper mantle material entrained onto the margins of the plume axis during its ascent though the upper mantle. This entrainment could have feasibly occurred deep at the base of the upper mantle or, alternatively, from shallow asthenospheric MORB.

C3. Gorgona depleted end member. A component with an even more depleted εHf composition than EPR MORB (εHf ~+17; εNd ~+10.5), as sampled by the Gorgona komatiites and depleted basalts, but with a negative ΔNb. This could be explained by a long-lived depleted source generated by partial melting during which a phase like garnet was residual, perhaps in the form of recycled MORB-source residue that has resided in the deep mantle for some time, allowing the $^{176}Hf/^{177}Hf$ ratios time to evolve to more radiogenic compositions, whilst retaining its MORB-like trace element compositions. A similar scenario has been suggested for the depleted high εHf basalts of the Reykajnes and Kolbeinsey Ridges

Name	$^{87}Sr/^{86}Sr$	$^{206}Pb/^{204}Pb$	$^{207}Pb/^{204}Pb$	$^{208}Pb/^{204}Pb$	^{3}He	εHf_i	εNd_i	ΔNb	Where sampled
Caribbean C1	0.7034	19.3	15.58	39.1	n.a.	+11	+6.5	>0 (+0.2)	DSDP Site 151
Caribbean C2	0.7024	18.5	15.51	38.1	n.a.	+13.5	+10	<0??	DSDP Site 146
Caribbean C3	0.7027	17.25	15.51	37.3	18.2	+17	+10.5	<0 (-0.5)	Gorgona komatiites
Galápagos G1a	0.7031	19.0	15.60	38.7	16.8	10	6.8	>0 (+0.1)	Fernandina
Galápagos G1b	0.7034	19.4	15.70	39.3	6.9	7	4.8	>0 (+0.2)	Pinta
Galápagos G2	0.7027	18.4	15.51	37.9	9?	15	9.9	<0 (-0.3)	Genovesa
Galápagos G3	0.7037	20	15.66	39.7	14	12.6	6.6	>>0 (+0.7)	Floreana

Table 6.3: Table showing principal geochemical components of the Caribbean plateau system, their compositions and where they are sampled. Galápagos ^{3}He data from Kurz & Geist (1999), Hf isotope data from this study and Blichert-Toft & White (2001), and other Galápagos isotope data from Blichert-Toft et al., 2001. Caribbean plateau data: this study, and other sources discussed in text. n.a. is an abbreviation for not analyed.

in Iceland, and possibly the Azores and Ascension Islands (Nowell et al., 1998; Kempton et al., 2000).

In fact, there appear to be many similarities between the Icelandic and Caribbean plume systems. Kempton et al. (2000) identified four individual components within the North Atlantic Igneous Province: 1) an enriched OIB-like component, 2) a depleted component with high εHf for a given εNd and with a ΔNb of near 0 or below and very high $^{3}He/^{4}He$ ratios, 3) a depleted component with a positive ΔNb, and 4) shallow MORB-source mantle that was present prior to plume emplacement. They envisaged the depleted component with positive ΔNb to be incorporated into the plume axis at great mantle depths (probably at the D" layer), along with the enriched component, resulting in partial mixing between these two components by the time the plume reaches the surface. The other depleted, high εHf component in the Iceland system is interpreted as hot depleted material entrained into the margins of the plume as it stalls at the transition zone between the lower and upper mantle, picking up an outer sheath from the thermal boundary layer above this discontinuity, before continuing to the surface.

A similar model may apply to the Caribbean plume system, with the main Caribbean enriched end member (C1) originating at the D" boundary and stalling at the 670 km discontinuity, gaining a depleted high ^{3}He outer sheath in the process. Although detailed modelling of the fluid dynamics involved is beyond the scope the this study, we would suggest as a hypothesis for future consideration that the Caribbean plume was less vigorous than Iceland. This could have encouraged greater entrainment of asthenosphere at shallow levels (Farnetani et al., 1995), resulting in an apparent binary mixing array between the C1 and C2 components.

6.9. The Caribbean plateau: a Galápagos source?

A Pacific origin for the Caribbean plateau is now almost universally accepted in recent literature (e.g. Burke et al., 1978; Pindell et al., 1988; Duncan and Hargraves, 1984; but see Meschede et al., 1998), especially with evidence such as the discovery of fragments of oceanic crust around the Caribbean region (e.g. Puerto Rico) that are closely associated with radiolarian chert containing fauna with a Pacific provenance (Montgomery et al., 1994).

Many petrologists cite the initiation of the Galápagos plume as the cause of this magmatism (e.g. Duncan and Hargarves, 1984; Richards et al., 1989; Hill, 1993; Hauff et al., 1997), an argument which is strengthened by the occurrence of the 65 Ma Quepos terrane, an accreted oceanic island complex on the Costa Rican margin that shares geochemical affinities with both the Caribbean plateau and the present day Galápagos islands (e.g. Sallares and

Danobeitia, 2001; Hauff et al., 2000b). This shows isotopic (Pb, Sr, Nd) and trace element similarities to both the neighbouring Caribbean plateau sequences found on the Costa Rican margin (e.g. the Nicoya Complex), and the Miocene Cocos and Carnegie aseismic ridges that are believed to form part of the Galápagos hotspot track (Hauff et al., 1997; Hauff et al., 2000b), hinting at a common origin for the Caribbean plateau, the Quepos Complex and the Galápagos islands. In addition, komatiites from Gorgona (Révillion et al., 2001; in press) and picrites from the Costa Rican Quepos Complex (Hauff et al., 2000b) both have high ^{3}He signatures: the Galápagos plume is one of the few plumes in existence today that also displays this feature (Graham et al., 1993), strengthening the connection between the Galápagos plume, the Quepos Complex, and the Caribbean Plateau.

Whilst trace element and existing isotope data for the Caribbean plateau support a Galápagos origin, the hypothesis nonetheless still remains controversial amongst tectonics workers. Recent kinematic and palinspastic reconstructions (Pindell, pers. com., 2001) suggest the Caribbean plateau formed much closer to the Americas than the Galápagos hotspot, which was as far away as 1000 km to the west at 90 Ma. In addition, as the oldest proven manifestations of the Galápagos plume are 15–20 m.y. old (Christie et al., 1992), yet the youngest Caribbean plateau sequences identified are at least 65 Ma (Sinton et al., 1998; Hauff et al., 2000b). This requires a long hotspot duration of >90 Ma (Sinton et al., 1998; Kerr et al., 1999; Walker et al., 1999), with an absence of any magmatic record for ca. 45–50 Ma of that time, possibly as a consequence of subduction at the Central American trench.

The εHf–εNd plot in Figure 6.5 gives us an insight into the relationship between the Caribbean Plateau and the Galápagos mantle plume. It is evident that the Galápagos field has a slightly shallower slope than the EPR MORB field, and is displaced to lower εHf and εNd. Hence there is little overlap between the two fields, unlike other isotopic systems (e.g. Pb). The DSDP and Aruba-defined Caribbean plateau array fit entirely within this field, along with the enriched Gorgona rocks. There is no overlap, however, with the depleted Gorgona basalts and komatiites. From this we can conclude that the Caribbean plateau is consistent with a Galapagos plume origin, as two of the end members required to explain the composition of the Caribbean plateau are also present in the Galápagos plume (Table 6.3). Component C1 is geochemically similar to Galápagos components G1a and G1b (distinguished on the basis of their ^{3}He ratios, for which no data exists for the C1 component), and component C2 is similar to component G2. The depleted Gorgona C3 component is not seen in the modern-day Galápagos plume, and equally, the distinctive Floreana G3 component of the Galápagos plume, which has high ΔNb (>0.6), and moderately high εHf is not recognised in the Caribbean plateau rocks. The former can be explained via the suggestion that the rocks on

Gorgona are believed to represent the ancient plumbing system of the Caribbean plateau (Révillion et al., 2000), and hence represent small magma batches that haven't been homogenised by magma chamber processes. They may feasibly sample plume compositions not preserved elsewhere. We must also consider that the Galápagos plume is thought to be waning in its intensity today, (Allan and Simpkin, 2001), and its isotopic composition may have changed over its >90 Ma history. Alternatively, there is far less Hf isotope data currently available for the older plateau rocks compared with the younger Galápagos samples, and it may be that this component, which is relatively rare in the Galápagos, has not yet been sampled among the older plateau sequences.

6.10. Conclusions

We have characterised the Caribbean plateau in terms of Hf-Nd isotopes in order to resolve the nature of its relationship to the Galápagos mantle plume. We have shown that the plume responsible for the Caribbean plateau was compositionally heterogeneous, comprising at least three distinct end members, including two depleted ones (Fig. 6.5). The enriched component appears to be typical OIB-source mantle. One depleted component has similar Hf-Nd isotopic characteristics to MORB. It has extensively mixed with the enriched component, forming the main Caribbean plateau array in εHf vs εNd.

The second depleted component is represented by the depleted basalts and komatiites on Gorgona, and is characterised by high εHf for a given εNd, negative ΔNb and high $^{3}He/^{4}He$ isotopic ratios [similar to the high εHf basalts sampled on the Reykjanes Ridge south of Iceland]. All evidence suggests that this component is related to the plume (high ^{3}He, high eruption temperatures); yet it has a depleted isotopic and trace element composition (and negative ΔNb), suggesting that it may represent depleted material entrained into the margins of the plume. This material was possibly derived from depleted mantle, which resides beneath the shallow convecting MORB-source asthenosphere. By analogy with Iceland (Kempton et al., 2000), this could be at the transition zone between upper and lower mantle.

New Hf isotopic data confirm that the Galápagos plume is also comprised of at least three, and probably four components, and overlaps almost entirely in Hf-Nd isotopic composition with the Caribbean plateau, with the exception of the depleted Gorgona rocks. This is consistent with the Caribbean plateau representing the initial outpourings from the ancestral Galápagos plume. The Gorgona komatiites and depleted basalts are unique in that they have been interpreted as the ancient plumbing system of the plateau, and most likely sample plume compositions not preserved elsewhere in the Caribbean-Galápagos system.

Chapter 7

Petrogenesis of the Washikemba Formation, and its relationship to the Caribbean Plateau

7.1. Introduction

In this chapter the geochemical data presented in Chapter 5 will be more fully interpreted, and integrated with field and geochronological information presented in earlier chapters. The aim of this chapter is to gain an insight into the petrogenesis of the Washikemba Formation and the geochemical nature of its source components. In particular, the relative importance of the mantle wedge, sediment and subduction components will be ascertained. An understanding of the source components of the Washikemba Formation, together with new geochronological and field constraints, will allow its relationship to the neighbouring Caribbean plateau and Aruba batholith to be evaluated. This will enable a model of the tectonic evolution of the Washikemba Formation to be constructed, so further constraining the Mesozoic evolution of the Caribbean region.

7.2. Summary of key constraints from earlier chapters

It was shown in Chapter 3 that there are two separate inliers of the Washikemba Formation: the Northern Complex and the Southern Complex. Both inliers are broadly lithologically similar, comprising intrusive dolerite, rhyodacite flows and sills and volcaniclastic sediments, but the Southern Complex is additionally noted for the presence of abundant pillow basalts and rhyodacite domes, the latter of which is completely absent in the Northern Complex.

In Chapter 4, new ^{40}Ar -^{39}Ar geochronological data yielded a minimum age of 95± 2 Ma for the Washikemba Formation, obtained from a rhyodacite sill in the Northern Complex. This is older than the bulk of the Caribbean plateau lithologies, along with the Aruba batholith, implying there is not a genetic link between the Washikemba Formation and the plateau.

As discussed in Chapter 5, the Formation represents a typical intra-oceanic arc sequence. It is believed to be broadly consanguineous, with the more silicic members being produced through fractional crystallisation of major (and probably anhydrous) phases from a mafic parent. The Southern Complex domes are geochemically unique, and cannot be accounted for by this process. It was speculated in Chapter 5 that the domes are from the same magmatic source as the rest of the Formation, but have experienced a separate differentiation event giving rise to the unique geochemical characteristics of the domes. In this Section 7.4, this model will be investigated and tested further, and alternative models presented.

7.3. Potential endmember magmas of the Washikemba Formation

In Chapter 5, it was shown that the Bonaire Washikemba Formation represents a Mesozoic intra-oceanic arc sequence, showing particular affinities with the modern-day Caribbean Lesser Antilles arc. In this section, the potential source compositions of the magmatic arc will be evaluated.

Most modern day models for the generation of arc magmatism invoke the modification of the mantle wedge by the addition of sediment (or sediment-derived melts) and aqueous fluids from the dehydrating slab (Arculus and Powell, 1986; Arculus, 1994; Davidson, 1996; Hawkesworth et al., 1994). This has the effect of lowering the solidus, thereby triggering partial melting of the mantle wedge. These partial melts may be then further modified in crustal magma chambers by fractionation (possibly combined with assimilation) processes, before being erupted in the island arc. The resulting volcanic products will be variable enriched in LILE's, U, Pb, and LREE relative to the HFSE. A generalised cartoon diagram showing the different subduction inputs is shown in Figure 7.1.

7.3.1. Mantle wedge

As illustrated in the cartoon described above and presented in Fig. 7.1, it is widely accepted that partial melting of the mantle above the descending slab, rather than the slab itself, is responsible for subduction zone magmatism, activated either by sediment-derived melts or aqueous fluids. In order to evaluate the sediment and fluid fluxes into the subduction zone, it is necessary to first consider the mantle wedge composition.

For the purposes of this discussion, and given that it is widely believed that the Caribbean arc system originated in the Pacific realm (Chapter 2), it is assumed that the presubduction mantle wedge of the arc responsible for the Washikemba Formation was Pacific MORB-source mantle. On a plot of εHf vs. εNd (Fig. 7.2a), the composition of Pacific MORB is well constrained from more than 40 analyses (Pearce et al., 1999; Kempton, unpubl.). Also plotted on this diagram are analyses of Mesozoic Pacific MORB from ODP Hole 801c (Pearce et al., 1999). All analyses of Mesozoic Pacific MORB fall within the modern day Pacific MORB field, thereby justifying the use of Pacific MORB as an analogue of the ancestral unmodified (presubduction) mantle wedge. Other possible mantle wedge compositions will be discussed in Section 7.5.1.1.

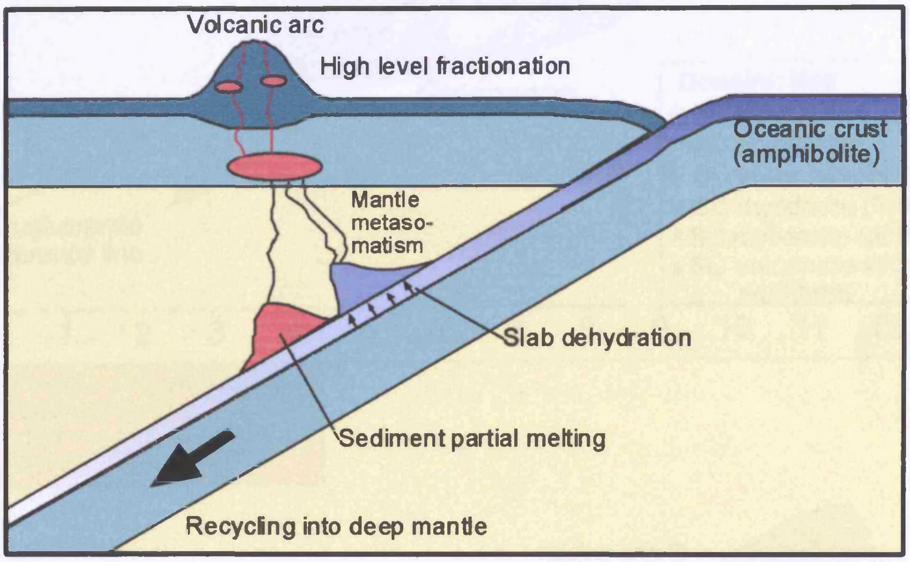

Fig. 7.1. Schematic cartoon showing process of generation of arc magmatism. After Wilson (1989) Davidson (1996) and Stolz et al. (1996).

7.3.2. Subducted sediment component

It is widely acknowledged that the trace element compositions of most arc sequences cannot be derived from simple melting of a typical MORB-source (e.g. Perfit et al., 1980; Arculus and Powell, 1986; Arculus, 1994; Davidson, 1994; Hawkesworth et al., 1994), but require the modification of the mantle wedge by the incorporation of slab-derived components. It is now becoming apparent that subducted sediment plays a role in arc magma genesis, as many isotopic tracers in arcs show a signature of subducted sediment (e.g. Kay et al., 1978; Sun, 1980; Ben Othmann et al., 1989; Patino et al., 2000). The discovery of high levels of ^{10}Be in arc lavas, for example, provides the strongest evidence of the presence of subducted sediments within arc magma sources (Tera et al., 1986; Edwards et al., 1993) as it has a solely cosmogenic origin, along with a comparatively short half life). In addition, two other indicators of the involvement of sediment in the source of island arc magmas are Pb isotopes and Ce anomalies. Most marine sediments contain very high concentrations of Pb relative to MORB (typically 20×; Davidson, 1996; Plank and Langmiur, 1998), ensuing that

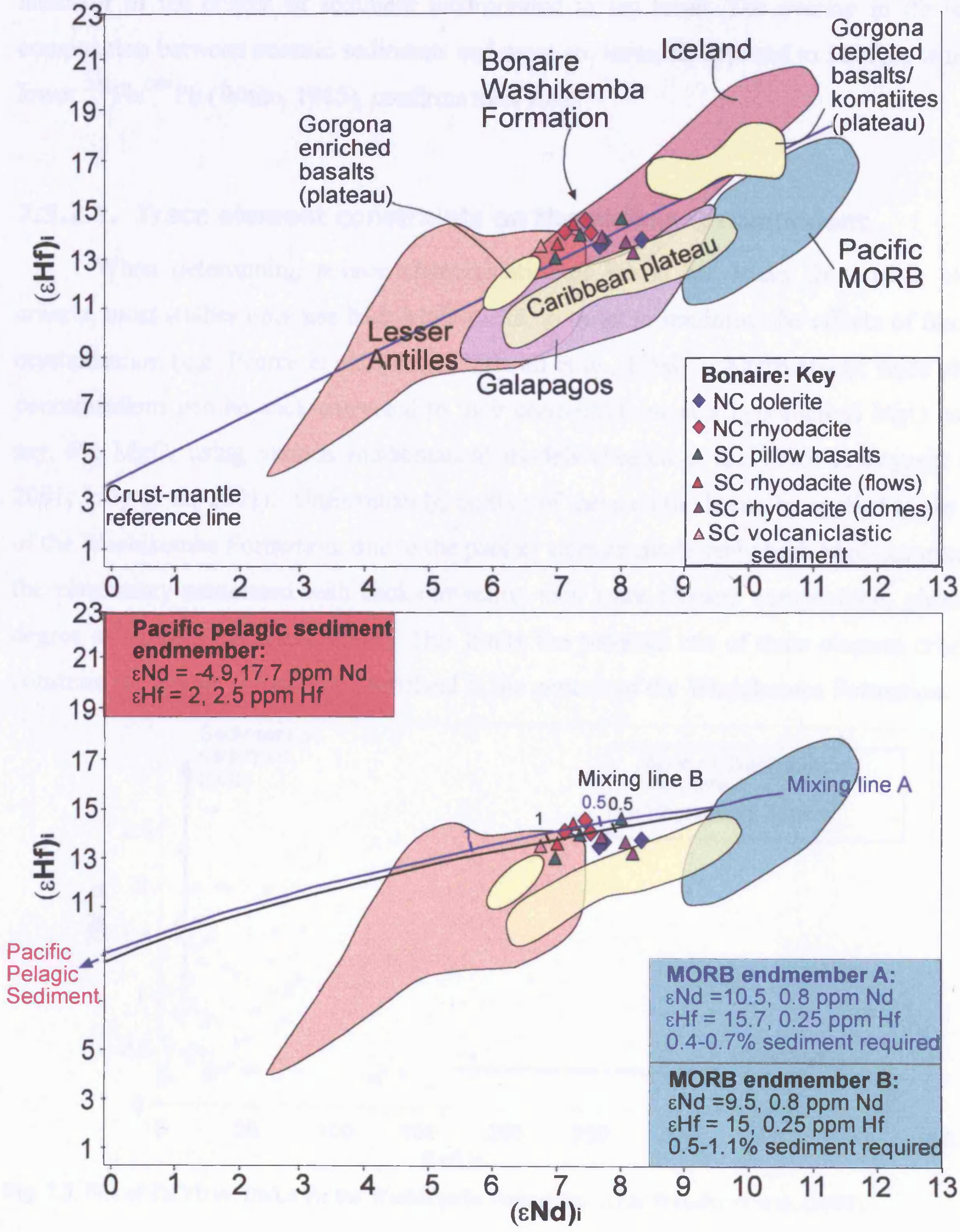

Fig. 7.2a. As presented in Section 5.8, plot of initial εHf vs. initial εNd for samples from the Bonaire Washikemba Formation with other fields shown for reference, all age corrected to the assumed age of emplacement. Data sources as for Fig. 5.27.

Fig. 7.2b. As above, but with sediment mixing lines drawn. Fields and annotations have been omitted for clarity. Mixing line A represents mixing between "average" MORB and "average" Pacfic pelagic sediment. Mixing line B represents a more realistic MORB endmember, with a slightly lower εHf and εNd. Pelagic sediment data from Pearce et al. (2000). Key as above.

Pb isotopes, providing that they have a distinct isotope composition, can provide a good indicator of the degree of sediment incorporated in arc lavas. The overlap in Pb isotopic composition between oceanic sediments and most arc lavas, as opposed to MORB, which has lower $^{207}Pb/^{204}Pb$ (White, 1985), confirms their role.

7.3.2.1. Trace element constraints on the sediment component

When determining source characteristics of island arc rocks from trace element criteria, most studies only use high MgO rocks, in order to minimise the effects of fractional crystallisation (e.g. Pearce et al., 1995; Thirlwall et al., 1996). Alternatively, trace element concentrations can be back-corrected to their concentrations at a hypothetical MgO content, say, 6% MgO, using various mathematical models (Pearce et al., 1995; Kobayashi et al., 2001; Jolly et al., 2001). Unfortunately, neither of these methods can be applied to the rocks of the Washikemba Formation, due to the paucity of even moderately high MgO samples, and the uncertainty associated with back-correcting their trace element composition, given their degree of alteration and evolution. This limits the potential use of trace element criteria to constrain the source components involved in the genesis of the Washikemba Formation.

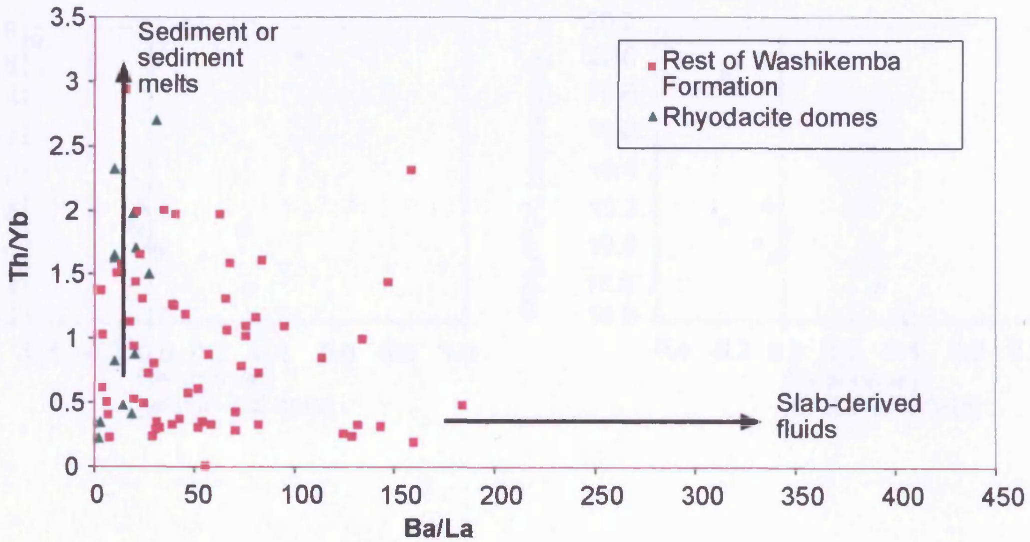

Fig. 7.3. Plot of Th/Yb vs. Ba/La for the Washikemba Formation. After Woodhead et al. (2001).

A plot of Th/Yb vs. Ba/La is frequently used as a method of distinguishing arcs dominated by sediment or sediment melts (high Th/Yb) from those dominated by slab-derived fluids (high Ba/La). Accordingly, the data from the Washikemba Formation is presented on such a diagram in Fig. 7.3. The Formation displays an approximately vertical trend, meaning that on the basis of this rationale, the subduction component of the Washikemba Formation is dominated by sediment rather than aqueous fluids. Interestingly, the present-day Lesser Antilles, along with the Sunda arc (Indonesia) also displays these characteristics, whereas the

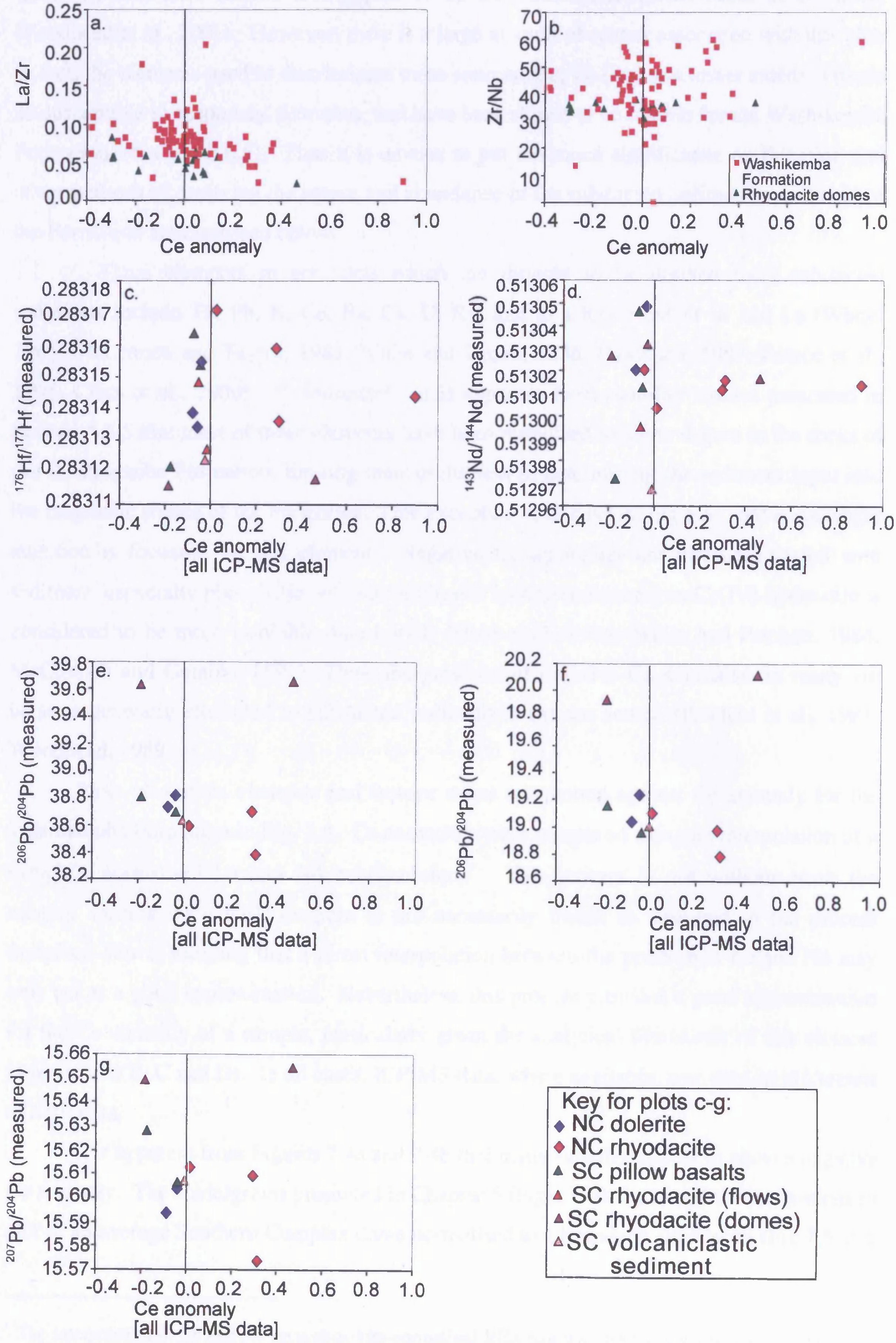

Fig. 7.4. Series of plots showing Ce anomalies vs. selected trace element (a, b) and isotope (c-g) parameters. Ce anomalies have been calculated from interpolation between La and Nd on REE plots.

Marianas and New Britain arcs appear to be fluid-dominated (MacDonald et al., 2000; Woodhead et al., 2001). However, there is a large amount of scatter associated with this plot. In fact, the elements used to discriminate these sources, Ba, Th (and to a lesser extent, Yb) are all susceptible to secondary alteration, and have been shown to be mobile for the Washikemba Formation. (Section 5.6.5). Thus it is unwise to put too much significance on this plot, and other methods of resolving the nature and abundance of the subducted sediment component of the Formation are discussed below.

Trace elements in arc lavas which are thought to be derived from subducted sediments include Th, Pb, K, Ce, Ba, Cs, U, Rb, and to a lesser extent Sr and La (White, 1985; McLennan and Taylor, 1981; White and Dupré, 1986; Davidson, 1987; Pearce et al., 1995; Class et al., 2000). Unfortunately, it is apparent from mobility studies presented in Section 5.6.5 that most of these elements have been mobilised to some degree in the rocks of the Washikemba Formation, limiting their usefulness in determining the sediment input into the magmatic source of the Formation. One exception to this is Ce (Fig 5.5), and accordingly attention is focussed on this element. Negative Ce anomalies are often associated with sediment, especially phosphatic red clay or abyssal marine sediments, as Ce(IV) hydroxide is considered to be more insoluble than La(III) (Hole et al., 1984; White and Patchett, 1984; McCulloch and Gamble, 1991) Thus, the presence of negative Ce anomalies in many arc lavas is generally attributed to subducted sediment in the arc source (Patchett et al., 1984; Woodhead, 1989.

Plots of various elements and isotope ratios are plotted against Ce anomaly for the Washikemba Formation in Fig. 7.4. Ce anomalies were computed using an interpolation of a sample's normalised La and Nd concentrations*. This process is not without error: the relative spacing on a REE diagram is not necessarily linear, as assumed in the process described above, meaning that a direct interpolation between the position of La and Nd may only act as a good approximation. Nevertheless, this process provides a good approximation for the Ce anomaly of a sample, particularly given the analytical limitations of this element (Appendices B, C and D). In all cases, ICP-MS data, where available, was used in preference to XRF data.

It is apparent from Figures 7.4a and 7.4b that many samples appear to show a negative Ce anomaly. The spidergrams presented in Chapter 5 (Figs. 5.19–5.22) and the multi-element plot of an average Southern Complex dome normalised to a Brandaris rhyodacite (Fig 7.5, red

* The interpolation of La and Nd on a chondrite-normalised REE plot was used to determine the expected Ce concentration, and the magnitude of the anomaly was determined relative to this, in a method similar to that discussed in Hole et al. (1984). The figure was then recalculated by subtracting 1 from it, so that 0 represented no anomaly, and positive values represented positive anomalies etc.

symbols) demonstrates that this feature is displayed almost exclusively by the Brandaris rhyodacites. However, as summarised in Chapter 5, these rhyodacites are otherwise geochemically indistinguishable from other Washikemba rhyodacites (with the exception of the rhyodacite domes), which are interpreted as fractionates of the Washikemba dolerites and basalts (Section 5.9.1). This makes an explanation for the origin of the Ce anomalies difficult, as they do not appear to correlate with any other geochemical parameter. As Figs. 7.4c–g demonstrate, there is little or no correlation between Hf, Nd or Pb isotope ratios and the magnitude of the Ce anomaly. It is thus considered that these anomalies are an artefact of analytical error. The reasons for this are as follows:

On Figs. 7.4a and b, it is evident that the magnitude of the anomalies scatter around a mean of zero, i.e. the amount of positive anomalies roughly correspond to the number of negative ones. The bulk of these data were obtained from XRF, as ICP-MS or ICP-OES data are not available. The low limit of precision for XRF analysis (6 ppm) means that much of the scatter in the data may be due analytical factors. This is supported by the fact that the Brandaris rhyodacites appear to more commonly display negative Ce anomalies than other lithological types- there are less ICP-MS and ICP-OES data available for this subgroup, meaning that XRF data may bias the dataset. However, plotting only ICP-MS and ICP-OES data does not necessarily eliminate the error. The determination of Ce anomalies involves accurate determination of Ce, La and Nd concentrations, and although XRF Ce data are significantly less reliable than other methods, for other elements such as La and Nd, ICP-OES data, at least, may not be significantly better (Appendices B, C). Accordingly, caution is placed on the over interpretation of Ce anomalies in this study.

7.3.2.2. Isotopic constraints on the sediment component

Pb isotopes are conventionally used as an index of sediment contribution to arcs (e.g. Smith et al., 1996; Peate et al., 1997; Ewart et al., 1998; Class et al., 2000; Munker, 2000 and Jolly et al., 2001), but are of limited use for the Washikemba Formation as unfortunately Pb appears to have suffered from secondary alteration processes (discussed in Section 5.6.5). Attention is therefore focussed on Hf-Nd isotope systematics.

Hf isotopes were originally considered to be resistant to subduction zone processes, meaning that they "see through" the effects of subduction, and hence can fingerprint the composition of the mantle wedge (Davidson et al., 1988; Pearce et al., 1999). A new study by Woodhead et al. (2001), of paired arc/back-arc settings, has revealed that Hf and HFSE are not as conservative as originally thought, and Hf isotopes almost always pick up a signature from the subducting slab. Nd isotopes have long been a useful tool in deciphering subduction components in arc lavas (Smith et al., 1996; Thirlwall et al., 1996; Davidson, 1997;

Encarnacion et al., 1999; Munker et al., 2000), thereby justifying the use of coupled Hf-Nd isotopes in unravelling the subduction signature of arc systems.

A Hf-Nd plot of the rocks of the Washikemba Formation is shown in Fig. 7.2a, based on the data presented in Section 5.8.3. Data from the Caribbean plateau, Iceland, Galápagos, Lesser Antilles and Pacific MORB (as an analogue of the ancestral mantle wedge) are also plotted, for reference.

The Washikemba Formation plots in a reasonably tight cluster in Hf-Nd space. This cluster is displaced distinctly to the lower εNd than the Pacific MORB field, and partially overlaps with the higher εHf-εNd portion of the Lesser Antilles field. If the Formation were to overlap with the Pacific MORB field, it would provide evidence that the mantle wedge was more or less unmodified by a subduction component, i.e. there was little or no sediment contamination of the Washikemba Formation. On the contrary, the displacement of the Formation away from the Pacific MORB field to lower εNd strongly implies the involvement of a low εHf-εNd component. Pelagic sediment has a low εHf-εNd composition, and is a possible candidate. This is supported by the overlap of the Washikemba Formation with the high εNd end of the Lesser Antilles field, as a role for sediment in the genesis of Lesser Antilles lavas is well known from numerous Pb, Sr, Nd and O isotopic studies (Thirlwall and Graham, 1984; White and Dupré, 1986; Davidson, 1995, 1996; Smith et al., 1996; Turner et al., 1996; Van Soest et al., 2002).

In fact, Fig. 7.2b demonstrates that the Washikemba Formation falls neatly on a simple mixing line (A) between average pelagic sediment (Pearce et al., 1999), and average Pacific MORB-source. The Nd and Hf concentrations of MORB mantle were approximated as follows, using the rationale of DePaulo and Johnson, 1979: For moderate degrees of melting, (i.e. the fraction of melt, F, is greater than 0.1, virtually all the incompatible elements go into the melt, and there is no relative fractionation of the REE (Hf, can be treated as a REE for the purposes of this calculation). The melt will therefore have the same REE pattern as the original source, with the concentrations increased by a factor of 1/F. As 10% melting is reasonable in a subduction zone setting, the trace element concentration of the mantle source will approximate F (i.e. 10%) of MORB.

Using these parameters (outlined on Fig. 7.2b), approximately 0.4–0.7% of sediment is required in the source of the Washikemba Formation volcanics. This is typical of most arcs. In order to assess the dependence of the model on the isotopic characteristics of the mantle source, a second mixing line is therefore presented, (B), using a mantle wedge more similar in isotopic composition to the Washikemba Formation. This yields slightly greater estimates of 0.5–1.1% of subducted pelagic sediment in the source of the Washikemba Formation. It should be mentioned that the scatter of the Washikemba Formation samples along the mixing line does not necessarily represent varying amounts of sediment in the source. This model uses single points as endmembers, and realistically it is more likely that each endmember is actually a compositional range, accounting for the variability along the array.

7.3.3. Slab-derived fluid component

Although sediment is clearly an important subduction-derived component in island arcs, in many cases mixing between likely sediment compositions and MORB fails to model the chemical composition of arc lavas (White and Dupré, 1986; Davidson, 1987). Many features of island-arc rocks cannot be explained without the involvement of hydrous fluids, for example the relative abundance of LILE's, Cl, H_2O, Sr, Ba and B in typical arc lavas (Stolper and Newman, 1994; Turner et al., 1997; Peacock and Hervig, 1999, Woodhead et al., 2001). Unfortunately, a trace element evaluation of the nature of the slab-derived component (if any) in the magmatic source of the Washikemba Formation faces similar difficulties to the sediment component. The intrinsic feature of fluid-mobile elements means that they are susceptible to low-temperature alteration processes, and hence cannot be quantitively evaluated for the Washikemba Formation, for which fluid-mobile elements have been mobilised. Thus, a slab derived fluid component remains entirely possible, but unquantifiable, in the genesis of the Washikemba Formation magmas.

7.4. Generation of the rhyodacite domes

In Section 5.9, it was suggested that the Southern Complex rhyodacite domes, which show trace element characteristics distinct to the bulk of the Washikemba Formation, but indistinguishable Hf-Nd isotope characteristics, were derived from a similar magmatic source, but experienced a separate crystal differentiation event. However, trace element modelling using TRACE3 (Nielsen, 1988), failed to account for the unique trace element compositions of the domes via fractional crystallisation from a mafic parent. Here, the aim is to reconcile the trace element and isotopic data, and come up with a satisfactory model for the genesis of the Southern Complex rhyodacite domes, and their relationship to the rest of the Washikemba Formation.

7.4.1. Summary of the geochemical characteristics of the rhyodacite domes

To summarise from Chapter 5, the Southern Complex rhyodacite domes are characterised by higher abundances of HFSE and REE (e.g. Zr concentrations of ca. 300 ppm, as opposed to ~60 ppm for the rest of the Formation). Of the major elements, SiO_2 is lower than other rhyodacites, and Al_2O_3 higher, but this is likely to be a consequence of the constant sum problem, and the mobilisation of most other major elements such as MgO and FeO, rather than illustrating any true difference. The reader is referred to Table 7.1 for a summary of the main distinctive geochemical features of the domes.

Element	% abundance (normalised to average Southern Complex rhyodacite flow)
Nb	361
Zr	276
Ta	274
Cr	263
Hf	219
La	187
Nd	185
Ga	159
Pr	157
Y	143
Ti	92
V	85
Zn	77
P	73
Sc	69

Table 7.1: Percentage abundance of selected trace elements in the Southern Complex rhyodacite domes, normalized to an average Southern Complex rhyodacite flow.

Fig. 7.5 shows a multi-element plot for an average rhyodacite dome, normalised to firstly, an average Brandaris rhyodacite (red symbols), and secondly, a Southern Complex flow (green symbols). Both sets of normalising data show similar patterns: the Ce peak for the Brandaris rhyodacites should be ignored, as mentioned in Section 7.3.2.1, as this is likely to be an analytical artefact, due to the paucity of high-quality ICP-MS data affecting the mean. This illustrates that of the elements plotted, only P, Ti, Yb and Lu abundances are not more abundant in the rhyodacite domes than other Washikemba Formation rhyodacites. Possible mechanisms for generating these abundances are discussed below.

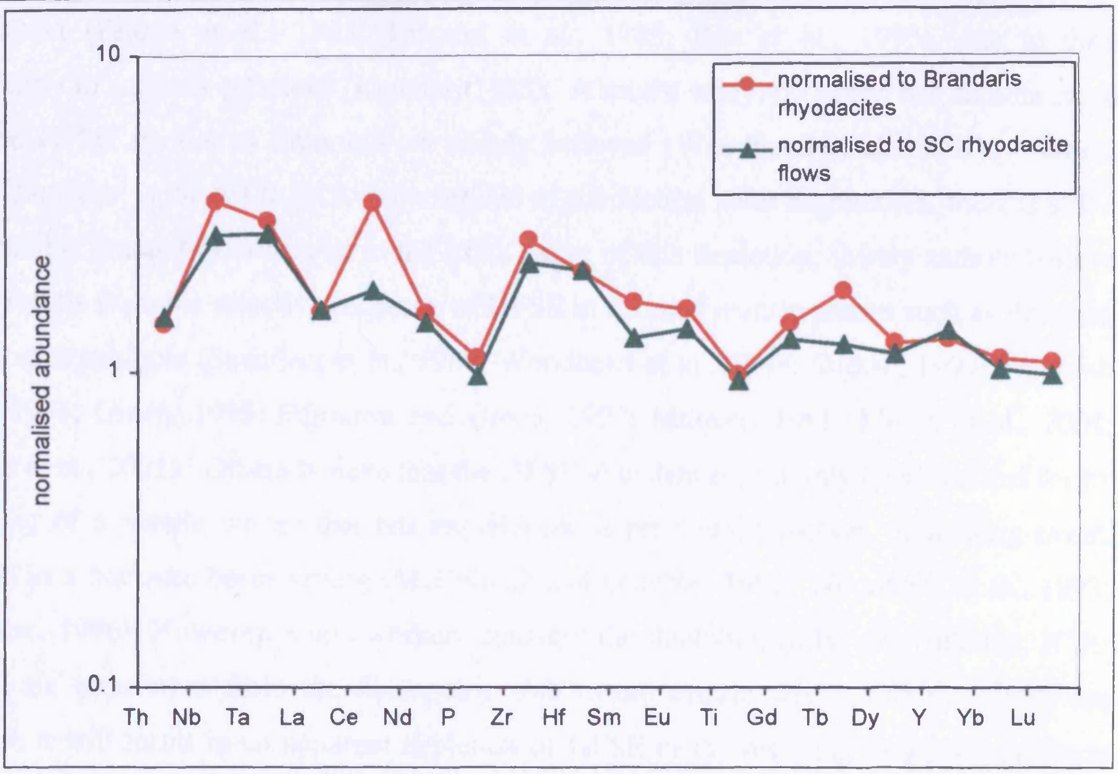

Fig. 7.5. Spidergram showing average Southern Complex rhyodacite dome, normalised to an average Southern Complex rhyodacite flow (green), and an average Brandaris rhyodacite (red).

7.4.2. Variation in subduction component?

As mentioned above, the rhyodacite domes are typified by higher La/Yb and REE enrichments than the rest of the Formation. It is thus tempting to assume that the distinct composition of the rhyodacite domes results from the incorporation of a greater component of sediment in the magmatic source of the domes. Nevertheless, the rhyodacite domes remain indistinguishable in terms of Hf-Nd isotopes (Fig. 7.2a), and plot at broadly the same point on the mixing array between the mantle source and sediment to the rest of the Formation (Fig. 7.2b), signifying their distinct composition is not a consequence of variable sediment incorporation. In addition, the rhyodacite domes are characterised by their Zr and Nb abundance, and both of these elements are unlikely to be soluble in aqueous fluids or siliceous sediment-derived melts (Pearce and Norry, 1979; Woodhead et al., 1993; Thirlwall et al., 1994). Consequently, a mantle source or fractional crystallisation origin of these anomalies is considered a much more likely hypothesis, and is discussed further beneath.

7.4.3. Source variation?

The distinct HFSE and REE concentration of the rhyodacite domes, as compared to neighbouring rhyodacite flows implies there must be a fundamental reason for the distinction, such as a variable mantle wedge composition. The HFSE concentrations of arc lavas are generally thought to be derived solely from the mantle wedge rather than from the subduction component (Pearce et al., 1983; Tatsumi et al., 1986; Bau et al., 1993), due to their immobility in aqueous solutions (Keppler, 1985). A recent study, however, has demonstrated that the HFSE are not as immobile as widely believed (Woodhead et al., 2001). Whilst HFSE depletion is known to be a characteristic of subduction zone magmatism, there is still a considerable amount of debate as to the exact cause of this depletion. Many authors believe that it results from the selective retention of HFSE in residual mantle phases such as ilmenite, rutile and amphibole (Saunders et al., 1980; Woodhead et al., 1993; Stimac, 1994; Thirlwall et al., 1994; Green, 1995; Fujinawa and Green, 1997; Munker, 1998; Moine et al., 2001; Tiepolo et al., 2001). Others believe that the HFSE abundances can only be accounted for by remelting of a mantle wedge that has experienced a previous depletion, or melting event, perhaps in a back-arc basin setting (McCulloch and Gamble, 1991; Woodhead et al., 1993; Davidson, 1996). However, some workers consider the depletion to be only relative: if the LILE's are transferred from the downgoing slab to the mantle wedge and the HFSE are retained, it will result in an apparent depletion of HFSE in the resulting magmatic products (Saunders et al., 1991).

Hf-Nd isotope systematics (Fig. 7.2a) demonstrate that the rhyodacite domes plot within the Washikemba Formation field, having isotopic ratios close to a Washikemba Formation average. As Hf is a HFSE and hence is wedge controlled (as discussed above) this shows that the rhyodacite domes have not experienced a separate mantle wedge-controlled magmatic event from the bulk of the Washikemba Formation. In addition, field evidence (Chapter 3) confirms that the rhyodacite domes and flows are coeval, rendering a separate magmatic source more unlikely.

Consequently it is likely that the rhyodacite domes were derived from a similar magmatic source to the remainder of the Washikemba Formation, and other possibilities of generating the trace element patterns are discussed in the sections below.

7.4.4. Variable degrees of melting of a similar source?

The relative LREE enrichment of the Southern Complex domes compared with the rest of the Formation (mean $(La/Yb)_N$ of >3 as opposed to 2, is consistent with the domes resulting from smaller degrees of melting of the mantle source region. However, although rare-earth element modelling using non-modal batch melting equations (e.g. Cox et al., 1979) can reproduce the REE patterns for reasonable degrees of melting of a typical MORB-source mantle, considerable uncertainties exist in the literature on the importance of residual phases in MORB mantle. This means that the HFSE concentrations of the source (let alone the resulting magmatic products) are not quantifiable, and cannot be modelled with any certainty.

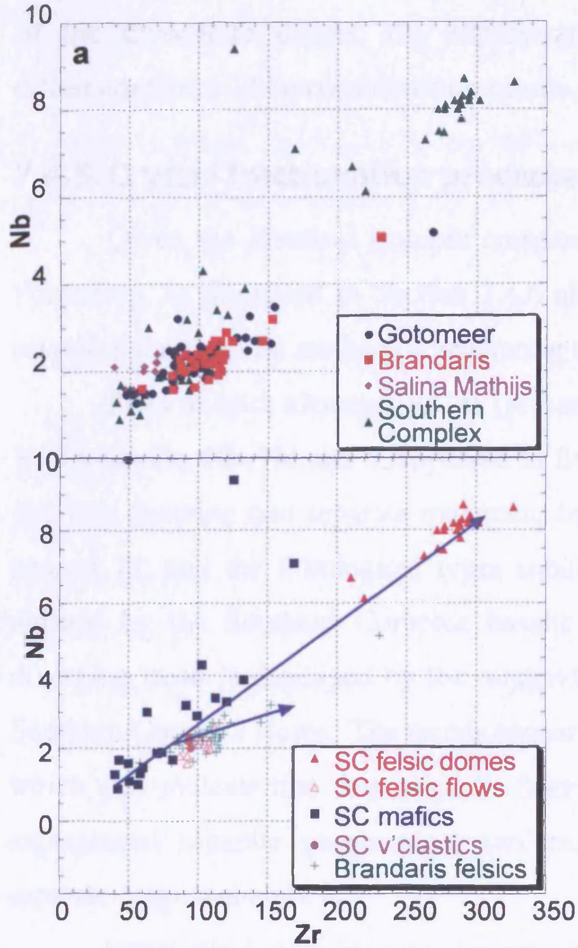

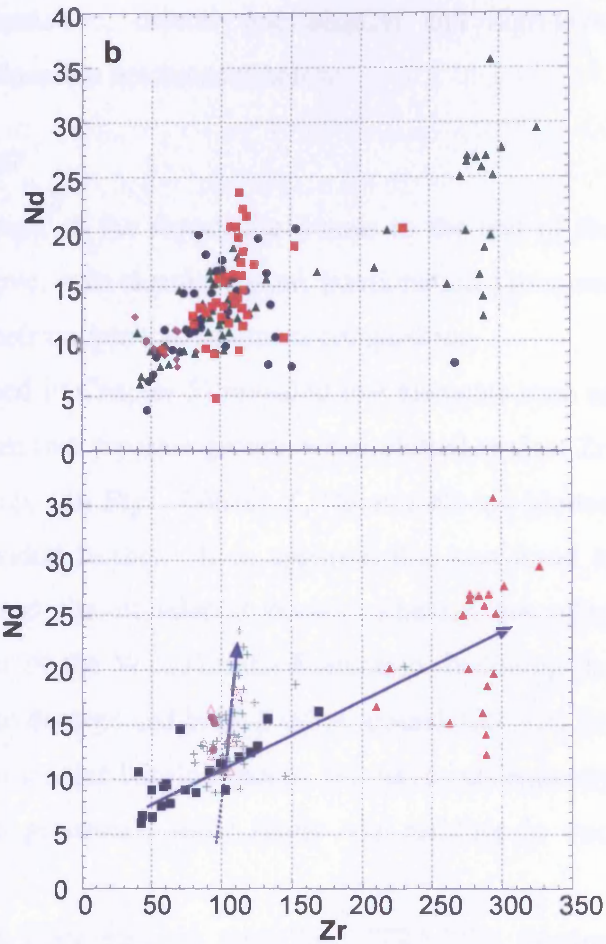

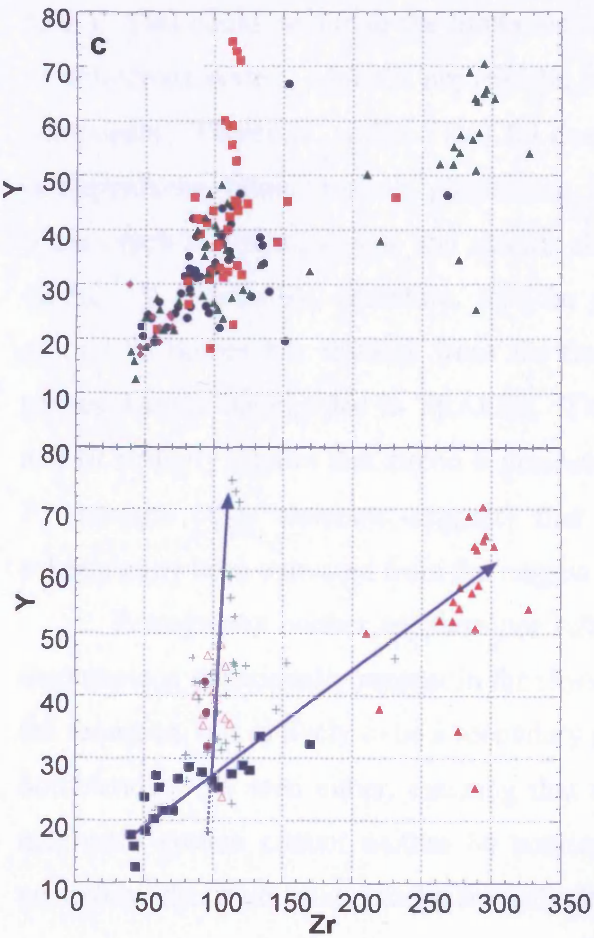

Fig. 7.6a. Plot of Zr vs. Nb for the Washikemba Formation, Bonaire, subdivided by area (upper plot) and subdivided by lithology for the Southern Complex and Brandaris areas (lower plot).

Fig. 7.6b. Plot of Zr vs. Nd for the Washikemba Formation, Bonaire, subdivided by area (upper plot) and subdivided by lithology for the Southern Complex and Brandaris areas (lower plot). Key as for Fig. 18a.

Fig. 7.6c. Plot of Zr vs. Y for the Washikemba Formation, Bonaire, subdivided by area (upper plot) and subdivided by lithology for the Southern Complex and Brandaris areas (lower plot). Key as for Fig. 18a.

On each plot it can be seen that the Washikemba formation appears to show two individual trends: one defined by the mafic Southern Complex lithologies and felsic domes, and the other defined by Southern Complex felsic flows, along with all lithologies from other areas. This implies two separate histories of magmatic evolution.

Hence, whilst variable degrees of source melting remains a viable process for the generation of the rhyodacite domes, the simpler alternative, crystal fractionation and high-level differentiation, will be considered as a more plausible mechanism below.

7.4.5. Crystal fractionation processes?

Given the identical isotopic composition of the rhyodacite domes to the rest of the Formation, as discussed in Section 7.4.6 above, subvolcanic crystal fractionation processes represent the simplest method of generating their unique trace element composition.

Plots of trace elements vs. Zr (presented in Chapter 5) revealed that elements such as Y, Sc, Cr, Co, Nb, Nd and V appeared to form two separate groups when plotted against Zr, possibly denoting two separate magmatic series. In Figs. 7.6a–c, Y, Nd and Nb are plotted against Zr, and the lithological types subdivided further. It is apparent that one trend is defined by the Southern Complex basalts and the rhyodacite domes, whereas the other diverging trend is displayed by the remainder of the Washikemba Formation, including the Southern Complex flows. The trends appear to diverge and branch off at around 100 ppm Zr, which may indicate that they originate from a similar basaltic parent, but have subsequently experienced separate geochemical evolution processes, most likely via residing in two separate magma chambers.

Nonetheless, this is not supported by trace element modelling (TRACE3; Section 5.9.1). This could be due to the limitations of the modelling programme: TRACE3 assumes an anhydrous system, which is not realistic for island arc rocks, for which H_2O is an intrinsic component. Therefore, whilst TRACE3 deals with major anhydrous phases such as olivine, orthopyroxene, clinopyroxene, plagioclase, spinel, ilmenite and pigeonite, it ignores minor phases such as zircon, sphene and apatite, along with hydrous phases such as amphibole and biotite. It is possible, therefore, that the distinct composition of the Southern Complex rhyodacite domes has resulted from the fractional crystallisation of one or more of these phases that are disregarded in TRACE3. The relative overabundance of REE along with Zr and Hf strongly implies that zircon is present in the system. In addition, the paucity of Sc and P, amongst other elements suggests that hornblende and apatite has fractionated and subsequently been extracted from the magma giving rise to the Southern Complex domes.

Petrography neither supports nor refutes this hypothesis. As detailed in Chapter 3, amphibole is occasionally present in the rhyodacite domes, but given the state of alteration of the sequence, this is likely to be a secondary phase. No convincing pseudomorphs of primary hornblende were seen either, meaning that the presence of phenocrystic hornblende in the magmatic system cannot neither be confirmed nor refuted. In addition, no zircon was positively identified in any rocks from the Washikemba Formation. Igneous zircons within these rocks, however, are likely to be very small (<0.1 mm) and may be difficult to identify even with a microscope, particularly as apatite is an abundant phenocrystic phase that can closely resemble zircon. Nonetheless, this provides the best explanation for the origin of the Southern Complex rhyodacite domes: they most likely originated from the same parent as the remainder of the sequence, but part way through the crystallisation process (at ~100 ppm Zr), the crystal mush (including zircon) was extracted from the system, leaving behind lighter mineral phases such as apatite and hornblende. This zircon-rich mush then underwent further crystallisation in a separate magma chamber, before being erupted as exogenous domes, probably on the flanks of the volcano (Fig. 7.7). The seriate texture displayed by the domes (as opposed to the porphyritic texture of the other rhyodacites) is consistent with this separate magma chamber and eruption history. This is supported by Zr/Sm ratios of 40–80 for the rhyodacite domes, whereas the rhyodacite flows have Zr/Sm ratios of <30, as Sm should behave similarly to Zr, unless zircon fractionation has occurred. The removal of hornblende and apatite is suggested by their pronounced negative P and Sc anomalies (Table 7.1). In addition, it is interesting that the differentiation event can be pinpointed at around 100 ppm Zr. In silicic peraluminous systems, this is the amount of Zr required to saturate the melt and prompt zirconium crystallisation, and is effectively independent of factors such as H_2O content and pressure (Watson, 1979; Watson and Harrison, 1983).

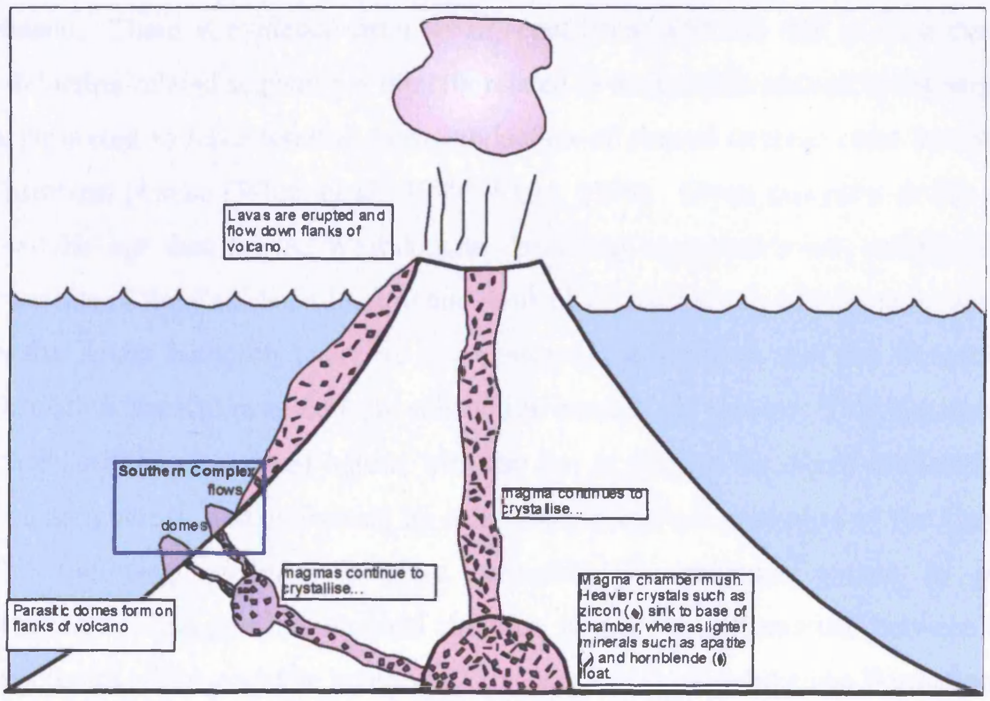

Fig. 7.7. Schematic model of the volcanic evolution of the Washikemba Formation, Bonaire, illustrating the model for the generation of the Southern Complex domes.

This model is supported by the literature. Numerous other studies acknowledge the role of accessory phases such as zircon, amphibole, ilmenite and rutile, in fractionating HFSE (Woodhead et al., 1993; Thirlwall et al., 1994; Fujinawa and Green, 1997; Muenker, 1998;

Moine et al., 2001; Tiepolo et al., 2001). For example, quoted partition coefficients of Nb and Zr in ilmenite associated with rhyolite are 51–71 and 1.0–1.4 respectively (Stimac and Hickmott; 1994), in broad agreement with observed patterns (Fig. 7.5) of Nb showing greater enrichment than Zr. In addition, experimentally determined partition coefficients for amphibole-melt pairs in basaltic systems at >0.5 GPa (Fujinawa and Green, 1997) demonstrate that D_{Zr} is consistently greater than D_{Hf}, consistent with the elevated Zr/Hf ratios (>41 as opposed to <39) observed for the rhyodacite domes. Further quantitive analysis is hampered by the scant data available for felsic magmatic systems, especially at the relevant shallow crustal *p-t* conditions. Nevertheless, it seem plausible that the involvement of minor phases such as zircon, amphibole and apatite in the fractionation of a similar parent magma to the remainder of the Washikemba Formation, would result in the generation of trace element compositions similar to those of the Southern Complex rhyodacite domes.

7.5. Relationship to the Caribbean Plateau and Aruba batholith

7.5.1. The Caribbean Plateau

As discussed in Chapter 1, the ultimate aim of this study is to evaluate the origin of an arc sequence that appears to be both temporarily and spatially associated with the Caribbean plateau. There is evidence from an adjacent island (Aruba) that at least one neighbouring subduction-related sequence is directly related to the oceanic plateau in the sense that it could is purported to have resulted from subduction of normal oceanic crust beneath the buoyant Caribbean plateau (White et al., 1999; White, 1999). Given that prior to this study, the best available age data for the Washikemba Formation suggested it was indistinguishable in age from that of the Caribbean Plateau and Aruba batholith, along with its geographical proximity to the Aruba batholith today, it is a reasonable hypothesis that the Bonaire Washikemba Formation has also resulted from subduction beneath the plateau. This hypothesis, along with others, will be considered below, with the aim of placing the island of Bonaire into a wider tectonic context, and evaluating its role in the Mesozoic evolution of the Caribbean region. The following sections, therefore, assemble the evidence gained in previous field, geochemical and geochronological chapters, in order to differentiate between three different hypotheses which could be invoked for the origin of the Washikemba Formation.

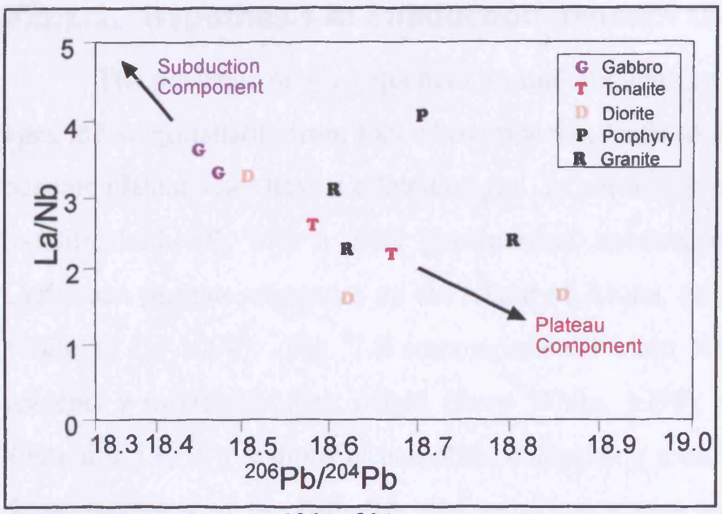

Fig 7.8a. Plot of La/Nb vs. $^{206}Pb/^{204}Pb$ for the Aruba batholith, adapted from White (1999).

Tonalites:
*Sr, Nd, Pb isotopes, and Zr-Nb-Y systematics similar to plateau
*produced from remelting of Caribbean plateau crust

Gabbros:
*Most primitive liquids of batholith
*High La/Nb requires a subduction zone origin
*Sr, Nd isotopes and Zr-Nb-Y systematics imply involvement of plume => mantle wedge had plume-like composition

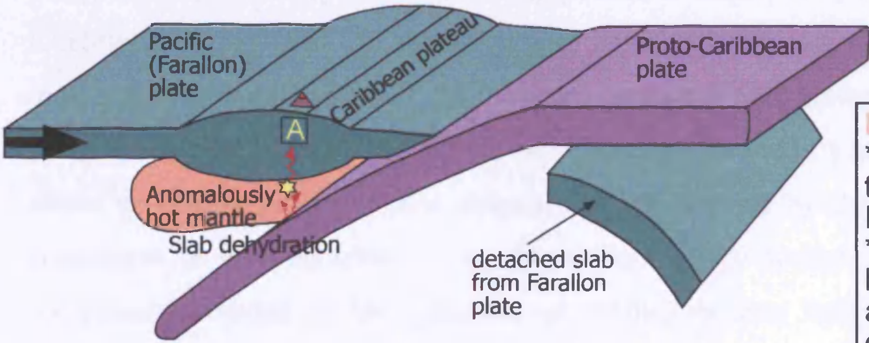

Diorites:
*Intermediate between tonalites and gabbros in La/Nb and Pb isotopes.
*Formed from mixing between slab component and plateau-derived component

Fig 7.8b. Cartoon model for the tectonic setting of the Aruba batholith, adapted from White (1999).

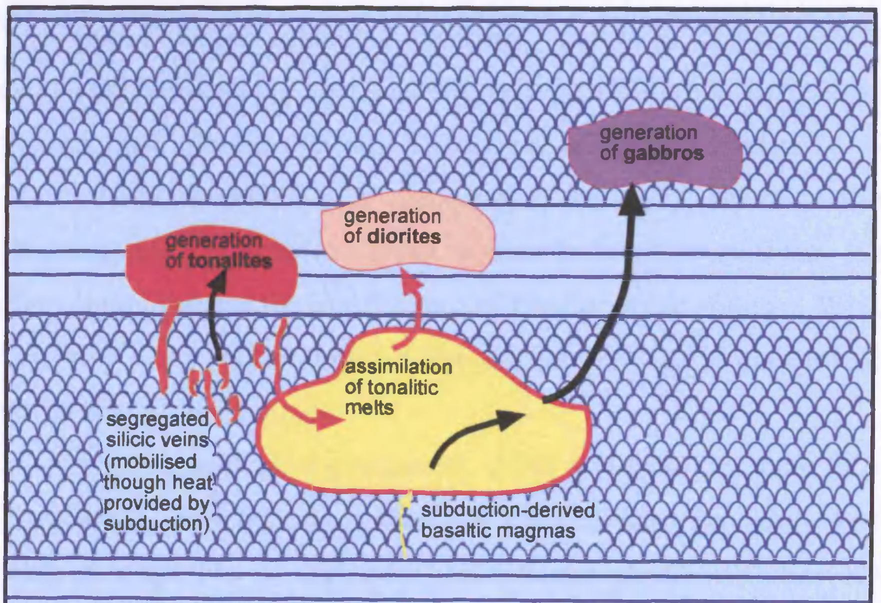

Fig. 7.8c. Model for the generation of the different members of the Aruba batholith, simplified from White (1999). The gabbros are derived from subduction beneath the plateau. The tonalites (in the simplest cases) represent partial melting of the plateau sequence, and the diorites represent interaction between tonalitic and gabbroic magmas.

7.5.1.1. Hypothesis A: Subduction beneath the Caribbean plateau?

The presence of arc sequences around the margins of the Caribbean plateau, often with ages indistinguishable from that of the plateau, leads to speculation that the island arc(s) and oceanic plateau may have a related origin. In particular, the Aruba batholith, a predominantly tonalitic batholith with a clear geochemical subduction signature, is seen to intrude the Caribbean plateau sequences on the island of Aruba, only 100 km to the west (White, 1999; White et al., 1999). Fig. 7.8 summarises the main elements of the Aruba batholith, and presents a model for their origin (from White, 1999). The Aruba batholith, described in Section 2.5.1, is a composite batholith, comprising tonalitic, dioritic and gabbroic members. Some members of the batholith (the tonalites) appear to show a more plateau-like affinity, whereas others (the gabbros) are more arc-like in geochemical character. This is illustrated by the negative correlation between La/Nb and $^{206}Pb/^{204}Pb$ (Fig. 7.8a; from White, 1999), where a high La/Nb, indicating a subduction component, is displayed by the gabbros, whereas in the tonalities, a high $^{206}Pb/^{204}Pb$ (in addition to other trace element and isotopic characteristics) indicates a plateau component. The diorites are transitional between the two. A model was proposed by White (1999; Fig 7.8b,c) where the tonalites were generated by the remelting of silicic veins associated with the plateau, and the gabbros by the addition of a subduction component to the anomalous (hot, plateau-like) mantle wedge. Interaction between these components resulted in the spectrum of lithologies seen today. The Aruba batholith, therefore, represents subduction of normal oceanic crust beneath the plateau, and the age constraints dictate that this must have immediately followed the subduction polarity reversal. The first order assumption considered, therefore, is that the Washikemba Formation represents the extrusive equivalent of the Aruba batholith, and hence results from subduction beneath the Caribbean plateau. This assumption is tested below.

1. *Field constraints.* On the island of Aruba, Caribbean plateau sequences are clearly observed, and the intrusive contact with the batholith is apparent. On the island of Bonaire, there is no evidence for any outcrops of the Caribbean plateau. Whilst this does not provide any proof that the Caribbean plateau was not involved, it does reveal that the relationship is not as obvious as on Aruba.

2. *Geochronological constraints.* New data from this study (Chapter 4) reveal that the Washikemba Formation is at least 95± 2 Ma in age. The Aruba batholith was dated by the same technique (Ar-Ar step heating) at the same lab (SURRC, East Kilbride) and yielded ages of 82–85 Ma. Providing these dates are valid, this indicates that the Washikemba Formation predates the Aruba batholith by at least 8, and possibly as much as 17 Ma. It is therefore, extremely unlikely that the Washikemba Formation represents the extrusive equivalent of the

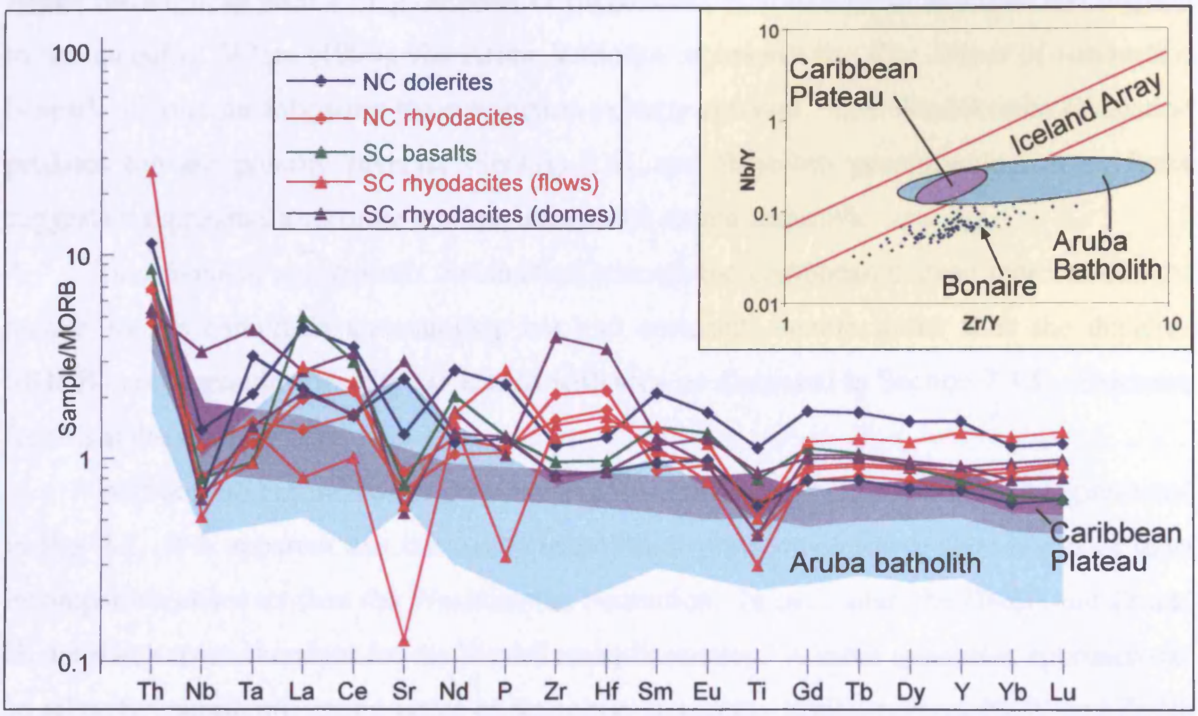

Fig. 7.9a. MORB-normalised spidergram for the Washikemba Formation, compared with the Aruba Lava Formation (i.e. Caribbean plateau, shaded purple) and the Aruba batholith (shaded green). Note the typically flat patterns of the Caribbean Plateau compared with the Washikemba Formation. **7.9b.** Nb/Y vs. Zr/Y plot for the Washikemba Formation (blue symbols) compared to the Aruba batholith (green fill) and the Aruba Lava Formation (i.e. Caribbean plateau, shaded purple).

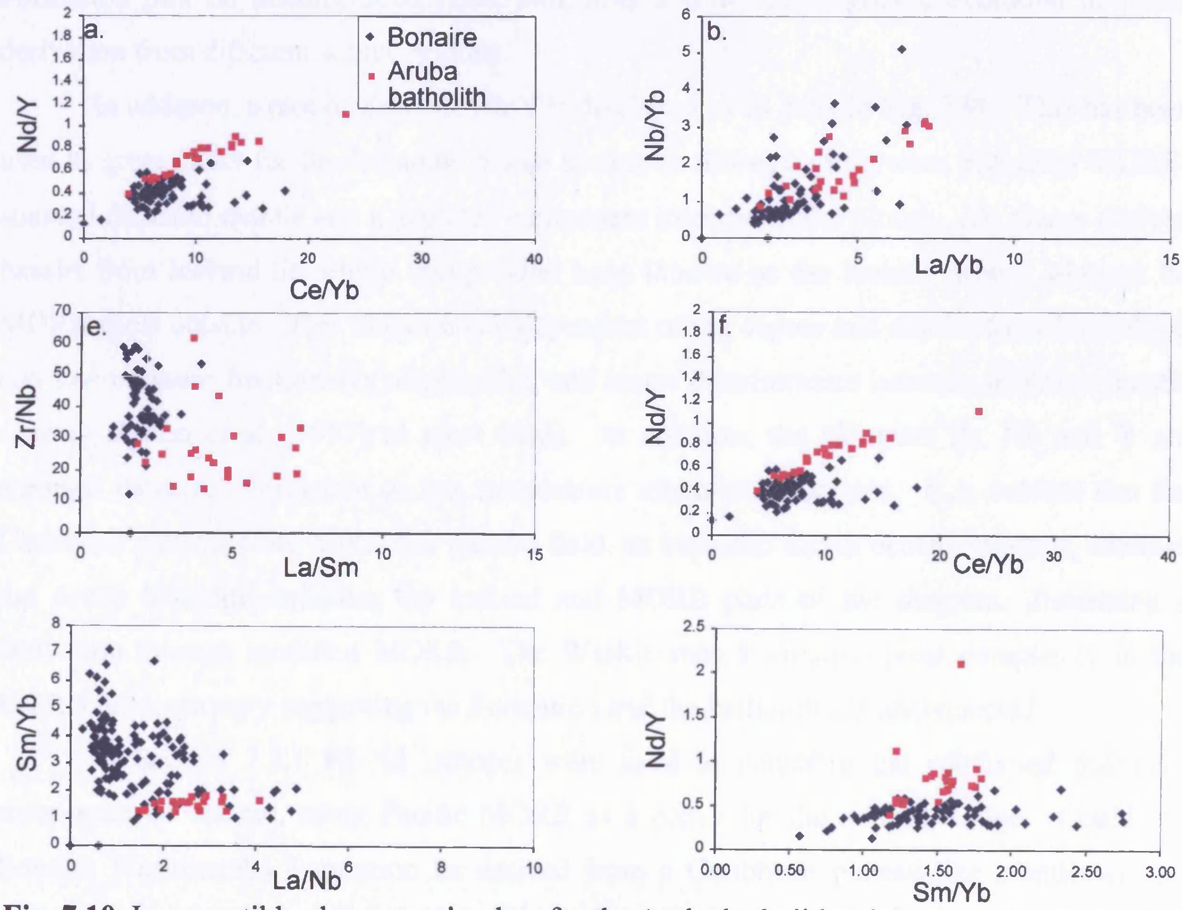

Fig. 7.10. Incompatible element ratio plots for the Aruba batholith (pink squares) compared with the Washikemba Formation, Bonaire (blue diamonds). Aruba data from White (1999).

Aruba batholith, as such a long duration of magmatism is unlikely. In addition, and implicit to the model of White (1999), the Aruba batholith represents the *first stages* of subduction beneath the plateau following the subduction polarity reversal. The Washikemba Formation predates the arc polarity reversal (Section 2.6), and therefore geochronological evidence suggests it represents a separate arc sequence to the Aruba batholith.

3. *Geochemical constraints.* Subduction beneath the Caribbean plateau requires that the mantle wedge comprises anomalously hot and enriched[1] mantle rather than the depleted MORB-source mantle normally associated with arcs, as discussed in Section 7.3.1. Evidence for this is discussed below.

A chondrite-normalised multi-element plot of the Washikemba Formation is presented in Fig. 7.9. It is apparent that the Aruba batholith displays much lower abundances of most incompatible elements than the Washikemba Formation. In particular, the HREE and Zr and Hf are much more abundant for the Washikemba Formation. A more quantitive approach can be taken by examining paired ratios of immobile elements. Ratios such as Nd/Y and Zr/Nb are thought to be resistant to low-pressure crystal fractionation processes, and are therefore indicative of source compositions. Fig. 7.10 shows various immobile trace element ratios plotted against one another. It is evident that the Aruba batholith and the Washikemba Formation plot on distinct trend lines, indicating a different magmatic evolution or likely derivation from different source regions.

In addition, a plot of Zr/Y vs. Nb/Y is displayed as an inset in Fig. 7.9b. This has been used to great effect for the Icelandic plume system to distinguish between entrained MORB-sourced depleted mantle and a depleted component intrinsic to the plume. All plume-derived basalts from Iceland lie within two parallel lines (known as the Iceland array), whereas N-MORB plots outside. This diagram is independent of the degree and depth of partial melting and low-pressure fractional crystallisation, and hence discriminates between different mantle sources (Fitton et al., 1997) in most cases. In addition, the elements Zr, Nb and Y are amongst those most resistant to low temperature alteration processes. It is evident that the Caribbean plateau plots within the Iceland field, as expected for an oceanic plateau, whereas the Aruba batholith straddles the Iceland and MORB parts of the diagram, illustrating a derivation through modified MORB. The Washikemba Formation plots completely in the MORB field, strongly suggesting the Formation and the batholith are unconnected.

In Section 7.2.1 Hf-Nd isotopes were used to constrain the subducted sediment component of the arc, using Pacific MORB as a proxy for the mantle wedge. Could the Bonaire Washikemba Formation be derived from a Caribbean plateau-like mantle wedge,

[1] Relative to primitive mantle.

(like the Aruba batholith) using Hf-Nd isotope criteria? As illustrated on Fig. 7.11, the main Caribbean plateau array extends to a εNd of +9 and a εHf of +13, although the Gorgona depleted komatiites have a higher εHf and εNd extending to +17 and +10 respectively (Chapter 6). As either of these could potentially represent suitable Caribbean plateau mantle wedge compositions, mixing between these potential components and the Pacific pelagic sediment of Fig. 7.2b is modelled in Fig. 7.11, using trace element characteristics specific to each source[2]. It is evident that neither one of these endmembers can interact with sediment to reproduce the compositions of the Washikemba Formation, strengthening the argument that the Caribbean plateau and the Formation are unrelated. Hence, field, geochronological and geochemical arguments refute the hypothesis, that the Washikemba Formation represents the extrusive equivalent of the Aruba batholith. By implication, the Formation was not a product of subduction of normal oceanic crust beneath the Caribbean plateau. Alternative hypotheses are considered below.

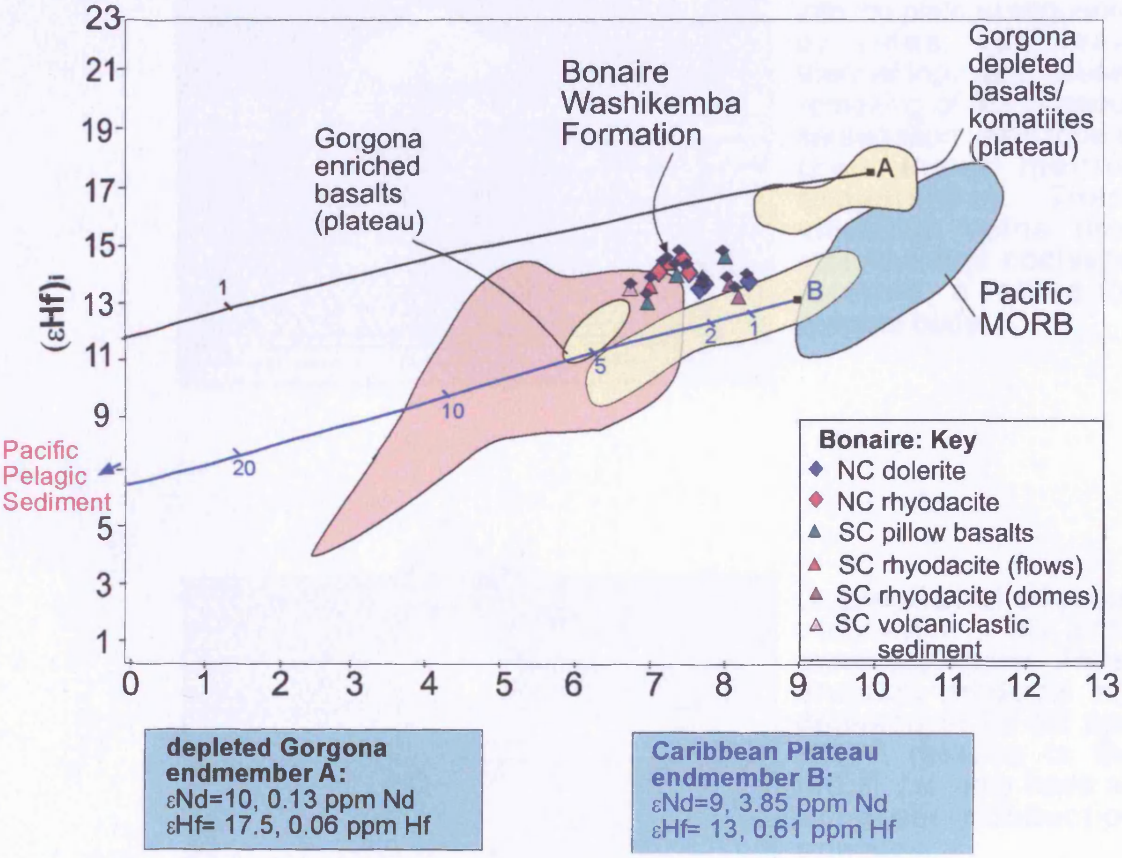

Fig. 7.11. Plot showing mixing in Hf-Nd isotope space between pelagic sediment (as for Fig. 7.2b) and different mantle wedge compositions. Many fields and annotations have been omitted for clarity. Mixing line A represents mixing between a depleted Gorgona-type source and pelagic sediment, whereas mixing line B represents a typical main Caribbean plateau-type mantle wedge. Numbers on mixing line refer to sediment %.

---

[2] As for Section 7.3.2.2, mantle source compositions were inferred from basalt compositions. For Gorgona, 15% melting was inferred (Arndt et al., 1997; Révillion et al., 1999), whereas for the main Caribbean plateau, 10% melting of the mantle source was assumed.

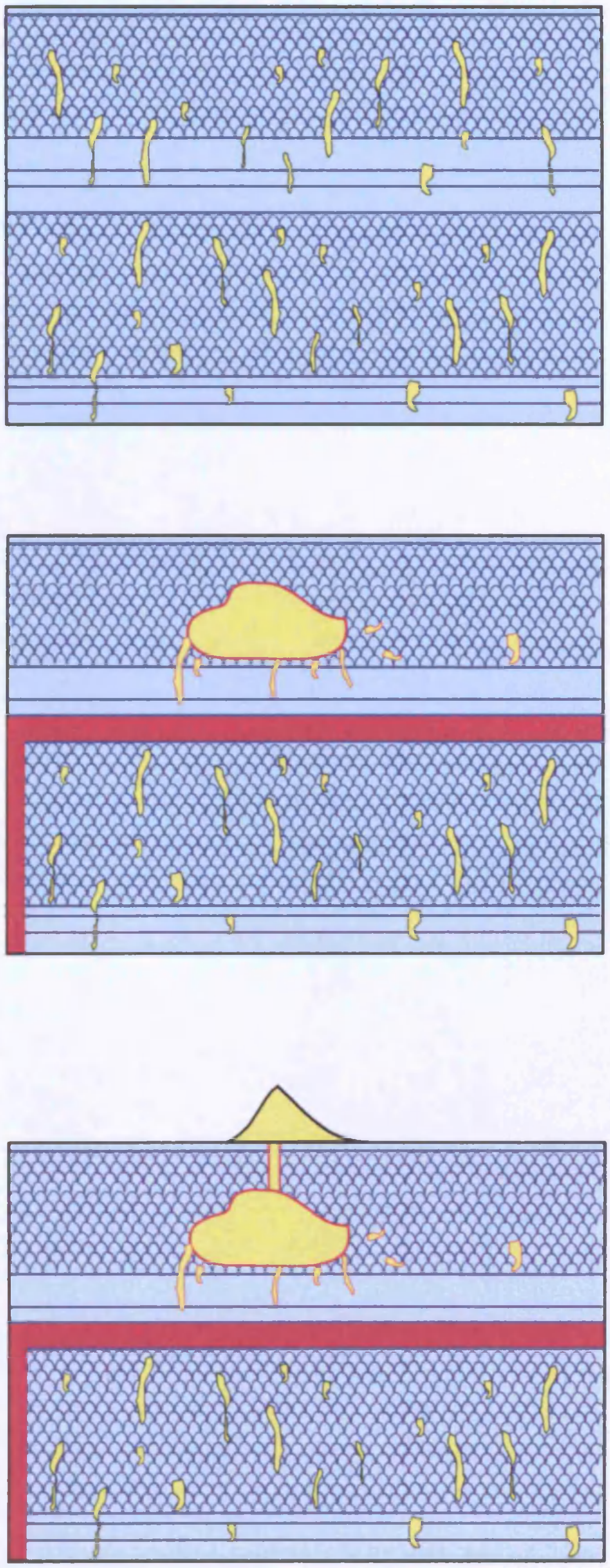

Fig. 7.12. Model for the generation of siliceous rocks from remelting of basaltic oceanic plateau sequences. Based on Marsh et al. (1991), Jonasson et al. (1992) and Jonasson (1994).

7.5.1.2. Hypothesis B: Remelting of the Caribbean plateau?

A second model for the generation of the rocks of the Washikemba Formation, speculates that the hydrous, commonly felsic rocks have been produced by partial melting of the thin, hot, basaltic crust of the plateau (Fig 7.12). Iceland represents an obvious example of this process, as rhyolite comprises 10–12% of its surface rocks, some of which has been attributed to partial melting of basalt (Marsh et al., 1991; Jonasson et al., 1992; Jonasson, 1994). A model is envisaged where silicic segregation veins and lenses within the basalt become consolidated as heating of the basalt proceeds. As they have a lower melting temperature than the basalt, they are able to migrate and coalesce, forming chemically heterogeneous magma chambers which will eventually erupt. The resulting volcanic products are significantly depleted in HFSE (e.g. Nb, Zr, Y) and HREE, i.e., they have a geochemical signature that superficially resembles that of island arcs (Johnasson et al., 1982).

1. *Geochronological evidence.* Hypothesis B appears to be a feasible model for the generation of the Washikemba Formation, given the close special and temporal relationship with the Caribbean plateau. However, as for Hypothesis A, it is contradicted by the new geochronological information available for the Washikemba Formation (Chapter 4), which indicates that the Formation predated plateau formation by a minimum of two million years. Whilst this does not entirely rule out the hypothesis, as it is likely that there would be a short time gap after the later stages of plateau magmatism (needed to provide thermal input to cause remelting) and the eventual eruption of silicic magma, it does render it more unlikely.
2. *Geochemical evidence.* An additional line of evidence comes from the plot of Nb/Y vs. Zr/Y presented as Fig. 7.9b and discussed above. The Washikemba Formation plots outside the tramlines, within the MORB-field, whereas the Caribbean plateau plots entirely within the array, as expected for plume-derived basalts. If the Washikemba Formation was derived from remelting of the Caribbean plateau lithologies, it would be likely to have the same Nb/Y and Zr/Y characteristics of the plateau, as these are thought to be ratios inherited from the source (Fitton et al., 1997; Pearce et al., 1999) rather than magmatic fractionation processes.
3. *Isotopic evidence.* Hf-Nd isotopes may shed a further light on the origin of the arc related sequence, as Hf-Nd isotopes are considered to be relatively resistant to fluid-related processes (i.e., subduction; e.g. Davidson, 1986, Pearce et al., 1999; Woodhead, 2001) and hence reveal information about the nature of the mantle source. The plot of εHf-εNd presented in Figure 7.2, it is apparent that the Washikemba Formation is significantly displaced off to the low εNd end of the Caribbean plateau array, and there

is no apparent isotopic overlap. In addition, as illustrated in Chapter 5 and Section 7.3, all trace element and isotopic evidence suggests that the Formation represents a typical arc sequence, and hence there is little reason to invoke alternative mechanisms of generating an apparent subduction signature. This provides support to the information already gleaned, that the Washikemba Formation is not derived from the Caribbean plateau.

Ergo, Hypothesis B is rejected: it is considered that geochronological and geochemical constraints preclude a derivation of the Washikemba Formation from remelting of the lower basaltic portions of the Caribbean plateau.

7.5.1.3. Hypothesis C: Accreted arc sequence unrelated to the Caribbean plateau?

A preferable solution is that the Bonaire Washikemba Formation represents part of an island arc that is entirely unconnected to the Caribbean plateau, but is now juxtaposed with oceanic plateau fragments on the margins of the Caribbean. This may not be such a coincidence as it first appears: as outlined in Chapter 2, most authors acknowledge that the plateau has moved from the Pacific realm, into the space created by the diverging Americas, and its buoyant nature would have ensured that any arc (or continent) fragment in its path may have been accreted to its leading edge and moved passively eastwards, together with the plateau.

Geochemical or isotopic evidence does not provide many constraints here, although they are both consistent with such an idea (e.g. the superficial similarity in Hf-Nd isotope compositions of the Washikemba Formation and the Lesser Antilles, as discussed in Section 7.2). Fortunately, attention can be focussed on the new geochronological data discussed in Chapter 4. The oldest reliable minimum age for the Washikemba Formation is 95±2 Ma. This is deemed to be older than at least the main phase of magmatism of the Caribbean plateau (Section 2.2.1) and hence it is difficult to accept a related origin. Instead, a more reasonable model may be the Washikemba Formation represents part of a pre-existing arc sequence. This arc has now somehow been juxtaposed on the margins of the Caribbean, along with dissected plateau sequences. A detailed model and mechanism for this is discussed below.

7.5.2. Detailed tectonic model of the origin and emplacement of the Washikemba Formation

A cartoon model for the origin and evolution of the arc sequence is presented in Figs. 7.13 and 7.14. As the Bonaire Washikemba Formation represents an arc sequence older than

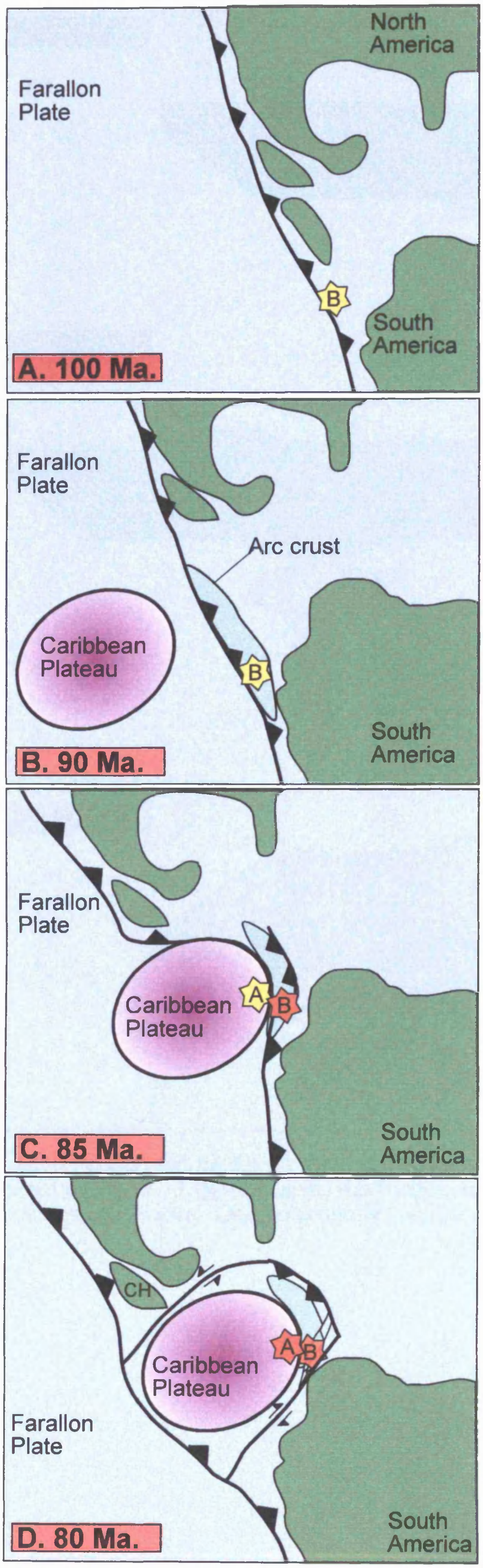

Fig. 7.13. Cartoon model for the origin and evolution of the Bonaire Washikemba Formation, in its wider tectonic context. General tectonic reconstructions after Pindell et al. (1990); White et al. (1999).

A. North and South America start to diverge, extending the length of the long-lived intra-American subduction zone.

B. At around 95 Ma, the Washikemba Formation is extruded as part of the intra-oceanic arc (represented by B). Note that yellow symbols represent active arc sequences, whereas orange ones denote inactive ones.
Meanwhile, at around 90 Ma, as the Pacific plate drifts eastwards over a hotspot, the Caribbean plateau is extruded onto Pacific crust.

C. The Caribbean plateau reaches the subduction zone, causing it to jam and and a new subduction zone to start to develop on the eastern side of the remnant arc. This has the opposite polarity, consuming Atlantic lithosphere as opposed to Farallon/Caribbean plateau. The Aruba batholith (A)is intruded into the Caribbean plateau, representing the first stages of subduction beneath the plateau.

D. The Caribbean plateau continues to move eastwards between the two Americas. The relict arc sequence is now accreted to the leading edge of the plateau. As the margins of the arc/plateau sequence get close to South America, numerous strike slip faults begin to dissect the sequence.
After 80 Ma, the Caribbean plateau moves further eastwards, causing the island arc sequence and portions of the plateau to be fragmented and accreted onto the Southern American margin.

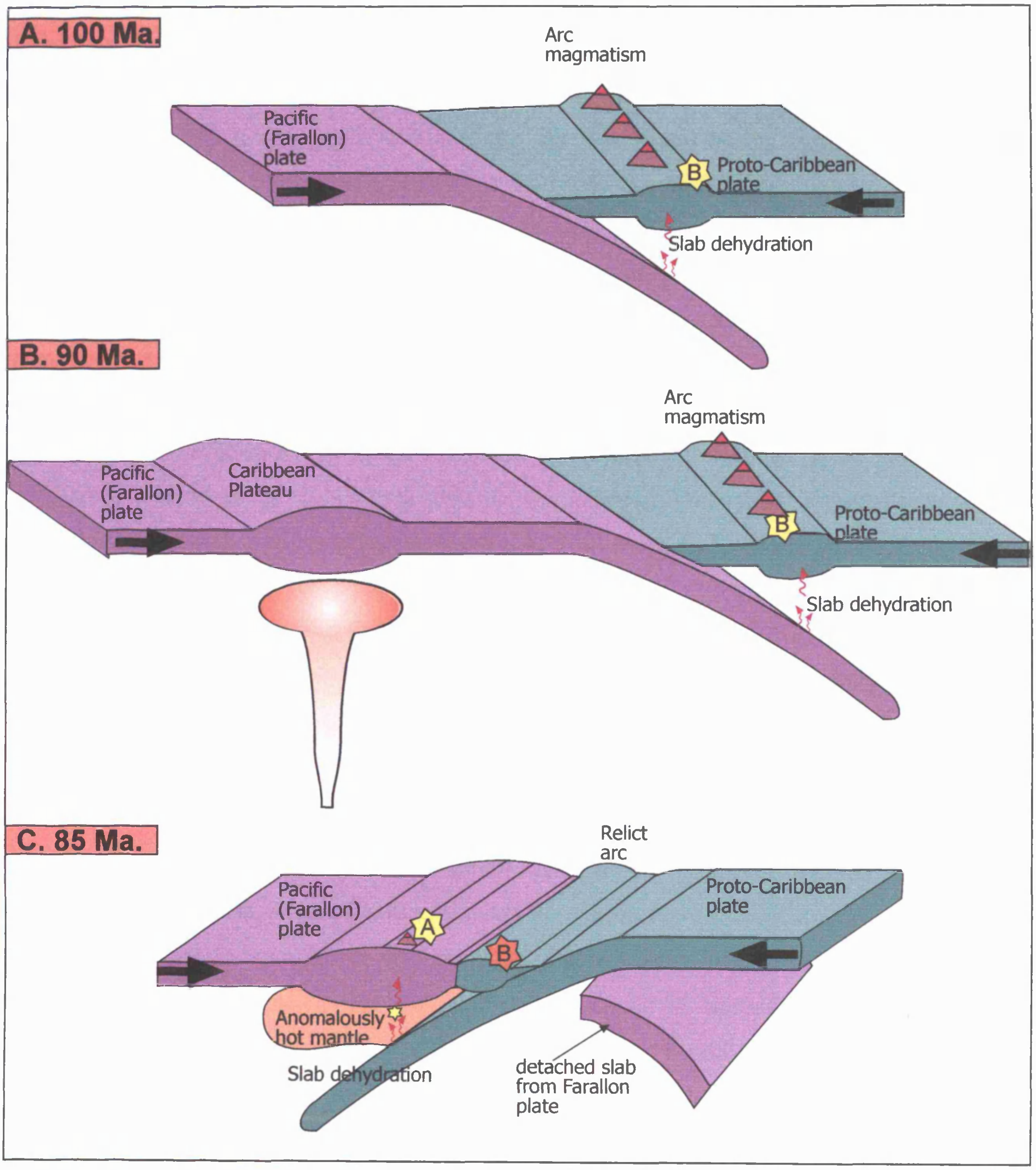

Fig. 7.14. Cartoon model for the origin and evolution of the Bonaire Washikemba Formation, based on Fig. 7.13. A represents the position of the Aruba batholith, whereas B represents the position of Bonaire. Orange symbols denote inactive arc sequences.

the Caribbean plateau, it is envisaged that it originated in the Pacific realm as part of the long-lived intra-American arc at >95 Ma. The Caribbean plateau was extruded onto Farallon crust shortly afterwards, and began to approach the subduction zone where proto-Caribbean crust was overriding and consuming Farallon crust. By this stage, the arc responsible for the Bonaire Washikemba Formation had become inactive. By 85 Ma, the buoyant and thick oceanic plateau had arrived at and subsequently clogged the subduction zone. This resulted in a new subduction zone (with opposite polarity) developing to the east of the now-relic arc sequence, as proto-Caribbean crust became subducted beneath the juxtaposed arc and plateau sequences. As the plateau continued to move passively between the two Americas, parts of the plateau and arc collided with the Southern Caribbean margin, causing the margins of the plateau to become dissected by strike-slip faults, and eventually accreted in slices onto the Southern Caribbean margin. This accounts for the present-day juxtaposition of plateau and arc rocks in the Dutch Antilles on the Southern Caribbean margin.

7.6. Implications for the tectonic evolution of the Caribbean

Section 7.5 concludes that the Bonaire Washikemba Formation represents part of an allochthonous, intraoceanic arc sequence that was swept up in front of the Caribbean plateau as it moved eastwards, and eventually accreted onto the northern margin of South America. This reveals that there was at least two stages of Mesozoic arc development in the Caribbean region: an earlier phase, which the Washikemba Formation represents, and a later phase of subduction beneath the margins of the Caribbean plateau itself, which is represented by the Aruba batholith. Due to the close spatial relationship between the leading edge of the plateau and the arc sequence, as predicted by the model presented above, one might also expect to see subduction occurring beneath the earlier stage arc, and a second stage arc being built on relict arc basement. This scenario is found in the Solomon Isles, where the attempted subduction and eventual obduction of the Ontong Java Plateau has resulted in a subduction polarity reversal, and is represented today by a complex collage of crustal units, including plateau, arc, arc developed on arc basement, and arc intercalated with plateau (Petterson et al., 1997; 1999). Thus, the Solomon Isles represents a modern-day analogue of the Southern Caribbean margin.

This model for the generation of the arc sequence on Bonaire, coupled with recent work on the origin of the neighbouring Aruba batholith (White, 1999; White et al., 1999) provides a basic framework for interpreting the many other arc sequences found around the margins of the Caribbean (Section 2.4), which could be dealt with in a future study.

7.7. Conclusions

The integration of field, geochronological, petrological and Hf-Nd isotopic data reveals that the Bonaire Washikemba Formation is part of an intra-oceanic arc essentially unrelated to the Caribbean plateau, although the Caribbean plateau remains indirectly responsible for the transport and probably the ultimate preservation of this arc sequence. The arc originated at the Mesozoic subduction zone developed between the Americas. Geochemical and isotopic constraints dictate that the subduction zone magmatism was dominated by input from subducted pelagic sediment, and that the mantle wedge was most likely normal depleted upper mantle, rather than anomalously hot mantle affected by a plume, as invoked for the nearby Aruba batholith (White, 1999; White et al., 1999). Low-pressure fractional crystallisation, of a common parent magma then produced all rock suites of the Washikemba Formation, with the unique composition of the Southern Complex domes resulting from fractionation of minor phases such as zircon, apatite and hornblende. Minor assimilation of local sediment resulted in the negative Ce anomalies displayed by some rock suites.

The arc sequence became inactive by 85 Ma, when the Caribbean plateau reached the subduction zone and caused it to jam, resulting in the development of a new subduction zone on the eastern side of the arc sequence, consuming Atlantic, as opposed to Farallon crust. Thus the relic arc became accreted onto the leading edge of the eastwards moving Caribbean plateau, and as it approached the South American continent, it became dissected by strike-slip faults and eventually fragmented. A collage of arc and plateau fragments from the leading edge of the plateau were thus accreted onto the margin of South America, and comprise the Dutch Antilles today.

7.8. Scope for further research

This study represents the first indepth study of the petrology, geochronology and volcanic evolution of the Cretaceous arc sequence on Bonaire, now juxtaposed together with oceanic plateau fragments on the Southern Caribbean margin. The adjacent oceanic plateau and batholith sequences (Curaçao and Aruba) have been well constrained from recent studies (Kerr et al., 1996a; White et al., 1999; White, 1999), and thus this study is the first of its kind to permit an integrated model of the relationship between the oceanic plateau, arc and batholith to be generated for the Dutch Antilles. This model can be used as a framework for interpreting other regions of the Caribbean: as detailed in Chapter 2, terranes of oceanic plateau, arc and tonalitic batholith affinity are found all over the Caribbean region, but their significance is still, largely, unexplained. In particular, similar studies of the arc sequences on the Southern Caribbean island of Tobago, along with those on the Jurassic La Desirade (now positioned on the main Lesser Antilles arc) may yield important insights into the complex Palaeozoic/Mesozoic evolution of the Caribbean plate. Further insights may still be gained by detailed geochronological analysis of the Caribbean plateau, and in particular the associated arc sequences, for which few reliable ages exist. In addition, interpretations of the evolution of the Caribbean region are presently hampered by the lack of seismic and geophysical data, particularly on the basement and subsurface structures, which could be rectified by detailed offshore geophysical surveys.

Finally, this study has demonstrated that Hf-Nd isotope systematics can be a powerful tool in two ways: firstly, in interpreting the relationship between plateau and associated arc rocks, particularly in altered and ancient successions. This could be directly applied to Archaean granite greenstone belts, and used to elucidate early subduction processes. Secondly, Hf-Nd isotope systematics can be invaluable in tracing ancestral oceanic plateaux to their mantle plumes, a common problem for many plateaux in existence today (Clounard and Bonneville, 2000), and this can be utilised to help tighten global plate reconstruction models.

References

Acton G. D., Galbrun B., and King J. W., 2000. Paleolatitude of the Caribbean plate since the late Cretaceous. *Proceedings of the Ocean Drilling Programme, Scientific Results* **165**, 149-173.

Allan J. F. and Simkin T., 2001. Ferandina Volcano's evolved, well mixed basalts: mineralogical and petrological constraints on the nature of the Galápagos plume. *Journal of Geophysical Research* **105** (B3), 6017-6041.

Alvarado G. E., Denyer, P. and Sinton, C.W., 1997. The 89 Ma Tortugal komatiitic suite, Costa Rica: Implications for a common geological origin of the Caribbean and Eastern Pacific region from a mantle plume. *Geology* **25** (5), 439-442.

Arculus R. J., 1994. Aspects of magma genesis in arcs. *Lithos* **33**, 189-208.

Arculus R. J. and Powell R., 1986. Source component mixing in the regions of arc magma generation. *Journal of Geophysical Research* **91**, 5913-5926.

Arndt N., Kerr, A.C. and Tarney, J., 1997. Dynamic melting in plume heads: the formation of Gorgona komatiites and basalts. *Earth and Planetary Science Letters* **146**, 289-301.

Avé Lallement H. G., 1996. Displacement partitioning and arc-parallel extension: example from the southeastern Caribbean plate margin. In: *Subduction: Top to Bottom*, Vol. 96, pp. 113-118.

Avé Lallement H. G., 1997. Transpression, displacement partitioning and exhumation in the eastern Caribbean/South American plate boundary. *Tectonics* **16**, 272-289.

Ayres L. D. and Peloquin A. S., 2000. Subaqeous, Paleproterozoic, metarhyolite dome-flow-cone complex, Flin-Flon greenstone belt, Manitoba, Canada. *Precambrian Research.* **101**, 211-235.

Ball M. M., Harrison C. G. A., and Supko P. R., 1969. Atlantic Opening and the structure of the Caribbean. *Nature* **223**, 167-168.

Bau M. and Knittel U., 1993. Significance of slab-derived partial melts and aqueous fluids for the genesis of tholeiitic and calc-alkaline island-arc basalts: evidence from Mt. Arayat, Philippines. *Chemical Geology* **105**, 233-251.

Beck C. M., Girard D., and DeWeber P., 1984. Volcanosedimentaire du Rio Guare: un element de la nappe ophiolitic de Lomo de Hierro, chaine Caraibe Venezuelienne. *Compte Rendus de Seances (D)* **299**, 337-342.

Beets D. J., Maresch W.V., Klaver G.Th, Mottana A., Bocchio R., Beunk F.F, and Monen H.P., 1984. Magmatic rock series and high-pressure metamorphism as constraints on the tectonic history of the southern Caribbean. In: *The Caribbean-South American plate boundary and regional tectonics*, Vol. Memoir **162** (ed. W. E. Bonini, Hargraves, R.B. and Shagam, R.). The Geological Society of America.

Beets D. J. and Lodder W., 1967. Indications for the presence of ignimbrites in the Cretaceous Washikemba Formation of the Isle of Bonaire, Netherlands Antilles. *Proc. K. Ak. Wet. Amsterdam (B)* **70**, 63-67.

Beets D. J., MacGillavry H. J., and Klaver G. T., 1977. Volcanic-sedimentary facies associations in the Washikemba Formation, Late Cretaceous, Bonaire. *Abstract of the 8th Geological Conference (Curaçao)*, 13-15.

Ben Othman D., White W. M., and Patchett J., 1989. The geochemistry of marine sediments, island arc magma genesis and crust-mantle recycling. *Earth and Planetary Science Letters.* **94**, 1-21.

Blichert-Toft J. and White W. M., 2001. Hf isotope geochemistry of the Galàpagos Islands. *Geochemistry, Geophysics, Geosystems* **2**.

Bocchio R., De Capitani L., Liborio G., Maresch W. V., and Mottana A., 1990. The eclogite-bearing series of Isla Margarita, Venezuela: geochemistry of metabasic lithologies in the La Rinconada and Juan Griego groups. *Lithos* **25**, 55-69.

Boland M. L., Pilatsig L. F., Ibadango C. E., McCourt W. J., Aspden J., and Hughes R., 2000. Geology of the Cordillera Occidental of Ecuador between 0-1N, pp. 70. Projecto de Desarrollo Minero y Control Ambiental, Informe 10.

Bouysse P., Schmidt-Effing R., and Westercamp D., 1983. La Desirade Island (Lesser Antilles) revisited; Lower Cretaceous radiolarian cherts and arguments against an ophiolitic origin for the basal complex. *Geology* **11** (4), 244-247.

Bowland C. L. and Rosencrantz E., 1988. Upper crustal structure of the western Colombian Basin, Caribbean Sea. *Bulletin of the Geological Society of America* **100**, 534-546.

Burke K., Fox P. J., and Sengör M. C., 1978. Buoyant ocean floor and the origin of the Caribbean. *Journal of Geophysical Research* **83** (B8), 3949-3954.

Campbell I. H. and Griffiths, R.W., 1990. Implications of mantle plume structure for the evolution of flood basalts. *Earth and Planetary Science Letters* **99**, 79-93.

Cas R. W. and Wright J. V., 1987. *Volcanic successions modern and ancient: a geological approach to processes, products and successions*. Allen and Unwin.

Case J. E., 1972. Tectonics of Colombian Andes; a progress report. *Transactions of the Caribbean Geological Conference Memorias - Conferencia Geologica del Caribe* **6**, 299.

Case J. E., Shagam, R. and Giegengack R.F., 1990. Geology of the northern Andes; an overview. In:*The Geology of North America*, Vol. Volume H, The Caribbean Region (ed. G. C. Dengo, J.E.), pp. 177-200. Geolgical Society of America.

Chown E. H., N'dah E., and Mueller W. U., 2000. The relation between iron-formation and low-temperature hydrothermal alteration in an Archaean volcanic environment. *Precambrian Research.* **101**, 263-275.

Christiansen R. L. and Lipman, 1966. Emplacement and thermal history of a rhyolite lava flow near Fortymile Canyon, southern Nevada *Bulletin of the Geological Society of America* **77** (7), 671-684.

Christie D. M., Duncan R. A., McBirney A. R., Richards M. A., White W. M., Harpp K. S., and Fox C. G., 1992. Drowned islands downstream from the Galápagos hotspot imply extended speciation times. *Nature* **355** (6357), 246-248.

Class C., Miller D. M., Goldstein S. L., and Langmuir C. H., 2000. Distinguishing melt and fluid subduction components in Umnak Volcanics, Aleutian Arc. *Geochemistry, Geophysics, Geosystems* **1**.

Cloos M., 1993. Lithospheric buoyancy and collisional orogenesis: subduction of oceanic plateaus, continental margins, island arcs, spreading ridges and seamounts. *Bulletin of the Geological Society of America* **105**, 715-737.

Clounard V. and Bonneville A., 2001. How many Pacific hotspots are fed by deep mantle plumes? *Geology* **29** (8), 695-698.

Cousineau P. A. and Bedard J. H., 2000. Sedimentation in a subaqueous arc/back arc setting: the Bobby Cove Formation, Snooks Arm Group, Newfoundland. *Precambrian Research* **101**, 111-134.

Cox K. G., Bell J. D., and Pankhurst R. J., 1979. *The interpretation of igneous rocks*. Chapman and Hall.

Dalrymple G. B. and Duffield W. A., 1988. High precision ^{40}Ar-^{39}Ar dating of Oligocene rhyolites from the Mogollon-Datil volcanic field using a continuous laser system. *Journal of Geophysical Research* **15** (5), 463-468.

Davidson J. P., 1987. Crustal contamination versus subduction zone enrichment: examples from the Lesser Antilles and implications for mantle source compositions of island arc rocks. *Geochemica Cosmochemica Acta* **51**, 2185-2198.

Davidson J. P., 1996. Deciphering mantle and crustal signatures in subduction zones (overview). In: *Subduction from top to bottom*, Vol. Geophysical Monograph (ed. G. E. Bebout, Scholl, D.W., Kirby, S.H. and Platt, J.P.), pp. 119-134. American Geophysical Union.

DePaulo D. J. and Johnson R. W., 1979. Magma genesis in the New Britain island arc: constraints from Nd and Sr isotopes and trace element patterns. *Contributions to Mineralogy and Petrology* **70**, 367-379.

Di Marco G., 1994. Les terraines accretes du sud du Costa Rica. Evolution tectonostratigraphique de la marge occidentale de la plaque Caraibe. Ph.D. thesis, Univ. Lausanne.

Diebold J. and Driscoll N. W., 1999. New insights on the formation of the Caribbean basalt province revealed by multichannel seismic images of volcanic structures in the Venezuelan Basin. In:*Caribbean basins* (ed. P. Mann), pp. 561-589. Elsevier.

Donnelly T. W., 1966. The geology of St. Thomas and St. John, Virgin Islands. In:*Caribbean Geological Studies*, Vol. Geological Society of America Memoir, **98** (ed. H. H. Hess), pp. 85-176.

Donnelly T. W., 1972. Deep water, shallow water and subareal island arc volcanism: example from the Virgin Islands. In:*Studies in Earth and Space Sciences, Geological Society of America Memoir*, Vol. 132 (ed. R. Shagam), pp. 401-414.

Donnelly T. W., 1985. Mesozoic and Cenozoic plate evolution of the Caribbean region. In: *The great American biotic interchange*, Vol. 4 (ed. F. G. Stehli and S. D. Webb), pp. 89-121. Plenum Press.

Donnelly T. W., 1989. Geologic history of the Caribbean and Central America. In: *The Geology of North America- an overview*, Vol. A (ed. A. W. P. Bally, A.R.), pp. 299-321. Geological Society of America.

Donnelly T. W., Beets, D., Carr, M. J., Jackson, T., Klaver, G., Lewis, J., Maury, R., Schellekens, H., Smith, A. L., Wadge, G., and Westercamp, D., 1990. History and tectonic setting of Caribbean magmatism In: *The Caribbean Region*, Vol. H (ed. G. Dengo and J. E. Case), pp. 339-374.

Donnelly T. W., 1994. The Caribbean Cretaceous basalt association: a vast igneous province that includes the Nicoya Complex of Costa Rica., 17-45.

Donnelly T. W. and Rogers J. J. W., 1967. Crust vs. mantle derivation of eastern Antillean igneous rocks (abs.). *EOS Transactions of the American Geophysical Union* **48**, 253.

Doyle M. G. and McPhie J., 2000. Facies architecture of a silicic intrusion-dominated volcanic centre at Highway-Reward, Queensland, Australia. *Journal of Volcanology and Geotherma Research* **99**, 76-96.

Draper G., Gutierrez, G. and Lewis, J.F., 1996. Thrust emplacement of the Hispaniola peridotite belt; Orogenic expression of the mid-Cretaceous Caribbean arc polarity reversal? *Geology* **24** (12), 1143-1146.

Driscoll N. W. and Diebold J. B., 1999. Tectonic and stratigraphic development of the eastern Caribbean; new constraints from multichannel seismic data. In: *Caribbean basins* (ed. P. Mann), pp. 591-626. Elsevier.

Druitt T. H., 1998. Pyroclastic density curents. In: *The Physics of Explosive Volcanic Eruptions*, Vol. 145 (ed. J. S. S. Gilbert, R.S.J.), pp. 145-182. Geological Society Special Publications.

Duncan R. A. H., R.B., 1984. Plate tectonic evolution of the Caribbean region in the mantle reference frame. In: *The Caribbean-South American plate boundary and regional tectonics*, Vol. Memoir 162 (ed. W. E. Bonini, Hargraves, R.B. and Shagam, R.), pp. 81-94. The Geological Society of America.

Echeverria L. M., 1980. Tertiary or Mesozoic komatiites from Gorgona Island, Colombia: field relations and geochemistry. *Contributions to Mineralogy and Petrology.* **73**, 253-256.

Echeverria L. M., 1980. Tertiary or Mesozoic komatiites from Gorgona Island, Colombia: field relations and geochemistry. *Contributions to Mineralogy and Petrology.* **73**, 253-256.

Edgar N. T. and Saunders J. B., 1971. *Initial Results of the Deep Sea Drilling Project - Leg 15.* Ocean Drilling Programme, Texas.

Edwards C. M. H., Morris J. D., and Thirlwall M. F., 1993. Separating mantle from slab signatures in arc lavas using B/Be and radiogenic isotope systematics. *Nature* **362**, 530-533.

Encarnacion J., Musaka S. B., and Evans C. A., 1999. Subduction components and the generation of arc-like melts in the Zambales ophiolite, Philippines: Pb, Sr and Nd isotopic evidence. *Chemical Geology* **156**, 343-357.

Ewart A., Collerson K. D., Regelous M., Wendt J. I., and Niu Y., 1998. Geochemical evolution within the Tonga-Kermadec-Lau-Back-arc systems: the role of varying mantle wedge composition in space and time. *Journal of Petrology* **39** (3), 331-368.

Farnetani C. G., Richards, M.A. and Ghiorso, M.S., 1996. Petrological models of magma evolution and deep crustal structure beneath hotspots and flood basalt provinces. *Earth and Planetary Science Letters* **143**, 812-94.

Faure G., 1986. *Isotope geology.* John Wiley.

Feighner M. A. and Richards M. A., 1995. Lithospheric structure and compensation mechanisms of the Galápagos Archipelago. *Journal of Geophysical Research, B, Solid Earth and Planets* **99** (4), 6711-6729.

Fisher R. V., Schmincke, H.-U., 1984a. *Pyroclastic Rocks.* Springer-Verlag.

Fisher R. V., 1984b. Submarine volcaniclastic rocks. In: *Marginal basin geology*, Vol. 16 (ed. B. P. H. Kokelaar, M.F.), pp. 5-29. Geological Society Special Publications.

Fisher R. V. and Smith G. A., 1991. Volcanism, tectonics and sedimentation. In: *Sedimentation in volcanic settings*, Vol. 45, pp. 1-5. Special Publication - Society of Economic Paleontologists and Mineralogists.

Fiske R. S., 1964. *Vertical grading of fragment density in subaqueous pyroclastic flows*. Geological Society of America.

Fitton J. G., Saunders A. D., Norry M. J., Hardarson B. S., and Taylor R. N., 1997. Thermal and chemical structure of the Iceland plume. *Earth and Planetary Science Letters* **153**, 197-208.

Francis E. H., 1983. Magma and Sediment-II. Problems of interpreting paleovolcanics buried in the stratigraphic column. *Journal of the Geological Society of London* **140**, 165-183.

Freydier C., Lapierre H., Ruiz J., Tardy M., Martinez-R J., and Coulon C., 2000. The early Cretaceous Arperos basin: an oceanic domain dividing the Guerro arc from nuclear Mexico evidenced by the geochemistry of the lavas and sediments. *Journal of South American Earth Sciences* **13**, 325-336.

Frisch W., Meschede M., and Sick M., 1992. Origin of the Central American ophiolites: evidence from paleomagnetic results. *Bulletin of the Geological Society of America* **104**, 1301-1314.

Frost C. D., Schellekens J. H., and Smith A. L., 1998. Nd, Sr and Pb isotopic characterisation of Cretaceous and Paleogene volcanic and plutonic island arc rocks from Puerto Rico. In: *Tectonics and Geochemistry of the Northeastern Caribbean*, Vol. 322 (ed. E. G. Lidiak and D. K. Larue), pp. 99-122. Geological Society of America.

Frost C. D. and Snoke A. W., 1989. Tobago, West Indies, a fragment of a Mesozoic oceanic island arc: petrochemical evidence. *Journal of the Geological Society of London.* **146**, 953-964.

Fujinawa A. and Green T. H., 1997. Partitioning behaviour of Hf and Zr between amphibole, clinopyroxene, garnet and silicate melts at high pressure. *European Journal of Mineralogy* **9**(2), 379-391.

Geist D., Naumann T., and Larson P., 1998. Evolution of Galápagos magmas: mantle and crustal fractionation without assimilation. *Journal of Petrology* **39** (5), 953-971.

Geldmacher J. and Hoernle K., 2000. The 72 Ma geochemical evolution of the Madeira Hotspot (eastern North Atlantic); recycling of Paleozoic (≤500 Ma) oceanic lithosphere. *Earth and Planetary Science Letters* **183** (1-2), 73-92.

Gill J. B., 1981. *Orogenic andesites and plate tectonics*. Springer Verlag.

Gomez A., Moreno M., and Pardo A., 1995. Edad y origen de Complejo metasedimentario de Aranzazu-Manizales en los alrededores de Manizales (Departamento de Caldas, Colombia. *Geologia Colombiana* **19**, 83-93.

Goossens P. J., Rose, W.I. and Flores, D., 1977. Geochemistry of theoleiites of the Basic Igneous Complex of northwestern South America. *Bulletin of the Geological Society of America* **88**, 1711-1720.

Graham D. W., Christie D. M., Harpp K. S., and Lupton J. E., 1993. Mantle plume helium in submarine basalts from the Galápagos platform. *Science* **262** (24 December), 2023-2027.

Green T. H., 1995. Significance of Nb/Ta as an indicator of geochemical processes in the crust-mantle system. *Chemical Geology* **120** (3-4), 347-359.

Greenly E., 1940. Studies in the Mona complex [pre-Cambrian, Wales]. *Geological Magazine* **77** (1), 50-53.

Griffiths R. W. and Campbell I. H., 1990. Stirring and structure in mantle starting plumes. *Earth and Planetary Science Letters* **99**, 66-78.

Gripp A. E. and Gordon R. G., 1990. Current plate velocities relative to the hotspots incorporating the NUVEL-1 global plate motion model. *Journal of Geophysical Research* **17** (8), 1109-1120.

Harland W. B., Armstrong R. L., Cox A. V., Craig L. E., Smith A. G., and Smith D. G., 1990. *A Geologic Time Scale 1989*. Cambridge University Press.

Harpp K. S. and White W. M., 2001. Tracing a mantle plume: isotopic and trace element variations of Galápagos seamounts. *Geochemistry, Geophysics, Geosystems* **2**.

Hauff F., Hoernle K., Schmincke H.-U., and Werner R., 1997. A Mid-Cretaceous origin for the Galápagos hotspot: volcanological, petrological and geochemical evidence from Costa Rican oceanic crustal segments. *Geologische Rundschau* **86**, 141-155.

Hauff F., Hoernle K., Tilton G., Graham D. W., and Kerr A. C., 2000a. Large volume recycling of oceanic lithosphere over short time scales: geochemical constraints from the Caribbean Large Igneous Province. *Earth and Planetary Science Letters* **174**, 247-263.

Hauff F., Hoernle K., van den Bogaard P., Alvarado G., and Garbe-Schonberg D., 2000b. Age and geochemistry of basaltic complexes in western Costa Rica: contributions to the geotectonic evolution of Central America. *Geochemistry, Geophysics, Geosystems* **1** (May 30).

Hawkesworth C. J., Gallagher, K., Hergt, J.M. andMcDermott, F., 1994. Destructive plate margin magmatism: geochemistry and melt generation. *Lithos* **33**, 169-188.

Hawkesworth C. J., Gallagher K., Hergt J. M., and McDermott F., 1993. Mantle and slab contributions in arc magmas. *Annual Review of Earth and Planetary Sciences* **21**, 175-204.

Hey R., Johnson G. L., and Lowrie A., 1977. Recent plate motions of the Galápagos area. *Bulletin of the Geological Society of America* **88**, 1385-1403.

Hill R. I., 1993. Mantle plumes and continental tectonics. *Lithos* **30**, 193-206.

Hoernle K., Werner R., Phipps Morgan J., Garbe-Schonberg D., Bryce J., and Mrazec J., 2000. Existence of complex spatial zonation in the Galápagos plume for at least 14 Ma. *Geology* **28**, 435-438.

Hole M. J., Saunders A. D., Marriner G. F., and Tarney J., 1984. Subduction of pelagic sediments; implications for the origin of Ce-anomalous basalts from the Mariana Islands. *Journal of the Geological Society of London* **141**, 453-472.

Jackson T. A. S., T.E., 1979. The tectonic significance of basalts and dacites in the Wagwater Belt, Jamaica. *Geological Magazine* **116** (5), 365-374.

Jaillard E., 1995. Basin development in an accretionary, oceanic-floored fore-arc setting: southern coastal Ecuador during Late Cretaceous-Late Eocene time. In: *Petroleum basins of South America*, Vol. 62 (ed. A. J. Tankard, Suarez S., R. and Welsink, H.J.), pp. 615-631. AAPG.

Jensen L. S., 1976. A new cation plot for classifying subvolcanic rocks. *Ontario Division of Mines Miscellaneous Paper* **66**.

Jolly W. T., Lidiak E. G., Dickin A. P., and Wu T.-W., 1998. Geochemical diversity of island arc rocks in eastern Puerto Rico. In: *Tectonics and Geochemistry of the Northeastern Caribbean*, Vol. 322 (ed. E. G. Lidiak and D. K. Larue), pp. 67-98. Geological Society of America.

Jolly W. T., Lidiak E. G., Dickin A. P., and Wu T.-W., 2001. Secular geochemistry of central Puerto Rican island arc Lavas- constraints on Mesozoic tectonism in the eastern Greater Antilles. *Journal of Petrology* **42** (12), 2197-2214.

Jónasson K., 1994. Rhyolite volcanism in the Krafla central volcano, north-east Iceland. *Bulletin of Volcanology*. **56**, 516-528.

Jónasson K., Holm P. M., and Pederson A. K., 1992. Petrogenesis of silicic rocks from the Króksfjördur Central Volcano, NW Iceland. *Journal of Petrology* **33**, 1345-1369.

Kay R. W., 1978. Aleutian magnesian andesites; melts from subducted Pacific Ocean crust. *Journal of Volcanology and Geothermal Research* **4** (2), 117-132.

Kelly K., Plank T., Farr L., Ludden J., Stadigel H., and Alt J., 2001. Subduction cycling of U, Th and Pb: perspectives from altered oceanic crust. *Journal of Conference Abstracts* **6** (384).

Kempton P. D., Fitton J. G., Saunders A. D., Nowell G. M., Taylor R. N., Hardarson B. S., and Pearson G. M., 2000. The Iceland plume in space and time: a Sr-Nd-Pb-Hf study of the North Atlantic rifted margin. *Earth and Planetary Science Letters* **177**, 255-271.

Keppler H., 1995. Experimental constraints on trace element transport by fluids in subduction zones (abstract). *EOS Transactions of the American Geophysical Union* **76** (46), 655.

Kerr A. C., Saunders, A.D., Tarney, J., Berry, N.H. and Hards, V.L., 1995. Depleted mantle-plume geochemical signatures: no paradox for plume theories. *Geology* **23** (9), 843-846.

Kerr A. C., Tarney, J., Marriner, G.F., Klaver, G.Th, Saunders, A.D and Thirlwall, M.F., 1996a. The geochemistry and petrogenesis of the late-Cretaceous picrites and basalts of Curaçao, Netherlands Antilles: a remnant of an oceanic plateau. *Contributions to Mineralogy and Petrology* **124**, 29-43.

Kerr A. C., Marriner G. F., Arndt N. T., Tarney J., Nivia A., Saunders A. D., and Duncan R. A., 1996b. The petrogenesis of Gorgona komatiites, picrites and basalts: new field, petrographic and geochemical constraints. *Lithos* **37**, 245-260.

Kerr A. C., Marriner, G.F., Tarney, J., Nivia, A., Saunders, A.D., Thirlwall, M.F. and Sinton, C., 1997a. Cretaceous basaltic terranes in western Colombia: Elemental, chronological and Sr-Nd isotopic constraints on the petrogenesis. *Journal of Petrology* **38**, 677-702.

Kerr A. C., Tarney, J., Marriner, G.F., Nivia, A and Saunders, A.D., 1997b. The Caribbean-Colombian Cretaceous Igneous Province: the internal anatomy of an oceanic plateau. In: *Large Igneous Provinces: Continental, Oceanic and Planetary Flood Volcanism*, Vol. Geophysical Monograph **100**, pp. 123-143. American Geophysical Union.

Kerr A. C., Iturralde-Vinent, M.A., Saunders, A.D., Babbs, T.L. and Tarney, J., 1999. A geochemical reconnaissance of Cuban Mesozoic volcanic rocks: implications for plate tectonic models of the Caribbean. *Bulletin of the Geological Society of America* **111**, 1581-1599.

Kerr A. C., Marriner G. F., Spadea P., Tarney J., Kempton P. D., Nivia A., and Saunders A. D., 2000. Cretaceous picrites and high-Mg basalts from SW Colombia: Implications for the plume source of the Caribbean oceanic plateau. *Journal of Geophysical Research.*

Kerr A. C., Tarney J., Kempton P. D., Spadea A., Nivia A., Marriner G. F., and Duncan R. A., 2002a. Pervasive mantle plume head heterogeneity: Evidence from the late Cretaceous Caribbean-Colombian Oceanic Plateau. *Journal of Geophysical Research* In press.

Kerr A. C., Aspden J. A., Tarney J., and Pilatasig L. F., 2002b. The nature and provenance of accreted oceanic terranes in western Ecuador: Geochemical and tectonic constraints. *Journal of the Geological Society (London)* In Press.

Kerr, A. C, White, R. V., Thompson, P. M. E., Tarney, J. and Saunders, A. D., 2002c. No oceanic plateau- no Caribbean plate? The seminal role of oceanic plateau(s) in Caribbean plate evolution. *American Association of Petroleum Geologists Memoir* In Press.

Kerrich R. and Wyman D. A., 1996. The trace element systematics of igneous rocks in mineral exploration; an overview. *Short Course Notes - Geological Association of Canada* **12**, 1-50.

Kesler L. G. and Bedard J. H., 2000. Epiclastic volcanic debrites- evidence of flow transformations between avalanche and debris flow processes, Middle Ordovician, Baie Verte Penninsula, Newfoundland, Canada. *Precambrian Research* **101**, 135-161.

Kesler S. E., Sutter J. F., Barton J. M., and C. S. R., 1991. Age of intrusive rocks in Northern Hispaniola. In: *Geologic and Tectonic Development of the North America-Caribbean Plate Boundary in Hispaniola*, Vol. 262 (ed. P. Mann, G. Draper, and J. F. Lewis), pp. 165-172. Geological Society of America.

Klaver G., 1976. The Washikemba Formation, Bonaire. MSc Thesis, Uttrecht, Netherlands.

Klaver G. T., 1987. The Curaçao lava formation: an ophiolitic analogue of the anomalous thick layer 2B of the mid-Cretaceous oceanic plateaus in the western Pacific and central Caribbean, Drukkerij Elinkwijk.

Kobayashi K. and Nakamura E., 2001. Geochemical evolution of Akagi volcano, NE Japan, implications for interaction between island-arc magma and lower crust, and generation of isotopically various magmas. *Journal of Petrology* **42** (12), 2303-2331.

Kurz M. D. and Geist D., 1999. Dynamics of the Galápagos hotspot from Helium isotope geochemistry. *Geochemica et Geocosmica Acta* **63** (23/24), 4139-4156.

Lapierre H., Dupuis, V., Mercier de Lepinay, B., Tardy, M., Ruiz, J., Maury, R.C., Hernandez, J. and Loubet, M., 1997. Is the Lower Duarte igneous complex (Hispaniola) a remnant of the Caribbean plume-generated oceanic plateau? *The Journal of Geology* **105**, 111-120.

Lapierre H., Bosch, D., Dupuis, V. and others, 2000. Multiple plume events in the genesis of the peri-Caribbean Cretaceous oceanic plateau province. *Journal of Geophysical Research* **105** (B4), 8403-8421.

Le Maitre R. W., Bateman P., Dudek A., Keller J., LeBas M. J., Sabine P. A., Schmid R., Sorensen H., Streckeisen A., Woolley A. R., and Zanettin B., 1989. *A classification of igneous rocks and a glossary of terms.* Blackwell.

Leat P. T., Livermore R. A., Millar I. L., and Pearce J. A., 2000. Magma supply in back-arc spreading centre segment E2, East Scotia Ridge. *Journal of Petrology* **41** (6), 845-866.

Lebras M., Megard F., Dupuy C., and Dostal J., 1987. Geochemistry and tectonic setting of pre-collision Cretaceous and Paleogene volcanic rocks of Ecuador. *Bulletin of the Geological Society of America.* **99**, 569-578.

Lebron M. C. and Perfit M. R., 1993. Stratigraphic and petrochemical support subduction polarity reversal of the Cretaceous Caribbean Island arc. *Journal of Geology* **101**, 389-396.

Lebron M. C. P., M.R., 1994. Petrochemistry and tectonic significance of Cretaceous island-arc rocks, Cordellera Oriental, Dominican Republic. *Tectonophysics* **229**, 69-100.

Lewis J. F., Hames W. E., and Draper G., 1999. Late Juriassic oceanic crust and Upper Cretaceous Caribbean Plateau picritic basalts exposed in the Duarte Igneous Complex, Hispaniola: a discussion. *The Journal of Geology* **107**, 505-508.

Lewis J. F., Perfit M., Horan S., and Diaz d., 1995. Geochemistry and petrotectonic significance of early island arc bimodal volcanism in the Greater Antilles arc. *Geological Society of America, 1995 annual meeting*, 227.

Lewis J. F. D., G., 1990. Geology and Tectonic evolution of the northern Caribbean margin. In: *The Geology of North America*, Vol. Volume H, The Caribbean Region (ed. G. C. Dengo, J.E.), pp. 77-140. The Geological Society of America.

Lidiak E. G. and Jolly W. T., 1996. Circum-Caribbean granitoids; characteristics and origin. *International Geology Review* **38**, 1098-1133.

Lowe D. R., 1982. Sediment Gravity Flows. *Journal of Sedimentary Petrology* **52** (1), 0279-0297.

Macdonald R., Hawkesworth C. J., and Heath E., 2000. The Lesser Antilles volcanic chain: a study in arc magmatism. *Earth Science Reviews* **49**, 1-76.

Mahoney J. J., 1987. An isotopic survey of Pacific ocean plateaus: implications for their nature and origin. In: *Seamounts, Islands and Atolls* (ed. B. H. Keating, P. Fryer, R. Batiza, and G. W. Boehlert), pp. 207-220. American Geophysical Union.

Mann P., Schubert, C and Burke , K., 1990. Review of Caribbean neotectonics. In: *The Geology of North America*, Vol. Volume H, The Caribbean Region (ed. G. C. Dengo, J.E.), 307-338. The Geological Society of America.

Mann P., Draper G., and Lewis J. F., 1991. An overview of the geologic and tectonic development of Hispaniola. In: *Geologic and Tectonic Development of the North America-Caribbean Plate Boundary in Hispaniola*, Vol. 262 (ed. P. Mann, G. Draper, and J. F. Lewis), 1-28. Geological Society of America.

Marsh B. D., Gunnarsson B., Congdon R., and Carmody R., 1991. Hawaiian basalt and Icelandic rhyolite: indicators of differentiation and partial melting. *Geologische Rundschau* **80** (2), 481-510.

Mattinson J. M., Fink L. K. J., and Hopson C. A., 1980. Geochronologic and isotopic study of the La Desirade Island Basement Complex. *Contributions to Mineralogy and Petrology.* **71**, 237-245.

Mauffret A. and Leroy S., 1997. Seismic stratigraphy and structure of the Caribbean igneous province. *Tectonophysics* **283**, 61-104.

McBirney A. R., 1993. Differentiated rocks of the Galápagos hotspot. In: *Magmatic Processes and Plate Tectonics*, Vol. **76** (ed. H. M. Prichard, T. Alabaster, N. B. W. Harris, and C. R. Neary), pp. 61-69. Geological Society.

McCourt W. J. and Aspden J. A., 1987. A plate tectonic model for the Phanerozoic evolution of central and southern Colombia. In: *Transactions of the Tenth Caribbean Geological Conference, Cartagena de Indias, Colombia* (ed. H. Duque-Caro), 38-47. INGEOMINAS.

McCulloch M. T. and Gamble J. A., 1991. Geochemical and geodynamical constraints on subduction zone magmatism. *Earth and Planetary Science Letters* **102**, 358-374.

McDonough W. F. and Sun S.-s., 1995. The composition of the Earth. *Chemical Geology* **120**, 223-253.

McGuire W. J., 1996. Volcano instability; a review of contemporary themes. In: *Volcano instability on the Earth and other planets*, Vol. 110, pp. 1-23. Geological Society Special Publications.

McKenzie D. P. and Bickle M. J., 1988. The volume and composition of melt generated by extension of the lithosphere. *Journal of Petrology* **29**, 625-679.

McLennan S. M. and Taylor S. R., 1981. Role of subducted sediments in island-arc magmatism: constraints from REE patterns. *Earth and Planetary Science Letters* **54**, 423-430.

McPhie J., Doyle M., and Allen R., 1993. *Volcanic textures: a guide to the interpretation of textures in volcanic rocks.* University of Tasmania.

Meschede M., 1998. The impossible Galápagos connection: geometric constraints for a near-American origin of the Caribbean plate. *Geologische Rundschau* **87**, 200-205.

Meschede M. F., W., 1998. A plate tectonic model for the Mesozoic and Early Cenozoic history of the Caribbean plate. *Tectonophysics* **296**, 269-291.

Middlemost E. A. K., 1975. The basalt clan. *Earth Science Reviews* **11** (4), 337-364.

Moine B. N., Gregoire M., O'Reilly S. Y., Sheppard S. M. F., and Cottin J. Y., 2001. High field strength element fractionation in the upper mantle: evidence from amphibole-rich composite mantle xenoliths from the Kerguelen islands (Indian Ocean). *Journal of Petrology* **42** (11), 2145-2167.

Montgomery H., Pessagno E. A., and Munoz I. M., 1992. Jurassic (Tithonian) radiolaria from La Desirade (Lesser Antilles): premliminary palaentological tectonic implications. *Tectonics* **11** (6), 1426-1432.

Montgomery H., Pessagno E. A. J., Lewis J. F., and Schellekens J., 1994. Paleogeography of Jurassic fragments in the Caribbean. *Tectonics* **13** (2), 725-732.

Munker C., 1998. Nb/Ta fractionation in a Cambrian arc/back arc system, New Zealand; source constraints and application of refined ICPMS techniques. *Chemical Geology* **144**, 23-45.

Munker C., 2000. The isotope and trace element budget of the Cambrian Devil River arc system, New Zealand: identification of 4 source components. *Journal of Petrology* **41** (6), 759-788.

Munker C. and Crawford A. J., 2000. Cambrian arc evolution along the SE Gondwana active margin: a synthesis from Tasmania-New Zealand-Australia-Antarctic correlations. *Tectonics* **19** (3), 415-432.

Nicolaysen K., Frey F. A., Hodges K. V., and the shipboard scientific party, 2000. ^{40}Ar-^{39}Ar geochronology of flood basalts from the Kerguelen Archipelago, southern Indian Ocean; implications for Cenozoic eruption rates of the Kerguelen plume. *Earth and Planetary Science Letters* **174** (3-4), 313-328.

Nielsen R. L., 1988. A model for the simulation of combined major and trace element liquid lines of descent. *Geochimica et Cosmochimica Acta* **52**, 27-38.

Nivia A., 1996. The Bolivar mafic-ultramafic complex, SW Colombia: the base of an obducted plateau. *Journal of South American Earth Sciences.* **9**, 59-68.

Nowell G. M., Kempton P. D., Noble S. R., Fitton J. G., Saunders A. D., Mahoney J. J., and Taylor R. N., 1998. High precision Hf isotope measurements of MORB and OIB by thermal ionisation mass spectrometry: insights into the depleted mantle. *Chemical Geology* **149**, 211-233.

Patino L. C., Carr M. J., and Feigenson M. D., 2000. Local and regional variations in Central American arc lavas controlled by variations in sediment input. *Contributions to Mineralogy and Petrology.* **138**, 265-283.

Peacock S. M. and Hervig R. L., 1999. Boron isotopic composition of subduction-zone metamorphic rocks. *Chemical Geology* **160** (4), 281-290.

Pearce J. A., Baker P. E., Harvey P. K., and Luff I. W., 1995. Geochemical evidence for subduction fluxes, mantle melting ad fractional crystallisation beneath the South Sandwich island arc. *Journal of Petrology* **36** (4), 1073-1109.

Pearce J. A., Kempton P. D., Nowell G. M., and Noble S. R., 1999. Hf-Nd element and isotopic perpective on the nature and provenance of mantle and subduction components in Western Pacific arc-basin systems. *Journal of Petrology* **40** (11), 1579-1611.

Pearce J. A. and Norry M. J., 1979. Petrogenetic implications of Ti, Zr, Y and Nb variations in volcanic rocks. *Contributions to Mineralogy and Petrology.* **69**, 33-47.

Peate D. W., Pearce J. A., Hawkesworth C. J., Colley H., Edwards C. M. H., and Hirose K., 1997. Geochemical variations in Vanatu Arc Lavas: the role of subducted material and a variable mantle wedge composition. *Journal of Petrology* **38** (10), 1331-1358.

Perfit M. R., Gust D. A., Bence A. E., Arculus R. J., and Taylor S. R., 1980. Chemical characteristics of island-arc basalts: implications for mantle sources. *Chemical Geology* **30**, 227-256.

Petterson M. G., Neal, C.R., Mahoney, J.J., Kroenke, L.W., Saunders, A.D., Babbs, T.L., Duncan, R.A., Tolia, D. and McGrail, B., 1997. Structure and deformation on north and central Malaita, Solomon Islands; tectonic implications for the Ontong Java Plateau-Solomon arc collision, and for the fate of oceanic plateaus. *Tectonophysics* **283**, 1-33.

Petterson M. G., Babbs, T.L., Neal, C.R., Mahoney, J.J., Saunders, A.D., Duncan, R.A., Tolia, D., Magu, R., Qopoto, C, Mahoa, H and Natogga, D., 1999. Geological-tectonic framework of Solomon Islands, SW Pacific; crustal accretion and growth in an intra-oceanic setting. *Tectonphysics* **301**, 35-60.

Pijpers P. J., 1933. Geology and Paleontology of Bonaire. Ph.D. Thesis.

Pindell J. L., 1985. Plate-tectonic Evolution of the Gulf of Mexico and Caribbean Region. Ph.D. Thesis.

Pindell J. L. and Barrett S. F., 1990. Geologic evolution of the Caribbean region: a plate tectonic perspective. In: *The Caribbean region*, Vol. vol. H (ed. G. Dengo and J. E. Case), pp. 405-432. Geological Society of America.

Pindell J. L., Higgs R., and Dewey J. F., 1998. Cenozoic palinspastic reconstruction, paleogeographic evolution and hydrocarbon setting of the northern margin of South America. In:

Paleogeographic Evolution and non-glacial Eustasy, Nothern South America, Vol. No. 58, pp. 45-85.

Plank T. and Langmuir C. H., 1988. An evaluation of the global variations in the major element chemistry of arc basalts. *Earth and Planetary Science Letters* **90**, 349-370.

Priem H. N. A., Andriessen, P.A.M, Beets, D.J., Boelrijk, N.A.I.M., Herbeda, E.H., Verdurmen, E.A.Th and Verschure, R.H., 1979. K-Ar and Rb-Sr dating in the Cretaceous island-arc succession of Bonaire, Netherlands Antilles. *Geologie en Mijnbouw* **58** (3), 367-373.

Révillon S., Arndt N. T., Hallot E., Kerr A. C., and Tarney J., 1999. Petrogenesis of picrites from the Caribbean Plateau and the North Atlantic magmatic province. *Lithos* **49**, 1-21.

Révillon S., Chauvel C., Arndt N. T., Pik R., Martineau F., Fourcade S., and Marty B., 2002. Heterogeneity of the Caribbean plateau mantle source: new constraints from Sr, O and He isotope compositions of olivine and clinopyroxene. *Earth and Planetary Science Letters* In Press.

Reynaud C., Lapierre, H., Jaillard, E., Benitez, S., Berrones, G. and Mascle, G., 1996.. Mineralogical and geochemical characterisation of Middle Cretaceous to Paleocene oceanic and continental volcanic rocks from southwestern Ecuador. *Third ISAG*, 633-636.

Reynaud C., Jaillard E., Lapierre H., Mamberti M., and Mascle G. H., 1999. Oceanic plateau and island arcs of southwestern Ecuador: their place in the geodynamic evolution of northwestern South America. *Tectonophysics* **307**, 235-254.

Richards M. A., Duncan R. A., and Courtillot V. E., 1990. Flood basalts and hotspot tracks: plume heads and tails. *Science* **246**, 103-107.

Richards M. A. and Griffiths R. W., 1989. Thermal entrainment by deflected mantle plumes. *Nature* **342** (6252), 900-902.

Rickwood P. C., 1989. Boundary lines within petrologic diagrams which use oxides of major and minor elements. *Lithos* **22** (4), 247-263.

Rollinson H. R., 1993. *Using geochemical data: evaluation, presentation and interpretation.* Longman.

Royse K., Kempton P. D., and Darbyshire, P.D.F., 1998. Procedure for the analysis of rubidium-strontium and samarium-neodymium isotopes at the NERC Isotope Geosciences Laboratory. *NIGL Report Series* **121**. 28 pp.

Sallares V. and Danobeitia J. J., 2001. Lithospheric structure of the Costa Rican Isthmus: Effects of subduction zone magmatism on an oceanic plateau. *Journal of Geophysical Research* **106** (B1), 621-643.

Santamaria F. and Schubert C., 1974. Geochemistry and geochronology of the Southern Caribbean-Northern Venezuela plate boundary. *Bulletin of the Geological Society of America* **7**, 1085-1098.

Saunders A. D., Tarney, J., Kerr, A.C. and Kent, R.W., 1996. The formation and fate of large oceanic igneous provinces. *Lithos* **37**, 81-95.

Saunders A. D., Tarney J., and Weaver S. D., 1980. Transverse geochemical variations across the Antarctic Peninsula; implications for the genesis of calc-alkaline magmas. *Earth and Planetary Science Letters* **46** (3), 344-360.

The following image type has poor quality text due to the nature of the material.

Image quality is best available.

Schellekens J. H., 1998a. Composition, metamorphic grade and origin of metabasites in the Bermeja Complex, Puerto Rico. *International Geology Review* **40**, 722-747.

Schellekens J. H., 1998b. Geochemical evolution and tectonic history of Puerto Rico. In: *Tectonics and Geochemistry of the Northeastern Caribbean*, Vol. 322 (ed. E. G. Lidiak and D. K. Larue), pp. 35-66. Geological Society of America.

Schellekens J. H., Montgomery H., Joyce J., and Smith A. L., 1990. Late Jurassic to Late Cretaceous development of island arc crust in southwestern Puerto Rico. In: *Transactions of the 12th Caribbean geological conference*, Vol. 12 (ed. D. K. Larue and G. Draper), pp. 268-281.

Sen G., Hickey-Vargas R., Waggoner D. G., and Maurrasse F., 1988. Geochemistry of basalts from the Duimisseau Formation, southern Haiti: implications for the origin of the Caribbean Sea crust. *Earth and Planetary Science Letters* **87**, 423-437.

Sha L.-K., Chapell, B.W., 1991. Apatite chemical composition, determined by electron microprobe and laser-ablation inductively coupled plasma mass spectrometry, as a probe into granite petrogenesis. *Geochimica et Cosmochimica Acta* **63** (22), 3861-3881.

Shagam R., 1960. Geology of the Central Aragua, Venezuela. *Bulletin of the Geological Society of America* **71**, 249-302.

Sharma A. and Rajamani V., 2000. Major element, REE, and other trace element behavior in amphibolite weathering under semiarid conditions in southern India. *Journal of Geology* **108** (4), 487-496.

Sharp W. D. and Snoke A. W., 1988. Tobago, West Indies; Geochronological study of a fragment of a composite Mesoaoic oceanic island arc. *Geological Society of America, Abstracts with programs* **20**, 60.

Silver E. A., Case J. E., and MacGillavry H. J., 1975. Geophysical study of the Venezuelan Borderland. *Bulletin of the Geological Society of America* **86**, 213-226.

Sinton C. W., Duncan, R.A., Storey, M., Lewis, J. and Estrada, J.J., 1998. An oceanic flood basalt province within the Caribbean plate. *Earth and Planetary Science Letters* **155** (3-4), 221-235.

Sinton C. W. and Duncan R. A., 1992. Temporal evolution of the Caribbean Cretaceous basalt province, results of ^{40}Ar-^{39}Ar dating. *EOS Transactions of the American Geophysical Union* **73**, 532.

Sinton C. W. and Duncan R. A., 1997. Nicoya Peninsula, Costa Rica: A single suite of Caribbean oceanic plateau magmas. *Journal of Geophysical Research* **102** (B7), 15507-15520.

Sinton C. W., Duncan R. A., and Storey M., 1993. ^{40}Ar-^{39}Ar ages from Gorgona Iosland, Colombia, and the Nicoya Peninsula, Costa Rica (abstract). *EOS Transactions of the American Geophysical Union* **73**, 532.

Sinton C. W., Sigurdsson H., and Duncan R. A., 2000. Geochronology and petrology of the igneous basement at the Lower Nicaraguan Rise, Site 1001. *Proceedings of the Ocean Drilling Programme, Scientific Results* **165**, 233-236.

Smit J., 1977.. Planktonic formaniferal faunas from the upper part of the Washikemba Formation, Bonaire. *8th Caribbean Geological Conference*, 192-193.

Smith C. A., Sisson V. B., Ave Lallemant H. G., and Copeland P., 1999. Two contrasting pressure-temperature-time paths in the Villa de Cura blueschist belt Venezuela: Possible evidence for

Late Cretaceous initiation of subduction in the Caribbean. *Bulletin of the Geological Society of America* **111** (6), 831-848.

Smith T. E., Thirlwall, M.F. and Macpherson, C., 1996. Trace element and isotope geochemistry of the volcanic rocks of Bequia, Grenadine Islands, Lesser Antilles Arc: a study of subduction enrichment and intra-crustal contamination. *Journal of Petrology* **37** (1), 117-143.

Snoke A. W. and Noble P. J., 2001. Ammonite-radiolarian assemblage, Tobago Volcanic group, Tobago, West Indies- Implications for the evolution of the Great Arc of the Caribbean. *GSA Bull* **113** (2), 256-264.

Snoke W., 1990. An evaluation of the petrogenesis of the accreted Mesozoic island arc of the southem Caribbean. In: *Transactions of the Second Geological Conference of the Geological Society of Trinidad and Tobago*, pp. 222-230.

Spadea P. and Espinosa A., 1996. Petrology and chemistry of late Cretaceous volcanic rocks from the southernmost segment of the Western Cordillera of Colombia (South America). *Journal of South American Earth Sciences* **9**, 79-90.

Speed R. C. and Smith-Horowitz P. L., 1998. The Tobago Terrane. *Internation Geology Review* **40**, 805-830.

Steiger R. H. and Jaeger E., 1977. Subcommission on geochronology; convention on the use of decay constants in geo- and cosmochronology. *Earth and Planetary Science Letters* **36** (3), 359-362.

Stimac J. and Hickmott D., 1994. Trace-element partition co-efficients for ilmenite, orthopyroxene and pyrrhotite in rhyolite determined by micro-PIXE analysis. *Chemical Geology* **117**, 313-330.

Stöckhert B., Maresch, W.V., Brix, M., Kaiser, C., Toetz, A., Kluge, R. and Krückhans-Lueder, G., 1995. Crustal history of Margarita Island (Venezuela) in detail: constraint on the Caribbean plate-tectonic scenario. *Geology* **23** (9), 787-790.

Stolper E. and Newman S., 1994. The role of water in the petrogenesis of Mariana Trough magmas. *Earth and Planetary Science Letters* **121**, 293-325.

Stoltz A. J., Jochum K. P., Spettel B., and Hofmann A. W., 1996. Fluid and melt-related enrichment in the subarc mantle: evidence from Nb/Ta variations in island-arc basalts. *Geology* **24** (7), 587-590.

Sun C.-H. and Stern R., 2001. Genesis of Mariana shoshonites; contribution of the subduction component. *Journal of Geophysical Research, B, Solid Earth and Planets* **106** (1), 589-608.

Sun S. S., 1980. Lead isotopic study of young volcanic rocks from mid-ocean ridges, ocean islands, and island arcs. *Philosophical Transactions of the Royal Society of London.* **A297**, 409-445.

Tardy M., Lapierre, H., Feydier, C., Coulon, C., Gill, J.-B., Mercier de Lepinay, B., Beck, C., Martinez, R., J., Talavera M., O., Ortiz H., E., Stein, G., Bourdier, J-L. and Yta, M., 1994. The Guerrero suspect terrane (western Mexico) and coeval arc terranes (the Greater Antilles and the Western Cordillera of Colombia): a late Mesozoic intra-oceanic arc accreted to cratonal America during the Cretaceous. *Tectonophysics* **230**, 49-73.

Tatsumi Y., Hamilton D. L., and Nesbit R. W., 1986. Chemical characteristics of fluid phase released from a subducted lithosphere and origin of arc magmas; evidence from high-pressure experiments and natural rocks. *Journal of Volcanology and Geothermal Research* **29**, 293-309.

Tera F., Brown L., Morris J., Sacks I. S., Klein J., and Middleton R., 1986. Sediment incorporation in island-arc magmas; inferences from ^{10}Be. *Geochimica et Cosmochimica Acta* **50** (4), 535-550.

Thirlwall M. F., Graham, A.M., Arculus, R.J., Harmon, R.S. and Macpherson, C.G., 1996. Resolution of the effects of crustal assimilation, sediment subduction and fluid transport in island arc magmas: Pb-Sr-Nd-O isotope geochemistry of Grenada, Lesser Antilles. *Geochimica et Cosmochimica Acta* **60** (2), 4785-4810.

Thirlwall M. F. and Graham A. M., 1984. Evolution of high-Ca, high-Sr C-series basalts from Grenada, Lesser Antilles; the effects of intra-crustal contamination. *Journal of the Geological Society of London* **141**, 427-445.

Thorpe R. S., Leat P. T., Mann A. C., Howell M. F., Reedman A. J., and Campbell S. D. G., 1993. Magmatic evolution of the Ordovician Snowdon volcanic centre, North Wales (UK). *Journal of Petrology* (4), 711-741.

Tiepolo M., Bottazzi P., Foley S. F., Oberti R., Vannucci R., and Zanetti A., 2001. Fraactionation of Nb and Ta from Zr and Hf at mantle depths: the role of titanian pargasite and kaersutite. *Journal of Petrology* **21**(1), 221-232.

Tistl M. and Salazar G., 1993. The tectonomagmatic evolution of north western South America. *Zbl. Geol. Palont. Teil I* **H 1/2**, 439-453.

Todt W., Cliff R. A., Hanser A., and Hofmann A. W., 1996. Evaluation of a ^{202}Pb-^{205}Pb double spike for high-precision lead isotope analysis. In: *Earth Processes: Reading the Isotope Code*, Vol. 95 (ed. S. R. Hart and A. Basu), pp. 429-437. *American Geophysical Union.*

Turner S., Hawkesworth C., Rogers N., Bartlett J., Worthington T., Hergt J., Pearce J., and Smith I., 1997. ^{238}U-^{230}Th disequilibria, magma petrogenesis, and flux rates beneath the depleted Tonga-Kermadec island arc. *Geochimica et Cosmochimica Acta* **61** (22), 4855-4884.

Turner S., Hawkesworth C., vanCalsteren P., Heath E., Macdonald R., and Black S., 1996. U-series isotopes and destructive plate margin magma genesis in the Lesser Antilles. *Earth and Planetary Science Letters* **142**, 191-207.

Van Soest M. C., Hilton D. R., Macpherson C. G., and Mattey D. P., 2002. Resolving sediment subduction and contamination in the Lesser Antilles island arc: a combined He-O-Sr isotope approach. *Journal of Petrology* **43** (1), 143-170.

Vervoort J. D. and Blichert-Toft J., 1999. Evolution of the depleted mantle; Hf isotope evidence from juvenile rocks through time. *Geochimica et Cosmochimica Acta* **63** (3-4), 533-556.

Wadge G., Jackson, T.A., Isaacs, M.C. and Smith, T.E., 1982. The ophiolitic Bath-Dunrobin Formation, Jamaica: significance for Cretaceous plate margin evolution in the north-western Caribbean. *Journal of the Geological Society of London* **139**, 321-333.

Wadge G. M., R., 1985. Cretaceous tholeiites of the northern continental margin of South America: the Sans Souci Formation of Trinidad. *Journal of the Geological Society, London* **142**, 297-308.

Walker R. J., Storey M., Kerr A. C., Tarney J., and Arndt N. T., 1999. Implications of 187 Os heterogeneities in a mantle plume: Evidence from Gorgona Island and Curaçao. *Geochemica et Cosmochemica Acta* **63** (5), 713-728.

Watson E. B., 1979. Zircon saturation in felsic liquids: experimental results and applications to trace element geochemistry. *Contributions to Mineralogy and Petrology.* **70**, 407-419.

Watson E. B. and Harrison T. M., 1983. Zircon saturation revisited: temperature and composition effects in a variety of crystal magma types. *Earth and Planetary Science Letters* **64**, 295-304.

Weber J. C., Dixon T. H., De MEts C., Ambeh W. B., Jansma P., Mattioli G., Saleh J., Sella G., Bilham R., and Perez O., 2001. GPS estimate of relative motion between the Caribbean and South American plates, and geological implications for Trinidad and Venezuela. *Geology* **29** (1), 75-78.

White R. S. and Dupre B., 1986. Sediment subduction and magma genesis in the Lesser Antilles; isotopic and trace element constraints. *Journal of Geophysical Research* **91** (6), 5927-5941.

White R. V., Tarney, J., Kerr, A.C., Saunders, A.D., Kempton, P.D., Pringle, M.S. and Klaver, G.Th, 1999. Modification of an oceanic plateau, Aruba, Dutch Caribbean: implications for the generation of continental crust. *Lithos* **46** (1), 43-68.

White R. V., 1999. Tonalite intrusions associated with an oceanic plateau, Aruba, Dutch Caribbean, Ph.D. thesis. Univ. Leicester.

White W. M., 1985. Sources of oceanic basalts: Radiogenic isotopic evidence. *Geology* **13**, 115-118.

White W. M. and Hofmann A. W., 1978. Geochemistry of the Galápagos Islands: implications for mantle dynamics and evolution. *Carnegie Institute of Washington Yearbook*, 596-606.

White W. M., McBirney A. R., and Duncan R. A., 1993. Petrology and geochemistry of the Galápagos Islands: portrait of a pathological mantle plume. *Journal of Geophysical Research* **98** (B11), 19533-19563.

White W. M. and Patchett J., 1984. Hf-Nd-Sr isotopes and incompatible element abundances in island arcs: implications for magma origins and crust-mantle evolution. *Earth and Planetary Science Letters* **67**, 167-185.

Wilson M., 1989. *Igneous Petrogenesis- a global tectonic approach.* Chapman and Hall.

Woodhead J., Eggins S., and Gamble J., 1993. High field strength and transition element systematics in island arc and back-arc basalts: evidence for multiphase melt extraction and a depleted mantle. *Earth and Planetary Science Letters* **114**, 491-504.

Woodhead J. D., 1989. Geochemistry of the Mariana Arc (western Pacific); source composition and processes. *Chemical Geology* **76**, 1-24.

Woodhead J. D., Hergt J., Davidson J. P., and Eggins S. M., 2001. Hafnium isotope evidence for "conservative" element mobility during subduction zone magmas. *Earth and Planetary Science Letters* **192**, 331-346.

Yamada E., 1984. Subaqueous pyroclastic flows; their development and their deposits. In:*Marginal basin geology*, Vol. 16 (ed. B. P. H. Kokelaar, M.F.), pp. 29-37. Geological Society Special Publications.

Yonce G. ,1997. Geological Map of Southern Bonaire. Unpublished internal report.

Young K.,1972. Ammonites from Puerto Rico and the Virgin Islands. *Transactions of the 6th Caribbean Geological Conference, Margarita. p 469.*

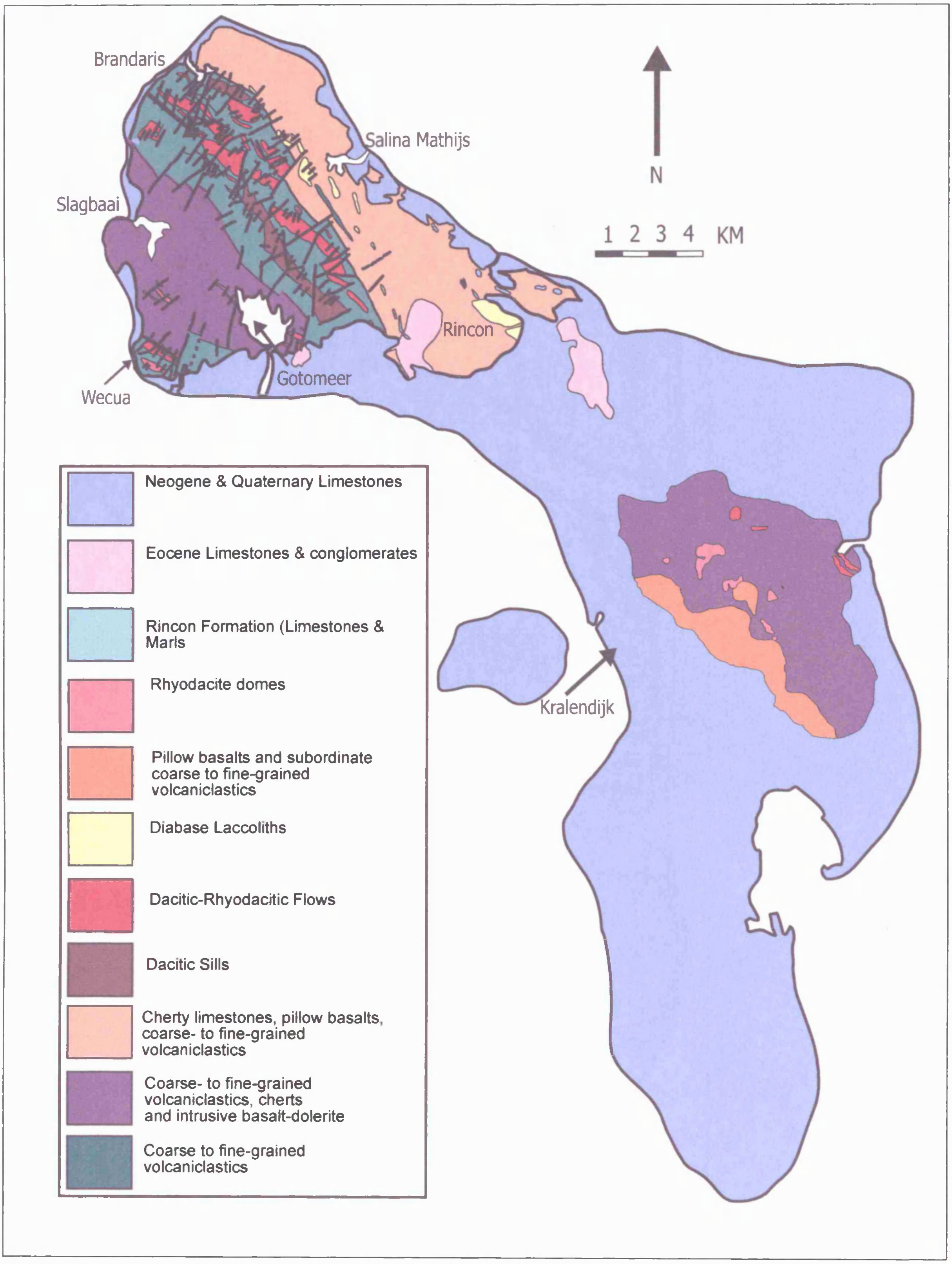

Map A.1. Geological map of Bonaire, Dutch Antilles. After Klaver, 1976, and this study.

Appendix A
Map A.2
Map of the Northern Complex showing sampling sites and localities mentioned in text.
See Tables A.1 to A.4 for details.
N

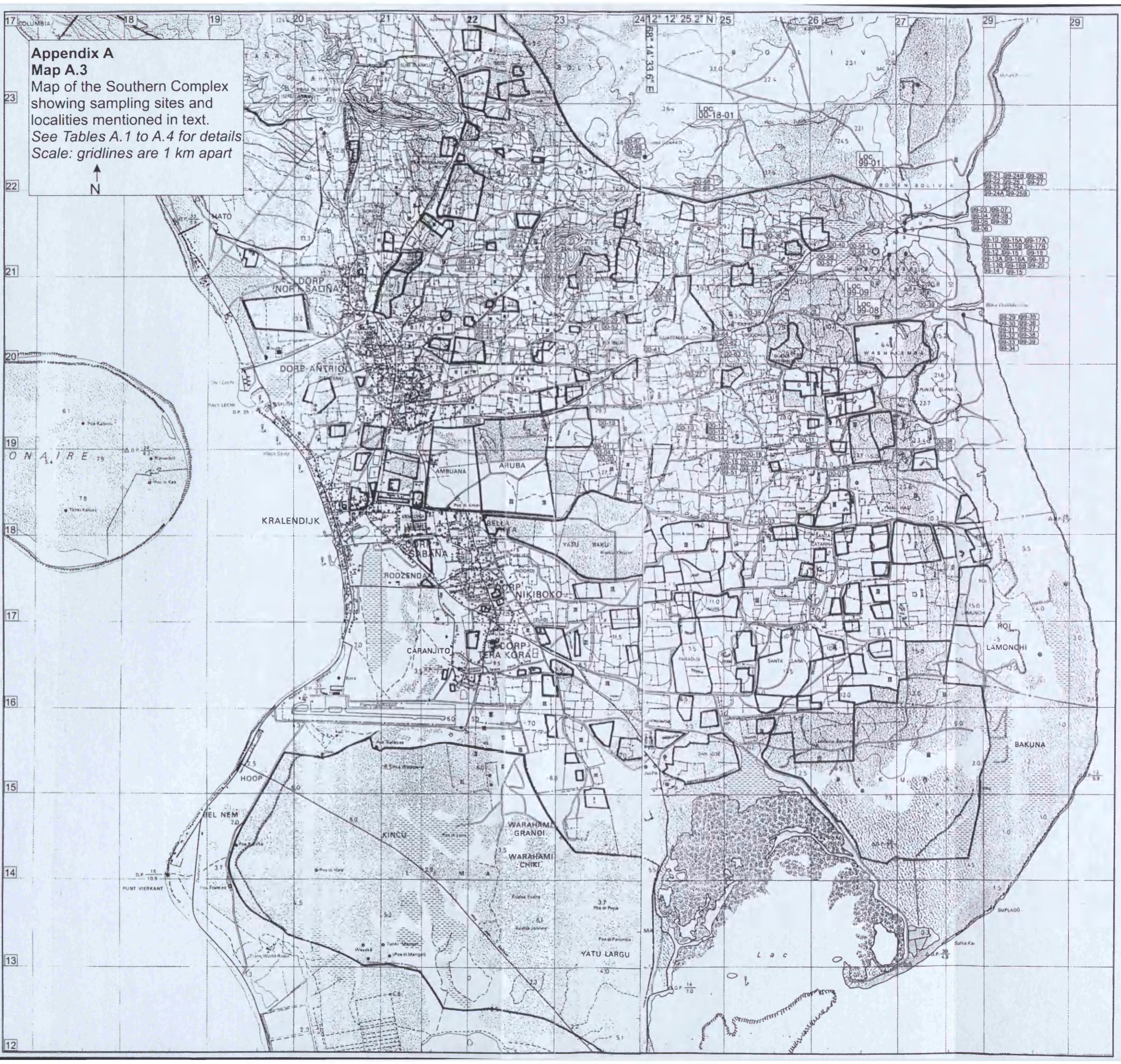

Appendix A
Map A.3
Map of the Southern Complex showing sampling sites and localities mentioned in text.
See Tables A.1 to A.4 for details
Scale: gridlines are 1 km apart

Table 1: 1994 Field season. Collected by John Tarney and Andrew C. Kerr.

Rock Number	Grid Reference	Locality Description	Rock type//field notes	Hand Specimen Description	Thin Section Description	XRF	Isotope/ Ar-Ar?	Photo–micrographs
BON 94–01		From beside shores of lake Gotomeer, across from rhyodacitic island.	Felsic volcaniclastic. Fine-grained. Very pale roadside exposure.	Fine-grained welded volcaniclastic, sandy yellow–white in colour. Demonstrates two sets of laminations: 1. Alternating wavy dark and light bands, several mm apart, with thickening varying from 1/2 to 2 mm. Probably represents original sedimentary layering. 2. late–stage colour banding on a scale of several cm's– result of varying oxidation. The average grainsize is <0.5 mm, and the rock displays a sugary texture.	Homogenous rock, consisting of fine-grained matrix– microcrystalline rounded quartz, feldspar and magnetite.	Y		
BON 94–02		Further 0.5 km along road after island.	Dolerite. Very altered dolerite but reasonably fresh centres to spheroidally weathered dolerite. Medium-grained–core sampled. Moderately fresh.	Medium-grained equigranular dark greenish rock. Consists of 60% dark pyroxene and 40% plagioclase, forming "blobs". Also some dark laths, 1–1.5 mm (hornblende?) Weathered faces show orange tinge and white powdery patches probably representing plagioclase.	Clinopyroxene (0.5 mm) is now partially pseudomorphed by pumpellyite. Spiky plagioclase and possible K–feldspar phenocrysts (55%, 1.5mm) are extremely turbid. Magnetite is also relatively abundant, comprising 5% (<0.5 mm), and there are some calcite patches.	Y		
BON 94–03		Further along road.	Elongate clasts in volcaniclastic rock. Some clasts fragmental, fine-grained, Possible Mn concretions?	Fine-grained rock, brown in colour, with an average grain size 0.3 mm. Phases consist of small rounded quartz grains, and 30% tiny feldspar laths.	This homogenous volcaniclastic rock consists of glassy, very fine-grained material (ash and magnetite), with elongated wisps defining the texture.	Y		
BON 94–04		1–2 km after park entrance.	Dolerite. Quite fresh, medium-grained. Loose block on surface from diabase laccolith.	Medium-grained dark greenish rock: slightly coarser than BON–94–2 and slightly fresher, enabling the mineralogy to be easier determined. A mafic black phase comprises 30%, which weathers out, 3 to 4 mm in diameter, with a squat form. A whitish, more transparent feldspar comprises 20%, with some lath–like crystals <1 mm. The remainder of the rock consists of grey–green secondary minerals.	Relatively fresh dolerite with five main phases: 1. plagioclase (50% rock, average <1 mm) displays zoning and sometimes undulose extinction. Some grains are so opaque they don't show interference colours, and others show moderate degrees of weathering. The cores are noticably more weathered than the margins. 2. Olivine (0.5 mm, <<1%) is distinguishable by its clear pale yellow colour (no inclusions) and very high relief with characteristic fracture patterns. Not an abundant phase, and ppl view shows it has now been altered to serpentine. 3. clinopyroxene (30%) often shows its charactersitic twinning and 2° colours. It is relatively fresh. 4. orthopyroxene (5%) is hard to find, but is distinguished by its dusty, pale olive-green colour. In xpl it can be seen that it is very coroded, but preserved sections show characteristic	Y		

Rock Number	Grid Reference	Locality Description	Rock type//field notes	Hand Specimen Description	Thin Section Description	XRF	Isotope/ Ar-Ar?	Photo–micrographs
					high 1st order interference colours. The weathering product is very similar, but less extreme, than clinopyroxene weathering in 94–3. Magnetite (15%) is present.			
BON 94–05		From second laccolith along road.	Dolerite. In situ. Centre of spheroidally weathered dolerite. Medium-grained.	Also similar to BON 94–2, with slightly more felsics. This may be due to increased weathering making the feldspars more visible, white and powdery. There are some patches of iron staining.	This isn't as well preserved as BON 94–4. There are two varieties of pyroxenes: orthopyroxene (15%) is severely altered to clays and serpentine, again bright green and irregular in shape. Clinopyroxene (30%) is fresher, but shows more fracturing and alteration than the previous section. Magnetite (15%) displays some well developed faces, as before. Olivine (<1%) is rare, and fairly altered. Fractures and edges are well defined by a pale brown weathering product, and the cores are entirely serpentine. Plagioclase (40%) forms dusty ares, and the laths can just about be distinguished in xpl in some areas, but not in others due to the degree of turbidity.	Y		
BON 94–06		0.5 km along road.	Rhyodacite. Lots of felsic boulders with plagioclase, quartz and chlorite amygdales. Fine-grained. Rounded vesicles.	This porphyritic rock is brown in colour and too fine-grained to determine mineralogy, although possible micro–phenocrysts of quartz and feldspar can be seen, giving a rhyodacite matrix. Porphyritic plagioclase comprises 10% of the rock and forms laths up to 1 cm in length, with an average size of <5 mm. Vesicles comprise 10% of the rock, with an average diameter of 1mm, but ranging up to 3mm. Most vesicles are infilled with quartz, although some have zeolites infilling in their characteristic radial manner.	K–feldspar (30%), possibly with some plagioclase forms the main porphyritic phase– partly altered, seriticised and turbid. Some form glomerocrysts, and others show rounded (resorbed) edges. Smaller phenocrysts of magnetite (1%) are <0.5 mm in size. The matrix (60%) consists of a spherulitic texture (<0.1 mm). Magnetite (5%) and feldspar (>20%) are also found in the matrix, but relatively altered now. Vesicles (<10%) are infilled with fresh quartz. A coating near the rim of fine-grained detrital material illustrates the swapped rims of the quartz.	Y		
BON 94–07		0.5 km along road.	Porphyritic rhyolite.	This porphyritic rock has a dove–grey very fine-grained matrix, probably comprising quartz and feldspar. The milky–white to translucent porphyritic feldspar is tabular rather than lath–like, and averages 4 mm in length. Irregular cavities form 5% of the rock, and are less than 2 mm in size, commonly infilled with quartz.	This rock displays a fine-grained felsic matrix (devitrified glass?) with no obvious feldspar present. Glomerocrysts are present, mainly of K–feldspar (20%, rounded and seriticised, possibly with some plagioclase), magnetite (4%) and partly altered clinopyroxene (1%). Well–developed spherulitic texture.	Y		

Rock Number	Grid Reference	Locality Description	Rock type//field notes	Hand Specimen Description	Thin Section Description	XRF	Isotope/ Ar-Ar?	Photo–micrographs
BON 94–08		Slagbaai–Gotomeer.	Felsic volcaniclastic rock.	This green–coloured fine-grained rock is present as small angular blocks <6 cm diameter, with medium to dark brown weathering patterns. There is some faint fine–scaled lamination defined by mafic wisps of material, and small quartz grains are rounded and show possible reaction rims.	This partially welded devitrified glass volcaniclastic is heterogeneous. Bands, several mm in thickness, vary from brown devitrified, cryptocrystalline material, with microphenocrysts of feldspar, to what looks like a sandstone, with angular quartz and fresh feldspar (both plagioclase and K–feldspar) in a fine matrix. Some lithic fragments are visible– mainly feldspathic volcaniclastics. Occasional feldspar phenocrysts (1 mm) can be seen.	Y		
BON 94–09			Dacite. Feldsparphyric lava with quartz phenocrysts with areas of segregated material.	This quartz and feldspar porphyry contains irregular xenoliths (comprising 10% of the rock) ranging widely in size from 10–30 mm. The feldspar (40% rock) is in the form of tablets <5 mm in length, and the quartz (20%) is rounded, but a similar size. The matrix is a very fine-grained blue–grey colour, containing quartz and feldspar.	Glomerocrysts of quartz, plagioclase and possibly altered pyroxene comprise 40% of the rock. Plagioclase is strongly resorbed and normally–zoned, with sericite on some margins, but otherwise surprisingly fresh. The quartz is very fresh looking, <3 mm, with resorbed edges, whereas the pyroxene is probably clinopyroxene (due to similarities with other, less altered crystals, but now is altered to sericite). Segregated areas (10%) are visible, noticable by the abundance of opaques, but indistinguishable in xpl.	N	Ar-Ar	00-08-21 00-08-22
BON 94–10		Further along road 1 km.	Dacite. Phenocrysts sub–alligned.	This is identical to BON 94–9, demonstrating a thick weathered red rind.	This rock is similar to above, with 15% phenocrysts, generally smaller than above (average 2mm), and glomerocrysts of very turbid feldspar (possibly K–feldspar). Some zoned plagioclase is surprisingly fresh. Segregated material comprises 10%, generally felspathic, magnetite rich, with very unclear boundaries. One 2 mm (xenocrystic?) clinopyroxene is visible, along with several smaller crystals.	Y		00-08-23
BON 94–11			Rhyodacite.	This buff–coloured rock has a medium-grained matrix mainly comprising quartz, averaging 1 mm in size, and some microphenocrysts of feldspar. Tiny mafic grains are just visible to the naked eye. The rock has a sugary texture, and weathered surfaces display black dendritic (probably manganese) mineralisation radiating in from the surface.	This weathered–looking rock consists mainly of a brown ~microcrystalline heterogeneous matrix. Very small phenocrysts are just distinguishable of quartz and feldspar.	Y		

Rock Number	Grid Reference	Locality Description	Rock type//field notes	Hand Specimen Description	Thin Section Description	XRF	Isotope/ Ar-Ar?	Photo–micrographs
BON 94–12			Dacite.	Pinky–brown fine-grained matrix encloses plagioclase phenocrysts averaging 1 mm in length. Vesicles comprise 10% of the rock, ranging in size from <0.5 to 3 mm. Most are infilled with quartz, although some are lined with detrital iron.	Feldspar phenocrysts (predominantly K–feldspar) form 20% or more of the rock. They often don't form laths, but are diamond shape with unusual sanidine twinning, <1 mm in length and fairly turbid. The matrix is "spiky", mainly consisting of feldspars and possibly areas of strained quartz. An almost "globular" texture can be seen in ppl– spherulites.	Y		
BON 94–13			Basalt/Dolerite	A ~fine-grained basaltic rock, with some faint green discolouration in places due to weathering. A felsic phase comprises 30%, with 2 mafic phases (one greenish) making up the rest. A chalky–white weathering surface implies feldspar degredation, and there is also some red–brown weathering material on the margins.	This rock is nearly aphanitic. Several corroded crystals of (probably) clinopyroxene, full of inclusions and fractures are visible– squat, euhedral and ~0.5 mm in diameter, some surrounded by magnetite. In the matrix, many small high relief grains, full of inclusions can be see, similar size to magnetite (25%)– these could also be clinopyroxene (25%). Plagioclase (50%) is also visible.	Y		00-08-02
BON 94–14		200–300m further along.	Rhyodacite.	This is a mid–brown coloured rock, with a dark–brown weathering rind. There are some sparse (5%) phenocrysts of feldspar, with a sub–parallel allignment, averaging 1mm in size. There are some vesicles, 2 mm diameter, partly infilled with quartz. The matrix is dull and fine-grained, probably containg quartz and feldspar, albeit hard to distinguish.	There are two phenocrystic phases visible: feldspar, (mainly K–feldspar, if not all), <2 mm in length, comprising 10% of the rock, and showing a sub–parallel alignment. The matrix displays a trachytic texture, and is comprised of spiky laths of feldspar (K–feldspar+plagioclase?), comprising 50%, 15% magnetite and 15% of a pale brown patchy mineral, possible a replacement amphibole. The matrix is surprisingly fresh. Rounded quartz comprises the remaining 5%.	Y		
BON 94–15		After Playa Funchi	Fine-grained rhyodacite. Sugary texture.	This fine-grained laminated rock displays a colour varying from buff–coloured to pale grey parallel to the laminations. The laminations suggest this is a volcaniclastic, and the phases are mainly quartz and feldspar (indistinguishable at this level) with 5% very fine-grained mafics.	Microcrystalline and homogeneous rock. Glassy quartz and some magnetite is visible in a crypto–crystalline matrix. Brown clays are also visible.	Y		
BON 94–16			Basalt.	This is a fine-grained green–brown rock with a red–brown weathered crust. Vesicles comprise 10%, some infilled with detrital iron, and range in size from <0.5–8 mm. Some quartz is also present in a similar size range to the vesicles, although whether this represents a late stage infilling is uncertain. The matrix is comprised of 50% feldspar and a greenish pyroxene.	This fine-grained rock mainly consists of spiky feldspars (60%, type unknown). Quartz clasts, slightly larger than the feldspar (20%), are distinguishable by their lack of inclusions in ppl and their degree of roundness. A more interstitial, brown phase is seen once again, possible a replacement of amphibole. Patches of fresh looking quartz grains, 0.5 mm in diameter and displaying sutured contacts probably represent infilled vesicles, although there is no visible rim.	Y		

Rock Number	Grid Reference	Locality Description	Rock type//field notes	Hand Specimen Description	Thin Section Description	XRF	Isotope/ Ar-Ar?	Photo–micrographs
BON 94–17		Slagbaai. Near shore.	Dioritic rock near coast.	This medium-grained green rock displays an equigranular texture, consisting of plagioclase (30%), with some well formed grains averaging 1 mm in length, and more mafic phases. The mafics can be subdivided into an elongate dull green phase, comprising 40%, and a stubbier darker phase.	This is a very complex rock which is not significantly altered. A bright green phase is quite dominant both as phenocrysts and smaller anhedral "blobs" in the matrix. It shows anomalous interference colours and is difficult to identify. Feldspar (definitely K–feldspar, but possible plagioclase) remains an abundant (50% rock) phase, and clinopyroxene (20%) is just distinguishable as poorly preserved grains, still showing inclined extinction and twinning. Both magnetite and quartz are also present as small grains.	Y		
BON 94–19		Slagbaai. Near shore.	Rhyodacite with xenoliths.	This has three main phases: white phenocrystic plagioclase (30%), ranging in size from 5–20 mm, elongate green pyroxene comprising 30%, and a coarser brown phase, up to 4 mm in diameter, which may be quartz. The remaining 10% is visible as very fine-grained Fe–oxydroxide.	Xenoliths are quite dominant (25%) in this rock, generally 1 mm in size, displaying a weathered looking matrix with outlines of feldspar visible. One large specimen, 3–4 mm in diameter, is clearly a fine-grained acidic rock, with the feldspars demonstrating a trachytic texture, and a faint reaction rim present. The matrix surrounding the xenolthis displays flow structures around them, defined by detrital (clay?) material. Some porphyritic feldpars (mainly K–feldspar) are visible, very corroded and with some resorbed edges– xenocrysts? One large relict crystal of clinopyroxene is apparent, with only the margins remaining.	Y		
BON 94–20			Rhyodacite. Flow banded felsite sill.	This rock is buff–coloured and displays laminations on a scale of 2 mm. It is fairly fine-grained with a similar sugary texture to other samples. It displays a black weathered crust of manganese, which is confirmed by the dendritic patterns seen on some surfaces.	This rock consists of very few (<1%) phenocrysts of strained quartz and feldspar (definitely K–feldspar), albeit difficult to distinguish. The matrix is homogenous, consisting of quartz and feldspar (again only K–feldspar distinguished) in a speckly matrix.	Y		
BON 94–21		Southern Complex Seru Grande rhyodacite dome.	Klaver's rhyodacite dome (plug) flowing over or intruding andesitic basalt.	This vesicular, buff–to–pinky–brown coloured rock has a sugary texture, and a possible sub–parallel orientation of the phenocrystic plagioclase (<3 mm in length, 35% rock). Some vesicles are elongate and orientated sub–parallel to the phenocrystic plagioclase. These have been partially infilled with quartz, some with lovely large euhedral crystals.	This rock consists (80%) of both plagioclase and K–feldspar. (K–feldspar > plagioclase), demonstrating a trachytic texture. Rounded quartz (10%) is <.5 mm in diameter, and the remaining 10% is comprised of magnetite and brown clays / Fe–oxyhydroxide.	Y		
BON 94–22		Southern Complex Adjacent to Seru Grande.	Rhyodacite dome.	A fine-grained, smooth blue–grey rock which displays a fine–brown weathering crust. Thin laminations are defined by parallel wavy wisps of more mafic material. Many dull plagioclase microphenocrysts are visible, about 1 mm in length, matrix consists of feldspar and quartz.	Porphyritc microphenocrysts (10%) of plagioclase and (predominantly) K–feldspar, some very seriticised, show a sub parallel alignment and are found in an almost microcrystalline matrix of quartz and feldspar.	Y		

Rock Number	Grid Reference	Locality Description	Rock type//field notes	Hand Specimen Description	Thin Section Description	XRF	Isotope/ Ar-Ar?	Photo–micrographs
BON 94–23		Southern Complex Rhyodacite dome.	Fresher rhyodacite. Might be more mafic. Plagioclasecrystals more grey.	Medium brown–grey, it consists of randomly–orientated micro–phenocrysts of feldspar (30%), <7 mm in length, athough most average 1 mm. Fine-grained quartz (<1 mm) comprises 60% of the rock, and very fine-grained mafics make up the last 10%. Some manganese mineralisation can be seen on the surface.	Microphenocrysts of both K–feldspar (55%) and plagioclase (20%), show a continuous range of grain sizes, the largest being 1 mm in diameter. Quartz (15%), infilling vesicles and magnetite (10%) is present.	Y		
BON 94–24		Southern Complex Rhyodacite dome. East of Seru Grande (in small quarry).	Rhyodacite dome.	This dull rock has a pale green–white groundmass and consists of 10% round, rusty–brown patches <1 mm in diameter, surrounding fine vesicles/cavities. There are 10% plagioclase phenocrysts, <1.5 mm in length, and a greenish glassy phase (possibly quartz) comprises 30%. A pale–pink phase, probably feldspar (40%) is found in the matrix, along with less than 5% of very fine-grained mafics which appear to be associated with the quartz.	This is identical to BON 94–23, but with slightly more plagioclase and correspondingly less quartz.	Y		
BON 94–25		By roadside– flat area.	Andesite.	This medium-grained rock displays a green and bumpy texture, and crushed with extreme ease, despite its hard appearance, in the fly press. The phenocrysts present are quartz, 1–4 mm in size, and pyroxene (now pumpellyite?) displaying a shiny dark surface. The largest phenocrysts are 2 mm, but generally 1–1.5 mm. The green colour may be the result of weathered quartz, whereapon the rock will consist of 50% quartz, 30% a more mafic phase, and finally 20% of brown rusty patches which may have originally been K–feldspar.	This rock is very open textured– consisting of many (20%) irregular "holes" or green chlorite and infilled with calcite. Could the green mineral be chlorite? Feldspar (50%) is extremely seriticised and turbid, ranging from 0.1–1 mm in length, with a random orientation. Some clinopyroxene (15%) is distinguishable as small high relief grains.	N		00-08-24 00-08-25
BON 94–26			Minor intrusion– loose block.	This is fine-grained, grey–green in colour and consists of 50% phenocrysts of quartz, 1 mm or less. In addition, plagioclase (20%) is present, along with a more mafic phase– biotite or hornblende.	Quartz grains (average 1 mm) display undulose extinction and are outlined by spiky feldspar and magnetite. Chlorite forms rings surrounding the quartz and there are also large vughs filled with calcite.	N		

Table 2: 1996 Field season. Collected by Rosalind V. White and John Tarney.

Rock Number	Grid Reference	Locality Description	Rock type/ Field Notes	Hand Specimen Description	Thin Section Description	XRF	Isotope/ Ar-Ar?	Photo–micrograph
BON 96–06	12°14'36"N 068°22'17"W	Inlet of Gotomeer, at lakeshore. Gently folded interbedded cherts and volcaniclastics, dipping 30° to 020°N .	Chert.	Dark black and dull chert, faintly banded. Weathered surface represented by mid–brown fine-grained material.	No thin section taken.	N		
BON 96–07	12°14'36"N 068°22'17"W	Inlet of Gotomeer, at lakeshore. Gently folded interbedded cherts and volcaniclastics, dipping 30° to 020°N.	Felsic volcaniclastic rock.	Medium-grained volcaniclastic rock, very prominently banded (1–2 mm scale). Displays sandstone–like/sugary texture. Yellow–brown in colour, some bands slightly darker. Orange weathering surface with some pockets of dendritic manganese. Weathered surface displays a sheen– desert varnish effect?	This fine-grained volcaniclastic rock has an average grain size of <0.1 mm and consists of quartz, feldspar and some interstitial brown clay material. The banding represents a concentration of interstitial brown clays.	Y		
BON 96–08	12°14'36"N 068°22'17"W	Inlet of Gotomeer, at lakeshore. Gently folded interbedded cherts and volcaniclastics, dipping 30° to 020°N.	Chert.	Very well banded chert? (looks like volcaniclastic). Colour in bands varies from blue/black to pale yellow, averaging 1.5 mm. Rock displays graduation from darker to paler bands over 3 cm. Darker part shows pale orange spots 1 mm in diameter, with an irregular shape, which appear to be independent of banding. Oxidation spots?	No thin section taken.	N		
BON 96–09	12°14'30"N 068°22'15"W	Still on Gotomeer shore.	Coarse-grained conglomerate, with rhyolitic 2–3 cm clasts.	Coarse, heterogeneous, rhyolitic welded irregular volcaniclastic rock with a lumpy crust. Mid green in colour with no signs of banding. Feldspar forms white tablets, often creamy, <2 mm in length. Some crystalline fragments display a well–defined cleavage, shinier than the matrix and <7 mm. They display a habit similar to hornblende, and weather in easily–strongly cleaved surface remains. There are many small angular clasts, one displays a metallic crystalline sheen, 1 cm diameter, with a red halo surrounding it for 1 cm.	Abundant phenocrysts of rounded (resorbed edges?) and often strongly zoned feldspar showing undulose extinction are visible. Large rounded quartz phenocrysts are also apparent, and they all have the appearance of xenocrysts. Some small microphenocrysts of clinopyroxene can also be seen, 0.1–0.2 mm in size. A large xenolith with irregular embayed edges comprises half the slide, and several smaller xenoliths 0.5 mm in diameter are also visible, distinguishable by the abundance of opaques and resulting brown colour.	N		
BON 96–10	12°14'39"N	~100m from	Dolerite	This dolerite is green–grey in colour, fine to medium-	This dolerite is very altered and appears	Y		

Rock Number	Grid Reference	Locality Description	Rock type/ Field Notes	Hand Specimen Description	Thin Section Description	XRF	Isotope/ Ar-Ar?	Photo–micrograph
	068°22'17"W	**BON 96–9** on shore.		grained (1 mm), with a brown weathered crust. It consists of 50% fine pale elongated clasts of plagioclase, and 50% of a medium–dark green/black phase.	extremely turbid in thin–section. Olive–green / orange patches, often irregular and averaging 0.25 mm in size comprise 25%. These sometimes have a core of Clinopyroxene (20%), indicating that they may be replacing it. Are these patches pumpellyite? Or chlorite/clays? They may be pumpellyite, with some possible prehnite in the interstites. Clinopyroxene (20%) is often fairly corroded and fractured, up to 1 mm in size. Plagioclase (45%) is extremely seriticised and displays an interlocking texture. Opaques, cubic in habit, comprise the remaining 10%.			
BON 96–11	12°14'43"N 068°22'34"W	~100m from **BON 96–9** on shore.	Porphyritic rhyodacite.	Porphyritic rhyodacite. Fresh surface shows very fine-grained mid–dark grey, almost dull glassy groundmass. Porphyritic feldspar displays lovely euhedral crystals, <4 mm in length (average 2 mm). Some vughs are infilled with a detrital orange–white mineral, similar to the weathered crust. Some irregular fractures on surface. Upon fracturing, it can be seen to be very weathered throughout.	This rock consists of glomerocrysts of turbid and seriticised alkali feldspar (30%), .5–3mm in length. A small inclusion of a xenolith can be seen, consisting of interlocking intergranular alkali feldspar, surrounded by opaques with an interstitial brown detrital mineral, average grainsize being less than 0.5 mm in size. The groundmass of the host rock consists of small feldspars and micro–crystalline material.	Y		
BON 96–12	12°14'38"N 068°22'14"W	Near road (WP003).	Dolerite.	Medium-grained dolerite, identical to **BON 96–10**.	This is similar to **BON 96–10** but is slightly less corroded. One olivine phenocryst is present, along with several smaller ones, and opaque oxides comprise 20% of the rock. Olive–green/orange patches, often irregular and averaging 0.25 mm in size comprise 25%. These sometimes have a core of clinopyroxene (20%), indicating that they may be replacing it. These patches are probably pumpellyite, with some possible prehnite in the interstites.	Y		
BON 96–13	12°15'58"N 068°22'32"W	Car in lay–by at col between Juwa and Seru Palmita. Top of small hillocks (WP004).	Rhyodacite/ Dacite sill.	Fairly weathered looking sill, pale green in colour. Feldspar phenocrysts, some of which are fresh, are <4 mm in length, averaging 2 mm. Abundant bright green weathered spots, of a similar size to the feldspar, indicate the remains of another phase. There appears to be abundant quartz in the matrix. The matrix displays an almost sugary texture.	This rhyodacite consists of tabular phenocrysts of alkali feldspar, possibly microperthitic, but very turbid, in a finer–grained matrix of mainly alkali feldspar with possibly some plagioclase. Small quartz phenocrysts are present, some very small opaques, and some interstitial patches of green alteration are present. Note: This rock borders on microgranite in terms of grainsize.	Y		
BON 96–14	12°16'07"N 068°22'41"W	Car in lay–by at col between Juwa and Seru Palmita. Top of small hillocks (WP005).	Rhyodacite.	Porphyritic dacite? The feldspar is <3 mm in length, and comprises 20%. Another porphyritic phase is more mafic, irregular, and <2 mm in length– possibly hornblende? The matrix is fine-grained but not glassy– almost sugary, but contains lots of quartz, pale to mid–grey in colour.	Phenocrysts comprise 10% of this rock and consist of plagioclase and alkali feldspar, 1–2 mm in size. Several feldspars form glomerocrysts along with a detrital interstitial orange/brown mineral. Are these xenocrysts? The matrix has a spiky random texture as defined by feldspar and	Y		

Rock Number	Grid Reference	Locality Description	Rock type/ Field Notes	Hand Specimen Description	Thin Section Description	XRF	Isotope/ Ar-Ar?	Photo–micrograph
					some quartz, 0.25 mm in size. Some interstitial quartz and many tiny opaques can be seen, and the rock displays a slight trachytic texture, with the spiky feldspar wrapping itself around the phenocrysts.			
BON 96–15	12°16'08"N 068°22'39"W (*–46W)	To the north of **BON 96–14**. contact with sill (lots of vughs) and overlying volcaniclastic rocks.	Green coarse-grained volcaniclastic rock.	This green chloritised coarse-grained volcaniclastic rock contains many clasts <2 cm, with some indication of flattening. The clasts form mainly more mafic elongate "blebs". Some clasts are rhyodacite fragments others are just visible as powdery white patches. Occasional feldspar phenocrysts can be seen, and overall this rock may display a eutaxitic texture.	This is an extremely heterogeneous lapilli volcaniclastic rock consisting of many clasts of rhyodacite etc. in a heterogeneous micro–crystalline matrix.	N		
BON 96–16	12°16'08"N 068°22'46"W (*–46W)	To the north of **BON 96–14**.	Felsic volcaniclastic rock.	Fine-grained, poorly–banded ash volcaniclastic rock, orange–brown in colour. The rock displays an almost sugary texture and a black weathered crust still partially remains.	This extremely fine-grained volcaniclastic rock is well sorted and consists of subangular fragments of quartz (feldspar may be present, but too fine-grained to determine) in a microcrystalline matrix. The crystal fragments average 0.05 mm in size.	Y		
BON 96–17	12°16'08"N 068°22'46"W (*–46W)	To the north of **BON 96–14**. Next ridge along from **BON 96–16**.	Purplish porphyritic (plagioclase) rhyodacite, forming rounded clasts in coarse agglomerate.	This porphyritic rhyodacite is purple–brown in colour with a glassy matrix. The phenocrysts are solely feldspar (60% rock), averaging 1 mm in size. Some occasional iron–rich spots can be seen, (<3 mm) Abundant vughs can be seen, <3 mm and mostly sub-rounded. The rhyodacite is a clast (10 x 6 x 5 cm) in a coarse-grained welded volcaniclastic rock, fragments of which can be seen on the borders of the clast.	Phenocrysts consist of seriticised feldspar and one very fractured clinopyroxene crystal. 2 mm in length, suggesting a xenocrystic source. The matrix consists of mainly quartz with some feldspar, average grain size 0.1 mm. The feldspar displays almost a seriate texture. Some crystals of clinopyroxene <0.3 mm are apparent, and again the degree of fracturing suggests they may be xenocrystic. Several elongate vughs appear to be infilled with calcite. This rock is not a typical rhyodacite.	Y		
BON 96–18	12°16'21"N 068°22'29"W	To the north of **BON 96–14**. Orange ridge of altered and porphyritic (but not as much as before) rhyodacite. Poorly developed columnar jointing in base suggests flow not sill.	Porphyritic Rhyodacite.	This pink porphyritic rhyodacite displays an orange colour on more weathered surfaces. Some occasional vughs show a sub–parallel orientation and are sub–rounded, <5 mm diameter. Feldspar forms the porphyritic phase (25% of rock), milky–white in colour and <3 mm in length. The matrix is almost sugary and fine-grained.	Broad and stubby porphyritic K–feldspar comprises 20% of this rock. They are surrounded by a matrix of spiky feldspar, interstitial dirty–looking quartz and blobs of an orange detrital mineral < 0.1 mm in diameter.	Y		
BON 96–19	12°10'14"N	By road on way	Felsic volcaniclastic	This medium to fine-grained volcaniclastic rock	This fragmental rock consists of altered sub–	Y		

Rock Number	Grid Reference	Locality Description	Rock type/ Field Notes	Hand Specimen Description	Thin Section Description	XRF	Isotope/ Ar-Ar?	Photo-micrograph
	(*–20N) 068°14'55"W (–*00W)	to Lagoen to east of disused quarry, on N side of road.	rock.	consists of elongate black wisps with sub-parallel allignment, (2–3 mm), in a mid-brown/grey ash groundmass. Some white powdery weathered patches can be seen.	rounded crystals in a matrix of finer-grained crystals, ash and possibly devitrified glass, with some small streaks of brown clay minerals. Quartz, plagioclase and k-feldspar comprise the larger fragments, 0.1 mm in size.			
BON 96–20	12°10'14"N (*–20N) 068°14'55"W (–*00W)	By road on way to Lagoen to east of disused quarry, on N side of road.	Coarse volcaniclastic rock.	This coarse-grained welded volcaniclastic rock is not as green as other similar volcaniclastics- the black/red/white/brown patches suggests the influence of weathering. It is massive, irregular and lumpy, and the clasts are very similar to those in **BON 96–9**. Similar black elongate shards are also seen. Some green–blue clasts, 1–2 cm in diameter can be seen, like **BON 96–9**, but most clasts are difficult to determine, due to their irregular form.	Coarse-grained conglomerate, consisting of angular clasts of rhyodacite, crystals, and matrix.	Y		
BON 96–21	12°10'14"N (*–20N) 068°14'55"W (–*00W)	By road on way to Lagoen to east of disused quarry, on N side of road.	Greenish–blue clast from coarse-grained conglomerate.	Green–blue weathered quartzose clast, 7 x 4 x 4 cm. It is very fine-grained, with very weathered margins, and is identical to smaller clasts seen in all the coarse welded volcaniclastics. Note: Some weathered surfaces still remain after splitting.	Consists of microphenocrysts (0.2 mm) of stubby feldspar (both plagioclase and K–feldspar) in a homogenous quartz–rich microcrystalline groundmass (90%).	Y		
BON 96–22	12°10'57"N 068°13'09"W	By road intersection near Lagoen. dipping 45/300, slump structures, graded beds.	Fine-grained volcaniclastic rock.	This chalky–white/sandy–yellow volcaniclastic rock is well bedded, displaying fine laminations, 1–3 mm in size. The laminations are not distinct enough to see signs of cross–bedding structures. There are indications of some black (Mn?) mineralisation on the outer rims, and a small amount of late–stage veining can be seen.	This homogenous looking rock consists of subordinate amounts of fine-grained crystal fragments in a microcrystalline glassy groundmass. The crystal fragments are <0.1 mm in size, rounded, and consist of k–feldspar, plagioclase and quartz.	Y	Hf, Nd, Pb, Sr	
BON 96–23	12°10'57"N 068°13'09"W	By road intersection near Lagoen. dipping 45/300, slump structures, graded beds.	Chert.	This is a similar grain–size to **BON 96–22**, but varies in terms of its colour, which is mink–brown/grey. The very sharp fracture seen is almost reminiscent of chert.	Mcrocrystalline chert.	Y		
BON 96–24	12°10'57"N 068°13'09"W	By road intersection near Lagoen. dipping 45/300, slump structures, graded beds.	Rhyodacite.	This porphyritic rhyodacite is dark–grey and dull in colour, and fine-grained. Feldspar forms the clear porphyritic phase, although fresh–looking quartz forms lovely euhedral crystals in elliptical blobs (<10 mm) which may be amygdoidal or primary.	Stubby phenocrysts of K–feldspar (<2 mm) which are seriticised and turbid, and sometimes form glomerocrysts comprise 20% of this rock. The matrix is comprised of spiky feldspar (both K–feldspar and plagioclase) with small interstitial quartz, distinguishable by a brown clay mineral coating in ppl.	Y		
BON 96–25	12°10'42"N 068°13'52"W	Up a side road which started from landward side of dry lake.	(Trachy)rhyodacite.	Porphyritic rhyodacite, purple/grey in colour, although the purple may represent more weathered areas. Several types of phenocrysts are present: 1. salmon–pink, often euhedral crystals, (K–feldspar?) averaging 1.5 mm in length and comprising <10% of rock. 2. Smaller	A trachytic texture is very dominant, which is divided into several domains. This is even visible in ppl as opaques, clays and devitrified glass define the outline of spiky feldspar (both K–feldspar and plagioclase) averaging 0.2 mm in	Y		

Rock Number	Grid Reference	Locality Description	Rock type/ Field Notes	Hand Specimen Description	Thin Section Description	XRF	Isotope/ Ar-Ar?	Photo–micrograph
				elongate tabular crystals, white in colour (plagioclase or quartz?), comprising 20%. The final phase (20%) consists of rounded, irregular, and possibly embayed quartz phenocrysts, <2 mm in diameter. The matrix is dark grey and not glassy.	length. Phenocrystic feldspar (K–feldspar, possibly with plagioclase) are very corroded and totally seriticised in places, showing irregular edges and averaging 1 mm in length. Round vesicles are very dominant and are defined by the concentration of opaques around the margins and are infilled with quartz or calcite.			
BON 96–26	12°10'23"N 068°14'48"W	Further up side road, disused quarry.	(Trachy)rhyodacite.	This vesicular rhyodacite is pale/buff–grey coloured. More skeletal k–feldspar phenocrysts are <5mm in length and comprise 25% of the rock. The vesicles (25%) vary from <1 mm to 4 mm, and are rounded and randomly orientated. They are lined with orange/brown acicular minerals, and the rock displays a sugary texture. Dendritic manganese is visible on the weathered surfaces.	Phenocrysts of K–feldspar <1.5 mm in length, some showing ragged edges, display a seriate texture to matrix size. The matrix consists of spiky feldspar, interstitial quartz, opaques and brown clays. The matrix is relatively coarse with an average grainsize of 0.1 mm.	Y		
BON 96–27	12°10'23"N 068°14'48"W	Further up side road, disused quarry.	(Trachy)rhyodacite.	This is similar to **BON 96–26** but without vesicles and is slightly more buff coloured.	This rock displays a seriate texture, with k–feldspar and subordinate amounts of plagioclase varying in size from 2–0.1 mm, with interstitial quartz and opaques. Many small patches of red–brown clays are present.	Y	Hf, Nd, Pb, Sr	
BON 96–28	12°10'23"N 068°14'48"W	Further up side road, disused quarry.	(Trachy)rhyodacite.	Again this is similar to **BON 96–26** but the feldspar demonstrates a sub parallel orientation and is slightly smaller (<3 mm). Upon splitting, a lovely large amygdale infilled with euhedral quartz can be seen.	Phenocrysts of K–feldspar with occasional plagioclase comprise 20% of the rock, but illustrate a seriate texture ranging to a matrix size (1 mm–0.1 mm). The matrix is principally K–feldspar, with some opaques and quartz.	Y		
BON 96–29	12°10'42"N(*) 068°15'11"W (*)	Cliffs of Ceru Grande (S side)	(Trachy)rhyodacite.	Red/brown massive rhyodacite. Feldspar phenocrysts are euhedral and shiny, up to 1 cm, but generally 2 mm in length. Lithophysae are less than 1 cm in size, irregular, and partially infilled with radiating euhedral quartz, averaging 3 mm in length. This rock is very crumbly when split.	Spiky K–feldspar, 1–2 mm in length comprises 15% of the rock and has a sub–parallel orientation, with some grains displaying ragged edges. The matrix is relatively fine-grained and displays a trachytic texture, and there are some irregular vughs partially infilled with quartz.	Y	Hf, Nd, Pb, Sr	
BON 96–30		In the park– W of Gotomeer. Car parked at flamingo observation point (point 24 on park route). Samples from lakeshore N of car.	Porphyritic rhyodacite.	Amygdaloidal rhyodacite? The quartz amygdales are <5 mm in diameter, very round and some remain unfilled. They comprise 10% of the rock. Some feldspar phenocrysts can be seen (<5%), less than 5 mm in length. The matrix is red/brown in colour.	There are abundant quartz infilled vesicles present in this rock, <2 mm in size, along with quartz veining. Occasional K–feldspar phenocrysts are present, generally <0.5 mm in size, although one elongate phenocryst was seen 1.5 mm in length. The matrix is fine-grained and is mainly comprised of spiky feldspar <2 mm, along with interstitial magnetite.	Y		
BON 96–31		In the park– W of Gotomeer. Car parked at flamingo	Dolerite.	This spheroidally weathered dolerite is grenade shaped, and may be too corroded to obtain decent results. An irregular mafic phase, 1 mm in size, comprises 60% of the rock, and a weathered green/brown, more interstitial	This dolerite is extremely weathered and borders on basalt in grain–size terms (0.5–1 mm). It consists of lots of spiky plagioclase, seriticised and turbid, and patches of a pale green/orange	Y		

Rock Number	Grid Reference	Locality Description	Rock type/ Field Notes	Hand Specimen Description	Thin Section Description	XRF	Isotope/ Ar-Ar?	Photo–micrograph
		observation point (point 24 on park route). Samples from lakeshore N of car.		phase can also be distinguished.	alteration mineral which may represent the alteration of (clino?) pyroxene. Some of these patches have small quartz crystals inside. Fine-grained cubic opaques comprise 5% of the rock.			
BON 96–32		In the park– W of Gotomeer. Car parked at flamingo observation point (point 24 on park route). Samples from lakeshore N of car.	Rhyodacite.	This is the same as **BON 96–33**, but occasional feldspar phenocrysts (<2 mm) can be seen, along with quartz phenocrysts (<5 mm), rounded and irregular in shape. Each of these phases comprises 10% of the rock, and irregular calcite veining is fairly dominant throughout.	This sample is extensively quartz veined and consists (10%) of phenocrysts of feldspar (predominantly K–feldspar) <1 mm in size. The matrix consists of spiky feldspar (again, predominantly K–feldspar) and interstitial quartz and opaques, with an average grainsize of <0.25 mm.	Y		
BON 96–33		In the park– W of Gotomeer. Car parked at flamingo observation point (point 24 on park route). Samples from lakeshore N of car.	Rhyodacite.	This massive green coloured rock may be a fine-grained volcaniclastic rock but is more likely to be a chloritised igneous rock. It displays an almost sugary texture, with branching calcite veins throughout, <2 mm in width. These are impossible to avoid when crushing.	This aphyric rock consists principally of spiky feldspar (both plagioclase and K–feldspar) 0.1–0.3 mm in length and outlined by opaques and interstitial green chlorite/clays. This may represent devitrified glass.	Y		
BON 96–34	12°15'53"N 068°21'54"W	Roadside, near cattlegrid.	Rhyodacite.	This porphyritic rhyodacite shows a sub–parallel orientation of phenocrysts and mineral–lined vughs. It consists of 25% translucent quartz phenocrysts, ranging from 0.5–4 mm in size, and 25% feldspar phenocrysts, generally 1–2 mm. In addition, partially infilled vughs 4–5 mm in size comprise 10% of the rock. The dark blue–grey matrix shows some signs of weathering.	Extremely turbid phenocrysts of feldspar (mainly K–feldspar) have an irregular shape and display a sub–parallel orientation. The matrix is made up of spiky feldspar (displaying a trachytic texture) with interstitial quartz and opaques. Some quartz-rimmed round vesicles, 0.5–3 mm in diameter comprise 10% of the rock. This rock is similar to **BON 96–36**, except for the trachytic texture.	Y		
BON 96–35	12°16'00"N 068°21'28"W	Roadside near official park entrance.	Dacitic fine-grained volcaniclastic rock.	This dark–grey/brown rock is fine-grained. It displays a strange pattern of elongate lenticles <10 mm in length and 1 mm width, with sub–parallel alignment.	This ash–rich volcaniclastic rock consists of parallel bands of rounded grains (30%) in a brown clay and opaques–rich matrix. The grains are <0.05 mm in diameter, and although some plagioclase can be seen, most grains consist of clays, probably representing the degradation of feldspar. The elongate lenticles visible in	Y		

Rock Number	Grid Reference	Locality Description	Rock type/ Field Notes	Hand Specimen Description	Thin Section Description	XRF	Isotope/ Ar-Ar?	Photo–micrograph
					handspecimen represent slight concentrations of iron.			
BON 96–36		Ceru Mangel. Klaver's lava tube locality.	Dacite.	This felsic massive rock is pale grey/brown in colour. Feldspar phenocrysts (50%) range from 1–3 mm in length and are weathered–looking and possibly sub–parallel. Some small round vesicles (5%) are present, with some mineral development on the edges. The fine-grained sugary groundmass is pale–grey/brown in colour.	Phenocrysts/glomerocrysts of K–feldspar, with occasional plagioclase, are often stubby, turbid, fractured and have irregular edges. They are <2 mm in length and comprise 20%. The matrix is feldspar rich (dominantly K–feldspar) with quartz and opaques. Some small round vesicles are visible.	Y		
BON 96–37	12°15'18"N 068°24'05"W	Iguana stop, along the ridge back towards roads and then down. Columnar jointed.	(Trachy)rhyodacite.	Similar to **BON 96–36**, this is a slightly darker mid green/grey massive rock, with no crystals but some fine vughs <1 mm. It is fresh–looking, but thin section work is needed to identify it.	This aphyric igneous rock consists mainly of spiky feldspar 0.1 mm in length, with abundant small opaques and abundant quartz. Occasional microphenocrysts of k–feldspar and some fairly round vesicles are apparent.	Y		

Table 3: 1999 Field season. Collected by the author in this study.

Rock Number	Grid Ref	Locality	Field notes	Hand Specimen Description	Thin Section Description	XRF	Isotope/ Ar-Ar?	Photo micrographs
BON 99–01			Blue rhyodacite.	Squat quartz–feldspar porphyry, extremely rich in phenocrysts, with 20% brown patches of segregated material 3–30 mm in size. Dark blue matrix.	Altered slide. Consists of quartz, plagioclase, K–feldspar– altered, all seriticised, turbid. The rock displays an almost seriate texture. Segregated material consists of concentrations of acicular opaque minerals.	N		
BON 99–02	09603066	Seru Palmita summit.	Rhyodacite flow.	~30% sanidine, 0.5–1 mm in length. Matrix is sandy–pinky brown, fine-grained and fresh with some almond shaped vesicles infilled with (weathered–in) brown powdery material. Extremely hard.	One of the fresher rhyodacites seen. K–feldspar and plagioclase phenocrysts are clear, and matrix is not very turbid.	Y		
BON 99–03	27252168	Lagoen.	Coarse-grained white/grey sandstone.	A heterogeneous weathered sandstone consisting of ~30% irregular white albite ~1–3 mm in size, ~10% small quartz and ~20% black irregular blobs <2 mm in size. The matrix is weathered, brown–green in colour with a white precipitate.	Very heterogeneous sandstone with lots of lithic clasts– some very feldspathic and others totally altered to prehnite. Feldspars are in very varying states of alteration, and some xenolithic fragments with a granophyric tecture show classic perlitic fractures (recrystalline ash).	N		
BON 99–04	27252168	Lagoen.	Olivine basalt dyke.	This consists of 5% lovely fresh olivine phenocrysts, the largest being >10 mm in size. Elongate cavities (vesicles?) are infilled with black powdery material and pale pink crystalline quartz (?)	Matrix of feldspar, opaques and a pale–green interstitial phase (pumpellyite replacing pyroxene?) along with occasional glomero/ phenocrysts of pyroxene, plagioclase and olivine.	Y		00-08-14 00-08-15 00-08-16
BON 99–05	27222168	Lagoen.	Coarse-grained white sandstone.	This volcaniclastic rock is bumpy, powdery, very weathered and heterogeneous. Examination of fresher surfaces show the bumps are formed by albite with subordinate quartz.	Irregular angular fragments of quartz and feldspar (both plagioclase and K–feldspar, some complexly zoned) along with lithic fragments (fine-grained igneous, fissile mudstone, tube pumice and several showing clear perlitic fractures– relic glass?) in a heterogeneous matrix of brownish microcrystalline quartz.	N		00-05-03 00-05-04
BON 99–06	27212168	Lagoen.	Coarse-grained volcaniclastic rock.	This is a coarse-grained, pale brown/yellow volcaniclastic bumpy sandstone with a superficial growth of crystalline fibres– probably gypsum or NaCl or epsom salts from seawater.	This weathered rock consists of crystal fragments (quartz, plagioclase, K–feldspar) in a microcrystalline quartz matrix (granophyric texture).	N		
BON 99–07	27212168	Lagoen.	Coarse-grained volcaniclastic rock.	Consists (>50%) of broken fragments of crystals (albite? 1–5 mm in size) which weather out. Also, micro–vesicular clasts of rhyodacite less than 1 cm are apparent. The matrix consists of brown/blue spots of altered material.	This extremely weathered section consists of fragments of seriticised feldspar with subordinate amounts of quartz and extremely corroded and altered igneous clasts in a microcrystalline quartz matrir. Tiny opaque minerals are extremely abundant in patches.	N		
BON 99–08	27192168	Lagoen.	Basalt. Fine-grained altered grey dyke with quartz amygdules.	This green–grey basalt is ~fine-grained, consisting of ~20% feldspar, 40% orange/brown phase and 40% of a dark brown phase. Some large fresh quartz < 5 mm in size is visible– these may be amygdular as they are coated in a brown cement.	This is stacked full of spiky feldspar with interstitial domains of pale yellow areas and some opaques.	Y		
BON 99–09	27192168	Lagoen.	Coarse-grained	This consists of >50% of white broken albite crystals,	Consists of extremely variably–altered feldspar,	N		

Rock Number	Grid Ref	Locality	Field notes	Hand Specimen Description	Thin Section Description	XRF	Isotope/ Ar-Ar?	Photo micrographs
			volcaniclastic rock. Red/brown clastic unit with white speckles. White, subangular irregular clasts, 0.5–2 mm. No bedding. Red, fine-grained matrix.	0.5 mm in size, some subordinate quartz and 10% lithics ~10 mm in size. in a brown powdery matrix. Pumice? These elements are difficult to distinguish due to the degree of weathering. Crystal fibres– see **BON 99–6.**	very angular in shape, with some angular lithics (both igneous and chert) with occasional quartz, in a heterogeneous matrix of microcrystalline quartz and smears of an orange–brown detrital substance.			
BON 99–10	27012152	Lagoen.	Basalt. Very friable powdery rock consisting of olivine crystals (60%, now weathered to pale–green powder) in brown matrix.	This coarse brown powder now only consists of 2–3mm green patches, which probably represent the remains of olivine and now consists of talc and calcite (?).		N		
BON 99–11	27032153	Lagoen.	Pumice breccia. Green clasts from 2 m into conglomerate succession.	These extremely regular knobbly clasts are 2–5 mm in size and sky–blue to brown in colour. Is this colour diagenetic? Some surfaces show broken albite crystals and this may possibly be identical to **BON 99–9** with diagenetic nodule formation.	This pumice breccia is similar to **BON 99–12**. Abundant pumice (~30%) can be seen, again in varying orientations. Fragments of devitrified glass can be identified by a perlitic fracture and this sample is even more heterogeneous than **BON 99–12**.	N		
BON 99–12	27042154	Lagoen.	Pumice breccia. Variety of clasts from 7–9 m into conglomerate succession.	One clast is clearly angular and represents a fragmented bit of pink/brown rhyodacite with some small ~1 mm vesicles and albite crystals. The other speciments are too weathered to ascertain.	This pumice breccia consists of >60% relict tube pumice (the vesicles of which appear to have been infilled with a brown detrital mineral) in random orientations, which confirms the deposit was originally non–welded. In addition, broken phenocrysts and glomerocrysts of seriticised feldspar are found, along with corroded lithic fragments (igneous) and more rounded devitrified glass fragments, some several mm in size, which are recognised by their pronounced perlitic texture.	N		00-05-07 00-05-08
BON 99–13A	27042154	Lagoen.	Rhyodacite clasts from conglomerate– banded rhyodacite and others.	These angular fragments consist of very fine-grained blue/red/brown rhyodacite, with small plagioclase phenocrysts ~ 1 mm.	This rhyodacite consists of a relatively homogenous microcrystalline quartz and feldspar matrix with xenocrystic feldspar (both K–feldspar and plagioclase). Some feldspar laths are either fragmented or rounded and resorbed, although not too seriticised, showing evidence for a xenocrystic origin. Some additional (xenocrystic) mineral fragments are visible– their high relief, squat form and birefringence (up to 1st order sensitive tint) suggest it is orthopyroxene, but one grain shows distinct inclined extinction relative to one strong cleavage, and therefore it may be xenocrystic clinopyroxene.	N		
BON 99–13B	27042154	Lagoen.	Pumice breccia. Clasts from conglomerate–	**BON 99–13b** consists of a 5 cm clast with an extremely weathered outside which looks encrusted in pumice,	Complex slide. Consists of an amalgamation of rock types but essentially a large scoriaceous clast	N		00-05-15 00-05-16

Rock Number	Grid Ref	Locality	Field notes	Hand Specimen Description	Thin Section Description	XRF	Isotope/ Ar-Ar?	Photo micrographs
			banded rhyodacite etc.	crystals and cement. Is there fresh rhyodacite on the inside?	with feldspar phenocrysts in a heterogeneous matrix consisting of relict tube pumice, lithic clasts and areas displaying a clear perlitic texture with small feldspar laths. Other areas seem to display a clear granophyric texture. Is the matrix essentially an ignimbrite? But there is no eutaxitic fabric. Therefore, perhaps this is just a heterogeneous breccia and the areas with a perlitic texture are coherent lava fragments in a pumaceous ashy matrix.			00-05-17
BON 99–14	27042154	Lagoen.	Fragment of conglomeratic unit.	This mid–brown unit consists of poorly–sorted ~subrounded clasts of pumice/scoria 2–20 mm in size mixed with lithics	Thin section not taken.	N		
BON 99–15A	27042154	Lagoen.	Scoria– clasts in conglomerate.	One large 100 mm broken scoria clast with some infilled vesicles is present.	Abundant vesicles are varible in size and are infilled with quartz. Abundant spiky plagioclase is found in the interstites, forming the matrix, and phenocrysts of albitised plagioclase are sometimes glomerocrystic. Several xenoliths are visible: the rounded type are an unvesicular version of the same lithology whereas the other is more corroded and is mainly represented by opaques.	N		
BON 99–15B	27042154	Lagoen.	Rhyodacite clasts in conglomerate.	Albite–rich rhyodacite (common clast type).	Consists of large stubby very albitised feldspar (mainly plagioclase, some K–feldspar) which may be xenocrystic in origin as extremely angular and some are fragmented, displaying undulose extinction. Large vesicles are rimmed with brown iron oxides and infilled with quartz. Groundmass consists of opaques and spiky feldspars.	N		
BON 99–16A	27052155	Lagoen.	Dolerite. Slab from middle of composite dyke.	Appears very altered. Coarse-grained with weathered olivine, a mafic phase (pyroxene?) and lots of calcite veining.	Extremely distinctive rock– large phenocrysts of clinopyroxene (50%, <6 mm) with abundant twins are partially corroded, fragmented and rimmed with calcite. An anhedral patch of orange detrital mineral and cubic opaques may represent another corroded phase. The groundmass consists of feldspar with interstitial medium relief mineral– clinopyroxene?	N		00-05-26
BON 99–16B	27052155	Lagoen.	Basalt. Slab from edge of composite dyke.	Mid–brown, vesicular rock with some weathered albite < 3 mm in size.	Distinctive spiky texture displayed by feldspar (0.25 mm) with abundant (30%) blobs of opaques. Clusters of radiating orange minerals (pumpellyite?) replace pyroxene or olivine, both in the groundmass and as phenocrysts, and rim cavities that may represent vesicles or the removal of crystals.	Y		
BON 99–17A	27072157	Lagoen.	Volcaniclastic sandstone.	This poorly–sorted sandstone contains clasts of aphyric	This is a poorly sorted sandstone. It's packed full	N		

Rock Number	Grid Ref	Locality	Field notes	Hand Specimen Description	Thin Section Description	XRF	Isotope/ Ar-Ar?	Photo micrographs
				pink rhyodacite and green pumice (?), all ~10 mm in size with a few albite crystals. The matrix is difficult to determine.	of tube pumice, with vesicles now infilled with pumpellyite/zeolites. There's a huge clast in the centre of the slide of scoriaceous pumice, and some incredibly fresh plagioclase crystals. A core of olivine is surrounded by zeolites and/or low temperature alteration minerals.			
BON 99–17B	27072157	Lagoen.	Secondary chert.	This mid–brown, grey, medium to fine-grained rock has 1 mm albite crystals and shows parallel, colour–defined laminations.	Very fine-grained rock consisting of occasional angular fragments of quartz and feldspar in a microcrystalline matrix with orange/brown patches.	N		
BON 99–18	27072157	Lagoen.	Secondary chert/ volcaniclastic sandstone sample from grey unit.	Grey, fine-grained volcaniclastic sandstone with some chert development.	Very fine-grained rock consisting of occasional angular fragments of quartz and feldspar in a microcrystalline matrix with orange/brown patches.	N		
BON 99–19	27072157	Lagoen.	Chert. Grey, hard fine-grained unit.	This is fine-grained, mid–brown/grey.	Homogenous microcrystalline quartz with brown mottled areas and occasional crystal fragments. One faint green fossil fragment comprised of a fine circular net structure is visible (radiolaria).	N		
BON 99–20	27072157	Lagoen.	Chert.	This grey, fine-grained hard rock is probably a fine-grained ash, being dense and aphyric in the middle and more powdery and carious at the base and top. The 100 mm sequence has laminations that are slightly convolute.	Stacked full of radiolaria, which are easily distinguished as the brown mottled mineral forms in the interstites. Some internal structure can be distinguished– some radial. Slight evidence of compaction in places. Radiolaria are poorly preserved.	N		
BON 99–21	27202160	Lagoen.	Chert.	This is fairly fine-grained, dove grey with a chalky feel and has faint approximately parallel laminations defined by discontinuous white blebs <40 mm (average 10 mm). One large sample is present– 70 mm long and 40 mm wide and weathers in.	Stacked full of radiolaria, which are easily distinguished as the brown mottled substance forms in the interstites. Some internal structure can be distinguished– some radial. Slight evidence of compaction in places.	N		
BON 99–22	27202160	Lagoen.	Chert. Finely laminated grey rock– hard and sharp fracture.	Similar to **BON 99–20** and clearly not rhyodacite– looks sedimentary– with a clear grading of grainsize– looks turbiditic.	Very fine-grained. Apparent radiolaria present.	N		
BON 99–23	27202162	Lagoen.	Stripey rock, convolute laminations. Loose blocks within ash.	The stripes are defined by 1–4 mm wide laminations– dove–grey/brown/black. Very distinctive. The convolutions are present of a scale of <1 mm to 5 cm.	Homogeneous, fine-grained, microcrystalline with some poorly preserved radiolaria defined by coarser–grained quartz.	N		
BON 99–24A	27202162	Lagoen.	Rhyodacite clasts in brown conglomerate.	Clast of rhyodacite coated in matrix. Polymictic, with red/blue clasts 1–40 mm.	Clast is mid–brown in colour, with glomerocrysts of seriticised plagioclase (and K–feldspar?). Its fine-grained matrix is difficult to confirm as rhyolitic. The surrounding matrix shows no evidence of chilling and is a heterogeneous mix of lithic clasts, crystal fragments and nearly isotropic material, possibly with a weak perlitic fracture.	N		
BON 99–24B	27202162	Lagoen.	Brown conglomerate, polymictic, with red/blue	This is an altered, crumbly, poorly sorted, heterogeneous lithology consisting of >50% altered	Extremely heterogeneous.	N		

Rock Number	Grid Ref	Locality	Field notes	Hand Specimen Description	Thin Section Description	XRF	Isotope/ Ar-Ar?	Photo micrographs
			clasts 1–40 mm.	brown lithics and some broken crystals (albite?) in a paler altered matrix. Some large broken and angular rhyodacite clasts >4 cm are present.				
BON 99–25	27222168	Lagoen.	Brown conglomerate, polymictic, with red/blue clasts 1–40 mm.	This is a crumbly brown heterogeneous lithology, consisting ~40% of broken crystals (mainly albite; < 3 mm, some quartz) and the lithic clasts present are irregular, brown and 2–30 mm in size– altered rhyodacite or mud? No bedding.	Extremely altered volcaniclastic lithology with occasional perlitic glass fragments.	N		
BON 99–25A	27222168	Lagoen.	See slight convolute bedding with partings of a coarser sandstone between the layers.	Pale brown/grey coloured rock. Convolute lamination defined by 3 different lithologies: discontinuous lenses <3 cm long of pink/brown finely/faintly laminated fine-grained material (mud?), in a medium-grained weathered crystal–rich sandstone. This appears to be contained within a harder, fine-grained pink unit.	Alternating bands of fine-grained ash (granophyric texture) with occasional crystal fragments and a streaky texture defined by dark elongate blebs. These alternate with coarser layers of very angular crystal fragments.	N		
BON 99–26	27222168	Lagoen.	Brown conglomerate, polymictic, with red/blue clasts 1–40 mm.	Brown/green, coarse-grained, relatively crumbly and weathered sandstone. Poorly sorted, consists of angular albite and quartz crystals and some elongate <3 mm long mafic fine-grained blebs– possibly compressed rhyodacite?	Consists of 1–2 mm fragments (moderately angular) of K–feldspar with quartz, plagioclase and rock fragments (mainly igneous, some chert?) in a microcrystalline groundmass with lots of pumpellyite and prehnite.	N		
BON 99–27	27222168	Lagoen.	Trachytic dyke intrusive into conglomerate	Brown, vesicular (20%, <1 mm, some elonagate 2 cm cavities) fine-grained basalt? Mineralogy too fine-grained to be determined in hand specimen.	This fine-grained igneous rock has a matrix comprised of spiky plagioclase and small ragged opaques with interstital orange coloured areas (prehnite/ pumpellyite?) Are these all replacing pyroxene? There's no pyroxene remaining. There are some phenocrysts of feldspar: blocky seriticised K–feldspar, and some plagioclase appears glomerocrystic. Is the rock actually intermediate or is the K–feldspar xenocrystic? There does appear to be K–feldspar in the matrix too so therefore probably a trachyte.	Y	Hf, Nd, Pb, Sr	
BON 99–28	26742162	Lagoen.	Fine-grained volcaniclastic sandstone.	Fine-grained distal turbidite? At base dark coloured fine-grained chert with sole marks at top from erosive unit above. This unit (Bouma A) is medium-grained with rough sub–parallel laminations, <1 mm in size. Laminations are defined by coarser–grained, more carious pale ash alternating with darker fine-grained material. After 1 cm, the laminations begin to become more planar, normally graded and fainter (B) and after 4 cm see faint fine-grained cross–laminations (C). Above this see 3 cm of homogeneous fine-grained ash (D) and then end of sample. Don't see top of sequence. Way up criteris present.	Fine-grained homogenous quartz/feldspar ash.	N		
BON 99–29	27342138	Washikemba.	Crystal–rich sandstone. Blue grey unit, medium-grained sandstone.	Medium-grained mid–brown crystal–rich sandstone, with faint laminations.	Relatively poorly sorted with lots of angular fragments of predominantly feldspar in a brown matrix comprised of prehnite, pumpellyite and	N		

Rock Number	Grid Ref	Locality	Field notes	Hand Specimen Description	Thin Section Description	XRF	Isotope/ Ar-Ar?	Photo micrographs
					clay minerals.			
BON 99–30	27342138	Washikemba.	Coarse-grained sandstone.	Coarse-grained very poorly sorted heterogeneous sandstone consisting of sub–angular albite and quartz crystals <1–3 mm (>60%) and sub–rounded rhyodacite and other lithics (30%) <1 cm in size. Matrix is brown and powdery.	An extremely poorly sorted immature sandstone with very angular fragments of quartz and feldspar (mainly) with a very complex history (resorbed edges, complex twinning, seriticised and fractured). There are many lithics– all igneous and feldspathic. The matrix is brown in colour, consisting of clays, pumpellyite and prehnite. Some small round globules are visible which are outlined by a brown mineral– are these relic perlitic texture? Possibly.	N		00-07-35 00-07-36 00-07-37 00-07-38
BON 99–31	27182138	Washikemba.	Coarse brown volcaniclastic?	Medium-grained sandstone consisting of subangular to subrounded quartz and feldspar fragments (<1mm) in a brown powdery matrix.	Very poorly sorted, packed with fine-grained igneous lithics (>50%) which appear more rounded than the crystal fragments. The cement is pumpellyite/clays.	N		
BON 99–32	27182138	Washikemba.	Fine-grained volcaniclastic rock.	Brown/grey fine-grained ash.	This looks like banded fine-grained ash with 10% radiolaria which are poorly preserved but infilled with quartz.	N		00-07-33 00-07-34
BON 99–33	27182138	Washikemba.	Red fine-grained uniform sandstone.	Brown/grey fine-grained homogenous ash.	Brown/grey fine-grained homogenous ash with quartz and feldspar fragments.	N		
BON 99–34	27182138	Washikemba.	Fine to medium-grained sandstone with very convoluted bedding.	Brown ~fine-grained sandstone with faint parallel laminations several mm in scale, defined by darker bands.	Brown/grey fine-grained homogenous ash with quartz and feldspar fragments.	N		
BON 99–35	27172133	Washikemba.	Blocks of purple porphyritic.rhyodacite in conglomerate.	Purple/grey rhyodacite with 20% porphyritic feldspar (some albitised) and 10% vesicles (~round, <1.5 mm, some with rim/infilling of quartz). Matrix is ~fine-grained. Small amount of fresh blue rhyodacite in interior.	A “crazy paving” like texture is visible– a result of the polishing process, as present in many sections. The matrix is a result of quartz and feldspars, all showing signs of shearing and looking fairly disturbed with lots of inclusions. Some large squat K–feldspar with small quatrz/sericite inclusions are visible. The brown more altered area is due to a concentration of patches of prehnite/pumpellyite with chlorite.	Y	Hf, Nd, Pb, Sr	
BON 99–36	27172133	Washikemba.	Dense purple fine-grained rock– volcaniclastic sandstone.	Very weathered brown fine-grained rock. Possibly altered rhyodacite, but more likely to be volcaniclastic rock. Can distinguish many feldspar minerals <2 mm in size.	This is an incredibly altered slide consisting of very altered volcaniclastic rock (possibly like **BON 99–05**) but every phase is so altered and turbid that determining any primary mineralogy is difficult.	N		
BON 99–37	27172133	Washikemba.	Coarse ash grading down into conglomerate.	Medium-grained medium–brown weathered crystal–rich sandstone.	Homogeneous microcrystalline ash.	N		
BON 99–38	27152133	Washikemba.	Massive unit– welded ash?	Pale grey/brown welded ash. 10% irregular cavities (0.1–30 mm).	Consists of crystal fragments and some pumice (elongate outlines and infilled with a granophyric mosaic), which are moderately well–sorted in a very fine-grained microcrystalline matrix. There is a very weak sub–parallel orientation.	N		00-07-31 00-07-32

Appendix A- Sample Information. Table 3: 1999 Field Season.

Rock Number	Grid Ref	Locality	Field notes	Hand Specimen Description	Thin Section Description	XRF	Isotope/ Ar-Ar?	Photo micrographs
BON 99–39	27152133	Washikemba.	Non–conglomeratic layer from within conglomerate.	Extremely crystal–rich sample. Consists of subangular quartz and feldspar in equal proportions in small amount of matrix and surrounded by small (<1 mm) cubic opaques comprising >20% of the rock.	Extremely heterogeneous rock with feldspar, quartz, tube pumice and lithic fragments, <2 mm in size, in a chaotic fine-grained microcrystalline matrix with pumpellyite /clays.	N		00-07-27 00-07-28 00-07-29 00-07-30
BON 99–40	21972115	Angola.	Loose blocks of rhyodacite.	Pink/brown rhyodacite consisting 30% of spiky porphyritic feldspar and 20% irregular vesicles, infilled with quartz.	Consists of lots of very seriticised K–feldspar and plagioclase (glomerocrysts?) in a feldspathic matrix. There is some alignment of the feldspar and vesicles, which are infilled with quartz and biotite. This rock displays a seriate texture.	N		
BON 99–41	21972115	Angola.	Loose blocks of rhyodacite.	Pink/brown rhyodacite consisting 30% of spiky porphyritic feldspar and 20% irregular vesicles, infilled with quartz.	Consists of lots of very seriticised K–feldspar and plagioclase (glomerocrysts?) in a feldspathic matrix. There is some alignment of the feldspar and vesicles, which are infilled with quartz and biotite. This rock displays a seriate texture.	N		
BON 99–42	22972115	Near Angola.	Rhyodacite.	Mid brown weathered fine-grained rhyodacite (looks like ash) with 20% phenocrysts of feldspar and some quartz and epidote veining– impossible to avoid on crushing.	All phenocrysts of feldspar (plagioclase and K–feldspar) look very turbid, some resorbed, others fragmented– all look like they're xenocrystic. Quartz infills an irregular vugh– it appears to have a very strange texture and is highly fractured. Pumpellyite here has high relief, is pleochroic olive green, and interference colours up to top second order.	Y		
BON 99–43	22762156	Near Angola.	0.5 m thick crystal–rich volcaniclastic layer.	Sub–angular quartz and feldspar <2 mm in size dominate this brown rock, with a powdery brown/green matrix.	As hand specimen.	N		
BON 99–44	22762156	Near Angola.	Very fine-grained volcaniclastic.	Sandy–brown homogenous fine-grained ash, feels chalky. Faint ~parallel laminations defined by grainsize.	Typcially altered dolerite with mafic phases replaced by pumpellyite and clays.	N		
BON 99–45	22602235	Near Angola.	Rhyodacite.	Purple/grey rhyodacite with 20% large (5mm) round vesicles lined with quartz. Consists of 30% albitised feldspar.	As hand specimen.	Y		
BON 99–46	22602235	Near Angola.	Very fine-grained volcaniclastic.	Medium-grained hard mid–brown sandstone. Difficult to determine composition.	Homogenous ash with opaques, quartz and feldspar.	N		
BON 99–47	22152024	Quarry near "Food King".	Very fine-grained volcaniclastic.	Chalk–like fine-grained ash. See faint mm– scale parallel laminations defined by darker bands.	Homogenous ash with opaques, quartz and feldspar.	N		
BON 99–48	22152024	Quarry near "Food King".	Dolerite– weathered, intruded into ash.	Very weathered green/grey dolerite with ~10% feldspar	Too weathered for petrographic analysis.	N		
BON 99–49	22152024	Quarry near "Food King".	Basalt (top), intruded into ash (slightly chilled).	Weathered fine-grained sample. Impossible to identify in hand specimen.	Loaded with spiky plagioclase with prehnite/pumpellyite in the interstites (replacing clinopyroxene?).	N		
BON 99–50	25231883	Hill, 500m NW of Orinoco.	Orange/tan rhyodacite from dome.	Very fresh rhyodacite with <20% porphyritic spiky feldspar and no vesicles. Extremely hard rock.	Relatively fresh rock– different to the NC– consists of seriate–textured feldspar with subordinate amounts of quartz.	Y		
BON 99–51	25261883	Hill, 500m NW	Basalt from base of cliff	Fine-grained weathered basalt with 10% irregular	Homogenous microcrystalline ash with iron	Y		

Rock Number	Grid Ref	Locality	Field notes	Hand Specimen Description	Thin Section Description	XRF	Isotope/ Ar-Ar?	Photo micrographs
		of Orinoco.	beneath rhyodacite.	cavities <1 mm in size.	staining.			
BON 99–52	25261883	Hill, 500m NW of Orinoco.	Basalt from base of cliff beneath rhyodacite.	~Fresh dolerite/basalt.	Stacked full of feldspar (plagioclase and K–feldspar) displaying a seriate texture. Corroded pyroxene (clinopyroxene?) is found in the interstites, partially replaced by prehnite and pumpellyite.	Y		
BON 99–53	10262833 Locality 99-16	Gotomeer lake.	Chert. Dark blue/red fine-grained unit.	Blue–black/brown chert, consisting of wavy laminations several mm in width.	Extremely iron rich banded microcrystalline mush with some radiolarites very poorly preserved.	N		
BON 99–54	10262833 Locality 99-16	Gotomeer lake.	Very coarse, finely laminated sandstone.	Brown very coarse-grained sandstone, consisting entirely of subrounded feldspar and quartz crystals, 1–2 mm in size. A rough parallel foliation is visible.	As hand specimen. Matrix is recrystalline ash.	N		
BON 99–55	10262833 Locality 99-16	Gotomeer lake.	Fine-grained sandstone.	Banded chert/fine ash: consists of alternating laminations of pale brown ash and dark blue chert over a mm–scale. Cross–lamination present.	Microcrystalline ash with very well developed micro-laminations.	N		
BON 99–56	10532798 Locality 99-19	Gotomeer lake.	Coarse-grained conglomerate, blue/green in colour.	Heterogeneous breccia, consisting of subangular feldspar (40%) and mafic blebs 1–10mm in size (lithics?), in a brown powdery matrix. Elongate (2 cm) blebs of mudstone are present.	Consists of many lithic fragments, some scoria, some (tube) pumice, and some amazing perlitic–fractured clasts, all in a fine-grained heterogeneous matrix consisting of altered pumice and ash.	N		00-07-17 00-07-18 00-07-19 00-07-20 to 26
BON 99–57	10482802 Locality 99-20	Gotomeer lake.	Fine-grained sedimentary rip–up clasts in coarse-grained conglomerate.	Dense, fine-grained, brown lens ~ 10 cm in diameter. No fresh surfaces.	Fine-grained homogeneous ash with some crystal fragments (feldspar) and lots of opaques.	N		
BON 99–58	10442805 Locality 99-21	Gotomeer lake.	Coarse-grained grey volcaniclastic.	Medium-grained brown sandstone similar to **BON 99–54.**	As hand specimen. Very homogenous.	N		
BON 99–59	10442805 Locality 99-21	Gotomeer lake.	Planar laminated, blue/grey well–bedded fine-grained sandstone.	Brown fine-grained ash alternating with harder blue material (chert?) with sub–parallel laminations several mm in size.	Homogeneous microcrystalline ash with laminations defined by grainsize– turbiditic?	N		00-06-09 00-06-10 00-06-11
BON 99–60	10442805 Locality 99-21	Gotomeer lake.	Chert lenses within **BON 99–59.**	Wavily–laminated chert. Consists of dark blue/black laminations alternating with brown, with discontinuous lenses of creamy–white material.	Microcrystalline ash with very well developed micro-laminations.	N		
BON 99–61	Locality 99-22	Gotomeer lake.	Basalt.	Very weathered green/grey rock with ~5% round vesicles 2–10 mm, partially infilled with quartz, zeolites and clays. Some fresh surfaces show a green basalt.	Aphyric basalt. Abundant small clinopyroxenes.	N		
BON 99–62	10102826 Locality 99-27	Gotomeer lake.	Crumbly and massive volcaniclastic rock, fining up with some large angular chert fragments (<15 cm).	Coarse-grained poorly sorted sandstone consisting of >40% feldspar and subordinate quartz along with angular rhyodacite clasts 2–15 mm. Brown and powdery matrix.	Poorly sorted heterogeneous mix of igneous lithic fragments and crystals.	N		
BON 99–63	10102826 Locality 99-27	Gotomeer lake.	Crumbly and massive volcaniclastic rock, fining up with some large angular chert fragments	Very coarse-grained sandstone consisting of 30% angular feldspar fragments and many lithic clasts (rhyodacite and chert?). Several pale yellow powdery patches are visible: these have weathered in and must	Very heterogeneous lithic breccia consisting of angular igneous and volcaniclasticaceous fragments, abundant pumice (no tube evidence) and ash, along with many crystal fragments.	N		00-07-12 00-07-13 00-07-14 00-07-15

Rock Number	Grid Ref	Locality	Field notes	Hand Specimen Description	Thin Section Description	XRF	Isotope/ Ar-Ar?	Photo micrographs
			(<15 cm).	represent the remains of some less–resistant lithic clast or pumice.				00-07-16
BON 99–64	10106281 Locality 99-28	Gotomeer lake.	Well–bedded fissile shales interbedded with fine-grained sandstone. Strange weathering texture.	Fine-grained mid–brown sandstone with a dark exterior distinguished by a strange weathering texture: pale blobs on the dark exterior (2–20 mm) weather in and give a swiss–cheese appearance.	Homogeneous microcrystalline ash.	N		
BON 99–65	09982830 Locality 99-29	Gotomeer lake.	Coarse-grained conglomerate.	Consists (40%) of angular feldspar fragments and angular mafic lithic clasts (20% chert? shale? basalt?) in a green/brown matrix.	Angular lithic breccia consisting of fine-grained plagioclase–phyric igneous fragments (one with a 2 mm clinopyroxene phenocryst in) and crystals fragments with subordinate amounts of pumice in a heterogeneous matrix comprised of ash.	N		00-07-08 00-07-09 00-07-10 00-07-11
BON 99–66	09682848 Locality 99-30	Gotomeer lake.	Cherts with convoluted bedding.	Chert but extremely weathered exterior nearly totally obscures laminations.	Microcrystalline chert. No fossils present. Very homogeneous.	N		
BON 99–67	09662867 Locality 99-31	Gotomeer lake.	Either crystal–rich volcaniclastic with fragments of basalt in or weathered rhyodacite with many inclusions.	Very coarse-grained crystal–rich poorly–sorted sandstone with a green coloured matrix. Contains many subangular basaltic and rhyolitic inclusions (10%; 10–40 mm in size)	Patches of coherent rhyodacite occasionally separated by fine-grained microcrystalline ash. This probably represents an autobreccia. One K–feldspar is bent into an s–shape.	N		
BON 99–68	09662867 Locality 99-31	Gotomeer lake.	Either crystal–rich volcaniclastic with fragments of basalt in or weathered rhyodacite with many inclusions.	Rhyodacite autobreccia? "Clast" of porphyritic rhyodacite 10 cm in diameter surrounded by what also looks like rhyodacite with abundant mafic inclusions (<1–3 cm)– could be basalt or mudstone. Also observe ragged clast with striated texture– could represent elongated tube pumice as no phenocrysts present.	Volcaniclastic rock. Consists of sub–rounded crystals of quartz and quartz <1 mm in size, along with irregular basaltic/andesitic xenocryst in an inhomogenous granophyric groundmass. See texture defined by regions of coarser granophyric intergrowth (possibly relic pumice) or subparallel elongate wisps of opaque material distorted around the crystals.	Cut in two?		
BON 99–69	09562857 Locality 99-32	Gotomeer lake.	Massively bedded sandstone.	Yellow/pale brown sedimentary rock– Consists of 25% sub angular albitised feldspar (most visible on weathered surface). On non–weathered surface, texture appears homogenous and non–clastic.	Homogenous altered rock consisting of a granophyric intergrowth, occasional weathered crystal fragments and stylolites.	N		
BON 99–70A	09182845 Locality 99-35	Gotomeer lake.	Coarse crystal rich sandstone, fining up.	Medium to coarse-grained sandstone, consisting of sub–angular feldspar in a yellow–brown powdery matrix. Weak foliation parallel to bedding?	Classic ash consisting of lots of fragments of quartz and feldspar in a prehnite– pumpellyite cement.	N		
BON 99–70	09182845 Locality 99-35	Gotomeer lake.	Top of coarse crystal rich sandstone, fining up.	Extremely fine-grained homogenous tan/dark brown sandstone– almost grading to mudstone. See a weak parallel lamination defined by colour and weathering in.	Monotonous fine-grained ash with crystal fragments and poorly–preserved radiolaria.	N		
BON 99–71	09132850 Locality 99-35	Gotomeer lake.	Clasts in coarse sandstone.	Heart–shaped clast 4 cm long of pink porphyritic rhyodacite in medium-grained tan coloured sandstone. Specimen is too altered to obtain thin section.	Too altered for petrographic analysis.	N		
BON 99–72	08862854 Locality 99-36	Gotomeer lake.	Dolerite. Weathered medium-grained rock– looks more	Medium-grained green coloured dolerite? Very feldspar rich. Fresh sample is too small for thin section, whereas other part is too weathered.	Stacked full of feldspar (plagioclase and K–feldspar) displaying a seriate texture. Corroded pyroxene (clinopyroxene?) is found in the	Y		

Rock Number	Grid Ref	Locality	Field notes	Hand Specimen Description	Thin Section Description	XRF	Isotope/ Ar-Ar?	Photo micrographs
			felsic than dolerite seen previously.		interstites, partially replaced by prehnite and pumpellyite. Borders with diorite in chemical composition.			
BON 99–73	08902850 Locality 99-37	Gotomeer lake.	Rhyodacite. Quartz–veined. Very similar to NE domes. As unweathered as possible.	Felsic fine-grained rock. Consists of 10% phenocrysts of feldspar <1 mm in size and eliptical quartz amygdules (10%). Difficult to avoid thin weathered crust.	Rhyodacite– fine-grained, nearly aphyric with occasional quartz amygdules.	Y		
BON 99–74	08902850 Locality 99-37	Gotomeer lake.	Rhyodacite. Quartz–veined. Very similar to NE domes. As unweathered as possible.	Felsic fine-grained rock. Consists of 10% phenocrysts of feldspar <1 mm in size and elliptical quartz amygdules (10%). Inclusion of red–brown rock present on surface, 3 cm in size. Too weathered for XRF.	This is similar to **BON 99–49** except more quartz is present– dacite? It consists of feldspar and quartz in a prehnite/pumpellyite matrix, which is very corroded. Occasional vesicles are quartz infilled.	N		
BON 99–75	12123164 Locality 99-39	Salina Mathijs.	Rounded sedimentary clast in massive clast–supported igneous unit.	Surfaces totally weathered.	Very fine-grained microcrystalline ash with lots of opaaques. See other clasts on margin of slide– i.e. igneous clast with igneous xenolith in.	N		
BON 99–76	12123164 Locality 99-39	Salina Mathijs.	Rounded slumped blocks of limestone in coarse-grained clastic unit.	Smoothed sample of finely–laminated (parallel) brown/grey limestone. Smells of sulphur when split.	Homogenous slide consisting of a microcrystalline matrix, no trace of fossils– Laminations consist of faint parallel wisps.	N		
BON 99–77	12213156 Locality 99-39	Salina Mathijs.	Clast–supported conglomerate (debris flow).	Very poorly–sorted clast–supported conglomerate, consisting of angular to subrounded clasts of rhyodacite and others, 1–30 mm in size.	Consists of clasts varying from angular to rounded (ash fragments tend to be angular). Clasts are igneous or volcaniclastic derived but are heterogeneous in terms of their colour/ degree of phenocrysts etc although most are plagioclase–phyric and probably andesite. Clast size ranges from 0.5–15 mm, and some of the smaller ones are discrete crystals (clinopyroxene and plagioclase). Interlocking grain boundaries and the matrix is subordinate and appears to be devitrified ash.	N		00-07-01 00-07-02 00-07-03 00-07-04 00-07-05 00-07-06 00-07-07
BON 99–78	12163101 Locality 99-39	Salina Mathijs.	Andesitic basalt. Fine-grained igneous clast in very poorly sorted conglomerate.	Fresh fine-grained blue igneous rock. Sparsely porphyritic. Irregularly shaped feldspar phenocrysts are present.	Well–defined trachytic texture displayed by plagioclase. See occasional glomerocrysts of plagioclase 1–2 mm in size, in matrix of turbid plagioclase <0.5 mm in length, with very occasional clinopyroxene.	Y		00-06-16 00-06-17
BON 9–79	11483126 Locality 99-39	Salina Mathijs.	Fine-grained grey aphyric rock.	Brown, fine-grained, aphyric basalt.	As hand specimen.	Y		
BON 99–80	11483126 Locality 99-39	Salina Mathijs.	Basalt/dolerite. Medium-grained pyroxene rich igneous rock– may not be in situ.	Perhaps a microdiorite– medium to coarse-grained rock consisting of interlocking grains of quartz and feldspar (50%) and a shiny black phase (40%– probably pyroxene). Very fresh.	Extremely fresh dolerite. Consists of interlocking grains of plagioclase and clinopyroxene, some rimmed with magnetite. There is also some olivine and perhaps a little orthopyroxene. Some plagioclase seems strained.	Y		00-06-22 00-06-23
BON 99–81	11483126 Locality	Salina Mathijs.	Basalt. Grey fine-grained rock with 20% vesicles,	Fine-grained fresh mafic rock dominated by amygdular quartz and zeolites (round, 1–10 mm in size).	Weathered spiky feldspar <0.5 mm in length surrounded by abundant opaques with some small	Y		00-06-18 00-06-19

Rock Number	Grid Ref	Locality	Field notes	Hand Specimen Description	Thin Section Description	XRF	Isotope/ Ar-Ar?	Photo micrographs
	99-39		<2 mm in size, rounded, now infilled with quartz		patches of clinopyroxene (?) some with strain shadows and areas of pumpellyite.			
BON 99–82	11483126 Locality 99-39	Salina Mathijs.	Fine-grained rhyodacite with porphyritic plagioclase and vesicles.	Fine-grained dark blue rhyodacite with large feldspar (20%) and irregular vesicles (some elongate) 1–20 mm, rimmed by subordinate amounts of quartz.	Calcite infilled vesicles. Glomerocrysts of K–feldspar and plagioclase in a fine-grained matrix of spiky feldspar and quartz. Some xenocrysts of pyroxene.	too small		
BON 99–83	11483126 Locality 99-39	Salina Mathijs.	Microdiorite. Medium to coarse-grained rock with pyroxene.	Phenocrystic plagioclase (40%) dominates this rock, in a fine-grained mafic matrix.	Classic fresh basalt– relatively unaltered, with phenocrystic plagioclase (some glomerocrysts) and fine-grained plagioclase, pyroxene and opaques in the groundmass. Most grains of pyroxene are altered to pumpellyite/prehnite. Several are altered to chlorite on the margins.	N		00-08-17 00-08-18 00-08-19
BON 99–84	11483126 Locality 99-39	Salina Mathijs.	Basalt. Grey fine-grained rock with 20% vesicles, <2 mm in size, rounded, now infilled with clays?	Amygdules have lining of clays and are infilled with white mineral– zeolites?	Basalt dominated by green amygdules (pumpellyite?) with spiky feldspar and clinopyroxene. Weathered. Some calcite infilling also.	Y		00-06-01
BON 99–85	11433126 Locality 99-39	Salina Mathijs.	Basalt breccia. Brecciated appearance created by brown fine-grained sub–angular fragments with blue and white calcite vesicular infillings.	Calcite/clay cemented clast–supported breccia, with aphyric purple amygdular angular rhyodacite clasts 1–10 cm in size.	As hand specimen.	N		
BON 99–86	11433126 Locality 99-39	Salina Mathijs	Basalt breccia. Brecciated appearance created by brown fine-grained sub–angular fragments with blue and white calcite vesicular infillings.	Calcite/clay cemented clast–supported breccia, with aphyric purple amygdular angular basalt clasts 1–10 cm in size.	Spectacular phenocrystic intermediate fine-grained igneous rock extensively veined by calcite. Basalt has patches of a bright green mineral– probe. K–feldspar phenocrysts are weathered and some are glomerocrystic. Clinopyroxene is fresh and abundant in a matrix rich in opaques and spiky feldspar.	N		00-06-24
BON 99–87	11373194 Locality 99-43	Near Salina Mathijs.	Fresh boulder of dolerite– but see in– situ weathered dolerite/basalt beside it.	Mosaic of pyroxene and feldspar, appears relatively fresh.	Lots of relatively fresh pyroxene (all clinopyroxene) surrounded by less fresh plagioclase, with some magnetite and Fe–oxyhydroxides. There is a mineral that shows 3rd order birefringence and slight green pleochroism– this may be olivine, although extensive probe analysis found all suspective olivine to be pyroxene.	Y	Hf, Nd, Pb, Sr	00-06-20 00-06-21
BON 99–88	10813228 Locality 99-45	Near Salina Mathijs.	Blue crystal–rich volcaniclastic rock.	Breccia/ very coarse-grained sandstone consisting of angular rhyodacite (and other) clasts 1–15 mm in size, along with crystal fragments. Extremely poorly sorted, clast supported (just) with blue and powdery matrix.	A lithic breccia consisting of igneous and ash lithic fragments along with complexly zoned fragmented feldspar with subordinate amounts of quartz in a heterogeneous ash matrix. A large perlite clast is also present.	N		00-06-02 00-06-03
BON 99–89	10553222	Near Salina	Porphyritic rhyodacite.	Blue rhyodacite with 40% stubby feldspar <3 mm in	Consists of large (1–3 mm) xenocrysts with	Y		

Rock Number	Grid Ref	Locality	Field notes	Hand Specimen Description	Thin Section Description	XRF	Isotope/ Ar-Ar?	Photo micrographs
	Locality 99-46	Mathijs.		size and subordinate amounts of fresh quartz phenocrysts. It contains ~5% inclusions.	resorbed edges. Quartz, K–feldspar, plagioclase, clinopyroxene and others. All appear to be out of chemical equilibrium. The plagioclase is seriticised, but the clinopyroxene appears fresh. Groundmass is irregular mosaic of quartz and feldspar (?)– granophyric?			
BON 99–90[PAT1]	10553222 Locality 99-46	Near Salina Mathijs.	Porphyritic rhyodacite with small basaltic (?) inclusions– loose fragment and possibly from blue coarse-grained conglomerate unit.	Blue rhyodacite with 40% stubby feldspar <3 mm in size and subordinate amounts of fresh quartz phenocrysts. It also contains ~20% inclusions–(basaltic?) with irregular edges, 1–40 mm in size.	Consists of 30% large (1–3 mm) xenocrysts with incredible resorbed edges. Quartz, K–feldspar, plagioclase, clinopyroxene and others. All appear to be out of chemical equilibrium. The plagioclase is seriticised, but the clinopyroxene appears fresh. Groundmass is irregular granophyric mosaic of quartz and feldspar. Irregular brown xenocrysts present 1 cm in diameter– no chilled margin visible, and comprised of a fine-grained mosaic of radiating corroded crystals– feldspar? Mainly composed of clays now.	N		
BON 99–91	10503222 Locality 99-46	Near Salina Mathijs.	Stripy fine-grained rock– flow banded rhyodacite?	Weathered fragment. Appear to be a rhyodacite and consists of several parallel more mafic bands, one 3 mm thick and the other 2 cm in width. Surrounding these are small–scale wispy parallel blebs, 0.1 mm in width.	Glomerocrysts of K–feldspar are seriticised, corroded, calcified and fractured, as are the occasional clinopyroxene. The matrix is fine-grained and consists of quartz and feldspar with some alignment of feldspar parallel to phenocryst margins.	N		
BON 99–92	10333234 Locality 99-47	Near Salina Mathijs.	Coarse-grained blue conglomerate, finer–grained here, crystal rich with rhyodacite clasts <2 cm. 1–2 mm grain size.	Coarse brown altered sandstone consisting of poorly sorted fragments of rhyodacite and other lithics, 1–20 mm in size, and crystal fragments. Pumice may also be present.	Consists of many subrounded clasts <5 mm in size, outlined by Fe–oxyhydroxide. Clasts are particularly heterogeneous– perlite, basalt and other fragments are present.	N		
BON 99–93	08952847 Locality 99-37	Gotomeer.	Black basalt overlying rhyodacite.	Black fine-grained basalt, possibly aphyric. Very altered.	Too weathered for petrographic analysis.	N		
BON 99–94	08952847 Locality 99-49	Gotomeer.	Fine-grained greenish rhyodacite with irregular vesicles (1–3 mm). Part of flow.	Relatively fresh green–coloured igneous rock. Occasional vesicles.	This fine-grained igneous rock consists of lots of ragged feldspar and quartz, all with interstitial chlorite, pumpellyite and prehnite. Several vesicles are calcite infilled.	N		
BON 99–95	08952847 Locality 99-49	Gotomeer.	Coarser–grained volcaniclastic.	Extremely weathered very coarse-grained sandstone consisting of lithic clasts and crystals <3 mm in size. Weak foliation defined by orientation of clasts.		N		
BON 99–96	08952847 Locality 99-49	Gotomeer.	Coarser–grained volcaniclastic, weathered, fines upward. 1–3 mm grainsize.	Brown weathered rock consisting of brown elongate wispy patches several mm in size– pumice(?), some lithics and crystal fragments. Too weathered to determine.	Fragmentary rock consisting of poorly–sorted angular fragments of volcaniclasticaceous rock and fine-grained plagioclase–phyric igneous rock with crystals (plagioclase, quartz). Many igneous rock fragments appear to have a jigsaw fit observed.	N		00-06-04
BON 99–97	08952847	Gotomeer.	Coarse-grained	Very poorly sorted breccia– clasts very angular, 1–20		N		

Rock Number	Grid Ref	Locality	Field notes	Hand Specimen Description	Thin Section Description	XRF	Isotope/ Ar-Ar?	Photo micrographs
	Locality 99-49		conglomerate/breccia.	mm in size in powdery brown matrix. ~Matrix supported?				
BON 99–98	08952836 Locality 99-50	Gotomeer.	Basalt. Isolated lump of fine-grained green rock.	Mid–brown fine-grained with tiny spiky feldspar visible.	Basalt is stacked full of spiky seriate–textured plagioclase with interstitial pumpellyite.	Y		
BON 99–99	08952836 Locality 99-50	Gotomeer.	Dolerite.	Fairly weathered dolerite	Plagioclase with interstitial corroded clinopyroxene and green pumpellyite.	N		
BON 99–100	08992823 Locality 99-51	Gotomeer.	Rhyodacite. Grey fine-grained igneous rock outcropping immediately N of parking place.	Grey/green fine-grained relatively fresh rock with some slight quartz veining	Relatively fresh rhyodacite with spiky feldspar, interstitial quartz and opaques with quartz amygdules.	Y		
BON 99–101	09052806 Locality 99-54	Gotomeer.	Andesite.	Grey/green andesite.	Consists of 1 mm turbid "blobs" which are actually glomerocrystic plagioclase, in matrix of opaques, turbid plagioclase, quartz, occasional clinopyroxene, and a brown alteration mineral.	Y		
BON 99–102	09222793 Locality 99-58	Gotomeer.	Fine-grained pale cherty sediment.	Pale brown fine-grained homogenous sediment with a sharp fracture. Chert?		N		
BON 99–103	09062818 Locality 99-59	Gotomeer.	Massive, structureless brown fine-grained unit. Could either be fine-grained volcaniclastic unit or basalt. Too weathered to determine.	Need to see fresh surface to identify.	Basalt. Stacked full of plagiolcase with patches of pumpellyite.	N		
BON 99–104	08952817 Locality 99-60	Gotomeer.	Fairly fresh microdiorite.	Beautiful trachitic texture visible in hand specimen.	Microdiorite. Consists of spiky interlocking feldspar with interstial quartz and feldspar, along with opaques.	Y	Hf, Nd, Pb, Sr	
BON 99–105	10562797 Locality 99-61	Gotomeer.	Basalt.	Weathered basalt	As hand specimen.	Y		
BON 99–106	10482730 Locality 99-64	Gotomeer.	Rhyodacite flow with columnar jointing.	Tan–coloured weathered rhyodacite with orientated elongate vesicles (10%) and albitised feldspar. Too weathered for XRF?	Too altered for petrographic analysis.	N		
BON 99–107	10342727 Locality 99-65	Gotomeer.	Slab of crystal–rich volcaniclastic (not in situ) with interesting texture for polishing.	On weathered surface see strange texture: subrounded apparent clasts of porphyritic rhyodacite outlined by a concentration of a white cement in a coarse sandstone matrix (similar to the other coarse volcaniclastic sandstones). This appears to rest on a medium-grained medium sandstone with an erosive contact between the two.	Too altered for petrographic analysis.	N		
BON 99–108	07153172 Locality 99-67	Brandaris.	Rhyodacite from top of Brandaris.	Pink/brown rhyodacite with weathered feldspar and no vesicles. Extremely weathered crust analysed as **BON 99–108W**	Too altered for petrographic analysis.	Y		

Rock Number	Grid Ref	Locality	Field notes	Hand Specimen Description	Thin Section Description	XRF	Isotope/ Ar-Ar?	Photo micrographs
BON 99–109	07153172 Locality 99-67	Brandaris.	Rhyodacite from top of Brandaris.	Pink/brown rhyodacite with weathered feldspar and no vesicles.	No thin section taken.	Y		
BON 99–110	07352165 Locality 99-67	Brandaris.	Clastic (?) rock associated with rhyodacite has lumpy texture here, despite columns.	Appears to be clastic– lumps 5 mm in diameter appear to be rhyodacite, with smaller lumps of rhyodacite in the interstites. Need to thin section.	Mucky slide. Clastic rock. Consists of slightly rounded fragments of seriticised K–feldspar and plagioclase, with magnetite in heterogeneous matrix, which appears to be comprised of 5 mm diameter irregular patches of quartz and feldspar. Unusual.	N		
BON 99–111	07203210 Locality 99-68	Brandaris.	Rhyodacite.	Pink rhyodacite. Appears sparsely porphyritic.	Seriticised squat feldspar phenocrysts in a matrix of quartz, feldspar and opaques.	Y		
BON 99–112	07743190 Locality 99-69	Brandaris.	Spherulitic rhyodacite.	Grey rhyodacite. Appears sparsely porphyritic.	Altered slide– turbid phenocrysts of feldspar and areas of infilled quartz in a matrix of quartz, feldspar and opaques– partially recrystalline so get areas of spherultites (i.e. bumpy texture).	Y		
BON 99–113	Locality 99-70	Brandaris.	Fine-grained yellow/white sediment.	Finely laminated tan coloured sediment with a chalky feel.	Microcrystalline ash.	N		
BON 99–114	07603212 Locality 99-71	Brandaris.	Hillock of rhyodacite without columns.	Tan coloured rhyodacite	Weathered rhyodacite with seriate texture	Y		
BON 99–115	09273373 Locality 99-73	Seru Mangel.	Coarse-grained conglomerate.	Bumpy massive rock, fresher surfaces are olive/khaki green and show elonglated pumice fragments <1.5 cm. Crude bedding–parallel foliation, irregular calcite mineralised veins and broad fining up. Klaver's "agglomerate".	Weathered rhyodacite with seriate texture.	N		
BON 99–116	09273373 Locality 99-73	Seru Mangel.	Sediment clast within agglomerate.	Brown fine-grained weathered clast. May be basalt or sediment.	Homogenous fine-grained sediment. Microcrystalline ash.	N		
BON 99–117	09273373 Locality 99-73	Seru Mangel.	Rhyodacite clast in agglomerate	Weathered dark blue rhyodacite.	Stubby K–feldspar in devitrified fine-grained matrix.	N		
BON 99–118	08953405 Locality 99-74	Seru Mangel.	White breccia– fragmental rhyodacite blocks in powdery orange/ white matrix. Tiny exposure.	Extremely poorly–sorted monomictic clast supported breccia with pale rhyodacite clasts varying from <1 mm to 100 mm in a tan coloured powdery matrix.	As hand specimen.	N		
BON 99–119	06222983 Locality 99-76	Slagbaai.	Dacite. Fresh sample of fine-grained igneous rock. Note: not in situ– from border between salt pans.	Dark grey fine-grained rock– very fresh on inside.	Fresh rock. Aphanitic, consists of feldspar (K–feldspar and plagioclase, < 1 mm in length) with interstitial subrounded quartz and opaques. Some pumpellyite is present, and is concentrated in domains. A small calcite vein cuts the rock.	Y		00-06-25
BON 99–120	06253006	Slagbaai.	Banded chert horizon–	Very similar in texture to **BON 99–64**. Strange		N		

Rock Number	Grid Ref	Locality	Field notes	Hand Specimen Description	Thin Section Description	XRF	Isotope/ Ar-Ar?	Photo micrographs
	Locality 99-78		black dense material with white blobs– iron development?	weathering texture only occurs at paler more sandy horizons.				
BON 99–121	06133017 Locality 99-78	Slagbaai.	Andesite. Loose fine-grained intermediate igneous rock.	Some calcite veining.	Calcite infilling pore spaces has affected Si content. Actually intermediate rock as consists soley of quartz, feldspar (predominantly K–feldspar) and opaques with lots of patches of calcite.	Y		
BON 99–122	06153022 Locality 99-78	Slagbaai.	Vesicular dolerite, infilled with calcite.	Dolerite / basalt- transitional in terms of grainsize.	K–feldspar with interstitial pumpellyite and opaques. Lots of calcite infilled vesicles.	N		
BON 99–123	07262638 Locality 99-79	Salina Tan.	Contact zone between andesite and "agglomerate"– fine-grained sharp–fractured rock.	Brown homogenous weathered basalt or volcaniclastic rock?	Homogenous fine-grained sandstone with crystal fragments and igneous lithic clasts in fine-grained ashy matrix.	N		
BON 99–124	07262638 Locality 99-79	Salina Tan.	Dolerite?	Very weathered unit. Medium-grained, but difficult to confirm non–clastic origin as too altered.	Altered rock– most likely dolerite with lots of pumpellyite development but very weathered.	N		00-06-05 00-06-06
BON 99–125	07256239 Locality 99-79	Salina Tan.	"Agglomerate".	Again, extremely weathered. Appears to consist of angular clasts of rhyodacite 1–30 mm in size in muddy brown matrix. Extremely poorly sorted. Clast supported?	Lithology very altered.	N		
BON 99–126	07182640 Locality 99-79	Salina Tan.	Fine-grained clast from "agglomerate".	Dark blue fine-grained clast. Faint fine parallel laminations and distinct grading over 30 mm, i.e. sedimentary rock.		N		
BON 99–128	07162643 Locality 99-80	Salina Tan.	Andesitic basalt. 50 cm wide dyke intruding agglomerate. Weathered.	Fine-grained aphyric brown andesitic basalt, but very weathered. Fresh green and fine-grained on the inside but lots of fracture surfaces which cannot be avoided due to the size of the sample.	Lovely spiky texture displayed by plagioclase/K–feldspar? Surrounded by quartz, lots magnetite and brown alteration phase. All feldspars very altered. Microvesicular.	Y		
BON 99–129	07312663 Locality 99-83	Salina Tan.	Dacite.		K–feldspar (and possibly plagioclase) with interstitial opaques and quartz. Trachytic texture.	Y		
BON 99–130	07312663 Locality 99-83	Salina Tan.	Dacite. Pale epidote–coloured rock.	Mid grey fine-grained aphyric rock. Fairly fresh on inside.	Very occasional phenocrysts of feldspar in matrix of corroded spiky feldspar defined by a coating of clay, along with quartz, magnetite and prehnite. Packed full of little round amygdules with a coating of Fe–oxide phase and radiating fibres of crystoballite (?) and quartz in the interior.	Y		
BON 99–131	07342670 Locality 99-84	Salina Tan.	Rhyodacite.	Grey rhyodacite with albitised irregular shaped feldspars. Irregular cavities infilled with quartz and zeolites?	Near–seriate texture with apparently altered phenocrysts.	Y		
BON 99–132	07372647 Locality	Salina Tan.	Rhyodacite. Typical clast from "agglomerate".	Grey rhyodacite identical to **BON 99–131**. See irregular cavities infilled with quartz and zeolites? Angular clast	Feldspar phenocrysts (K–feldspar and plagioclase; one really strained round K–	Y		

Rock Number	Grid Ref	Locality	Field notes	Hand Specimen Description	Thin Section Description	XRF	Isotope/ Ar-Ar?	Photo micrographs
	99-86			20 cm in diameter. 10% discontinuous quartz veining (+ cavity infilling) and possible epidote.	feldspar), areas of bright green mineral (probe?) in a matrix consisting of rounded quartz, opaques and fine-grained qf intergrowth. Strange fine-grained (<1mm) bumpy texture– spherulitic???			
BON 99–133	27432666 Locality 99-89	Salina Tan.	Agglomerate here seems to be harder and forms slabs– not easy to distinguish clasts from matrix.	See angular clasts of rhyodacite up to 60 mm in size, in places impossible to distinguish from matrix. Subangular clasts of brown material weathers in– (probably vesicular basalt as one larger clast has small round quartz inclusions– amygdules?) These clasts are 2–30 mm in size and possibly the rock represents autobrecciated rhyodacite with basaltic inclusions. Fresh surfaces are blue and crystalline with brown irregular (basaltic?) inclusions.	Very heterogeneous slide consisting of angular fragments of igneous clasts surrounded by wispy pumice, crystal fragments and ash. A dominant type if igneous clast is red in colour and consists of tiny spiky feldspar and (dominantly) round and oval structures with a rim of quartz. These oval structures are very probably vesicles but originally thought they could be radiolaria in chert. Also see some phenocrysts of plagioclase and K–feldspar within the clasts.	N		00-06-07 00-06-08
BON 99–134	27542664 Locality 99-90	Salina Tan.	Crystal–rich volcaniclastic rock Shows pronounced fabric parallel to bedding.	Foliated white–grey coloured rock consisting of feldspar and quartz crystals and probable elliptical lithic clasts <10 mm surrounded by partings of brwon/green fine-grained muddy material with a pronounced foliation.	As hand specimen.	N		
BON 99–135	09903275	Brandaris.	Chert nodule. Concretion– 2 pieces from track ending in Locality 48.	Dense, skittle shaped concretion with smooth hard, very dark brown crust. When split open, can see dark crust is 3 mm thick, with inner mid–brown band 1–3 mm wide, then 20 mm wide brown band and finally core (30 mm radius) of very dark fine-grained material. Very fresh. Look almost basaltic. Chert.	Consists of radiolaria (poorly preserved; no internal structure) and some shelly fragments and spines along with crystal fragments. Show to someone– a few curious ones. Note: sample was processed for achritarchs but none found.	N		
BON 99–136	Locality 99-19	Gotomeer.	Dolerite– freshest around, from Gotomeer lake near Locality 19.	Murky–green weathered rock. Can't be unequivocally distinguished as dolerite due to condition.	Too weathered for petrographic analysis.	Y		
BON 99–137	06572999 Locality 99-93	Slagbaai.	Upper part of dolerite layer.	Fairly weathered dolerite.	Elongate feldspar (mainly K–feldspar, if not all) with interstitial clinopyroxene. No olivine visible. Lots of cubic opaques in matrix, along with interstital pumpellyite.	N		
BON 99–138	06572999 Locality 99-93	Slagbaai.	Lower part of dolerite layer.	Fairly weathered dolerite.	Nice slide consisting of interlocking feldspar and clinopyroxene, with interstitial pumpellyite. As 99–137.	N		
BON 99–139	06572999 Locality 99-93	Slagbaai.	Larger vein in dolerite, white/ green, coarse-grained, epidote/ chlorite?	Extremely altered and weathered sample. Appears to be altered basalt with abundant epidote and chlorite mineralisation.		N		
BON 99–140	06542974 Locality 99-95	Slagbaai.	Green volcaniclastic rock.	Extremely coarse-grained volcaniclastic sandstone, green in colour. Consists of abundant crystal fragments and larger (< 10 mm) sub–angular red–brown (and some dark) lithic clasts in a green powdery matrix.	Crystal fragments (quartz, K–feldspar) in matrix of poorly–preserved tube pumice and some ash. One large lithic clast is comprised of spiky feldspar with intersitial opaques and pumpellyite (intermediate).	N		

Rock Number	Grid Ref	Locality	Field notes	Hand Specimen Description	Thin Section Description	XRF	Isotope/ Ar-Ar?	Photo micrographs
BON 99–141	06542974 Locality 99-95	Slagbaai.	Hard, crystal–rich volcaniclastic rock.	Either crystal–rich volcaniclastic tuff or (more likely) an extremely weathered grey/purple rhyodacite, blue/green on inside.	Not sure whether this is a weathered rhyodacite with a granophyric matrix or (more likely) a finegrained volcaniclastic sandstone with occasional crystal fragments (crystals are slightly rounded) with possibly a few wisps of tube pumice.	N		
BON 99–142	06542974 Locality 99-95	Slagbaai.	Rhyodacite.	Very weathered. Many large (2–20 mm) vesicles partially infilled with quartz and zeolites? Too many weathered fracture sufaces for sensible geochemical analysis.	Rhyodacite with many small interstitial clinopyroxene grains. Seriate texture.	N		
BON 99–143	08393375 Locality 99-96	Lower grounds of Seru Mangel.	Andesite–dacite Fine-grained aphyric quartzose rock– very fresh.	Green/grey fine-grained aphyric fresh rock	Doesn't appear fresh in thin section. Turbid slide, consisting of spiky trachytic feldspar with interstitial quartz and opaques with an abundant orange/green detrital iron phase.	Y		
BON 99–144	08553395 Locality 99-97	Klaver's lava tube.	Rhyodacite– pink and sandy, spiky (albitised) plagioclase with round vesicles (mm–2 cm scale).		Seriticised squat feldspar phenocrysts in a matrix of quartz, feldspar and opaques. Some apatite in K–feldspar and groundmass	Y	Hf, Nd, Pb, Sr	
BON 99–145	08553395 Locality 99-97	20 m below Klaver's lava tube.	Rhyodacite– pink and sandy, spiky (albitised) plagioclase with round vesicles (mm–2 cm scale).		Seriticised squat feldspar phenocrysts in a matrix of quartz, feldspar and opaques.	Y		
BON 99–146	08253374 Locality 99-98	Top of ridged hill SE of Seru Mangel.	Rhyodacite sill or flow?	Pink and sandy rhyodacite with some fresh spiky feldspars.	Turbid (possibly fragmented) feldspar (mainly K–feldspar) in a matrix of quartz and feldspar, with some clays and opaques. Not very fresh.	Y		
BON 99–147	08243356 Locality 99-99	Summit of ridged hill SE of Seru Mangel (90m).	Rhyodacite. Pinky, sandy lava with orange weathered patches inside.	Lots of spiky albitised plagioclase	Seriticised squat feldspar phenocrysts in a matrix of quartz, feldspar and opaques. Weathered.	Y		
BON 99–148	08343550 Locality 99-99	Half way between path and 90m summit.	Rhyodacite. Pinky, sandy lava with orange weathered patches inside.	Lots of spiky albitised plagioclase	Weathered rhyodacite with porphyritic texture, with lots of orange detrital volcaniclastic in the matrix.	Y		
BON 99–149	08443355 Locality 99-101	Excellent outcrop 10 m high beside path on low ground, south of Seru Mangel.	Fine-grained volcaniclastic.	Grey/green fine-grained sandstone with planar fine–scale laminations. Strange texture defined by small–scale brown wisps that appear to have a sub–parallel orientation, and some brown roughly circular blobs ~ 1 mm in size.	As hand specimen.	N		
BON 99–150	08443355 Locality 99-101	Excellent outcrop 10 m high beside path	Dacite.	Either aphyric lava or fine-grained homogenous mid–brown sandstone. Homogenous, with occasional small (~1 mm) irregular cavities.	Altered lava as lots of angular feldspar with a sub–parallel orientation along with some quartz, opaques and brown clays etc that once	Y		

Rock Number	Grid Ref	Locality	Field notes	Hand Specimen Description	Thin Section Description	XRF	Isotope/ Ar-Ar?	Photo micrographs
		on low ground, south of Seru Mangel.			represented primary igneous matrix.			
BON 99–151	08343315 Locality 99-102	Seri Camina.	Rhyodacite. Very weathered buff coloured rock.	Similar to **BON 99–150** but with orientated vesicles 1–10 mm partially infilled with quartz.	Abundant spiky feldspar present in the matrix. Lots of quartz amygdules. Feldspar phenocrysts are quite turbid.	Y		
BON 99–152	08363319 Locality 99-102	Seri Camina.	Finer–grained volcaniclastic with clasts in. Grades from medium-grained "agglomerate".	Extremely weathered fine-grained unit.	Extremely heterogenous breccia/sandstone consisting of angular lithics (igneous) and crystals. Can't see any pumice. Matrix poor–where present it is brown and vfine-grained.	N		
BON 99–153	08363319 Locality 99-102	Seri Camina.	Blue "agglomerate".	Blue/green breccia with clasts varying from 2–20 mm. Very weathered.	Heterogeeous breccia of crystal fragments and possibly altered pumice in altered matrix.	N		
BON 99–154	08403323 Locality 99-102	Seri Camina.	Typical coarse lapilli–rich volcaniclastic rock.	Coarse-grained sandstone/ breccia consisting of extremely poorly sorted heterogeneous mix of angular rhyodacite (and other?) clasts, 1– 20 mm and possible relic pumice in a powdery white/brown matrix. Clast supported.	As hand specimen decription with lithic clasts of rhyodacite and ash.	N		
BON 99–155	08703395	Summit, Ceru Mangel.	Stumpy rhyodacite columns.	Weathered pink/grey rhyodacite with pink–tinged feldspar visible. Can't avoid brown weathered crust in analysis.	As hand specimen.	Y		
BON 99–156	08703400	20 m down from BON 99–155.	Stumpy rhyodacite columns.	Weathered pink/grey rhyodacite with pink–tinged feldspar visible and occasional round vesicles (1–3 mm)	As hand specimen.	Y		
BON 99–157	05543057	Slagbaai.	Finely–fractured dolerite.	Finer grained dolerite with strange texture defined by pale bumps <0.5 mm in diameter comprising 30% of rock.	Seriate textured intermediate rock consisting of feldspar (plagioclase and K–feldspar) with corroded clinopyroxene (can't see any olivine or orthopyroxene, but difficult to spot as corroded) and interstitial pumpellyite.	N		
BON 99–158	10312705 Locality 99-103	Parking place with view of Gotomeer and the island.	Massive white bed with planar blue laminations defined by increased resistance to weathering and possible coarser grains. Some chert development?	Sandy brown/white finely laminated fine-grained rock.	Homogenous granophyric texture with occasional weathered crystal fragments and laminations defined by presence of wispy stylolites and grainsize variations.	N		
BON 99–159	10312705 Locality 99-103	Parking place with view of Gotomeer and the island.	Massive bed, weathers out, red/ brown. Increasingly clear laminations defined by alternating white/red clay as ascend sequence.	Homogenous pale fine-grained sediment with occasional very faint laminations.	As hand specimen.	N		
BON 99–160	10312705 Locality	Parking place with view of	Fine-grained mid–brown sandstone, finely	As field notes.		N		

Rock Number	Grid Ref	Locality	Field notes	Hand Specimen Description	Thin Section Description	XRF	Isotope/ Ar-Ar?	Photo micrographs
	99-103	Gotomeer and the island.	laminated, defined by darker horizons.					
BON 99–161	10312705 Locality 99-103	Parking place with view of Gotomeer and the island.	Irregular lenses of sand mm's thick, elongated parallel to bedding, in a fine-grained sandstone matrix.	As field notes.		N		
BON 99–162	10312705 Locality 99-103	Parking place with view of Gotomeer and the island.	Fine-grained fissile, chocolate–brown mudstone.	As field notes.		N		
BON 99–163	06372938 Locality 99-104	Slagbaai.	Dolerite–diorite Top of layer.	Very weathered crust– cannot avoid.	Fresh rock, equigranular, with plagioclase and K–feldspar (<1 mm in length) with interstitial opaques and pumpellyite. The pumpellyite often appears to have a core of clinopyroxene.	Y		00-06-26 00-06-27
BON 99–164	06372938 Locality 99-104	Slagbaai.	Base of next layer of dolerite/diorite.	Typical dolerite, but with small (1–10 mm) round growths of white powdery radiating minerals (zeolites?) coated by a black substance (1%).	Dioritic in composition. Consists of feldspar (all similar sized) with interstitial weathered material.	N		
BON 99–165	06372938 Locality 99-104	Slagbaai.	Top of next layer of dolerite/diorite.	Typical dolerite, but with occasional round growths <1 mm in size as described in **BON 99–164.** Altered.	Not a dolerite as abundant K–feldspar. Diorite with felspar and lots of opaques with interstitial clays/pumpellyite.	Y		
BON 99–166	09033089 Locality 99-107	Kimeterio.	Massive rhyodacite sill?	Bright pink rhyodacite with sparse irregular feldspars.	Altered slide– consists of weathered feldspar fine-grained fragments in a fine-grained matrix of feldspar, quartz and opaques.	Y		
BON 99–167	09303096 Locality 99-109	East Kimeterio.	Very fresh rhyodacite with columnar jointing.	Very fresh grey medium-grained rock– equigranular and feldspar rich with 30% green/grey powdery phase– weathered pyroxene?	Phenocrysts of K–feldspar and plagioclase in a matrix of plagioclase, K–feldspar, quartz and a brown detrital weathering phase.	Y		
BON 99–168	09603095 Locality 99-109	East Kimeterio.	Columnar jointed rhyodacite.	Orange–brown rhyodacite, sparse irregular feldspars.	Near–seriate textured rhyodacite with interstitial pumpellyite. Difficult to see how fresh the feldspar are.	Y		
BON 99–169	11173079 Locality 99-110	Green/yellow road south of Kibra Karati (Washington).	Pink rhyodacite.	Orange–brown rhyodacite with 10% round vesicles 1–10 mm.	Turbid possibly fragmented feldspar (mainly K–feldspar) in a matrix of quartz and feldspar, with some clays and opaques. Not very fresh.	Y		
BON 99–170	11133257 Locality 99-112	where yellow and green roads split, east of Caracao.	Loose dolerite block.	Fresh blue–green dolerite.	Dolerite consists of slightly corroded clinopyroxene and very turbid plagioclase. Cannot see any olivine, nor orthopyroxene, but see some areas of chlorite.	Y		
BON 99–171	07953407 Locality 99-113	Pos Mangel.	Plagioclase–phyric orange powdery rhyodacite.	Orange–brown rhyodacite with sparse irregular cavities.	Weak trachytic texture defined by feldspar in a matrix of quartz and feldspar.	Y		
BON 99–172	08343447 Locality 99-114	1/2 way along track between Pos Magel and	Fresh blue rhyodacite, quartzose and sparkly.	Distinctive blue rhyodacite with abundant quartz and more occasional feldspar phenocrysts.	Not as fresh as expected. Consists of occasional phenocrysts of feldspar (very seriticised, one totally round => xenocryst?) in a turbid matrix of	N		

Rock Number	Grid Ref	Locality	Field notes	Hand Specimen Description	Thin Section Description	XRF	Isotope/ Ar-Ar?	Photo micrographs
		main road.			quartz, magnetite with a clear granophyic texture. Is this from the top of the flow?			
BON 99-173	06523402 Locality 99-115	Base of Pichi Lang.	Very fresh pink vesicular plagioclase-phyric rhyodacite.	Pink brown rhyodacite with 10% vesicles (some quartz infilled) showing elongation direction.	Phenocrysts of predominantly K-feldspar and plagioclase in a fine-grained matrix of quartz, feldspar and red amorphous clay mineral. Vesicles are filled with fresh interlocking quartz. Trachytic alignment of feldspar in matrix (and possibly also phenocrysts).	Y	Hf, Nd,	00-06-33
BON 99-174	06673304 Locality 99-116	Base of Shishribana.	Rhyodacite.	Purple/dark grey rhyodacite with abundant small feldspar glomerocrysts and irregular cavities partially infilled with quartz.	Globular texture of matrix defined by rounded quartz blobs surrounded by murky brown areas which contain tiny skeletal feldspar. These appear to be minature spherulites. Phenocrysts of feldspar are also seriticised, turbid and abundant. Irregular vughs are infilled with radiating crystoballite(?).	Y		00-06-28 00-06-29 00-06-30
BON 99-175	06673304 Locality 99-116	Base of Shishribana.	Rhyodacite.	Blue-grey rhyodacite, yet no stubby feldspar phenocrysts. Vesicular- slightly elongate quartz amygdules 1-20 mm comprise 10% of the rock. Pink radiating zeolites are visible.	Well developed spherulites. Visible in hand specimen- 0.5 mm in diameter. However, don't see radial fibres- in xpl see lots spiky feldspar. Spherulites partially recrystalised to quartz and feldspar mosaic. Also round quartz amygdules and very seriticised K-feldspars are present.	Y		00-06-31
BON 99-176	06353187 Locality 99-117	Main road, due west of Brandaris.	Orange columnar coarse-grained rhyodacite.	Sandy texture.	Altered section with very seriticised K-feldspars in a murky matrix of feldspar and quartz with much Fe-oxyhydroxide which gives a sandy texture.	Y		
BON 99-177	06372938 Locality 99-104	Slagbaai.	Fine-grained black rock- basalt?	Very weathered.	Consists of seriticised strained plagioclase (undulose extinction) with many small intersitial opaques and small patches of chlorite/ pumpellyite. Occasional phenocrysts of seriticised altered plagioclase, and some clinopyroxene in matrix. See large glomerocrystic xenocryst consisting of quartz and clinopyroxene with 120° grain boundaries- the clinopyroxene is strained and fractured, and the quartz is fresh. There are a few other large clinopyroxene leading out from this which also appear xenocrystic.	N		00-06-32
BON 99-178	12203144	Beside junction of green/yellow track with exit.	Loose dolerite boulder.	Fresh dolerite.	No thin section taken.	Y		
BON 99-179	06332671 Locality 99-105	Wecua.	Loose rhyodacite.	Pink/brown weathered rhyodacite with sparse small elongate vesicles.	No thin section taken.	N		
BON 99-180	06332671 Locality	Wecua.	Loose rhyodacite.	Pink/grey rhyodacite with occasional elongate vesicles generally <1 mm in size, one 10 mm specimen. Some	Huge glomerocryst of feldspar, opaques with some interstitial chlorite, and some phenocrysts of	Y	Hf, Nd, Pb, Sr	

Rock Number	Grid Ref	Locality	Field notes	Hand Specimen Description	Thin Section Description	XRF	Isotope/ Ar-Ar?	Photo micrographs
	99-105			vesicles are infilled with apple green epidote.	feldspar in matrix of fine-grained quartz and feldspar (granophyric texture). Some apatite in K–feldspar and groundmass.		Ar-Ar	
BON 99–181	06332671 Locality 99-105	Wecua	Loose rhyodacite.	Orange–brown fresh rhyodacite, no visible vesicles.	No thin section taken.	Y		
BON 99–182	05533058 Locality 99-106	Slagbaai–beside house.	Fresh dolerite boulder.	Fresh dolerite, rich in felsics. Note: geochemistry suggests this boulder is actually from Salina Mathijs. Possible.	Freshest dolerite seen so far. Distinguished by abundant fresh clinopyroxene (>20%) and another phase (orthopyroxene?) now pseudomorphed by chlorite surrounded by less well–preserved (turbid, corroded) plagioclase.	Y	Hf, Nd,	00-06-34 00-06-35 00-06-36
BON 99–183	07623302 Locality 99-118	Track north of Brandaris ascent.	Rhyodacite.	Orange–grey rhyodacite, sparsely phyric. No vesicles.	Fine-grained rhyodacite, consisting of matrix of quartz, feldspar, pumpellyite and lots of opaques with occasional phenocrysts/ glomerocrysts of seriticised and turbid feldspar rimmed by magnetite and opaques. Some fresh quartz is present– probably amygdular in origin (very small vesicles) as fresh and different in character to everything else. Are the glomerocrysts xenocrystic?	N		
BON 99–184	08153276 Locality 99-119	Old viewpoint south of road near Seru Camina.	Pink vesicular (quartz infilled) rhyodacite, no columns. Possible fracture patterns parallel to bedding.	Weathered brown outside, completely fresh inside of fresh blue/black rhyodacite with irregular vugs infilled with quartz and zeolite in middle. Some quartz veining.	A globular texture in the groundmass is apparent, defined by brown patches that are comprised of radiating crystals: spherulites. These are surrounded by quartz and very fine-grained skeletal feldspar. Some phenocrysts of very seriticised K–feldspar (occasional plagioclase and quartz; too seriticised for Ar–Ar) are present, with irregular vughs infilled with crystoballite.	Y		
BON 99–185	08313298 Locality 99-121	Seru Camina.	Columnar–jointed rhyodacite.	Pink/grey rholite. Sugary texture. No vesicles but occasional irregular vughs are infilled with a powdery red//brown clays and Fe–oxyhydroxide.	No thin section taken.	Y	Ar-Ar	
BON 99–186	08303290 Locality 99-122	Seru Camina.	Freshest possible rhyodacite.	Weathered orange/brown weathered rhyodacite with occasional irregular vughs infilled with powdery orange substance.	Fine-grained rhyodacite, consisting of matrix of quartz, feldspar, pumpellyite and lots of opaques with occasional phenocrysts of seriticised and turbid feldspar and opaques.	N		
BON 99–187	06373048 Locality 99-129A	Slagbaai lake–north.	Clast in "agglomerate" for thin–section identification.	Green/brown/grey finely laminated fine-grained rock with complex convolute laminations.	No thin section taken.	N		
BON 99–188	06003074 Locality 99-124	Slagbaai lake–north.	Basalt dyke– edge to middle.	Weathered green basalt.	Not as weathered as expected. Fine-grained basalt with abundant fresh clinopyroxene (excellent cleavage) <0.5 mm in size, surrounded by seriticised feldspar and patches of chlorite. Much less pumpellyite present than other sections. Also, a phase with no cleavage but interference colours identical to orthopyroxene. Some pyroxenes seem	N		

Rock Number	Grid Ref	Locality	Field notes	Hand Specimen Description	Thin Section Description	XRF	Isotope/ Ar-Ar?	Photo micrographs
					strained.			
BON 99–189	06003074 Locality 99-124	Slagbaai lake–north.	Weathered sample of whole dyke.	Weathered sample– see progressive coarse-grained towards middle and resistant grey nodule (>1 cm wide) development at this point.	No thin section taken.	N		
BON 99–190		Rincon roadcut.	Sediment from basal part of sequence of Rincon road cutting.	Fine-grained homogenous sediment.	No thin section taken.	N		
BON 99–191		Rincon roadcut.	Sediment from basal part of sequence of Rincon road cutting	Quartz veined brown fine-grained sediment with faintly convolute small–scale laminations.	No thin section taken.	N		
BON 99–192		Rincon roadcut.	Sediment from basal part of sequence of Rincon roadcutting.	Fine-grained homogenous sediment.	No thin section taken.	N		
BON 99–193		Rincon roadcut.	Grey–blue sandstone grade rock. Grades coarse–fine–coarse.	Distinct grading over 3 cm scale. Sediment has chalky feel.	No thin section taken.	N		
BON 99–196	11723240 Locality 99-130	Near Salina Mathyijs.	Weathered green pillow basalt.	Weathered basalt with some 1 cm diameter amygdules.	Spiky seriticised plagioclase interlocking with opaques and orange/brown areas of pumpellyite. In areas can see that pumpellyite clearly pseudomorphing a mineral phase– pyroxene. Can also see occasional well–preserved clinopyroxene, but never orthopyroxene. The pumpellyite displays beautiful textures. Matrix average size 0.5 mm, but some phenocrysts (plagioclase) up to 1.7 mm. Can see plagioclase wrapping itself around pumpellyite (pseudomorphing clinopyroxene?).	Y		
BON 99–197	Locality 99-132		Dolerite/diorite.	Pijper's quartz–hornblende rock. Hornblende is secondary.	No thin section taken.	N		
BON 99–198	Locality 99-132		Weathered brown basalt.	Too weathered for meaningful analysis?	Consists of seriticised plagioclase with intersititial opaques and orange areas of pumpellyite replacing pyroxene. Also observe small (<0.5 mm) clinopyroxene. A seriate texture from 1.25–0.25 mm is displayed.	N		

Table 4: 2000 Field season. Collected by the author in this study.

Rock Number	Grid Reference	Locality Description	Rock type/ Field Notes	Hand Specimen Description	Thin Section Description	XRF	Isotope/ Ar-Ar?	Photo micrographs
BON 00–01	23331912	Southern Complex Locality 2–05 Quarry near Aruba.	Relatively fresh basalt.	Relatively fresh green basalt consisting of pyroxene, plagioclase, and possibly olivine <1 mm in size, with possible phenocrysts of clinopyroxene >5 mm in size.	Consists of spiky plagioclase (and some K–feldspar) with clinopyroxene and abundant pumpellyite which is probably replacing olivine.	Y	Hf, Nd, Pb, Sr	
BON 00–02	24871820	Southern Complex Locality 2–11 Near base of succession.	Basalt.	Amygdular fine-grained green basalt. Amygdules 1–10 mm in diameter. The basalt is ~fine-grained, with lots of weathered surfaces.	Calcite–infilled amygdules. Consists of lots of spiky plagioclase showing skeletal textures, with interstitial weathered clinopyroxene. Olivine replaced by pumpellyite?	Y		
BON 00–03		Southern Complex Locality 2–13 Near base.	Cherty ironstone.	Red/blue chert. Irregular laminations.	Cherty ironstone. Consists of interlocking quartz (looks neomorphic, widely different grainsizes in patches) with irregular patches of haematite intimately associated with the quartz and also precipitated veinlets of black iron material. Essentially a vein of quartz and hematite.	N		
BON 00–04	23571894	Southern Complex Locality 2–4 Quarry near Aruba.	Basalt pillow	Mafic rock with black blobs ~1mm in diameter, comprising ~30% of the rock. Are these infilled vesicles? Some possibly have a calcite core and lots of tiny calcite veins which are impossible to avoid.	Consists of lots of spiky skeletal plagioclase, with interstitial weathered clinopyroxene.	Y		
BON 00–05	23571894	Southern Complex Locality 2–05 Quarry near Aruba	Basalt pillow.	Fresh mafic rock consisting of interlocking plagioclase and pyroxene. Grains are <1mm in size, and rock is transitional towards a dolerite.	Relatively fresh rock (as fresh as **BON 00–01**). Consists of lots of spiky plagioclase, with interstitial weathered clinopyroxene. Clinopyroxene appears to have crystallised first.	Y		
BON 00–06		Locality 3–5, near base.	Rhyodacite breccia (calcite?).	Angular fragments– autobreccia. Jigsaw–fit fragments 1–20 mm in size. Poorly sorted.	As hand specimen description.	N		
BON 00–07	26391877	Southern Complex Locality 3–8.	Quartz diorite.	Very variably altered rock.	Altered rock consisting of lots of plagioclase, clinopyroxene (subophitic texture– clinopyroxene surrounds euhedral plagioclase) and cubic opaques with lots of areas infilled with calcite– probably not vesicles but replacement minerals.	Y		
BON 00–08		Southern Complex Locality 3–10, end of path to east.	Layered crystal–rich volcaniclastic tuff– welded?	Typical crystal–rich volcaniclastic tuff. No real evidence for welding.	Heterogeneous clastic rock, consisting of stubby fragmented crystals of K–feldspar and some plagioclase, in a microcrystalline matrix of devitrified ash and a brown wispy substance that wraps around the phenocrysts.	N		00-08-01
BON 00–09		Southern Complex	Layered crystal–rich volcaniclastic tuff–	Clastic brown rock, consisting of heterogeneous mix of fresh looking K–feldspar and plagioclase, quartz and	Heterogeneous clastic rock, consisting of stubby fragmented crystals of K–feldspar and some	Y		

Rock Number	Grid Reference	Locality Description	Rock type/ Field Notes	Hand Specimen Description	Thin Section Description	XRF	Isotope/ Ar-Ar?	Photo micrographs
		Locality 3–10, end of path to east.	welded?	pumice wisps. No discernible fabric can be seen.	plagioclase, in a microcrystalline matrix of devitrified ash and a brown wispy substance that wraps around the phenocrysts. Some lithic fragments are present: angular perlite and a feldspar–rich igneous rock with interstital pumpellyite which has very irregular wavy margin. Some of the K–feldspar is approaching sensitive tint colour as the section is thick.			
BON 00–10	24531915	Southern Complex Locality 4–3.	Bedded crystal–rich volcaniclastic tuff	Crystal –rich volcaniclastic, green in colour with lots of small lithics and crystals.	Poorly sorted. Consists of rounded feldspar grains, a variety of (possibly. rounded) igneous clasts and scoria, in a sparse fine-grained ashy matrix.	N		
BON 00–11	26021911	Southern Complex Locality 4–8, cattle ranch near top.	Pillow basalt. Altered sample.	A green/grey ~fine-grained rock with many many weathered fractured surfaces that can't be avoided on crushing. White and black patches <0.5 mm in diameter are abundant– are they pyroxene and plagioclase or are the white patches amygdules?	Very spiky turbid feldspar with interstital opaques and pumpellyite with some remaining clinopyroxene. Some skeletal plagioclase and opaques– indicative of quenching.	Y		
BON 00–12	24971912	Southern Complex Locality 4–22.	Rhyodacitic dome.	Very fine-grained purple hard rhyodacite. Spiky pink feldspar. Looks siliceous. Very splintery with lots of fracture surfaces.	Trachytic alignment of feldspar. Seriate texture. Small veinlets and vesicles infilled with quartz.	Y	Ar-Ar	
BON 00–13	24971912	Southern Complex Locality 4–22.	Rhyodacitic dome, strange weathering texture.	Probably an autobreccia.	Autobreccia. Consists of subangular patches of coherent weathered rhyodacite surrounded by small amounts of fine-grained material– probably a mix of ash and clays, but can't tell as very weathered. Almost jigsaw fit texture present in places.	N		
BON 00–14	24971912	Southern Complex Locality 4–22.	Rhyodacitic dome, strange texture.	Small altered sample. Clay rich. No phenocrysts visible. Possible clastic texture– "lumps" 1–3 mm in diameter, defined by colour and grain size variations.		N		
BON 00–15	25221876	Southern Complex Locality 5–02, orienteering dome.	Rhyodacite from dome.	Friable very weathered rock with lots of quartz and epidote mineralisation with vesicles infilled with Fe-oxyhydroxide. Some spiky fresh feldspar is present.	Seriate textured rock (0.2–2 mm) consisting of turbid plagioclase and K–feldspar with interstitial pumpellyite.	Y		
BON 00–16	25441894	Southern Complex Locality 5–09.	Brown green clastic unit with interesting texture for thin sectioning.	Mottled green crystal–rich volcaniclastic tuff with lots of sub–rounded to sub–angular black fine-grained fragments– basalt?	Interesting slide– consists of many angular fragments of rhyodacite (autobrecciated) with matrix of brown alteration material. Possibly just very weathered rhyodacite. But not typical clastic rock. Feldspar phenocrysts are squat and seriticised. Occasional clinopyroxene.	N		
BON 00–17	25321883	Southern Complex Locality 5–05.	Altered chilled basalt or seds? Right next to contact.	Fine-grained coherent igneous clast	Must be coherent igneous rock as see lots of fine spiky feldspar phenocrysts. K–feldspar appears amazingly fresh– perhaps worth probing. Matrix is very altered and very fine grained– perhaps	N		00-08-09 00-08-10 00-08-11

Rock Number	Grid Reference	Locality Description	Rock type/ Field Notes	Hand Specimen Description	Thin Section Description	XRF	Isotope/ Ar-Ar?	Photo micrographs
					was glass and now devitrifed and altered to clays although could be clastic from its texture.			
BON 00–18	25321883	Southern Complex Locality 5–05.	Basalt, altered, but no more than usual.	A moderately altered, green rock with globular plagioclase, dark clinopyroxene and pumpellyite replacing olivine. Soft to crush.	Basalt/dolerite consisting of turbid plagioclase and elongate clinopyroxene which is very corroded and fractured, along with elongate and skeletal opaques and abundant pumpellyite. Not as fresh as **BON 00–01** or **BON 00–34**.	Y		
BON 00–19	24021920	Southern Complex Locality 5–14 Basal part succession.	Massive non–vesicular rhyodacite–flow?	Very hard rock– silicifed? Consists of fresh looking laths of feldspar up to 10 mm long in fine-grained dark matrix.	Seriate textured rock consisting of plagioclase and K–feldspar 0.2–1 mm in size, with some interstitial quartz. The feldspar is turbid, but has no sericite development.	Y	Ar-Ar	
BON 00–20	23022114	Southern Complex Locality 5–18, Ceru Grande top.	Rhyodacite, non vesicular.	Buff coloured weathered rhyodacite consisting of orange infilled vesicles and albitised feldspar in a powdery matrix. Very soft.	Seriate textured rock consisting of plagioclase and K–feldspar 0.2–1 mm in size, with some interstitial quartz. The feldspar is turbid, but has no sericite development.	Y		
BON 00–21	22982116	Southern Complex Locality 5–19 Ceru Grande, top.	Rhyodacite: Rounded cobbles within lava. Flow top? Look like lapilli.	Brown rounded fragments 1–20 mm in diameter.	Too weathered for meaningful petrographic analysis.	N		
BON 00–22	23002118	Southern Complex Locality 5–20, Ceru Grande, top.	Red irregular patches within rhyodacite.	Elongate fabric defined by elongate patches of fine-grained brick red material 1–20 mm in length with a white rim, in a pink altered rhyodacite. Perhaps infilled vesicles. Or flow structures.	The patches are not infilled vesicles as have phenocrysts of feldspar within–generally coarser grained than the material surrounding it. But contain more holes and concentrations of iron minerals. Prob result of differential weathering.	N		
BON 00–23	23052124	Southern Complex Locality 5–22.	Greener rhyodacite with quartz amygdules.	Plagioclase and quartz– phyric fine-grained green rock with quartz amygdules.	Lovely fresh seriate and trachytic textured fine-grained rock consisting of K–feldspar and plagioclase with interstitial pumpellyite (?). Good possibility for Ar–Ar.	Y	Ar-Ar	
BON 00–24	23202106	Southern Complex Locality 5–25	Rhyodacite on track.	Pink fresh rhyodacite.	Very fresh looking rhyodacite with seriate texture. Full of K–feldspar and plagioclase that appear very fresh.			
BON 00–25	23202106	Southern Complex Locality 5–25	Basalt on track.	Green, altered very fine-grained rock. Shot through with calcite veins.	Calcite–veined weathered rock consisting of very turbid feldspar and a lot of "alteration material" in the interstites, with a tiny amount of clinopyroxene remaining.	Y		
BON 00–26	22041929	Southern Complex Locality 6–02, south of Lagoen rd.	Fresh basalt from large block– not in situ.	Very calcite fractured weathered mafic fine-grained green rock.	Fine-grained rock consisting of plagioclase with interstitial clinopyroxene and quartz blobs (undulose extinction or multiple subgrains). No Calcite apparent..	Y		00-08-12
BON 00–27	24921990	Southern	Hard crystal–rich	As every other crystal–rich volcaniclastic tuff (1 mm	Homogenous beddded volcaniclastic consisting	N		

Rock Number	Grid Reference	Locality Description	Rock type/ Field Notes	Hand Specimen Description	Thin Section Description	XRF	Isotope/ Ar-Ar?	Photo micrographs
		Complex Locality 6–11.	volcaniclastic tuff for thin sectioning.	sized crystals) with a weak foliation.	of sparse subrounded feldspar in a fine-grained granophyric matrix. Foliation defined by wisps of haematite.			
BON 00–28	25922055	Southern Complex Locality 6–22.	Purple vesicular basalt.	Calcite amygdules are very abundant and are 0.2–3 mm in diameter. The rock is fine-grained and purple in colour.	Amydules infilled with either calcite or quartz are abundant, varying from 2–10 mm in size. Occasional seriticised phenocrysts of plagioclase are present in a matrix of spiky plagioclase, opaques and pumpellyite. Segregated vesicles are abundant.	Y		00-08-02 00-08-03 00-08-04
BON 00–29	23632054	Southern Complex Locality 7–8 JT's quarry.	Pink vesicular rhyodacite with irregular steam holes.	Rhyodacite with pink spiky K–feldspar and plagioclase in a quartzose matrix. Lots of irregular round steam holes ca. 1 mm in diameter,	Very fresh looking rhyodacite with seriate texture. Full of K–feldspar and plagioclase that appear very fresh. Good for Ar–Ar.	Y	Ar-Ar	
BON 00–30		Southern Complex Locality 7–13.	Welded volcaniclastic fragment from road?	Silicified volcaniclastic conisisting of pumice <1 cm in length, with a preferred orientation– welded?	Fine-grained rock with occasional feldspar crystals– from thin section could be either igneous or volcaniclastic– only field relations say it's volcaniclastic. No evidence of welding– i.e. no fiamme, euataxitic texture, perlite, pumice.	N		
BON 00–31		Southern Complex Locality 7–13.	Bright blue clastic material.	Fragmentary blue rock with a weak undulating coarse foliation and a patchy blue colour. Essentially just a volcaniclastic.	Too altered for petrographic analysis.	N		
BON 00–32	24382125	Southern Complex Locality 7–15.	Dolerite. Not in situ– fresh rock.	Fresh medium-grained rock– lots of black pyroxene and some plagioclase in a green matrix.	Section consisting of interlocking clinopyroxene and turbid feldspar, along with pumpellyite replacing orthopyroxene or olivine (?). Almost aphanitic texture.	Y		00-08-05 00-08-06
BON 00–33	12°15' 00.2"N 68°18' 37.1"E	Locality 7–16 RINCON.	Pillow basalt. Weathered.	Very very altered– no need to split!	So altered can deduce nothing about this in thin section. Consists of more irregular holes than anything else, and the remainder of the rock is principally brown iron–rich material with traces remaining of plagioclase outlines and possibly clinopyroxene.	Y		
BON 00–34	22621967	Southern Complex Locality 8–2.	Fresh basalt. Not in situ but not far away.	Consists of lots of spiky plagioclase <1 mm in size in a green matrix. Transitional to dolerite.	One of the freshest basalts seen so far. Consists of spiky plagioclase (and some K–feldspar) with abundant clinopyroxene and pumpellyite which is probably replacing olivine.	Y	Hf, Nd	00-08-34 00-08-34
BON 00–35	25322054	Southern Complex Locality 8–8.	Coarse-grained blue conglomerate. Sample for xrd.	Poorly laminated fine-grained ash	Fine-grained ash. Brown small patches. No traces of fossils.	N		
BON 00–36		Southern Complex Locality 8–12.	Well-bedded crystal –rich volcaniclastic for thin sectioning.	Sample for polishing.	None obtained.	N		
BON 00–37	22462132	Southern Complex Locality 10–3.	Fine-grained sandstone with white coating accentuating convolute	Sample for polishing.	None obtained.	N		

Rock Number	Grid Reference	Locality Description	Rock type/ Field Notes	Hand Specimen Description	Thin Section Description	XRF	Isotope/ Ar-Ar?	Photo micrographs
			bedding.					
BON 00–38	22722249	Southern Complex Locality 10–7.	Blue rhyodacite with elongate vesicles infilled with quartz.	Blue fresh rhyodacite with lots of elongate quartz vesicles.	Seriticised squat feldspar in a fine-grained matrix of feldspar and quartz.	Y		
BON 00–39	20702735	Southern Complex Locality 11–04, Washikemba.	Rhyodacite flow with polygonal jointing.	Not very fresh. Sandy texture.	Occasional stubby K–feldspar and plagioclase phenocrysts in a spiky fine-grained matrix with some patches of pumpellyite. The phenocrysts look relatively fresh.	Y		
BON 00–40	21352630	Southern Complex Locality 11–13, Lagoen rd, near Lagoen.	Dolerite.	Not very fresh medium-grained dolerite.	Very fresh in thin section. Unaltered clinopyroxene displays a sub-ophitic texture with plagioclase. Olivine is entirely pseudomorphed by chlorite and/or pumpellyite. Some develoment of skeletal magnetite denotes quenching.	Y		
BON 00–41		Southern Complex Basalt quarry from last year.	Basalt/dolerite fresh sample. Intrusive.	Fine-grained green basalt. Riddled with calcite veins.	Spiky K–feldspar and plagioclase with interstitial pumpellyite and small amounts of clinopyroxene still remaining.	Y		
BON 00–42	121434.2 682151.8	Locality 15–1 Gotomeer.	Heterogeneous pumaceous crystal–rich volcaniclastic tuff for thin section.	Lots of green pumice– green/brown in colour.	Angular to occasionally subrounded K-feldspar and lithic clasts (some flow-banded rhyolites, with microlites).	N		
BON 00–43	121434.2 682151.8	Locality 15–1 Gotomeer.	Weathered dolerite for icp.	Weathered crumbly green dolerite.	Too weathered for meaningful petrographic analysis.	Y		
BON 00–44	121434.2 682151.8	Locality 15–1 Gotomeer.	Fresh grey aphyric rock– basalt.	Fresh extremely hard rock with some round vesicles <2 mm in diameter.	Consists of small spiky plagioclase (non-skeletal) and pumpellyite/clays. Some calcite development in vesicles.	Y		
BON 00–45	121430.5 682158.4	Locality 15–2 Gotomeer	Dolerite, fairly weathered.	Typical dolerite	Appears intermediate in composition as large proportion of plagioclase. Interstitial abundant opaque minerals and some psuedomorphed clinopyroxene (now pumpellyite).	Y		
BON 00–46		Locality 15–3, Gotomeer, 50 m south of causeway to island.	Loose boulder of rhyodacite with unfilled vesicles and a purple hue.	Weathered sample.	Too altered for petrographic analysis.	N		
BON 00–47	121440.7 682432.5	Locality 15.5, south of playa frans just opposite track to other beach.	Fresh (on inside) diorite (quartz infilled).	Mafic igneous rock with K–feldspar laths and quartz vesicles.	Intermediate medium-grained rock. Many minerals have been plucked out by polishing process- only plagioclase remains.	Y		
BON 00–48	121440.7 682432.5	Locality 15.5, south of Playa Frans just	Diorite- fairly fresh.	Intermediate fine-grained rock, lots of epidote and quartz veining. Patchy.	Consists predominantly of ~skeletal feldspar and abundant vugh/vesicles now infilled with calcite.	Y		

Rock Number	Grid Reference	Locality Description	Rock type/ Field Notes	Hand Specimen Description	Thin Section Description	XRF	Isotope/ Ar-Ar?	Photo micrographs
		opposite track to other beach.						
BON 00–49	20692300	Seru Grande, Locality 15–7.	Rhyodacite with no copper or quartz development, with crazy paving type bedding.	Typical rhyodacite. Hard.	Well-developed seriate texture displayed by K-feldspar.	Y		
BON 00–50	20852298	Seru Grande, Locality 15–8.	Rhyodacite.	Sandy, not very fresh rhyodacite.	Well-developed seriate texture displayed by feldspars.	Y		
BON 00–51		Locality 5–25, Seru Grande.	Rhyodacite.	Some orange weathered patches.	Seriate-textured rhyodacite. Predominantly K-feldspar.	Y		
BON 00–52		JT's quarry.	Really fresh rhyodacite for Ar–Ar?	Amazingly fresh grey rhyodacite. Suitable for isotope analysis.	Seriate-textured rhyodacite. Predominantly K-feldspar. Section cut slightly thick.	Y	Hf, Nd	
BON 00–53	21852673	Basalt flow, altered, for ICP.		Green very altered rock.	Too weathered for meaningful petrographic analysis.	N		
BON 00–54	21332645	Locality 11–12, Lagoen rd near Lagoen.	Very altered pillow basalts.	Green very altered rock.	Too weathered for meaningful petrographic analysis.	N		
BON 00–55			Chery ironstone.	Blue chert with green and white horizons	Recrystalline chert. Different colour horizons are the result of different grain sizes of recrystallised silica.	N		
BON 00–56			Cross–bedded crystal–rich volcaniclastic tuff from "ignimbrite".	Very fresh and crystalline on inside. See only very occasional amounts of pumice.	Angular feldspars with a preferential orientation, in a matrix of recrystalline material. Clear evidence for reworking.	N		
BON 00–57			Bright green volcaniclastic fragment.		Too weathered for meaningful petrographic analysis.	N		
BON 00–58	121619.7 682422.5	Locality 16–1, Slagbaai.	Dolerite loose boulder.	Typical dolerite.	Altered dolerite. Abundant seriticed plagioclase forms a poorly-developed sub-ophitic texture with clinopyroxene. The clinopyroxene is now partially replaced by pumpellyite. Calcite infills vughs.	Y		
BON 00–59	121609.0 682403.0	Locality 16–2, track north of Slagbaai.	Dolerite on side of track.	Very very weathered. Lots of fracture surfaces. Analysis may be poor.	As handspecimen. Well-developed alteration mineral e.g. pumpellyite. Plagioclase appears skeletal (hollow, branched).	Y		
BON 00–60	121634.7 682422.3	Locality 16–9, Salina Wayaka.	Clastic rock with pumice and lithics (1 cm diameter). Interesting texture for hand specimen/thin section.	Lithic rich sample. Weathered.	Abundant angular lithics including scoria and flow-banded rhyodacite, with very little matrix. Clasts are normally well-preserved.	N		
BON 00–61	121634.9 682430.0	West of 16–10, Salina Wayaka.	Dolerite– particularly abundant here.	Two many fracture surfaces for analysis.	Too weathered for meaningful petrographic analysis.	N		
BON 00–62	121021.1 681356.8	Locality 17–3.	Rhyodacite. P ossibly flowtop as slightly brecciated? Some quartz veining.	Chalcedony amygdules. So many fractured surfaces probably not worth analysing.	Too weathered for meaningful petrographic analysis.	N		

Rock Number	Grid Reference	Locality Description	Rock type/ Field Notes	Hand Specimen Description	Thin Section Description	XRF	Isotope/ Ar-Ar?	Photo micrographs
BON 00–63	121024.5 681358.4	Locality 17–4.	Pillow basalt– exposure in cliff face.	Not fresh enough for analysis.	Too weathered for meaningful petrographic analysis.	N		
BON 00–64	121020.9 681355.2	Locality 17–5	Basalt in situ.		Basalt is dominated by round vesicles (40%) now entirely infilled with calcite. Plagioclase is skeletal, clearly indicating quenching.			
BON 00–65	121141.8 681430.8	Locality 18–3 20 m to NE of last locality. Seru Korai.	Rhyodacite.	Not very fresh– lots of albitised feldspar. Fresher on inside. Sandy yellow in colour.	Glomerocrysts of seriticised squat K-feldspar with some plagioclase in a slightly spherulitic groundmass. Altered.	Y		
BON 00–67	121139.0 681433.0	Locality 18–4.	Rhyodacite. Poorly exposed lava flow along strike from house.	White weathered surface. Looks like columns.	Consists of ~squat K-feldspar in a fine-grained recrystalline matrix with some iron development.	Y	Hf, Nd	
BON 00–68	121121.9 681410.6	Locality 18–21.	Rhyodacite Lava here in situ. Crazy paving.	Not very fresh.	Glomerocrysts of seriticised K-feldspar with some plagioclase in a spherulitic groundmass. Altered.	Y		
BON 00–69	121121.9 681410.6	Near Locality 18–21.	Rhyodacite. Fragment in road. Quartz rich.	Weathered, blue in colour. Too weathered for XRF.	Too weathered for meaningful petrographic analysis.			

Appendix B

XRF Analytical technique

B.1. Sample Preparation

Samples were prepared for XRF at the University of Leicester. Weathered crust was removed from the rock sample, using a hand splitter, and the remainder was split into 3 cm^3 chips. These were placed in the University of Leicester flypress and reduced to small gravel-sized chips. Any additional weathered material adhering to the surface of the chips was removed at this stage.

50 cc of gravel-sized sample was then placed in an Agate Tema© swing mill and each sample was ground for ~15 minutes, until it had attained a floury texture. An agate mill was used rather than tungsten-carbide, in order to minimise surface contamination of Nb and Ta. Once a rock powder was produced, fusion beads were prepared, for major element analysis. ~5 g aliquots of sample were placed in a low temperature (~110°C) oven overnight, and then a measured amount of sample was put in a ceramic crucible, which was weighed and then placed in a 950°C muffle furnace for 1 to 1.5 hours. After ignition, the sample was allowed to briefly cool before being placed in a dessicator until it has reached room temperature. The cooled samples is then reweighed. Loss of ignition (LOI) was determined using the formula:

$$\text{LOI}=\frac{100\times(crucible+sample)_{before}-(crucible+sample)_{after}}{(crucible+sample)_{before}+sample}$$

To make the fusion bead, 0.8000g of sample was placed in a Pt/Au crucible, along with 4.0000 g of lithium tetraborate-metaborate flux. In addition, a further amount of flux was added to correct for the loss of ignition of the flux. This was determined at the beginning of every new day. The crucible was then heated to ~1200°C for ~12 minutes on a Spartan gas burner, in order to melt and homogenise the rock. The crucible was periodically swirled and shaken, in order ensue homogenisation. After this time, the molten rock+flux was poured into a Pt/Al casting plate, and was rapidly air cooled, before being tapped out, labelled and eventually bagged.

Powder pellets for trace element determinations were made by mixing 7 grams of dry powder with ~20 drops of Moviol 88 wood glue, until the mixture felt moist but not wet. This mixture was then carefully poured in a casting die, the plunger depressed, and the whole die was placed in an electric hydraulic press until 10 tons of force had been applied. The resulting pellet was then ejected and dried overnight at room temperature, prior to analysis.

B.2. Machine Conditions

Prepared samples were analysed for selected major and trace elements using a Philips PW1400 wavelength-dispersive X-ray fluorescence mass spectrometer, with a 3kw anode X-ray tube. The machine was run by N. G. Marsh at the University of Leicester. Limits of detection for each element are listed in Table B.1.

Element	Detection Limit	Counting time on peak (seconds)	Counting time on background (seconds)
SiO_2	0.065	20	5
TiO_2	0.0015	40	20
Al_2O_3	0.0064	30	15
Fe_2O_3	0.0024	25	10
MnO	0.0018	50	25
MgO	0.18	50	20
CaO	0.0024	25	10
Na_2O	0.22	50	20
K_2O	0.0024	50	20
P_2O_5	0.0019	50	25
Traces			
Rb	0.5	80	50
Sr	0.7	80	50
Ba	3.1	100	160
Zr	0.7	80	50
Nb	0.6	100	50
Y	0.6	80	50
Sc	4.2	100	100
V	7.0	100	40
Cr	6.5	100	40
Co	2.7	100	40
Ni	2.6	40	20
Cu	1.4	60	30
Zn	1.1	40	20
Ga	1.8	40	20
La	3.5	160	80
Ce	6	160	160
Nd	2.34	160	160

Table B.1. Limits of detection and minimum counting times for XRF analyses.

B.3. Rock Standards

A variety of international and in-house reference materials were analysed with each batch of samples, in order to assess the accuracy and precision of the XRF. These are listed in Table B. 2. (majors) and B.3 (traces).

AV denotes agreed value

Batch	Standard	SiO_2	TiO_2	Al_2O_3	Fe_2O_3	MnO	MgO	CaO	Na_2O
BON 94	**ARSiO2**	99.41	0.00	0.10	0.01	0.01	0.00	0.08	0.14
BON 96	**ARSiO2**	99.45	0.00	0.02	0.01	0.01	0.00	-0.01	0.20
BON 99	**ARSiO2**	99.84	0.00	0.03	0.03	0.01	0.12	0.01	0.03
BON 00	**ARSiO2**	99.57	0.01	0.04	-0.01	0.00	0.02	0.04	0.07
AV	**ARSiO2**	**99.63**	**0.01**	**0.02**	**0.01**	**0.01**	**0.00**	**0.00**	**0.59**
BON 94	**BCS372/1**	20.14	0.15	5.12	3.32	0.06	1.27	64.55	0.27
BON 96	**BCS372/1**	20.21	0.16	5.09	3.29	0.06	1.50	64.69	0.29
BON 99	**BCS372/1**	20.27	0.18	4.86	3.38	0.06	1.61	65.18	0.29
AV	**BCS372/1**	**20.50**	**0.16**	**3.77**	**4.82**		**2.42**	**64.80**	**0.10**
BON 99	**DTS-1**	40.59	0.01	0.14	9.03	0.14	49.98	0.11	-0.07
AV	**DTS-1**	**40.41**	**0.01**	**0.19**	**6.97**	**0.12**	**49.59**	**0.17**	**0.02**
BON 94	**JP-1**	42.96	0.01	0.66	8.53	0.12	44.86	0.48	-0.06
BON 96	**JP-1**	42.83	0.01	0.64	8.41	0.12	44.91	0.48	-0.01
AV		**42.39**		**0.62**	**8.34**	**0.12**	**44.72**	**0.56**	**0.02**
BON 00	**JSI-1**	62.15	0.84	18.66	7.33	0.06	2.61	1.57	2.46
AV	**JSI-1**	**59.35**	**0.73**	**17.62**	**2.45**	**0.06**	**2.48**	**1.43**	**2.20**
BON 96	**MRG-1**	38.61	3.87	8.46	17.96	0.17	13.33	14.69	0.83
BON 99	**MRG-1**	39.35	3.89	8.08	17.94	0.17	13.23	14.89	0.92
AV	**MRG-1**	**39.09**	**3.77**	**8.46**	**17.93**	**0.17**	**13.55**	**14.71**	**0.74**
BON 94	**NIM-G**	75.54	0.09	11.93	2.01	0.02	-0.01	0.72	3.60
BON 96	**NIM-G**	75.95	0.09	11.90	1.99	0.02	-0.01	0.73	3.45
BON 99	**NIM-G**	76.26	0.11	12.02	2.04	0.03	0.11	0.76	3.55
BON 00	**NIM-G**	75.74	0.11	11.96	2.21	0.02	-0.01	0.81	3.37
AV	**NIM-G**	**75.70**	**0.09**	**12.08**	**2.02**	**0.02**	**0.06**	**0.78**	**3.36**
BON 94	**W-1**	52.40	0.94	15.14	11.21	0.17	6.47	10.84	2.33
BON 96	**W-1**	52.36	1.02	14.98	11.14	0.17	6.52	10.85	2.17
BON 00	**W-1**	52.33	1.07	14.99	11.04	0.16	6.83	11.10	2.20
AV	**W-1**	**52.46**	**1.07**	**15.00**	**11.11**	**0.17**	**6.62**	**11.00**	**2.16**

Batch	Standard	K_2O	P_2O_5	Total
BON 94	**ARSiO2**	0.01	0.01	99.77
BON 96	**ARSiO2**	0.06	0.01	99.75
BON 99	**ARSiO2**	0.04	0.01	100.12
BON 00	**ARSiO2**	0.01	0.01	99.76
AV	**ARSiO2**	**0.07**	**0.01**	**100.32**
BON 94	**BCS372/1**	0.73	0.08	96.82
BON 96	**BCS372/1**	0.72	0.09	97.23
BON 99	**BCS372/1**	0.74	0.09	96.65
AV	**BCS372/1**	**0.49**	**0.08**	**97.14**
BON 99	**DTS-1**	0.03	0.01	99.96
AV	**DTS-1**	**0.00**	**0.00**	**97.47**
BON 94	**JP-1**	0.07	0.01	99.77
BON 96	**JP-1**	0.07	0.01	99.60
AV		**0.00**		**99.22**
BON 00	**JSI-1**	3.17	0.20	99.04
AV	**JSI-1**	**2.01**	**0.09**	**88.42**
BON 96	**MRG-1**	0.26	0.07	99.27
BON 99	**MRG-1**	0.24	0.07	98.77
AV	**MRG-1**	**0.18**	**0.08**	**99.95**
BON 94	**NIM-G**	4.96	0.01	99.54
BON 96	**NIM-G**	4.98	0.01	99.77
BON 99	**NIM-G**	5.03	0.01	99.91
BON 00	**NIM-G**	5.06	0.01	99.28
AV	**NIM-G**	**4.99**	**0.01**	**99.11**
BON 94	**W-1**	0.62	0.14	100.16
BON 96	**W-1**	0.61	0.13	99.86
BON 00	**W-1**	0.67	0.13	100.53
AV	**W-1**	**0.64**	**0.13**	**100.36**

AV denotes agreed value

Batch	Standard	Sc	V	Cr	Co	Ni	Cu	Zn	Ga	Rb
BON 94	BCR-1	31.5	389.9	0.0	49.6	11.3	23.8	125.7	22.3	47.4
BON 96	BCR-1	30.3	392.8	0	48.5	11.6	22.8	127.9	22.3	47.7
BON 99	BCR-1	30.9	396.5	-6.0	49.2	20.6	30.6	126.6	21.6	47.9
BON 00	BCR-1	32.2	394.9	-2.1	48.1	11.1	24.6	129.5	22.3	47.5
AV	BCR-1	**33**	**407**	**16**	**37**	**13**	**19**	**130**	**22**	**47**
BON 94	BCS313/1	0.0	6.3	10.5	0.0	0	0	0	0	0
BON 96	BCS313/1	0	6.5	11.1	0	0	0	0	0	0
BON 99	BCS313/1	0.1	9.5	9.8	-3.0	-3.5	-4.6	0.3	1.1	0.0
AV	BCS313/1	**0**	**0**	**-1**	**0**	**0**	**0**	**0**	**0**	**0**
BON 94	BE-N	26.5	242.1	369.5	57.3	281.7	80.5	121.3	17.1	47.3
BON 96	BE-N	26.7	247.2	372	58.8	278.8	81.6	120.3	16.2	48.8
BON 99	BE-N	n.a.	n.a.	n.a.	n.a.	275.7	84.8	123.2	16.8	48.8
BON 00	BE-N	24.3	251.2	394.8	58.3	285.1	86.1	126.2	17.4	48.2
AV	BE-N	**22**	**235**	**360**	**60**	**267**	**72**	**120**	**17**	**47**
BON 94	BHVO-1	32.6	308.9	289.2	50.4	121.9	136.1	103.1	21.5	9.8
BON 96	BHVO-1	29.3	311.6	283.1	51.1	122.7	135.9	102.1	21.4	9.8
BON 99	BHVO-1	32.2	310.8	294.7	51.3	125.5	131.4	105.0	21.7	10.7
BON 00	BHVO-1	31.5	309.7	296.7	48.3	121.7	141.2	103.1	21.5	9.7
AV	BHVO-1	**32**	**317**	**289**	**45**	**121**	**136**	**105**	**21**	**11**
BON 94	BIR-1	40.0	314.9	388.8	49.2	164.3	126.9	67	15.4	0.8
BON 96	BIR-1	40.6	309.3	385.7	48.9	163.7	127.6	67.6	15.9	0
BON 99	BIR-1	42.0	316.8	395.3	51.8	163.6	117.4	71.8	16.5	1.6
BON 00	BIR-1	41.5	306.4	404.8	50.4	167.6	127.1	71.3	16.7	0.8
AV	BIR-1	**44**	**313**	**382**	**51**	**166**	**126**	**71**	**16**	**1**
BON 94	BOB-1	37.3	227.4	276.5	44.1	107	66	68.2	15.2	5.2
BON 96	BOB-1	36.5	232	280.1	43.4	110.9	67.1	69	15.4	6
BON 99	BOB-1	34.9	225.9	270.5	45.9	106.8	67.5	66.5	15.9	6.0
BON 00	BOB-1	35.5	218.9	279.0	43.7	105.5	67.5	65.5	15.0	6.0
AV	BOB-1		**234**	**304**		**115**		**63**	**16**	**6**
BON 94	BR	24.4	249.3	360.2	57.1	289.7	88.1	163.3	16.8	48.4
BON 96	BR	25.8	245.4	367.3	58.1	289.8	90.1	163.5	16.7	49.3
BON 99	BR	n.a.	n.a.	n.a.	n.a.	280.8	88.9	163.1	17.1	49.5
BON 00	BR	27.0	251.4	377.5	57.3	283.8	84.9	160.6	17.6	48.5
AV	BR	**25**	**235**	**380**	**52**	**260**	**72**	**160**	**19**	**47**
BON 94	G-2	4.0	41.7	4.2	5.2	1.8	9.4	83.3	21.8	167.4
BON 96	G-2	3.5	39.9	5.5	5.6	2.6	9.8	83.8	22.2	168.6
BON 99	G-2	3.8	40.8	6.0	5.7	1.5	10.0	81.4	21.4	167.3
BON 00	G-2	5.3	36.7	2.1	5.1	1.3	8.8	84.5	22.0	169.3
AV	G-2	**4**	**36**	**9**	**5**	**5**	**11**	**86**	**23**	**170**
BON 94	GSP-1	5.1	52.9	17.2	9.3	11.9	41.3	103.9	23	244.6
BON 96	GSP-1	5.8	54.4	19.4	9.2	11.7	39.8	102.7	22.9	247.2
BON 99	GSP-1	5.4	55.4	18.9	10.7	11.5	33.2	100.7	21.0	245.3
BON 00	GSP-1	5.5	47.8	17.5	9.8	11.2	34.3	103.5	22.0	248.4
AV	GSP-1	**6**	**53**	**13**	**7**	**9**	**33**	**104**	**23**	**254**
BON 94	JA-1	29.0	104.9	5.2	21.0	2.4	39.9	86.4	17.4	11.3
BON 96	JA-1	30.9	100.4	6	20.7	2.6	38.5	85.4	17.1	10.7
BON 99	JA-1	n.a.	n.a.	n.a.	n.a.	4.6	42.0	94.9	17.5	11.1
BON 00	JA-1	29.7	102.2	-6.8	20.5	0.1	42.5	85.5	17.5	10.8
AV	JA-1	**28**	**105**	**7**	**12**	**2**	**42**	**91**	**17**	**12**
BON 94	JA-2	21.8	111.7	385.7	25.4	129.9	27.4	63.2	16.7	72.2
BON 96	JA-2	19.6	114.8	390.4	26.5	129.8	28.3	64.4	16.9	72.3
BON 99	JA-2	n.a.	n.a.	n.a.	n.a.	121.2	27.4	63.5	16.8	71.7
AV	JA-2	**20**	**130**	**465**	**30**	**142**	**29**	**63**	**16**	**68**
BON 99	JB-1A	n.a.	n.a.	n.a.	n.a.	130.1	56.6	79.5	18.2	37.5
AV	JB-1A	**28**	**220**	**415**	**40**	**140**	**56**	**82**	**18**	**41**
BON 00	JB-2	51.3	567.8	-2.3	49.5	11.6	219.4	107.1	16.2	6.4
AV	JB-2	**54**	**578**	**27**	**40**	**14**	**227**	**110**	**17**	**6**
BON 00	JB-3	35.6	337.8	29.1	41.1	32.0	190.0	93.3	20.6	14.9
AV	JB-3	**33**	**383**	**60**	**36**	**39**	**198**	**106**	**21**	**13**
BON 94	JGB-1	39.5	653.8	35.1	60.4	26.3	85	115.9	18.8	6.9

AV denotes agreed value

Batch	Standard	Sr	Y	Zr	Nb	Ba	Ce	La	Nd
BON 94	**BCR-1**	333.7	38.9	195.2	12.2	730.6	66.8	26.6	31
BON 96	**BCR-1**	333.1	38.7	193.2	12.7	725.9	59.1	30.3	30.2
BON 99	**BCR-1**	327.7	38.7	196.5	12.6	740.8	64.2	28.9	28.0
BON 00	**BCR-1**	326.6	38.3	193.2	12.4	740.0	63.6	28.4	29.4
AV	**BCR-1**	**330**	**38**	**190**	**14**	**681**	**54**	**25**	**29**
BON 94	**BCS313/1**	0	0	27.8	0	0.0	0	0	0
BON 96	**BCS313/1**	0	0	27.6	0	0	0	0	2.1
BON 99	**BCS313/1**	1.1	0.0	27.8	0.0	-6.6	-1.5	1.9	1.5
AV	**BCS313/1**	**0**	**0**	**0**	**0**	**0**	**0**	**0**	**0**
BON 94	**BE-N**	1383.1	30	272.3	110.4	1008.1	174.6	88.6	70.6
BON 96	**BE-N**	1381.8	30	272.8	109.9	1001.1	175.3	88	70.1
BON 99	**BE-N**	1368.9	30.4	274.6	109.9	n.a.	168.7	87.5	69.6
BON 00	**BE-N**	1348.6	30.9	271.0	109.9	1013.3	169.6	92.9	70.0
AV	**BE-N**	**1370**	**30**	**265**	**100**	**1025**	**152**	**82**	**70**
BON 94	**BHVO-1**	397.5	28.3	177	19.1	122.8	49.9	15.2	27.3
BON 96	**BHVO-1**	393.2	28	178.7	18.2	123.5	53.1	14.6	27.6
BON 99	**BHVO-1**	392.5	28.2	178.1	18.9	136.2	47.0	16.3	23.3
BON 00	**BHVO-1**	385.2	28.3	173.7	18.3	142.0	47.0	16.0	26.6
AV	**BHVO-1**	**403**	**28**	**179**	**19**	**139**	**39**	**16**	**25**
BON 94	**BIR-1**	107.6	13.5	17.1	1.5	16.1	15.8	0	4
BON 96	**BIR-1**	108.5	13.6	14.8	1.7	23.1	8.2	0	2.4
BON 99	**BIR-1**	108.6	14.2	17.9	0.0	11.7	7.8	-1.2	3.5
BON 00	**BIR-1**	106.7	13.8	16.2	0.0	18.4	2.9	-0.8	1.6
AV	**BIR-1**	**108**	**16**	**22**	**2**	**8**	**3**	**1**	**3**
BON 94	**BOB-1**	193.7	27.5	104.2	5.2	41.1	16.2	0	11.4
BON 96	**BOB-1**	193.7	29.1	102.8	5	37.8	22.1	6.4	11.5
BON 99	**BOB-1**	194.3	26.2	105.5	4.8	42.9	15.0	3.8	10.3
BON 00	**BOB-1**	190.9	27.7	100.6	4.9	36.7	16.1	4.1	11.7
AV	**BOB-1**	**190**	**26**	**100**	**5**	**44**	**15**	**6**	**11**
BON 94	**BR**	1396.3	30.6	279.6	111.9	1024.0	157.6	84.4	66
BON 96	**BR**	1394.9	31.5	281.5	111.9	1011.6	162.6	83	64.3
BON 99	**BR**	1361.1	30.3	273.4	110.4	n.a.	159.2	84.2	67.4
BON 00	**BR**	1345.7	30.8	274.2	110.4	1040.4	169.9	85.7	67.2
AV	**BR**	**1320**	**30**	**250**	**98**	**1050**	**151**	**82**	**65**
BON 94	**G-2**	478.4	11	319.1	12	1882.6	144.7	89.9	50.1
BON 96	**G-2**	481.9	11.7	321.3	12.5	1893	148.3	89.5	52.5
BON 99	**G-2**	477.7	12.2	316.7	12.3	1874.4	144.2	89.9	49.9
BON 00	**G-2**	471.7	12.2	318.5	12.0	1882.5	146.1	90.2	50.2
AV	**G-2**	**478**	**11**	**309**	**12**	**1882**	**160**	**89**	**55**
BON 94	**GSP-1**	224.9	25.4	514.9	24.8	1233.1	286.6	122.4	134.2
BON 96	**GSP-1**	229.3	26.4	520.2	25.5	1248.9	285.1	122.3	137.2
BON 99	**GSP-1**	237.5	32.1	553.9	27.0	1319.0	304.7	127.7	145.8
BON 00	**GSP-1**	235.1	31.1	543.5	26.6	1318.7	306.8	129.6	145.3
AV	**GSP-1**	**234**	**26**	**530**	**28**	**1310**	**399**	**184**	**196**
BON 94	**JA-1**	258.1	31.3	83.2	1.8	330.0	0	5	11.1
BON 96	**JA-1**	259.2	31.9	84.5	1.9	321.5	7.1	5.3	11.7
BON 99	**JA-1**	257.0	31.1	84.7	1.6	n.a.	3.6	4.9	10.4
BON 00	**JA-1**	252.7	31.0	82.3	1.5	316.8	4.7	4.0	10.2
AV	**JA-1**	**266**	**31**	**87**	**2**	**307**	**13**	**6**	**11**
BON 94	**JA-2**	249.6	18.8	119.9	10	337.0	31.6	15.3	13.3
BON 96	**JA-2**	249.8	18.8	120.5	9.8	334.6	31	15.9	14.1
BON 99	**JA-2**	248.2	19.2	120.4	9.5	n.a.	29.0	16.0	14.9
AV	**JA-2**	**252**	**18**	**119**	**10**	**317**	**33**	**16**	**14**
BON 99	**JB-1A**	444.4	24.8	139.9	27.9	n.a.	69.7	40.2	29.3
AV	**JB-1A**	**443**	**25**	**144**	**27**	**497**	**67**	**38**	
BON 00	**JB-2**	172.3	25.7	49.8	0.8	239.7	12.9	0.5	6.9
AV	**JB-2**	**178**	**26**	**52**	**1**	**208**	**7**	**2**	**7**
BON 00	**JB-3**	404.6	28.2	96.1	2.2	252.4	26.9	9.3	16.5
AV	**JB-3**	**395**	**28**	**99**	**2**	**251**	**21**	**9**	**17**
BON 94	**JGB-1**	328	11.6	28	2.6	67.3	21.4	0	6.5

Appendix B- Table B.3 *XRF trace element standards*

Batch	Standard	Sc	V	Cr	Co	Ni	Cu	Zn	Ga	Rb
BON 94	**JGB-1**	2.0	126.1	95.8	44.7	23.8	85.1	116.1	18.8	6.4
BON 96	**JGB-1**	38.7	657.9	31.8	63.6	26.2	88	116.9	19.5	5.6
BON 96	**JGB-1**	40.1	677.9	35	63.3	25.7	86.4	115.5	19.3	6.7
BON 99	**JGB-1**	n.a.	n.a.	n.a.	n.a.	30.9	89.5	115.8	19.4	6.8
BON 00	**JGB-1**	39.7	654.6	14.4	62.1	24.4	86.1	113.3	19.2	5.6
AV	**JGB-1**	**37**	**640**	**59**	**62**	**25**	**87**	**111**	**19**	**4**
BON 94	**JP-1**	6.5	32.4	2978.2	68.5	2442.6	9.7	52.5	1.6	0
BON 96	**JP-1**	10.3	29.2	2968.4	69	2440.6	9.7	51.9	1.7	0
BON 99	**JP-1**	n.a.	n.a.	n.a.	n.a.	2437.3	10.2	53.3	2.3	0.8
BON 00	**JP-1**	7.9	28.5	2948.8	67.9	2444.2	5.0	48.1	1.5	-0.1
AV	**JP-1**	**7**	**29**	**2970**	**116**	**2460**	**6**	**30**	**1**	
BON 94	**JR-1**	4.3	9.6	23.4	0.0	2.2	1.4	30	15.6	250.8
BON 96	**JR-1**	3.8	8.3	25	0	2.6	0.9	30	15.9	251.3
BON 00	**JR-1**	5.5	9.9	1.6	-0.7	0.5	-1.2	27.8	16.0	252.0
AV	**JR-1**	**5**		**2**	**1**	**1**	**1**	**30**	**18**	**257**
BON 94	**JR-2**	4.5	7.9	7.4	0.0	0	0	25.4	16.6	299.2
BON 96	**JR-2**	5.5	7.3	8.9	0	1.9	0	25.1	17.2	297.9
BON 99	**JR-2**	n.a.	n.a.	n.a.	n.a.	-0.8	-1.8	24.2	16.6	302.0
BON 00	**JR-2**	4.4	6.2	2.7	-1.6	0.1	-1.1	25.0	16.3	298.0
AV	**JR-2**	**6**		**3**	**0**	**1**	**1**	**27**	**18**	**297**
BON 94	**JR-3**	0.0	2.4	6.7	9.0	4.6	6	204.2	36.7	462.9
BON 96	**JR-3**	0	6.2	6.6	9.3	4	4.8	203.3	36.5	463.2
BON 99	**JR-3**	n.a.	n.a.	n.a.	n.a.	4.6	5.4	201.4	37.2	467.2
BON 00	**JR-3**	-0.5	3.0	3.6	9.2	1.9	2.0	202.5	37.6	466.9
AV	**JR-3**			**3**	**1**	**1**	**2**	**204**		**458**
BON 94	**MA-N**	0.0	9.0	5.9	0.0	14.2	138.5	240.4	60.4	3791.5
BON 96	**MA-N**	0	9.3	8	0	14.5	137.7	240.6	60.8	3788.8
BON 99	**MA-N**	-4.1	11.9	3.3	-17.9	12.0	122.5	237.8	60.8	3762.5
BON 00	**MA-N**	-3.0	7.0	2.2	-21.4	15.1	139.9	241.1	60.4	3800.1
AV	**MA-N**	**0.2**	**0.2**	**3.0**	**0.5**	**3.0**	**140.0**	**220.0**	**59.0**	**3600**
BON 94	**MRG-1**	54.9	571.1	533.5	82.2	196.6	133.7	203.2	17.8	9
BON 96	**MRG-1**	55.7	564	526.9	81.4	196.4	133.3	206.2	17.3	8.3
BON 99	**MRG-1**	53.4	560.3	522.6	82.7	200.0	137.4	203.2	17.3	8.1
BON 00	**MRG-1**	54.8	580.4	533.2	82.6	200.2	143.3	203.1	17.4	8.9
AV	**MRG-1**	**55**	**526**	**430**	**87**	**193**	**134**	**191**	**17**	**9**
BON 94	**NIM-G**	2.2	5.1	17.8	0.0	5.3	8.1	52.1	27.2	316.7
BON 96	**NIM-G**	0	6.3	19.9	0	5.3	6.8	52.9	26.7	315.9
BON 99	**NIM-G**	0.3	7.6	16.0	1.4	5.6	5.2	51.0	27.6	316.9
BON 00	**NIM-G**	0.5	4.4	14.7	1.2	4.8	6.9	53.4	27.9	317.2
AV	**NIM-G**	**1**	**2**	**12**	**4**	**8**	**12**	**50**	**27**	**320**
BON 94	**PCC-1**	7.9	32.8	2720.0	67.2	2396.9	12.6	44	1.5	0
BON 96	**PCC-1**	8.7	34.5	2731.9	68.4	2399.2	12.4	44.2	1.7	0
BON 99	**PCC-1**	n.a.	n.a.	n.a.	n.a.	2403.3	11.0	44.1	2.1	0.1
BON 00	**PCC-1**	8.9	32.7	2742.9	66.8	2393.6	8.0	44.3	2.0	-0.8
AV	**PCC-1**	**8**	**31**	**2730**	**112**	**2380**	**10**	**42**	**1**	**0**
BON 94	**STM-1**	0.0	5.1	7.9	12.2	0	2.3	235.6	34.4	115.5
BON 96	**STM-1**	0	4.8	8	11.1	3.2	4	235.8	34.2	116.1
BON 99	**STM-1**	0.1	7.7	6.4	12.2	3.3	5.7	234.7	34.7	117.9
BON 00	**STM-1**	0.9	4.6	4.2	11.9	0.7	4.2	237.1	35.3	118.1
AV	**STM-1**	**1**	**9**	**4**	**1**	**3**	**5**	**235**	**36**	**118**
BON 94	**W-1**	32.2	251.7	112.1	45.6	72	114.6	85.7	17.6	22.1
BON 96	**W-1**	34.7	255.6	108.9	46.2	71.6	114	86.4	17.5	22.2
BON 99	**W-1**	n.a.	n.a.	n.a.	n.a.	74.4	107.9	86.6	18.0	22.6
BON 00	**W-1**	35.0	254.1	104.7	44.7	71.7	111.4	86.1	18.2	21.1
AV	**W-1**	**35**	**257**	**119**	**47**	**75**	**113**	**84**	**17**	**21**

XRF trace element standards

Batch	Standard	Sr	Y	Zr	Nb	Ba	Ce	La	Nd
BON 94	**JGB-1**	327.5	10.4	26.9	2.6	0.0	22.7	0	6.2
BON 96	**JGB-1**	329.4	10.2	29.2	2.7	73.2	21.5	0	4.5
BON 96	**JGB-1**	330	11.8	30.4	3.2	73.6	23.1	0	5.8
BON 99	**JGB-1**	327.6	11.6	29.4	2.6	n.a.	17.8	2.8	6.1
BON 00	**JGB-1**	323.3	9.2	31.4	2.9	64.3	19.6	3.8	4.5
AV	**JGB-1**	**321**	**11**	**13**	**3**	**63**	**8**	**6**	
BON 94	**JP-1**	0	0	4.5	0	11.2	0	0	0
BON 96	**JP-1**	0	0	4.5	0	10.2	0	0	0
BON 99	**JP-1**	0.8	-2.1	6.0	0.9	n.a.	1.0	-2.1	-1.1
BON 00	**JP-1**	2.2	-2.0	7.9	0.5	1.9	3.9	-0.1	1.1
AV	**JP-1**		**1**	**6**	**1**	**17**			
BON 94	**JR-1**	27.1	45.6	97.4	16.2	48.4	37	21.2	23.7
BON 96	**JR-1**	27.5	46	95.7	16	46	33	21.8	23.9
BON 00	**JR-1**	28.9	45.9	98.6	16.0	41.6	35.6	20.6	23.7
AV	**JR-1**	**30**	**46**	**102**	**16**	**40**	**49**	**28**	
BON 94	**JR-2**	7.7	52.1	94.8	19.2	21.9	28.2	15.8	20.3
BON 96	**JR-2**	6.6	52.2	93.9	18.8	25	28.5	16.1	20.7
BON 99	**JR-2**	7.8	51.0	92.9	18.9	n.a.	25.5	15.6	19.7
BON 00	**JR-2**	9.4	51.9	96.2	18.9	18.5	25.6	16.2	19.7
AV	**JR-2**	**8**	**51**	**99**	**19**	**39**	**38**	**18**	
BON 94	**JR-3**	9.2	174	1675.7	573.7	68.5	311.5	159	103.4
BON 96	**JR-3**	8.7	175.5	1670.6	573.6	62.3	308.8	155.4	102.4
BON 99	**JR-3**	8.7	173.3	1668.4	584.3	n.a.	306.9	158.8	102.0
BON 00	**JR-3**	10.9	174.4	1665.1	574.1	59.7	309.9	158.4	101.9
AV	**JR-3**	**9**							
BON 94	**MA-N**	89.6	0	28.8	172.2	70.9	9.5	37.6	1.1
BON 96	**MA-N**	89.5	0	27.1	170.5	67.6	9.4	37.1	0
BON 99	**MA-N**	90.5	13.8	30.7	170.5	57.8	14.0	38.3	1.1
BON 00	**MA-N**	90.6	14.7	29.0	170.2	55.4	3.7	37.7	0.1
AV	**MA-N**	**84.0**	**0.4**	**25.0**	**173.0**	**42.0**	**0.9**	**38.0**	**0.4**
BON 94	**MRG-1**	270.3	15	107.7	20.3	44.7	52.9	10.5	20.3
BON 96	**MRG-1**	265.4	13.6	105	19.7	36.4	53.9	8.8	21.1
BON 99	**MRG-1**	267.1	15.3	104.0	20.3	65.4	50.2	9.8	22.2
BON 00	**MRG-1**	264.1	14.2	107.9	20.1	68.1	47.3	7.9	17.9
AV	**MRG-1**	**266**	**14**	**108**	**20**	**61**	**28**	**19**	
BON 94	**NIM-G**	11.1	141	280.9	56.1	105.0	189.6	106.8	70.3
BON 96	**NIM-G**	9.5	140.6	277.5	55.8	115.8	187.9	105.8	69.8
BON 99	**NIM-G**	10.6	141.5	278.5	56.0	104.3	191.8	106.4	72.1
BON 00	**NIM-G**	12.7	140.9	277.1	56.2	108.7	196.9	107.3	71.1
AV	**NIM-G**	**10**	**143**	**300**	**53**	**120**	**195**	**109**	
BON 94	**PCC-1**	0	0	0	0	0.0	0	0	0
BON 96	**PCC-1**	0	0	0	0	0	0	0	0
BON 99	**PCC-1**	0.0	-2.2	1.4	0.6	n.a.	1.1	-1.2	0.2
BON 00	**PCC-1**	1.9	-1.6	3.4	0.3	-8.2	1.1	0.1	-0.8
AV	**PCC-1**	**0**	**0**	**10**	**1**	**1**	**0**	**0**	
BON 94	**STM-1**	712.4	48.8	1355.1	267.2	613.1	248.6	135.1	78.3
BON 96	**STM-1**	717.3	49	1355.1	268.6	613.2	245.9	136.6	78.5
BON 99	**STM-1**	712.4	49.0	1356.8	269.5	605.9	249.3	135.3	79.3
BON 00	**STM-1**	703.6	49.6	1369.2	267.2	610.7	251.2	138.2	79.9
AV	**STM-1**	**700**	**46**	**1210**	**268**	**560**	**259**	**150**	
BON 94	**W-1**	190	23.6	96.4	7.3	159.8	30.1	8.4	10.4
BON 96	**W-1**	190.1	23.4	95.4	7.6	169	33.3	9.2	13.2
BON 99	**W-1**	188.4	23.4	99.1	7.4	n.a.	28.7	11.6	12.5
BON 00	**W-1**	185.5	24.5	95.1	7.1	165.5	24.7	12.0	15.1
AV	**W-1**	**186**	**26**	**99**	**10**	**162**	**24**	**15**	

Appendix C

ICP Analytical technique

C.1. Introduction

Two different Inductively Coupled Plasma (ICP)-based techniques were utilised in this study. A subset of 56 samples were analysed by Inductively Coupled Plasma Optical Emission Spectroscopy (ICP-OES) at the University of Leicester, specifically for the determination of REE. In addition, 18 samples were analysed by Inductively Coupled Plasma Mass Spectroscopy (ICP-MS) at the University of Cardiff, for the determination of selected trace elements and REE. The purpose of this was twofold: to serve as a comparison with other analytical methods used, and for the high precision determination of Lu, Hf, Sm and Nd concentrations for isotope analysis. The results of both these techniques are presented in Table D.2, and the techniques are outlined below.

C.2. ICP-OES Analytical technique

C.2.1. Sample preparation

Open vessel digestion (rather than microwave) was used for this method as there was little petrographic evidence for the presence of heavy mineral phases (Chapter 3). 0.300 grams of ignited powder were weighed into a clean Teflon beaker, to which perchloric acid and hydrofluoric acid were added. The mixture was placed on a hotplate for ~4 hours until it became solid, then more perchloric acid was added and the procedure was repeated. After the addition of 50 ml of 1.7M hydrochloric acid, the resulting solution was placed on a hotplate for ~10 minutes until dissolution was complete. The solutions were then loaded into columns in order to chemically separate the REE. For each batch of 6 samples, one standard and one blank was added.

Quartz glass columns of 180 mm length and 8 mm internal diameter were used. The columns have a 100 ml reservoir at the top and a plug of quartz glass wool, to act as a sinter, at the bottom. 5g of resin (Dowex AG 50W-8X, 200-400 mesh) was loaded on to the columns in 1.7M HCl and settled at a height of 130 mm. The resin was washed with 50 ml of 6M HCl, followed by 50 ml of de-ionised water and the pH adjusted to match that of the sample solutions with 50 ml of 1.7M HCl.

After sample loading, all the major constituents, including Ca and Fe which are potential spectral interferences in the ICP-OES, and most of the trace elements in the solution were then eluted, by washing the resin with a further 100 ml of 1.7M HCl. This fraction was discarded. The REE, which are quantitatively held on the resin, were then eluted by washing with 80 ml of 6M HCl. This fraction was collected in 100 ml Pyrex beakers and evaporated to dryness on a sand bath at c. 110°C. The samples were converted to nitrates by the addition of 4 ml of 16M HNO_3 and then re-dissolved in 3 ml of 5% HNO_3 and stored in polypropylene tubes prior to analysis. After use, the columns were cleaned in the same way as before their first use and then re-used for the next batch of samples.

C.2.2. **Analysis**

Analysis was carried out at the University of Leicester, using a Philips PV 8060 ICP-OES. The sample solution is carried in an aerosol in argon to the centre of the plasma flame where it reaches a temperature of about 8000 K. At this extreme temperature atomisation of the analyte solution occurs. The basis for all emission spectrometry is that atoms or ions in an energised state will spontaneously revert to a lower energy state and emit a photon of light energy, at a characteristic wavelength, as they do. For quantitative analysis it is assumed that the intensity of light emitted is proportional to the concentration of the element in solution. The light emitted by the atoms of the elements in the ICP is focused into a spectrometer where a diffraction grating resolves the light into its component wavelengths. The intensity of light emitted at each given wavelength is then converted to an electrical signal by photomultiplier tubes located at specific wavelengths for each element line. Using calibration lines that relate elemental concentration with intensity of light emitted, the electrical signal is converted into a concentration measurement.

Detection limits for the ICP-OES are detailed in Table C.1 below.

Element	La	Ce	Pr	Nd	Sm	Eu	Gd	Dy	Er	Yb	Lu
Limit of detection (ppm)	0.8	0.9	0.9	1.0	0.5	0.15	0.8	0.7	0.8	0.14	0.08

Table C.1. Limits of detection for ICP-OES analysis. From E. Mansley, pers. com.

C.2.3. International standards

International standards are presented in Table C.2., along those for the ICP-MS technique. It is apparent that there is a reasonable correlation between agreed values and values obtained in this study.

C.3. ICP-MS analysis

C.3.1. Sample preparation

For ICP-MS analysis, samples were prepared at the University of Leicester. Samples were prepared samples in batches of 8 including a blank and a standard. 200 mg of sample was accurately weighed into a clean microwave vessel and 10 ml of HF was added. A rupture membrane was added to the cap of each vessel, which was then secured. A pressure-regulating cap was placed on one of the vessels in every batch. The vessels were then evenly distributed in the microwave carousel, the pressure sensing line was secured to the appropriate vessel cap, and the microwave was set to the HF program. After cooling and pressure reduction, the pressure release valves were opened and the dissolved samples were transferred to Teflon beakers. 3 ml of concentrate Primar HNO_3 was added to each of the beakers, which were then slowly evaporated to incipient dryness and the procedure was repeated. 5–6 ml 5M Primar HNO_3 was then added, and the solution warmed on the hotplate until it appeared clear. This was then diluted with UHQ water to 50 ml, in centrifuge tubes.

C.3.2. Analysis

ICP-MS analysis was carried out at the University of Cardiff by Dr. Laurence Coogan. The machine used was a Perkin Elmer Elan 5000, and W-2 was used as a drift monitor during analysis.

C.3.3. International standards

International standards and procedural blanks are presented in Table C.2., along those for the ICP-OES technique. It is apparent that there is a reasonable correlation between agreed values and values obtained in this study.

ICP-OES

AV denotes agreed value

Batch	Standard	La	Ce	Pr	Nd	Sm	Eu	Gd	Dy	Er	Yb	Lu
Batch 1	**JB-1a**	35.21	65.20	7.07	23.46	5.20	1.62	5.07	4.14	2.37	2.12	0.32
Batch 2	**JB-1a**	35.55	65.43	6.13	22.02	4.97	1.55	4.67	3.97	2.18	1.97	0.31
Batch 3	**JB-1a**	34.95	64.22	6.42	24.82	5.87	1.55	4.63	4.41	2.46	2.12	0.32
Batch 4	**JB-1a**	34.34	62.94	6.77	25.05	5.57	1.43	4.23	3.76	2.16	1.30	0.18
Batch 5	**JB-1a**	34.03	62.95	6.33	22.69	5.40	1.49	4.73	4.26	2.36	1.81	0.25
AV	**JB-1a**	**37.60**	**65.90**	**7.30**	**26.00**	**5.07**	**1.46**	**4.67**	**3.99**	**2.18**	**2.10**	**0.33**
Batch 6	**JR-1**	19.94	46.40	5.95	24.26	5.94	0.38	5.32	5.56	4.08	4.01	0.62
Batch 7	**JR-1**	19.31	50.07	5.10	22.17	5.21	0.34	4.88	5.67	3.74	4.21	0.62
Batch 8	**JR-1**	20.02	49.10	5.24	23.74	5.19	0.30	4.74	5.80	3.79	4.38	0.64
AV	**JR-1**	**19.70**	**47.20**	**5.58**	**23.30**	**6.03**	**0.3**	**5.83**	**5.69**	**0.3**	**4.55**	**0.71**

ICP-MS

AV denotes agreed value

Date	Standard	ID	Rb	Sr	Y	Zr	Nb	Ba	La	Ce	Pr	Nd	Sm
May-00	**JB1A**	Pat 1-7	42.80	511.38	23.30	152.23	29.98	442.28	37.44	65.40	7.01	25.08	4.82
May-00	**JB1A**	Pat 2-7	43.41	525.28	23.68	155.23	30.33	421.72	39.12	67.76	7.12	26.01	5.04
May-00	**JB1A**	Pat 3-7	43.52	524.56	23.92	154.40	30.74	429.80	39.17	67.05	7.23	25.82	5.02
AV	**JB1A**		**39.20**	**442**	**24.00**	**144.00**	**26.90**	**504.00**	**37.60**	**65.90**	**7.30**	**26.00**	**5.07**
May-00	**Blank**	Pat 1-8	0.27	1.6857	0.11	0.15	0.00	0.85	0.07	0.14	0.02	0.07	0.02
May-00	**Blank**	Pat 2-8	0.16	0.2199	0.01	0.17	0.02	0.36	0.02	0.03	0.01	0.02	0.00
May-00	**Blank**	Pat 3-6	0.04	1.2917	0.03	0.29	0.02	1.19	0.02	0.03	0.00	0.03	0.01
Nov-00	**Blank**	P1-6	0.03	1.2193	0.23	0.03	0.00	3.11	0.04	0.04	0.01	0.03	0.01
Nov-00	**Blank**	P2-6	0.03	0.5574	0.16	0.04	0.00	2.45	0.03	0.04	0.00	0.02	0.00

ICP-MS *continued*

Standard	Eu	Gd	Tb	Dy	Ho	Er	Tm	Yb	Lu	Hf	Ta	Pb	Th
JB1A	1.56	5.18	0.77	4.20	0.79	2.15	0.31	1.97	0.31	3.77	1.97	6.41	8.78
JB1A	1.66	5.48	0.79	4.39	0.82	2.30	0.32	2.04	0.30	3.84	1.87	6.83	8.58
JB1A	1.63	5.31	0.77	4.34	0.82	2.19	0.33	2.01	0.31	3.79	2.07	6.21	8.55
AV	**1.46**	**4.67**	**0.69**	**3.99**	**0.71**	**2.18**	**0.33**	**2.10**	**0.33**	**3.41**	**1.93**	**6.76**	**9.03**
JG1	0.60	1.55	0.28	1.70	0.35	1.02	0.14	0.90	0.15	1.19	0.53	2.88	0.48
JG1	0.63	1.64	0.29	1.81	0.35	1.01	0.15	0.90	0.14	1.15	0.24	2.85	0.47
JG1													
Blank	0.00	0.02	0.00	0.01	0.00	0.02	0.00	0.01	0.00	0.00	0.00	1.04	0.03
Blank	0.00	0.00	0.00	0.01	0.00	0.00	0.00	0.00	0.00	0.01	0.01	0.80	0.00
Blank	0.00	0.01	0.00	0.01	0.00	0.00	0.00	0.01	0.00	0.01	0.00	1.04	0.00
Blank	0.00	0.01	0.00	0.00	0.00	0.00	0.00	0.00	0.00	0.01	0.03	1.79	0.00
Blank	0.00	0.00	0.00	0.00	0.00	0.00	0.00	0.00	0.00	0.01	0.00	1.64	0.00

Appendix D

Major and Trace Element Data

D.1. Data presented

Three techniques have been used in obtaining major and trace element data: XRF, ICP-MS and ICP-OES. Major and trace element data collected for samples listed in Appendix A are outlined in Tables D.1 and D.2.

D.2. Discussion of data format

Major and trace element data collected for samples listed in Appendix A are outlined in Tables D.1 and D.2. Table D.1 consists of optimised major and trace element data, i.e., the data used for this study, where ICP-MS data (where available) took precedence over ICP-OES data and XRF. This data has been filtered: some of the more altered samples that were disregarded from any subsequent interpretation have been omitted, for clarity. A lithological code is assigned to individual samples: this is detailed in the key at the base of each page of the table. Table D.2 consists of all existing trace and rare earth element data obtained using the ICP-MS and ICP-OES techniques. This enables the reader to disregard analyses from a particular technique, if required, or allow a comparison between the different techniques.

D.3. Data quality

Plots showing comparisons of different techniques are shown in Fig. D.1. Plots of Ce XRF data compared with ICP-MS and ICP-OES are shown in plots (a) and (b). It is apparent that there is only a reasonable agreement between ICP-MS and XRF data, and possibly even less of an agreement between the XRF and ICP-OES techniques. For low (<10 ppm) Ce concentrations, it is likely that this is due to poor precision of the XRF technique. This is supported by the high limits of detection (6 ppm; Table B.1) of Ce compared to other elements, and by comparison with the standards, especially those with low Ce concentrations

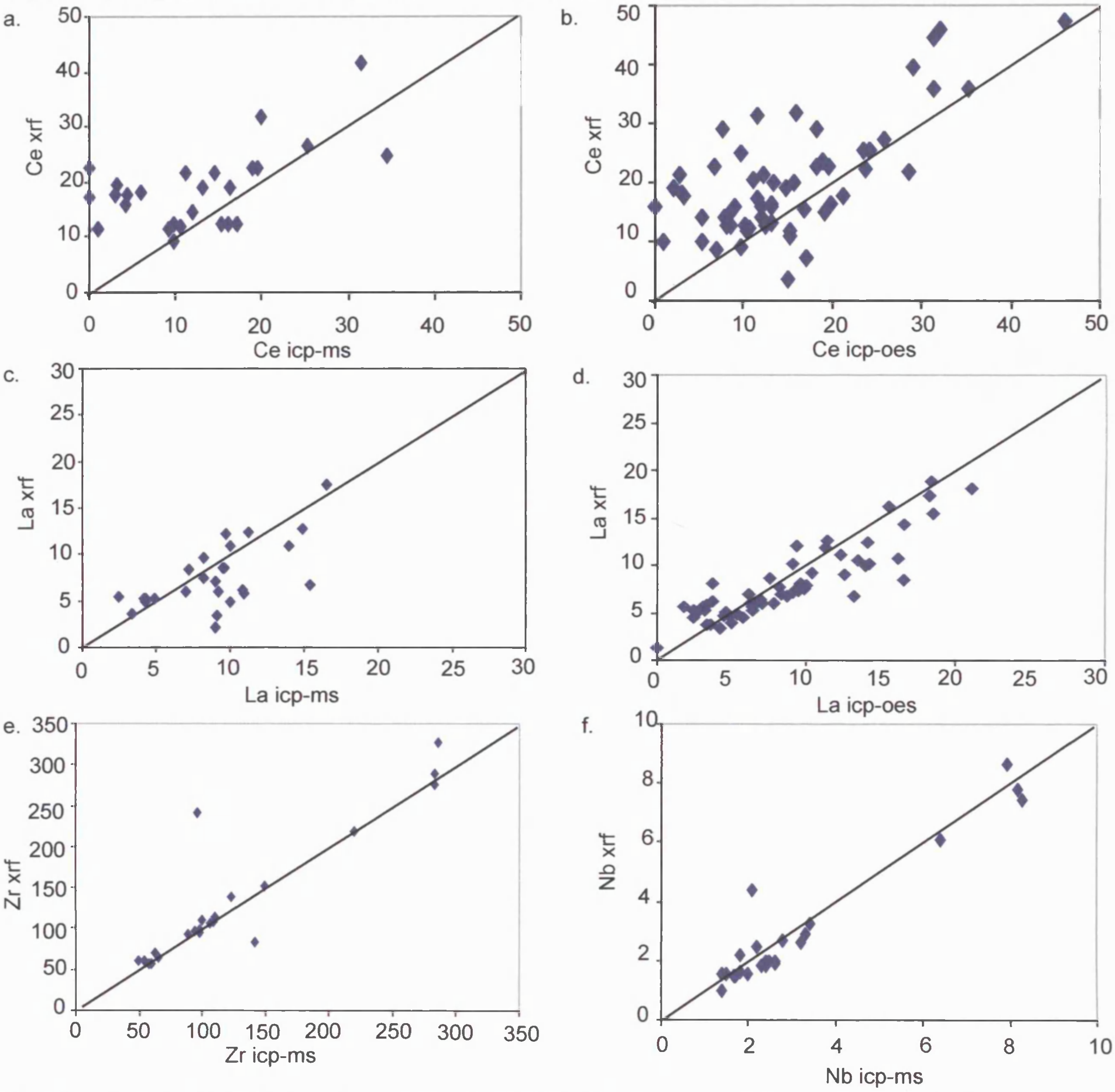

Fig. D1. Plots comparing different analytical techniques for selected elements. See text for discussion.

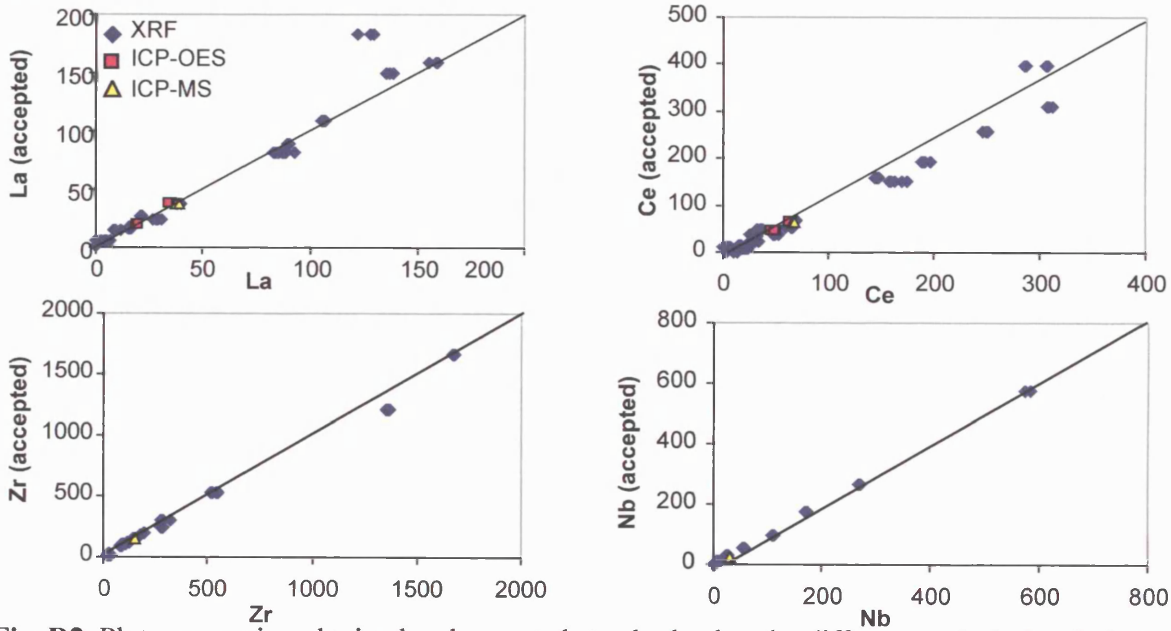

Fig. D2. Plots comparing obtained and accepted standard values by different analytical techniques for selected elements.

(Table B.2). It is for this reason that ICP-MS and ICP-OES Ce data are used in preference to XRF, where available.

La (XRF) only shows a reasonable to good agreement with ICP-MS and ICP-OES data. It appears that for low concentrations (<15 ppm) ICP-OES, rather than ICP-MS, correlates better with XRF data. However, the XRF limit of detection of La is 3.5 ppm (Table B.1), and therefore, throughout this work, where available, ICP-OES and ICP-MS data are used in preference to XRF data.

Both Zr and Nb show a near perfect correlation between XRF and ICP-Ms data. There are several outliers, however. For the prominent outlier with higher Zr (XRF), this could be attributed to poor sample dissolution for ICP-MS, which could also be responsible for the high Nb (XRF) outlier. However, the good correlation between the techniques justifies the use of Nb and Zr ICP-MS, along with XRF data.

Appendix D-Table D.1: Major and trace element data

	GOTOMEER					
Sample no	**BON 94-3**	**BON 94-8**	**BON 96-7**	**BON 94-19**	**BON 94-2**	**BON 96-10**
Bead	LF12670	LF12675	LF12764	LF12684	LF12669	LF12766
Pellet	L33719	L33724	L33880	L33733	L33718	L33881
Lithology	v	v	v	v	d	d
	quartz					weathered
majors						
SiO_2	76.32	50.72	76.87	74.37	52.18	52.82
TiO_2	0.49	0.30	0.36	0.43	1.06	0.81
Al_2O_3	7.65	8.66	9.99	12.09	14.21	14.84
Fe_2O_3	4.82	3.90	3.01	4.34	8.46	12.65
MnO	0.09	0.18	0.04	0.10	0.22	0.19
MgO	1.41	1.55	1.17	1.14	3.70	4.91
CaO	1.10	17.07	0.58	1.15	9.01	5.75
Na_2O	1.20	1.68	4.31	5.45	4.88	4.05
K_2O	3.42	1.12	1.18	0.66	0.93	1.06
P_2O_5	0.11	0.12	0.10	0.10	0.21	0.11
SO_3	n.a.	n.a.	n.a.	n.a.	n.a.	n.a.
LOI	2.02	14.87	1.48	1.29	5.80	2.13
traces						
Pb*	15.6	4.9	2.1	54.2	3.9	n.d.
Rb*	40.9	15.1	10.2	6.4	12.5	12.5
Ba*	1849.5	802.1	459.5	305.9	695.1	446.6
Th*	0.8	2.7	3.3	2.0	1.0	2.5
U*	n.d.	1.8	n.d.	n.d.	0.5	n.d.
Nb*	n.d.	2.1	1.9	2.5	2.2	1.5
La*	7.6	9.7	6.9	8.6	8.5	n.d.
Ce*	n.d.	n.d.	16.0	16.3	19.0	10.4
Sr	57.5	379.5	51.9	180.6	266.8	302.1
Nd*	6.3	8.8	11.2	15.3	14.3	6.9
Zr*	48.2	95.8	86.2	104.8	81.1	51.5
Y*	20.4	30.9	38.8	39.1	35.2	24.3
Sc	14.0	21.5	10.2	16.8	27.5	36.6
Co	18.2	11.6	6.5	11.7	26.4	47.1
V	94.8	76.3	33.9	49.3	321.5	284.6
Cr	17.4	8.8	6.0	12.8	91.3	n.d.
Cu	65.2	36.4	40.5	33.2	99.6	169.3
Ga	8.7	10.5	10.7	13.9	18.1	16.2
Ni	15.7	4.6	14.3	4.5	21.8	15.0
Zn	71.3	44.1	88.1	61.7	66.9	58.3
Hf *	n.a.	n.a.	n.a.	n.a.	2.52	n.a.
Ta	n.a.	n.a.	n.a.	n.a.	0.21	n.a.
REE						
La	n.a.	n.a.	6.92	n.a.	8.46	n.a.
Ce	n.a.	n.a.	15.96	n.a.	18.99	n.a.
Pr	n.a.	n.a.	2.30	n.a.	2.97	n.a.
Nd	n.a.	n.a.	11.24	n.a.	14.35	n.a.
Sm	n.a.	n.a.	3.82	n.a.	4.08	n.a.
Eu	n.a.	n.a.	1.14	n.a.	1.60	n.a.
Gd	n.a.	n.a.	3.90	n.a.	4.87	n.a.
Tb	n.a.	n.a.	n.a.	n.a.	0.86	n.a.
Dy	n.a.	n.a.	4.96	n.a.	5.37	n.a.
Ho	n.a.	n.a.	n.a.	n.a.	1.13	n.a.
Er	n.a.	n.a.	3.01	n.a.	3.22	n.a.
Tm	n.a.	n.a.	n.a.	n.a.	0.49	n.a.
Yb	n.a.	n.a.	3.11	n.a.	3.19	n.a.
Lu	n.a.	n.a.	0.46	n.a.	0.49	n.a.
Y	n.a.	n.a.	38.8	n.a.	35.2	n.a.
other data ?			*icp-oes*		*icp-ms*	

* denotes ICP-MS data used where available

Key:	
r rhyodacite	rd rhyodacite dome
d dolerite	b basalt
v volcaniclastic	an andesite
di diorite	

	GOTOMEER						
Sample no	**BON 96-12**	**BON 96-31**	**BON 99-72**	**BON 99-104**	**BON 99-121**	**BON 99-136**	**BON 99-163**
Bead	LF12768	LF12786	LF13358	LF13367	LF13374	LF13380	LF13391
Pellet	L33883	L33901	L34287	L34296	L34303	L34309	L34320
Lithology	d	d	d	d	d	d	d
		weathered	weathered	fresh	calcite	weathered	layered
majors							
SiO_2	68.80	53.86	56.97	58.68	50.76	46.72	56.01
TiO_2	0.70	1.21	1.56	1.41	1.19	1.13	1.40
Al_2O_3	13.38	15.51	14.45	13.45	13.18	14.48	14.24
Fe_2O_3	5.15	10.25	9.25	9.50	8.96	9.15	10.38
MnO	0.25	0.13	0.15	0.12	0.18	0.11	0.10
MgO	2.04	4.80	4.12	2.56	3.87	2.33	4.30
CaO	0.74	3.81	2.90	3.26	8.59	19.60	3.56
Na_2O	5.36	4.43	4.82	6.07	5.11	0.43	4.74
K_2O	1.22	1.38	1.35	0.22	0.44	0.05	1.52
P_2O_5	0.18	0.18	0.24	0.27	0.20	0.21	0.23
SO_3	n.a.	n.a.	0.03	0.04	0.03	0.03	0.02
LOI	2.35	3.24	4.89	2.71	7.54	4.66	2.85
traces							
Pb*	n.d.	3.0	2.7	2.2	n.d.	1.0	1.6
Rb*	5.1	15.7	17.3	2.3	3.7	1.5	20.9
Ba*	249.0	867.0	1336.8	80.5	232.9	24.3	689.3
Th*	1.1	2.2	3.1	1.4	3.3	3.6	1.4
U*	n.d.	n.d.	0.4	0.4	0.6	0.5	0.6
Nb*	1.5	2.5	2.4	3.2	2.5	2.4	2.5
La*	1.4	6.4	9.3	11.0	6.1	5.0	9.8
Ce*	3.5	19.6	7.3	26.4	16.2	19.3	21.6
Sr	239.6	376.8	338.3	177.4	108.7	21.4	193.5
Nd*	3.7	10.7	12.0	19.7	10.9	14.4	15.8
Zr*	46.8	77.9	104.7	84.0	82.0	93.6	109.9
Y*	22.1	31.5	38.9	42.1	29.0	25.8	34.6
Sc	33.9	38.2	32.6	27.3	35.4	34.2	32.1
Co	45.0	38.7	35.3	32.4	33.4	30.6	37.3
V	285.4	383.3	383.0	234.4	325.6	370.8	334.5
Cr	7.4	77.9	13.5	n.d.	15.8	143.1	43.7
Cu	42.4	125.9	366.7	10.9	118.2	131.7	176.9
Ga	16.5	19.0	16.2	16.9	13.6	46.1	15.6
Ni	11.3	17.9	25.2	6.2	19.0	22.2	21.9
Zn	57.9	99.9	70.5	43.3	66.6	75.5	68.3
Hf *	n.a.	n.a.	n.a.	2.58	n.a.	n.a.	3.10
Ta	n.a.	n.a.	n.a.	0.27	n.a.	n.a.	0.24
REE							
La	1.35	n.a.	n.a.	10.98	n.a.	n.a.	9.76
Ce	3.54	n.a.	n.a.	26.41	n.a.	n.a.	21.59
Pr	0.56	n.a.	n.a.	4.15	n.a.	n.a.	3.31
Nd	3.66	n.a.	n.a.	19.71	n.a.	n.a.	15.76
Sm	1.31	n.a.	n.a.	5.45	n.a.	n.a.	4.36
Eu	0.85	n.a.	n.a.	1.69	n.a.	n.a.	1.63
Gd	2.67	n.a.	n.a.	6.18	n.a.	n.a.	5.04
Tb	n.a.	n.a.	n.a.	1.11	n.a.	n.a.	0.89
Dy	3.89	n.a.	n.a.	6.80	n.a.	n.a.	5.51
Ho	n.a.	n.a.	n.a.	1.39	n.a.	n.a.	1.12
Er	2.33	n.a.	n.a.	3.99	n.a.	n.a.	3.28
Tm	n.a.	n.a.	n.a.	0.56	n.a.	n.a.	0.50
Yb	2.29	n.a.	n.a.	3.45	n.a.	n.a.	3.27
Lu	0.39	n.a.	n.a.	0.53	n.a.	n.a.	0.50
Y	22.1	n.a.	n.a.	42.1	n.a.	n.a.	34.6
other data ?	*icp-oes*			*icp-ms*			*icp-ms*

* denotes ICP-MS data used where possible

Key:	
r rhyodacite	rd rhyodacite dome
d dolerite	b basalt
v volcaniclastic	an andesite
di diorite	

Appendix D-Table D.1: Major and trace element data

	GOTOMEER						
Sample no	**BON 99-165**	**BON 99-182**	**BON00-43**	**BON00-45**	**BON00-47**	**BON00-48**	**BON00-58**
Bead	LF13392	LF13404	LF15009	LF15011	LF15012	LF15013	LF15019
Pellet	L34321	L34333	L35821	L35823	L35824	L35825	L35831
Lithology	d	d	d	di	di	d	d
	layered			weathered	quartz		
majors							
SiO_2	56.45	50.57	52.54	56.20	60.29	49.53	48.76
TiO_2	1.44	0.86	1.38	1.43	0.75	0.97	0.99
Al_2O_3	14.04	17.65	14.29	14.77	14.67	13.82	13.80
Fe_2O_3	10.36	10.27	11.82	10.11	5.78	9.59	10.72
MnO	0.10	0.17	0.16	0.11	0.20	0.21	0.25
MgO	3.93	4.58	6.06	4.27	1.16	4.84	4.78
CaO	3.61	8.51	1.72	3.54	5.77	10.54	8.83
Na_2O	4.66	4.27	4.86	5.15	7.34	4.14	4.40
K_2O	1.11	0.99	0.91	1.78	0.35	0.08	0.92
P_2O_5	0.25	0.16	0.21	0.23	0.25	0.13	0.14
SO_3	0.02	0.02	n.a.	n.a.	n.a.	n.a.	n.a.
LOI	3.28	2.89	3.65	2.27	4.48	6.30	5.87
traces							
Pb*	n.d.	2.5	n.d.	5.1	1.8	n.d.	2.5
Rb*	11.3	19.1	7.6	15.4	2.0	0.3	9.3
Ba*	556.3	165.6	520.9	1003.9	259.0	80.0	623.2
Th*	2.3	0.6	2.8	3.2	4.3	2.8	0.7
U*	0.7	0.2	0.5	0.5	2.1	0.1	0.3
Nb*	2.7	1.6	2.6	2.0	2.8	1.3	1.5
La*	8.4	5.2	6.9	7.5	12.0	4.5	5.0
Ce*	20.5	12.2	17.8	19.2	31.3	11.0	11.5
Sr	149.0	294.3	144.5	223.3	182.4	146.0	321.9
Nd*	16.0	9.0	12.0	12.7	19.3	8.5	9.2
Zr*	110.7	56.8	86.5	105.6	126.8	54.0	65.5
Y*	36.1	19.4	31.2	37.5	27.7	23.6	22.1
Sc	31.2	25.4	39.1	28.1	22.1	41.5	35.5
Co	36.3	36.7	44.1	34.3	22.0	39.2	41.5
V	305.6	256.8	383.6	367.7	145.2	328.5	354.1
Cr	57.5	35.5	75.9	n.d.	n.d.	1.0	182.8
Cu	140.5	106.4	n.a.	n.a.	n.a.	n.a.	n.a.
Ga	16.1	18.6	n.a.	n.a.	n.a.	n.a.	n.a.
Ni	17.5	23.3	15.1	19.3	2.7	12.1	13.4
Zn	67.4	61.5	78.5	78.2	73.2	73.6	87.9
Hf *	n.a.	1.64	n.a.				
Ta	n.a.	0.22	n.a.	n.a.		n.a.	n.a.
REE							
La	n.a.	5.23	6.85	7.50	12.04	4.54	n.a.
Ce	n.a.	12.23	17.79	19.16	31.27	10.99	n.a.
Pr	n.a.	1.88	2.58	2.54	4.49	1.56	n.a.
Nd	n.a.	9.02	12.05	12.67	19.34	8.50	n.a.
Sm	n.a.	2.55	3.66	4.06	5.00	2.49	n.a.
Eu	n.a.	0.98	1.28	1.34	1.20	0.96	n.a.
Gd	n.a.	2.99	4.74	5.23	4.97	3.48	n.a.
Tb	n.a.	0.53	n.a.	n.a.	n.a.	n.a.	n.a.
Dy	n.a.	3.16	4.78	5.79	3.89	4.18	n.a.
Ho	n.a.	0.66	n.a.	n.a.	n.a.	n.a.	n.a.
Er	n.a.	1.90	3.08	3.28	2.69	2.44	n.a.
Tm	n.a.	0.27	n.a.	n.a.	n.a.	n.a.	n.a.
Yb	n.a.	1.70	2.56	3.22	2.14	2.47	n.a.
Lu	n.a.	0.27	0.36	0.48	0.34	0.35	n.a.
Y	n.a.	19.4	31.2	37.5	27.7	23.6	n.a.
other data ?		*icp-ms*	*icp-oes*	*icp-oes*	*icp-oes*	*icp-oes*	

* denotes ICP-MS data used where possible

Key:

r rhyodacite	rd rhyodacite dome
d dolerite	b basalt
v volcaniclastic	an andesite
di diorite	

Appendix D-Table D.1: Major and trace element data

	GOTOMEER						
Sample no	**BON00-59**	**BON 94-16**	**BON 94-17**	**BON 99-100**	**BON 99-101**	**BON 99-105**	**BON 99-119**
Bead	LF15020	LF12682	LF12683	LF13365	LF13366	LF13368	LF13373
Pellet	L35832	L33731	L33732	L34294	L34295	L34297	L34302
Lithology	d	b	b	b	an	b	an
	weathered	quartz		quartz		weathered	
majors							
SiO_2	53.38	67.50	51.73	68.27	60.02	53.74	63.91
TiO_2	1.13	0.68	0.89	0.76	0.97	1.39	1.25
Al_2O_3	14.93	14.47	14.40	13.25	14.76	14.34	12.85
Fe_2O_3	11.67	6.21	13.08	6.11	9.55	11.65	7.69
MnO	0.14	0.10	0.21	0.11	0.11	0.14	0.12
MgO	5.01	1.82	3.70	2.44	2.93	5.96	2.10
CaO	4.93	0.94	7.01	1.13	1.90	2.08	3.27
Na_2O	5.47	7.35	4.03	6.68	6.46	5.85	5.11
K_2O	0.70	0.16	1.09	0.16	0.29	0.08	1.22
P_2O_5	0.16	0.31	0.15	0.30	0.15	0.20	0.20
SO_3	n.a.	n.a.	n.a.	0.04	0.04	0.03	0.03
LOI	2.04	1.80	3.57	2.12	2.43	4.11	2.27
traces							
Pb*	n.d.	28.4	2.6	1.3	1.5	0.6	2.5
Rb*	6.8	0.8	12.4	0.9	3.7	n.d.	13.7
Ba*	329.8	110.3	461.4	155.2	158.8	56.3	695.8
Th*	2.1	1.1	n.d.	3.1	3.2	3.6	2.7
U*	n.d.	2.1	n.d.	1.1	n.d.	0.5	0.5
Nb*	1.6	2.6	1.5	2.1	1.8	2.4	2.4
La*	5.8	10.0	4.4	11.0	6.7	7.5	6.7
Ce*	15.4	17.2	17.4	16.5	16.3	19.4	7.5
Sr	306.8	88.9	407.9	108.8	162.6	92.5	126.7
Nd*	11.0	16.5	11.0	17.4	11.1	11.9	11.1
Zr*	75.5	100.3	59.9	101.1	80.3	82.6	81.5
Y*	28.3	34.0	26.7	32.5	23.8	25.8	32.9
Sc	35.0	20.8	33.0	19.6	37.1	39.9	30.7
Co	43.6	17.3	43.8	17.9	36.4	41.8	27.3
V	352.1	70.5	357.1	73.6	265.0	387.2	319.9
Cr	n.d.	17.6	67.0	1.0	180.1	84.0	201.4
Cu	n.a.	12.8	207.1	3.4	102.3	11.7	124.8
Ga	n.a.	16.8	19.1	14.3	15.0	18.0	14.3
Ni	13.6	n.d.	13.0	n.d.	9.3	21.1	15.7
Zn	64.0	64.0	83.2	60.0	68.3	45.0	74.6
Hf *							
Ta	n.a.	n.a.	n.a.	n.a.	n.a.	n.a.	n.a.
REE							
La	5.76	n.a.	n.a.	n.a.	n.a.	n.a.	n.a.
Ce	15.39	n.a.	n.a.	n.a.	n.a.	n.a.	n.a.
Pr	2.18	n.a.	n.a.	n.a.	n.a.	n.a.	n.a.
Nd	11.02	n.a.	n.a.	n.a.	n.a.	n.a.	n.a.
Sm	3.34	n.a.	n.a.	n.a.	n.a.	n.a.	n.a.
Eu	1.26	n.a.	n.a.	n.a.	n.a.	n.a.	n.a.
Gd	4.57	n.a.	n.a.	n.a.	n.a.	n.a.	n.a.
Tb	n.a.	n.a.	n.a.	n.a.	n.a.	n.a.	n.a.
Dy	4.87	n.a.	n.a.	n.a.	n.a.	n.a.	n.a.
Ho	n.a.	n.a.	n.a.	n.a.	n.a.	n.a.	n.a.
Er	2.96	n.a.	n.a.	n.a.	n.a.	n.a.	n.a.
Tm	n.a.	n.a.	n.a.	n.a.	n.a.	n.a.	n.a.
Yb	2.42	n.a.	n.a.	n.a.	n.a.	n.a.	n.a.
Lu	0.35	n.a.	n.a.	n.a.	n.a.	n.a.	n.a.
Y	28.3	n.a.	n.a.	n.a.	n.a.	n.a.	n.a.
other data ?	*icp-oes*						

* denotes ICP-MS data used where possible

Key:	
r rhyodacite	rd rhyodacite dome
d dolerite	b basalt
v volcaniclastic	an andesite
di diorite	

	GOTOMEER						
Sample no	**BON 99-128**	**BON 99-129**	**BON00-44**	**BON 94-1**	**BON 94-10**	**BON 94-15**	**BON 96-11**
Bead	LF13375	LF13376	LF15010	LF12668	LF12677	LF12681	LF12767
Pellet	L34304	L34305	L35822	L33717	L33726	L33730	L33882
Lithology	b	an	b	r	r	r	r
	weathered	quartz					porphyric
majors							
SiO_2	55.36	66.23	52.27	77.63	79.23	78.71	81.04
TiO_2	1.14	0.92	1.16	0.35	0.38	0.35	0.29
Al_2O_3	16.00	12.90	12.66	11.79	10.79	11.14	9.92
Fe_2O_3	12.69	6.48	9.95	2.89	1.95	2.06	1.68
MnO	0.20	0.12	0.21	0.03	0.06	0.02	0.02
MgO	2.06	3.17	4.55	0.48	0.17	0.32	0.27
CaO	1.30	1.30	6.82	0.15	1.62	0.30	0.44
Na_2O	5.72	5.41	5.17	5.18	5.21	5.17	4.38
K_2O	0.45	0.75	0.04	1.56	0.83	1.48	1.66
P_2O_5	0.21	0.36	0.18	0.04	0.07	0.05	0.06
SO_3	0.03	0.03	n.a.	n.a.	n.a.	n.a.	n.a.
LOI	3.43	2.31	6.92	1.15	0.99	0.95	0.43
traces							
Pb*	1.1	1.1	n.d.	3.6	6.5	22.7	n.d.
Rb*	4.8	4.6	n.d.	18.3	3.0	11.6	21.4
Ba*	190.8	306.8	33.7	993.3	264.7	482.6	820.3
Th*	2.7	2.6	3.5	3.5	1.3	1.8	2.8
U*	0.1	1.0	0.5	2.6	0.9	n.d.	n.d.
Nb*	1.9	2.3	2.0	5.2	2.7	2.5	2.0
La*	7.9	9.6	8.7	5.5	6.2	9.2	5.9
Ce*	16.6	13.6	21.3	n.d.	19.2	17.3	n.d.
Sr	126.9	115.9	55.9	31.8	99.8	62.5	145.7
Nd*	9.0	16.4	14.4	8.0	10.3	7.8	8.9
Zr*	71.2	97.2	73.3	268.0	139.8	134.5	95.7
Y*	24.6	32.7	25.8	46.3	28.6	37.1	24.6
Sc	33.1	22.5	36.0	9.3	7.9	10.0	7.3
Co	45.8	21.2	35.9	6.2	3.6	4.2	3.7
V	342.6	106.3	364.5	38.2	29.1	23.3	31.2
Cr	7.9	60.6	96.0	n.d.	28.2	21.8	n.d.
Cu	102.4	23.1	n.a.	49.8	27.2	16.3	2.6
Ga	16.7	14.6	n.a.	12.2	11.8	12.6	5.3
Ni	15.7	0.9	13.5	2.9	2.9	2.7	1.7
Zn	90.8	79.3	78.7	10.0	52.5	74.3	23.0
Hf *					4.37		
Ta	n.a.	n.a.	n.a.	n.a.	0.20	n.a.	n.a.
REE							
La	7.94	n.a.	8.66	n.a.	6.19	9.23	n.a.
Ce	16.56	n.a.	21.32	n.a.	19.16	17.32	n.a.
Pr	1.96	n.a.	2.95	n.a.	2.21	1.81	n.a.
Nd	8.99	n.a.	14.35	n.a.	10.33	7.80	n.a.
Sm	2.86	n.a.	4.06	n.a.	3.05	2.30	n.a.
Eu	1.11	n.a.	1.42	n.a.	0.82	0.85	n.a.
Gd	3.29	n.a.	4.60	n.a.	3.58	3.53	n.a.
Tb	n.a.	n.a.	n.a.	n.a.	0.70	n.a.	n.a.
Dy	3.91	n.a.	5.04	n.a.	4.66	5.32	n.a.
Ho	n.a.	n.a.	n.a.	n.a.	1.04	n.a.	n.a.
Er	2.27	n.a.	2.98	n.a.	3.20	3.47	n.a.
Tm	n.a.	n.a.	n.a.	n.a.	0.51	n.a.	n.a.
Yb	2.07	n.a.	2.55	n.a.	3.50	3.01	n.a.
Lu	0.26	n.a.	0.43	n.a.	0.55	0.52	n.a.
Y	24.6	n.a.	25.8	n.a.	28.6	37.1	n.a.
other data ?	*icp-oes*		*icp-oes*		*icp-ms*	*icp-oes*	

* denotes ICP-MS data used where possible

Key:	
r rhyodacite	rd rhyodacite dome
d dolerite	b basalt
v volcaniclastic	an andesite
di diorite	

	GOTOMEER						
Sample no	**BON 96-30**	**BON 96-32**	**BON 96-33**	**BON 99-131**	**BON 99-132**	**BON 99-166**	**BON 99-168**
Bead	LF12785	LF12787	LF12788	LF13378	LF13379	LF13393	LF13394
Pellet	L33900	L33902	L33903	L34307	L34308	L34322	L34323
Lithology	r	r	r	r	r	r	r
	quartz	calcite	calcite	calcite, epidote	clast		
majors							
SiO_2	70.68	71.55	49.74	79.45	76.88	70.32	71.14
TiO_2	0.72	0.75	1.09	0.49	0.45	0.79	0.78
Al_2O_3	12.32	12.16	12.74	10.17	9.72	12.59	12.48
Fe_2O_3	5.07	5.12	8.90	2.31	2.44	5.36	4.74
MnO	0.07	0.08	0.15	0.02	0.03	0.13	0.13
MgO	1.63	1.92	3.97	0.42	0.96	1.30	0.82
CaO	1.15	1.45	6.84	0.68	0.40	0.43	0.57
Na_2O	5.79	5.48	4.82	4.94	2.16	4.83	6.11
K_2O	0.25	0.21	1.64	0.78	4.61	2.58	1.01
P_2O_5	0.18	0.19	0.20	0.09	0.09	0.18	0.27
SO_3	n.a.	n.a.	n.a.	0.03	0.03	0.03	0.03
LOI	1.77	1.96	5.64	0.92	1.06	1.44	1.15
traces							
Pb*	n.d.	n.d.	n.d.	1.7	0.9	2.5	n.d.
Rb*	1.6	0.9	11.6	7.8	30.9	13.6	5.7
Ba*	160.6	378.0	532.1	260.5	879.2	848.5	426.3
Th*	2.3	2.6	1.6	3.1	4.3	0.8	3.0
U*	n.d.	n.d.	n.d.	0.5	0.4	0.5	n.d.
Nb*	2.4	2.6	2.6	3.3	2.8	1.9	2.2
La*	6.4	6.5	6.1	12.0	9.9	5.9	8.3
Ce*	10.3	7.4	12.2	9.6	6.8	17.9	8.5
Sr	101.5	67.4	85.7	172.3	66.5	111.2	141.6
Nd*	14.5	14.6	11.8	13.3	16.2	9.5	15.8
Zr*	112.2	111.6	85.9	136.1	132.8	103.8	105.3
Y*	44.4	41.1	32.5	33.8	38.6	22.0	43.9
Sc	19.0	18.2	34.4	9.0	10.2	19.6	19.3
Co	14.2	14.2	34.7	3.1	4.2	12.5	10.6
V	27.9	28.2	388.5	19.3	24.8	24.7	21.4
Cr	4.5	6.0	16.0	23.0	43.4	14.1	20.8
Cu	454.5	213.0	163.8	0.0	3.2	3.0	n.d.
Ga	12.8	12.5	16.8	9.2	8.2	15.0	15.8
Ni	n.d.	n.d.	16.5	n.d.	n.d.	0.7	n.d.
Zn	26.7	25.4	72.4	59.7	38.3	99.8	32.0
Hf *						3.37	
Ta	n.a.	n.a.	n.a.	n.a.	n.a.	0.15	n.a.
REE							
La	n.a.	n.a.	n.a.	n.a.	n.a.	5.92	n.a.
Ce	n.a.	n.a.	n.a.	n.a.	n.a.	17.94	n.a.
Pr	n.a.	n.a.	n.a.	n.a.	n.a.	1.99	n.a.
Nd	n.a.	n.a.	n.a.	n.a.	n.a.	9.49	n.a.
Sm	n.a.	n.a.	n.a.	n.a.	n.a.	2.74	n.a.
Eu	n.a.	n.a.	n.a.	n.a.	n.a.	1.21	n.a.
Gd	n.a.	n.a.	n.a.	n.a.	n.a.	3.29	n.a.
Tb	n.a.	n.a.	n.a.	n.a.	n.a.	0.60	n.a.
Dy	n.a.	n.a.	n.a.	n.a.	n.a.	3.75	n.a.
Ho	n.a.	n.a.	n.a.	n.a.	n.a.	0.81	n.a.
Er	n.a.	n.a.	n.a.	n.a.	n.a.	2.36	n.a.
Tm	n.a.	n.a.	n.a.	n.a.	n.a.	0.36	n.a.
Yb	n.a.	n.a.	n.a.	n.a.	n.a.	2.46	n.a.
Lu	n.a.	n.a.	n.a.	n.a.	n.a.	0.38	n.a.
Y	n.a.	n.a.	n.a.	n.a.	n.a.	22.0	n.a.
other data ?						*icp-ms*	

* denotes ICP-MS data used where possible

Key:	
r rhyodacite	rd rhyodacite dome
d dolerite	b basalt
v volcaniclastic	an andesite
di diorite	

Appendix D-Table D.1: Major and trace element data

	GOTOMEER					BRANDARIS	
Sample no	**BON 99-180**	**BON 99-181**	**BON 99-73**	**BON 99-130**	**BON 99-98**	**BON 94-8**	**BON 96-16**
Bead	LF13402	LF13403	LF13411	LF13377	LF13409	LF12675	LF12771
Pellet	L34331	L34332	L34340	L34306	L34338	L33724	L33886
Lithology	r	r	r	da	an	v	v
	epidote		quartz				
majors							
SiO_2	72.81	73.61	68.20	66.45	54.75	50.72	76.50
TiO_2	0.53	0.55	0.83	0.78	1.34	0.30	0.40
Al_2O_3	12.83	13.22	12.46	12.16	15.02	8.66	11.95
Fe_2O_3	2.98	2.73	6.58	4.45	8.50	3.90	3.25
MnO	0.09	0.04	0.08	0.05	0.15	0.18	0.02
MgO	0.83	0.56	2.10	0.86	3.55	1.55	0.58
CaO	0.78	0.30	1.24	8.07	4.35	17.07	0.13
Na_2O	6.15	6.54	5.95	3.72	6.05	1.68	4.33
K_2O	1.72	1.87	0.12	0.09	1.30	1.12	2.54
P_2O_5	0.12	0.14	0.20	0.37	0.20	0.12	0.08
SO_3	0.02	0.03	0.04	0.03	0.06	n.a.	n.a.
LOI	0.71	0.88	1.98	2.22	4.96	14.87	1.44
traces							
Pb*	2.6	n.d.	1.5	0.7	0.5	4.9	n.d.
Rb*	6.0	14.2	1.3	n.d.	13.4	15.1	22.5
Ba*	445.0	332.7	131.3	15.3	981.9	802.1	1533.2
Th*	0.6	2.4	2.4	2.6	3.0	2.7	5.1
U*	0.5	0.8	0.2	0.8	1.2	1.8	1.5
Nb*	2.7	3.5	2.4	2.4	2.2	2.1	5.1
La*	3.4	11.1	8.4	10.9	9.2	9.7	14.2
Ce*	12.3	31.6	11.3	13.5	6.3	n.d.	18.4
Sr	94.1	36.2	108.3	31.2	133.7	379.5	52.9
Nd*	7.6	20.3	14.6	17.9	11.3	8.8	20.3
Zr*	151.3	154.1	118.3	89.1	82.0	95.8	230.9
Y*	19.6	66.8	46.6	31.3	31.6	30.9	46.0
Sc	10.6	12.2	18.9	23.6	40.4	21.5	9.1
Co	6.3	5.5	18.3	13.8	30.8	11.6	7.4
V	21.4	17.0	32.9	120.2	372.1	76.3	28.6
Cr	25.0	18.9	1.6	9.8	9.0	8.8	3.9
Cu	n.d.	n.d.	17.4	8.7	109.3	36.4	5.8
Ga	14.1	13.5	15.3	21.7	16.6	10.5	11.7
Ni	n.d.	n.d.	0.5	0.6	16.8	4.6	n.d.
Zn	79.5	48.8	32.2	26.0	76.1	44.1	23.8
Hf *	4.36						
Ta	0.20	n.a.	n.a.	n.a.	n.a.	n.a.	n.a.
REE							
La	3.45	11.10	n.a.	n.a.	n.a.	n.a.	n.a.
Ce	12.30	31.62	n.a.	n.a.	n.a.	n.a.	n.a.
Pr	1.53	4.22	n.a.	n.a.	n.a.	n.a.	n.a.
Nd	7.63	20.25	n.a.	n.a.	n.a.	n.a.	n.a.
Sm	2.27	6.31	n.a.	n.a.	n.a.	n.a.	n.a.
Eu	0.93	1.75	n.a.	n.a.	n.a.	n.a.	n.a.
Gd	2.82	6.93	n.a.	n.a.	n.a.	n.a.	n.a.
Tb	0.54	n.a.	n.a.	n.a.	n.a.	n.a.	n.a.
Dy	3.51	7.67	n.a.	n.a.	n.a.	n.a.	n.a.
Ho	0.79	n.a.	n.a.	n.a.	n.a.	n.a.	n.a.
Er	2.28	3.89	n.a.	n.a.	n.a.	n.a.	n.a.
Tm	0.36	n.a.	n.a.	n.a.	n.a.	n.a.	n.a.
Yb	2.40	3.00	n.a.	n.a.	n.a.	n.a.	n.a.
Lu	0.37	0.38	n.a.	n.a.	n.a.	n.a.	n.a.
Y	19.6	66.8	n.a.	n.a.	n.a.	n.a.	n.a.
other data ?	*icp-ms*	*icp-oes*					

* denotes ICP-MS data used where possible

Key:	
r rhyodacite	rd rhyodacite dome
d dolerite	b basalt
v volcaniclastic	an andesite
di diorite	

Appendix D-Table D.1: Major and trace element data

	BRANDARIS						
Sample no	**BON 94-13**	**BON 99-143**	**BON94-6**	**BON 94-7**	**BON 94-11**	**BON 94-12**	**BON 94-14**
Bead	LF12679	LF13381	LF12673	LF12674	LF12678	LF12793	LF12680
Pellet	L33728	L34310	L33722	L33723	L33727	L33908	L33729
Lithology	d	b	r	r	r	r	r
			porphyritic	porphyritic			
majors							
SiO_2	54.30	62.91	77.25	78.24	72.78	75.96	72.52
TiO_2	0.81	0.84	0.54	0.38	0.39	0.60	0.76
Al_2O_3	15.90	14.33	11.17	10.56	12.00	11.31	13.32
Fe_2O_3	11.33	7.07	2.27	1.87	3.89	2.42	4.06
MnO	0.14	0.15	0.09	0.06	0.07	0.04	0.05
MgO	3.31	3.60	0.19	0.26	1.64	0.14	1.18
CaO	8.54	1.27	0.86	1.13	0.48	0.23	0.73
Na_2O	3.22	5.31	4.70	4.48	3.61	5.68	6.85
K_2O	1.11	1.76	1.81	1.79	3.46	1.52	0.89
P_2O_5	0.19	0.27	0.22	0.06	0.08	0.14	0.22
SO_3	n.a.	0.02	n.a.	n.a.	n.a.	n.a.	n.a.
LOI	0.81	1.98	0.71	0.84	2.01	0.69	1.03
traces							
Pb*	8.0	0.7	3.1	2.5	3.8	1.9	27.1
Rb*	15.4	20.8	12.6	11.9	22.0	8.1	5.7
Ba*	371.2	769.3	961.4	1802.9	905.0	311.2	225.5
Th*	0.6	2.4	1.2	2.1	1.1	2.8	1.0
U*	n.d.	0.1	n.d.	2.5	n.d.	1.9	1.7
Nb*	1.6	2.2	2.3	2.9	2.3	2.3	2.4
La*	4.9	10.0	9.2	11.7	10.3	8.1	9.4
Ce*	13.0	10.6	n.d.	n.d.	n.d.	7.1	14.3
Sr	242.0	194.7	110.8	122.6	43.8	41.1	59.5
Nd*	9.2	13.5	13.1	12.4	11.4	13.2	15.7
Zr*	58.3	96.7	85.3	119.5	116.1	93.8	98.5
Y*	21.7	32.3	46.1	31.8	33.5	41.3	43.5
Sc	32.9	23.4	14.6	7.9	14.4	12.2	20.5
Co	34.5	21.8	3.8	3.2	10.8	5.0	8.7
V	360.4	104.4	15.0	41.3	68.0	10.8	13.9
Cr	18.2	221.2	10.9	3.0	59.3	6.8	5.4
Cu	230.1	8.2	6.7	34.3	5.7	n.d.	3.9
Ga	20.9	16.6	12.1	10.2	11.7	13.2	13.6
Ni	12.1	2.2	2.2	2.6	5.0	n.d.	n.d.
Zn	81.0	52.6	68.1	50.7	62.3	63.7	79.1
Hf *							
Ta	n.a.	n.a.	n.a.	n.a.	n.a.	n.a.	n.a.
REE							
La	n.a.	n.a.	n.a.	n.a.	n.a.	n.a.	n.a.
Ce	n.a.	n.a.	n.a.	n.a.	n.a.	n.a.	n.a.
Pr	n.a.	n.a.	n.a.	n.a.	n.a.	n.a.	n.a.
Nd	n.a.	n.a.	n.a.	n.a.	n.a.	n.a.	n.a.
Sm	n.a.	n.a.	n.a.	n.a.	n.a.	n.a.	n.a.
Eu	n.a.	n.a.	n.a.	n.a.	n.a.	n.a.	n.a.
Gd	n.a.	n.a.	n.a.	n.a.	n.a.	n.a.	n.a.
Tb	n.a.	n.a.	n.a.	n.a.	n.a.	n.a.	n.a.
Dy	n.a.	n.a.	n.a.	n.a.	n.a.	n.a.	n.a.
Ho	n.a.	n.a.	n.a.	n.a.	n.a.	n.a.	n.a.
Er	n.a.	n.a.	n.a.	n.a.	n.a.	n.a.	n.a.
Tm	n.a.	n.a.	n.a.	n.a.	n.a.	n.a.	n.a.
Yb	n.a.	n.a.	n.a.	n.a.	n.a.	n.a.	n.a.
Lu	n.a.	n.a.	n.a.	n.a.	n.a.	n.a.	n.a.
Y	n.a.	n.a.	n.a.	n.a.	n.a.	n.a.	n.a.
other data ?							

* denotes ICP-MS data used where possible

Key:	
r rhyodacite	rd rhyodacite dome
d dolerite	b basalt
v volcaniclastic	an andesite
di diorite	

Appendix D-Table D.1: Major and trace element data

	BRANDARIS						
Sample no	**BON 94-20**	**BON 96-14**	**BON 96-18**	**BON 96-34**	**BON 96-36**	**BON 96-37**	**BON 99-02**
Bead	LF12685	LF12770	LF12773	LF12789	LF12791	LF12792	LF13348
Pellet	L33734	L33885	L33888	L33904	L33906	L33907	L34277
Lithology	r	r	r	r	r	r	r
		porphyritic	porphyritic	porphyritic	porphyritic	porphyritic	
majors							
SiO_2	76.46	70.13	74.09	76.02	66.95	66.64	72.87
TiO_2	0.42	0.72	0.65	0.57	0.67	0.67	0.56
Al_2O_3	11.59	13.66	12.65	10.57	13.28	14.23	13.38
Fe_2O_3	2.66	6.03	3.32	1.98	3.91	5.23	3.26
MnO	0.05	0.12	0.04	0.08	0.09	0.07	0.10
MgO	0.69	1.51	0.42	0.18	1.37	2.66	0.74
CaO	0.16	0.51	0.17	1.82	0.49	0.87	0.39
Na_2O	3.77	6.40	5.08	3.73	6.42	3.95	6.44
K_2O	3.45	0.42	2.24	1.27	1.04	4.34	1.61
P_2O_5	0.06	0.19	0.05	0.20	0.20	0.29	0.15
SO_3	n.a.	n.a.	n.a.	n.a.	n.a.	n.a.	0.03
LOI	1.18	1.48	1.23	0.69	1.71	1.82	0.89
traces							
Pb*	35.8	0.0	1.7	2.2	2.6	0.0	0.8
Rb*	34.3	2.1	15.4	11.5	6.7	36.3	15.4
Ba*	981.7	172.4	464.8	874.3	289.8	1353.1	551.2
Th*	1.1	2.7	3.1	2.0	3.5	2.5	3.7
U*	1.6	n.d.	n.d.	n.d.	n.d.	1.5	0.9
Nb*	2.7	2.4	2.3	2.1	2.5	2.2	3.2
La*	9.1	6.1	7.8	8.1	11.2	9.7	11.0
Ce*	n.d.	9.9	n.d.	n.d.	14.4	11.0	13.8
Sr	52.8	117.2	61.2	191.7	70.8	104.0	54.1
Nd*	10.3	12.2	15.9	13.0	20.5	15.4	18.7
Zr*	145.4	101.0	103.1	86.6	107.2	103.3	152.9
Y*	37.8	36.9	37.5	42.2	60.1	33.1	45.3
Sc	8.3	20.2	15.8	17.3	18.4	16.4	12.3
Co	5.3	14.7	6.9	2.5	9.0	16.4	6.9
V	39.2	24.6	12.6	11.2	10.2	60.4	18.8
Cr	n.d.	25.7	17.1	7.3	5.6	n.d.	34.2
Cu	21.1	2.2	n.d.	n.d.	n.d.	2.1	n.d.
Ga	12.4	16.3	11.9	12.0	17.8	13.9	15.0
Ni	4.3	n.d.	n.d.	n.d.	n.d.	n.d.	n.d.
Zn	141.7	27.6	103.4	76.5	75.5	61.3	63.9
Hf *							
Ta	n.a.	n.a.	n.a.	n.a.	n.a.	n.a.	n.a.
REE							
La	n.a.	n.a.	n.a.	n.a.	n.a.	n.a.	n.a.
Ce	n.a.	n.a.	n.a.	n.a.	n.a.	n.a.	n.a.
Pr	n.a.	n.a.	n.a.	n.a.	n.a.	n.a.	n.a.
Nd	n.a.	n.a.	n.a.	n.a.	n.a.	n.a.	n.a.
Sm	n.a.	n.a.	n.a.	n.a.	n.a.	n.a.	n.a.
Eu	n.a.	n.a.	n.a.	n.a.	n.a.	n.a.	n.a.
Gd	n.a.	n.a.	n.a.	n.a.	n.a.	n.a.	n.a.
Tb	n.a.	n.a.	n.a.	n.a.	n.a.	n.a.	n.a.
Dy	n.a.	n.a.	n.a.	n.a.	n.a.	n.a.	n.a.
Ho	n.a.	n.a.	n.a.	n.a.	n.a.	n.a.	n.a.
Er	n.a.	n.a.	n.a.	n.a.	n.a.	n.a.	n.a.
Tm	n.a.	n.a.	n.a.	n.a.	n.a.	n.a.	n.a.
Yb	n.a.	n.a.	n.a.	n.a.	n.a.	n.a.	n.a.
Lu	n.a.	n.a.	n.a.	n.a.	n.a.	n.a.	n.a.
Y	n.a.	n.a.	n.a.	n.a.	n.a.	n.a.	n.a.
other data ?							

* denotes ICP-MS data used where possible

Key:	
r rhyodacite	rd rhyodacite dome
d dolerite	b basalt
v volcaniclastic	an andesite
di diorite	

Appendix D-Table D.1: Major and trace element data

	BRANDARIS						
Sample no	**BON 99-108**	**BON 99-111**	**BON 99-112**	**BON 99-114**	**BON 99-144**	**BON 99-145**	**BON 99-146**
Bead	LF13369	LF13370	LF13371	LF13372	LF13382	LF13383	LF13384
Pellet	L34298	L34299	L34300	L34301	L34311	L34312	L34313
Lithology	r	r	r	r	r	r	r
			spherulitic				
majors							
SiO_2	73.17	74.03	71.19	76.78	70.74	71.29	71.51
TiO_2	0.82	0.83	0.80	0.66	0.75	0.76	0.76
Al_2O_3	12.18	12.61	12.26	11.08	12.92	13.05	12.85
Fe_2O_3	4.65	3.87	3.88	2.26	3.81	4.31	4.29
MnO	0.12	0.09	0.11	0.07	0.07	0.06	0.06
MgO	0.96	0.93	1.76	0.31	0.88	0.98	0.93
CaO	0.61	0.36	0.36	0.57	0.41	0.47	0.33
Na_2O	5.60	6.56	6.05	6.75	5.57	5.89	5.79
K_2O	0.97	0.56	0.63	0.08	2.15	1.96	1.76
P_2O_5	0.17	0.17	0.17	0.22	0.13	0.19	0.15
SO_3	0.03	0.03	0.03	0.04	0.04	0.03	0.03
LOI	1.36	1.31	1.71	1.50	1.43	1.23	1.26
traces							
Pb*	5.1	0.7	n.d.	1.2	3.0	n.d.	2.9
Rb*	10.9	4.0	5.8	15.4	12.4	17.1	11.6
Ba*	565.8	249.4	180.1	415.2	644.4	647.0	517.5
Th*	3.1	2.6	3.5	3.1	0.8	3.3	1.9
U*	0.5	n.d.	0.3	1.0	0.5	0.5	1.7
Nb*	2.4	2.7	2.3	2.3	1.9	2.3	2.7
La*	15.8	9.1	10.5	13.7	4.9	6.8	10.4
Ce*	17.3	22.5	9.7	13.4	16.1	20.0	9.3
Sr	43.1	69.4	81.8	52.8	115.8	119.9	78.1
Nd*	21.4	13.0	16.0	18.2	9.1	13.9	20.5
Zr*	118.5	115.4	115.0	115.9	113.5	112.4	110.9
Y*	71.1	52.7	45.1	44.8	22.7	55.7	59.2
Sc	20.4	15.5	17.9	18.6	18.0	21.0	19.6
Co	11.0	8.1	8.2	11.4	8.4	9.9	9.7
V	25.2	23.4	21.1	22.3	12.4	14.4	11.7
Cr	12.8	14.1	42.7	11.8	15.7	16.1	8.8
Cu	n.d.	n.d.	n.d.	1.2	n.d.	n.d.	n.d.
Ga	15.8	14.3	15.1	15.0	14.3	14.8	14.7
Ni	n.d.	n.d.	n.d.	n.d.	n.d.	n.d.	n.d.
Zn	69.2	36.2	36.1	73.6	71.6	72.8	56.4
Hf *					3.50		
Ta	n.a.	n.a.	n.a.	n.a.	0.16	n.a.	n.a.
REE							
La	n.a.	9.12	n.a.	n.a.	4.89	6.78	n.a.
Ce	n.a.	22.53	n.a.	n.a.	16.06	19.96	n.a.
Pr	n.a.	3.05	n.a.	n.a.	1.87	3.01	n.a.
Nd	n.a.	13.04	n.a.	n.a.	9.12	13.93	n.a.
Sm	n.a.	3.87	n.a.	n.a.	2.72	4.16	n.a.
Eu	n.a.	1.47	n.a.	n.a.	0.97	1.31	n.a.
Gd	n.a.	5.74	n.a.	n.a.	3.21	5.37	n.a.
Tb	n.a.	n.a.	n.a.	n.a.	0.60	n.a.	n.a.
Dy	n.a.	6.21	n.a.	n.a.	3.96	5.82	n.a.
Ho	n.a.	n.a.	n.a.	n.a.	0.84	n.a.	n.a.
Er	n.a.	3.73	n.a.	n.a.	2.48	3.20	n.a.
Tm	n.a.	n.a.	n.a.	n.a.	0.39	n.a.	n.a.
Yb	n.a.	3.57	n.a.	n.a.	2.58	3.04	n.a.
Lu	n.a.	0.50	n.a.	n.a.	0.42	0.45	n.a.
Y	n.a.	52.7	n.a.	n.a.	22.7	55.7	n.a.
other data ?		*icp-oes*			*icp-ms*		

* denotes ICP-MS data used where possible

Key:
r rhyodacite — rd rhyodacite dome
d dolerite — b basalt
v volcaniclastic — an andesite
di diorite

Appendix D-Table D.1: Major and trace element data

	BRANDARIS						
Sample no	**BON 99-147**	**BON 99-148**	**BON 99-150**	**BON 99-151**	**BON 99-155**	**BON 99-156**	**BON 99-171**
Bead	LF13385	LF13386	LF13387	LF13388	LF13389	LF13390	LF13396
Pellet	L34314	L34315	L34316	L34317	L34318	L34319	L34325
Lithology	r	r	r	r	r	r	r
	weathered	weathered	weathered	weathered	weathered		
majors							
SiO_2	69.67	71.00	67.64	74.75	72.03	70.95	68.44
TiO_2	0.77	0.76	0.77	0.77	0.75	0.79	0.86
Al_2O_3	13.18	13.27	14.28	12.18	12.12	12.98	14.41
Fe_2O_3	4.02	4.32	5.30	4.25	2.86	4.44	3.63
MnO	0.07	0.07	0.08	0.07	0.07	0.08	0.06
MgO	1.61	1.21	1.64	1.10	0.47	1.67	0.86
CaO	0.39	0.44	0.85	0.35	1.63	0.60	0.39
Na_2O	6.16	5.55	5.77	6.49	4.14	5.23	6.32
K_2O	1.38	1.78	2.51	0.19	1.45	1.94	2.93
P_2O_5	0.20	0.14	0.32	0.17	0.19	0.21	0.22
SO_3	0.04	0.02	0.03	0.04	0.03	0.03	0.04
LOI	1.64	1.52	1.63	1.48	3.08	1.73	1.43
traces							
Pb*	2.5	2.2	0.5	4.7	8.7	2.8	2.1
Rb*	8.9	12.1	23.2	0.7	6.0	18.2	17.4
Ba*	382.2	820.5	1335.4	111.5	198.1	861.4	627.5
Th*	3.7	4.2	5.1	4.5	1.0	2.6	3.1
U*	1.6	0.3	1.0	1.6	0.5	1.0	0.2
Nb*	2.1	2.4	2.6	2.2	1.8	2.3	2.7
La*	10.2	14.7	11.0	7.5	6.0	7.6	9.7
Ce*	8.3	9.0	4.6	6.2	17.7	22.8	6.6
Sr	54.3	83.1	118.3	44.1	49.1	117.5	37.5
Nd*	17.2	23.6	14.1	16.1	11.6	13.5	17.0
Zr*	114.4	113.0	109.0	109.3	106.1	110.8	123.7
Y*	45.4	74.6	32.4	40.1	31.3	42.5	44.8
Sc	20.2	20.3	19.0	19.4	18.1	21.4	17.2
Co	9.6	10.2	13.9	9.2	5.8	11.1	8.2
V	11.6	14.2	60.7	20.2	12.2	16.2	15.1
Cr	37.7	7.2	2.9	47.1	7.9	3.3	22.6
Cu	n.d.	n.d.	1.9	1.9	n.d.	n.d.	n.d.
Ga	17.3	15.1	14.5	13.7	13.3	15.1	14.8
Ni	n.d.	n.d.	n.d.	n.d.	n.d.	n.d.	n.d.
Zn	70.7	84.0	55.0	67.3	63.9	89.7	161.4
Hf *					3.29		
Ta	n.a.	n.a.	n.a.	n.a.	0.16	n.a.	n.a.
REE							
La	n.a.	n.a.	n.a.	n.a.	5.96	7.57	n.a.
Ce	n.a.	n.a.	n.a.	n.a.	17.75	22.80	n.a.
Pr	n.a.	n.a.	n.a.	n.a.	2.42	2.78	n.a.
Nd	n.a.	n.a.	n.a.	n.a.	11.64	13.49	n.a.
Sm	n.a.	n.a.	n.a.	n.a.	3.57	4.25	n.a.
Eu	n.a.	n.a.	n.a.	n.a.	1.23	1.30	n.a.
Gd	n.a.	n.a.	n.a.	n.a.	4.49	4.55	n.a.
Tb	n.a.	n.a.	n.a.	n.a.	0.84	n.a.	n.a.
Dy	n.a.	n.a.	n.a.	n.a.	5.49	5.51	n.a.
Ho	n.a.	n.a.	n.a.	n.a.	1.16	n.a.	n.a.
Er	n.a.	n.a.	n.a.	n.a.	3.46	3.23	n.a.
Tm	n.a.	n.a.	n.a.	n.a.	0.53	n.a.	n.a.
Yb	n.a.	n.a.	n.a.	n.a.	3.47	3.08	n.a.
Lu	n.a.	n.a.	n.a.	n.a.	0.54	0.46	n.a.
Y	n.a.	n.a.	n.a.	n.a.	31.3	42.5	n.a.
other data ?					*icp-ms*	*icp-oes*	

* denotes ICP-MS data used where possible

Key:	
r rhyodacite	rd rhyodacite dome
d dolerite	b basalt
v volcaniclastic	an andesite
di diorite	

	BRANDARIS						
Sample no	**BON 99-173**	**BON 99-174**	**BON 99-175**	**BON 99-176**	**BON 99-184**	**BON 99-185**	**BON 99-148**
Bead	LF13397	LF13398	LF13399	LF13400	LF13405	LF13406	LF13408
Pellet	L34326	L34327	L34328	L34329	L34334	L34335	L34337
Lithology	r	r	r	r	r	r	r
		quartz	zeolites		quartz, epidote		weathered
majors							
SiO_2	77.31	79.89	76.94	70.51	78.09	68.79	51.62
TiO_2	0.67	0.61	0.71	0.81	0.63	0.80	1.11
Al_2O_3	10.87	9.45	11.83	12.27	10.23	12.66	13.85
Fe_2O_3	2.40	2.19	2.45	5.28	2.22	4.56	11.21
MnO	0.08	0.09	0.07	0.09	0.10	0.14	0.14
MgO	0.22	0.21	0.16	1.51	0.34	2.17	4.29
CaO	0.44	0.59	0.68	0.30	0.84	0.40	9.74
Na_2O	5.60	5.63	6.85	5.96	5.04	6.13	3.43
K_2O	1.12	0.47	0.29	1.25	1.09	0.90	0.16
P_2O_5	0.18	0.15	0.22	0.17	0.20	0.21	0.16
SO_3	0.02	0.03	0.07	0.03	0.03	0.04	0.02
LOI	0.55	0.65	0.57	1.51	0.59	2.01	4.59
traces							
Pb*	4.2	1.0	1.9	4.2	2.4	6.7	n.d.
Rb*	5.3	2.8	2.7	12.3	7.6	5.3	2.3
Ba*	364.7	527.8	3786.9	658.8	381.7	300.1	80.0
Th*	0.4	3.1	2.7	4.6	2.4	2.7	2.3
U*	0.6	1.0	0.9	0.9	0.7	n.d.	0.7
Nb*	1.6	1.9	2.0	2.3	2.4	2.4	1.6
La*	2.3	8.1	9.5	9.2	8.1	7.8	4.9
Ce*	11.5	n.d.	n.d.	8.0	3.2	3.7	14.6
Sr	90.3	65.9	90.8	43.3	103.2	67.1	60.1
Nd*	4.7	12.3	9.3	14.7	12.6	13.2	11.5
Zr*	96.7	80.2	89.4	116.7	90.0	102.5	80.8
Y*	18.2	30.5	39.3	43.6	41.9	37.3	26.3
Sc	13.9	13.6	14.7	17.6	16.2	21.7	35.7
Co	3.9	3.2	3.3	13.6	3.0	11.6	40.5
V	18.2	22.2	38.3	27.6	12.7	30.3	345.1
Cr	17.6	18.8	11.5	9.7	10.3	4.8	18.5
Cu	n.d.	n.d.	n.d.	5.9	n.d.	n.d.	36.6
Ga	11.3	8.7	7.9	14.8	10.3	16.2	23.2
Ni	n.d.	n.d.	n.d.	2.7	n.d.	n.d.	25.8
Zn	59.9	62.7	90.2	68.0	78.8	68.1	56.2
Hf *	2.97						
Ta	0.12	n.a.	n.a.	n.a.	n.a.	n.a.	n.a.
REE							
La	2.28	n.a.	n.a.	n.a.	n.a.	n.a.	n.a.
Ce	11.54	n.a.	n.a.	n.a.	n.a.	n.a.	n.a.
Pr	0.96	n.a.	n.a.	n.a.	n.a.	n.a.	n.a.
Nd	4.74	n.a.	n.a.	n.a.	n.a.	n.a.	n.a.
Sm	1.62	n.a.	n.a.	n.a.	n.a.	n.a.	n.a.
Eu	0.67	n.a.	n.a.	n.a.	n.a.	n.a.	n.a.
Gd	2.11	n.a.	n.a.	n.a.	n.a.	n.a.	n.a.
Tb	0.43	n.a.	n.a.	n.a.	n.a.	n.a.	n.a.
Dy	2.82	n.a.	n.a.	n.a.	n.a.	n.a.	n.a.
Ho	0.63	n.a.	n.a.	n.a.	n.a.	n.a.	n.a.
Er	1.93	n.a.	n.a.	n.a.	n.a.	n.a.	n.a.
Tm	0.31	n.a.	n.a.	n.a.	n.a.	n.a.	n.a.
Yb	2.05	n.a.	n.a.	n.a.	n.a.	n.a.	n.a.
Lu	0.31	n.a.	n.a.	n.a.	n.a.	n.a.	n.a.
Y	18.2	n.a.	n.a.	n.a.	n.a.	n.a.	n.a.
other data ?	*icp-ms*						

* denotes ICP-MS data used where possible

Key:	
r rhyodacite	rd rhyodacite dome
d dolerite	b basalt
v volcaniclastic	an andesite
di diorite	

Appendix D-Table D.1: Major and trace element data

	BRANDARIS		SALINA MATHIJS			
Sample no	**BON 99-146B**	**BON 99-108W**	**BON 96-35**	**BON 94-4**	**BON 94-5**	**BON 99-87**
Bead	LF13410	LF13412	LF12790	LF12671	LF12672	LF13364
Pellet	L34339	L34341	L33905	L33720	L33721	L34293
Lithology	r	r	v	d	d	d
		weathered rind		fresh		fresh
majors						
SiO_2	72.82	72.09	67.67	49.70	51.45	49.13
TiO_2	0.79	0.80	0.33	0.68	0.80	0.73
Al_2O_3	12.98	12.09	6.68	18.70	17.25	17.67
Fe_2O_3	4.36	4.61	3.42	10.46	10.79	9.34
MnO	0.06	0.10	0.19	0.16	0.17	0.16
MgO	0.92	0.91	1.49	4.28	4.31	4.49
CaO	0.33	0.56	7.60	8.52	6.33	8.11
Na_2O	5.93	6.15	2.01	4.17	4.84	4.84
K_2O	1.86	1.04	1.84	0.97	2.01	0.63
P_2O_5	0.16	0.19	0.09	0.17	0.16	0.15
SO_3	0.04	0.03	n.a.	n.a.	n.a.	0.03
LOI	1.33	1.19	7.51	2.61	2.68	3.47
traces						
Pb*	2.5	12.7	6.2	2.5	3.2	1.1
Rb*	11.4	10.1	20.8	16.1	27.3	10.7
Ba*	543.4	765.2	298.0	275.6	514.2	300.2
Th*	3.6	2.4	2.0	0.5	n.d.	0.6
U*	1.2	0.8	n.d.	0.1	n.d.	0.2
Nb*	2.2	2.0	2.1	1.6	2.2	1.5
La*	12.5	14.3	7.0	5.3	0.0	5.5
Ce*	12.8	18.2	n.d.	12.4	15.3	12.1
Sr	79.6	61.4	127.9	299.8	258.5	332.3
Nd*	19.5	22.1	12.2	9.3	8.3	8.7
Zr*	112.6	115.9	38.4	51.8	68.5	60.4
Y*	59.1	72.8	30.0	18.5	23.9	19.3
Sc	18.9	19.2	18.4	25.1	24.7	26.4
Co	10.1	10.9	11.6	36.1	35.5	34.5
V	13.7	25.9	88.1	228.7	255.8	218.8
Cr	19.9	24.7	34.4	15.6	14.2	23.2
Cu	n.d.	0.2	67.0	154.4	152.6	51.0
Ga	15.2	15.7	8.0	21.4	20.4	18.3
Ni	0.5	n.d.	20.6	24.7	19.2	24.6
Zn	60.3	61.7	127.4	49.3	68.0	55.5
Hf *				1.22		1.76
Ta	n.a.	n.a.	n.a.	0.18	n.a.	0.42
REE						
La	n.a.	n.a.	n.a.	5.27	n.a.	5.50
Ce	n.a.	n.a.	n.a.	12.45	n.a.	12.12
Pr	n.a.	n.a.	n.a.	1.93	n.a.	1.80
Nd	n.a.	n.a.	n.a.	9.32	n.a.	8.71
Sm	n.a.	n.a.	n.a.	2.58	n.a.	2.48
Eu	n.a.	n.a.	n.a.	1.02	n.a.	0.99
Gd	n.a.	n.a.	n.a.	2.94	n.a.	2.83
Tb	n.a.	n.a.	n.a.	0.52	n.a.	0.52
Dy	n.a.	n.a.	n.a.	3.12	n.a.	3.19
Ho	n.a.	n.a.	n.a.	0.62	n.a.	0.66
Er	n.a.	n.a.	n.a.	1.74	n.a.	1.93
Tm	n.a.	n.a.	n.a.	0.26	n.a.	0.27
Yb	n.a.	n.a.	n.a.	1.60	n.a.	1.81
Lu	n.a.	n.a.	n.a.	0.25	n.a.	0.28
Y	n.a.	n.a.	n.a.	18.5	n.a.	19.3
other data ?				*icp-ms*		*icp-ms*

* denotes ICP-MS data used where possible

Key:	
r rhyodacite	rd rhyodacite dome
d dolerite	b basalt
v volcaniclastic	an andesite
di diorite	

Appendix D-Table D.1: Major and trace element data

	SALINA MATHIJS						
Sample no	**BON 99-170**	**BON 99-178**	**BON 99-196**	**BON00-33**	**BON 99-78**	**BON 99-79**	**BON 99-80**
Bead	LF13395	LF13401	LF13407	LF15005	LF13359	LF13360	LF13361
Pellet	L34324	L34330	L34336	L35817	L34288	L34289	L34290
Lithology	d	d	b	b		di	di
			weathered			clast	clast
majors							
SiO_2	48.07	49.71	48.96	46.22	55.78	51.73	51.94
TiO_2	0.85	0.79	1.11	1.10	1.15	1.10	1.17
Al_2O_3	18.09	17.53	15.69	16.08	16.32	15.67	15.43
Fe_2O_3	10.46	9.97	10.21	11.81	6.77	10.37	11.95
MnO	0.14	0.16	0.20	0.12	0.27	0.14	0.17
MgO	4.89	4.63	5.35	7.13	1.29	4.31	3.92
CaO	9.51	7.78	5.99	7.11	5.85	9.36	10.19
Na_2O	3.81	4.24	5.78	2.07	6.29	4.29	3.06
K_2O	0.96	1.36	0.71	0.37	2.48	1.19	0.56
P_2O_5	0.15	0.17	0.23	0.19	0.23	0.20	0.11
SO_3	0.03	0.06	0.03	n.a.	n.a.	n.a.	n.a.
LOI	3.31	2.58	5.65	6.91	2.92	1.66	1.09
traces							
Pb*	0.6	0.7	0.6	0.5	1.1	n.d.	2.1
Rb*	18.8	21.1	4.9	2.2	27.8	14.6	5.6
Ba*	200.6	345.1	291.4	184.5	1167.3	338.1	257.4
Th*	2.5	2.5	1.1	3.3	2.9	3.4	3.1
U*	n.d.	0.5	0.6	n.d.	n.d.	0.1	0.9
Nb*	1.6	2.1	2.4	2.0	2.0	2.0	0.0
La*	5.1	5.1	6.1	4.6	6.2	4.0	5.6
Ce*	13.9	12.6	15.8	11.9	5.8	12.7	14.7
Sr	417.4	314.2	430.7	170.7	236.0	247.6	385.2
Nd*	9.8	8.7	10.9	9.1	9.0	11.0	10.1
Zr*	46.2	60.2	69.3	59.5	82.7	67.6	46.3
Y*	18.4	21.9	22.1	19.6	28.2	24.4	17.0
Sc	27.8	26.2	47.8	48.1	33.8	43.4	36.5
Co	38.8	36.1	37.0	47.2	19.6	36.1	53.3
V	267.6	224.5	386.9	380.1	358.7	373.8	574.5
Cr	37.5	50.4	54.2	18.7	n.d.	34.6	n.d.
Cu	113.5	107.2	182.7	n.a.	145.2	127.4	116.9
Ga	19.0	19.1	17.8	n.a.	10.1	17.2	18.8
Ni	29.9	25.8	18.1	23.9	5.4	25.8	27.9
Zn	44.0	44.4	76.4	98.9	94.1	73.1	70.3
Hf *							
Ta	n.a.	n.a.	n.a.	n.a.	n.a.	n.a.	n.a.
REE							
La	5.11	5.06	6.13	4.56	n.a.	4.05	5.57
Ce	13.86	12.60	15.76	11.88	n.a.	12.71	14.68
Pr	2.01	1.86	2.26	1.69	n.a.	1.94	2.14
Nd	9.85	8.68	10.89	9.10	n.a.	10.96	10.09
Sm	3.24	2.78	3.51	3.12	n.a.	3.73	3.34
Eu	0.91	0.91	1.10	1.21	n.a.	1.03	1.26
Gd	3.82	2.84	3.41	4.25	n.a.	4.36	4.43
Tb	n.a.	n.a.	n.a.	n.a.	n.a.	n.a.	n.a.
Dy	4.34	3.29	3.98	4.82	n.a.	4.49	4.69
Ho	n.a.	n.a.	n.a.	n.a.	n.a.	n.a.	n.a.
Er	2.46	1.93	2.23	3.12	n.a.	2.61	3.10
Tm	n.a.	n.a.	n.a.	n.a.	n.a.	n.a.	n.a.
Yb	1.98	1.58	1.95	2.63	n.a.	2.12	2.61
Lu	0.28	0.30	0.30	0.39	n.a.	0.29	0.38
Y	18.4	21.9	22.1	19.6	n.a.	24.4	17.0
other data ?	*icp-oes*	*icp-oes*	*icp-oes*	*icp-oes*		*icp-oes*	*icp-oes*

* denotes ICP-MS data used where possible

Key:

r rhyodacite	rd rhyodacite dome
d dolerite	b basalt
v volcaniclastic	an andesite
di diorite	

Appendix D-Table D.1: Major and trace element data

	SALINA MATHIJS		SOUTHERN COMPLEX			
Sample no	**BON 99-81**	**BON 99-84**	**BON 96-19**	**BON 96-20**	**BON 00-09**	**BON00-07**
Bead	LF13362	LF13363	LF12774	LF12775	LF14670	LF14999
Pellet	L34291	L34292	L33889	L33890	L35659	L35811
Lithology	d	d	v	v	v	d
	clast	clast		coarse		
majors						
SiO_2	47.04	49.04	69.25	68.06	71.98	47.72
TiO_2	0.97	1.18	0.61	0.73	0.60	1.52
Al_2O_3	12.26	14.55	12.79	12.83	13.59	15.69
Fe_2O_3	9.48	11.94	5.61	5.63	3.10	8.23
MnO	0.32	0.23	0.09	0.12	0.10	0.22
MgO	2.74	4.80	2.14	2.95	1.07	5.20
CaO	14.51	6.77	0.66	0.67	0.70	16.17
Na_2O	3.69	4.94	3.76	1.62	6.42	4.89
K_2O	1.00	0.24	3.40	5.65	1.55	0.92
P_2O_5	0.21	0.19	0.20	0.22	0.17	0.24
SO_3	n.a.	n.a.	n.a.	n.a.	n.a.	n.a.
LOI	7.92	5.31	2.26	2.19	1.13	9.20
traces						
Pb*	n.d.	1.6	9.2	2.6	4.4	n.d.
Rb*	8.3	2.3	38.1	81.9	11.3	13.5
Ba*	312.1	59.9	1707.3	1617.8	506.9	220.1
Th*	1.4	1.6	3.0	3.1	1.3	4.9
U*	0.7	n.d.	n.d.	n.d.	0.5	n.d.
Nb*	1.5	2.2	2.3	2.2	2.0	3.3
La*	4.4	4.5	7.9	8.5	8.7	6.2
Ce*	10.5	15.1	n.d.	n.d.	19.4	16.5
Sr	200.3	155.5	112.2	47.2	121.0	321.0
Nd*	9.1	7.6	12.8	15.7	15.2	12.5
Zr*	55.2	69.4	94.1	93.0	94.9	120.7
Y*	23.9	22.0	37.3	42.2	31.8	28.9
Sc	37.8	38.7	18.1	18.0	12.3	31.9
Co	33.8	45.4	14.9	14.2	6.6	31.5
V	353.5	399.4	81.4	64.4	22.1	239.0
Cr	19.1	1.4	n.d.	n.d.	14.5	200.3
Cu	193.2	213.4	15.3	14.4	3.8	67.3
Ga	14.2	15.3	13.2	15.1	14.4	14.6
Ni	14.4	12.6	2.2	2.9	n.d.	81.8
Zn	84.2	108.8	79.7	95.2	74.9	57.1
Hf *						
Ta	n.a.	n.a.	n.a.	n.a.	n.a.	n.a.
REE						
La	n.a.	n.a.	n.a.	n.a.	7.32	6.22
Ce	n.a.	n.a.	n.a.	n.a.	17.60	16.50
Pr	n.a.	n.a.	n.a.	n.a.	2.52	2.47
Nd	n.a.	n.a.	n.a.	n.a.	11.88	12.53
Sm	n.a.	n.a.	n.a.	n.a.	3.81	3.86
Eu	n.a.	n.a.	n.a.	n.a.	1.51	1.49
Gd	n.a.	n.a.	n.a.	n.a.	4.54	4.74
Tb	n.a.	n.a.	n.a.	n.a.	n.a.	n.a.
Dy	n.a.	n.a.	n.a.	n.a.	4.94	5.22
Ho	n.a.	n.a.	n.a.	n.a.	n.a.	n.a.
Er	n.a.	n.a.	n.a.	n.a.	2.92	3.23
Tm	n.a.	n.a.	n.a.	n.a.	n.a.	n.a.
Yb	n.a.	n.a.	n.a.	n.a.	2.41	2.44
Lu	n.a.	n.a.	n.a.	n.a.	0.34	0.38
Y	n.a.	n.a.	n.a.	n.a.	31.8	28.9
other data ?					*icp-oes*	*icp-oes*

* denotes ICP-MS data used where possible

Key:
r rhyodacite — rd rhyodacite dome
d dolerite — b basalt
v volcaniclastic — an andesite
di diorite

Appendix D-Table D.1: Major and trace element data

	SOUTHERN COMPLEX						
Sample no	**BON00-32**	**BON00-40**	**BON 99-04**	**BON 99-08**	**BON 99-27**	**BON 99-51**	**BON 99-52**
Bead	LF15004	LF15008	LF13349	LF13350	LF13351	LF13356	LF13357
Pellet	L35816	L35820	L34278	L34279	L34280	L34285	L34286
Lithology	d	d	b	b	b	b	b
			dyke	dyke	dyke		
majors							
SiO_2	48.42	46.88	49.01	48.44	50.59	51.46	48.77
TiO_2	1.02	1.30	0.89	0.85	0.99	1.92	1.07
Al_2O_3	18.51	17.74	18.00	17.83	16.21	16.43	13.99
Fe_2O_3	8.46	8.96	10.51	10.52	11.99	9.50	12.79
MnO	0.13	0.17	0.24	0.24	0.25	0.19	0.21
MgO	5.86	8.02	6.66	8.18	7.14	6.34	3.88
CaO	7.52	6.83	3.87	2.29	1.03	4.77	10.03
Na_2O	5.53	4.15	3.97	5.01	6.07	5.49	3.50
K_2O	1.02	1.18	1.06	1.05	0.32	0.34	0.59
P_2O_5	0.13	0.23	0.11	0.10	0.15	0.23	0.15
SO_3	n.a.	n.a.	0.03	0.03	0.03	0.03	0.03
LOI	4.81	4.96	5.28	6.08	4.87	3.61	4.90
traces							
Pb*	n.d.	n.d.	1.5	n.d.	4.0	n.d.	1.8
Rb*	10.4	9.0	8.6	9.6	3.8	4.1	10.0
Ba*	215.4	792.9	721.8	606.8	247.7	451.9	374.3
Th*	3.1	2.2	2.5	3.4	1.0	1.4	0.7
U*	n.d.	0.1	0.9	1.0	1.2	0.4	0.3
Nb*	3.0	9.4	1.1	0.9	1.9	3.9	1.5
La*	5.3	9.7	4.9	3.8	12.5	8.1	5.3
Ce*	12.6	16.0	9.8	8.8	22.4	17.1	12.3
Sr	280.6	693.0	202.4	147.9	99.8	372.9	407.5
Nd*	7.9	13.1	6.6	6.0	14.6	15.6	9.6
Zr*	63.3	125.6	50.4	42.2	70.5	132.9	60.3
Y*	21.6	28.1	18.3	15.8	21.6	33.5	25.3
Sc	28.8	26.6	45.1	46.7	39.4	34.9	40.5
Co	30.5	35.3	40.4	41.1	44.7	37.7	48.0
V	220.8	182.2	311.0	296.7	318.5	271.9	384.2
Cr	121.9	146.0	46.6	40.2	27.7	193.1	159.9
Cu	n.a.	n.a.	132.2	117.2	156.9	67.7	161.3
Ga	n.a.	n.a.	18.9	16.9	19.7	16.1	17.4
Ni	49.6	90.7	24.8	34.4	24.1	65.6	18.9
Zn	40.9	53.4	66.7	59.8	77.5	67.7	89.5
Hf *					1.98		1.74
Ta	n.a.	n.a.	n.a.	n.a.	0.13	n.a.	0.19
REE							
La	5.32	n.a.	4.91	3.83	12.50	n.a.	5.27
Ce	12.63	n.a.	9.80	8.78	22.39	n.a.	12.28
Pr	1.65	n.a.	1.23	1.35	3.36	n.a.	1.98
Nd	7.87	n.a.	6.60	6.04	14.64	n.a.	9.64
Sm	2.46	n.a.	2.16	2.20	3.72	n.a.	3.02
Eu	0.95	n.a.	0.89	0.70	1.35	n.a.	1.26
Gd	3.03	n.a.	2.85	2.21	4.09	n.a.	3.61
Tb	n.a.	n.a.	n.a.	n.a.	0.70	n.a.	0.67
Dy	3.34	n.a.	3.33	2.74	4.07	n.a.	4.19
Ho	n.a.	n.a.	n.a.	n.a.	0.78	n.a.	0.89
Er	1.61	n.a.	1.88	1.58	2.22	n.a.	2.51
Tm	n.a.	n.a.	n.a.	n.a.	0.32	n.a.	0.38
Yb	1.59	n.a.	1.74	1.48	1.97	n.a.	2.35
Lu	0.22	n.a.	0.26	0.23	0.29	n.a.	0.36
Y	21.6	n.a.	18.3	15.8	21.6	n.a.	25.3
other data ?	*icp-oes*		*icp-oes*	*icp-oes*	*icp-ms*		*icp-ms*

* denotes ICP-MS data used where possible

Key:	
r rhyodacite	rd rhyodacite dome
d dolerite	b basalt
v volcaniclastic	an andesite
di diorite	

Appendix D-Table D.1: Major and trace element data

	SOUTHERN COMPLEX						
Sample no	**BON 00-01**	**BON 00-02**	**BON 00-04**	**BON 00-05**	**BON 00-11**	**BON 00-18**	**BON 00-25**
Bead	LF14752	LF14753	LF14754	LF14755	LF14756	LF14757	LF14758
Pellet	L35750	L35751	L35752	L35753	L35754	L35755	L35756
Lithology	b	b	b	b	b	b	b
	flow		pillow		pillow		calcite
majors							
SiO_2	51.41	48.18	47.59	50.85	42.61	49.85	49.89
TiO_2	1.32	0.96	0.92	1.35	1.69	1.52	1.03
Al_2O_3	15.55	14.05	14.95	15.61	15.73	16.26	15.20
Fe_2O_3	11.47	10.90	13.46	11.66	9.09	8.03	11.44
MnO	0.15	0.21	0.17	0.15	0.14	0.18	0.15
MgO	4.73	3.38	4.73	4.73	4.76	5.51	4.45
CaO	6.53	11.02	8.80	7.68	15.37	8.36	7.73
Na_2O	5.59	4.09	3.65	5.38	2.86	5.52	3.55
K_2O	0.55	0.70	0.33	0.22	0.10	0.41	0.67
P_2O_5	0.17	0.14	0.10	0.16	0.25	0.20	0.15
SO_3	n.a.	n.a.	n.a.	n.a.	n.a.	n.a.	n.a.
LOI	2.60	6.07	5.05	2.94	6.68	4.22	5.53
traces							
Pb*	2.5	1.9	0.9	n.d.	0.9	n.d.	1.7
Rb*	3.8	7.5	3.4	1.1	0.8	4.1	7.1
Ba*	235.8	461.1	186.2	82.5	32.9	419.5	500.2
Th*	0.9	2.8	3.2	3.8	3.3	1.9	2.5
U*	0.3	n.d.	n.d.	n.d.	n.d.	n.d.	n.d.
Nb*	2.9	1.3	1.3	3.2	7.1	3.4	1.6
La*	6.0	5.7	8.1	6.0	7.7	5.7	5.2
Ce*	14.7	13.9	20.0	15.1	21.8	16.0	4.8
Sr	115.7	251.6	235.1	67.5	72.7	338.4	313.1
Nd*	11.5	9.4	10.8	10.8	16.3	12.1	9.1
Zr*	99.5	58.2	40.0	91.2	169.2	112.5	49.7
Y*	26.5	27.3	17.6	27.8	32.3	27.5	23.8
Sc	n.a.	n.a.	n.a.	n.a.	n.a.	n.a.	n.a.
Co	44.4	43.7	56.1	43.8	41.1	32.4	45.0
V							
Cr	72.4	117.7	69.7	8.2	282.4	204.4	n.d.
Cu	95.1	138.9	189.4	68.0	49.7	63.1	107.7
Ga	17.2	15.4	18.2	19.2	20.6	15.8	15.6
Ni	0.3	n.d.	n.d.	n.d.	n.d.	n.d.	n.d.
Zn	71.3	87.5	90.7	59.8	69.9	65.9	79.0
Hf *							
Ta	n.a.	n.a.	n.a.	n.a.	n.a.	n.a.	n.a.
REE							
La	6.33	5.69	8.12	5.96	7.73	5.66	n.a.
Ce	15.86	13.91	19.96	15.11	21.77	16.03	n.a.
Pr	2.20	1.86	2.54	2.17	3.17	2.21	n.a.
Nd	11.17	9.39	10.76	10.81	16.25	12.10	n.a.
Sm	3.61	3.14	3.45	3.30	5.00	3.73	n.a.
Eu	1.44	1.20	1.30	1.36	1.78	1.44	n.a.
Gd	4.82	3.82	4.30	4.40	5.58	4.50	n.a.
Tb	n.a.	n.a.	n.a.	n.a.	n.a.	n.a.	n.a.
Dy	4.58	4.34	4.64	4.11	5.12	4.56	n.a.
Ho	n.a.	n.a.	n.a.	n.a.	n.a.	n.a.	n.a.
Er	2.67	2.74	2.57	2.33	3.14	2.72	n.a.
Tm	n.a.	n.a.	n.a.	n.a.	n.a.	n.a.	n.a.
Yb	2.65	2.42	1.94	2.41	3.21	2.43	n.a.
Lu	0.43	0.38	0.31	0.36	0.48	0.36	n.a.
Y	26.5	27.3	17.6	27.8	32.3	27.5	n.a.
other data ?	*icp-oes*	*icp-oes*	*icp-oes*	*icp-oes*	*icp-oes*	*icp-oes*	

* denotes ICP-MS data used where possible

Key:	
r rhyodacite	rd rhyodacite dome
d dolerite	b basalt
v volcaniclastic	an andesite
di diorite	

Appendix D-Table D.1: Major and trace element data

	SOUTHERN COMPLEX						
Sample no	**BON00-26**	**BON00-28**	**BON00-34**	**BON00-41**	**BON00-64**	**BON 94-21**	**BON 94-23**
Bead	LF15002	LF14759	LF14760	LF14761	LF15021	LF12686	LF12688
Pellet	L35814	L35757	L35758	L35759	L35833	L33735	L33737
Lithology	b	b	b	b	b	rd	r
			fresh		calcite	quartz	
majors							
SiO_2	51.88	48.63	49.79	52.51	42.47	71.58	71.29
TiO_2	1.14	0.71	1.19	1.16	1.15	0.50	0.51
Al_2O_3	14.76	11.82	14.96	14.48	13.73	15.04	14.65
Fe_2O_3	11.17	6.59	13.14	11.95	5.77	3.61	3.86
MnO	0.12	0.09	0.16	0.14	0.15	0.05	0.07
MgO	4.85	3.12	4.66	5.01	4.34	0.46	0.54
CaO	6.07	13.11	6.91	4.56	16.29	0.40	0.80
Na_2O	3.60	5.28	5.37	5.10	4.29	7.69	8.44
K_2O	1.03	0.32	0.39	0.23	1.08	1.23	0.25
P_2O_5	0.16	0.20	0.11	0.16	0.20	0.11	0.13
SO_3	n.a.	n.a.	n.a.	n.a.	n.a.	n.a.	n.a.
LOI	4.06	10.75	2.71	3.71	11.24	1.11	0.93
traces							
Pb*	1.3	n.d.	2.7	1.1	n.d.	0.0	14.3
Rb*	10.4	3.9	2.6	2.5	9.0	8.8	1.6
Ba*	669.5	74.4	109.8	108.7	825.0	941.4	106.9
Th*	2.2	3.8	0.5	2.8	3.5	1.7	1.8
U*	n.d.	n.d.	0.2	n.d.	0.9	n.d.	n.d.
Nb*	1.9	1.7	1.0	1.7	4.3	7.5	8.0
La*	5.3	4.7	3.7	5.3	8.1	14.9	16.3
Ce*	15.6	10.1	9.1	12.9	3.3	19.5	39.5
Sr	307.0	118.3	70.3	92.1	301.1	103.3	93.9
Nd*	9.1	6.7	7.6	8.8	9.1	25.0	25.0
Zr*	74.1	43.1	56.9	81.9	102.6	272.5	272.1
Y*	26.8	12.5	20.3	28.6	25.4	55.2	52.0
Sc	38.8	n.a.	n.a.	n.a.	29.5	10.8	12.2
Co	42.1	24.0	50.7	47.6	26.1	6.8	7.2
V	342.4				227.0	13.3	25.9
Cr	165.7	109.3	n.d.	17.0	237.0	112.2	8.7
Cu	n.a.	23.8	270.1	205.2	n.a.	6.4	9.4
Ga	n.a.	9.5	18.2	19.7	n.a.	20.4	20.2
Ni	19.7	n.d.	n.d.	n.d.	146.1	3.7	2.4
Zn	109.3	46.1	85.9	77.8	62.8	58.2	86.4
Hf *							
Ta	n.a.	n.a.	n.a.	n.a.	n.a.	n.a.	n.a.
REE							
La	n.a.	4.67	3.76	5.27	n.a.	n.a.	16.31
Ce	n.a.	10.08	8.91	12.86	n.a.	n.a.	39.47
Pr	n.a.	1.37	1.27	1.75	n.a.	n.a.	5.00
Nd	n.a.	6.74	6.67	8.85	n.a.	n.a.	25.04
Sm	n.a.	2.13	2.20	2.84	n.a.	n.a.	6.16
Eu	n.a.	0.77	0.94	1.01	n.a.	n.a.	1.83
Gd	n.a.	2.20	2.83	3.69	n.a.	n.a.	5.78
Tb	n.a.	n.a.	n.a.	n.a.	n.a.	n.a.	n.a.
Dy	n.a.	2.43	3.28	4.22	n.a.	n.a.	6.58
Ho	n.a.	n.a.	n.a.	n.a.	n.a.	n.a.	n.a.
Er	n.a.	1.53	1.64	2.41	n.a.	n.a.	3.73
Tm	n.a.	n.a.	n.a.	n.a.	n.a.	n.a.	n.a.
Yb	n.a.	1.29	1.23	1.94	n.a.	n.a.	3.60
Lu	n.a.	0.19	0.17	0.28	n.a.	n.a.	0.53
Y	n.a.	12.5	20.3	28.6	n.a.	n.a.	52.0
other data ?		*icp-oes*	*icp-oes*	*icp-oes*			*icp-oes*

* denotes ICP-MS data used where possible

Key:	
r rhyodacite	rd rhyodacite dome
d dolerite	b basalt
v volcaniclastic	an andesite
di diorite	

	SOUTHERN COMPLEX						
Sample no	**BON 94-24**	**BON 96-26**	**BON 96-27**	**BON 96-28**	**BON 96-29**	**BON 99-42**	**BON 99-50**
Bead	LF12689	LF12781	LF12782	LF12783	LF12784	LF13353	LF13355
Pellet	L33738	L33896	L33897	L33898	L33899	L34282	L34284
Lithology	rd	rd	rd	rd	rd	rd	rd
				quartz	quartz		
majors							
SiO_2	69.87	72.34	72.37	71.15	72.48	77.97	70.03
TiO_2	0.53	0.53	0.54	0.54	0.52	0.57	0.60
Al_2O_3	15.19	14.01	14.31	14.60	14.08	11.59	14.21
Fe_2O_3	3.94	3.87	3.78	4.02	3.39	2.35	4.26
MnO	0.08	0.08	0.05	0.08	0.05	0.06	0.09
MgO	0.85	0.89	0.89	0.96	1.10	0.17	0.75
CaO	0.99	0.63	0.41	0.77	0.42	0.25	0.76
Na_2O	7.86	7.75	7.17	7.11	7.70	6.98	7.76
K_2O	1.02	0.14	0.93	1.15	0.27	0.16	0.73
P_2O_5	0.14	0.12	0.13	0.12	0.12	0.10	0.15
SO_3	n.a.	n.a.	n.a.	n.a.	n.a.	0.03	0.03
LOI	1.07	0.97	1.07	1.02	1.11	0.51	1.23
traces							
Pb*	1.7	n.d.	0.8	n.d.	0.8	3.7	n.d.
Rb*	8.5	0.0	6.1	10.3	0.2	1.8	5.5
Ba*	220.8	25.9	155.6	373.6	12.6	38.1	150.6
Th*	2.8	4.2	2.2	4.1	0.6	1.3	3.0
U*	n.d.	n.d.	0.7	n.d.	0.6	0.5	0.3
Nb*	8.0	8.1	7.5	8.7	7.8	6.1	8.3
La*	16.1	15.8	11.0	16.7	6.7	12.9	15.5
Ce*	32.8	27.5	22.4	28.3	24.8	32.0	35.8
Sr	74.8	57.3	98.7	107.8	73.1	39.0	108.1
Nd*	26.4	26.9	20.1	26.9	12.3	20.1	19.7
Zr*	276.8	277.2	276.4	290.6	288.6	219.6	293.9
Y*	54.1	57.4	34.5	57.8	25.3	38.0	65.0
Sc	11.2	10.1	12.3	10.6	9.9	9.0	12.7
Co	7.2	7.3	7.6	7.9	6.5	3.9	8.7
V	11.9	10.3	17.2	10.1	15.3	21.4	15.7
Cr	13.5	8.8	7.4	9.2	7.0	5.2	19.8
Cu	2.5	n.d.	n.d.	n.d.	n.d.	n.d.	n.d.
Ga	19.5	18.2	17.0	17.4	18.6	12.7	19.3
Ni	1.9	n.d.	n.d.	n.d.	n.d.	1.2	n.d.
Zn	61.4	47.7	60.4	59.6	50.2	37.9	45.9
Hf *					7.01	5.27	
Ta	n.a.	n.a.	n.a.	n.a.	0.57	0.42	n.a.
REE							
La	n.a.	n.a.	10.06	n.a.	6.70	12.89	15.53
Ce	n.a.	n.a.	22.80	n.a.	24.76	32.05	35.80
Pr	n.a.	n.a.	3.27	n.a.	2.68	4.51	4.23
Nd	n.a.	n.a.	15.59	n.a.	12.27	20.12	19.68
Sm	n.a.	n.a.	5.24	n.a.	3.30	5.19	5.84
Eu	n.a.	n.a.	1.70	n.a.	0.94	1.57	2.05
Gd	n.a.	n.a.	4.50	n.a.	3.76	5.77	6.84
Tb	n.a.	n.a.	n.a.	n.a.	0.69	1.06	n.a.
Dy	n.a.	n.a.	4.83	n.a.	4.36	6.46	7.24
Ho	n.a.	n.a.	n.a.	n.a.	0.91	1.30	n.a.
Er	n.a.	n.a.	2.82	n.a.	2.72	3.93	3.27
Tm	n.a.	n.a.	n.a.	n.a.	0.42	0.56	n.a.
Yb	n.a.	n.a.	2.91	n.a.	2.86	3.66	3.65
Lu	n.a.	n.a.	0.46	n.a.	0.44	0.56	0.49
Y	n.a.	n.a.	34.5	n.a.	25.3	38.0	65.0
other data ?			*icp-oes*		*icp-ms*	*icp-ms*	*icp-oes*

* denotes ICP-MS data used where possible

Key:	
r rhyodacite	rd rhyodacite dome
d dolerite	b basalt
v volcaniclastic	an andesite
di diorite	

	SOUTHERN COMPLEX						
Sample no	**BON00-12**	**BON 00-015**	**BON 00-015w**	**BON 00-019**	**BON 00-020**	**BON00-23**	**BON00-29**
Bead	LF15000	LF14671	LF14672	LF14673	LF14674	LF15001	LF15003
Pellet	L35812	L35660	L35661	L35662	L35663	L35813	L35815
Lithology	rd	rd	rd	rd	rd	rd	rd
majors							
SiO_2	74.27	71.17	70.47	68.71	70.63	58.95	70.16
TiO_2	0.54	0.58	0.59	0.60	0.63	1.38	0.59
Al_2O_3	13.54	14.46	14.42	14.82	15.24	16.62	14.67
Fe_2O_3	3.24	3.97	4.03	4.30	4.14	7.38	4.10
MnO	0.04	0.06	0.07	0.09	0.03	0.16	0.07
MgO	0.07	0.50	0.50	0.78	0.52	3.00	0.91
CaO	0.25	0.35	0.36	1.52	0.15	2.49	0.84
Na_2O	7.28	7.46	7.50	6.90	7.44	7.43	7.88
K_2O	0.99	0.96	0.87	1.42	0.97	0.97	0.60
P_2O_5	0.10	0.08	0.08	0.13	0.05	0.40	0.13
SO_3	n.a.	n.a.	n.a.	n.a.	n.a.	n.a.	n.a.
LOI	0.59	0.93	1.08	1.02	1.36	2.55	1.08
traces							
Pb*	0.1	n.d.	n.d.	n.d.	0.8	n.d.	n.d.
Rb*	7.2	6.4	6.5	12.5	6.7	7.2	3.0
Ba*	163.1	122.5	99.9	379.9	169.2	284.0	110.1
Th*	3.9	5.1	4.3	3.8	6.1	2.8	4.2
U*	0.8	0.9	0.3	0.1	1.2	0.8	0.7
Nb*	7.3	8.3	8.2	8.4	8.2	6.7	8.0
La*	8.5	12.4	16.0	18.8	17.4	10.5	10.7
Ce*	22.1	29.1	27.2	46.1	47.4	25.4	27.2
Sr	61.1	81.2	94.2	188.6	84.1	151.5	72.5
Nd*	15.2	18.5	25.9	25.2	27.7	16.7	16.1
Zr*	262.6	289.6	287.6	295.5	301.8	210.2	285.9
Y*	52.1	63.5	64.1	65.8	64.1	50.1	56.6
Sc	9.6	12.5	11.0	13.2	11.8	20.8	12.0
Co	4.8	8.0	7.6	8.9	8.0	21.1	7.9
V	16.4	11.7	9.2	9.8	9.4	88.4	9.9
Cr	4.8	48.3	25.8	21.5	5.2	87.1	2.2
Cu	n.a.	0.9	n.d.	n.d.	n.d.	4.7	n.a.
Ga	n.a.	17.6	17.3	19.0	19.8	19.4	n.a.
Ni	0.1	0.0	n.d.	n.d.	n.d.	1.2	n.d.
Zn	54.7	65.4	65.3	59.2	69.7	86.2	47.0
Hf *							
Ta	n.a.	n.a.	n.a.	n.a.	n.a.	n.a.	n.a.
REE							
La	8.49	12.37	n.a.	18.81	17.40	10.49	10.74
Ce	22.09	29.14	n.a.	46.11	47.39	25.36	27.15
Pr	3.17	3.76	n.a.	5.68	6.08	3.50	3.60
Nd	15.17	18.53	n.a.	25.17	27.66	16.67	16.07
Sm	3.80	5.42	n.a.	7.46	7.25	5.20	4.77
Eu	1.29	1.84	n.a.	2.40	2.28	1.84	1.57
Gd	4.34	6.07	n.a.	7.77	6.64	6.02	5.22
Tb	n.a.	n.a.	n.a.	n.a.	n.a.	n.a.	n.a.
Dy	3.70	6.05	n.a.	7.79	5.78	5.72	5.50
Ho	n.a.	n.a.	n.a.	n.a.	n.a.	n.a.	n.a.
Er	2.12	3.53	n.a.	4.67	3.11	2.69	3.18
Tm	n.a.	n.a.	n.a.	n.a.	n.a.	n.a.	n.a.
Yb	1.99	3.14	n.a.	4.37	2.64	1.89	2.56
Lu	0.31	0.47	n.a.	0.64	0.36	0.22	0.34
Y	52.1	63.5	n.a.	65.8	64.1	50.1	56.6
other data ?	*icp-oes*	*icp-oes*		*icp-oes*	*icp-oes*	*icp-oes*	*icp-oes*

* denotes ICP-MS data used where possible

Key:	
r rhyodacite	rd rhyodacite dome
d dolerite	b basalt
v volcaniclastic	an andesite
di diorite	

	SOUTHERN COMPLEX						
Sample no	**BON00-49B**	**BON00-50B**	**BON00-51**	**BON00-52**	**BON 94-22**	**BON 96-22**	**BON 96-24**
Bead	LF15014	LF15016	LF15017	LF15018	LF12687	LF12777	LF12779
Pellet	L35826	L35828	L35829	L35830	L33736	L33892	L33894
Lithology	rd	rd	rd	rd	r	r	r quartz
majors							
SiO_2	71.00	69.45	69.56	69.31	73.74	79.04	79.20
TiO_2	0.58	0.60	0.58	0.58	0.50	0.37	0.56
Al_2O_3	14.55	15.06	14.68	15.02	10.90	9.75	10.76
Fe_2O_3	3.76	4.52	3.90	4.06	1.94	3.29	2.03
MnO	0.05	0.05	0.05	0.08	0.05	0.03	0.05
MgO	0.54	0.61	1.10	0.87	0.10	0.85	0.12
CaO	0.45	0.54	0.45	1.40	0.58	0.33	0.59
Na_2O	7.21	6.64	7.44	7.46	6.62	4.84	4.71
K_2O	1.51	2.29	1.28	1.42	0.19	0.71	1.87
P_2O_5	0.13	0.14	0.13	0.13	0.10	0.04	0.17
SO_3	n.a.	n.a.	n.a.	n.a.	n.a.	n.a.	n.a.
LOI	1.06	1.12	1.08	1.27	0.52	1.58	0.51
traces							
Pb*	n.d.	n.d.	n.d.	1.7	12.1	6.0	n.d.
Rb*	11.7	19.5	10.0	13.0	n.d.	5.7	10.6
Ba*	375.1	593.8	314.4	324.4	102.5	190.0	948.9
Th*	5.3	4.2	4.3	2.4	1.3	1.3	2.3
U*	0.9	0.6	0.6	0.8	n.d.	1.2	0.0
Nb*	8.2	8.2	8.1	8.6	2.6	2.0	1.8
La*	18.2	24.5	10.2	17.6	10.7	7.5	6.6
Ce*	44.4	39.9	25.3	41.8	12.3	17.3	n.d.
Sr	84.5	188.7	108.1	93.7	86.7	55.9	95.8
Nd*	26.8	35.7	14.1	29.4	17.7	10.8	13.4
Zr*	283.6	294.1	288.3	326.9	112.1	106.5	87.3
Y*	68.9	70.4	50.9	54.0	35.5	23.8	39.9
Sc	10.5	10.4	12.4	11.1	10.2	11.3	16.1
Co	6.8	9.1	8.1	7.4	3.2	8.3	2.9
V	8.3	9.0	14.9	9.4	7.7	95.0	11.4
Cr	27.3	5.6	28.5	19.6	7.3	25.7	6.5
Cu	n.a.	n.a.	n.a.	n.a.	1.1	45.2	n.d.
Ga	n.a.	n.a.	n.a.	n.a.	14.4	8.7	11.7
Ni	n.d.	n.d.	0.1	n.d.	1.8	8.9	n.d.
Zn	67.1	50.9	48.7	54.3	84.3	68.7	60.9
Hf *						3.26	
Ta	n.a.	n.a.	n.a.	n.a.	n.a.	0.18	n.a.
REE							
La	18.20	n.a.	10.18	14.37	n.a.	7.54	n.a.
Ce	44.39	n.a.	25.25	35.94	n.a.	17.27	n.a.
Pr	6.18	n.a.	3.08	4.83	n.a.	2.39	n.a.
Nd	26.78	n.a.	14.09	22.48	n.a.	10.79	n.a.
Sm	7.02	n.a.	3.86	5.95	n.a.	2.93	n.a.
Eu	1.99	n.a.	1.25	2.06	n.a.	0.78	n.a.
Gd	6.12	n.a.	3.98	6.68	n.a.	3.31	n.a.
Tb	n.a.	n.a.	n.a.	n.a.	n.a.	0.62	n.a.
Dy	5.75	n.a.	3.93	5.99	n.a.	4.08	n.a.
Ho	n.a.	n.a.	n.a.	n.a.	n.a.	0.86	n.a.
Er	3.30	n.a.	2.12	3.58	n.a.	2.55	n.a.
Tm	n.a.	n.a.	n.a.	n.a.	n.a.	0.41	n.a.
Yb	3.07	n.a.	1.58	3.63	n.a.	2.69	n.a.
Lu	0.43	n.a.	0.21	0.56	n.a.	0.42	n.a.
Y	68.9	n.a.	50.9	54.0	n.a.	23.8	n.a.
other data ?	*icp-oes*		*icp-oes*	*icp-oes*		*icp-ms*	

* denotes ICP-MS data used where possible

Key:	
r rhyodacite	rd rhyodacite dome
d dolerite	b basalt
v volcaniclastic	an andesite
di diorite	

	SOUTHERN COMPLEX						
Sample no	**BON 99-35**	**BON 99-45**	**BON00-38**	**BON00-39**	**BON00-50**	**BON00-65**	**BON00-67**
Bead	LF13352	LF13354	LF15006	LF15007	LF15015	LF15022	LF15023
Pellet	L34281	L34283	L35818	L35819	L35827	L35834	L35835
Lithology	r	r	r	r	r	r	r
	clast		quartz				
majors							
SiO_2	78.54	73.00	77.64	69.49	69.33	71.07	71.37
TiO_2	0.64	0.82	0.64	0.81	0.74	0.73	0.76
Al_2O_3	10.61	12.69	11.24	13.31	13.52	13.35	13.76
Fe_2O_3	1.99	4.73	2.49	5.27	4.82	4.67	5.05
MnO	0.07	0.07	0.11	0.12	0.07	0.09	0.08
MgO	0.23	0.95	0.13	2.06	1.10	0.91	1.01
CaO	0.81	0.17	0.97	0.45	0.40	0.53	0.38
Na_2O	6.28	5.63	6.35	5.98	5.41	6.04	6.67
K_2O	0.11	2.09	0.09	1.38	2.55	2.18	1.16
P_2O_5	0.32	0.14	0.18	0.23	0.23	0.27	0.19
SO_3	0.03	0.04	n.a.	n.a.	n.a.	n.a.	n.a.
LOI	0.52	0.82	0.50	1.67	1.52	1.17	1.24
traces							
Pb*	4.0	n.d.	2.7	n.d.	1.4	n.d.	3.8
Rb*	0.9	0.5	n.d.	10.9	22.9	16.7	9.2
Ba*	54.8	253.6	85.0	465.2	601.3	534.4	265.6
Th*	0.8	2.6	3.6	2.9	3.1	4.7	1.4
U*	1.2	0.1	0.1	0.4	0.6	0.7	0.6
Nb*	1.6	2.3	1.8	2.2	2.2	2.3	2.0
La*	7.1	12.7	7.2	6.1	7.1	8.1	8.6
Ce*	17.7	29.0	21.2	13.9	2.8	19.3	21.7
Sr	79.3	57.3	120.0	69.5	62.4	66.4	73.6
Nd*	12.1	15.3	16.4	10.5	13.4	13.8	18.5
Zr*	92.6	96.1	92.5	101.5	108.6	105.5	109.0
Y*	37.0	46.5	35.2	39.5	36.4	48.3	44.9
Sc	16.1	16.9	15.7	21.4	18.6	18.9	22.2
Co	3.2	3.9	4.3	12.0	9.8	9.5	10.9
V	17.9	20.0	7.8	16.3	11.9	11.6	8.9
Cr	8.6	16.9	11.6	3.6	2.9	9.9	n.d.
Cu	n.d.	n.d.	n.a.	n.a.	n.a.	n.a.	n.a.
Ga	10.9	11.9	n.a.	n.a.	n.a.	n.a.	n.a.
Ni	n.d.	n.d.	n.d.	n.d.	n.d.	n.d.	n.d.
Zn	72.6	71.8	77.1	73.3	89.6	71.4	71.7
Hf *	2.91						
Ta	0.13	n.a.	n.a.	n.a.	n.a.	n.a.	n.a.
REE							
La	7.05	12.73	7.21	6.12	n.a.	8.09	7.86
Ce	17.65	28.95	21.15	13.95	n.a.	19.29	20.32
Pr	2.51	3.58	3.06	1.91	n.a.	2.77	2.74
Nd	12.14	15.30	16.40	10.50	n.a.	13.80	13.86
Sm	3.71	5.01	4.88	3.40	n.a.	4.31	4.20
Eu	1.19	1.52	1.24	1.21	n.a.	1.48	1.21
Gd	4.37	4.75	4.59	4.27	n.a.	5.40	4.11
Tb	0.83	n.a.	n.a.	n.a.	n.a.	n.a.	n.a.
Dy	5.42	5.48	4.91	4.94	n.a.	5.44	4.34
Ho	1.23	n.a.	n.a.	n.a.	n.a.	n.a.	n.a.
Er	3.67	2.89	3.08	2.85	n.a.	3.37	2.61
Tm	0.57	n.a.	n.a.	n.a.	n.a.	n.a.	n.a.
Yb	3.83	2.78	2.40	2.88	n.a.	3.60	2.71
Lu	0.60	0.41	0.39	0.42	n.a.	0.53	0.42
Y	37.0	46.5	35.2	39.5	n.a.	48.3	44.9
other data ?	*icp-ms*	*icp-oes*	*icp-oes*	*icp-oes*		*icp-oes*	*icp-oes*

* denotes ICP-MS data used where possible

Key:	
r rhyodacite	rd rhyodacite dome
d dolerite	b basalt
v volcaniclastic	an andesite
di diorite	

Appendix D-Table D.1: Major and trace element data

	SOUTHERN COMPLEX
Sample no	**BON00-68**
Bead	LF15024
Pellet	L35836
Lithology	r weathered
majors	
SiO_2	75.36
TiO_2	0.68
Al_2O_3	12.27
Fe_2O_3	3.02
MnO	0.06
MgO	0.45
CaO	0.31
Na_2O	5.89
K_2O	1.27
P_2O_5	0.12
SO_3	n.a.
LOI	0.90
traces	
Pb*	0.6
Rb*	8.2
Ba*	437.0
Th*	3.7
U*	0.1
Nb*	2.1
La*	7.0
Ce*	18.3
Sr	80.5
Nd*	11.9
Zr*	100.3
Y*	40.8
Sc	18.7
Co	6.1
V	9.6
Cr	5.2
Cu	n.a.
Ga	n.a.
Ni	n.d.
Zn	95.1
Hf *	
Ta	n.a.
REE	
La	6.96
Ce	18.32
Pr	2.54
Nd	11.91
Sm	3.52
Eu	0.96
Gd	3.51
Tb	n.a.
Dy	3.21
Ho	n.a.
Er	1.81
Tm	n.a.
Yb	1.91
Lu	0.27
Y	40.8
other data ?	*icp-oes*

* denotes ICP-MS data used where possible

Key:	
r rhyodacite	rd rhyodacite dome
d dolerite	b basalt
v volcaniclastic	an andesite
di diorite	

Appendix E

Radiogenic isotope analysis

E.1. Pb, Nd and Sr isotopic analysis

E.1.1. Sample selection and preparation

Care was taken in sample selection to choose the most unaltered samples representative of each lithological type. These are summarised in Table E.1. Samples were crushed to a fine powder in a tungsten carbide mill at the University of Leicester, in order to avoid potential Pb contamination induced by the agate mill. Samples were then prepared for isotope analysis at National Isotope Geosciences Laboratory under the supervision of Dr Pamela Kempton. Full details of the procedures followed are found in Kempton, 1995 and Royse et al., 1998. Samples were not acid leached prior to dissolution. This was decided as the rocks of the Bonaire Washikemba Formation have experienced such a high degree of alteration (Chapter 3 and Section 5.3). Acid leaching serves to remove secondary phases in slightly altered rocks, in order that the primary igneous phases remain. However, in the case of the Washikemba Formation, secondary phases comprise most of the mineralogy (Chapter 3), and therefore acid leaching may remove material containing original isotope ratios. Hence, the unleached powders were utilised for sample digestion. The results of this study are presented in Tables E.2 to E.6.

Sample number	Rock type	Region	Detail	Isotopes analysed
BON 96-22	Fine-grained volcaniclastic	Southern Complex		Pb, Sr, Hf, Nd
BON 96-27	Rhyodacite	Southern Complex	Dome	Pb, Sr, Hf, Nd
BON 96-29	Rhyodacite	Southern Complex	Dome	Pb, Sr, Hf, Nd
BON 99-27	Basalt	Southern Complex	Dyke	Pb, Sr, Hf, Nd
BON 99-35	Rhyodacite	Southern Complex		Pb, Sr, Hf, Nd
BON 99-87	Dolerite	Northern Complex	Salina Mathijs	Pb, Sr, Hf, Nd
BON 99-104	Microdiorite	Northern Complex	Gotomeer	Pb, Sr, Hf, Nd
BON 99-144	Rhyodacite	Northern Complex	Seru Mangel	Pb, Sr, Hf, Nd
BON 00-01	Basalt	Southern Complex	Pillow	Pb, Sr, Hf, Nd
BON 99-180	Rhyodacite	Northern Complex	Wecua	Pb, Sr, Hf, Nd
BON 99-182	Dolerite	Northern Complex	Salina Mathijs	Hf, Nd
BON 99-173	Rhyodacite	Northern Complex	Brandaris	Hf, Nd
BON 00-52	Rhyodacite	Southern Complex	Dome	Hf, Nd
BON 00-34	Basalt	Southern Complex		Hf, Nd
BON 00-67	Rhyodacite	Southern Complex	Flow	Hf, Nd

Table E.1. Summary of lithologies selected for isotope analysis.

E.1.2. **Dissolution chemistry**

Approximately 150–200 mg of powder was accurately weighed into a clean Savillex© beaker. The amount of sample weighed was dependent on the Pb content of the sample. Approximately 0.5 ml of 16M TD HNO_3 and 2 mls of TD 29M HF were then added to the beakers, which were left on a hotplate over a weekend. After this interval, the lids were removed from the beakers, and the HF-HNO_3 sample solution was evaporated to near dryness on the hotplate. A further 2–3 mls of TD 6M HCl were added, the beakers sealed, and returned to the hotplate for 30 minutes. The samples which had then dissolved were evaporated to dryness, and for those which hadn't, the final acid procedure was repeated, adding the acid in 1 ml volumes, until complete dissolution was achieved. Finally, 1M HBr was then added to the dried and dissolved sample residue, and the beakers were left cold overnight.

E.1.3. **Pb separation**

Chemical separation of Pb was done in columns made of 1 ml polypropylene pipette tips with a porous (35 microns) polyethylene frit in the tip. Prior to use, the columns were cleaned with QD 6M HCl, followed by H_2O, and 15–25 μl of resin was then added to the column. The resin was washed following the same procedure as for the columns, and then was preconditioned with 0.5CV 1M HBr.

Sample was transferred to the column by pipette. Prior to transferring the sample, the pipette tip was cleaned by drawing up and discarding 1 ml of HBr. Once the samples were transferred onto the columns, the dissolution beakers were rinsed with Milli-Q H_2O, filled with TD 6M HCl, sealed and left standing on the hotplate until needed later to collect the Pb fraction from the columns. The samples were then eluted with 0.5 ml of 1M HBr, followed by 1 ml of 1 M HBr, and the elution repeated before the Pb fraction was collected by adding 1CV of TD 6M HCl to the column. This column procedure was then repeated, and the final product collected in cleaned 1 ml Savillex© beakers. 3μl of 1M phosphoric acid was then added to the collection beakers, in order to make the Pb fraction easier to load onto the filaments.

E.1.4. **Sr and Nd chemical separation**

The eluent from the first pass on the Pb columns was collected in cleaned Savillex© beakers, together with any undissolved material remaining in the dissolution beakers. Excess bromine was removed from the collected material by adding several drops of HNO_3 to the beaker. The sample was then dried down on a hotplate in a fume cupboard before 2 mls of 2.5M HCl was added and left overnight to dissolve. The sample was then centrifuged for 5 minutes at 3000 rpm.

Sr columns were preconditioned using HCl, before the centrifuged sample transferred. After this had completely drained through the resin, 3 stages of 1 ml of 2.5M HCl were eluted, then the Sr was collected under 10 ml of 2.5M HCl. Following Sr collection, 9 ml of 6M HCl was eluted, and the REE collected under 11 ml of the same acid. Both the collected Sr and REE fractions were then evaporated to dryness.

Nd was separated from the REE using HCl preconditioned REE columns. The REE collected fraction was carefully loaded, then the columns were washed with 3 stages of 1 ml of 0.25M HCl, then the Nd was collected in 4 mls of 0.3M HCl. 2μl of chlorophosphonazo III was added to the collected Nd before being evaporated to dryness, prior to analysis.

E.1.5. **Sample loading**

Sr was loaded onto an out-gassed single-Ta filament, and Nd onto an outgassed double-Ta filament. Pb was loaded in class 100 HEPA-filtered cupboards using the silica gel method onto a single rhenium filament (Akishin et al., 1957; Cameron et al., 1969).

E.1.6. **Mass spectrometric analysis**

Analysis of Sr, Nd and Pb isotopes were carried out using a Finnegan MAT 262 Thermal Ionisation Mass Spectrometer (TIMS) in static mode, and are presented in Table E. 2 (Pb), Tables E.4 and E.5 (Sr), and Table E.6 (Nd). In addition, a dual run of Pb was analysed on the VG P54 Plasma Ionisation Mass Multi-collector Spectrometer (PIMMS), in order to provide a statistical test of the PIMMS machine's capabilities. These are presented Table E.3, and are statistically compared below.

E.1.7. **Blanks and reference materials**

Blanks and reference materials used are detailed in the appropriate sections in Tables E.2 to E.6.

E.1.8. **A comparison of Pb isotope analysis by PIMMS and TIMMS**

The results obtained by TIMS and PIMMS are compared in Table E.8. TIMS is a better established method of obtaining Pb data at NIGL, but PIMMS can yield better results, providing the machine conditions are favourable. Analysing the Washikemba Formation samples by two different methods will help to establish the PIMMS method of Pb isotope analysis at NIGL.

It is clear from Table E.8 that in general there is an excellent correlation between the results obtained from both techniques, with the difference between Pb isotopic ratios for the techniques typically being about 0.01. One notable exception stands out: BON 96-29 yields significantly higher Pb isotopic ratios for TIMS than PIMMS (about 0.4 for $^{206}Pb/^{204}Pb$ and $^{208}Pb/^{204}Pb$). Removing this from the dataset lowers the standard deviation to less than 0.04 for each isotopic ratio. Considering the data, it is apparent that the TIMS technique has yielded the anomalous results: BON 96-29 is a rhyodacite dome, along with BON 96-27. Their trace element characteristics are markedly homogenous, yet their TIMS Pb isotope ratios are significantly different. Given that there is good agreement between both PIMMS and TIMS data for BON 96-27, but not for BON 96-29, it is concluded that PIMMS data should be used in preference to TIMS for at least sample BON 96-29. Therefore, for the sake of consistency, PIMMS Pb data is used throughout this work, except where otherwise stated.

E.2. Sr analysis of apatite mineral separates

The aim of this experiment was to investigate whether the high $^{87}Sr/^{86}Sr$ ratios of the Formation are a result of alteration, as was assumed on the basis of their trace element characteristics, or whether they do indeed represent magmatic values. The rationale behind this is that primary igneous apatites should preserve their initial isotopic ratio, even if the whole rock has been reset, as they are a lot less susceptible to alteration than other major phases.

E.2.1. Sample selection

Samples were selected on the basis of thin section petrography. Care was taken to ensure that, of the samples for which isotopic data already existed, samples containing the greatest amount of phenocrystic apatite (and the largest average grain size) were chosen. Two rhyodacites, BON 99-180 and BON 96-29 were selected: despite their whole rock ratios not being the highest of the Washikemba Formation, the abundance of apatite (~1%, ~0.5 mm in length) meant that the experiment was most likely to succeed.

E.2.2. Sample preparation and mineral separation

Samples were prepared at the crushing facilities at NIGL. The samples were first split into as small fragments as possible (~1 cm) using the handsplitter. The residue from this was placed in the jawcrusher, and run through 5 times, cleaning the apparatus between each sample. The output from this stage was then placed in a diskmill until the average grainsize was about 1 mm, and then the fine sand was placed in a mechanical sieve, with a 600μm mesh, sieved for 15 minutes and repeated. Any material that did not go through the sieve at this point was reground using the diskmill, and then resieved.

The heavy minerals were then separated from the lighter ones in the <600μm fraction, using the NIGL "superpanner" table. One spoonful at a time, the sample was placed onto one end of the superpanner, which was set to vibrate at its highest setting. The gradient of the table was gradually increased, in order that the heavy mafic minerals were preferentially retained at the top of the table. These were extracted, using a pipette and dried in a 100°C oven.

At this stage, heavy liquids were used to remove other non-magnetic minerals such as quartz and feldspar. As apatite has a specific gravity of ~3, Two density beads (2.98 and 3.01) were used to separate the mineral, using methyl iodide diluted with acetone.

The resulting mineral separate was then placed in a Franz magnetic separator, in order to extract any magnetic minerals such as magnetite. In addition, it was possible to remove non-magnetic minerals that frequently contain magnetic inclusions, such as zircon and epidote. The resulting fraction was then handpicked, using tweezers and a binocular microscope, before the apatites were transferred to a glass beaker and placed in an ultrasonic bath for 20 minutes, to remove any associated material. In total, 121μg of apatites were obtained from BON 99-180, and 56μg from BON 96-29.

E.2.3. **Isotopic analysis**

The dried apatite separates were placed in Savillex© beakers, prior to chemical dissolution and analysis as for whole rock procedures (described in Section E.1). The apatites were analysed for Sr and Nd isotopes, and these results are presented in Table E.5. The limited quantity of sample resulted in relatively poor analyses (i.e. 20 ratios for BON 96-29 and 5 ratios for BON 99-180. Nonetheless, as presented in Section 5.8.2.1, the data quality is sufficient to prove that the Sr isotope ratios of the Washikemba Formation have been artificially raised by secondary alteration processes, and therefore the hypothesis is correct.

E.3. Hf isotope analysis

E.3.1. **Sample preparation**

Sufficient amount of whole rock powder was weighed into a 60ml Savillex© bomb to ensure recovery of ~1 μg of Hf. 2mls of 16M HNO_3 was then added, along with 10–12 mls of 29M HF, prior to being sealed placed on a 120°C hotplate overnight, and then evaporated the next day.

The sample dissolution procedure invariable produces a fluoride precipitate, which may contain some Hf. In addition, Hf may adhere to the walls of the dissolution bomb or centrifuge tube. The sample conditioning process is designed to recover as much of the available Hf as possible by using a 4N hydrofluoric acid leaching procedure. Depending on the weight of sample initially dissolved, 2–4mls of 4N HF was added to the dry sample residue and sealed and agitated. This slurry was then transferred to clean 12 ml HDPP centrifuge tubes and centrifuged at 4000–5000 rpm for 90 mins. When the sample has been centrifuged, it was decanted into the centrifuge tubes and centrifuged once more. A final 2mls of 4N HF was directly to the sample residues in the centrifuge tubes before a final centrifuging stage.

E.3.2. **Chemical separation**

The 4^+ ions, Ti-Zr-Hf, are strongly adsorbed onto the BioRad anion exchange resin AGl-X8 in dilute 4N HF, whereas major elements and other trace elements are not. Therefore, the separation and purification of Hf for isotopic analysis starts with loading the dissolved sample onto a large anion exchange column, eluting the undesired elements with 4N HF and stripping off the Ti-Zr-Hf with 1N HF–1N HCI. These anion exchange columns were thoroughly cleaned prior to sample loading. 3–6mls of 4N HF were eluted, followed by 200mls and then a further 30 mls. The solutions were then collected in 60 mls of 1N HF-1N HCI, and 20 to 30µl of 36.6N H_2SO_4. was added to the collection beaker. These were dried down on a hotplate overnight, prior to the second column procedure.

1ml of 0.52N H_2SO_4–5% H_2O_2 was first added to the sample residue, which was then pipetted along with the sample, into the second stage columns. The sample beakers were washed with a further 1 ml of 0.52N H_2SO_4 - 5% H_2O_2, which was then added to the appropriate columns. After the first wash has eluted, an additional wash consisting of 1ml of 0.52N H_2SO_4 - 5% H_2O_2 was eluted, and then 12 mls of 0.52N H_2SO_4 - 5% H_2O_2. Once this had eluted through the column, the Hf fraction was collected using 13mls of 1N HF-2N HCI. Collected samples were then dried down on a hotplate in a fume cupboard.

E.3.3. **Mass spectrometric analysis**

Hf separates collected during ion exchange chemistry that are to be run by plasma ionization multi-collector mass spectrometry (PIMMS) must be dissolved in a dilute solution of nitric acid (~2%) and 0.1M HF. The samples were therefore transferred into 1ml micro-centrifuge tubes in a dilute solution of nitric acid (~2%) and 0.1M HF, and placed in the autosampler rack of the PIMMS. The results of this study are presented in Table E.3.

Appendix E- Table E.2

Batch #	Sample	TIMMS $^{206}Pb/^{204}Pb$ measured	error	TIMMS $^{207}Pb/^{204}Pb$ measured	error	TIMMS $^{208}Pb/^{204}Pb$ measured	error	TIMMS $^{206}Pb/^{204}Pb$ corrected	TIMMS $^{207}Pb/^{204}Pb$ corrected	TIMMS $^{208}Pb/^{204}Pb$ corrected
P207:1	**BON 96-22**	18.974	1	15.561	1	38.470	2	19.007	15.606	38.633
P207:2	**BON 96-27**	19.898	2	15.603	1	39.459	3	19.933	15.648	39.627
P207:3	**BON 96-29**	20.080	2	15.609	1	39.467	3	20.115	15.654	39.635
P207:4	**BON 99-27**	19.115	2	15.583	2	38.625	4	19.149	15.628	38.789
P207:5	**BON 99-35**	19.077	2	15.568	1	38.439	4	19.111	15.613	38.602
P207:6	**BON 99-87**	18.992	2	15.549	1	38.579	3	19.025	15.594	38.743
P207:7	**BON 99-104**	19.208	1	15.559	1	38.636	1	19.241	15.604	38.801
P207:8	**BON 99-144**	18.962	1	15.564	1	38.541	3	18.995	15.609	38.705
P207:9	**BON 99-180**	18.752	1	15.529	1	38.231	1	18.785	15.574	38.393
P207:10	**BON 00-01**	18.933	1	15.561	1	38.532	3	18.966	15.606	38.696
P207:11	**JB1**	18.33184	0	15.51512	0	38.49750	0	18.364	15.560	38.661
P207:12	**blank**	452 pg						452 pg		

Sample	U	Th	Pb	$^{206}Pb/^{204}Pb$ initial	$^{207}Pb/^{204}Pb$ initial	$^{208}Pb/^{204}Pb$ initial
BON 96-22	1.20	1.32	6.02	18.82676	15.598	38.570
BON 96-27	0.72	2.17	0.80	19.09926	15.609	38.821
BON 96-29	0.63	0.63	0.79	19.37682	15.620	39.396
BON 99-27	1.17	1.03	4.02	18.88537	15.616	38.715
BON 99-35	1.23	0.84	3.99	18.83296	15.600	38.541
BON 99-87	0.18	0.62	1.09	18.87628	15.587	38.578
BON 99-104	0.39	1.37	2.24	19.08375	15.597	38.623
BON 99-144	0.49	0.82	2.99	18.84670	15.603	38.625
BON 99-180	0.55	0.56	2.65	18.59888	15.565	38.333
BON 00-01	0.33	0.89	2.54	18.84898	15.601	38.595

Corrected values have been corrected for mass bias and normalised to average for 20/7/00 to 21/7/00 (for standard loads ~75ng) .
$^{206}Pb/^{204}Pb$ correction factor: 16.90594±.00453 (1 sigma, n= 10)
$^{207}Pb/^{204}Pb$ correction factor: 15.44418±.00546 (1 sigma, n=10)
$^{208}Pb/^{204}Pb$ correction factor: 36.54529±.01398 (1 sigma, n= 10)
All normalised to accepted values (15.4891, 16.9356 and 36.7006, respectively) of Todt et al., 1996.

Batch #	Sample	PIMMS $^{206}Pb/^{204}Pb$ measured	error	PIMMS $^{207}Pb/^{204}Pb$ measured	error	PIMMS $^{208}Pb/^{204}Pb$ measured	error	PIMMS $^{206}Pb/^{204}Pb$ corrected	PIMMS $^{207}Pb/^{204}Pb$ corrected	PIMMS $^{208}Pb/^{204}Pb$ corrected
P206:1	**BON 96-22**	19.416096	3	16.1100227	2	40.302201	3	19.015	15.618	38.669
P206:2	**BON 96-27**	20.323426	6	16.1212359	5	41.249395	5	19.899	15.623	39.560
P206:3	**BON 96-29**	20.132263	4	16.1223878	4	40.962592	4	19.714	15.627	39.294
P206:4	**BON 99-27**	19.495838	5	16.1110977	5	40.379307	5	19.085	15.609	38.710
P206:5	**BON 99-35**	19.532615	4	16.1220358	3	40.305044	3	19.116	15.614	38.619
P206:6	**BON 99-87**	19.434059	6	16.1007105	5	40.42987	6	19.019	15.592	38.735
P206:7	**BON 99-104**	19.662066	4	16.1230213	4	40.520095	3	19.241	15.612	38.817
P206:8	**BON 99-144**	19.399476	4	16.1224801	3	40.403022	3	18.982	15.610	38.699
P206:9	**BON 99-180**	19.192086	4	16.0856612	4	40.084091	3	18.779	15.573	38.391
P206:10	**BON 00-01**	19.403137	6	16.1197847	5	40.417697	5	18.977	15.597	38.678
P206:11*	**JB-1**		3		3		3	18.349	15.558	38.638
P206:12	**blank**	18.6621		15.9548		39.9547		144 pg		
P206:13	**BHVO**	19.028097	4	16.0054969	4	39.625893	4	18.701	15.597	38.285

*solution ran out before end; result on edited ratios

Sample	U	Th	Pb	$^{206}Pb/^{204}Pb$ initial	$^{207}Pb/^{204}Pb$ initial	$^{208}Pb/^{204}Pb$ initial
BON 96-22	1.20	1.32	6.02	18.867512	15.655422	38.769772
BON 96-27	0.72	2.17	0.80	19.098887	15.629927	38.920856
BON 96-29	0.63	0.63	0.79	19.015289	15.638364	39.224182
BON 99-27	1.17	1.03	4.02	18.855001	15.642258	38.800432
BON 99-35	1.23	0.84	3.99	18.871129	15.646095	38.721423
BON 99-87	0.18	0.62	1.09	18.903249	15.630409	38.734143
BON 99-104	0.39	1.37	2.24	19.116331	15.650211	38.8035
BON 99-144	0.49	0.82	2.99	18.866713	15.647973	38.783433
BON 99-180	0.55	0.56	2.65	18.625481	15.609826	38.49381
BON 00-01	0.33	0.89	2.54	18.893034	15.636941	38.740545

Corrected values have been corrected for mass bias and normalised to average for 28/11/00 to 7/12/00
(for standard loads ~75ng) .

$^{206}Pb/^{204}Pb$ correction factor: 16.936532 ±.001457 (1 sigma, n= 42)

$^{207}Pb/^{204}Pb$ correction factor: 15.48716± .002045(1 sigma, n=42)

$^{208}Pb/^{204}Pb$ correction factor: 36.698691±.0033554 (1 sigma, n= 42)

All normalised to accepted values (15.4891, 16.9356 and 36.7006, respectively) of Todt et al., 1996.

Table E.3: Sr isotope data

Batch#	Sample #	$^{87}Sr/^{86}Sr$ measured	error	$^{87}Sr/^{86}Sr$ normalized	Rb	Sr	$^{87}Sr/^{86}Sr$ Initial
P207:1	**96-22**	0.706410	5	0.706407	5.75	66.31	0.7060863
P207:2	**96-27**	0.704545	4	0.704542	6.07	99.00	0.70431516
P207:3	**96-29**	0.704362	4	0.704359	0.15	48.90	0.70434736
P207:4	**99-27**	0.706507	5	0.706504	3.77	125.39	0.70639277
P207:5	**99-35**	0.705603	6	0.705600	0.94	79.16	0.70555596
P207:6	**99-87**	0.704086	7	0.704083	10.70	399.35	0.70398385
P207:7	**99-104**	0.704164	4	0.704161	2.31	221.12	0.70412232
P207:8	**99-144**	0.704991	5	0.704988	12.38	103.52	0.70454551
P207:9	**99-180**	0.704990	5	0.704987	6.00	54.43	0.70457898
P207:10	**00-01**	0.704843	7	0.704840	3.76	116.00	0.70484002
P207:11	**JB1**	0.704144	5	0.704141			
P207:12	**blank**	1080pg					
P207:13	**BHVO**	0.703466	6	0.703463			

Batch P207 normalised to machine average 0.710243 ± 11 (1 sigma, n =11). Accepted value of NBS 987 = 0.71024

Table E.4: Apatite Sr and Nd isotope data

		$^{87}Sr/^{86}Sr$ measured	error	$^{143}Nd/^{144}Nd$ measured	error	$^{43}Nd/^{144}Nd$ normalized
P222:13	**BON 96-29 apatite**[1]	0.70335	7	0.513072	6	0.51303
P222:13	**Nd concentration**			1059.72	0.0252	
P222:13	**Sm concentration**			289.27	0.00961	
P222:14	**BON 99-180 apatite**[2]	0.703	1.1	0.513085	5	0.51304
P222:14	**Nd concentration**			949.56	0.01994	
P222:14	**Sm concentration**			270.99	0.00645	
P222:15	**Nd blank**			60pg		
P222:15	**Sm blank**			9 pg		

[1] Obtained on 20 ratios

[2] Obtained on 5 ratios

Table E.5: Nd isotope data

Batch#	Sample #	$^{143}Nd/^{144}Nd$ measured	error	$^{143}Nd/^{144}Nd$ normalized	Sm	Nd	$^{143}Nd/^{144}Nd$ initial	εNd
P207:1	**BON 96-22**	0.513018	5	4.999511	2.93	10.79	0.512873	6.76
P207:2	**BON 96-27**	0.513077	3	2.999707	5.53	23.70	0.512946	8.17
P207:3	**BON 96-29**	0.513066	3	2.999707	3.30	12.27	0.512922	7.72
P207:4	**BON 99-27**	0.513022	5	4.999511	3.72	14.64	0.512883	6.96
P207:5	**BON 99-35**	0.513054	4	3.999609	3.71	12.14	0.512897	7.23
P207:6	**BON 99-87**	0.513071	4	3.999609	2.48	8.71	0.512922	7.71
P207:7	**BON 99-104**	0.513099	4	3.999609	5.45	19.71	0.512953	8.31
P207:8	**BON 99-144**	0.513061	4	3.999609	2.72	9.12	0.512907	7.42
P207:9	**BON 99-180**	0.513065	3	2.999707	2.27	7.63	0.512911	7.50
P207:10	**BON 00-01**	0.513063	4	3.999609	3.55	11.46	0.512905	7.38
P222:1	**BON 99-182**	0.513084	5	4.999384	2.55	9.02	0.513021	7.43
P222:2	**BON 99-173**	0.513077	5	4.999384	1.62	4.74	0.513014	7.29
P222:3	**BON 00-52**	0.513095	4	3.999507	7.75	29.45	0.513032	7.64
P222:4	**BON 00-34**	0.513110	4	3.999507	2.41	7.62	0.513047	7.93
P222:5	**BON 00-67**	0.513058	5	4.999384	5.74	18.49	0.512995	6.92
P207:11	**JB1**	0.512834	5	4.999511				
P207:12	**blank**	195pg						
P207:13	**BHVO**	0.513034	5	4.999511				

Batch P207 normalized to MAT262 J&M average of 0.511175 ± 13 (1 sigma, n=14)
Batch P222 normalized to MAT 262 J&M for 5/2/01 to 12/2/01 = 0.511188±9 (1 sigma, n=14)
Accepted value for J&M = 0.511125

Table E.6: Hf isotope data

Batch #	Sample #	$^{176}Hf/^{177}Hf$ (172 corr) meas.	1 SD abs	$^{176}Hf/^{177}Hf$ 172 normalised	Lu	Hf	Epsilon Hf (t=88)	initial Hf
H90:1	**BON 96-22**	0.283173	4	0.283127	0.424	3.26	13.46	0.283082
H90:2	**BON 96-27**	0.283187	6	0.283116	0.746	7.79	13.36	0.283093
H90:3	**BON 96-29**	0.283163	4	0.283118	0.444	7.01	13.70	0.283103
H90:4	**BON 99-27**	0.283167	3	0.283122	0.2856	1.98	13.13	0.283090
H90:5	**BON 99-35**	0.283216	3	0.283171	0.6039	2.91	14.35	0.283121
H90:6	**BON 99-87**	0.283187	3	0.283138	0.2805	1.76	13.58	0.283100
H90:7	**BON 99-104**	0.283196	2	0.283155	0.5305	2.58	13.78	0.283105
H90:8	**BON 99-144**	0.283209	3	0.283159	0.4158	3.50	14.67	0.283130
H90:9	**BON 00-01**	0.283199	3	0.283154	0.427	2.69	14.14	0.283111
H106:1	**BON 99-180**	0.283191	2	0.283136	0.3653	4.3578	14.16	0.283116
H106:2	**BON 99-182**	0.283190	3	0.283135	0.2674	1.64	13.43	0.283095
H106:3	**BON 99-173**	0.283200	2	0.283145	0.3132	2.9719	14.27	0.283119
H106:4	**BON 00-52**	0.283179	3	0.283124	0.9072	9.8319	13.66	0.283102
H106:5	**BON 00-34**	0.283214	3	0.283164	0.3329	2.88	14.88	0.283131
H106:6	**BON 00-67**	0.283198	3	0.283148	0.7821	4.5849	13.84	0.283102
H90:10	**pk-G-D12**	0.283104	3					

Batch 90 average JMC 475 for 1/8/00 to 5/8/00 = 0.282205±8 (1 sigma, n-37)
Batch H106 average JMC 475 for 31/01/01 p.m. to 01/02/01 a.m. = 0.282215±6.9, 1 sigma, n=6
Agreed value of JMC 475 is 0.28216 (Nowell et al., 1998).

Appendix E- Table E.8

Sample	PIMMS $^{206}Pb/^{204}Pb$ corrected	PIMMS $^{207}Pb/^{204}Pb$ corrected	PIMMS $^{208}Pb/^{204}Pb$ corrected	TIMS $^{206}Pb/^{204}Pb$ corrected	TIMS $^{207}Pb/^{204}Pb$ corrected	TIMS $^{208}Pb/^{204}Pb$ corrected
BON 96-22	19.015	15.618	38.669	19.007	15.606	38.633
BON 96-27	19.899	15.623	39.560	19.933	15.648	39.627
BON 96-29	19.714	15.627	39.294	20.115	15.654	39.635
BON 99-27	19.085	15.609	38.710	19.149	15.628	38.789
BON 99-35	19.116	15.614	38.619	19.111	15.613	38.602
BON 99-87	19.019	15.592	38.735	19.025	15.594	38.743
BON 99-104	19.241	15.612	38.817	19.241	15.604	38.801
BON 99-144	18.982	15.610	38.699	18.995	15.609	38.705
BON 99-180	18.779	15.573	38.391	18.785	15.574	38.393
BON 00-01	18.977	15.597	38.678	18.966	15.606	38.696

Appendix F

Publications and presentations resulting from this study

F.1. Publications

Thompson, P.M.E., Kempton, P.D., White, R.V., Kerr, A.C., Tarney, J., Saunders, A.D. and Pringle, M.S. Elemental, isotopic and geochronological constraints on an island arc sequence associated with the Cretaceous Caribbean Plateau: the Washikemba Formation, Bonaire, Dutch Antilles. *In Prep.*

Thompson, P.M.E., Kempton, P.D., White, R.V., Kerr, A.C., Tarney, J., Saunders, A.D. and Fitton, J.G. Hf-Nd isotope constraints on the origin of the Cretaceous Caribbean plateau and its relationship to the Galápagos plume. *Submitted to EPSL.*

Kerr, A.C., White, R.V., Thompson, P.M.E., Tarney, J., Saunders, A.D., 2002. No Oceanic Plateau- No Caribbean plate? The Seminal Role of Oceanic Plateau(s) in Caribbean Plate Evolution. *In Press.*

F.2. Oral and Poster presentations

Thompson, P.M.E., Kempton, P.D., White, R. V., Saunders, A. D., Kerr, A.C and Tarney, J., 2002. Hf-Nd isotopic sysytematics of the Gorgona komatiites and implications for their relationship to the Caribbean plateau. *Goldschmidt, Davos, Switzerland.*

Thompson, P.M.E., White, R. V., Kerr, A. C., Tarney, J. & Saunders, A. D. 2001. The significance of island arcs associated with oceanic plateaux: a perspective from Bonaire, Dutch Caribbean. *Invited seminar (November, 2001),* University of Lausanne, Switzerland.

Thompson, P.M.E., Kempton, P.D.,White, R.V.W., Kerr, A.C., Tarney, J., and Saunders, A. D. 2001. New Hf-Nd evidence supports a heterogeneous plume source for the Caribbean Plateau. *International Symposium on South American Isotope Geology,* Pucon, Chile.

Thompson, P.M.E., White, R. V., Kerr, A. C., Tarney, J. & Saunders, A. D. 2001. The role of the Cretaceous Caribbean intra-oceanic arc system in Caribbean tectonic evolution. *Intra-Oceanic Subduction Zones Meeting*, Burlington House, UK.

Thompson, P.M.E., Kempton, P.D. Tarney, J., Saunders, White, R.V.W., and Kerr, A.C., 2001. Hf-Nd systematics of an arc sequence associated with the Cretaceous Caribbean oceanic plateau. *Goldschmidt International Geochemical Conference,* Virginia, US.

Thompson, P.M.E., Kempton, P.D. White, R.V., Tarney, J., Saunders and Kerr, A.C., 2001. New Isotopic and Geochronological Constraints on the Origin of an Island Arc Sequence Associated with the Cretaceous Caribbean Oceanic Plateau. *International Caribbean Workshop*, Leicester, UK.

Thompson, P.M.E., Kempton, P.D., Pringle, M.S, Tarney, J., Saunders, White, R.V.W., and Kerr, A.C., 2001. Geochronological and Isotopic constraints on the origin of an island arc sequence associated with the Caribbean plateau. *EUG,* Strasbourg, France.

Thompson, P.M.E., Kempton, P.D. Tarney, J., Saunders, White, R.V.W., and Kerr, A.C., 2001. The geochemical origin of an island arc sequence associated with the Cretaceous Caribbean oceanic plateau. *Volcanic and Magmatic Studies Group*, Durham, UK.

Thompson, P.M.E., Tarney, J., White, R.V.W., Saunders, A.D., Kempton, P.D. and Kerr, A.C., 2000. The Geochemical and Tectonic Origin of Island Arcs Associated with the Caribbean Oceanic Plateau. *Goldschmidt International Geochemical Conference*, Oxford.

Thompson, P.M.E., White, R., V., Tarney, J., Kempton, P.D., Kerr, A.C., and Saunders, A., D. 1999. The association between island arcs, tonalitic batholiths and oceanic plateaux in the Netherlands Antilles: implications for continental growth. *International Symposium for Andean Geodynamics, p. 749-753.* IRD, Gottingen, Germany.